

UNIVERSITY OF LONDON  
IMPERIAL COLLEGE OF SCIENCE & TECHNOLOGY  
DEPARTMENT OF ELECTRICAL ENGINEERING

MODULATION TRANSFER FUNCTIONS OF A.C.  
SERVOMECHANISM COMPONENTS

---

Thesis submitted for the degree of  
Doctor of Philosophy  
in the Faculty of Engineering

by

Farouk Bashandy KHALAFALLA  
B.Sc.(Hons), D.I.C., Grad. I.E.E.

May 1967

ABSTRACT

The main purpose of the work presented in this thesis was the development of more refined and systematic methods for the analysis and representation of various aspects of a.c. servo mechanisms, based on more realistic assumptions. Emphasis has been placed upon expanding the ideas in the area of a.c. compensation particularly with reference to chopper networks. Extensions and modifications of the available experimental techniques have been attempted, with the aim of obtaining more accurate results and overcoming practical limitations. To establish the necessary criteria on which accurate and efficient design for a.c. servomechanisms could be based, multiplication and rotary modulation transfer functions of idealised carrier channels between modulator and demodulator, have been studied in detail.

The 2-axis general theory of machines has been applied to the analysis of the 2-phase servomotor, the synchro-system and the a.c. tachometer, resulting in improved description to their dynamic behaviour. Because either a modulation or a demodulation process is effected in each of these components, it is not sufficient to obtain an explicit transfer function to describe each isolated component. It is necessary in dealing with a.c. servomechanisms, to correlate various components characteristics in order that an overall open-loop and closed-loop transfer functions may be obtained. Considerable weight has been given to the development of mathematical models and block diagram representations for various components and their interrelationships.

Compensation plays a significant part in the design of servomechanisms as an effective solution to the problems relevant to the system stability and to the improvement of the overall dynamic characteristics. The a.c. tachometer, as a simplest type of compensation, has been rigorously analysed, and its contribution

to the system response has been demonstrated. A synthesis method has been developed to realize linear compensating networks for specified multiplicative and rotary modulation transfer functions. Particular attention has been given to chopper class of networks which has recently emerged as a superior type of a.c. compensation specially when the carrier frequency deviation is large. These networks consist of passive electric elements interconnected by one or more 3-terminal synchronous switches. A design procedure of a transistor 3-terminal switch suitable for this application and its driving circuit, capable of operating with positive and negative fly-time, has been presented in detail. To facilitate the development of new networks, methods have been developed whereby configurations and responses of chopper networks can be modified and expanded. This has been achieved by extending the application of the duality concept to 3-terminal chopper networks and by exploiting the negative fly-time capabilities of the switch. Exact analysis of various chopper networks has been attempted using Z-transform and bounded forms of their multiplicative and rotary modulation transfer functions have been achieved. Previously, several authors have developed approximate methods of analysis for simple configurations of such networks using equivalent time-invariant electric networks. A portion of this thesis is devoted to a reformulation of this method in such a way as to be applicable to more general and complex configurations of chopper networks. Practical investigations have been performed on a selected number of chopper networks under various operating conditions, and the experimental results have been compared with the theoretical results obtained by both the exact and approximate methods.

To determine experimentally the modulation frequency response of a.c. servomechanisms, a test signal in the form of suppressed-carrier amplitude-modulated wave is required. Although conventional electronic modulators may be considered as simplest means by which such signal can be produced, they suffer from the serious draw-back

that the ratio modulating frequency to carrier frequency of the generated wave, for practical reasons, is limited to about 10%. As a result, the system modulation frequency response can be obtained over only a small range which may not give adequate information for the design purposes. A simple scheme has therefore been developed whereby the available commercial electronic modulators and demodulators can extend their working range of the ratio modulating frequency to carrier frequency. This scheme does not involve any modification to the basic circuits incorporated in the commercial electronic modulators and demodulators. The principle of the proposed scheme is based on artificially raising the frequency of the signal before being applied to the modulator, (or demodulator), and thus avoiding the non-flat portion of the frequency characteristics of various circuits incorporated. To accomplish this, the signal may be modulated on to a second high carrier before passing through these circuits whose output may then be demodulated by the same high carrier in order to recover the required signal. The processes of modulation and demodulation on the second high carrier have been achieved by means of square-wave modulators and demodulators, which have been designed and used in conjunction with a commercial modulator-demodulator set in such a way as to check the effectiveness of the proposed theory.

ACKNOWLEDGMENTS

The work described in this thesis was carried out in the Electrical Engineering Department of the Imperial College of Science and Technology, London, under the supervision of Professor D.G.O. Morris, D.Sc., F.I.E.E., of Pahlavi University, Shiraz, Iran. Dr. Morris was formerly University Reader at Imperial College and the author wishes to express his gratitude and indebtedness for his helpful guidance, constant encouragement and keen interest throughout the course of the work.

The author expresses his thanks to Dr. P.H.G. Allen, Dr. M.J. Short, and members of the staff of Power Systems and Machines for their valuable comments and helpful advice. Thanks are also extended to Mr. D. Pedder and Mr. H. Hardie for occasional assistance in the laboratory. Advice received from several colleagues on the use of the computer is highly appreciated.

The author wishes to place on record his sincere gratitude to his friend Dr. O.P. Malik for his encouragement and invaluable discussions. The author wishes to express appreciation of the facilities provided by the Electrical Engineering Department of the Imperial College of Science and Technology, London.

Finally, the author wishes to acknowledge with thanks the grant of study leave by Cairo University, which enabled him to undertake this work.

LIST OF CONTENTS

	<u>page no.</u>
Abstract	2
Acknowledgments	5
List of Contents	6
List of Figures	20
<u>Nomenclature:</u> a) List of symbols	33
i) Principal symbols	33
ii) Subscripts	35
iii) Superscripts	35
b) List of abbreviations	35
c) General notes	36
<u>CHAPTER 1</u> : INTRODUCTION	38
1.1 General features of a.c. servo- mechanisms	38
1.2 Principle of operation of a typical modulated-carrier positional control system	38
1.3 Problems associated with the design of a.c. servomechanisms	41
1.4 Review of previous work	42
1.4.1 General	42
1.4.2 Two-phase servo-motor	43
1.4.3 Error-detector	47
1.4.4 Techniques of compensation	48
1.4.4.1 Load compensation	49
1.4.4.2 A.c. tachometer feedback	50
1.4.4.3 Tandem compensation	53
1.5 Scope of the present work	91
1.5.1 Analysis of the basic components of a.c. servomechanisms	93

1.5.2 Compensation of a.c. systems	96
1.5.3 Experimental investigations	98
1.5.4 Scheme for extending the practical range of operation of commercial electronic modulators and demodulators	99
1.6 Original contribution	100
<u>CHAPTER 2</u> : ANALYSIS OF THE BASIC COMPONENTS OF A.C. SERVOMECHANISMS	
2.1 Introduction	103
2.2 Two-phase servomotor	104
2.2.1 Formulation of the dynamic equations	104
2.2.1.1 Voltage equations	104
2.2.1.2 Torque equation	107
2.2.2 Representation of the 2-phase servo-motor dynamic behaviour by a mathematical model	115
2.2.3 Complex frequency block diagram representation of the 2-phase servo-motor	118
2.3 Error-detector in the form of a transmitter-coincidence transmitter synchro-system	121
2.3.1 General	121
2.3.2 Analysis	123
2.3.2.1 Operating conditions of the postulated coincidence- transmitter rotor	124

2.3.2.2	Operating conditions of the postulated transmitter rotor	125
2.3.2.3	Boundary conditions	126
2.3.3	Representation by a mathematical model	128
2.3.4	Complex frequency block diagram representation	129
2.4	Open-loop and closed-loop responses of the uncompensated system	131
2.4.1	Formulation of the modulation transfer functions for the uncompensated a.c. servomechanism	132
2.4.1.1	System with a potentiometer-bridge as error-detector	132
2.4.1.2	System with a synchro-pair as error-detector	134
2.4.2	Complex frequency block diagram representation of the uncompensated a.c. servomechanism	135
2.4.2.1	System with a potentiometer-bridge as error-detector	135
2.4.2.2	System with a synchro-pair as error-detector	137
2.5	General discussion	139
<u>CHAPTER 3</u>	: COMPENSATION OF A.C. SERVOMECHANISMS	141
3.1	Introduction	141
3.2	A.c. tachometer	143
3.2.1	General	143
3.2.2	Analysis	144



3.2.3	Representation by a mathematical model	146
3.2.4	Complex frequency block diagram representation	147
3.2.5	Positional control a.c. servo-mechanism compensated by a.c. tachometer	149
3.3	Linear networks	150
3.3.1	General	150
3.3.2	Multiplicative modulation transfer function	152
3.3.3	Method of synthesising the transfer function from the multiplicative modulation transfer function	156
3.3.4	Rotary modulation transfer function	158
3.3.5	Method of synthesising the transfer function from the rotary modulation transfer function	162
3.4	Chopper networks	163
<u>CHAPTER 4</u>	: ANALYSIS OF CHOPPER NETWORKS	164
4.1	Introduction	164
4.1.1	General	164
4.1.2	Analysis techniques	166
4.1.3	Chopper network configurations	167
4.2	Application of the exact analytical approach	170
4.2.1	Development of block diagram representation	170

4.2.2	Derivation of the Z-transform of the voltage appearing across the capacitor	182
4.2.3	Determination of the output voltage	184
4.2.3.1	Contribution during the periods $nT \leq t < (n+\delta)T$	185
4.2.3.2	Contribution during the periods $(n + \frac{1}{2})T \leq t < (n + \frac{1}{2} + \delta)T$	186
4.2.3.3	Contribution during the periods $(n+\delta)T \leq t < (n + \frac{1}{2})T$ and $(n + \frac{1}{2} + \delta)T \leq t < (n+1)T$	188
4.2.4	Derivation of the multiplicative modulation transfer function	191
4.2.5	Closed form for the multiplicative modulation transfer function	193
4.2.6	Derivation of the rotary modulation transfer function	201
4.2.7	Noise study	203
4.3	Application of the approximate analytical approach	205
4.3.1	Derivation of the voltage appearing across the capacitor at the switching instants	205
4.3.2	Derivation of the chopper network response	207
4.3.3	Determination of equivalent time-invariant passive electric network	209
4.3.3.1	Phase-lag aspect	209
4.3.3.2	Phase-lead aspect	215
4.3.4	Derivation of the multiplicative modulation transfer function	218
4.3.4.1	Phase-lag aspect	218
4.3.4.2	Phase-lead aspect	222

<u>CHAPTER 5</u>	: MODULATION FREQUENCY RESPONSES OF CHOPPER NETWORKS	224
5.1	General	224
5.2	Experimental investigations	225
5.2.1	Tests performed	225
5.2.2	Apparatus used for measuring the modulation frequency response	225
5.2.3	Variable frequency supply	232
5.3	Effects of the various factors on the modulation frequency response	234
5.3.1	Variations of the passive electric elements	235
5.3.2	Fly-time of the synchronous switches	240
5.3.3	Carrier frequency deviation	247
5.3.4	Phase variations of the demodulation carrier reference	249
5.3.5	Phase variations of the modulation carrier reference	250
5.3.6	Combined effect of changing simultaneously the modulation and demodulation carrier references	252
5.3.7	Rotary modulation	252
5.4	Comparison of results	261
5.4.1	Experimental results versus theoretical calculations by the exact method	263
5.4.2	Experimental results versus theoretical calculations by the approximate method	269

5.4.3	Exact theoretical method versus approximate theoretical method	270
5.5	Records of wave forms	271
<u>CHAPTER 6</u>	: BREADBOARD MODEL OF A POSITIONAL CONTROL A.C. SERVO-MECHANISM - (Specifications, Construction, and Preliminary Studies).	279
6.1	Introduction	279
6.2	Component's specifications	280
6.2.1	Load	280
6.2.2	Servomotor	280
6.2.3	Error-detector	282
6.2.4	Gear train	283
6.3	Servo amplifier	284
6.3.1	General design considerations	284
6.3.2	Design requirements and specifications	285
6.3.3	Amplifier transistor circuit design	287
6.3.3.1	List of principal symbols	288
6.3.3.2	Output stage	289
6.3.3.3	Middle stages	297
6.3.3.4	Input stages	302
6.3.3.5	Negative feedback loop	309
6.3.4	Amplifier overall performance	310
6.4	Practical determination of the relevant parameters of the transmitter-coincidence transmitter magstrip-system	314
6.4.1	Static test	316

6.4.2	Dependence of the parameters $k_s$ and $\mu_s$ on the angular misalignment $\gamma_s$ and the magnetic flux density in the transmitter	319
6.4.3	Effect of the carrier frequency variation on the average values of the parameters $k_s$ and $\mu_s$	321
6.4.4	Effect of the transmitter magnetic flux density on the average values of the parameters $k_s$ and $\mu_s$	328
6.4.5	Input characteristics of the static transmitter-coincidence transmitter mag-slip-system for different values of the energising carrier frequency	330
<u>CHAPTER 7</u>	: POSITIONAL CONTROL A.C. SERVOMECHANISM - PRACTICAL INVESTIGATIONS	334
7.1	General	334
7.2	Techniques of measuring the modulation frequency response of the a.c. system	336
7.2.1	Error-detector in the form of a potentiometer-bridge	336
7.2.2	Error-detector in the form of a transmitter-coincidence transmitter mag-slip-system	340
7.2.3	Simulation of the mag-slip-system by means of a potentiometer-bridge in cascade with a differentiator	344
7.3	Experimental results of the uncompensated system modulation frequency responses	346
7.3.1	System with a potentiometer-bridge error-detector	346

7.3.2 System with a magslip-system error-detector	352
7.4 Experimental results of the compensated system modulation frequency responses	358
7.4.1 System with a potentiometer- bridge error-detector	358
7.4.2 System with a magslip-system error- detector	363
7.5 Transient response test considerations	368
7.6 Step-function response test results for the a.c. system with a potentiometer- bridge as error-detector	372
7.6.1 System uncompensated	372
7.6.2 System compensated	376
7.7 Step-function response test results for the a.c. system with a magslip-system as error-detector	379
7.7.1 System uncompensated	379
7.7.2 System compensated	382
 <u>CHAPTER 8</u> : SCHEME FOR EXTENDING THE PRACTICAL RANGE OF OPERATION OF COMMERCIAL ELECTRONIC MODULATORS AND DEMODULATORS	   386
8.1 General	386
8.2 Practical limitations	387
8.2.1 A practical modulator	388
8.2.2 A practical demodulator	390
8.3 Principle of operation of a proposed scheme for overcoming the practical limitations	  391

8.3.1	Theory of the scheme's operation	392
8.3.2	Criteria for the calculation of the auxiliary carrier frequency	394
8.4	Practical realization of the scheme	396
8.4.1	Possible positions of the square- wave modulators and demodulators	396
8.4.2	Design and construction of a transistor square-wave modulator and/or demodulator	398
8.4.2.1	The specified requirements	401
8.4.2.2	Selected components and the values of the designed parameters	402
8.4.3	General discussion	402
8.5	Practical investigations into the performance of the scheme	403
8.5.1	General test arrangement	403
8.5.2	Comparison of the results	407
8.5.3	Oscillograms illustrating the principle of operation of the scheme	411
<u>CHAPTER 9</u>	: CONCLUSIONS	413
9.1	Review and summary of work done	413
9.2	Suggestions for further work	427
BIBLIOGRAPHY		431

<u>APPENDIX A</u>	: ANALYTICAL REDUCTION OF VARIOUS EXPRESSIONS	445
A.1	Approximate expression for matrix $\Delta_1$	445
A.2	" " " " $\Delta_2$	446
A.3	" " " $e_{a1}$	446
<u>APPENDIX B</u>	: ANALYSIS OF THE DOUBLE-SWITCH SINGLE-CAPACITOR CHOPPER NETWORK SHOWN IN FIG.4.1.3b	448
B.1	Application of the exact analytical approach	448
B.1.1	Derivation of the Z-transform of the voltage appearing across the capacitor	448
B.1.2	Determination of the output voltage	449
B.1.2.1	Contribution during the periods $nT \leq t < (n+\delta)T$ and $(n+0.5)T \leq t < (n+0.5+\delta)T$	449
B.1.2.2	Contribution during the periods $(n+\delta)T \leq t < (n+0.5)T$ and $(n+0.5+\delta)T \leq t < (n+1)T$	451
B.1.3	Derivation of the multiplicative modulation transfer function	452
B.1.4	Closed form for the multiplicative modulation transfer function	453
B.2	Application of the approximate analytical approach	455
B.2.1	Derivation of the voltage appearing across the capacitor at the switching instants	455



B.2.2	Derivation of the chopper network response	456
B.2.3	Determination of equivalent time-invariant passive electric network	458
B.2.3.1	Phase-lag aspect	458
B.2.3.2	Phase-lead aspect	460
B.2.4	Derivation of the multiplicative modulation transfer function	461

APPENDIX C : ANALYSIS OF THE CASCADED INVERTED

DOUBLE-SWITCH DOUBLE-CAPACITOR CHOPPER NETWORK SHOWN IN FIG. 4.1.3c.

462

C.1	Application of the exact analytical approach	462
C.1.1	Derivation of the Z-transform of the voltage appearing across the capacitor	462
C.1.2	Determination of the output voltage	463
C.1.2.1	Contribution during the periods $nT \leq t < (n+\delta)T$	463
C.1.2.2	Contribution during the periods $(n+0.5)T \leq t < (n+0.5+\delta)T$	465
C.1.2.3	Contribution during the periods $(n+\delta)T \leq t < (n+0.5)T$ and $(n+0.5+\delta)T \leq t < (n+1)T$	465
C.1.2.4	Contribution during the periods $nT \leq t < (n+\delta)T$	466
C.1.2.5	Contribution during the periods $(n+0.5)T \leq t < (n+0.5+\delta)T$	467
C.1.3	Derivation of the multiplicative modulation transfer function	467

C.1.4 Closed form for the multiplicative modulation transfer function	469
C.2 Application of the approximate analytical approach	471
C.2.1 Derivation of the voltage appearing across the capacitor at the switching instants	471
C.2.2 Derivation of the chopper network response	472
C.2.3 Determination of equivalent time-invariant passive electric network	474
C.2.3.1 Phase-lag aspect	474
C.2.3.2 Phase-lead aspect	476
C.2.4 Derivation of the multiplicative modulation transfer function	478
 <u>APPENDIX D</u> : SOLUTION OF EQUATIONS ASSOCIATED WITH THE ANALYSIS OF CHOPPER NETWORKS	 479
D.1 Solution for function $F_a(s)$	479
D.2 " " " $F_b(s)$	482
D.3 Z-transform of function $Q_1(s)$	483
 <u>APPENDIX E</u> : DATA OF THE BREADBOARD MODEL COMPONENTS	 484
E.1 Mechanical load	484
E.2 Servo-motor	484
E.3 Error-detector	486
E.3.1 Transmitter and coincidence-transmitter	486
E.3.2 Potentiometer-bridge	487

E.4 Photographs for the breadboard model  
components assembly and the  
measuring instruments

487

CHAPTER I : DESIGN OF A TRANSISTOR 3-TERMINAL  
SYNCHRONOUS SWITCH AND ITS DRIVING  
CIRCUIT (see list of contents on  
page 493)

CHAPTER II : DERIVED CHOPPER NETWORKS AND METHODS  
OF MODIFYING THEIR RESPONSES (see  
list of contents on page 556)

LIST OF FIGURES

	<u>page no.</u>
Fig. 1.2.1 : Schematic diagram of a typical modulated-carrier positional control system.	39
Fig. 1.5.1 : A potentiometer-bridge error-detector.	94
Fig. 1.5.2 : Mathematical model representation of a potentiometer-bridge error-detector.	94
Fig. 1.5.3 : Complex frequency block diagram representation of potentiometer-bridge error-detector.	94
Fig. 2.2.1 : Diagrammatic representation of 2-phase servo-motor and its equivalent generalised 2-axis machine.	105
Fig. 2.2.2 : Mathematical model representation of 2-phase servo-motor.	116
Fig. 2.2.3 : Complex frequency block diagram representation of 2-phase servo-motor.	120
Fig. 2.3.1 : Diagrammatic representation of a transmitter-coincidence transmitter synchro-system and its equivalent generalised 2-axis machine.	122
Fig. 2.3.2 : Mathematical model representation of a synchro-system error-detector.	130
Fig. 2.3.3 : Complex frequency block diagram representation of a synchro-system error-detector.	130
Fig. 2.4.1 : Closed-loop block diagram of an uncompensated a.c. servomechanism with a potentiometer-bridge as error-detector.	136
Fig. 2.4.2 : Closed-loop block diagram of an uncompensated a.c. servomechanism with a synchro-pair as error-detector.	138

Fig. 3.2.1	: Mathematical model representation of a.c. tachometer.	148
Fig. 3.2.2	: Complex frequency block diagram representation of a.c. tachometer.	148
Fig. 3.2.3	: Closed-loop block diagram of a positional control a.c. servomechanism compensated by a feedback a.c. tachometer.	151
Fig. 3.3.1	: Ideal a.c. system with multiplicative modulation and demodulation.	153
Fig. 3.3.2	: Processes to obtain the M.M. impulse response and M.M.T.F. from specified impulse response and T.F. respectively.	153
Fig. 3.3.3	: Processes to obtain the impulse response and T.F. from specified M.M. impulse response and M.M.T.F. respectively.	153
Fig. 3.3.4	: Ideal a.c. system with rotary modulation and multiplicative demodulation.	159
Fig.3.3.5:	: Processes to obtain the R.M. impulse response and R.M.T.F. from specified impulse response and T.F. respectively.	159
Fig. 3.3.6	: Processes to obtain the impulse response and T.F. from specified R.M. impulse response and R.M.T.F. respectively.	159
Fig. 4.1.1	: Diagram for deriving the response of a chopper network to M.M. signal.	165
Fig. 4.1.2	: Diagram for deriving the response of a chopper network to R.M.signal.	165
Fig. 4.1.3	: Three prototypes of chopper networks considered in the analysis.	169

		22
Fig. 4.2.1	: Periodic functions of time useful for the analysis of chopper networks.	172
Fig. 4.2.2	: Block diagram representation of the single-switch double-capacitor chopper network illustrated in Fig. 4.1.3a.	175
Fig. 4.2.3	: Block diagram representation of the double-switch single-capacitor chopper network illustrated in Fig. 4.1.3b.	180
Fig. 4.2.4	: Block diagram representation of the cascaded inverted double-switch double-capacitor chopper network illustrated in Fig. 4.1.3c.	181
Fig. 4.2.5	: Paths of integrations along the line $c-j\omega$ to $c+j\omega$ and in the right half of the P-plane.	197
Fig. 4.2.6	: Path of integration in the left half of the P-plane.	197
Fig. 4.2.7	: Rotary modulator and its equivalent arrangement.	202
Fig. 4.3.1	: Circuit diagrams of the equivalent phase-lag time-invariant passive electric networks.	213
Fig. 4.3.2	: Circuit diagrams of the equivalent phase-lead time-invariant passive electric networks.	217
Fig. 4.3.3	: Diagram illustrating the instant at which the peak of the demodulation reference carrier occurs relative to the switching instant.	220
Fig. 4.3.4	: Frequency response locus of the equivalent d.c. networks shown in Fig. 4.3.1.	220

		23
Fig. 4.3.5	: Frequency response locus of the equivalent d.c. networks shown in Fig.4.3.2.	221
Fig. 5.2.1	: Equipment set-up for measuring the modulation frequency responses of chopper networks.	226
Fig. 5.2.2	: Equipment set-up for measuring the d.c. modulation transference.	230
Fig. 5.2.3	: Schematic diagram of a system for changing frequency.	233
Fig. 5.3.1	: M.M. frequency response loci of single-switch double-capacitor chopper network.	236
Fig. 5.3.2	: M.M. frequency response loci of double-switch single-capacitor chopper network.	237
Fig. 5.3.3	: M.M. frequency response loci of cascaded inverted double-switch double capacitor chopper network.	238 & 239
Fig. 5.3.4	: Variation of d.c. modulation transference with the normalized time constant $\tau/T$ .	241
Fig. 5.3.5	: Variation of the normalized equivalent d.c. network frequency $\omega_n/\Omega$ with the normalized time constant $\tau/T$ .	242
Fig. 5.3.6	: The dependence of the normalized frequency $\omega_m/\Omega$ on the normalized time constant $\tau/T$ .	243
Fig. 5.3.7	: The dependence of the peak phase shift on the normalized time constant $\tau/T$ .	244
Fig. 5.3.8	: M.M. frequency response loci of single-switch double-capacitor chopper network illustrating the effect of the fly-time of the incorporated synchronous switch.	245

- Fig. 5.3.9 : Variation of d.c. modulation transference with the normalized fly-time of the synchronous switch. 246
- Fig. 5.3.10 : M.M. frequency gain and phase responses of single-switch double-capacitor chopper network under different values of carrier frequency. 248
- Fig. 5.3.11 : M.M. frequency response loci of single-switch double-capacitor chopper network illustrating the effect of varying the phase of the demodulation reference. 253
- Fig. 5.3.12 : M.M. frequency response loci of single-switch double-capacitor chopper network illustrating the effect of varying the phase of the modulation reference. 254
- Fig. 5.3.13 : M.M. frequency response loci of single-switch double-capacitor chopper network illustrating the effect of varying simultaneously the phases of the modulation and demodulation references. 255
- Fig. 5.3.14 : Plot of the d.c. modulation transference as a function of the phase of the demodulation reference. 256
- Fig. 5.3.15 : Dependence of the maximum d.c. modulation transference and the corresponding phase of the demodulation reference upon the phase of the modulation reference. 257
- Fig. 5.3.16 : A practical differentiating circuit. 258
- Fig. 5.3.17 : Frequency response of the differentiating circuit shown in Fig. 5.3.16. 258



Fig. 5.3.18	:	R.M. frequency response loci of single-switch double-capacitor chopper network illustrating the effect of varying the phase of the demodulation reference.	260
Fig. 5.3.19	:	R.M. frequency gain and phase responses of single-switch double-capacitor chopper network under different values of carrier frequency.	262
Fig. 5.4.1	:	M.M. frequency response loci of single-switch double-capacitor chopper network.	264
Fig. 5.4.2	:	See caption of Fig. 5.4.1	265
Fig. 5.4.3	:	M.M. frequency response loci of double-switch single-capacitor chopper network.	266
Fig. 5.4.4	:	Variation of the d.c. modulation transference with the normalized time constant $\tau/T$ .	268
Fig. 5.5.1	:	Steady-state response of single-switch double-capacitor chopper network subject to S.C.A.M. wave.	272
Fig. 5.5.2	:	See caption of Fig. 5.5.1.	273
Fig. 5.5.3	:	Steady-state response of single-switch double-capacitor chopper network subject to R.M. wave.	274
Fig. 5.5.4	:	See caption of Fig. 5.5.3.	275
Fig. 5.5.5	:	" " " " " .	276
Fig. 5.5.6	:	" " " " " .	277
Fig. 6.3.1	:	Blocked-rotor open-circuit characteristics of the servomotor.	290
Fig. 6.3.2	:	Open-circuit impedance characteristics of the servomotor.	291

Fig. 6.3.3	:	No-load characteristics of the servomotor.	292
Fig. 6.3.4	:	A transistor circuit for the servo-amplifier.	294
Fig. 6.3.5	:	Complete small-signal circuit model for the stage 2 of the servo-amplifier.	306
Fig. 6.3.6	:	Simplified low-frequency circuit model for the stage 2 of the servo-amplifier (valid up to 20 kc.).	306
Fig. 6.3.7	:	Servo-amplifier frequency response for different settings of the gain control.	312
Fig. 6.3.8	:	Dependence of the servo-amplifier transfer admittance on frequency, for different settings of the gain control.	315
Fig. 6.4.1	:	Dependence of the parameters, $k_s$ and $\mu_s$ on the angular misalignment $\gamma_s$ for different values of the transmitter magnetic flux density.	320
Fig. 6.4.2	:	Dependence of the parameters $k_{sav}$ and $\mu_{sav}$ on the energization carrier frequency for two values of the transmitter magnetic flux density.	322
Fig. 6.4.3	:	Transfer locus of $\bar{k}_{sav}/E_s$ .	325
Fig. 6.4.4	:	" " " " .	326
Fig. 6.4.5	:	" " " " .	327
Fig. 6.4.6	:	Variation of the parameters $k_{sav}$ and $\mu_{sav}$ with the per-unit transmitter magnetic flux density for different values of the energization carrier frequency.	329
Fig. 6.4.7	:	Input characteristics of the static transmitter-coincidence transmitter mag-slip-system for different values of the energizing carrier frequency.	332

- Fig. 7.2.1 : Simulation of the sinusoidal angular-displacement disturbance of the reference potentiometer shaft by means of an injected S.C.A.M. wave. 338
- Fig. 7.2.2 : Simulation of the sinusoidal angular-displacement disturbance of the transmitter mag slip shaft by means of an injected R.M. wave. 342
- Fig. 7.3.1 : Nichols diagram for the system under different carrier-frequency of energization. 347
- Fig. 7.3.2 : Closed-loop modulation frequency response of the uncompensated system under different carrier-frequency of energization. 349
- Fig. 7.3.3 : Nichols diagram for the system showing the effects of varying the phase of the 2-phase servomotor reference excitation. 350
- Fig. 7.3.4 : Closed-loop modulation frequency response of the uncompensated system showing the effect of varying the phase of the 2-phase servomotor reference excitation. 351
- Fig. 7.3.5 : Nichols diagram for the system showing the effect of varying the energization carrier-frequency. 353
- Fig. 7.3.6 : Closed-loop modulation frequency response of the uncompensated system under different carrier-frequency of energization. 354
- Fig. 7.3.7 : Nichols diagram for the system showing the effect of the phase variations of the error-detector reference excitation. 355
- Fig. 7.3.8 : Closed-loop modulation frequency response of the uncompensated system showing the effect of varying the phase of the error-detector reference excitation. 357

- Fig. 7.4.1 : Closed-loop modulation frequency response of the compensated system under different carrier-frequency of energization. 361
- Fig. 7.4.2 : Closed-loop modulation frequency response of the compensated system showing the effect of varying the phase of the 2-phase servomotor reference excitation. 362
- Fig. 7.4.3 : Closed-loop modulation frequency response of the compensated system under different carrier-frequency of energization. 365
- Fig. 7.4.4 : Closed-loop modulation frequency response of the compensated system showing the effect of varying the phase of the error-detector reference excitation. 366
- Fig. 7.5.1 : Circuit arrangement suitable for the transient response test of the servomechanism with potentiometer-bridge as error-detector. 370
- Fig. 7.6.1 : Step-function response of the uncompensated system with a potentiometer-bridge as error-detector. 374
- Fig. 7.6.2 : Step-function response of the compensated system with a potentiometer-bridge as error-detector. 377
- Fig. 7.7.1 : Step-function response of the uncompensated system with a synchro-pair as error-detector. 380
- Fig. 7.7.2 : Step-function response of the compensated system with a synchro-pair as error-detector. 384
- Fig. 8.2.1 : Block diagram of a practical electronic modulator. 389

Fig. 8.2.2	: Block diagram of a practical electronic demodulator.	389
Fig. 8.4.1	: A transistor square-wave modulator or demodulator.	400
Fig. 8.5.1	: Test arrangement for measuring the carrier converter response when compensated by the proposed scheme.	405
Fig. 8.5.2	: Carrier converter gain response.	408
Fig. 8.5.3	: Carrier converter phase response.	409
Fig. 8.5.4	: Wave-form oscillograms of signal appearing at various points along an electronic modulator compensated by the proposed scheme.	412
Fig. E.2.1	: Average performance curve for 35 v winding.	485
Plate E.4.1	: Breadboard model assembly of the positional control a.c. servomechanism.	488
Plate E.4.2	: a) Servo-amplifier transistor circuit. b) 3-terminal synchronous switch. c) Driving circuit for the synchronous switch.	488 488 488
Plate E.4.3	: Equipment set-up for measuring the modulation frequency response of chopper network.	489
Plate E.4.4	: Square-wave modulators and demodulators required to realize the principle of operation of the scheme proposed in Chapter 8.	489
Fig. I.1	: Representation of a 3-terminal synchronous switch.	499
Fig. I.2	: Alternative representation of 3-terminal synchronous switch and its state-time relationship.	501

Fig. I.3	:	Single diode-bridge circuit operating as a Z.F.T. 3-terminal synchronous switch.	503
Fig. I.4	:	Double diode-bridge circuit capable of operating as a P.F.T and/or N.F.T. 3-terminal synchronous switch.	505
Fig. I.5	:	Transistor switch circuit capable of operating as a P.F.T and/or N.F.T. 3-terminal synchronous switch.	506
Fig. I.6	:	Transistor 2-terminal synchronous switch.	508
Fig. I.7	:	Steady-state response of pulse-transformer to rectangular waves for the conditions of maximum and minimum ON/OFF period ratios.	508
Fig. I.8	:	Representation of the 2-terminal synchronous switch shown in Fig. I.6.	515
Fig. I.9	:	Circuit used to set up the pulse-transformer response equations during ON period of the switch.	515
Fig. I.10	:	Circuit used to set up the pulse-transformer response equations during OFF period of the switch.	515
Fig. I.11	:	Variation of $R_2$ with $\Delta$ , as given by Eq.4.14.	525
Fig. I.12	:	" " $R_2'$ with $R_1$ , as given by Eq. 4.55.	525
Fig. I.13	:	Variation of $Q_2$ with $X$ , as given by Eq.4.69.	529
Fig. I.14	:	" " $Q_1$ " $\Delta$ , " " " Eq.4.60.	529
Fig. I.15	:	Plot of the calculated values of various pulse-transformer parameters with respect to $\Delta$ .	538
Fig. I.16	:	A transistor driving circuit for 3-terminal synchronous switch.	540

Fig. I.17	: Wave-forms at various points of the driving circuit, shown in Fig.I.16, for positive, zero, and negative d.c. bias.	542
Fig. I.9.1	: Approximate equivalent circuit of a pulse-transformer including capacitances and resistances.	548
Fig. I.9.2	: Approximate equivalent circuit for the calculation of the rise-time response.	548
Fig. I.9.3	: Approximate equivalent circuit for the calculation of the flat-top response.	548
Fig.. I.9.4	: Approximate equivalent circuits used to calculate the decay-time response.	549
Fig. I.9.5	: Switching-speed test circuit.	553
Fig.II.1	: Representation of a 3-terminal synchronous switch and its state-time relationship.	562
Fig.II.2	: Double-pole single-throw switch.	564
Fig.II.3	: a) 2-terminal synchronous switch and its dual. b) State-time relationship of the 2-terminal synchronous switch and its dual shown in (a).	564
Fig.II.4	: Illustration of the process of dual construction of a P.F.T. 3-terminal synchronous switch.	566
Fig.II.5	: Single:switch double-capacitor chopper network and its derived networks.	569
Fig.II.6	: Illustration of the process of dual construction of a part of the chopper network shown in Fig. II.5a.	572

Fig.II.7	: Double-switch single-capacitor chopper network and its derived networks.	573
Fig.II.8	: Parallel double-switch double-capacitor chopper network and its dual.	592
Fig.II.9	: Parallel double-switch double-capacitor chopper network and its derived networks (circuit is treated as a 3-terminal network I,II,III).	594
Fig.II.10	: Parallel double-switch double-capacitor chopper network and its derived networks (circuit is treated as a 3-terminal network I,IV,III).	595
Fig.II.11	: Cascaded inverted double-switch double-capacitor chopper network and its derived networks.	599
Fig.II.12	: Illustration of the process of dual construction of a part of the chopper network shown in Fig.II.11a.	600
Fig.II.13	: Triple-switch single-capacitor chopper network and its derived networks.	604
Fig.II.14	: Modified single-switch double-capacitor chopper network and its dual, practicable for full range of fly-time operation of synchronous switch.	608
Fig.II.15	: Circuits illustrating the use of operational amplifiers for obtaining modified responses.	610
Fig.II.16	: Circuits illustrating the use of transformers for obtaining modified responses.	612



NOMENCLATURE

a) LIST OF SYMBOLS

Most commonly used symbols and notations are defined below. Any symbol not given below will be explained where used in the text. To refer to various situations and operating conditions, any of the subsequently defined principal symbols may be used in conjunction with any of the subscripts or superscripts listed hereafter.

i) Principal symbols

$t$	:	time (independent variable)
$p$	:	differentiation with respect to time $(\frac{d}{dt})$ , <u>or</u> complex frequency variable
$\sum$	:	summation
$\int$ , $\oint$	:	integration and closed line integration
$\mathcal{L}$ , $\mathcal{L}^{-1}$	:	Laplace transform and inverse Laplace transform
$s$	:	Laplace complex frequency variable
$Z$	:	Z-transform ( $e^{Ts}$ ), <u>or</u> operational impedance
*	:	signifies convolution in the s-domain
$\mathcal{R}$	:	real part of
$j$	:	operator $\sqrt{-1}$
$T$	:	period of carrier wave
$\Omega$	:	carrier frequency, in radians/second
$\omega_m$	:	modulation frequency, in radians/second
$\tau$	:	time constant
$u_0(t-nT)$	:	Dirac pulse at $t=nT$
$u_{-1}(t-nT)$	:	unit-step function with discontinuity at $t=nT$
$x$	:	input signal
$y$	:	output signal

v	:	voltage associated with chopper networks
E	:	amplitude of carrier excitation voltage
e	:	voltage, <u>or</u> base of the natural logarithms
i	:	current
P	:	power
$T_m$	:	gross mechanical torque
$T_{cf}$	:	torque due to static or coulomb friction
$T_v$	:	torque due to unbalanced or gravitational force
R	:	resistance, <u>or</u> residue
L	:	total self inductance, <u>or</u> integer number
M	:	mutual inductance, <u>or</u> a function of time
G	:	conductance
Y	:	admittance
$\theta, \phi, \psi,$	:	phase angles associated with various carrier excitations, in radians
.	:	carrier excitations, in radians
$\gamma$	:	angular shaft position, in radians
$\Gamma$	:	angular spread of the potentiometer winding, in radians
F	:	coefficient of viscous friction, <u>or</u> a function of time
J	:	moment of inertia
n	:	gear ratio with respect to the reference, <u>or</u> integer number
m	:	integer number
$\delta$	:	proportion of conducting period of a switch to carrier period
$\epsilon$	:	error, <u>or</u> infinitesimal quantity
A	:	gain of amplifier
$g(t)$	:	impulse response
$G(s)$	:	transfer function
$G_o(s), G_c(s)$	:	open-loop and closed-loop transfer function

ii) Subscripts

m	:	2-phase servomotor, <u>or</u> mechanical, <u>or</u> modulation
p	:	potentiometer-bridge
s	:	synchro-system, <u>or</u> stator
t	:	a.c. tachometer, <u>or</u> transpose
R	:	reference
L	:	load
d, D	:	direct axis with respect to rotor and stator of electric machine
q, Q	:	quadrature axis with respect to rotor and stator of electrical machine
O	:	zero sequence component, <u>or</u> open-loop
A, B, C	:	stator phases of actual machine
a, b	:	rotor phases of actual machine
md	:	modulator
de	:	demodulator
mm	:	multiplicative modulation
rm	:	rotary modulation
r	:	rotor, <u>or</u> rotary

iii) Superscripts

.	:	rate of change with respect to time
*	:	conjugate, <u>or</u> implying that the function associated with this superscript is in sampled form

b) LIST OF ABBREVIATIONS

T.F.	:	transfer function
M.M.	:	multiplicative modulation
R.M.	:	rotary modulation

S.C.A.M.	:	suppressed-carrier amplitude-modulation
P.F.T.	:	positive fly-time
Z.F.T.	:	zero fly-time
N.F.T.	:	negative fly-time
R.H.S.	:	right hand side
L.H.S.	:	left hand side

c) GENERAL NOTES

i) For the sake of convenience, equations, diagrams, and tables will be referred to by three Arabic figures separated by dots. The first figure indicates the chapter number, the second figure indicates the section number and the third figure indicates the number of equation, diagram or table.

For the Appendices, capital alphabetic letters (A,B,C,...etc.) are used in the place of the first figure in order to make the reference easier.

In the two reports which are submitted with this thesis as supplements and treated in the text as Chapters I and II respectively, the equations, diagrams and tables were originally not assigned by three figures. However, they will be referred to in the same manner as mentioned above (with I and II in the place of the first figure) in order to maintain the consistency throughout the text.

ii) \* : When this symbol appears between two quantities, it indicates that the two quantities are convoluted. When the same symbol appears as a superscript of a certain quantity, it indicates either the Z-transform of the quantity, or the conjugate of the quantity.

iii) Negative and positive subscripts are introduced to enable functions of the complex frequency variable and carrier frequency to be written in abbreviated form. For example:

$$G_{\pm}(s) \equiv G(s_{\pm} \pm j\Omega)$$

## CHAPTER 1

### INTRODUCTION

#### 1.1 General features of a.c. servomechanisms

A.c. or carrier-systems, in which the low-frequency information is transmitted by means of a modulated high-frequency carrier, have numerous advantages over d.c. systems. The problem of d.c. drift in the amplifiers is eliminated and the various components are simple, rugged and reliable. Synchros have no wire-spacing noise component of potentiometers. Two-phase servo-motors are commutator free. The high-frequency carrier permits miniaturization and greater power per unit weight. The information can be modulated on to a second higher frequency carrier for telemetering.

Because of all these advantages, a.c. or carrier-systems have acquired a wide scope of application particularly in the fields of industry, instrumentation, computers and air-borne equipment.

#### 1.2. Principle of operation of a typical modulated-carrier positional control system.

An a.c. servomechanism controlling the output-shaft position  $\gamma_L$  is shown in Fig. 1.2.1. A transmitter-coincidence transmitter synchro-system is employed to detect the error signal  $\mathcal{E}$  which appears as the envelope of a modulated signal. The modulation effected in the synchro-system is in the form of rotary modulation<sup>1,2</sup> which differs from the simple multiplicative modulation, a type which takes place in potentiometers and choppers.

The actuating signal, produced by the synchro-system, is

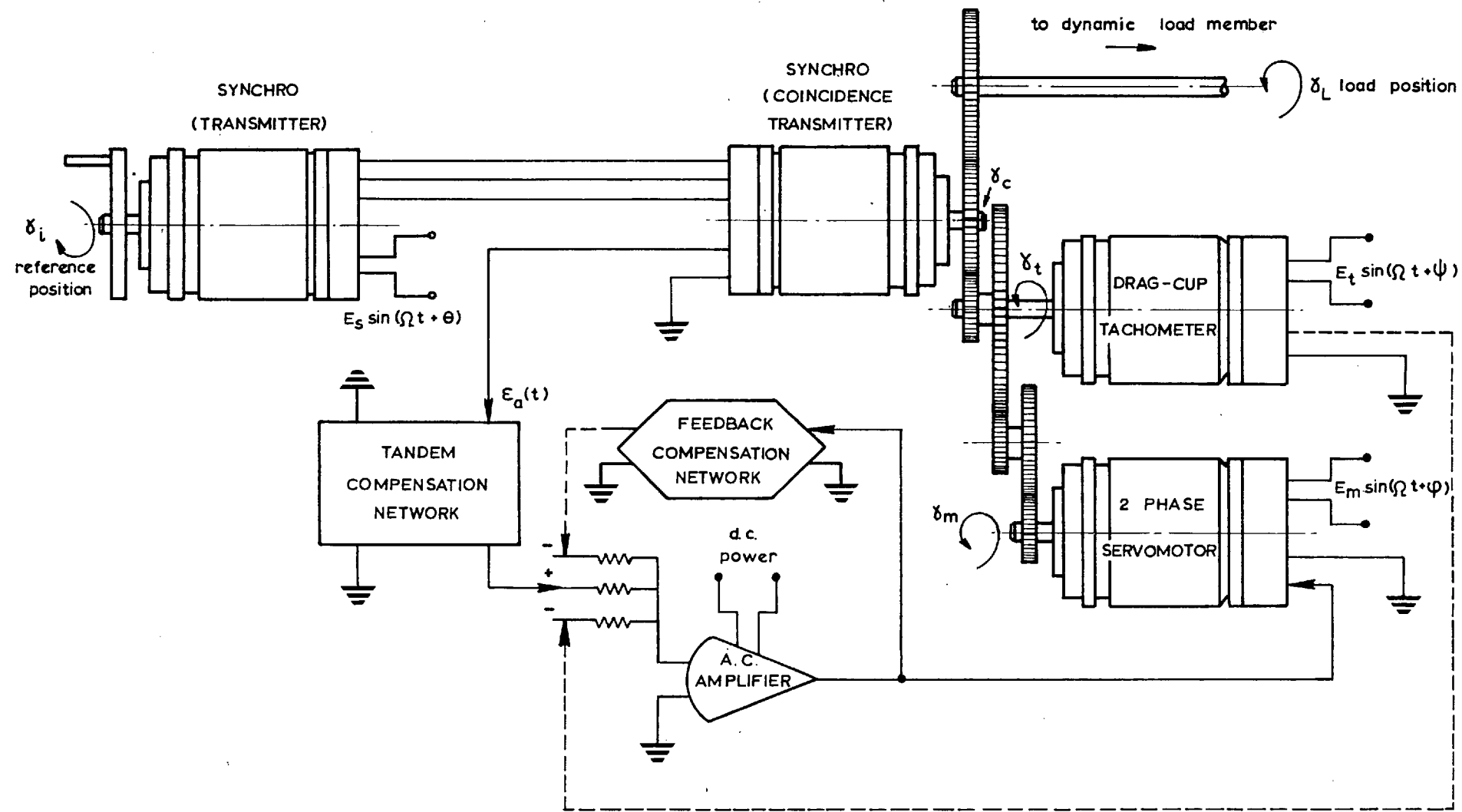


FIG. 1.21

SCHMATIC DIAGRAM OF A TYPICAL MODULATED - CARRIER POSITIONAL CONTROL SYSTEM

amplified using an a.c. servoamplifier, which drives the control winding of a 2-phase servomotor. The reference winding of that servomotor is excited by a fixed voltage at the carrier frequency. The 2-phase servomotor, which is utilized as the power member, is coupled to the load member by an appropriate gear train.

When the system is either found unstable or its overall performance does not satisfactorily meet the specified requirements, one of the following compensating techniques may be employed:

- i) Tandem compensation in which the compensating networks or devices are inserted in cascade with the main error channel.
- ii) Feedback compensation in which the compensating devices may be placed either in the main feedback path (for instance, the case of a.c. tachometer), or in a subordinate feedback path (e.g. using a compensating network in a minor loop around the a.c. servoamplifier).
- iii) Load compensation.
- iv) Any combination of the above three methods. Where the first two methods are illustrated in Fig. 1.2.1.

It is also possible, to a limited extent, to change the system performance either by changing the components parameters thus obtaining different time constants, or by adjusting the gain, hence altering both the steady-state performance, the phase, and gain margins. Small modification of the transmission characteristics can be achieved by adjustment of the phase of the demodulation reference <sup>1,2,3</sup>, a method which may be easily used as a final refinement to achieve the optimal system performance.



### 1.3 Problems associated with the design of a.c. servomechanisms

As it has been shown above, the conventional a.c. servomechanism is characterized by the transmission of the data as the envelope of a suppressed-carrier amplitude-modulated signal. The proper design of such system therefore depends on a knowledge of the change in transfer functions of the various components produced by the modulation and demodulation processes.

The modulation and demodulation can be considered with good approximation, as linear operations when the signal bandwidth is very small (less than 10%) compared to the carrier-frequency as usually the case in communications systems. In a.c. control systems, however, the signal frequencies may approach the same order of magnitude as the carrier frequency. This necessitates the use of an exact analysis of the various components in order that accurate and reliable results may be obtained.

Large deviations in carrier frequency (particularly common in air-borne equipment) and changes in the carrier phase in the various components and networks raise two significant problems. The variations in the carrier result in variations in the modulation transfer functions of tuned compensators<sup>76-81</sup> and in the dynamic behaviour of the 2-phase servomotors<sup>2,19,27,79</sup> and synchros<sup>2,27</sup>.

In order to assess the stability and general performance of an a.c. servomechanism, its modulation frequency response has to be obtained experimentally. Such experiment requires a test signal in the form of suppressed-carrier amplitude-modulated wave. Although such signal can be easily generated by conventional electronic modulators, nevertheless, for practical reasons, the ratio modulating frequency to carrier frequency is limited to about 10%. Furthermore, quantities such as the output and the error

appear as amplitude modulated electric signals which require to be demodulated in order that the attenuation and phase shift of their envelopes may be measured. If the demodulation process is accomplished by electronic means, a limitation on the ratio modulating frequency to carrier frequency of almost 10% again has to be imposed on the signals to be measured, otherwise distortion will take place leading to inaccurate results. In view of this practical limitation, the system frequency response can be obtained over only a small range. This may not give an adequate information for the design purposes.

#### 1.4 Review of previous work

##### 1.4.1 General

In the recent years, particularly during the last two decades, there has been a considerable amount of work performed on the various aspects of a.c. servomechanisms. Methods of analysis, synthesis, and design techniques for these systems have been developed to meet their rapidly expanding field of application. The growing realization of the potentialities and numerous advantages of the a.c. systems over their counterpart the d.c. systems explains their continually increasing demand at present and forecasts the prospects of more new exploitations in the future.

The vast contributions of various authors have resulted so far in a better understanding of the basic principles involved in the operation of a.c. servomechanisms, and in much improved descriptions of their basic components. To formulate the present work on a sound basis and to specify the various areas where further development is needed, a careful study should be made of the previous work published in this field.

In this section, therefore, it is intended to outline a general survey of the previous work in the relevant topics.

#### 1.4.2 Two-phase servo-motor.

Over the years 2-phase servomotors have received considerable attention. References 4 to 21 give a selected bibliography which deals with servomotor analysis from various points of view.

Of previous work performed on induction-motor transients, Stanley<sup>4</sup> has derived differential equations for both 2-phase and 3-phase motors. By employing perturbation analysis about a steady-state condition (thus making the equations linear and their solution more simple), he then obtained current and speed transients.

Koopman<sup>5</sup> has presented an analysis to the 2-phase servomotor based on the symmetrical component technique. The derived equations, therefore, are only applicable to the steady-state performance. Later, Bond<sup>6</sup> used the same technique of analysis but in a more condensed form.

By adopting linear approximation for the curves of the torque-speed characteristics, Brown<sup>7</sup> represented the 2-phase servomotor by a transfer function with a single time constant. In high bandwidth applications, however, this representation is not valid as a phase shift greater than 180 degrees was observed<sup>8</sup>. A second high-frequency break point was therefore suggested by Brown<sup>8</sup>. Nevertheless, his theoretical results, which involve some linearising assumptions, do not give close agreement with his observations.

Hopkin<sup>9</sup> was primarily concerned with the transient response aspect of the 2-phase servomotor to certain specified inputs. By assuming a torque equation linearly related to the speed, he was able to set up a differential equation with variable coefficients. The solution of this equation for a step input function to the control winding was obtained whose form appears as if the motor response is governed by only one time constant. It is noticed, however, that the experimental results suggest a second time constant on which Hopkin commented that, for most cases, it is sufficiently small to be neglected. Chang<sup>10</sup> developed a transient performance description on the basis of the equivalent circuit. He noted that the effect of the reference winding on the electrical transients is small enough and thus only the control winding equivalent circuit was considered, taking into account the effect of finite driving amplifier output impedance. Chang's analysis, however, does not provide adequate information about the performance or design of the 2-phase servomotor.

Mikhail and Fett<sup>11</sup> have developed an expression for the electric torque as a function of the stator currents and motor speed. In transforming the equation to the complex frequency domain, with the aim of establishing a transfer function, they failed to use the complex convolution technique<sup>124</sup> required to solve the terms appearing as multiplication of two time functions.

Kutvinov<sup>12</sup> considered the special features in the determination of the coefficients of the transfer function of a 2-phase motor for amplitude and phase modulations. In his analysis, the effect of non-linearity in the motor control characteristics has been included. However, the expression obtained for the transfer function is too

complex to be of any practical value.

References 13 and 14 are primarily concerned with the derivation of suitable design criteria rather than performance description. Solutions of the air-gap equation<sup>14</sup> have been obtained for the fictitious conditions of flux forcing and current forcing; the operating condition will, in practice, lie between these two conditions. The analysis developed is suitable only for the steady-state operation of the 2-phase servomotor.

By assuming linear and parallel curves for the torque-speed characteristics, Lohte<sup>15</sup> derived the steady-state torque equation as depending on the square of the control signal, ~~and linearly dependent on the square of the control signal~~, and linearly dependent on the motor speed. From this, he proceeded to obtain the dynamic characteristics described by a differential equation of the first order, but with variable coefficients. The author then deduced a transfer function in terms of amplitude so that the behaviour of the motor can be studied by a series of Nyquist diagrams.

Using a more physical approach of simplifying and idealising the configuration of the induction motor, West et al<sup>16</sup> obtained a relationship between the torque and rapid variations of stator-supply frequency about a fixed base frequency. With a good deal of assumptions, the developed analysis enables the frequency response and graphical solution (phase-plane) for the transient to be obtained. The analysis, also, suggests a fairly simple analogue simulator.

Hughes et al<sup>17</sup> considered the analogue simulation of

the induction machine with the aim of providing a convenient general model from which both starting transient and unbalanced operation of the machine may be predicted. The equations employed for the simulation have been derived on the basis of the 2-axis general theory of machines<sup>122</sup>, which give a mathematical model identical to that derived by Stanley<sup>4</sup>. Law and Schmitz<sup>18</sup> have adapted Stanley's fundamental differential equations of the 2-phase induction motor to a form amenable to the solution on a large-scale digital computer employed as an analogue device. In this way, it was possible to eliminate difficulties previously associated with analogue computer inaccuracies. The authors presented calculated and measured transient curves showing the behaviour of the servomotor under a variety of operating conditions, involving sinusoidal excitation through non-linear discontinuous impedances.

Wilson<sup>19</sup> derived an analytical expression for the modulation transfer function of the 2-phase servomotor. His analysis is, again, based on the generalised 2-axis machine theory, although he adopted more simplifying assumptions in addition to those involved in the theory in order to arrive at the analytical solution. With the modulation transfer function developed, he was able to study the effects of carrier frequency drift and phase misalignment on the locations of the poles and zeros in the complex frequency plane.

Rogers<sup>20</sup> presented a linearised analysis of the induction machine speed transients due to small voltage and torque disturbances. Discussion of the effects of supply frequency on these transients was included. A graphical

method (root-locus) was used rather than the more traditional frequency approach, for synchronising and damping torques, which could well be followed at the design stage to predict transient performance.

Hesmondhalgh and Driver<sup>21</sup> were fundamentally concerned with the development of an earlier theory<sup>14</sup>, so that it may be applied directly to the design of the a.c. servomotor. As such, the paper does not directly contribute to the performance analysis.

#### 1.4.3 Error-detector

One of the fundamental reasons for the existence of carrier control systems is the availability of numerous transducing devices which either generate or are driven by modulated carrier signals. Classification of the basic electromechanical transducers are given in Reference 22, accompanied by description of their mechanical and electrical constructions. References 22 and 23 describe the basic principles of these devices in a fairly general and simplified manner.

In a.c. servomechanisms, the most common types of error-detectors employed are:

- i) Potentiometer-bridge (resistive class of transducer, commutating type),
- ii) Synchro-systems (magnetic-field class of transducer, variable-transformer type).

For a.c. excited linear potentiometer-bridge, the output is in the form of suppressed-carrier amplitude modulated wave<sup>22,23</sup> (S.C.A.M.), provided that any load

which is connected across the output terminals is much greater than the potentiometer total resistance. On the other hand, Morris<sup>1</sup> has shown that the output from variometers and related devices (such as synchros, magslips, ... etc.) does not consist simply of S.C.A.M. as is commonly supposed, but includes a tachometric voltage which may usefully be employed for stabilization purposes<sup>1,2</sup>. To distinguish this type of modulation from the multiplicative type (S.C.A.M.), Morris proposed the term rotary modulation (R.M.). His analysis, however, is based on the assumption of negligible impedance of the excited winding; i.e. flux forcing condition, and therefore its validity is limited in practice.

#### 1.4.4 Techniques of compensation

In general, the design of a.c. servomechanisms is carried out to provide not only system stability, but also overall characteristics such that certain prescribed performance specifications are satisfied. If, however, these requirements are not met, gain adjustment may be attempted as a first step for its simplicity, and if this in turn does not offer the best possibility of matching the specifications, one has to resort to some compensation technique suitable to the system under consideration.

Compensation, principally, involves one or more of the following mathematical processes operating on either the output or error information

- i) Proportional,
- ii) Differentiation,
- iii) Integration.



In practice, these operations are realised approximately by devices and electric networks which may be classified as below:

- I Load compensation.
- II A.c. tachometer feedback.
- III Tandem compensation
  - a) Passive electric networks
    - i) Linear.
    - ii) Non-linear.
  - b) Active networks
    - i) Linear.
    - ii) Non-linear.
    - iii) General.
  - c) Periodically-switched linear networks or chopper networks.

#### 1.4.4.1 Load compensation

This type of compensation can be introduced using electromechanical compensating networks<sup>24-26</sup>. Since compensation is effected entirely mechanically and on the low-frequency signal (the output-shaft rotation), rather than on the modulated signal, it is insensitive to carrier frequency deviations.

Low-frequency filters<sup>2</sup> of great stability can be built with mechanical elements whose inertias and spring constants are invariant. Coulomb friction and stiction are the main difficulties in filters of this kind.

Viscous dampers attached to the motor shaft are in common use<sup>2,23,27</sup>. One type of viscous damper consists

of a container of viscous fluid in which the rotor is immersed. This arrangement works well, but the fluid is usually sensitive to temperature. The same effect can be obtained with eddy-current dampers which eliminate some of the temperature problem. Both the fluid and eddy-current dampers increase the velocity-lag error which is usually undesirable.

Acceleration dampers<sup>27</sup> act more in the manner of a lead network and provide damping in the transient period without increasing the velocity-lag error.

Oscillation damper<sup>28</sup> (tuned or untuned) can be used to change the apparent characteristics of the load. Hall<sup>28</sup> has demonstrated that oscillation dampers can be employed to obtain the equivalent of tachometer feedback.

Truxal<sup>27</sup> mentioned three significant ways in which mechanical networks are less flexible than the electrical counterparts. These are given below:

- i) The mechanical realisation of mutual mass is frequently troublesome,
- ii) A centering problem exists in the practical use of dampers,
- iii) The dampers are actually characterized by more nearly a square law than a linear relation between force and velocity.

#### 1.4.4.2 A.c. tachometer feedback

The a.c. tachometer, or induction generator, is very similar in both appearance and construction to the

small 2-phase induction motor. Its principle of operation<sup>22</sup> is such that one of the stator winding (reference) is excited by the carrier signal. At stand-still no coupling exists between the two windings, so that no electro-motive force (e.m.f.) is induced in the quadrature winding. When the rotor revolves, the conductor cuts the field due to the exciting winding, and the induced rotational e.m.f. causes a rotor current to flow in the quadrature axis, setting up space-quadrature flux at carrier frequency and inducing an e.m.f. into the quadrature winding. In simple theory, the rotational induced rotor e.m.f. is proportional to speed, so that the quadrature flux and induced e.m.f. in the quadrature-axis winding are both proportional to speed. The a.c. tachometer is usually employed to generate speed information signal for negative feedback stabilisation.

Due to the similarity of construction, the analysis of a.c. tachometer has pursued a similar pattern as that of the 2-phase servomotor. Frazier<sup>29</sup> applied the symmetrical components technique to the equivalent circuit of the machine. In this way, he established the steady-state characteristic equation for the output voltage. In a later paper, Frazier<sup>30</sup> presented an analytical analysis of the drag-cup a.c. tachometer when excited by a current source. Chang<sup>10</sup>, in his treatment, considered the a.c. tachometer behaviour as equivalent to an ideal modulator followed by a linear network. The linear network takes into account not only the equivalent circuit of the a.c. tachometer winding, but also any correcting network connected to the output terminals.

Knox<sup>31</sup> was primarily interested in determining criteria suitable for good speed-voltage linearity, and in finding

out the means of minimising the errors introduced by the variation of operating conditions. He employed a more physical approach to the analysis by which he was able to derive an approximate expression for the output voltage.

References 32 and 34 present performance analysis to the a.c. drag-cup tachometer when used to measure the shaft angular acceleration. In this application, one winding is excited with direct current and the output voltage from the other winding is found, using coupled-circuit theory, approximately proportional to the acceleration. The analysis showed that ideal characteristics are exhibited for low frequencies and small speed variations, and that small rotor time constants are necessary if this ideal range is to be large.

Trickey<sup>33</sup> developed a general method of performance calculation, based on the same circuit equations, when the a.c. machine is used for three applications; phase converter, a.c. tachometer generator, and single-phase brake. The treatment given provides useful information from the design view-point. Reference 14 also gives design criteria for the a.c. tachometer, though using a different approach. The analysis given in this reference has been developed from first principles using winding data and physical dimensions. Emphasis has been placed on the importance of the rotor time-constant as a design criterion, while the effect of rotor leakage reactance on the performance has been shown to be negligible. The performance characteristics are, however, only applicable to the steady-state operation.

#### 1.4.4.3 Tandem compensation

In both load and simple feedback compensation, the compensating device is operating on the output signal, which is not a modulated wave, thus the same principles apply for a.c. and d.c. systems. In tandem compensation, however, the compensation network is to operate on the envelope of a modulated signal as shown in Fig. 1.2.1. Synthesis of such networks, therefore, represents a major problem in a.c. systems design.

##### a) Passive electric networks.

##### i) Linear

Demodulation-compensation-remodulation provides one of the simplest procedures for the design of linear networks<sup>23,27</sup>. Since the resulting a.c. system is no different than d.c. system, the root-locus method and Guillemin's procedure are directly applicable<sup>27</sup>. Although such schemes have been used extensively, not only because of the ease of design but also for the relative insensitivity to carrier frequency variations, the amount of equipment involved is excessive for many applications. Furthermore, the additional modulators and demodulators will result in generation of undesirable high harmonic noise which usually must be suppressed by filters. These harmonic suppression filters, however, introduce phase lags which often reduce the relative stability of the system.

Modification of the dynamic characteristics of the information by means of linear passive networks inserted in the carrier channel has been examined by a great many authors. In the author's opinion, Morris<sup>1</sup> was the pioneer in giving a fairly general analysis to such

networks which enables the modulation frequency response to be directly determined from the simple frequency response of the network. Two treatments were presented in the paper based on graphical and symbolic techniques. In a more recent paper by Douce and Edwards<sup>35</sup>, a similar graphical approach was described, though the treatment given by Morris is more general in three important aspects (as pointed out in Reference 36):

1. The modulation response locus may be found directly for any phase relationship between the modulation and demodulation reference carriers.
2. The graphic and trigonometric treatments are accompanied by a symbolic analysis in terms of the "j" notation. The method is then not extremely laborious analytically.
3. The paper gives a treatment of both multiplicative and rotary modulation systems.

In an unpublished article<sup>37</sup>, Morris attempted to establish a basis for the analysis of the dynamic shaping of a signal modulated by a carrier by means of determining the transmission characteristics of each sideband separately, and then combining the results. The developed basic analysis was then applied to simple first-order RC networks for deriving their multiplicative modulation responses from their simple harmonic frequency responses using three techniques of analysis, trigonometric, diagrammatic, and symbolic. The graphical method employed depends on extensive use of the frequency calibration of the frequency response locus. In order to extend the application of this method to second-order networks, Morris<sup>38</sup> developed simple procedures to calibrate the frequency of the second-order loci.

Several analytical approaches<sup>39-44</sup> have been devised for determining the exact envelope transfer functions of linear networks. Chang<sup>40</sup> and Candy<sup>41</sup> introduced the concept of the doubly-complex variable which enables vector expressions to be derived for impedances, admittances, and transfer ratios of linear electrical circuits. With the application of bifid operators<sup>45</sup>, Candy<sup>41</sup> was able to obtain the response of circuits to non-sinusoidal amplitude modulated signals. References 42 to 44 present derivations for arbitrary envelope functions. Panzer<sup>43</sup> derivations are the most rigorous and complete. His analysis is based on Laplace transform technique and the treatment covers cascaded elements and closed loops employing elements of all types (modulator, demodulator, and linear network) in any configuration.

A review of the various analysis described in the literature referred to above clearly shows that synthesis of linear passive networks which may modify the envelope of the modulated signal in the same way that d.c. compensation networks operate cannot be physically realized. However, adequate approximations can be obtained in a wide variety of cases.

Blanton<sup>46</sup> has shown that the a.c. compensation characteristics should, theoretically, have symmetrical amplitude response and skew-symmetrical phase response around the carrier frequency, both considered on arithmetic frequency scale basis. This condition cannot be realized by linear passive networks except for the trivial case of  $\Omega = 0$ . However, within a limited frequency band on either side of the carrier frequency  $\Omega$ , physically realizable networks, exhibiting geometrical symmetry

rather than arithmetic symmetry about  $\Omega$ , can provide good approximation. With narrow-band information frequency, there are two standard techniques for this approximation: the low-pass band-pass transformation,<sup>47-49</sup> which can be used regardless of the form of the transfer function of the equivalent d.c. network; and the approximation by a transfer function with poles on the negative real axis in order that the network may be RC<sup>50-57</sup> (e.g., twin-T, bridge-T).

Carlson and Truxal<sup>58</sup> presented a direct approach to the synthesis of carrier compensation networks through a logical application of pole-zero concepts of network synthesis. The technique used is based on choosing a combination of poles and zeros which is realizable and approximately gives the desired overall gain and phase characteristics.

Gronner<sup>59</sup> employed the trigonometrical relations and approximations given below

$$j\omega_m = j(\omega - \Omega) \approx j \frac{(\omega - \Omega)(\omega + \Omega)}{2\Omega} \approx \frac{\Omega^2 + (j\omega)^2}{2j\Omega} \quad 1.4.1$$

(where  $\omega_m$  is the modulation frequency)

which led, on substitution into the transfer functions of standard d.c. compensation networks, to resonant, modified resonant, symmetrical parallel, and bridged-T networks.

A somewhat different approach to the synthesis procedure has been described by Hellerman<sup>60</sup>. The technique adopted requires the availability of a



quadrature input signal (i.e., a signal with the same modulation as the original signal, but on the quadrature carrier). Each of these signals is then passed through separate linear networks  $H_D(S)$  and  $H_Q(S)$ , and the responses are added to form a single modulated output signal with zero quadrature. Hellerman proves that both  $H_D(S)$  and  $H_Q(S)$  are realizable, provided that  $H_D(P)$  is realizable as a "low-pass prototype network". This method is obviously not suitable in practice as the quadrature signal is generally not available.

In developing Carlson and Truxal work, Levenstien<sup>44</sup> has shown that the synthesis of envelope networks can be treated in a fashion analogous to the approximation problem of classical network synthesis. The steps proposed are summarised below:

1. Approximate the specified  $H_D(P)$  by a function having the permissible pole-residue pattern.
2. Compute the  $H_Q(P)$  corresponding to the selected  $H_D(P)$ .
3. Optimize the parameters of the selected  $H_D(P)$  to minimize the difference between the actual and desired  $H_D(P)$  and  $H_Q(P)$ , based on a prescribed "goodness" criterion.
4. Derive  $H(S)$  from the optimized  $H_D(P)$  according to the relationship

$$H_D(S) = \mathcal{R} H(S - j\Omega) \quad 1.4.2$$

5. Synthesise the network from  $H(S)$  by conventional circuit synthesis.

The "error" or "goodness" criterion chosen to optimize

the selected  $H_D(P)$  essentially determines the detailed structure of the network and its parameter values. For example, approximation of  $H_D(P)$  by conjugate complex poles leads to real poles of  $H(S)$  which permits synthesis by RC networks, whereas approximation of  $H_D(P)$  by triplets and quadruplets leads to complex poles of  $H(S)$  and hence RLC networks. Weiss<sup>61</sup>, in continuing Levenstein's work, has shown that a particular set of optimization criteria leads to the conventional low-pass band-pass approximation, and at the same time to the currently used RC lead networks. Weiss has also shown that the only practical network which can be synthesised is the bi-quadratic lead network. The bi-quadratic lag network is impractical because of the large coil Q's required; higher order functions are impractical because several tuned circuits must be kept aligned.

Sapfirov<sup>62</sup> treated the ideal sinusoidal modulator and demodulator as linear elements with periodical coefficients which allowed the a.c. system to be described by linear differential equations with periodical coefficients. An approximate synthesis procedure was then developed based on the assumption of negligible high harmonic signal components, and that the poles and zeros of the modulation transfer function should lie at distances very small compared with the carrier frequency.

Synthesis through the use of low-pass to band-pass techniques, described in detail in the literature<sup>47-49</sup>, results in passive RLC networks. Although this type of network has the advantage of providing a wide variety of transfer functions, it is very limited in practice due to the stray magnetic field and non-linearities introduced by actual inductors, excessively high Q requirements,

high cost of special coils, the necessity of very large values of inductance, and large weight and size. For these reasons there has been considerable emphasis on employing RC compensating networks particularly of parallel-T and bridged-T configurations<sup>50-57</sup>. Both RLC and RC networks have, however, the serious drawback of being considerably sensitive to carrier frequency deviations as they exhibit the notch-characteristics.

ii) Non-linear

Comparatively little development is detected in this field which may be attributed to the supersedence of the chopper networks which will be discussed later in this Section. Diporse<sup>63</sup> has shown that phase lead of the envelope of a modulated carrier can be achieved with non-linear networks which are independent of the carrier frequency. The network employed utilizes d.c. current-controlled rectifiers as variable carrier-frequency admittances.

Another type of non-linear differentiator incorporating Deltamax or square-hysteresis-loop cores as memory devices to compare each half-cycle amplitude with the following half cycle has been introduced by Scorgie<sup>64</sup>. Clegg<sup>65</sup> suggested the use of a class of networks which employs diodes as the non-linear elements.

b) Active networks.

i) Linear

It has been widely recognised that by combining passive RC networks with active elements (such as

transistors), considerable advantage other than isolation can be obtained among which:

1. The ability to realize RC active networks that have the flexible characteristics of RLC passive networks but do not require inductors.
2. The ability to reduce the effect of parasitic resistances in inductors and subsequently allowing the realization of a.c. compensating networks with characteristics approaching, or even exceeding, the desired characteristics of designs based on the use of ideal conductors.

There are several ways in which active elements can be introduced into compensating network design. Two of the more common active network synthesis techniques are:

1. Techniques which combine active circuits and RC elements in a form of feedback configuration<sup>66,67</sup>.
2. Designs which use the active circuits as negative impedance converters<sup>68-70</sup>.

## ii) Non-linear

By polarizing thermistors with a steady alternating current of the same frequency as the carrier, the impedance of the thermistors to the envelope of modulated signal has been shown<sup>71</sup> to be equivalent to those obtained by RLC networks, provided that the carrier frequency is sufficiently high so that the thermistor resistance would vary in the same way as with d.c. polarized signal. Solbaken<sup>72</sup> used two thermistor elements connected in a four-arm-balanced-bridge to obtain an integration operation on modulated signals.

The suppressed-carrier amplitude-modulated wave being applied to the heater windings, which in turn varies the resistance of the beads, and hence a voltage appears across the output terminals of the bridge. However, due to the relatively slow action of the thermistors, circuits based on their use are only suitable to very low modulation frequency applications.

Levinson<sup>73</sup> has described a novel property of certain non-linear circuits, whereby the steady-state describing frequency response exhibits gain-phase relationships that are proven to be unrealizable by linear circuits. He showed and analysed several examples of non-linear circuits exhibiting gain reduction without phase change which are desirable features for servo stabilization.

Although chopper networks may suitably come under the heading of non-linear active networks, they are going to be reviewed separately in a later Sub-section for their special importance in the present work.

### iii) General

McDonald<sup>24,25</sup> has shown that low-frequency filters of great stability can be built with electro-mechanical networks. Two representative electro-mechanical networks are briefly described below:

1. A 2-phase motor driving a drag-cup tachometer performs the functions of demodulation-phase lag, and remodulation. The time constant of the phase lag can be adjusted by changing the inertia of the system. Connected in negative feedback around a carrier amplifier, this can provide a single real

zero (with respect to the information), whose time constant is controlled by the inertia, and a residual pole, whose position is controlled by the amplifier gain.

2. In the feedback branch of a carrier amplifier, a 2-phase torque motor for demodulation, a spring-mass-damping resonant system with torque input and position output, and an induction pick off for measuring position and remodulation can be placed. Connected in negative feedback, the overall system displays a pair of complex poles modulated on the carrier, but with poles also at carrier frequency. The inertia of the motor provides the low-pass characteristic needed for demodulation and is simultaneously useful in the resonant circuit.

The main disadvantages of such networks are the complexity, inflexibility of the design, cost, weight, and space.

Tustin<sup>74</sup> has described two possible devices:

1. The oscillating inductor as phase advancer,
2. The mechanical vibration absorber.

Apparently, no further investigations have been carried out into the first device, whereas the second device is, in fact, the load compensation technique discussed earlier.

Volz<sup>75</sup> effectively employed the technique of demodulation - d.c. electrical passive network - remodulation to obtain phase correction for the envelope of the modulated signal. Although this method is insensitive to carrier frequency drift, it is usually undesirable because of the

low-pass filters required for the demodulation, and because both processes (demodulation and remodulation) take noise which is outside the band of information frequencies and beat it into the signal, where it cannot be removed.

c) Periodically-switched linear networks or chopper networks.

In assessing the relative advantages of the aforementioned tandem compensation methods, the linear passive networks can be regarded as the most superior in terms of ease of design and construction, adjustment, size, weight, power requirement, and cost. However, since these networks (bridge-T, twin T, and RLC networks) possess notch characteristics which must be tuned to the carrier frequency, the success of their operation largely depends on the stability of the carrier frequency. Unfortunately, in some important applications, for example, in airborne control systems where the need to keep the physical weight and space of the system to a minimum prevents the use of suitable frequency regulating equipment; the carrier frequency fluctuates considerably.

The adverse effects of the carrier frequency drifts have been studied by several authors, some<sup>76-81</sup> of whom have revealed that within a definable range of carrier frequency variation, the original compensating network still provides adequate system compensation. One of the earliest attempts to achieve the specified form of compensating network whose characteristics are approximately independent of the carrier frequency over a narrow band of drift was outlined by Notthoff<sup>76</sup>. He proposed the use of fourth-order transfer functions as an approximation to

the ideal characteristics. Double twin-T network can realize these characteristics, in which one twin-T is adjusted for an amplitude minimum at the carrier frequency minus the desired bandwidth, and the other is adjusted for an amplitude minimum at the carrier plus the desired bandwidth. Nashman et al<sup>78</sup> have presented an exact method of analysis of a.c. notch networks which includes both the effects of carrier frequency variations and motor field misalignments. Mehelish and Murphy<sup>79</sup> studied the effects of carrier frequency variations on the performance of tuned compensators and on the closed-loop performance of a complete carrier control system taking into account the change in the servomotor characteristics with the carrier frequency. They presented an experimental technique devised for analysing this problem based on the assumption that the 2-phase servomotor transfer function can be described by one time constant. They further concluded that the effect of carrier frequency drift on the a.c. transfer function of the tuned compensating network decreases with the increase of the pole/zero ratio. Hence, since the bridged-T network usually provides a larger pole/zero ratio than its RLC counterpart, the RC circuit is superior in this respect. However, as the pole/zero ratio increases, the effect of noise in the system increases. It is therefore necessary to compromise between a design which yields a small signal-to-noise ratio and one which yields a system that is very sensitive to changes in carrier frequency. Weiss<sup>80</sup> has shown that the behaviour of the overall modulation transfer function due to changes in the carrier frequency can be best studied in terms of pole and zero migrations in the complex frequency plane. Nagrath and Arya<sup>81</sup>



modified the available complicated exact expressions of the in-phase and quadrature envelope transfer functions<sup>44</sup> for notch-type networks in a manner to be wieldable for practical network design under the condition of predetermined carrier frequency drift.

Smith<sup>2</sup> has shown that small carrier-frequency drifts can be compensated for by a fixed shift in the phase of the demodulator reference carrier. This phase shift results in zeros movements in the complex frequency plane, and therefore may be adjusted to suitably relocate these zeros to give extra phase lead. If, however, either the carrier-frequency drift or its rate of change is large enough, an automatic phase shifter must be used. Smith<sup>2</sup> described a system of this type in which a sample twin-T adjusted for full rejection is employed, with the positions of the poles and zeros with respect to the  $j\omega$ -axis identical to the positions of the poles and zeros in the twin-T used in the actual system, with respect to the line representing the phase shift on which the zeros have been adjusted in the actual system. A ring bridge demodulator follows the sample-T and delivers a direct current whose polarity depends on which side of the origin the demodulated zero falls. This controls the saturable reactor in the carrier reference-phase-shift circuit. Tracking between the sample-T and the system-T becomes important when the frequency deviation is large. Small phase errors will make large differences in the demodulated zero location and in the carrier rejection ratio. However, the zero location at large frequency shifts can be vernier-adjusted with a small RC frequency-dependent phase shifter in the feedback reference to the sample demodulator.

One of the detrimental effects of carrier-frequency drift, apart from the possible loss of the compensating properties of the in-phase envelope transfer function of the tuned network, is the increase of the quadrature signal<sup>77</sup>, which in turn may:

1. Saturate the amplifier thus limiting linear operation,
2. Cause excessive heating of the servomotor control winding.

Such quadrature signal may introduce considerable error in some applications such as in a null type recorder using a.c. servo system. Although the error due to the quadrature signal can be eliminated by adjusting the carrier excitation to the two windings of the servomotor at phase quadrature<sup>77</sup>, the risk of the amplifier saturation and heating problems still remain. Furthermore, it is practically very difficult to obtain exact phase adjustments. Methods<sup>82-84</sup> have, therefore, been developed to surmount all the aforementioned problems, whose principle of operation is based on injecting a quadrature signal of appropriate magnitude and anti-phase to that generated in the system so as to suppress it before amplification. If the carrier-frequency drift and hence the quadrature signal are not stable, the suppression must be controlled automatically. An auxiliary servosystem operating on the quadrature signal may be used, where the shaft of the servomotor is coupled to the sliding contact of a potentiometer energised by a quadrature carrier. The quadrature voltage picked up by this potentiometer is then fed back and added to the original signal for quadrature suppression before feeding the servoamplifier. However, the disadvantage of this system, apart from the extra weight, space and cost, is

that the same problem of exact quadrature carrier phase adjustment, as in the main loop, also exists. Williams and Payne<sup>82</sup> introduced a quadrature suppression device based on sampling technique, involving vibrator-type synchronous switches. The switches are arranged in such a way as to sample the signal at the instants where the quadrature component passes through zero, and thus transmit only the in-phase component. Damping was obtained by using RC elements in conjunction with the switches similar in form to phase-lag RC chopper network (as will be discussed later). Hutcheon and Harrison<sup>83</sup> outlined an electronic system whose principle of operation is analogous to that of the auxiliary servo-system mentioned earlier. The system is basically a quadrature generator employing two thermistors whose heaters are connected differentially and driven from a transistor demodulator. The corresponding thermistor beads act as a variable voltage divider which is used to control a suppression signal of precise quadrature phase. The main drawback of this device is the slow action of the thermistors. Constable<sup>84</sup> was fundamentally interested in removing the quadrature component generated in synchros<sup>1</sup> particularly desirable when employed as signal generators. He found that perfect integration is the answer. As an approximation, he used phase-lag networks, which are only suitable for a particular carrier frequency. This method is therefore not suitable under variations in carrier frequency.

A direct method of compensating for carrier-frequency drifts is to automatically retune the notch network so that the null follows the carrier frequency<sup>85,86</sup>. Shurr<sup>85</sup> accomplished this by employing an auxiliary servo-loop

consisting of a frequency detection network, amplifier, and a servomotor. He applied this self-adapting technique to a bridge-T network, with which he investigated the relative advantages of returning by varying either both resistances or only the shunt resistance. The auxiliary servomotor is operated such that it simultaneously changes the parameters in the frequency detection network to automatically provide proper positioning of the parameters which were shifted in the main notch network. Shurr used a sample bridged-T in the auxiliary-loop with source and load impedances matching the corresponding values in the actual system. The output of the sample-T is in-phase with the reference excitation of the auxiliary 2-phase motor when the notch frequency is equal to the carrier frequency. If the carrier frequency changes, the phase of the amplified output signal from the sample-T changes, and hence developing a torque in the auxiliary servomotor. This causes rotation of the motor shaft resulting in resistance adjustment in both the actual and sample-T networks until both are returned to the new carrier-frequency value. Although in varying the shunt resistance only, the minimum point of each notch varies slightly in magnitude and the transfer function does not remain constant, it is still more preferable to varying simultaneously the two resistances in view of the complexity of the latter. In a recent paper by Douce and Edwards<sup>86</sup>, a description of a system to track the carrier-frequency changes using a novel variable-null parallel-T filter in a feedback loop is outlined. The paper explains a means of increasing the notch sharpness of the null parallel-T network by including it in a feedback loop with a high gain amplifier; rendering the filter to be suitable for stabilizing a.c. systems of

very low natural frequency. Although the notch frequency of the parallel-T network can be adjusted by varying one of several combinations of two components simultaneously, accurate ganging is required to maintain a null over a wide frequency range. A simpler method<sup>87</sup> is, however, possible where the null is adjusted by a single potentiometer feeding the low-pass-T of the parallel-T network. A condition for this potentiometer to be of negligible resistance can be satisfied in practice by including an emitter-follower immediately after it. In principle, the self-adaptive-filter loop is similar to that used by Shurr. A perturbing signal at the quadrature carrier is added to the main-loop servosystem error signal and the sum is applied to the filter. This perturbation signal gives zero output when the filter is tuned to the carrier frequency. If the filter is off tune, this perturbation signal appears in the filter output which, on being phase-sensitive rectified using a reference signal that is in phase quadrature with it, produces motor torque for the auxiliary tracking-loop, which is used to alter the potentiometer setting. The paper suggests the possible use of high-speed electronic multiplier in place of the motor of the auxiliary loop. The main disadvantage of this method lies in the fact of possible cross-coupling between the tracking loop and main control system, which results due to the appearance of a quadrature component for the servosystem error signal at the off tune filter output. This signal, in addition to the perturbation signal, will operate the auxiliary tracking circuit. To reduce such effect, the perturbation signal may be made very large in comparison with the main system error signal.

From the above survey, it is evident that the methods and techniques so far developed to compensate for carrier-frequency deviations in a.c. servomechanisms, in order to enable notch passive compensating networks to be used effectively, have resulted in more complexity, cost, size, and weight. These are contrary to the original objectives in selecting the linear passive networks in the first place. Recently, a new class of networks referred to as switched or chopper networks has been developed which excludes the aforementioned disadvantages. While its characteristics are independent of changes in the carrier frequency. Because of these advantages, there is a rapid expansion in its applications as demodulating compensators in a.c. servomechanisms in spite of the disadvantage of generating noise in the form of harmonics of the carrier frequency (due to the switching process involved).

Basically, the chopper networks consist of passive electric networks (usually of RC passive elements) whose elements are interconnected by switches operating in synchronism with the carrier. Their principle of operation is therefore very similar to demodulation - d.c. compensation-remodulation all performed simultaneously instead of in sequence as in the conventional approach.

Several methods have been developed for the analysis of chopper networks<sup>88-111</sup> based on two simplifying assumptions:

1. All the transformers and diodes associated with the synchronous switches are ideal,

2. Switching is instantaneous. This implies that the reference carrier signal controlling the switching is either a square-wave, or that its amplitude is very large compared to the signal to be switched.

In this respect, Bolie<sup>88</sup> has made an early contribution, confining his attention to a single-switch RC chopper network operating in its lagging mode. His analysis is based on the fact that the network is linear for each of the switching intervals, and hence linear differential equations can be readily solved and initial conditions matched at the switching instants. Bolie, in his treatment, adopted the assumptions of infinite load resistance and that  $\delta T \ll RC$ . With these assumptions, he obtained the response of the chopper network to a step function, and found that its expression is closely related to the response of a simple d.c. lag network with a time constant of  $RC/\delta$ .

A general method of analysis has been developed by Murphy and Egan<sup>89,90</sup> which is based on the formulation of equivalent block diagrams coupled with Laplace and Z-transform techniques. They applied their analysis to the chopper network configuration used by Bolie<sup>88</sup>, but in both its phase-lag and phase-lead modes of operation. Their investigations, however, were confined to the simple case when the input modulation signal is in the form of a step-function. The results of their investigations again confirmed those of Bolie in that the behaviour of the chopper networks discussed, under step-function modulation of the carrier, have the same effect as first-order d.c. lead or lag networks acting

directly on the step-function input. For the lagging mode of operation, they extended their analysis to the case of finite load resistance, and thus found that the effective lag time constant of the chopper network is  $R_{\text{eff}} C/6$ , where  $R_{\text{eff}}$  is the equivalent of the parallel combination of  $R$  and the load resistance. They also found that the effective lead time-constant is dependent on the phase of the carrier with respect to the switching voltage.

Goster<sup>91</sup> showed that a sinusoidal modulator in series with an ON/OFF synchronous switch can be represented by an ideal sampler followed by a block of a linear transfer function, provided that the maximum data frequency is very small compared to the carrier frequency (the representation becomes exact at zero modulation frequency). Making use of this, he was able to represent the chopper network by an approximate open-loop sampled-data system which is different from the exact closed-loop sampled-data system representation developed earlier by Murphy and Egan. This has resulted in a much simpler method of analysis. Applying this technique to obtain the response of the chopper network analysed by Murphy and Egan in both its phase-lead and phase-lag modes of operation when subject to a step-function, Goster arrived at the same results.

Bohn's<sup>92</sup> analysis is based on setting up linear differential equations to describe the chopper network during the switching intervals. Solving these linear differential equations can be done easily, but matching the initial conditions at the switching instants can be extremely complicated except for the case of input



step-function modulation carrier. In obtaining the response of three demodulator lead type chopper networks (presented by Tustin<sup>93</sup>, Lyons<sup>94</sup> and Truxel<sup>22</sup>), Bohn<sup>92</sup> confirmed the results obtained by Murphy and Egan<sup>89,90</sup> and Goster<sup>91</sup>, through the use of sampled-data systems. By invoking the assumption that the envelope is a slowly-varying function of time as compared to the carrier frequency, Bohn was thus able to compute the amplitude of the envelope using quasi-stationary Fourier analysis. He noted that this amplitude, which is effectively the output modulation function, changes with time in a way similar to the response of a d.c. phase advance network subject to input step-function. In this way, Bohn derived an "equivalent" d.c. network which operates on the data in an analogous fashion as the chopper network operates while the data is carried on a carrier. Such equivalence is only valid when the basic assumption ( $\omega_m/\Omega \ll 1$ ,  $\omega_m$  is data frequency) is satisfied. In a later paper, Bohn<sup>95</sup> applied his approximate method to derive the equivalent d.c. network for a double-switch single-capacitor chopper network<sup>96</sup> when the switches are operating with zero fly-time. In an attempt to develop a simple practical design procedure for phase-lead and phase-lag chopper networks to meet specifications on a.c. system performance, Knox and Murphy<sup>97,98</sup> used the concept of the equivalent time-invariant passive electric networks<sup>90,92,95</sup>. They determined the parameters of the equivalent network in terms of those of the chopper network employing the assumption invoked by Bohn ( $\omega_m/\Omega \ll 1$ ), and hence applying the quasi-stationary Fourier analysis. Developing a set of design curves, they showed that the design procedure can become very simple, and that a great freedom in selecting the characteristics of the network

can be achieved by adjusting the time constant  $\tau$ , the carrier phase  $\theta$  (where  $\theta$  is defined as the phase of the carrier signal with respect to the gating signal), and the dwell time  $\delta$ , instead of being limited to adjustment of  $\tau$  only as has been done in earlier work by Bohn<sup>92,95</sup>. The chopper networks considered by Knox and Murphy are:

1. Double-switch single-capacitor type operating in its phase-lead mode,
2. Double-switch double-capacitor type operating in its phase-lag mode.

While working out the various equations from basic principles, the author has found certain mistakes in the signs of some expressions given by Knox and Murphy in their article of Reference 97. It may be worthwhile to give the corrections here as below:

The signs of

1. The term  $(\tau\Omega \cos \theta - \sin \theta)$  in Eqn. 4, and
2. The term  $\beta K_2$  in Eqn. 10

should be reversed.

Following similar steps, Negrath and Pratap<sup>99</sup> analysed Lyon's<sup>94</sup> lag chopper network (double-switch single-capacitor type originally patented by Whiteley<sup>96</sup>) and presented useful design curves, which again are only valid for the condition  $\omega_m/\Omega \ll 1$ .

Weiss<sup>100</sup> was fundamentally interested to verify the experimentally and intuitively derived behaviour of chopper networks proposed by some earlier

investigators<sup>94,101-104</sup>. He, therefore, attempted to give a rigorous steady-state analysis of an idealized model of the chopper network (in the form of double-switch single capacitor)<sup>96</sup>, with the objective to show that the envelope driving-point impedance is a capacitive reactance. Although, he restricted his analysis to the simplest case of zero fly-time switches, the resulting expressions are extremely complicated, so that he had to resort to some approximation to prove that the major term is carrier-frequency independent. His principal conclusion is, however, that since the envelope response of the chopper network is different for the cases of current excitation and voltage excitation, one cannot achieve a unique envelope model of the chopper network.

To study the transient response of chopper networks, Walker and Wilson<sup>105</sup> presented a simple analysis, based on the use of the Laplace Transform, for the double-switch single-capacitor chopper network<sup>96</sup>. Although they claimed the validity of their analysis for any value of fly-time of the switches, a thorough study of their work can reveal that it is only limited to the zero fly-time case. To prove this, it may be best done by examining Eqn. 6. The physical meaning of this equation may be explained as that the RC network of Fig. 7 (Reference 105) is energized from a source of voltage  $e$  which is connected through a fictitious ideal reversing switch of zero fly-time and shunted by a fictitious ON/OFF switch which acts as short-circuit to both the source and the RC network during the fly-time of the actual switch. This, in fact, does not represent the actual case, since the RC network remains open-circuit, and not short-circuit, during the fly-time. To simulate this, however, an additional correcting voltage must be introduced at each switching

instant in the form of a Dirac pulse, whose magnitude is equal to the voltage appearing across the capacitor at the same instant. The polarity of such voltage must be applied such that its resulting current drawn by the RC network will cancel the current flowing due to the charge on the capacitor, and thus giving the effect as if the RC network is open-circuited (this technique has been applied in the exact analysis outlined in Section 4.2, which has resulted in developing a closed-loop sampled-data system<sup>89,90</sup> capable of computing the voltage across the capacitor at the switching instants). In the limiting case of zero fly-time, however, the effect of instant short-circuiting of the fictitious ON/OFF shunt switch on the RC circuit becomes immaterial, since instant short-circuit and instant open-circuit theoretically have the same effect. Therefore, no additional voltage is needed, and Eqn. 6 as well as the subsequent derivations in Reference 105 consequently become valid.

Whiteley's<sup>96</sup> double-switch single-capacitor chopper network has recently attracted the attention of more investigators<sup>106-110</sup>. References 106 to 108 have dealt with the chopper network in its phase-lead mode of operation, while Reference 109 dealt with it in its phase-lag mode of operation. The approach to the analysis followed in these articles is basically concerned with deriving the transfer function using the Laplace Transform technique. After neglecting the high harmonic terms appearing in the output (on the grounds that these terms will be damped out by the filtering action of the induction motor), and the function in the term linearly related to the input was thus regarded as the transfer function. The expression of this transfer function is in the form of infinite summation, which the authors (of

the References 106 to 109) had to approximate by taking only the first term in addition to the constant term. The resulting approximate expression of the transfer function was shown to be bi-quadratic similar to those of the well-known notch networks. In examining the notch frequency (deduced from the bi-quadratic expression of the approximate transfer function), it was found related to the carrier frequency and thus any variation in the carrier frequency is reflected in a change of the notch position, which may suggest that the chopper network operates as if automatically self-tuned.

The analysis given in References 106 to 109 is limited to the case of zero fly-time operation of the switches. Any attempt to extend its application to positive fly-time operation, the initial condition values at the switching instants have to be taken into consideration in the manner explained above in discussing Reference 105. It may also be worthwhile to point out that the harmonic terms of the chopper network given by Eqn. 23 (Reference 107) do not include all the possible combinations. To work out the correct expression for the output signal of the chopper network, the relevant equations 11, 19, 20 given in Reference 107 may be reproduced here below:

$$X(s) = G(s) V'(s) \quad 1.4.3$$

$$V'(s) = \sum_m \frac{2}{jm\pi} \left[ V(s - jm\omega_s) - V(s + jm\omega_s) \right],$$

$$m = 1, 3, 5, \dots, \infty \quad 1.4.4$$

and

$$V_o(s) = \sum_n \frac{2}{jn\pi} \left[ X(s - jn\omega_s) - X(s + jn\omega_s) \right],$$

$$n = 1, 3, 5, \dots, \infty \quad 1.4.5$$

where the various parameters are as defined in the Reference.

Thus, substituting Eqns. 1.4.3 and 1.4.4 in Eqn. 1.4.5, one may express the output signal  $V_o(s)$  as :

$$V_o(s) = \sum_n \sum_m \frac{4}{nm\pi^2} \left[ G(s - jn\omega_s) \left\{ V[s + j(m-n)\omega_s] - V[s - j(m+n)\omega_s] \right\} + G(s + jn\omega_s) \left\{ V[s - j(m-n)\omega_s] - V[s + j(m+n)\omega_s] \right\} \right] \quad 1.4.6$$

To obtain the fundamental component of the output, one may substitute  $n=m$  in the above expression and collect the terms associated with  $V(s)$ . This will yield an expression similar to that obtained from Eqn. 23 (of Reference 107). To obtain any harmonic component, however, a similar technique can be applied, for example, if  $h$  represents the index of the required harmonic ( $h$  is even integer because both  $n$  and  $m$  are odd integers), then :

$m-n = h$  is substituted in the terms  $V[s_{\pm j}(m-n)\omega_s]$

and

$m+n = h$  " " " " "  $V[s_{\pm j}(m+n)\omega_s]$

of Eqn. 1.4.6. This will yield an expression different from that obtained from Eqn. 23 (of Reference 107). The reason for this difference has resulted from the fact that Eqn. 23 has been derived from Eqns. 19 and 20 (reproduced above as Eqns. 1.4.4 and 1.4.5 respectively) only for the condition  $n=m$ , which led to the exclusion of many terms. It must be emphasized, however, that the subsequent derivations in References 107 and 109 were fortunately not affected by this, since they depend only on the fundamental component which is, nevertheless, correct.

Continuing the work outlined in References 106 to 109, Wilson<sup>110</sup> presented an attempt for formulating an exact modulation model for two chopper network configurations:

1. Double-switch single-capacitor (see Reference 96),
2. Single-switch double-capacitor.

His investigation is limited to phase-lead mode of operation of the chopper network, and under the condition of zero-fly-time switches. The basis of his analysis depends on deriving the modulation transfer function from the transfer function obtained by the method previously propounded by him and Walker<sup>107,108</sup>. In computing the modulation frequency response of double-switch single-capacitor chopper network by this method and the approximate method developed by Bohn<sup>92,95</sup>, Wilson discovered a considerable difference on which he commented

that it may be attributed to the approximation involved in Bchn's method. The author of this thesis, however, does not entirely agree with Wilson's comment because he believes that in deriving the modulation transfer function from the transfer function, Wilson has inadvertently neglected two other terms which may contribute a large part to the modulation transfer function. The following analysis may help clearing this viewpoint:

In examining Eqn. 1.4.6, the output of the chopper network can be shown to contain a fundamental component and even harmonics of the carrier. It is possible, therefore, to rearrange it in the more suitable form:

$$\begin{aligned}
 V_0(s) &= Y_0(s) V(s) + Y_{+2}(s)V(s+j2\omega_s) + Y_{-2}(s)V(s-j2\omega_s) \\
 &+ Y_{+4}(s)V(s+j4\omega_s) + \dots\dots\dots \\
 &= \sum_{n=-\infty}^{n=\infty} Y_{2n}(s) V(s+j2n\omega_s) \qquad 1.4.7
 \end{aligned}$$

Where

$$n = 0, 1, 2, 3, \dots\dots\dots \text{integer}$$

and  $Y_{2n}(s)$  represents the functions associated with the various output signal components, with the post-subscript indicating the index of the harmonic.

If the input signal is in the form of suppressed-carrier amplitude-modulated wave, i.e. :



$$V(t) = x(t) \sin(\omega_s t + \theta) \quad 1.4.8$$

Where  $x(t)$  = is the data signal,

$\omega_s$  = is the carrier frequency,

and  $\theta$  = is the phase of the modulation carrier.

Applying the Laplace transform to both sides of Eqn. 1.4.8, gives

$$V(s) = \frac{1}{2j} \left[ e^{j\theta} x(s-j\omega_s) - e^{-j\theta} x(s+j\omega_s) \right] \quad 1.4.9$$

Substituting Eqn. 1.4.9 into Eqn. 1.4.7, the output signal can be written in terms of the data signal, thus

$$V_0(s) = \frac{1}{2j} \sum_{n=-\infty}^{n=\infty} Y_{2n}(s) \left[ e^{j\theta} x \left\{ s + j(2n-1)\omega_s \right\} - e^{-j\theta} x \left\{ s + j(2n+1)\omega_s \right\} \right] \quad ..1.4.10$$

To determine the transmission characteristics of the chopper network with respect to the data signal, the envelope of the output voltage  $V(s)$  should be compared with the input data signal  $x(s)$ . To accomplish this, the envelope may first be recovered by a demodulation process. The output of the demodulator may be written in general as:

$$y(t) = V_0(t) \sin(\omega_s t + \phi) \quad 1.4.11$$

where  $\phi$  is the phase of the demodulation carrier.

On applying the Laplace transform, Eqn. 1.4.11 becomes

$$y(s) = \frac{1}{2j} \left[ e^{j\phi} V_0(s-j\omega_s) - e^{-j\phi} V_0(s+j\omega_s) \right] \quad 1.4.12$$

which gives on substitution into Eqn. 1.4.10

$$\begin{aligned} y(s) = & \frac{1}{4} \sum_{n=-\infty}^{n=\infty} \left[ e^{j(\phi-\theta)} Y_{2n}(s-j\omega_s) + e^{-j(\phi-\theta)} Y_{2n}(s+j\omega_s) \right] \\ & \times \{s+2jn\omega_s\} \\ & - \frac{1}{4} \sum_{n=-\infty}^{n=\infty} e^{j(\phi+\theta)} Y_{2n}(s-j\omega_s) \times \{s+2j(n-1)\omega_s\} \\ & - \frac{1}{4} \sum_{n=-\infty}^{n=\infty} e^{-j(\phi-\theta)} Y_{2n}(s+j\omega_s) \times \{s+2j(n+1)\omega_s\} \end{aligned}$$

..1.4.13

Since the high harmonic components are assumed to be considerably attenuated by the 2-phase servomotor, they can be neglected without committing a serious error. Thus, only the fundamental component has to be considered which may be deduced from Eqn. 1.4.13 by substituting:

$n = 0$  in the first term,

$n = 1$  in the second term,

and  $n = -1$  in the third term.

Therefore,

$$\begin{aligned}
 y(s)_{\text{fundamental}} &= \frac{1}{4} \left[ \left\{ e^{j(\phi - \theta)} Y_0(s - j\omega_s) + e^{-j(\phi - \theta)} Y_0(s + j\omega_s) \right\} \right. \\
 &\quad \left. - \left\{ e^{j(\phi + \theta)} Y_{+2}(s - j\omega_s) + e^{-j(\phi + \theta)} Y_{-2}(s + j\omega_s) \right\} \right] x(s) \\
 &= G_m(s) x(s) \qquad \qquad \qquad 1.4.14
 \end{aligned}$$

where  $G_m(s)$  is the modulation transfer function.

Eqn. 1.4.14 shows that the modulation transfer function depends not only on the transfer function  $Y_0$ , but also on the functions  $Y_{+2}$  and  $Y_{-2}$  associated with the signal harmonic components of double carrier frequency appearing in the chopper network output (see Eqn. 1.4.7).

In this respect, Wilson's analysis considers only the contribution of the transfer function  $Y_0$  (whose approximate expression is given by Eqn. 10, Reference 110) to the modulation transfer function, and does not take into account the contribution by the other two terms  $Y_{+2}$  and  $Y_{-2}$ .

In considering the single-switch double-capacitor chopper network, Wilson pursued an analogous procedure by first deriving the transfer function and then deducing the modulation transfer function from it. Again, in this process he did not take into account the terms corresponding to  $Y_{+2}$  and  $Y_{-2}$  given above for the double-switch single-capacitor chopper network. Furthermore, in deriving the transfer function, Wilson did not take into account the effect of the initial conditions at the switching instants which must be introduced in this network even with zero-fly-time operation of the switch. This is because each capacitor is open-circuited for half the carrier

period plus twice the fly-time of the switch (see Fig. 3, Reference 110), while Wilson's analysis suggests it to be short-circuited through the effective resistance (equal to the parallel combination of  $R$  and  $R_1$  seen in Fig. 3, Reference 110) during the same period. Therefore, the argument given earlier in connection with Reference 105 also applies here. As a consequence, it may be concluded that the expression for the transfer function given by Wilson is not exact in the first place, and thus the subsequent derivations depending on it.

Schlesinger<sup>111</sup> has shown that by employing an input transformer, one can introduce a d.c. channel in parallel with the chopper network. By adding the output signals from the d.c. and chopper network channels in different ratios by means of a summing amplifier, it is possible to control the d.c. transference, and hence obtain a wide variety of modulation transfer characteristics.

#### 1.4.5 Analysis of closed-loop a.c. servomechanisms

In a.c. feedback control systems where modulated signals are developed in and transmitted through a portion of the control loop, the conventional analysis and synthesis techniques employed for d.c. servomechanisms cannot be directly applied. The application of such techniques can, however, be extended to the a.c. servomechanisms if the modulated-carrier sections of the control loop are represented by equivalent transfer functions.

Now, it is widely recognized (see the selective References 1 to 3, 35 to 48, 58 to 62) that these equivalent transfer functions of the modulated-carrier sections are effectively the modulation transfer functions, provided

that both the modulator and demodulator are assumed ideal sinusoidal multipliers, and that the generated carrier harmonics will be suppressed by a low-pass filter situated just after the demodulator. On this basis, by approximating the 2-phase servomotor by an ideal demodulator followed by a low-pass filter, the synchro-pair by an ideal modulator and summer, and by assuming a linear transfer function for the modulated-carrier section, Tou<sup>42</sup> was able to derive the closed-loop and open-loop of the a.c. control system and hence apply the conventional design techniques. However, the approximate representations for the 2-phase motor and the synchro-pair are far from being realistic (as will be seen in Chapter 2).

Vlasov<sup>112</sup> has followed similar analysis employing the same approximate description of the 2-phase motor as Tou's, but considered the notational voltage in the synchro-pair neglected by Tou which resulted in a better representation, though the effect of the electric impedance circuits is still neglected. His analysis, however, takes into account the effect of any phase-misalignment between the modulator and phase-detector reference carrier excitations. Furthermore, he considered the a.c. system when employing single-phase commutator motor under the conditions of both field-control and armature control. In two subsequent papers, Vlasov<sup>113,114</sup> presented the analysis of more elaborate a.c. control systems stabilized by a differentiating 4-terminal network in the forward carrier-path, and velocity feedback. In an attempt to give better description to the 2-phase servomotor, he examined the two extreme cases of flux forcing<sup>113</sup> (and thus neglecting the resistance of the control winding in comparison with its inductive reactance) and current forcing<sup>114</sup> (and thus neglecting the inductive reactance of the control winding

with respect to the resistance). Further simplifying assumptions were adopted to enable the derivation of linear differential equations with periodic coefficients. These assumptions include: negligible reference winding resistance, negligible leakage flux in the stator and rotor, and very small control signals compared with the reference excitation signal. Vlasov<sup>114</sup>, in his analysis, represented the a.c. tachometer by an ideal modulator followed by an ideal differentiating element. This again, as will be seen in Chapter 3, cannot be considered as an accurate representation. In a recent paper, Sapiro<sup>62</sup> pursued an analogous technique as that outlined by Vlasov<sup>113</sup> and adopting the same description of the 2-phase servomotor. He showed that this can result in a representation by an ideal demodulator followed by a block of transfer function of low-pass filter, which is similar to the representation given earlier by Tou<sup>42</sup>.

A thorough investigation into a closed-loop a.c. system with the carrier channel enclosed between an ideal modulator and an ideal half-wave diode phase-detector has been outlined by L'vov<sup>115</sup>. L'vov showed that the input and output signals of each element in the system-loop can be represented by a Fourier harmonic series with amplitudes varying with time. Each amplitude of these harmonics corresponds to an equivalent closed-loop system consisting of a linear transfer function. In this way, more accurate overall open-loop and closed-loop transfer functions of the system can be obtained by taking into account the effect of various harmonics, in addition to the fundamental signal, particularly in case the low-pass filter situated after the half-wave demodulator is not providing adequate attenuation to the high harmonic components. Later, in the same

article, L'vov demonstrated his analysis by applying it to an a.c. system comprising a d.c. motor stabilized by a tachometer feedback loaded by an RC differentiating circuit. The output from a selsyn-pair is first demodulated by a half-wave diode demodulator and added to the output from the stabilizing minor feedback loop before feeding a servo amplifier which drives the d.c. motor. The analysis of such a system is, however, relatively easy because it does not employ a 2-phase induction motor to which no apparent satisfactory simple description is yet available.

Stein and Thaler<sup>116</sup>, in their study of the 2-phase servomotor, have arrived at the conclusion that the behaviour of the 2-phase motor cannot be described by a simple linear transfer function of single time constant, i.e.,

$$G(s) = \frac{k}{s(1+s\tau)} \quad 1.4.15$$

where  $k = \frac{\text{stalled torque at rated voltage}}{\text{rated voltage}}$

and  $\tau = \frac{\text{moment of inertia}}{\text{coefficient of viscous friction}}$

as it may appear at first sight. Experimental investigations have showed that both  $k$  and  $\tau$  are not constant, but dependent on the amplitude of the control voltage  $e_D$ . A modification was therefore suggested based on the assumption that the torque-speed characteristics are straight lines, but not parallel (only valid for motor speeds up to approximately 50% of the synchronous speed), and hence  $k$  and  $\tau$  may be replaced by  $k_1$  and  $\tau_1$ , respectively, such that:

$$k_1 = \frac{k}{F + \left| \frac{\partial T_m}{\partial \gamma_m^*} \right|} \quad 1.4.16$$

and

$$\tau_1 = \frac{J}{F + \left| \frac{\partial T_m}{\partial \gamma_m^*} \right|} \quad 1.4.17$$

where

$F$  is the coefficient of viscous friction,

$J$  is the moment of inertia,

$T_m$  is the motor developed torque,

and  $\gamma_m^*$  is the motor shaft speed.

Since the torque-speed characteristics are not parallel straight lines, their slope  $\partial T_m / \partial \gamma_m^*$  is a function of the amplitude of the control winding voltage. As a result, in replacing  $k$  and  $\tau$  by  $k_1$  and  $\tau_1$  in the transfer function expression given by Eqn. 1.4.15, the resulting transfer function becomes dependent on the input control signal, and thus the 2-phase motor can be considered as a non-linear element. On this basis, Stein and Thaler<sup>117</sup> presented an analysis for closed-loop a.c. system employing 2-phase motor based on the describing function technique. From the experimentally determined torque gain  $k_1$  and time constant  $\tau_1$  versus the control voltage amplitude  $V_c$ , they found that the following functions can give good agreements with the experimental curves

$$k_1 = \frac{G}{\cosh(F V_c)} \quad 1.4.18$$

$$\text{and} \quad \tau_1 = \frac{E}{\cosh(F V_c)} \quad 1.4.19$$



if the constants  $G$ ,  $E$ , and  $F$  are appropriately chosen. Using these relations, a set of the inverse frequency response curves for the 2-phase motor can be plotted with  $V_c$  as a parameter. With this plot superimposed on a Nichol's diagram for the linear part of the a.c. system, Stein and Thaler showed that the closed-loop frequency response of the a.c. system can be determined by a simple graphical method. In the same article, they developed an analytical method for calculating the describing function of the 2-phase motor using Fourier analysis. In a further paper, Stein<sup>118</sup> studied the influences of the 2-phase motor non-linear characteristics on the transient response of an a.c. system. His analysis was carried out by means of the phase-plane method. He considered first a simple uncompensated system with only a servo-amplifier preceding the 2-phase motor in the forward path with unity feedback. He then proceeded to derive a second order differential equation for the error signal, from which he deduced that the natural frequency is independent of  $V_c$ , but the damping ratio is dependent on  $V_c$  and hence on the error signal. Stein then showed how to calculate the phase trajectories and isoclines with the help of the torque-speed characteristics of the 2-phase motor. He repeated the same analysis for the simple system when compensated by means of tachometer feedback which he represented as an ideal differentiating element. The conclusions he reached were that the tachometer feedback affects only the damping ratio with the result of decreasing the influence of the motor and thus increasing the system linearity. The work outlined in References 116 to 118 provides very useful analysis of a.c. systems employing 2-phase motor. However, the methods adopted depend on the experimental determination of the torque-speed characteristics of the

motor which may limit their exploitation in the synthesis of new systems. Furthermore, the papers<sup>116-118</sup> do not give rigorous analysis to either the error-detector or the tachometer.

References 119 and 120 demonstrate the application of conventional design techniques to hybrid servosystems. In these systems, d.c. sections within the closed-loops are provided so that compensation can be effected by means of d.c. networks. Thereby, one may avoid the complexity involved in designing satisfactory a.c. compensation networks particularly under carrier-frequency drift. The system of Bailey and Ziniuk<sup>119</sup> employs an output potentiometer energised by direct voltage. The sliding-contact voltage of this potentiometer, being proportional to the output shaft position, is feedback through either a resistance or a capacitor to allow a choice to be made between position and rate mode of operations by means of a switch. In this way, the use of tachometer feedback is avoided in order to reduce the inertia on the output shaft, thereby improving the acceleration properties of the system. In the position mode of operation, the output signal is feedback through a resistance to the summing point of a d.c. input amplifier, while compensation is accomplished by a lead-lag network in a minor loop connected around the d.c. amplifier. Cox and Johannessen<sup>120</sup>, on the other hand, employed the principle of demodulation - d.c. compensation - remodulation applied on the output signal of an a.c. tachometer in a minor feedback loop. Their emphasis is fundamentally placed on displaying the effective use of magnetic devices and transistors to perform the functions of amplification, modulation, and demodulation.

Although there are several types of control systems which involve amplitude-modulation processes, viz., single-sinusoid carrier signal systems, sampled-data systems, finite pulse-width systems, and modulated systems which use square-wave carrier signals, there seems to be little relation between most of the analytical techniques used in connection with each of these various types of systems. To allow an interchange of the pertinent techniques now available to take place, with respect to the analysis and synthesis of such systems, Ivey<sup>121</sup> has attempted to establish a common basis from which these various control system types can be derived. His attempt resulted in a general classification for amplitude-modulated carrier control systems.

#### 1.5. Scope of the present work

In view of the general survey conducted in the previous section, a conclusion can be drawn that despite the numerous publications on the various aspects of a.c. servomechanisms, the basic problems outlined in Section 1.3 do not seem to have been completely solved. Furthermore, as it is widely recognized<sup>2,23,27</sup>, the application of more refined and systematic methods to the design of a.c. servomechanisms is still lagging behind similar applications to d.c. systems. This is mainly because the designers are still confronted with extremely wide range of problems to which inadequate attention has been given so far. The following points summarise the basic obstacles facing the designers at present:

- i) There still appears to be no completely adequate simple description to the characteristics of various a.c. system components.

- ii) Difficulties associated with the realization of appropriate a.c. compensation designed to operate on the envelope of a modulated signal.
- iii) The existence of practical limitations which may be considered mainly responsible for holding back many experimental investigations to be carried out with sufficient scope.

In this thesis, therefore, it is intended to deal with these problems with the object of seeking more rigorous and accurate solutions. The realization of this aim requires the development of basic concepts and powerful techniques of analysis, illustrated whenever possible by comprehensive mathematical models, block diagrams and/or equivalent circuits in order to increase the physical insight.

In addition to tackling the various problems associated with a.c. servomechanisms, the present work includes new developments, amplification and modification of existing ideas, and extension of the scope of application of known concepts.

With such broad lines in mind, it is very difficult to treat all the topics in a homogenous manner. More emphasis is placed on areas where little or no attention previously given. More details and background information will be provided only wherever it is found needed.

To cope with the various problems outlined above and to present the various new developments, the plan of the present work has been divided into a number of logical steps. These steps are briefly outlined in the subsequent sub-sections.

### 1.5.1 Analysis of the basic components of a.c. servomechanisms.

Before effective studies could be made on the overall a.c. servomechanism, the basic components should be adequately analysed on reliable theoretical basis. Chapter 2 is therefore devoted to the analysis of

- a) 2-phase servomotor, and
- b) transmitter-coincidence transmitter synchro-system error-detector,

by applying the generalised 2-axis theory of machines<sup>122</sup>, and adopting more realistic assumptions. Emphasis is placed on treating these components, not as isolated units as usually has been done by previous investigators<sup>4-34</sup>, but as integrated parts of the system.

The analysis of potentiometer-bridge error-detector has been attempted by many authors<sup>22,23,27</sup> in the past, but the way of presenting the results of the analysis differs. It would be, therefore, appropriate to reformulate its analysis hereafter in order to make it compatible with the analysis of the other basic a.c. components outlined in Chapter 2, which is necessary for further use in the present work.

- i) Analysis of an error-detector in the form of a potentiometer-bridge.

Fig. 1.5.1 shows a diagrammatic representation of linear potentiometer-bridge in which the sliding contact shaft position of potentiometer 1 ( $\gamma_{p1}$ ) represents the command signal, whereas the shaft position of potentiometer 2 ( $\gamma_{p2}$ ) represents either the actual output or a proportion of it according to whether the sliding contact

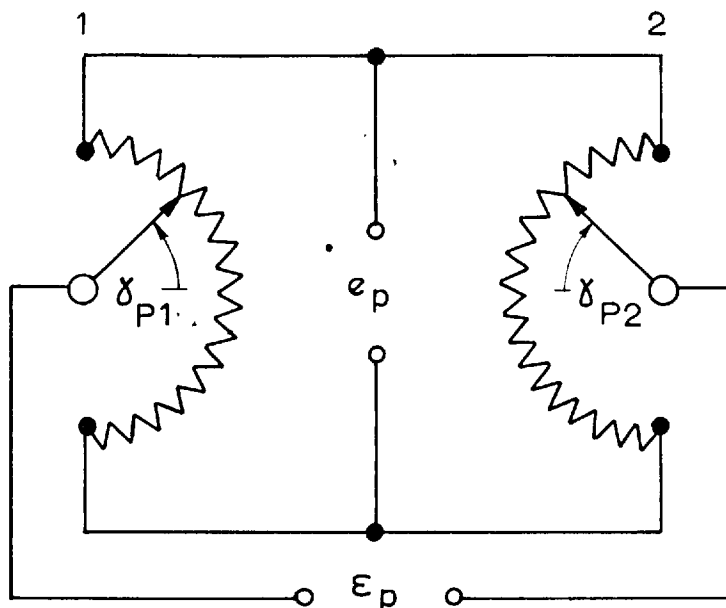


FIG. 1.5.1

A POTENTIOMETER - BRIDGE ERROR DETECTOR

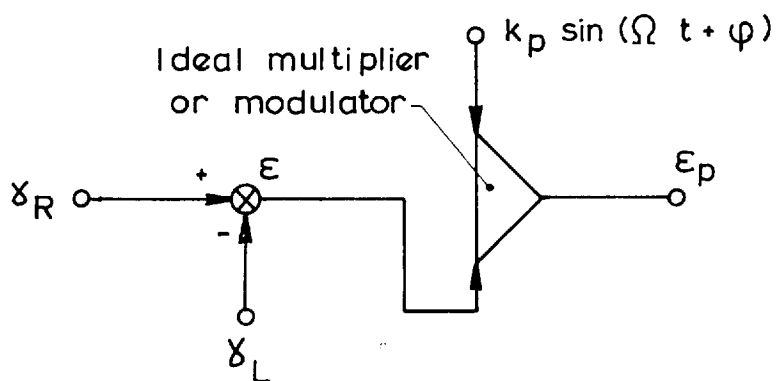


FIG. 1.5.2

MATHEMATICAL MODEL REPRESENTATION OF A  
POTENTIOMETER - BRIDGE ERROR DETECTOR

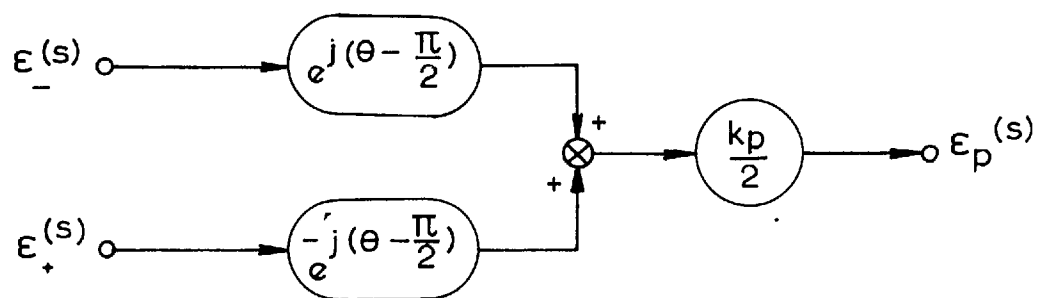


FIG. 1.5.3

COMPLEX FREQUENCY BLOCK DIAGRAM REPRESENTATION  
OF POTENTIOMETER - BRIDGE ERROR DETECTOR

shaft is solidly coupled to the load shaft, or coupled to it through an appropriate gear-train.

The potentiometers are wound in cylindrical form with maximum angular displacement  $\Gamma$ . In general, the potentiometer-bridge is energised by a carrier signal in the form of

$$e_p = E_p \sin(\Omega t + \theta) \quad 1.5.1$$

Assuming smoothly distributed winding and negligible backlash in the gear system, the voltage difference appearing between the two sliding contacts may be written as

$$\begin{aligned} \mathcal{E}_p &= \frac{e_p}{\Gamma} (\gamma_{p1} - \gamma_{p2}) \\ &= k_p \mathcal{E} \sin(\Omega t + \theta) \end{aligned} \quad 1.5.2$$

where

$$\mathcal{E} = \gamma_R - \gamma_L \quad 1.5.3$$

and

$$k_p = \frac{n_L}{n_p} \cdot \frac{E_p}{\Gamma} \quad 1.5.4$$

#### ii) Representation by a mathematical model

Eqn. 1.5.2 shows that the potentiometer-bridge measures the error  $\mathcal{E}$  and produces an actuating signal  $\mathcal{E}_p$  in the form of a suppressed-carrier amplitude-modulated wave. These functions can be represented by a summer in cascade with an ideal modulator as shown in Fig. 1.5.2.

#### iii) Complex frequency block diagram representation

By taking the Laplace transform of both sides of

Eqn. 1.5.2, making use of the complex convolution integral<sup>124</sup> and method of residue<sup>125,126</sup>, it is easy to deduce the following expression

$$\mathcal{E}_p(s) = \frac{k_p}{2} \left[ e^{j(\theta - \pi/2)} \mathcal{E}_-(s) + e^{-j(\theta - \pi/2)} \mathcal{E}_+(s) \right]$$

..1.5.5

which can be translated into the block diagram shown in Fig. 1.5.3.

### 1.5.2 Compensation of a.c. systems

The role of compensation, as a means of modifying the servo-system performance characteristics to meet certain specified requirements as well as for the stability purposes, is widely recognized. Many a.c. compensation techniques have been developed and are already in common use. The applications of some of these methods are still, however, very limited due to the lack of adequately accurate analysis, and the non-availability of simple and comprehensive descriptions to their behaviour. The present work considers three types of compensation:

#### i) A.c. tachometer feedback

The first part of Chapter 3 provides a rigorous analysis to this type of a.c. compensation using the 2-axis general theory of machines<sup>122</sup>. From the analysis, comprehensive mathematical model and complex frequency block diagram representations can be deduced, which can be easily integrated with their correspondings pertinent to the 2-phase servomotor and synchro-system error-detector



(or potentiometer-bridge error-detector) to form the overall block diagram representation.

ii) Tandem linear networks

The remaining part of Chapter 3 is devoted to the presentation of a new method of a.c. linear networks synthesis. The method is based on the derivation of the transfer function from the specified modulation transfer function, and then applying the conventional theories of linear networks to the resulting transfer function. This method of synthesis is believed to be more general and flexible than the available methods. In addition, it is applicable not only to multiplicative modulation systems but also to rotary modulation systems.

iii) Tandem chopper networks

Recently<sup>88-111</sup>, there has been considerable interest in chopper networks in view of their superior qualities over other types of a.c. compensation in terms of size, weight, cost and reliability, while their characteristics are insensitive to carrier frequency drifts. To simplify the analysis of such networks, most of the previous authors have adopted the assumption of step-function input modulating signal without establishing the validity of the same. In addition, all the authors confined their approximate analysis to only a few types of chopper networks with very simple configurations and under restricted operating conditions. Some references<sup>89,90,94,97,98,108,110</sup> give few experimental results for very special cases which neither provide sufficient assessment to the approximations involved in the analysis nor determine their limits of validity under various modes of operation.

In Chapter 4, two methods of analysis are given. One of these methods is exact and employs the Z-transform and modified Z-transform techniques<sup>125,126</sup>. The second method is approximate and is based on some techniques developed by earlier authors<sup>97-99</sup>.

In addition to tackling the problems associated with the analysis of chopper networks, the present work includes:

- a) Design of superior type of transistor 3-terminal synchronous switch with wide operational capabilities to suit the newly developed chopper networks requirements, and to secure wider applications in other possible fields. This is presented in Chapter I.
- b) The extension of existing techniques of linear networks, such as the duality concept, to chopper networks which enables new developments in this sphere. This is given in Chapter II.

### 1.5.3 Experimental investigations

i) To check the validity of the propounded theoretical analysis of chopper networks, extensive experimental investigations have been carried out on a representative number of chopper networks under various modes of operation, and for the both cases of suppressed-carrier amplitude-modulated and rotary modulated wave forms of the input signal. The experimental results obtained were then compared with those computed by both methods of analysis as outlined in detail in Chapter 5. Good agreement has been found between the results of the exact

theoretical analysis and those obtained experimentally. In contrast, wide differences between the Laboratory results and those calculated by the approximate theoretical analysis have been established, which become even more predominant under certain operating conditions.

ii) To study the stabilizing characteristics of chopper networks when inserted in the forward path of a practical a.c. servomechanisms, a breadboard model of a positional control a.c. system was designed and constructed in the Laboratory. Chapter 6 gives briefly the design details of the various components of the model and the results of the necessary preliminary experiments conducted on them.

Chapter 7 is devoted to the extensive studies performed on the a.c. system model with particular emphasis on investigating the effects of

- a) carrier frequency drifts,
- b) phase misalignment between the modulation and demodulation carrier references,

on the performance characteristics of the uncompensated system and the chopper network. Useful conclusions have been drawn from these investigations which suggest a simple method of automatic compensation for these effects, should they become detrimental to the overall system performance.

#### 1.5.4 Scheme for extending the practical range of operation of commercial electronic modulators and demodulators

In measuring the modulation frequency responses of a.c. systems, electronic modulators and demodulators form

basic units in the testing arrangement. For practical reasons, the commercial types of these equipment give reliable results only in the range of modulating frequencies not exceeding 10% of the carrier frequency. This limits the range of modulation frequency response obtainable experimentally to only a small value, which may, in some cases, provide insufficient information for the design purposes.

In Chapter 8, a scheme has been developed capable of extending the working range of modulation frequency to carrier frequency of the available electronic modulators and demodulators, thereby wider and more accurate studies could be carried out on a.c. systems. The operation of the proposed scheme has been realized by square-wave modulators and demodulators which can be integrated into the electronic modulators and demodulators to be compensated without the need of any modification to their circuitry. The practicability of the scheme has been verified by appropriate tests in the Laboratory.

#### 1.6. Original contribution

The points enumerated below briefly outline the original work presented in this thesis.

1. Although analysis of 2-phase servomotor based on the 2-axis general theory of machines has been previously attempted by several authors<sup>17,19</sup>, it is believed that this is the first time to translate the results (obtained by minimum simplifying assumptions) into useful mathematical model and complex frequency block diagram representations, and to emphasize the importance of considering the 2-phase motor (which comprises a demodulation process) in

combination with the error-detector (which comprises a modulation process) in order to obtain a meaningful modulation transfer function.

2. The extension of the application of the 2-axis general theory of machines to the analysis of error-detectors, in the form of a transmitter-coincidence transmitter synchro-pair, and to the a.c. tachometer, and also the systematic construction of block diagrams for each component as well as for the overall integrated a.c. system.
3. The development of a novel synthesis method to realize specified multiplicative modulation transfer functions and rotary modulation transfer functions by means of linear networks.
4. The establishment of design criteria for realizing high quality transistor 3-terminal synchronous switch and its appropriate driving circuit capable of operation with positive and negative fly-time. In effect, the work done in Chapter I may be considered, to the author's knowledge, to be original in its entirety.
5. The development of methods whereby configurations and responses of chopper networks can be modified and expanded. This has been achieved by extending the application of the duality concept to 3-terminal chopper networks and by exploiting the negative fly-time capabilities of the incorporated synchronous switches. Effectively, the entire work presented in Chapter II, as far as the author is aware, is believed to be original and the ideas involved are initially based on suggestions made by Professor D.G.O. Morris, D.Sc., F.I.E.E., to whom the author is deeply grateful.

6. The development of exact analysis to three configurations of RC chopper networks valid under all possible modes of operation, and the derivation of expressions necessary for the study of the generated noise in each type.
7. The reformulation of an available approximate analysis<sup>97-99</sup> to be applicable to more general and complex configurations of RC chopper networks.
8. Extensive experimental studies of the chopper networks behaviour when subject to both multiplicative and rotary modulated signals under various possible modes of operation. Also, the comparison of the experimental results with the theoretical results obtained by both the exact and approximate methods which allowed the assessment of their validity and the exposition of their limitations.
9. The demonstration of the stabilizing effects of chopper networks on the overall performance of a positional control a.c. breadboard system model designed and constructed in the Laboratory.
10. The development and testing of a scheme capable of extending the practical range of operation of commercial electronic modulators and demodulators which play a significant part in the equipment set up for measuring the modulation transfer functions of a.c. systems.

## CHAPTER 2

### ANALYSIS OF THE BASIC COMPONENTS OF A.C. SERVOMECHANISM

#### 2.1 Introduction

In general, the analysis and design of servomechanism are usually carried out in the first place, on a mathematical basis in order that time may be saved in reaching an optimum design. This implies that all the physical elements must be described by some mathematical form before their contributions to system performance can be satisfactorily related to determine the overall system response.

In this chapter, rigorous analysis is attempted for the basic components,

- i) 2-phase servomotor
- ii) error detector in the form of a synchro-pair

aiming at more realistic representation and better description. Emphasis is placed upon developing improved mathematical models and complex frequency block diagrams for each component which may throw more light on their dynamic behaviour. In addition, by joining properly the block diagrams of various components, a complete representation of the a.c. servomechanism can be constructed as will be shown in Section 2.4. This will allow the available techniques of block diagram manipulation to be applied. Furthermore, it enables both analogue and digital computers to be used to perform various studies on the a.c. servomechanisms.

The analysis of the 2-phase servomotor and the synchro-

system is based on the 2-axis general theory of electrical machines<sup>122</sup>.

Derivation of the various differential equations may be considerably simplified, without loss of accuracy, by means of the following generally accepted assumptions,

- i) Balanced rotor and stator windings.
- ii) Space harmonics in the flux-wave may be neglected.
- iii) Rotor is smooth and self inductance of various windings is independent of rotor position.
- iv) Negligible magnetic saturation.
- v) Hysteresis and eddy current effects are negligible.
- vi) Symmetrical conditions exist on the system, i.e. there is no zero-sequence component.

In formulating the dynamic equations for the 2-phase servomotor, some fundamental equations have been reproduced in order to provide the background for further manipulation, and to serve as references for the analysis of the synchro-system and the a.c. tachometer presented subsequently.

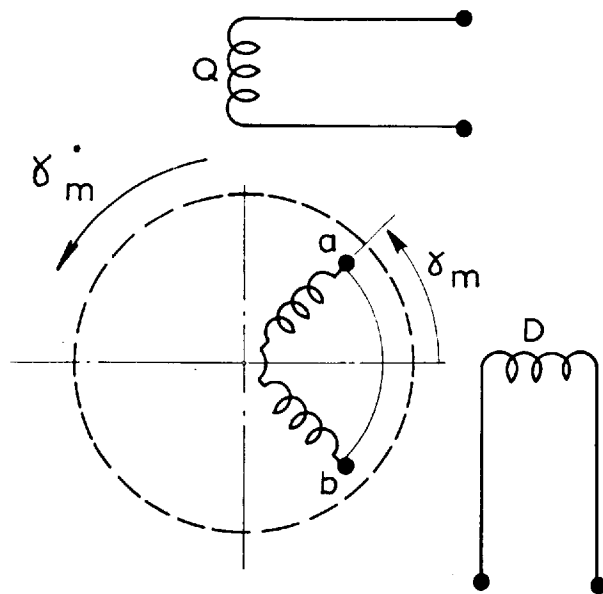
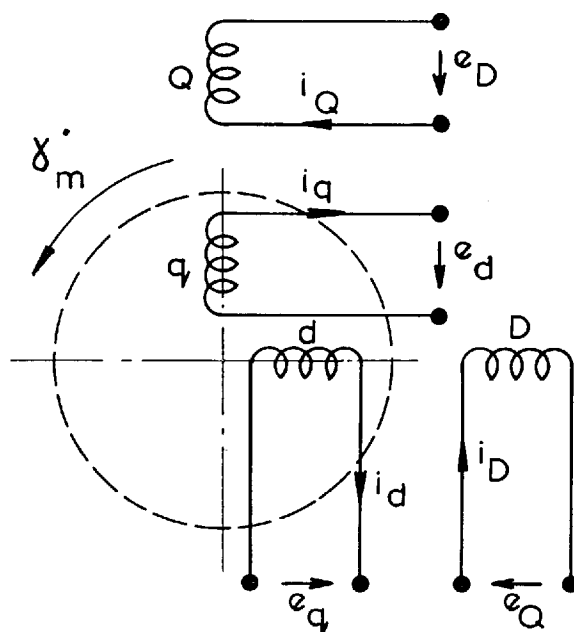
## 2.2 2-Phase Servomotor

### 2.2.1 Formulation of the dynamic equations

#### 2.2.1.1 Voltage equations

Fig. 2.2.1 shows a diagrammatic representation of the 2-phase servomotor and its equivalent generalised 2-axis machine. On the basis of the above assumptions, the voltages and



(a) ACTUAL MACHINE(b) EQUIVALENT GENERALIZED 2 - AXIS MACHINE

DIAGRAMATIC REPRESENTATION OF 2-PHASE SERVO MOTOR AND ITS EQUIVALENT GENERALISED 2-AXIS MACHINE.

FIG. 2.2.1.

currents of the general machine can be related by a generalised impedance matrix <sup>122</sup> as written below

$$\begin{bmatrix} e_D \\ e_Q \\ e_d \\ e_q \end{bmatrix} = \begin{bmatrix} R_D + L_D p & & M p & \\ & R_D + L_D p & & M p \\ M p & M \gamma'_m & R_d + L_d p & L_d \gamma'_m \\ -M \gamma'_m & M p & -L_d \gamma'_m & R_d + L_d p \end{bmatrix} \begin{bmatrix} i_D \\ i_Q \\ i_d \\ i_q \end{bmatrix} \quad 2.2.1$$

Equation 2.2.1 may be conveniently be written in the concise matrix form

$$[e] = [Z] \cdot [i_d] \quad 2.2.2$$

$$\text{Where } [Z] = [R] + [L] p + [G] \gamma'_m \quad 2.2.3$$

whereas

$$[R] = \begin{bmatrix} R_D & & & \\ & R_D & & \\ & & R_d & \\ & & & R_d \end{bmatrix}, [L] = \begin{bmatrix} L_D & & M & \\ & L_D & & M \\ M & & L_d & \\ & M & & L_d \end{bmatrix}$$

$$[G] = \begin{bmatrix} & & & \\ & & & \\ & M & & L_d \\ -M & & -L_d & \end{bmatrix}$$

2.2.4

The voltages and currents of the actual machine can be expressed in terms of those of the generalised machine by using an appropriate connection matrix<sup>122</sup> as given below,

$$\begin{array}{|c|c|} \hline e_D & i_D \\ \hline e_Q & i_Q \\ \hline e_d & i_d \\ \hline e_q & i_q \\ \hline \end{array} = \begin{array}{|c|c|c|c|} \hline 1 & & & \\ \hline & 1 & & \\ \hline & & \cos \gamma_m & \sin \gamma_m \\ \hline & & \sin \gamma_m & -\cos \gamma_m \\ \hline \end{array} \begin{array}{|c|c|} \hline e_D & i_D \\ \hline e_Q & i_Q \\ \hline e_a & i_a \\ \hline e_b & i_b \\ \hline \end{array} \quad 2.2.5$$

Or in a concise matrix form

$$[e_d, i_d] = [C] \cdot [e_a, i_a] \quad 2.2.6$$

#### 2.2.1.2 Torque equation

The electrical torque can be easily obtained from the gross mechanical power expression<sup>122</sup>. Therefore, it is appropriate to derive first the power equation. The input power of the machine can be written from its definition<sup>122</sup> as follows,

$$\begin{aligned} P &= \mathcal{R}[i] \cdot [e_t^*] \\ &= \mathcal{R}[i_t^*] \cdot [e] \end{aligned} \quad 2.2.7$$

Substituting Equations 2.2.2 and 2.2.3 into Equation 2.2.7, it gives

$$P = \mathcal{R} \left\{ [i_t^*] \cdot [R][i] + [i_t^*] \cdot [L] \cdot p \cdot [i] + [i_t^*] \cdot [G] \cdot \gamma_m [i] \right\} \quad 2.2.8$$

Where

$$\begin{aligned} \mathcal{R} [i_t^*] \cdot [R] \cdot [i] & \text{ represents the machine copper loss,} \\ \mathcal{R} [i_t^*] \cdot [L] \cdot p \cdot [i] & \text{ represents the machine magnetic stored energy per second, and} \\ \mathcal{R} [i_t^*] \cdot [G] \cdot \gamma_m \cdot [i] & \text{ represents the gross mechanical power, which is equal to} \\ & T_m \cdot \gamma_m \cdot \end{aligned}$$

Hence the electrical torque can be expressed as

$$\begin{aligned} T_m &= \mathcal{R} [i_t^*] \cdot [G] \cdot [i] \\ &= \mathcal{R} \end{aligned}$$

$i_D^*$	$i_Q^*$	$i_d^*$	$i_q^*$		$i_d$
					$i_Q$
		M		$L_d$	$i_d$
		-M		$-L_d$	$i_q$

2.2.9.

which gives on expansion

$$T_m = \mathcal{R} \left\{ M \left[ i_q i_d^* - i_D i_q^* \right] + L_d \left[ i_d^* i_q - i_q^* i_d \right] \right\} \quad 2.2.10$$

Since  $\mathcal{R} L_d \left[ i_d^* i_q - i_q^* i_d \right]$  represents the reluctance torque which is generally very small in comparison with the rotational torque, it may be neglected without much loss of accuracy. Also, in view of the fact that currents are real, the torque equation may thus be rewritten as

$$T_m = M [i_Q \cdot i_d - i_D \cdot i_q] \quad 2.2.11$$

Equation 2.2.11 gives an expression for the torque in terms of the equivalent 2-axis machine currents which are not known. It is, therefore, necessary to substitute these currents in terms of the actual machine known parameters and voltages, out of which

$$\left. \begin{aligned} e_Q & \text{ is known applied voltage, and} \\ e_a = e_b = 0 & \text{ as the rotor is squirrel cage, i.e.} \\ & \text{short circuited} \end{aligned} \right\} 2.2.12$$

By substituting Equation 2.2.6 into Equation 2.2.2, and pre-multiplying both sides of the resulting equation by the inverse matrix  $[C]^{-1}$ , the following expression can be obtained

$$[C]^{-1} \cdot [C] \cdot [e_a] = [C]^{-1} \cdot [Z] \cdot [C] \cdot [i_a] \quad 2.2.13$$

which may be reduced to

$$[e_a] = [Z'] \cdot [i_a] \quad 2.2.14$$

$$\text{where } [Z'] = [C]^{-1} \cdot [Z] \cdot [C] \quad 2.2.15$$

On expanding Equation 2.2.15, making use of Equations 2.2.4 and 2.2.5, and substituting the result into Equation 2.2.14, an expression relating the voltages and currents of the actual machine can be obtained.

$$\begin{array}{c|c|c|c|c} \begin{array}{c} e_D \\ e_Q \\ e_a \\ e_b \end{array} & = & \begin{array}{c|c|c|c} Z_D & & M_p \cos \gamma_m & M_p \sin \gamma_m \\ & Z_D & M_p \sin \gamma_m & -M_p \cos \gamma_m \\ M_p \cos \gamma_m & M_p \sin \gamma_m & Z_d & \\ M_p \sin \gamma_m & -M_p \cos \gamma_m & & Z_d \end{array} & \begin{array}{c} i_D \\ i_Q \\ i_a \\ i_b \end{array} & 2.2.16 \end{array}$$

Where

$$Z_D = R_D + L_D p \quad 2.2.17a$$

and  $Z_d = R_d + L_d p \quad 2.2.17b \quad 2.2.17$

In order to obtain the currents in terms of the known voltages, Equation 2.2.16 has to be inverted as follows<sup>123</sup>

$$\begin{bmatrix} i_D \\ i_Q \\ i_a \\ i_b \end{bmatrix} = \begin{bmatrix} \Delta_1^{-1} & & & \\ & & & \\ & & & \\ & & & \end{bmatrix} \begin{bmatrix} e_D \\ e_Q \\ e_a \\ e_b \end{bmatrix} \quad 2.2.18$$

$\begin{matrix} \Delta_1^{-1} & & & \\ & & & \\ & & & \\ & & & \end{matrix}$ 
 $\begin{matrix} -\Delta_1^{-1} & \alpha_{12} & \alpha_{22}^{-1} & \\ & & & \\ & & & \\ & & & \end{matrix}$ 
 $\begin{matrix} -\Delta_2^{-1} & \alpha_{21} & \alpha_{11}^{-1} & \\ & & & \\ & & & \\ & & & \end{matrix}$ 
 $\begin{matrix} \Delta_2^{-1} & & & \\ & & & \\ & & & \\ & & & \end{matrix}$

Where

$$\alpha_{11} = \begin{bmatrix} Z_D & \\ & Z_D \end{bmatrix}, \quad \alpha_{11}^{-1} = \frac{1}{Z_D} \begin{bmatrix} 1 & \\ & 1 \end{bmatrix}$$

$$\alpha_{12} = \alpha_{21} = \begin{bmatrix} M p \cos \gamma_m & M p \sin \gamma_m \\ M p \sin \gamma_m & -M p \cos \gamma_m \end{bmatrix}$$

$$\alpha_{22} = \begin{bmatrix} Z_d & \\ & Z_d \end{bmatrix}, \quad \alpha_{22}^{-1} = \frac{1}{Z_d} \begin{bmatrix} 1 & \\ & 1 \end{bmatrix} \quad 2.2.19$$

$$\Delta_1^{-1} = \alpha_{11}^{-1} - \alpha_{12}^{-1} \alpha_{21}$$

$$= Z_D \quad - M^2 p$$

1	
	1

$\cos \gamma_m \frac{p}{Z_d} \cos \gamma_m$	$\cos \gamma_m \frac{p}{Z_d} \sin \gamma_m$
$+\sin \gamma_m \frac{p}{Z_d} \sin \gamma_m$	$-\sin \gamma_m \frac{p}{Z_d} \cos \gamma_m$
$\sin \gamma_m \frac{p}{Z_d} \cos \gamma_m$	$\sin \gamma_m \frac{p}{Z_d} \sin \gamma_m$
$-\cos \gamma_m \frac{p}{Z_d} \sin \gamma_m$	$+\cos \gamma_m \frac{p}{Z_d} \cos \gamma_m$

2.2.20

$$\text{and } \Delta_2 = \alpha_{22} - \alpha_{21} \alpha_{11}^{-1} \alpha_{12}$$

$$= Z_d \quad - M^2 p$$

1	
	1

$\cos \gamma_m \frac{p}{Z_D} \cos \gamma_m$	$\cos \gamma_m \frac{p}{Z_D} \sin \gamma_m$
$+\sin \gamma_m \frac{p}{Z_D} \sin \gamma_m$	$-\sin \gamma_m \frac{p}{Z_D} \cos \gamma_m$
$\sin \gamma_m \frac{p}{Z_D} \cos \gamma_m$	$\sin \gamma_m \frac{p}{Z_D} \sin \gamma_m$
$-\cos \gamma_m \frac{p}{Z_D} \sin \gamma_m$	$+\cos \gamma_m \frac{p}{Z_D} \cos \gamma_m$

2.2.21

From Equation 2.2.18, since  $e_a = e_b = 0$ , it is therefore sufficient to obtain expressions for  $\Delta_1^{-1}$  and  $-\Delta_2^{-1} \alpha_{21} \alpha_{11}^{-1}$  in order to have a complete solution for the currents.

Unfortunately, it is extremely difficult to invert the matrices  $\Delta_1$  and  $\Delta_2$  so long as  $\gamma_m$  is an unknown function of time. However, some further assumptions may be adopted, particularly valid for small 2-phase servomotors, which enable the matrix inversion to be carried out approximately, yet without serious loss of accuracy. These assumptions may be stated as

$$R_D \gg L_D , \quad 2.2.22a$$

2.2.22

$$R_d \gg L_d \quad 2.2.22b$$

To illustrate the degree of validity of the above assumptions, the following are typical figures for a small 2-phase servomotor as quoted from Ref. 17:

$$R_D = 94 \text{ } \Omega , \quad L_D = 0.284 \text{ H}$$

$$R_d/L_d = 2400 \text{ S}^{-1} , \quad M^2/R_d = 5.16 \times 10^{-5} \text{ H.S}^{-1}$$

With the above assumptions, the matrices  $\Delta_1$  and  $\Delta_2$  can be considerably simplified and may be rewritten, with the help of the results of the Appendices A1 ~~and~~ A2, as follows

$$\Delta_1 = Z_s \begin{array}{|c|c|} \hline 1 & \\ \hline & 1 \\ \hline \end{array} \quad 2.2.23$$

and

$$\Delta_2 = Z_r \begin{array}{|c|c|} \hline 1 & \\ \hline & 1 \\ \hline \end{array} \quad 2.2.24$$

$$\text{Where } Z_s = Z_D - \frac{M^2}{R_d} p^2 \quad 2.2.25$$

$$\text{and } Z_r = Z_d - \frac{M^2}{R_D} p^2 \quad 2.2.26$$



Hence,

$$\Delta_1^{-1} = \frac{1}{Z_s}$$

1	
	1

2.2.27

and  $\Delta_2^{-1} = \frac{1}{Z_r}$

1	
	1

2.2.28

Equation 2.2.18 can thus be rewritten as

$i_D$	$1/Z_s$		$-\Delta_1^{-1} \alpha_{12} \alpha_{22}^{-1}$	$e_D$
$i_Q$		$1/Z_s$		$e_Q$
$i_a$	$-M \frac{p}{Z_r} (\cos \gamma_m \frac{1}{Z_D})$	$-M \frac{p}{Z_r} (\sin \gamma_m \frac{1}{Z_D})$		
$i_b$	$-M \frac{p}{Z_r} (\sin \gamma_m \frac{1}{Z_D})$	$M \frac{p}{Z_r} (\cos \gamma_m \frac{1}{Z_D})$	$\Delta_2^{-1}$	

2.2.29

Substituting Equation 2.2.5 into Equation 2.2.29 and rearranging, the currents  $i_d$  and  $i_q$  can be expressed in terms of the actual machine parameters as given below

$$i_d = -M \left[ \cos \gamma_m \cdot \frac{p}{Z_r} \left\{ \cos \gamma_m \cdot I_D + \sin \gamma_m \cdot I_Q \right\} \right. \\ \left. + \sin \gamma_m \cdot \frac{p}{Z_r} \left\{ \sin \gamma_m \cdot I_D - \cos \gamma_m \cdot I_Q \right\} \right]$$

2.2.30

$$\text{and } i_q = -M \left[ \sin \gamma_m \cdot \frac{p}{Z_r} \left\{ \cos \gamma_m \cdot I_D + \sin \gamma_m \cdot I_Q \right\} \right. \\ \left. - \cos \gamma_m \cdot \frac{p}{Z_r} \left\{ \sin \gamma_m \cdot I_D - \cos \gamma_m \cdot I_Q \right\} \right] \quad 2.2.31$$

$$\text{Where } I_D = e_D / Z_D \quad 2.2.32a$$

$$\text{and } I_Q = e_Q / Z_D \quad 2.2.32b$$

(2.2.32)

Usually, in designing small 2-phase servomotors, the rotor resistance  $R_d$  is intentionally made high enough to provide bigger stalling torque, more damping, better linearization of its dynamic performance and in addition, to avoid single phase operation on the reference phase alone. Depending on this fact and with the assumption expressed by Equation 2.2.22b,  $Z_r$  may be reasonably approximated to  $R_d$ . Consequently, Equations 2.2.30 and 2.2.31 can be very much simplified to

$$i_d = -\frac{M}{R_d} \left[ p I_D + \gamma_m \cdot I_Q \right] \quad 2.2.33$$

and

$$i_q = -\frac{M}{R_d} \left[ p I_Q - \gamma_m \cdot I_D \right] \quad 2.2.34$$

which on substitution into the torque equation, gives

$$T_m = \frac{M^2}{R_d} \left[ \left\{ i_D \cdot p \cdot I_Q - i_Q \cdot p \cdot I_D \right\} \right. \\ \left. - \gamma_m \cdot \left\{ i_D \cdot I_D + i_Q \cdot I_Q \right\} \right] \quad 2.2.35$$

### 2.2.2 Representation of the 2-phase servomotor dynamic behaviour by a mathematical model

The mathematical model is basically a translation of the dynamic equations, into a number of blocks, representing various mathematical operations, interconnected in such a way as to give the relationship between the controlling input signal and the controlled output. The controlling input signal for the 2-phase servomotor is  $e_D$  whereas the controlled output is  $\gamma_L$ . In order to obtain the relationship between  $e_D$  and  $\gamma_L$ , the electrical torque has to be related to the mechanics of the system. If the coulomb friction of both the motor and load is negligible and by regarding only their viscous friction and inertia torques, the following expression can be easily derived

$$T_m = [J \ p + F] \gamma_m \quad 2.2.36$$

If the backlash in the gear train is negligible, hence

$$\gamma_L = \frac{n_m}{n_L} \gamma_m \quad 2.2.37$$

Substituting Equations 2.2.36 and 2.2.37 into Equation 2.2.35 and rearranging, gives

$$\gamma_L = \frac{n_m}{n_L} \cdot \frac{1}{p} \cdot \frac{1}{F + Jp} \cdot \frac{M^2}{R_d} \left[ \left\{ \frac{e_D}{Z_s} \cdot \left( \frac{p}{Z_D} \cdot e_Q \right) - \frac{e_Q}{Z_s} \cdot \left( \frac{p}{Z_D} \cdot e_D \right) \right\} - \left( \frac{n_L}{n_m} p \cdot \gamma_L \right) \left\{ \left( \frac{e_D}{Z_s} \right) \cdot \left( \frac{e_D}{Z_D} \right) + \left( \frac{e_Q}{Z_s} \right) \cdot \left( \frac{e_Q}{Z_D} \right) \right\} \right] \quad 2.2.38$$

The mathematical model shown in Fig. 2.2.2 gives an exact translation of the nonlinear differential equation 2.2.38

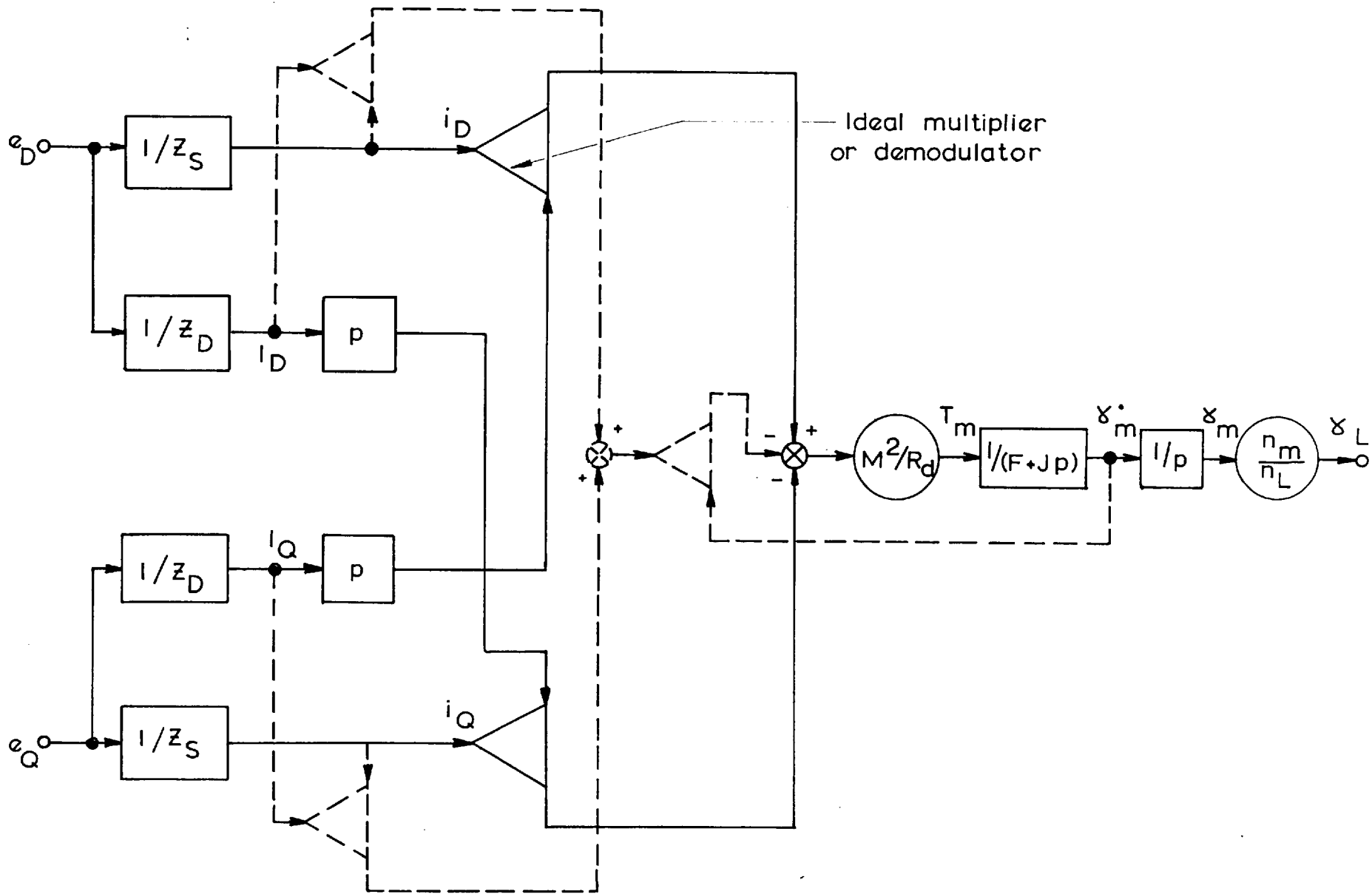


FIG. 2.22. MATHEMATICAL MODEL REPRESENTATION OF 2 - PHASE SERVOMOTOR

which describes the transient behaviour of 2-phase servomotor. In the model, ideal demodulators are employed to represent the operation of multiplication. It is interesting to notice the model symmetry which allows the interchangeability of  $e_D$  and  $e_Q$ , a process which can be feasibly performed on the actual machine.

Further simplification of the model can still be achieved by assuming negligible initial transients of the quadrature-axis currents  $i_Q$  and  $I_Q$ . This assumption is only valid when the excitation to the quadrature-axis is switched on a sufficiently long time before applying any controlling signal to the servomotor.

In general, the excitation to the quadrature-axis winding (reference winding) is in the form of

$$e_Q = E_m \sin (\omega t + \phi) \quad 2.2.39$$

On the basis of the above assumption, the currents can be directly deduced which may be written as follows

$$i_Q = \frac{E_m}{\sqrt{\left(R_D + \frac{M^2 \omega^2}{R_d}\right)^2 + L_D^2 \omega^2}} \sin (\omega t + \phi - \mu_1) \quad 2.2.40$$

$$\text{and } I_Q = \frac{E_m}{\sqrt{R_D^2 + L_D^2 \omega^2}} \sin (\omega t + \phi - \mu_2) \quad 2.2.41$$

Where

$$\mu_1 = \tan^{-1} \left[ \frac{L_D \omega}{R_D + \frac{M^2 \omega^2}{R_d}} \right] \quad 2.2.42$$

$$\text{and } \mu_2 = \tan^{-1} \left[ \frac{L_D \omega}{R_D} \right] \quad 2.2.43$$

### 2.2.3 Complex frequency block diagram representation of the 2-phase servomotor

On the basis of Equation 2.2.38, it is extremely difficult to construct a complex frequency block diagram due to the nonlinearity involved. However, if the motor speed  $\dot{\gamma}_m$  is reasonably small, the load shaft position may be thus approximated to

$$\gamma_L = \frac{n_m}{n_L} \cdot \frac{1}{p} \cdot \frac{1}{T + Jp} \cdot \frac{M^2}{R_d} \left\{ \frac{1}{Z_s} \cdot e_D \cdot \left( \frac{p}{Z_D} \cdot e_Q \right) - \frac{1}{Z_s} \cdot e_Q \cdot \left( \frac{p}{Z_D} \cdot e_D \right) \right\} \quad 2.2.44$$

which allows a simple block diagram to be constructed.

The above approximation is effectively analogous to the removal of the feedback path and the blocks drawn in dotted line in Fig. 2.2.2.

Assuming zero initial conditions of both the control voltage and load shaft position, or in mathematical terms

$$\begin{aligned} e_D &= 0 & , \text{ at } t = 0 & & 2.2.45a \\ \text{and } \gamma_L &= 0 & , \text{ at } t = 0 & & 2.2.45b \end{aligned} \quad \left. \vphantom{\begin{aligned} e_D &= 0 \\ \text{and } \gamma_L &= 0 \end{aligned}} \right\} 2.2.45$$

and on taking the Laplace transform of Equation 2.2.44, gives

$$\gamma_L(s) = \frac{n_m}{n_L} \cdot \frac{E_m}{2} \cdot \frac{M^2}{R_d} \cdot \frac{1}{S(F + Js)} \cdot \left[ Y_d \left\{ e^{j(\phi - \mu_2)} \frac{e_{D-}(s)}{Z_{s-}(s)} + e^{-j(\phi - \mu_2)} \frac{e_{D+}(s)}{Z_{s+}(s)} \right\} - Y_s \left\{ e^{j(\phi - \mu_1 - \pi/2)} \frac{s_{-} e_{D-}(s)}{Z_{D-}(s)} + e^{-j(\phi - \mu_1 - \pi/2)} \frac{s_{+} e_{D+}(s)}{Z_{D+}(s)} \right\} \right] \quad 2.2.46$$

$$\text{Where } Y_D = \frac{1}{\sqrt{R_D^2 + L_D^2 \Omega^2}} \quad 2.2.47$$

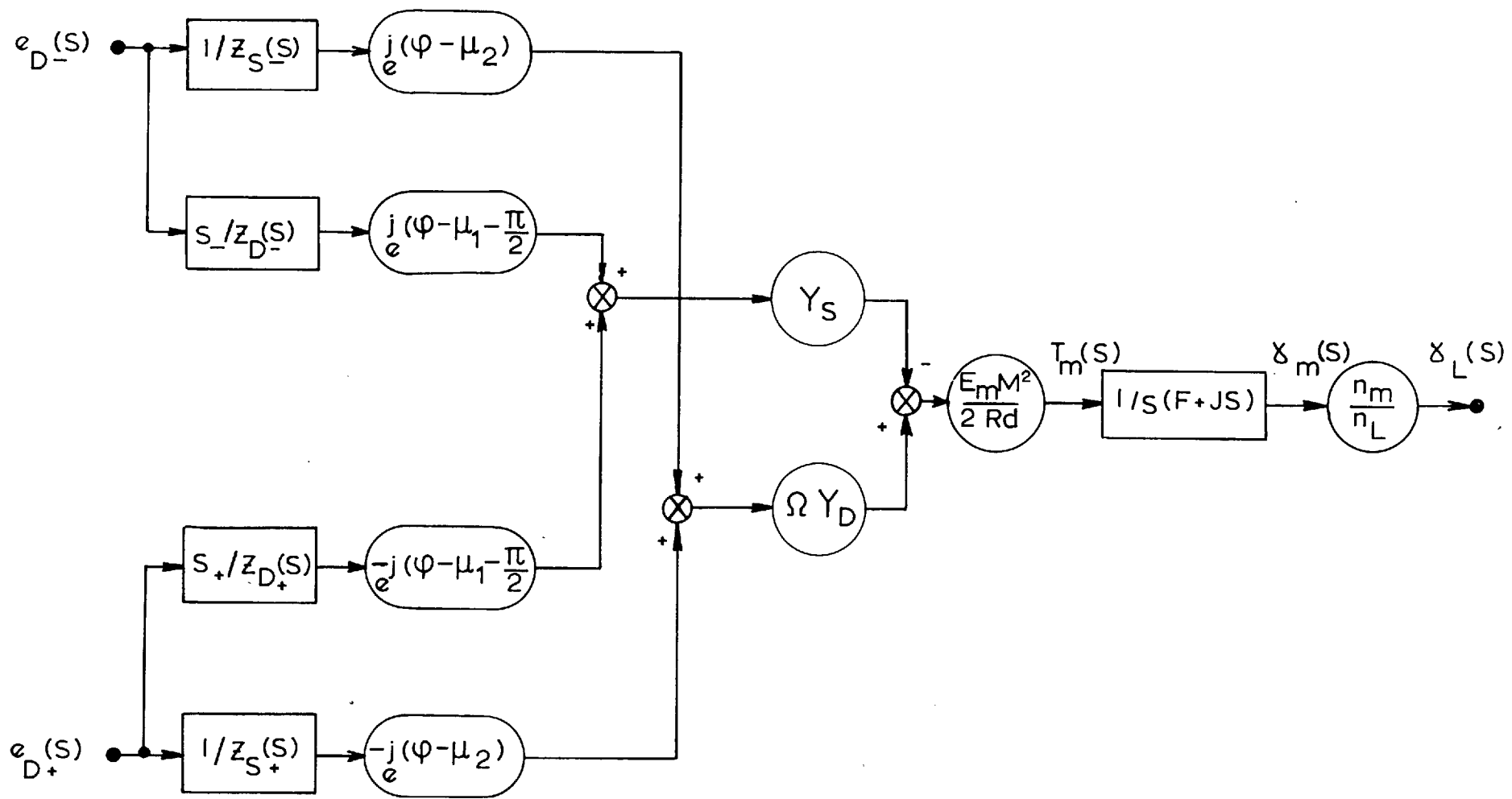
$$Y_s = \frac{1}{\sqrt{(R_D + \frac{M^2}{R_D}) \Omega^2 + L_D^2 \Omega^2}} \quad 2.2.48$$

The negative and positive subscripts are introduced to simplify writing the functions of the complex frequency variable in the way described below

$$e_{D\pm}(s) = e_D(s \pm j\Omega) \quad 2.2.49$$

With the help of Equation 2.2.46, a block diagram, which relates the output shaft position  $\gamma_L$  to the controlling input signal  $e_D$  in the complex frequency domain, can be constructed as illustrated in Fig. 2.2.3.

Because of the demodulation process involved in the



COMPLEX FREQUENCY BLOCK DIAGRAM REPRESENTATION OF 2-PHASE SERVOMOTOR

FIG. 2.2.3.



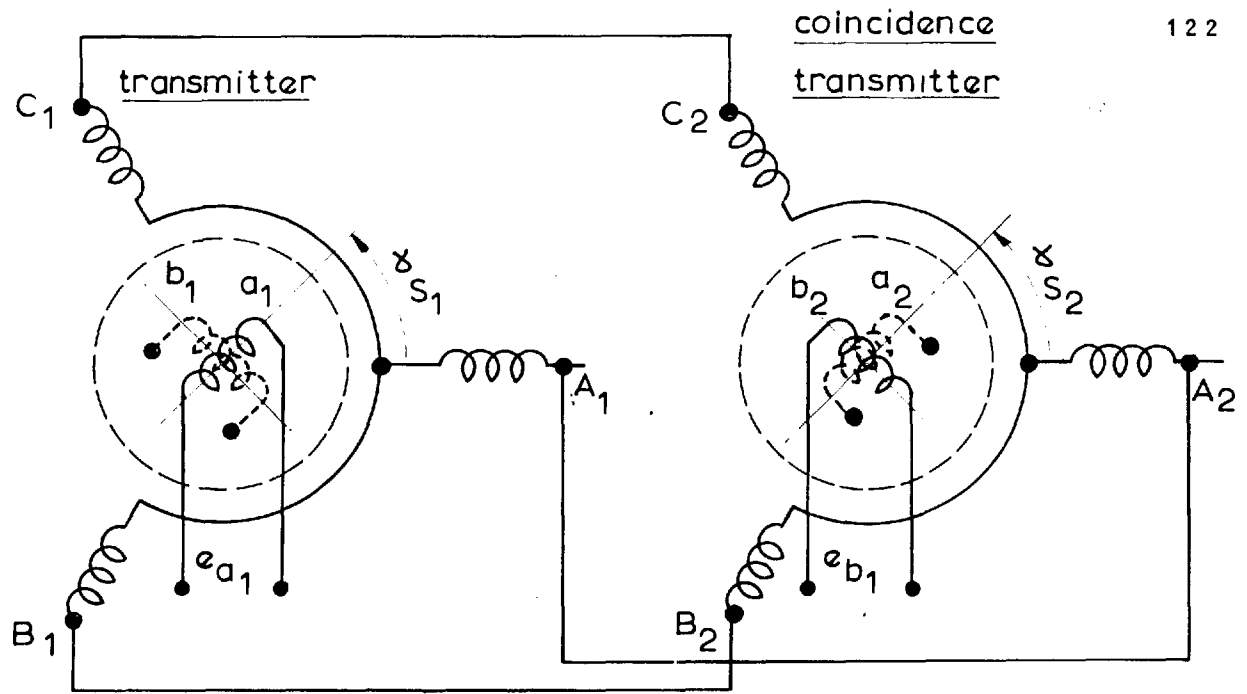
2-phase servomotor operation, the nature of the input signal is different **from** that of the output signal. This makes it insufficient to obtain an explicit transfer function to describe the 2-phase servomotor as an isolated component. However, by combining the 2-phase servomotor with another component whose operation involves a modulation process, it is possible to obtain a modulation transfer function for the combination as is shown in Section 2.4.

### 2.3 Error detector in the form of a transmitter-coincidence transmitter synchro-system

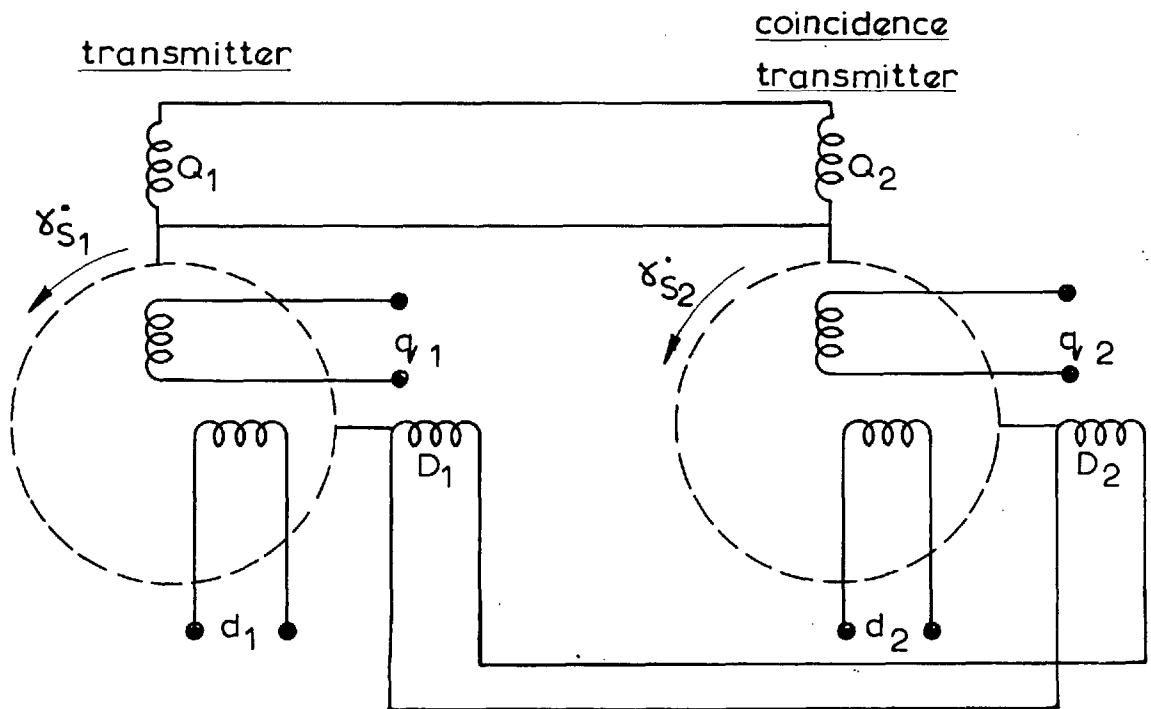
#### 2.3.1 General

Fig. 2.3.1 illustrates a diagrammatic representation of a transmitter-coincidence transmitter synchro system and its equivalent generalised 2-axis machine. The transmitter rotor position  $\gamma_{s1}$  represents the reference or command signal. The rotor shaft of the coincidence transmitter is coupled to the load shaft either solidly or through a gear system. Its position, accordingly, indicates either the actual output or proportion of it. The 3-phase stator winding of the transmitter is interconnected to its corresponding of the coincidence transmitter. The single-phase rotor winding of the transmitter is energized by a carrier signal, whereas the corresponding winding of the coincidence transmitter produces an actuating signal as a function of the position error.

In order to use a number of equations already derived for the 2-phase servomotor without modification, a fictitious winding is added orthogonally to the existing winding in the rotor so that the rotor may be considered as 2-phase wound. The effect of this fictitious winding on the finally derived response is nullified by assuming that both the voltage and current associated with it



(a) ACTUAL MACHINE



(b) EQUIVALENT GENERALIZED 2 AXIS MACHINE

DIAGRAMATIC REPRESENTATION OF A TRANSMITTER-COINCIDENCE TRANSMITTER SYNCHRO-SYSTEM AND ITS EQUIVALENT GENERALIZED 2-AXIS MACHINE

FIG. 2.31.

are null. In Fig. 2.3.1 the fictitious winding is shown in dotted line.

### 2.3.2. Analysis

In the subsequent analysis, derivation of the dynamic equations is based on the same general simplifying assumptions stated in 2.1 above.

Following similar steps as those employed in Sec. 2.2.1, it can be shown that Equations 2.2.1 to 2.2.4 are also applicable here provided that subscripts 1 and 2 are added to various variables and parameters to refer to the transmitter and coincidence transmitter respectively. The connection matrix, which relates the voltages and currents of the generalised 2-axis machine to the actual one, may be written as follows

$$\begin{array}{|c|c|} \hline e_D & i_D \\ \hline e_Q & i_Q \\ \hline e_o & i_o \\ \hline e_d & i_d \\ \hline e_q & i_q \\ \hline \end{array} = \begin{array}{|c|c|c|c|c|} \hline 1 & \cos(-\frac{2\pi}{3}) & \cos(-\frac{4\pi}{3}) & & \\ \hline & \sin(-\frac{2\pi}{3}) & \sin(-\frac{4\pi}{3}) & & \\ \hline 1/3 & 1/3 & 1/3 & & \\ \hline & & & \cos\gamma_s & \sin\gamma_s \\ \hline & & & \sin\gamma_s & -\cos\gamma_s \\ \hline \end{array} \begin{array}{|c|c|} \hline e_A & i_A \\ \hline e_B & i_B \\ \hline e_C & i_C \\ \hline e_a & i_a \\ \hline e_b & i_b \\ \hline \end{array} \quad 2.3.1$$

which may be rewritten in a concise form

$$\begin{bmatrix} e_d & i_d \end{bmatrix} = \begin{bmatrix} C_s \end{bmatrix} \cdot \begin{bmatrix} e_a & i_a \end{bmatrix} \quad 2.3.2$$

An expression for the impedance matrix  $[Z']$  may be derived in a similar manner as previously done in Sec. 2.2, which may be written as

$$[Z'] = [C_S]^{-1} \cdot [Z] \cdot [C_S] \quad 2.3.3$$

The matrix  $[Z']$  is apparently impossible to be evaluated because both  $[C_S]$  and  $[C_S]^{-1}$  are 5 x 5 matrices, whereas  $[Z]$  is 4 x 4 matrix. This difficulty has been resulted from considering the zero sequence component in the connection matrix  $[C_S]$  while neglecting the same in the impedance matrix  $[Z]$ . Therefore, matrix evaluation would become possible if the zero sequence impedance components are inserted back in the  $[Z]$  matrix. However, this will add another difficulty because of the unknown nature of the zero sequence impedance.

In order to circumvent the above difficulty, a fictitious machine may be postulated to act as an intermediate stage between the actual machine and the equivalent generalised 2-axis machine. The construction of this machine is such that its rotor is similar to that of the actual machine while its stator is similar to that of the generalised 2-axis machine. As a consequence, the connection matrix expressed by Equation 2.2.5 may be used to relate the voltages and currents of the postulated machine to those of the generalised 2-axis machine. Also, Equations 2.2.13 to 2.2.17 may be shown to be applicable without any modification.

#### 2.3.1.1 Operating conditions of the postulated coincidence transmitter rotor

- i) The voltage and current of the fictitious winding should be put to zero, or in mathematical terms

$$e_{a_2} = 0 \quad 2.3.4$$

$$i_{a_2} = 0 \quad 2.3.5$$

- ii) In actual practice, the rotor winding  $b_2$  feeds either an amplifier, whose input impedance is generally very high, or a compensating network, whose design is such that its input impedance is deliberately made high in order to avoid loading effect. Hence, the following assumption may be used without making serious errors

$$i_{b_2} = 0 \quad 2.3.6$$

Using the above constraints in Equation 2.2.16, the following expressions can be deduced

$$e_{D_2} = Z_{D_2} i_{D_2} \quad , \quad 2.3.7$$

$$e_{Q_2} = Z_{D_2} i_{Q_2} \quad , \quad 2.3.8$$

and

$$e_{b_2} = M_2 p \left[ \sin \gamma_{s2} \cdot i_{D_2} - \cos \gamma_{s2} \cdot i_{Q_2} \right] \quad 2.3.9$$

#### 2.3.2.2. Operating conditions of the postulated transmitter rotor

- i) As above, the conditions of the fictitious winding may be written as

$$e_{b_1} = 0 \quad 2.3.10$$

$$i_{b_1} = 0 \quad 2.3.11$$

- ii) The excitation to the winding  $a_1$  may, in general, be expressed as

$$e_{a_1} = E_s \sin(\omega t + \theta) \quad 2.3.12$$

On substituting the above conditions into Eqn. 2.2.16, the following expressions are deduced

$$e_{D_1} = Z_{D_1} \cdot i_{D_1} + M_1 p (\cos \gamma_{s1} \cdot i_{a_1}) \quad , \quad 2.3.13$$

$$e_{Q_1} = Z_{D_1} \cdot i_{Q_1} + M_1 p (\sin \gamma_{s1} \cdot i_{a_1}) \quad , \quad 2.3.14$$

and 
$$e_{a_1} = M_1 p [\cos \gamma_{s1} \cdot i_{D_1} + \sin \gamma_{s1} \cdot i_{Q_1}] + Z_{d_1} \cdot i_{a_1} \quad 2.3.15$$

### 2.3.2.3 Boundary conditions

From the knowledge that the stator windings of the transmitter are interconnected to those of the coincidence transmitter, the following boundary conditions may be set up,

$$e_{D_1} = e_{D_2} \quad \text{which may be replaced by } e_D \quad 2.3.16$$

$$e_{Q_1} = e_{Q_2} \quad \text{"} \quad e_{Q_2} \quad 2.3.17$$

$$i_{D_1} = -i_{D_2} \quad 2.3.18$$

$$i_{Q_1} = -i_{Q_2} \quad 2.3.19$$

In general practice, the transmitter and coincidence transmitter may be considered identical in design and construction except that the former one includes an extra damper winding. If the effect of this damper winding is negligible then,

$$Z_{D_1} = Z_{D_2} \quad \text{which may be replaced by } Z_{D_s} \quad 2.3.20$$

$$Z_{d_1} = Z_{d_2} \quad \text{"} \quad Z_{d_s} \quad 2.3.21$$

$$M_1 = M_2 \quad \text{"} \quad M_s \quad 2.3.22$$

Eliminating  $i_{D_1}$  and  $i_{Q_1}$  from Equations 2.3.13 and 2.3.14, give

$$e_D = \frac{M_s}{2} p (\cos \gamma_{s_1} \cdot i_{a_1}) \quad 2.3.23$$

and

$$e_Q = \frac{M_s}{2} p (\sin \gamma_{s_1} \cdot i_{a_1}) \quad 2.3.24$$

which on substitution into Equation 2.3.15 and 2.3.9, making use of Equations 2.3.7 and 2.3.8, give

$$e_{a_1} = Z_{d_s} \cdot i_{a_1} - \frac{M_s^2}{2} p \left[ \cos \gamma_{s_1} \cdot \frac{p}{Z_{D_s}} \cdot \cos \gamma_{s_1} + \sin \gamma_{s_1} \cdot \frac{p}{Z_{D_s}} \cdot \sin \gamma_{s_1} \right] i_{a_1} \quad 2.3.25$$

and

$$e_{b_2} = \frac{M_s^2}{2} p \left[ \sin \gamma_{s_2} \cdot \frac{p}{Z_{D_s}} \cdot \cos \gamma_{s_1} - \cos \gamma_{s_2} \cdot \frac{p}{Z_{D_s}} \cdot \sin \gamma_{s_1} \right] i_{a_1} \quad 2.3.26$$

Equations 2.3.25 and 2.3.26 may be considerably simplified by assuming that

$$L_{D_s} p \gg R_{D_s} \quad 2.3.27$$

which results in (see Appendix A3)

$$e_{a_1} = Z_{r_s} \cdot i_{a_1} \quad 2.3.28$$

Where

$$Z_{r_s} = R_{r_s} + p L_{r_s} \quad , \quad 2.3.29$$

$$R_{r_s} = R_{d_s} + \frac{M_s^2 R_{D_s}}{2 L_{D_s}^2} \quad , \quad 2.3.30$$

and

$$L_{r_s} = L_{d_s} - \frac{M_s^2}{2 L_{D_s}} \quad 2.3.31$$

Eliminating  $i_{a_1}$  and using the assumption expressed by Equation 2.3.27, Equation 2.3.26 reduces to

$$e_{b_2} = \frac{M_s^2}{2 L_{D_s}} p \left[ \sin(\gamma_{s_2} - \gamma_{s_1}) \cdot \frac{e_{a_1}}{Z_{r_s}} \right] \quad 2.3.32$$

### 2.3.3 Representation by a mathematical model

Further simplification of Equation 2.3.32 may be obtained by neglecting the initial transients of  $i_{a_1}$ , due to the excitation switching, thus

$$i_{a_1} = \frac{E_s}{\sqrt{R_{r_s}^2 + L_{r_s}^2 \omega^2}} \sin(\omega t + \theta - \mu_s) \quad 2.3.33$$

$$\text{where } \mu_s = \tan^{-1} \left\{ \frac{L_{r_s} \omega}{R_{r_s}} \right\} \quad 2.3.34$$

Also, if the servomechanism is behaving in a satisfactory manner, i.e. the error  $(\gamma_{s_1} - \gamma_{s_2})$  is very small, hence the following approximation may be adopted



$$\sin(\gamma_{s_1} - \gamma_{s_2}) \approx \gamma_{s_1} - \gamma_{s_2} \quad 2.3.35$$

Making use of Equations 2.3.33 and 2.3.34 and rearranging, the output of the synchro system may be rewritten as

$$e_{b_2} = -K_s p \left[ \epsilon \sin(\omega t + \theta - \mu_s) \right] \quad 2.3.35$$

Where

$$K_s = \frac{n_L}{n_S} \cdot \frac{M_s^2 E_s}{2 L_{D_S} \sqrt{R_s^2 + L_s^2 \omega^2}} \quad 2.3.36$$

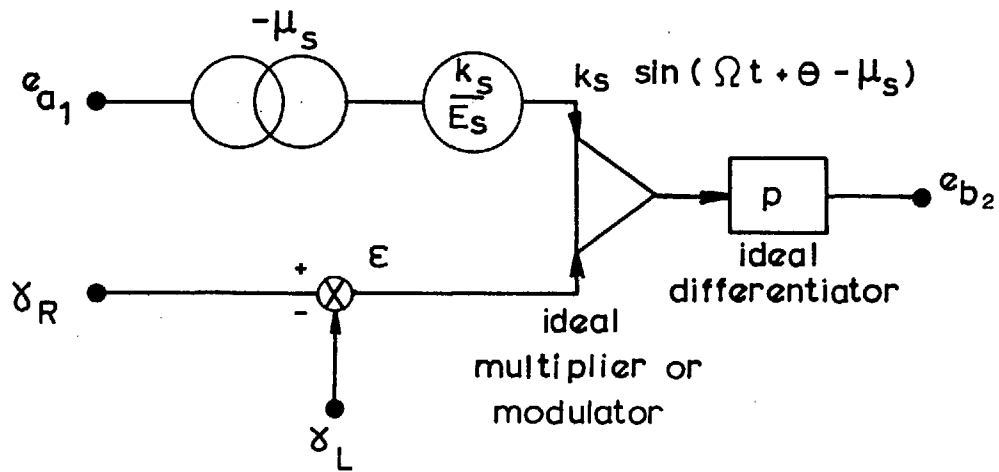
Equation 2.3.35 gives an expression for the output of the synchro system in the form of a rotary modulation with regard to the error .

In this respect, the rotary modulation may be defined as the rate of change of the multiplicative modulation with respect to time. The negative sign appearing in Equation 2.3.35 may be considered immaterial due to the fact that it can be reversed by either reversing the exciting voltage  $e_{a_1}$  or by interchanging the output terminals of the winding  $b_2$ .

In view of the potentiometer-bridge mathematical model, which represents essentially an actuating signal in the form of multiplicative modulation with reference to the error, an extension to that model, by adding an ideal differentiator, may be used to represent the behaviour of the synchro-pair. This model, is shown in Fig. 2.3.2.

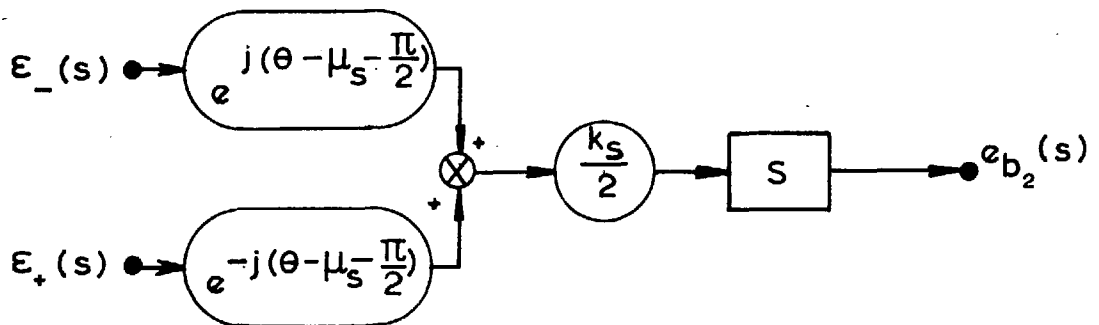
#### 2.3.4 Complex frequency block diagram representation

With the assumption of zero initial condition value of the error, or in mathematical terms



MATHEMATICAL MODEL REPRESENTATION OF  
A SYNCHRO SYSTEM ERROR - DETECTOR

FIG. 2.32



COMPLEX FREQUENCY BLOCK DIAGRAM REPRESENTATION  
OF A SYNCHRO SYSTEM ERROR DETECTOR

FIG. 2.33

$$\xi = 0 \quad , \quad \text{at } t = 0 \quad \quad \quad 2.3.37$$

the actuating signal, expressed by Equation 2.3.35, may be transformed into the complex frequency domain, using the Complex Convolution Integral and method of Residue, and thus may be expressed as

$$e_{b_2}(s) = \frac{K_s}{2} \cdot s \left[ e^{j(\theta - u_s - \pi/2)} \xi_{-}(s) + e^{-j(\theta - u_s - \pi/2)} \xi_{+}(s) \right]$$

2.3.38

According to Equation 2.3.38, a block diagram may be constructed, as shown in Fig. 2.3.3, which describes the synchro system response in the complex frequency domain.

In view of the fact that a modulation process is effected in the synchro-pair, it is not sufficient to formulate a transfer function for the input and output signals are of different nature. Though, if the synchro-pair is considered in conjunction with the 2-phase servomotor (where demodulation process is effected), as a closed loop system, a modulation transfer function for the combination can be obtained as will be shown in the subsequent section.

#### 2.4 Open-loop and closed-loop responses of the uncompensated system

In the preceding analysis, it has been shown that both the input and output signals associated with either of the basic components discussed above, are of different nature due to the involvement of either a modulation or a demodulation process. This leads to the fact that these components cannot individually be described by open-loop transfer functions as it is usually the

case with d.c. system components. However, by combining the components together, according to their interrelationships to form the closed-loop system, it is possible to formulate an overall open-loop and closed-loop modulation transfer functions in which, the contributions of various components are in implicit form. The basis of formulating these modulation transfer functions depends on the assumption that high harmonic components can be neglected.

The subsequent subsections are devoted to the formulation of the overall modulation transfer functions.

#### 2.4.1 Formulation of the modulation transfer functions for the uncompensated a.c. servomechanism

##### 2.4.1.1 System with a potentiometer-bridge as error-detector

According to Fig. 1.2.1, the output of the error-detector is fed to the control winding of the 2-phase servomotor after being amplified. In general, the transfer function of the servoamplifier is slightly dependent on frequency. This effect may be included in the transfer function of cascaded linear networks as will be dealt with in Section 3.3. In the present analysis, however, considerable simplification can be achieved by assuming that the servoamplifier exhibits a flat response, with gain  $A$  and zero phase shift, over the entire working frequency band. Consequently, the following relation can be deduced.

$$e_D(s) = A \xi_p(s) \quad 2.4.1.$$

which on substitution into Equations 2.2.46 and 1.5.5, gives

$$\gamma_{L^*}(s) = \frac{n_m}{n_L} \cdot \frac{E_m}{2} \cdot \frac{M^2}{R_d} \cdot \frac{K_p}{2} \cdot A \cdot \frac{1}{S(F+JS)}$$

$$\begin{aligned} & \left[ \Omega Y_D \xi(s) \left\{ e^{\frac{j(\varphi - \mu_2 - \theta + \pi/2)}{Z_{S-}(s)}} + e^{\frac{-j(\varphi - \mu_2 - \theta + \pi/2)}{Z_{S+}(s)}} \right\} \right. \\ & - Y_S \xi(s) \left\{ e^{\frac{j(\varphi - \mu_1 - \theta)}{Z_{D-}(s)}} + e^{\frac{-j(\varphi - \mu_1 - \theta)}{Z_{D+}(s)}} \right\} \\ & + \Omega Y_D \left\{ e^{\frac{j(\varphi - \mu_2 + \theta - \pi/2)}{Z_{S-}(s)}} \xi_{--}(s) + e^{\frac{-j(\varphi - \mu_2 + \theta - \pi/2)}{Z_{S+}(s)}} \xi_{++}(s) \right\} \\ & \left. + Y_S \left\{ e^{\frac{j(\varphi - \mu_1 + \theta)}{Z_{D-}(s)}} \xi_{--}(s) + e^{\frac{-j(\varphi - \mu_1 + \theta)}{Z_{D+}(s)}} \xi_{++}(s) \right\} \right] \end{aligned}$$

## 2.4.2.

Because of the presence of a pole at the origin and another pole situated on the left hand side of the real axis at a distance  $F/J$  in the  $S$ -plane, the 2-phase servomotor behaves, in a way, as a low-pass filter. The high frequency terms of Equation 2.4.2 may therefore be considered negligible which allows an open-loop modulation transfer function to be deduced,

$$\begin{aligned} \dot{G}_{op} = \frac{L(s)}{\xi(s)} = K_{op} \frac{1}{S(F+JS)} & \left[ \Omega Y_D \left\{ e^{\frac{j(\varphi - \mu_2 - \theta + \pi/2)}{Z_{S-}(s)}} \right. \right. \\ & + \left. \frac{e^{\frac{j(\varphi - \mu_2 - \theta - \pi/2)}{Z_{S+}(s)}}}{Z_{S+}(s)} \right\} - Y_S \left\{ e^{\frac{j(\varphi - \mu_1 - \theta)}{Z_{D-}(s)}} \right. \\ & \left. \left. + e^{\frac{-j(\varphi - \mu_1 - \theta)}{Z_{D+}(s)}} \right\} \right] \end{aligned} \quad 2.4.3.$$

Where

$$K_{o p} = \frac{n_m}{n_L} \cdot \frac{E_m}{2} \cdot \frac{M^2}{R_d} \cdot \frac{K_p}{2} \cdot A \quad 2.4.4$$

With the help of the simple relationship,

$$\xi(s) = \gamma_R(s) - \gamma_L(s) \quad 2.4.5$$

it is possible to deduce an expression for the closed-loop modulation transfer function, which may be written in terms of the open-loop modulation transfer function as given below

$$G_{c p} = \frac{\gamma_L(s)}{\gamma_R(s)} = \frac{G_{o p}}{1 + G_{o p}} \quad 2.4.6$$

#### 2.4.1.2 System with a synchro-pair as error-detector

On the basis of adopting the same above assumption concerning the servoamplifier, the synchro-system actuating signal may be related to the input signal to the control winding of the 2-phase servomotor by the expression,

$$e_D(s) = A e_{b2}(s) \quad 2.4.7$$

Using similar procedure as adopted above, an open-loop modulation transfer function can be obtained provided that high harmonic terms are neglected. This may be given as,

$$G_{o s} = \frac{\gamma_L(s)}{\xi(s)} = K_{o s} \cdot \frac{1}{S(F + Js)} \cdot \left[ \mu_{D-} \left\{ e^{j(\phi - \mu_2 - \theta + \mu_s + \pi/2)} \frac{S_-}{Z_{S-}(s)} + e^{-j(\phi - \mu_2 - \theta + \mu_s + \pi/2)} \frac{S_+}{Z_{S+}(s)} \right\} - Y_s \left\{ e^{j(\phi - \mu_2 - \theta + \mu_s)} \frac{S_-^2}{Z_{D-}(s)} + e^{-j(\phi - \mu_2 - \theta + \mu_s)} \frac{S_+^2}{Z_{D+}(s)} \right\} \right] \quad 2.4.8$$

Where

$$K_{o s} = \frac{n_m}{n_L} \cdot \frac{E_m}{2} \cdot \frac{M^2}{R_d} \cdot \frac{K_s}{2} \cdot A \quad 2.4.9$$

Again, the closed-loop modulation transfer function can be easily derived from Equation 2.4.9, and may be expressed in terms of  $G_{o s}$  as given below,

$$G_{c s} = \frac{G_{o s}}{1+G_{o s}} \quad 2.4.10$$

## 2.4.2 Complex frequency block diagram representation of the uncompensated a.c. servomechanism

### 2.4.2.1 System with a potentiometer-bridge as error-detector

The relationship expressed by Equation 2.4.1 may be rewritten in a more general form without violating its validity, hence

$$e_{D+}(s) = A \epsilon_{p+}(s) \quad 2.4.8$$

With the help of the above relationship, it is possible to join the block diagrams of the potentiometer-bridge and the 2-phase servomotor, shown in Figs. 1.5.3 and 2.2.3 respectively, where the signal is in the form of modulated carrier. The resulting block diagram of the combination is shown in Fig. 2.4.1. By introducing the reference signal  $\gamma_R$  and a summing point, the combined block diagram can be closed in the demodulated signal region, representing the uncompensated closed-loop system, according to the simple relationship expressed by Equation 2.4.5.

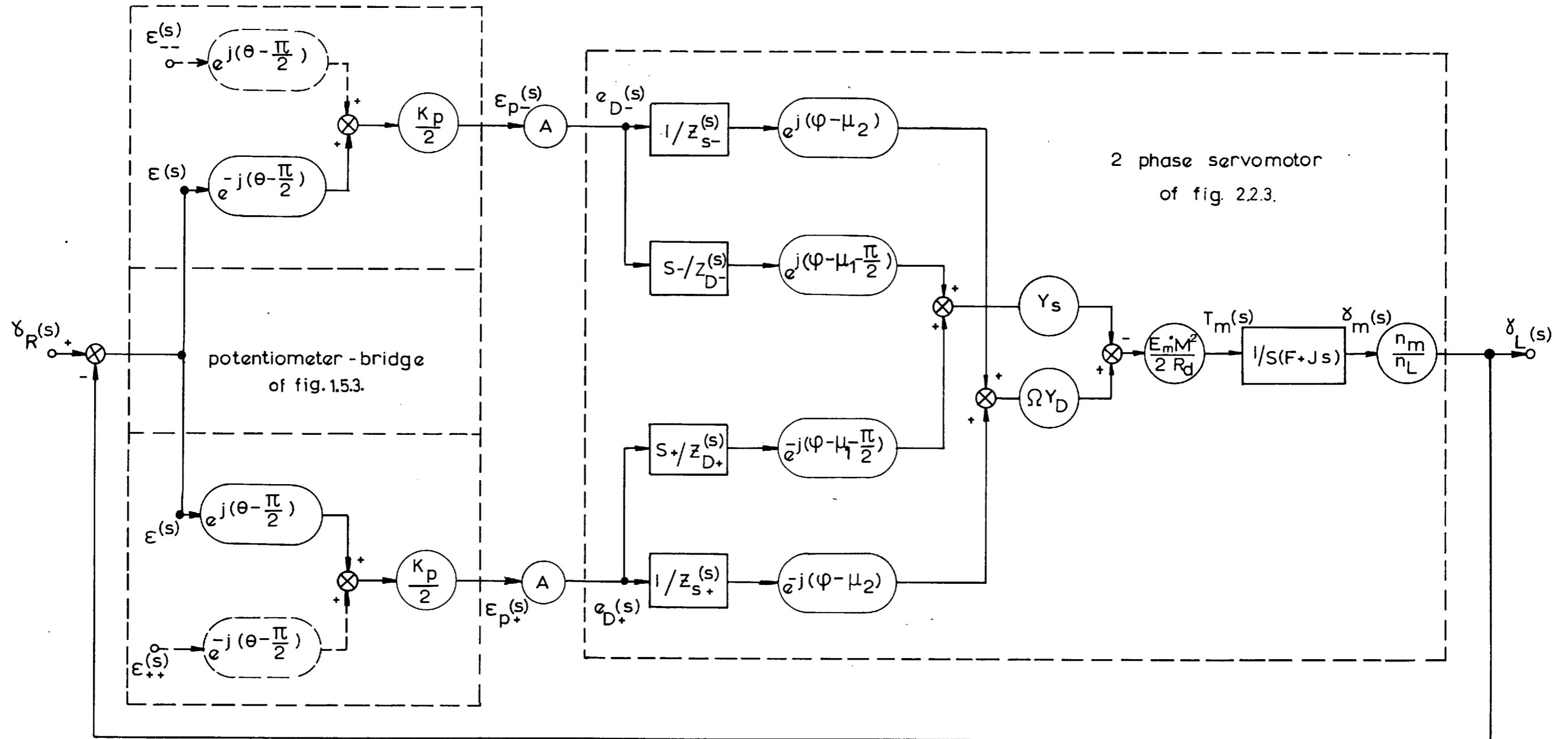


FIG. 2.4.1.

CLOSED - LOOP BLOCK DIAGRAM OF AN UNCOMPENSATED A.C. SERVOMECHANISM WITH A POTENTIOMETER - BRIDGE  
AS AN ERROR DETECTOR



Viewing the closed-loop block diagram of the uncompensated system of Fig. 2.4.1 it is noticed that in addition to the input reference signal  $Y_R$ , two other signals appear in such a way as if they are injected into the system from an outside source. These two signals are, in fact, high harmonic components at double the carrier frequency, generated by the modulation and demodulation processes involved in the system. Dotted line portion in Fig. 2.4.1 shows these noise signals in a distinct way.

Under the condition of neglecting the noise signals, it is possible to obtain from the block diagram, expressions for the open-loop and closed-loop modulation transfer functions which can be shown to be in conformity with the above mathematical formulation.

#### 2.4.2.2 System with a synchro-pair as error-detector

Following a similar pattern of steps as in 2.4.2.1 above, the synchro-pair block diagram shown in Fig. 2.3.3 may be joined to that of the 2-phase servomotor shown in Fig. 2.2.3 according to the boundary relationships in the modulated and demodulated signal zones. Equation 2.4.5 establishes the boundary relationship in the demodulated signal zone, whereas the general form of Equation 2.4.7, which may be expressed as,

$$e_{D+}(s) = A e_{b2+}(s) \quad 2.4.9$$

describes the boundary relationship in the modulated signal zone.

Fig. 2.4.2 shows the combined block diagram representing the uncompensated closed-loop system operated with a synchro-pair as error-detector. Due to the high frequency filtering action of the 2-phase servomotor, the effect of the high harmonic signals generated by the modulation and demodulation processes (illustrated

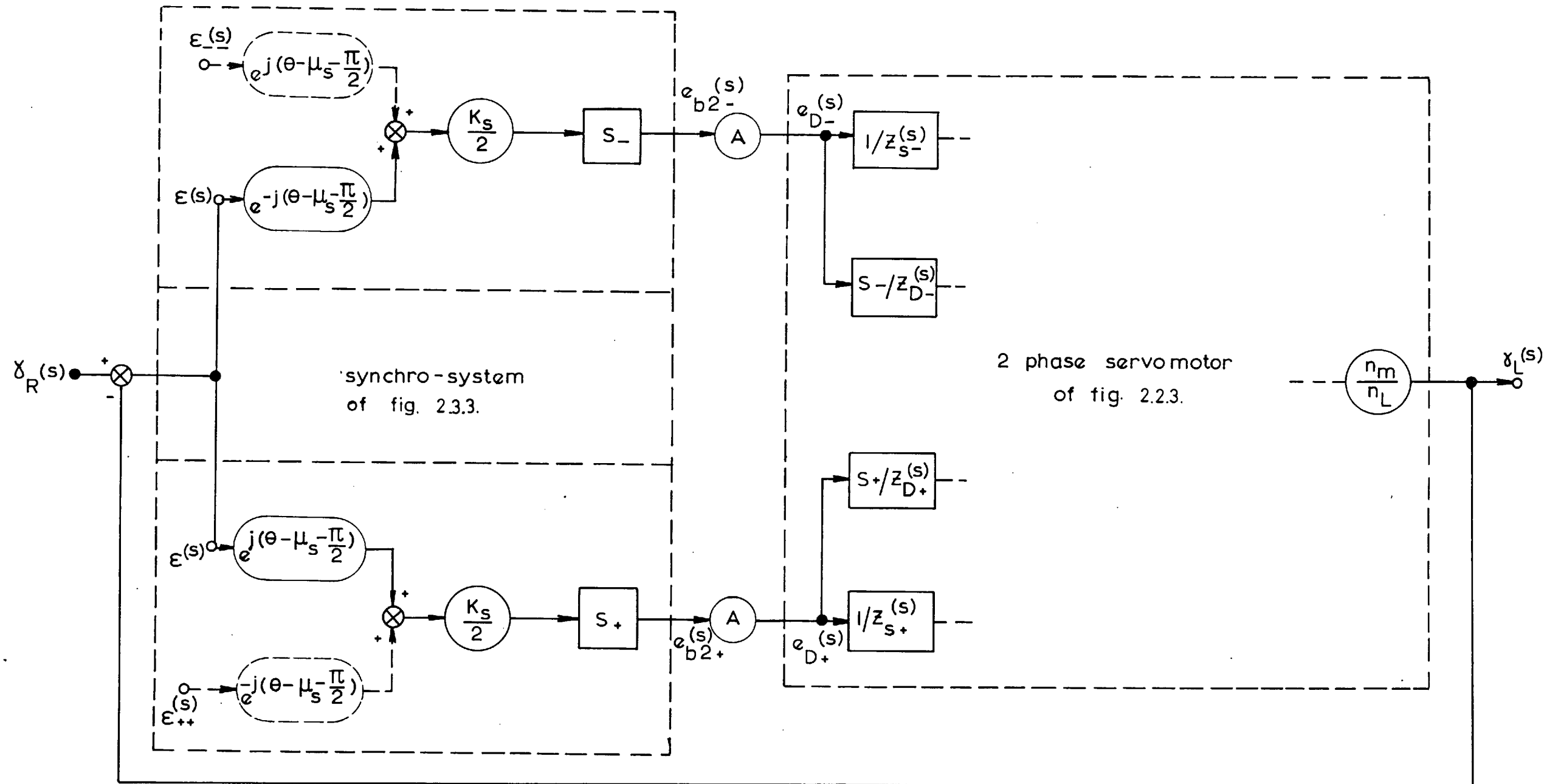


FIG. 2.4.2.

CLOSED-LOOP BLOCK DIAGRAM OF AN UNCOMPENSATED A.C. SERVOMECHANISM WITH A SYNCHRO-PAIR AS AN  
ERROR DETECTOR

in the figure by dotted line) on the system response may be considered negligible. On this basis, it becomes simple to derive from the block diagram expressions for the overall open-loop and closed-loop modulation transfer functions similar to those expressed by Equations 2.4.8 and 2.4.10 respectively.

The effect of the rotary modulation involved in the mechanism of the synchro-pair is to produce a new zero in the s-plane as can be easily deduced from the figure. This can usefully be employed for stabilization purposes <sup>1-3</sup> as an adjustment of this zero can be made to provide phase lead in the useful frequency range.

## 2.5 General discussion

As pointed out above, the a.c. servomechanism components, in which either a modulation or a demodulation process takes place cannot be described individually by transfer functions. However, by combining at least two of these components comprising a modulation and a demodulation process, renders it possible to obtain a modulation transfer function for the combination provided that the generated noise is neglected.

The significance of the system of equations described and the block diagrams developed above for representing the 2-phase servomotor and the synchro-pair lies in the fact that they are very adaptable, such that, the effect of other associated components, such as compensating devices, can easily be included (as will be dealt with in Chapter 3). Effect of the carrier frequency and phase variations on the system response can also easily be studied. Furthermore, the effect of changing the electrical and mechanical parameters of the various components can be investigated.

The analysis presented above was based on linearised conditions realised by generally accepted simplifying assumptions. However, it

provides a basis on which extensions and modifications could be made to account for the nonlinearities resulting from the gear backlash, coulomb friction and the high harmonic components generated by the modulation-demodulation process.

## CHAPTER 3

### COMPENSATION OF A.C. SERVOMECHANISMS

#### 3.1 Introduction

The principles of analysis and techniques developed in the previous chapter are readily applied to the design problem of a.c. servomechanisms. These techniques are particularly suitable for evaluating the performance characteristics of the overall uncompensated system once the parameter values are established, the loading conditions defined, and the input signals specified. Consequently, the absolute stability of the system can be checked, not only under normal operating conditions, but also when the system is subject to command signals, disturbing load variations, and realistic changes in loop parameters. Furthermore, a comparison between the performance obtained for the uncompensated servo-mechanism and the specified steady-state and dynamic performance would determine whether compensation is needed, and the way it should be effected.

Gain adjustment is certainly the most attractive procedure for accomplishing performance modifications to meet specified requirements, because it is the simplest and least costly method. The steady-state accuracy and band-width requirements can be achieved easily by this method. The effects of varying gain or changing parameter values correspond to motion of the system poles and zeros in the s-plane, which can rapidly be investigated by the use of root-locus method. Unfortunately, however, gain adjustment is seldom solely adequate until a

compensation procedure has reduced the problem to one which is within the range of gain adjustment.

In general, the design of an appropriate compensation can be accomplished in three stages:

- i) The choice of the compensator location in the system (e.g., in tandem, in the feedback loop, or in both).
- ii) The determination of the required dynamic characteristics of the compensator.
- iii) Physical realization (e.g., by RC network, a.c. tachometer, or....etc.), and synthesis of the various parameters of the practical compensator.

Stages (i) and (iii) require a good knowledge of the effect of various compensation techniques on both steady-state and transient performance of the a.c. system. Although many types of a.c. compensation are in common use, there is still neither a complete nor accurate analysis to some of them, which may be attributed to the difficulties encountered in realizing a.c. compensation designed to operate on the envelope of a modulated signal without affecting the carrier phase.

It is, therefore, the main object of this chapter and the next chapter to develop rigorous analysis and useful descriptions to three important types of a.c. compensation, viz:

- i) a.c. tachometer feedback
- ii) tandem linear networks
- iii) tandem chopper networks

## 3.2 A.c. tachometer

### 3.2.1 General

Tachometer feedback is a very common form of compensation. It usually represents the simplest means available. The signal fed back by the tachometer tends to increase the steady-state velocity-lag error. However, if a limiter is placed in the feedback path to provide saturation characteristics, it is frequently possible to obtain adequate damping in the transient period without excessive increases in velocity-lag error.

In general, tachometer feedback is used as inverse feedback and therefore tends to increase the bandwidth, which may be undesirable from the noise transmission point of view.

The following features show why tachometer feedback is an attractive compensator:

- i) Integrally constructed motor-tachometer units are available and very satisfactory.
- ii) This method of compensation is not very sensitive to changes in carrier frequency.
- iii) Tachometer feedback inherently reduces the destabilizing effects of gear backlash.

In the past, many authors<sup>14,22,29-33</sup> have attempted to describe the behaviour of the a.c. tachometer using different techniques of analysis. However, a simple and sufficiently accurate description of this device still does not seem to be available at present. In this Section, a rigorous analysis is going to be presented employing the 2-axis general theory of machines in order to offset these deficiencies.

### 3.2.2 Analysis

Because of the similarity between the construction of a.c. tachometer and 2-phase servomotor, the diagram of Fig. 2.2.1 may also be adopted to represent the a.c. tachometer and its equivalent generalised 2-axis machine. Again, the same basic assumptions, outlined in Section 2.1, are going to be used in deriving the dynamic equations.

By applying a similar procedure as in Sub-section 2.2.1, it is possible to arrive at the same results expressed by Eqns. 2.2.1 to 2.2.6 and 2.2.13 to 2.2.29 provided that the subscript  $t$  is used in conjunction with the various variables and parameters. At this stage, the operating conditions have to be set up in order to relate various expressions with the aim of formulating the response equation. The operating conditions may be given as below:

- i) Stator quadrature-axis winding  $Q_t$  is energised by a carrier signal whose general form is

$$e_{Qt} = E_t \sin(\omega t + \psi) \quad 3.2.1$$

- ii) The rotor is squirrel cage type which may be represented by short circuited windings, i.e.;

$$e_{at} = e_{bt} = 0 \quad 3.2.2$$

Expressions for the actual rotor currents can be obtained from Eqn. 2.2.29, which on substitution of the assumption

$$Z_{rt} \approx R_{rt} \quad , \quad 3.2.3$$



yield

$$i_{at} = -\frac{M_t}{R_{rt}} p \left[ \cos\gamma_t \left( \frac{1}{Z_{Dt}} \cdot e_{Dt} \right) + \sin\gamma_t \left( \frac{1}{Z_{Dt}} \cdot e_{Qt} \right) \right] \quad \dots 3.2.4$$

and

$$i_{bt} = -\frac{M_t}{R_{rt}} p \left[ \sin\gamma_t \left( \frac{1}{Z_{Dt}} \cdot e_{Dt} \right) - \cos\gamma_t \left( \frac{1}{Z_{Dt}} \cdot e_{Qt} \right) \right] \quad \dots 3.2.5$$

In general, the a.c. tachometer stator direct-axis winding  $D_t$  feeds either the a.c. servoamplifier with usually a high input impedance or a compensating network which is usually designed to provide a high input impedance in order to avoid loading problems. Consequently, it may be assumed that

$$i_{Dt} \approx 0 \quad 3.2.6$$

without committing a serious error. With this assumption, the a.c. tachometer output can be obtained in terms of rotor currents using Eqn. 2.2.16, thus

$$e_{Dt} = M_t p \left[ \cos\gamma_t \cdot i_{at} + \sin\gamma_t \cdot i_{bt} \right] \quad 3.2.7$$

Eliminating  $i_{at}$  and  $i_{bt}$  using Eqns. 3.2.4 and 3.2.5, Eqn. 3.3.7 becomes

$$e_{Dt} = -\frac{M_t^2}{R_{rt}} p \left[ \frac{p}{Z_{Dt}} \cdot e_{Dt} + \dot{\gamma}_t \cdot \left( \frac{1}{Z_{Dt}} \cdot e_{Qt} \right) \right] \quad 3.2.8$$

which may be rearranged to give

$$e_{Dt} = - \frac{n_L}{n_t} \cdot \frac{M_t^2}{R_{rt}} \cdot \frac{p Z_{Dt}}{\left[ Z_{Dt} + \frac{M_t^2}{R_{rt}} p^2 \right]} \left[ \dot{\gamma}_L \left( \frac{1}{Z_{Dt}} \cdot e_{Qt} \right) \right] \quad \dots 3.2.9$$

### 3.2.3 Representation by a mathematical model

After a sufficiently long time from the instant of applying the carrier excitation  $e_{Qt}$ , the current  $i_{Qt}$  reaches its steady-state which may be expressed as

$$i_{Qt} = \frac{E_t}{\sqrt{R_{Dt}^2 + L_{Dt}^2 \Omega^2}} \sin(\Omega t + \psi - \mu_t) \quad \dots 3.2.10$$

where

$$\mu_t = \tan^{-1} \left( \frac{L_{Dt} \Omega}{R_{Dt}} \right) \quad 3.2.11$$

Substituting Eqn. 3.2.10 into Eqn. 3.2.9 and rearranging gives

$$e_{Dt} = -k_t \frac{p Z_{Dt}}{\left[ Z_{Dt} + \frac{M_t^2}{R_{rt}} p^2 \right]} \left[ \sin(\Omega t + \psi - \mu_t) \cdot p \dot{\gamma}_L \right] \quad \dots 3.2.12$$

where

$$k_t = \frac{n_L}{n_t} \cdot \frac{M_t^2}{R_{rt}} \cdot \frac{E_t}{\sqrt{R_{Dt}^2 + L_{Dt}^2 \Omega^2}} \quad 3.2.13$$

Eqn. 3.2.12 describes the output of the a.c.

tachometer  $e_{Dt}$  as a function of the input  $\gamma_L$ . This function can be readily translated into the mathematical model shown in Fig. 3.2.1.

### 3.2.4 Complex frequency block diagram representation

Before taking the Laplace transform of Eqn. 3.2.12, it may first be rearranged in the more convenient form:

$$\left[ Z_{Dt} + M_t^2 p^2 / R_{rt} \right] e_{Dt} = -k_t p Z_{Dt} \left[ \sin(\Omega t + \psi - \mu_t) \cdot p \gamma_L \right]$$

..3.2.13

If the load shaft position is assumed to be initially zero with negligible higher order rate of change w.r.t. time, then

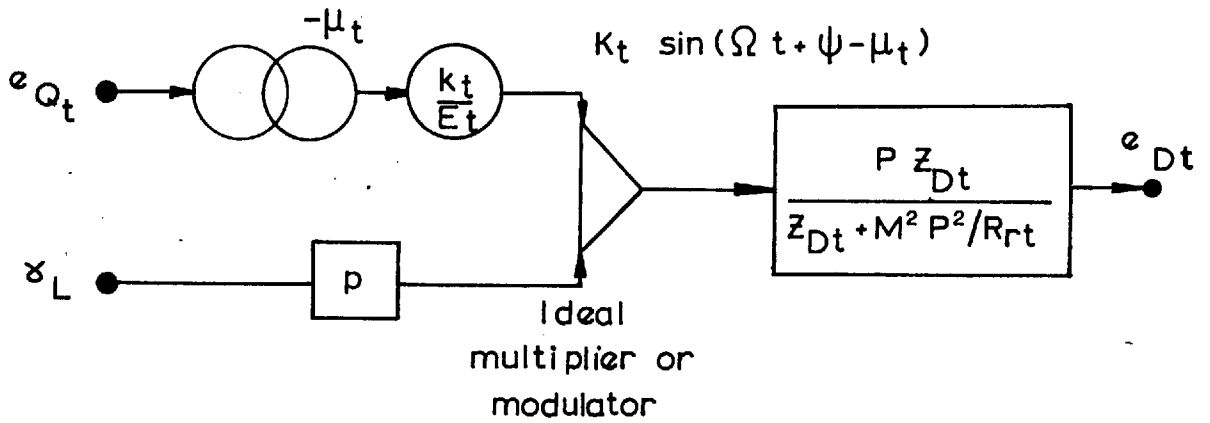
$$\gamma_L(0) = \dot{\gamma}_L(0) = \ddot{\gamma}_L(0) \dots \text{etc.} \approx 0$$

..3.2.14

The Laplace transform of the L.H.S. of Eqn. 3.2.13 is straightforward, whereas that of the R.H.S. would require the use of the Complex Convolution Integral<sup>124</sup> which, in turn, can be easily solved employing the method of Residue. Taking into account the results of Eqn. 3.2.14, Eqn. 3.2.13 can easily be transformed into the complex frequency domain yielding the expression

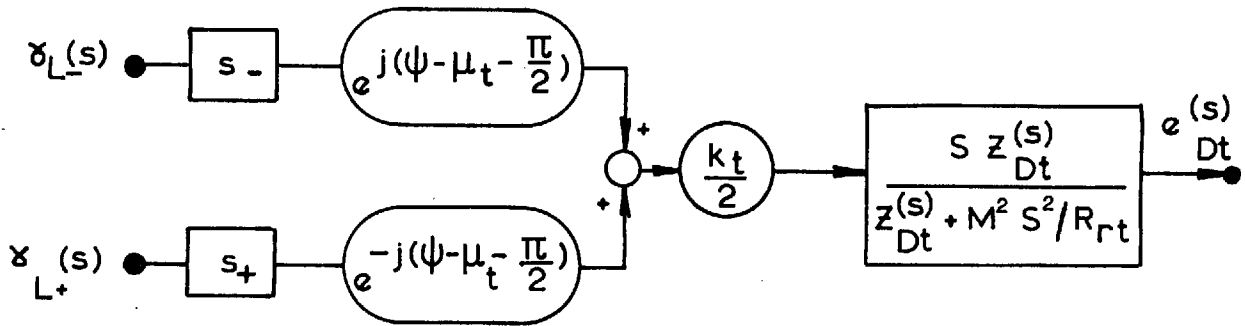
$$e_{Dt}(s) = \frac{k_t}{2} \frac{s Z_{Dt}(s)}{\left[ Z_{Dt}(s) + M_t^2 s^2 / R_{rt} \right]} \left[ e^{j(\psi - \mu_t - \pi/2)} s_- \gamma_{L-}(s) + e^{-j(\psi - \mu_t - \pi/2)} s_+ \gamma_{L+}(s) \right]$$

..3.2.15



MATHEMATICAL MODEL REPRESENTATION OF A.C. TACHOMETER

FIG. 3.2.1



COMPLEX FREQUENCY BLOCK DIAGRAM REPRESENTATION OF A.C. TACHOMETER

FIG. 3.2.2

On the basis of Eqn. 3.2.15, a complex frequency block diagram representing the dynamic behaviour of a.c. tachometer may be constructed as shown in Fig. 3.2.2. It is again evident that a transfer function for the isolated a.c. tachometer cannot be obtained because a modulation process is effected in it resulting in a change of the nature of the output signal in comparison with that of the input. However, by feeding the output of the a.c. tachometer back to the 2-phase servomotor (where a demodulation process is effected) and considering the combination, an overall modulation transfer function can be obtained (if high harmonic components are neglected) in which the effect of the a.c. tachometer is in implicit form. This treatment is deferred to the next Sub-section.

### 3.2.5 Positional control a.c. servomechanism compensated by a.c. tachometer

The positional control a.c. servomechanism shown in Fig. 1.2.1 is going to be considered as an illustrative example. To avoid undue complexity at this stage, the simplifying assumptions associated with the servo-amplifier adopted in Sub-section 2.4.1 will also be used here.

Formulation of the open-loop and closed-loop system responses can be considerably simplified if the system block diagram is first constructed. The complex frequency block diagrams representing the 2-phase servomotor, the synchro-pair and the a.c. tachometer shown in Figs. 2.2.3, 2.4.3, and 3.2.2 respectively, can be joined together according to the boundary conditions expressed below

$$e_{D\pm}(s) = A \left[ e_{b2\pm}(s) - e_{Dt\pm}(s) \right] \quad 3.2.16$$

The resulting block diagram is shown in Fig. 3.2.3. Clearly, the derivation of the overall open-loop and closed-loop modulation transfer function is straightforward provided that the high frequency filtering action of the 2-phase servomotor warrants the neglect of the high harmonic signals generated by the modulation and demodulation processes.

Such a complete representation of the a.c. system would enable the servo designer to apply more refined and systematic design techniques similar to those available for d.c. systems. Furthermore, it permits thorough studies to be easily carried out into the effects of carrier frequency drift, change in carrier phase, variations of electrical and mechanical parameters on the overall system performance.

### 3.3 Linear networks

#### 3.3.1 General

Although a.c. tachometer feedback compensation may be acceptable from the point of view of performance, the space available and the required geometry of the mechanical design may make it impossible to employ a motor with integrally mounted tachometer or to couple in a separate tachometer with gearing. Also, considerations of size and weight of electro-mechanical components set up a basic restriction to their use in some applications. Compensation by linear networks generally has the advantage in weight, size, reliability, and cost, but suffers from being very sensitive to carrier frequency drift.

In some applications, such as instrument servos,

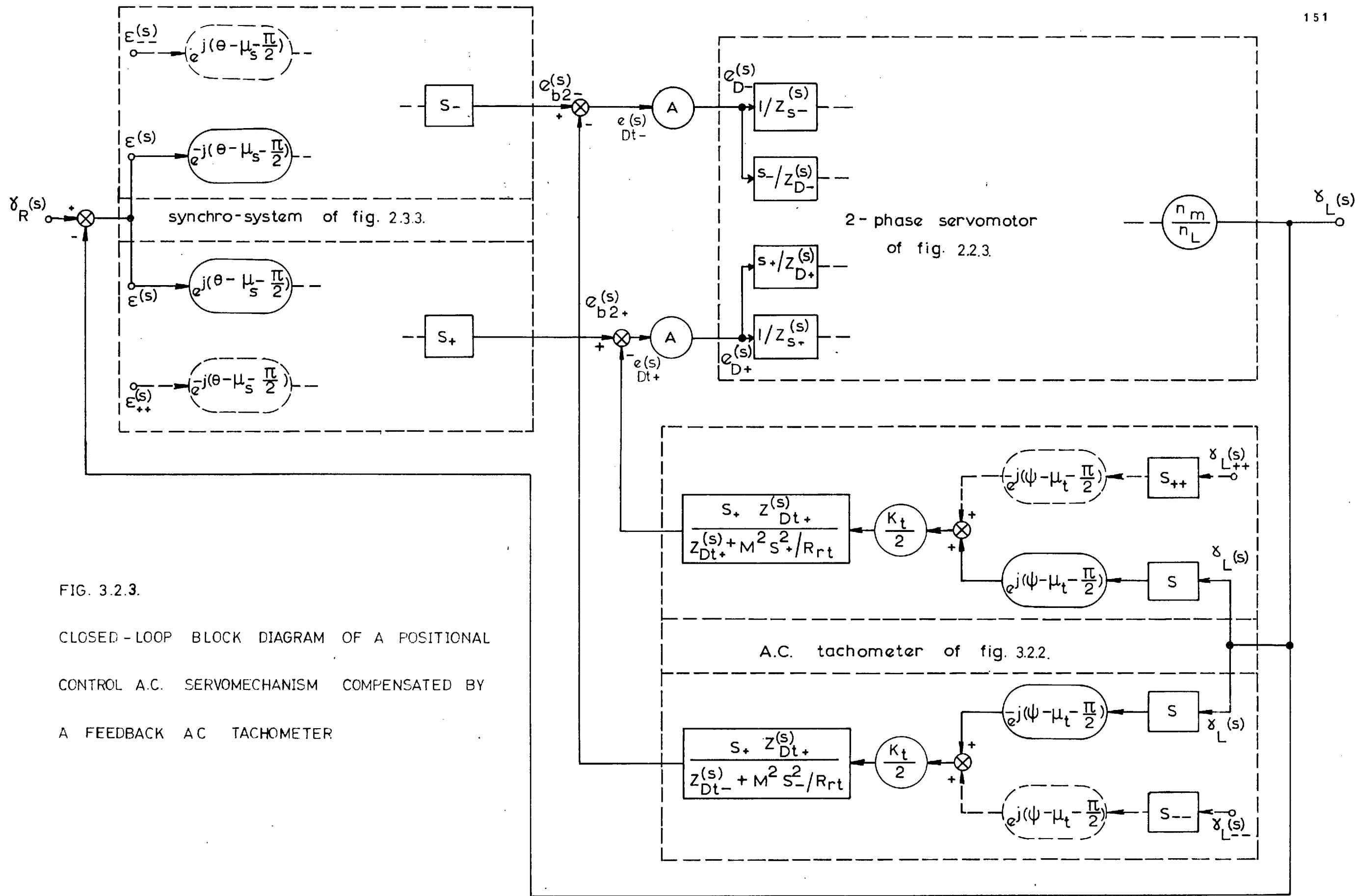


FIG. 3.2.3.  
 CLOSED-LOOP BLOCK DIAGRAM OF A POSITIONAL CONTROL A.C. SERVOMECHANISM COMPENSATED BY A FEEDBACK A.C. TACHOMETER

where the carrier frequency is adequately stable, linear network compensation emerges as the most superior type. The synthesis of a.c. compensation linear networks has received considerable attention<sup>46-62</sup> in recent years. However, the various techniques developed do not seem to provide a systematic general approach, and usually involve a great deal of approximation. In this Section, a general synthesis method is presented to realize specified multiplicative and rotary modulation transfer functions by means of linear networks.

### 3.3.2 Multiplicative modulation transfer function

Before considering the synthesis procedure, it would be appropriate to examine the relationship between the transfer function of a general linear network and its envelope transfer function. For this purpose, the ideal a.c. or carrier system shown in Fig. 3.3.1, in which a linear network is inserted in the carrier channel between an ideal modulator and demodulator, is going to be considered. Where the modulator and demodulator are sinusoidally excited by the voltages

$$E_{md} \sin(\Omega t + \theta) \quad \text{and} \quad E_{de} \sin(\Omega t + \emptyset)$$

..3.3.1

respectively.

Thus, the output of the modulator can be written as

$$x_1(t) = x(t) \cdot E_{md} \sin(\Omega t + \theta) \quad 3.3.2$$

where  $x(t)$  is the modulating signal.



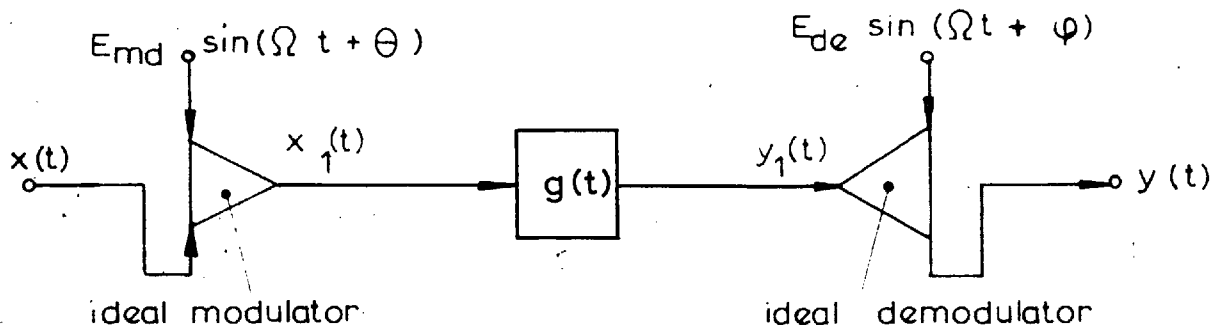


FIG. 3.3.1

IDEAL A.C. SYSTEM WITH MULTIPLICATIVE MODULATION AND DEMODULATION

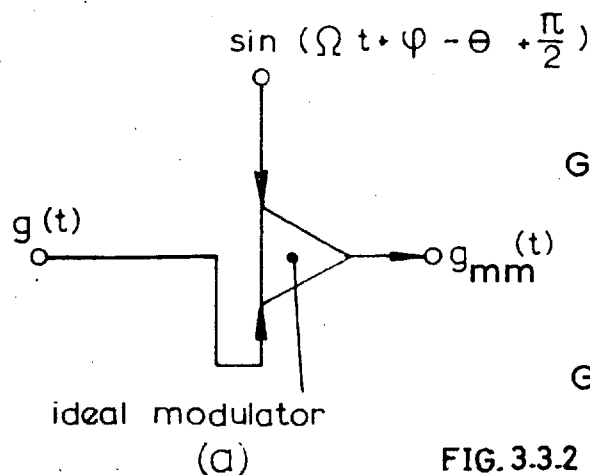
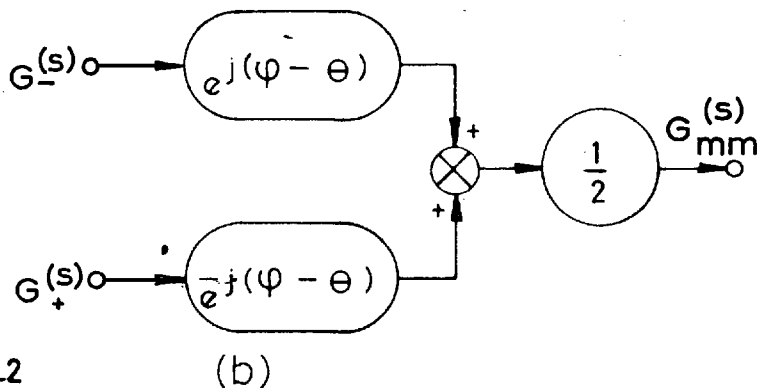


FIG. 3.3.2

PROCESS TO OBTAIN THE MULTIPLICATIVE MODULATION IMPULSE RESPONSE FROM A SPECIFIED IMPULSE RESPONSE



PROCESS TO OBTAIN THE MULTIPLICATIVE MODULATION TRANSFER FUNCTION FROM A SPECIFIED TRANSFER FUNCTION

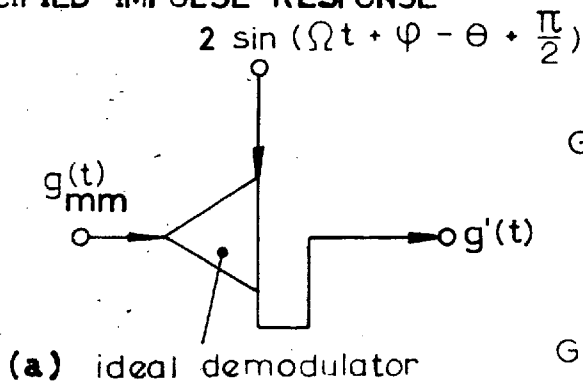
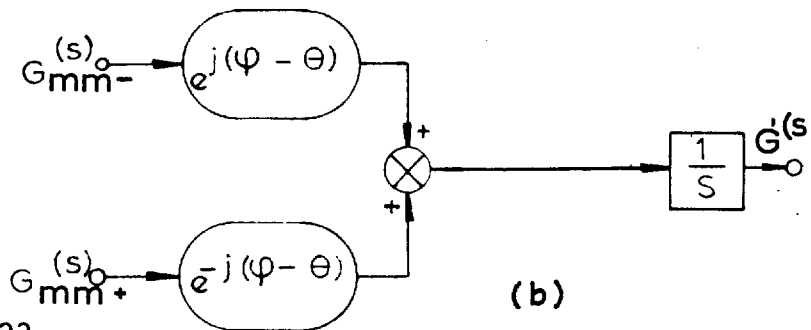


FIG. 3.33.

PROCESS TO OBTAIN THE IMPULSE RESPONSE FROM A SPECIFIED MULTIPLICATIVE MODULATION IMPULSE RESPONSE



PROCESS TO OBTAIN THE TRANSFER FUNCTION FROM A SPECIFIED MULTIPLICATIVE MODULATION TRANSFER FUNCTION

The Laplace transform of Eqn. 3.3.2 is

$$x_1(s) = \frac{E_{md}}{2} \left[ e^{j(\theta - \pi/2)} x_-(s) + e^{-j(\theta - \pi/2)} x_+(s) \right] \quad \dots 3.3.3$$

This signal is applied to the linear network whose transfer function is assumed to be  $G(s)$ . Therefore, the output from the network can be written as

$$y_1(s) = x_1(s) \cdot G(s) \quad 3.3.4$$

which on demodulation yields

$$y(s) = \frac{E_{de}}{2} \left[ e^{j(\phi - \theta)} y_{1-}(s) + e^{-j(\phi - \theta)} y_{1+}(s) \right] \quad \dots 3.3.5$$

Substituting Eqns. 3.3.3 and 3.3.4 into Eqn. 3.3.5, gives

$$y(s) = \frac{E_{md} E_{de}}{4} \left[ \left\{ e^{j(\phi - \theta)} G_-(s) + e^{-j(\phi - \theta)} G_+(s) \right\} x(s) - \left\{ e^{j(\phi + \theta)} G_-(s) x_{--}(s) + e^{-j(\phi + \theta)} G_+(s) x_{++}(s) \right\} \right] \quad \dots 3.3.6$$

Eqn. 3.3.6 shows that the output of the ideal a.c. system of Fig. 3.3.1 yields second harmonic terms in addition to the fundamental term. If these harmonic terms are neglected, a linear function can be obtained

which may be conveniently termed as "multiplicative modulation transfer function". This can be expressed as

$$G_{mm}(s) = \frac{y(s)/x(s)}{E_{md} E_{de}/2} \quad (\text{neglecting second harmonic components})$$

$$= \frac{1}{2} \left[ e^{j(\phi - \theta)} G_{-}(s) + e^{-j(\phi - \theta)} G_{+}(s) \right] \quad 3.3.7$$

where the division factor  $(E_{md} E_{de}/2)$  is introduced to make the multiplicative modulation response unity when

$$G(s) = 1, \quad \text{and} \quad \phi = \theta \quad 3.3.8$$

Eqn. 3.3.7 gives the relationship between the multiplicative modulation transfer function and the transfer function at any phase misalignment between the modulation and demodulation carrier references. The equation, in fact, shows how to deduce the former function when the latter is known. This process can be represented by the diagram shown in Fig. 3.3.2b.

The impulse response of the network  $g(t)$  is related to its transfer function  $G(s)$  in the wellknown manner

$$g(t) = \mathcal{L}^{-1} G(s) \quad 3.3.9$$

Correspondingly, a multiplicative modulation impulse response may be obtained from the multiplicative modulation transfer function, thus

$$g_{mm}(t) = \mathcal{L}^{-1} G_{mm}(s) \quad 3.3.10$$

Writing  $G_{mm}(s)$  in terms of  $G(s)$  and solving, it is easy to deduce that

$$g_{mm}(t) = g(t) \cdot \sin(\Omega t + \phi - \theta + \pi/2) \quad 3.3.11$$

This relationship can be described by the diagram shown in Fig. 3.3.2a, in which  $g_{mm}(t)$  is multiplicatively modulated to yield  $g(t)$ ; and thus the term multiplicative modulation used in association with the impulse response  $g_{mm}(t)$  appears to be very appropriate.

### 3.3.3 Method of synthesising the transfer function from the multiplicative modulation transfer function

If  $g_{mm}(t)$  is demodulated by a carrier signal of the form

$$2 \sin(\Omega t + \phi - \theta + \pi/2), \quad 3.3.12$$

the original impulse of the network is obtained provided that the second harmonic components are neglected. This implies that both the processes described by Eqns. 3.3.7 and 3.3.11 are approximately reversible (exactly reversible in the case of negligible high harmonic terms). This can be further explained in mathematical terms as below

$$g'(t) = g_{mm}(t) \cdot 2 \sin(\Omega t + \phi - \theta + \pi/2) \quad 3.3.13$$

and

$$G'(t) = e^{j(\phi - \theta)} G_{mm-}(s) + e^{-j(\phi - \theta)} G_{mm+}(s)$$

where  $g'(t)$  and  $G'(s)$  are slightly different in comparison with their correspondings  $g(t)$  and  $G(s)$  pertinent to the original network. The processes by which  $g'(t)$  and  $G'(s)$  are obtained from  $g_{mm}(t)$  and  $G_{mm}(s)$ , respectively, are illustrated by the diagrams a and b shown in Fig. 3.3.3.

To obtain the transfer function corresponding to a specified multiplicative modulation transfer function  $G_{mm}(s)$  with a better degree of accuracy, the following procedure may be employed:

- i) Apply Eqn. 3.3.14 to obtain  $G'(s)$ , which can be considered as a first approximation of the required transfer function.
- ii) Substitute the value of  $G'(s)$  in Eqn. 3.3.7 to obtain the corresponding  $G''(s)$ , which is expected to be different from the original  $G_{mm}(s)$  due to the approximation involved.
- iii) Evaluate the difference  $\left[ G''(s) - G_{mm}(s) \right]$ , and consider it as an error function on which the above two steps may be applied. This would allow a second approximation  $G'''(s)$  of the required transfer function to be obtained.
- iv) Better approximation can still be obtained by repeating the above steps. The number of repetitions depends on the required degree of accuracy.

Once the transfer function is obtained, the synthesis problem reduces to a conventional one, and the realization by a physical network can be accomplished by one of the procedures available for linear network realization.

### 3.3.4 Rotary modulation transfer function

In a.c. servomechanisms, the behaviour of the synchro-pair error-detector may be ideally represented by an ideal modulator followed by a differentiator, whereas that of the 2-phase servomotor may be ideally represented by an ideal demodulator followed by a filter. In this way, the a.c. system is reduced down to the ideal system shown in Fig. 3.3.4, where the filter after the demodulator is not considered and  $G(s)$  is the transfer function of a linear correcting network inserted between the synchro-pair and the servomotor.

From this figure, the output of the rotary modulator can easily be deduced as

$$\begin{aligned} x_2(t) &= p [x_1(t)] \\ &= p [x(t) \cdot E_{md} \sin(\Omega t + \theta)] \end{aligned} \quad 3.3.15$$

Transforming the above equation into the complex frequency domain by taking its Laplace transform, gives

$$\begin{aligned} x_2(s) &= \frac{E_{md}}{2} \cdot s \cdot \left[ e^{j(\theta - \pi/2)} x_-(s) + e^{-j(\theta - \pi/2)} x_+(s) \right] \\ &\quad - x(0) E_{md} \sin \theta \end{aligned} \quad 3.3.16$$

It follows that the output from the linear network is

$$y_1(s) = x_2(s) \cdot G(s) \quad 3.3.17$$

which on demodulation yields

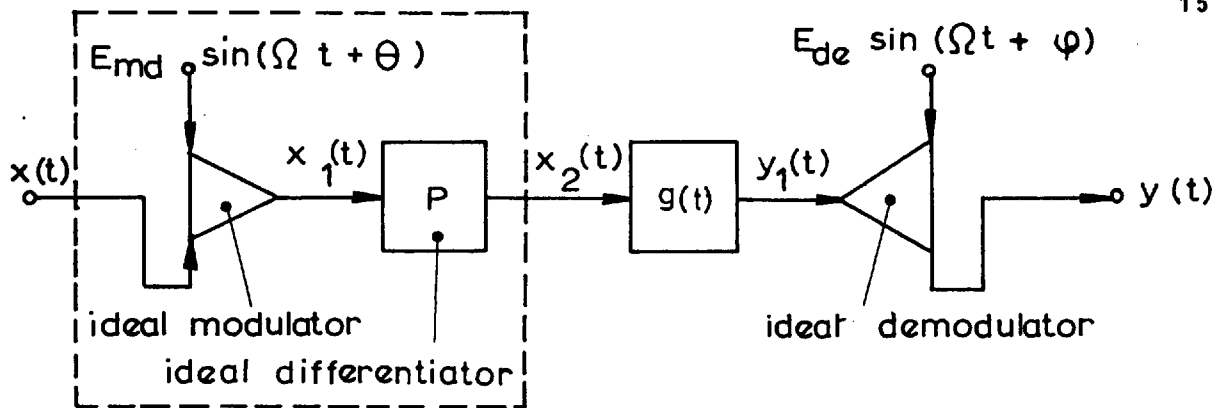


FIG. 3.3.4

IDEAL A.C. SYSTEM WITH ROTARY MODULATION AND MULTIPLICATIVE DEMODULATION

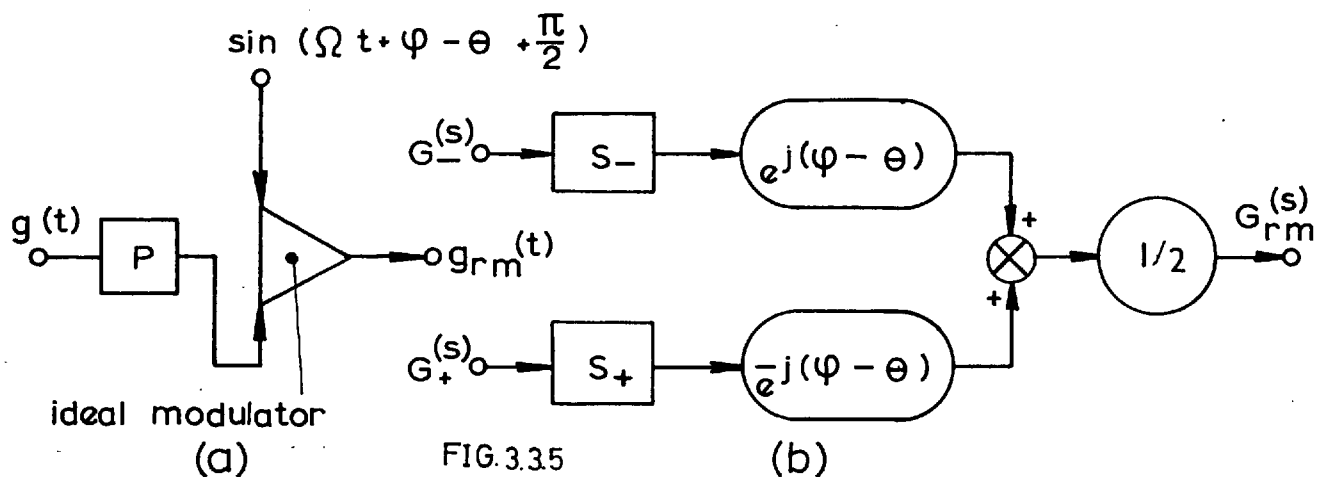


FIG. 3.3.5

PROCESS TO OBTAIN THE ROTARY MODULATION IMPULSE RESPONSE FROM A SPECIFIED IMPULSE RESPONSE

PROCESS TO OBTAIN THE ROTARY MODULATION TRANSFER FUNCTION FROM A SPECIFIED TRANSFER FUNCTION

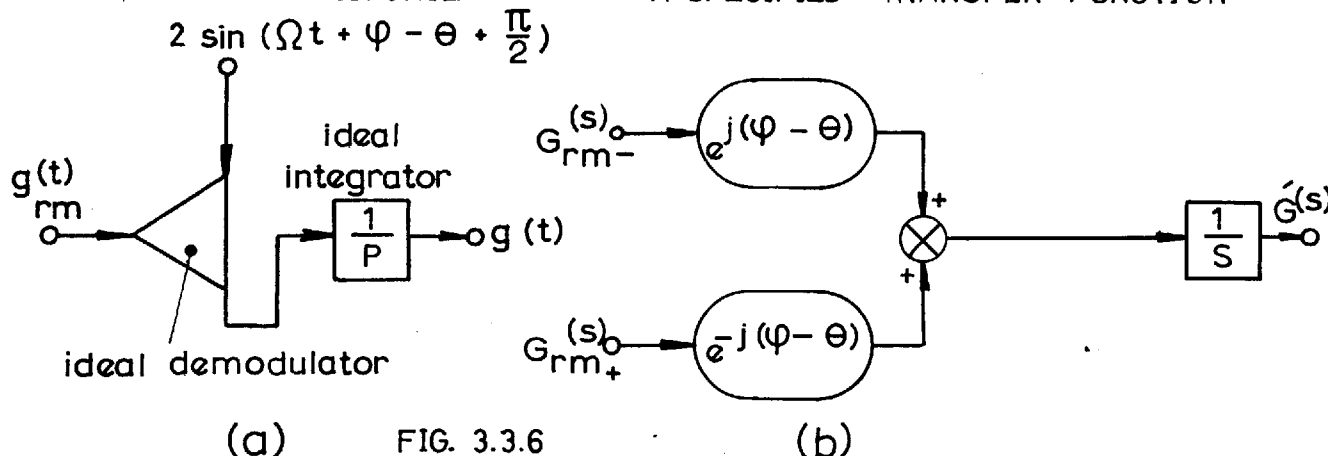


FIG. 3.3.6

PROCESS TO OBTAIN THE IMPULSE RESPONSE FROM A SPECIFIED ROTARY MODULATION IMPULSE RESPONSE

PROCESS TO OBTAIN THE TRANSFER FUNCTION FROM A SPECIFIED ROTARY MODULATION TRANSFER FUNCTION

$$\begin{aligned}
y(s) = & \frac{E_{md} E_{de}}{4} \left[ \left\{ e^{j(\phi - \theta)} s_- G_-(s) + e^{-j(\phi - \theta)} s_+ G_+(s) \right\} x(s) \right. \\
& - \left. \left\{ e^{j(\phi + \theta)} s_- G_-(s) x_{--}(s) + e^{-j(\phi + \theta)} G_+(s) x_{++}(s) \right\} \right] \\
& - \frac{E_{md} E_{de}}{2} \cdot x(0) \sin \theta \left[ e^{j(\phi - \pi/2)} G_-(s) + e^{-j(\phi - \pi/2)} G_+(s) \right]
\end{aligned}$$

..3.3.18

In this case, even with the assumption of negligible second harmonic components, a linear function relating the output and the input signals cannot be accomplished unless the further assumption of

$$x(0) \cdot \sin \theta = 0 \quad 3.3.19$$

is also established. This assumption states that either the signal initial value is zero,  $\theta = 0$ , or both simultaneously vanish. Under any one of these conditions, the resulting linear function, which may be appropriately termed as "rotary modulation transfer function  $G_{rm}(s)$ ", can be expressed as

$$\begin{aligned}
G_{rm}(s) = & \frac{y(s)/x(s)}{E_{md} E_{de} / 2} \quad (\text{neglecting second harmonic terms,} \\
& \text{and under the condition of} \\
& x(0) \sin \theta = 0)
\end{aligned}$$

$$= \frac{1}{2} \left[ e^{-j(\phi - \theta)} s_- G_-(s) + e^{-j(\phi - \theta)} s_+ G_+(s) \right]$$

..3.3.20



where the factor  $(E_{md} E_{de}/2)$  is introduced to make the rotary modulation response unity when

$$G(s) = 1, \text{ and } \phi = \theta \quad 3.3.21$$

The process of obtaining the rotary modulation transfer function from a given transfer function at any value of phase misalignment between the modulation and demodulation carrier references, described by Eqn. 3.3.20, is illustrated by the diagram shown in Fig. 3.3.5b.

If  $g(t)$  is the impulse response of the linear network whose transfer function is  $G(s)$ , correspondingly a rotary modulation impulse response  $g_{rm}(t)$  can be found such that

$$g_{rm}(t) = \int^{-1} G_{rm}(s) \quad 3.3.22$$

Writing  $G_{rm}(s)$  in terms of  $G(s)$  and solving for  $g_{rm}(s)$  results in

$$g_{rm}(t) = \sin(\Omega t + \phi - \theta + \pi/2) \cdot p g(t) \quad \dots 3.3.23$$

This is only valid when either  $g(0) = 0$  or  $\phi = \theta$ . Fig. 3.3.5a shows a diagram representing the process described by Eqn. 3.3.23.

### 3.3.5 Method of synthesising the transfer function from the rotary modulation transfer function

If  $g_{rm}(t)$  is first demodulated by a carrier signal of the form

$$2 \sin(\Omega t + \phi - \theta + \pi/2), \quad 3.3.24$$

and the result is then integrated, the original impulse transform of the network can be recovered provided that the second harmonic components are neglected. Thus, in mathematical terms

$$g'(t) = \frac{1}{p} \left[ 2 \sin(\Omega t + \phi - \theta + \pi/2) g_{rm}(t) \right] \quad \dots 3.3.25$$

which on taking the Laplace transform, gives

$$G'(s) = \frac{1}{s} \left[ e^{j(\phi - \theta)} G_{rm-}(s) + e^{-j(\phi - \theta)} G_{rm+}(s) \right] + \frac{G'(0)}{s} \quad 3.3.26$$

where  $g'(t)$  and  $G'(s)$  differ slightly from their correspondings  $g(t)$  and  $G(s)$  of the original network. Eqns. 3.3.25 and 3.3.26 can be translated into representative diagrams as shown in Fig. 3.3.6, where  $G'(0)$  was assumed to be zero.

With an analogous iterative procedure as that outlined in Section 3.3.3, it is possible to obtain more accurate values for  $g'(t)$  and  $G'(s)$ .

Synthesis of a specified rotary modulation transfer

function is thus accomplished in two steps: derivation of the transfer function from the specified rotary modulation transfer function in the manner explained above, and then realizing the resulting transfer function by a physical network employing one of the available methods of linear network synthesis.

### 3.4 Chopper networks

Despite the numerous advantages of linear passive compensating networks over many other types of a.c. compensation, they possess the serious drawback of being extremely sensitive to carrier frequency drift. That is why they cannot be employed in air-borne control systems where roughly regulated carrier frequency is common. In attempting to overcome this problem, several methods have been developed by which automatic returning<sup>2,82-87</sup> of the network can be achieved, but at the expense of size, weight, cost and reliability.

Recently chopper networks<sup>88-111</sup> have emerged as the most superior type of a.c. compensation in view of its insensitivity to carrier frequency fluctuations, while maintaining all the advantages of linear passive networks. This type of network consists basically of passive elements inter-connected by one or more 3-terminal switches which operate in synchronism with the carrier. Its principle of operation is thus very similar to demodulation - d.c. compensation - remodulation all performed simultaneously instead of in sequence as in the conventional approach.

The analysis of chopper networks constitutes a relatively big part of the present work, and it was thus decided to devote the whole next chapter to this purpose.

## CHAPTER 4

### ANALYSIS OF CHOPPER NETWORKS

#### 4.1 Introduction

##### 4.1.1 General

The purpose of the analysis presented in this chapter is mainly to obtain a mathematical form to describe the chopper network response to suppressed-carrier amplitude-modulated wave, so that its contribution to a.c. systems performance can satisfactorily be related, thereby enabling the overall system response to be determined. On this basis, the chopper networks under consideration are inserted between an ideal modulator and an ideal demodulator as shown in Fig. 4.1.1. The former produces the required input suppressed-carrier amplitude-modulated wave, whereas the latter is employed to recover the envelope of the output from the chopper network and thus may be compared with the modulating signal. To derive the response of the chopper networks when subject to rotary modulated signal, as in the case of using synchros as error-detectors, Fig. 4.1.2 is used.

Because of the non-linear nature of the modulation and demodulation operations as well as the switching processes incorporated in the chopper networks, the response of such networks is expected to be dependent on the input actuating signal  $x(t)$  (see Figs. 4.1.1 and 4.1.2). However, by neglecting the higher harmonic components, it is possible, as will be seen in this chapter, to obtain a response function independent of the input referred to as

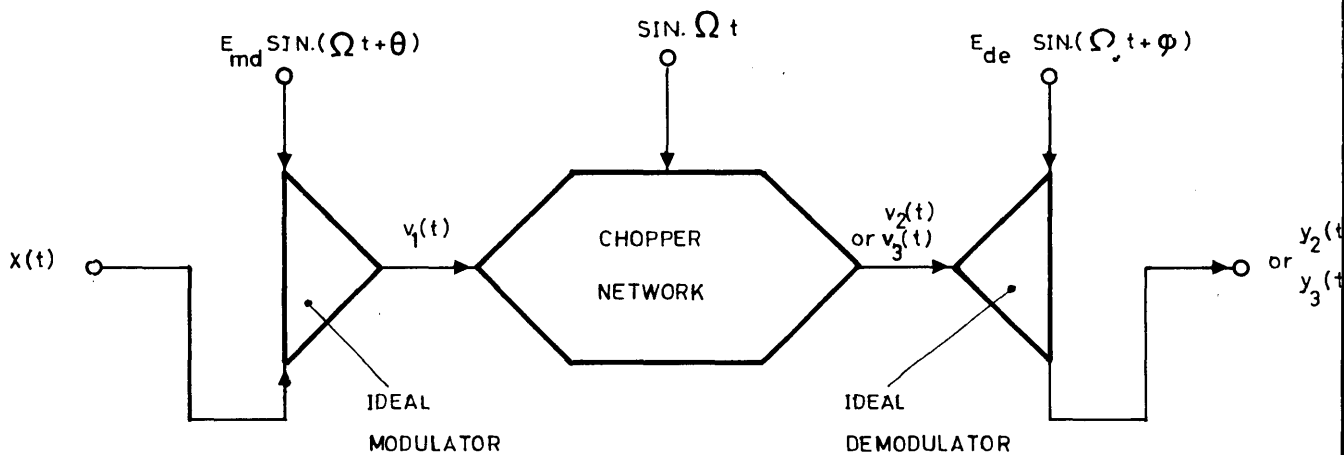


FIG. 4.1.1.

DIAGRAM FOR DERIVING THE RESPONSE OF A CHOPPER NETWORK TO MULTIPLICATIVE MODULATED SIGNAL

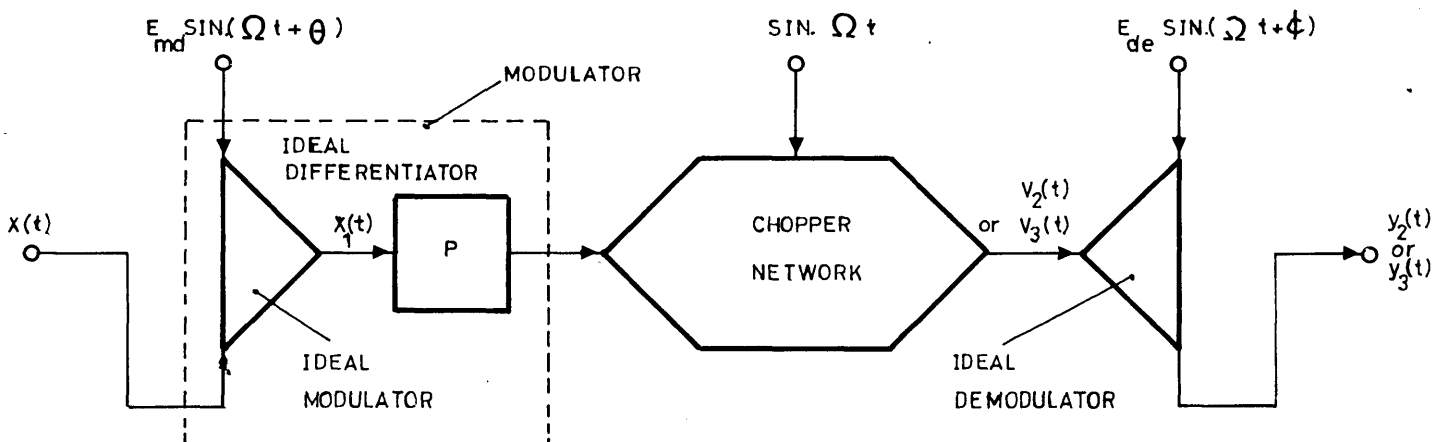


FIG. 4.1.2.

DIAGRAM FOR DERIVING THE RESPONSE OF A CHOPPER NETWORK TO ROTARY MODULATED SIGNAL

"modulation transfer function". Either the term multiplicative or rotary may be added to describe the type of the modulation.

#### 4.1.2 Analysis techniques

Previous contributions by many authors<sup>88-111</sup> have resulted in the development of several methods of analysis. Virtually all these methods depend on different simplifying assumptions with the common restriction of step-function input modulating signal. In addition, the application of these methods of analysis were usually confined to a few number of chopper networks with very simple configurations, and the treatment was only limited to restricted operating conditions. In some cases<sup>89,90,94,97,98,108,110</sup>, few experimental results were given for very special cases which neither provide sufficient assessment to the approximations involved nor determine their limits of validity under various modes of operation. Finally, neither of these available methods is suitable for evaluating the noise generated in the various chopper networks (due to the inherent switching mechanism), which may be very desirable in assessing their suitability in the various applications.

In an attempt to offset all the aforementioned deficiencies, two analytical approaches are going to be examined in detail:

##### i) Exact analytical approach

In this approach, the analysis is carried through-out in the complex frequency domain. The input modulating signal  $x(t)$  is treated as a general function of time. No further assumptions are imposed

other than that stated above concerning the neglect of the high harmonic terms appearing in the final output  $y(t)$ , which is essential for enabling the modulation transfer function to be determined.

This method of analysis although depends to some extent on some previous attempts<sup>89-91</sup> employing Z-transform and modified Z-transform techniques, it is believed to be new in its entirety and coverage.

ii) Approximate analytical approach

This approach is primarily based on methods previously developed by several authors<sup>97-99</sup>. Reformulation was necessary in order to make the method applicable to more general and complex configurations of chopper networks. The method depends essentially on the assumption that the envelope changes very slowly with respect to the carrier, which enables an equivalent time-invariant passive network to be determined.

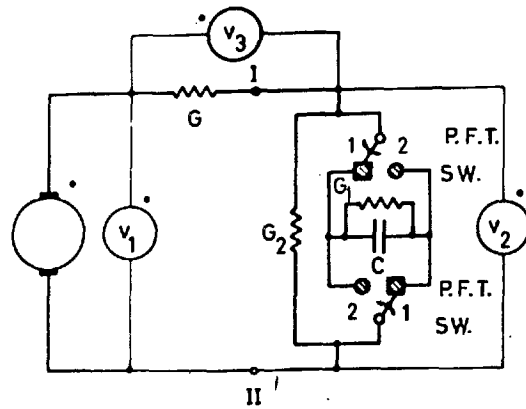
4.1.3 Chopper network configurations

According to the work presented in Chapter II, there are many types of chopper networks available. It would be very difficult to consider the analysis for all the types in one chapter. Therefore, a representative selection of only three RC prototypes are going to be considered in the subsequent analysis. These prototypes are:

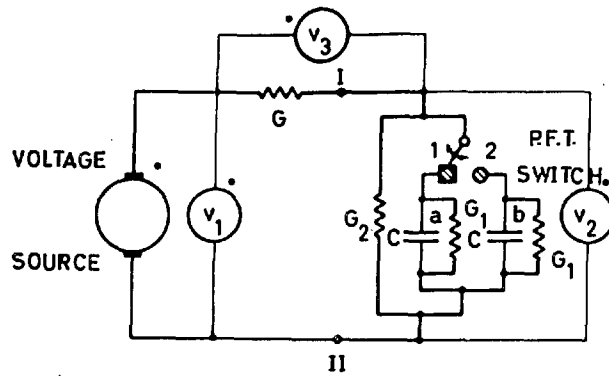
- i) Single-switch double-capacitor
- ii) Double-switch single-capacitor
- iii) Cascaded inverted double-switch double-capacitor

which are, for convenience, redrawn in Fig. 4.1.3. Since analogous steps can be used for analysing the various prototype chopper networks, the detailed analysis will be only confined to the single-switch double-capacitor chopper network, whereas the important formulae and final results corresponding to the other two prototypes will be directly given in Appendices B and C respectively.

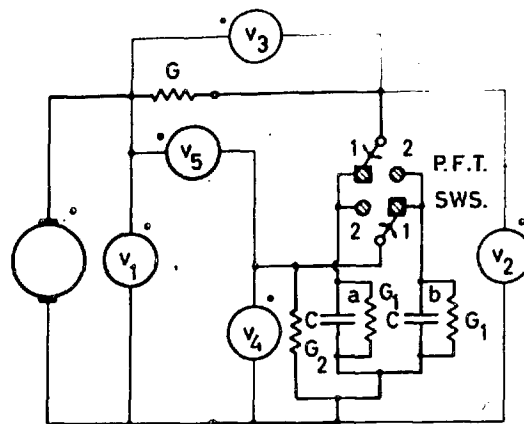




(a) Double-switch single-capacitor chopper network



(b) Single-switch double-capacitor chopper network



(c) Cascaded inverted double-switch double-capacitor chopper network

FIG. 4.13.

THREE PROTOTYPES OF CHOPPER NETWORKS CONSIDERED IN THE ANALYSIS

## 4.2 Application of the Exact Analytical Approach

### 4.2.1 Development of block diagram representation.

Consider the single-switch double-capacitor prototype chopper network shown in Fig. 4.1.3-a to be the one used in connection with the diagram of Fig. 4.1.1.

Ideally, the effect of the 3-terminal synchronous switch is to make contact with terminal 1 for

$$nT \leq t < (n+\delta)T, \quad n = 0, 1, 2, \dots, \quad 4.2.1$$

where

$$0 < \delta < 1/2 \quad 4.2.2$$

and to make contact with terminal 2 for

$$(n+1/2)T \leq t < (n+1/2+\delta)T \quad 4.2.3$$

On this basis, the 3-terminal synchronous switch has the effect of closing the circuit through branch a, which includes the parallel combination of c and  $G_1$ , thus impressing  $v_1(t)$  upon the resistance  $1/G$  in series with branch a for  $nT \leq t < (n+\delta)T$ , and opening the circuit for  $(n+\delta)T \leq t < (n+1)T$ , during which the capacitor discharges through its shunting resistance  $1/G_1$ . The identical process is applied to branch b but with a delay of  $T/2$ .

Considerable simplification can be achieved by breaking the 3-terminal synchronous switch into its equivalent two 2-terminal switches as outlined in Sub-section II.2.3.

- i) For  $nT \leq t < (n+\delta)T$ , the voltage  $v_2(t)$  is identical to the voltage appearing across the capacitor of

branch "a". This voltage may be considered as the superposition of three parts, each contributed to by a separate input as explained below:

a) Contribution due to  $v_1(t)$ :

By assuming that during the periods  $(n+\delta)T \leq t < (n+1)T$ ,  $n = 0, 1, 2, \dots$ , the 2-terminal switch, in series with branch a, is still closing the circuit, and the voltage  $v_1(t)$  is short-circuited (these assumptions are not true and their effect will be nullified in step "c" below), then the effect of  $v_1(t)$  can be obtained by replacing it by  $F_a(t)$  such that

$$F_a(t) = v_1(t) \cdot M_1(t) \quad 4.2.4$$

where

$$M_1(t) = \sum_{n=0}^{n=\infty} [U_{-1}(t-nT) - U_{-1}\{t-(n+\delta)T\}] \quad \dots 4.2.5$$

which is illustrated in Fig. 4.2.1.

In doing so, the voltage  $F_a(t)$  is continuously impressed on the linear network whose transfer function is

$$G(s) = \frac{1/\tau}{s+1/\tau_e} \quad 4.2.6$$

$$\text{where } \tau = c/G \quad 4.2.7$$

$$\text{and } \tau_e = c/(G+G_1+G_2) \quad 4.2.8$$

Therefore the contribution to  $v_2(t)$  due to  $F_a(t)$  can be directly written as

$$v_{21}(t) = \int_{\mathcal{L}}^{-1} F_a(s) G(s) \quad 4.2.9$$

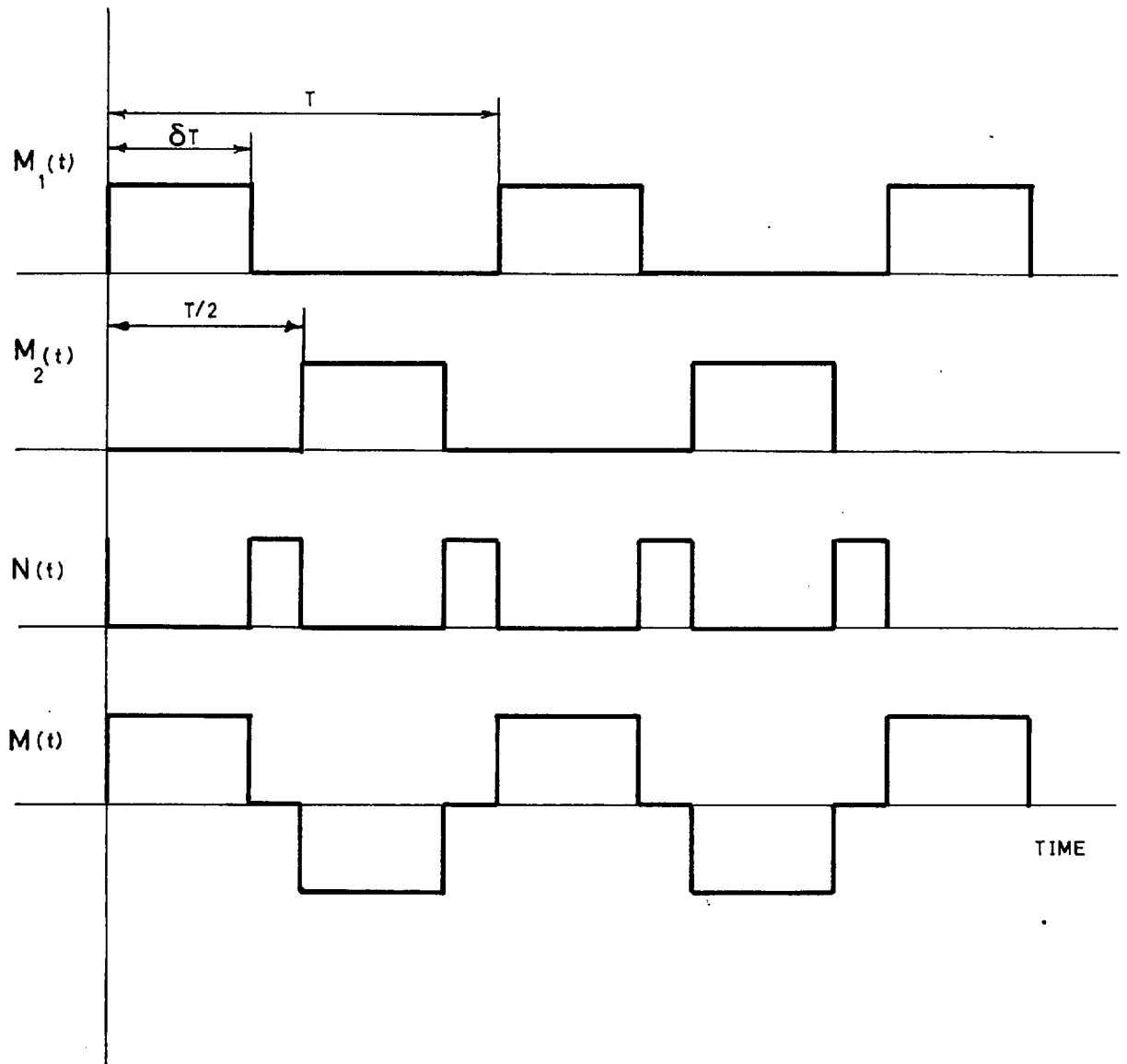


FIG. 4.2.1.

PERIODIC FUNCTIONS OF TIME USEFUL FOR THE ANALYSIS  
OF CHOPPER NETWORKS

- b) Contribution due to the charge appearing on the capacitor at  $t = nT$ :

This essentially represents the initial condition value of charge appearing at the switching instants  $t = nT$ ,  $n = 0, 1, 2, \dots$ , etc., which corresponds to the starting instants of the cyclic transient (see Sub-section I.4.2.4.3). Let the voltage across the capacitor due to this change be denoted by  $\lambda_{a2}(nT)$ . With the same assumption (as in "a" above) of permanent closure of the 2-terminal switch associated with branch a, the contribution to  $v_2(t)$  due to  $\lambda_{a2}(nT)$  can be expressed as

$$v_{22}(t) = \int_{\mathcal{L}}^{-1} \lambda_{a2}^*(s) \cdot \tau \cdot G(s) \quad 4.2.10$$

provided that the effect of  $\lambda_{a2}(mT)$  for  $m < n$  should be eliminated. This will be accomplished in step "c".

- c) Contribution due to  $F_a(t)$  for  $t < nT$  and  $\lambda_{a2}(mT)$  for  $m < n$  be eliminated:

This step is primarily introduced to counterbalance the effect of the wrong assumption made in steps a and b above. This is accomplished by computing first the voltage appearing across the capacitor at  $t = (n+\delta)T$  due to  $F_a(t)$  for  $t < nT$  and  $\lambda_{a2}(mT)$  for  $m < n$ , then nullifying that voltage by introducing an equal voltage but opposite in sense. Denoting this voltage by  $\lambda_{a1}\{(n+\delta)T\}$ , thus its contribution to  $v_2(t)$  can be written as

$$v_{23}(t) = \int_{\mathcal{L}}^{-1} \lambda_{a1}^*(s) \cdot Z_1^{-1} \cdot e^{(1-\delta)TS} \cdot \tau \cdot G(s)$$

The process of computing  $\lambda_{a1} \left\{ \begin{matrix} (n+\delta)T \\ 125, 126 \end{matrix} \right\}$  and  $\lambda_{a2}(nT)$  can be done using sampled-data system as illustrated by the block diagram shown in Fig. 4.2.2. A portion of the block diagram represents the signal flow in the time domain and the other portion in the s-domain. In doing so, convolution processes, which are not easy to represent by block diagrams, are replaced by multiplication processes, which can easily be represented, according to the mathematical rule that convolution in the s-domain corresponds to multiplication in the time domain and vice versa.

The voltage  $v_1(t)$  is derived from the input modulating signal  $x(t)$  according to the relation

$$v_1(t) = E_{md} \sin(\omega t + \theta) \cdot x(t) \quad 4.2.12$$

which is represented in the block diagram by an ideal modulator.  $F_a(t)$  is then derived from  $v_1(t)$  according to Eqn. 4.2.4 which may be represented by an ON-OFF switch functioning according to  $M_1(t)$ .

According to Eqns. 4.2.9, 4.2.10 and 4.2.11, the three signals  $F_a(s)$ ,  $\tau \lambda_{a2}^*(s)$  and  $\tau Z_1^{-1} e^{(1-\delta)TS} \lambda_{a1}^*(s)$  are simultaneously applied to the linear network with transfer function  $G(s)$  to give the voltage across the capacitor of branch a. This is valid only during the periods  $nT \leq t < (n+\delta)T$ ,  $n = 0, 1, 2, \dots$ . In order to compute the voltage across the capacitor at the instants  $(n+\delta)T$ , an ideal sampler may be introduced which operates at  $t = (n+\delta)T$ . The operation of sampling at  $t = (n+\delta)T$  is equivalent to advancing the signal to be sampled by  $\delta T$ , sampling at  $t = nT$ , and then delaying the resulting train of impulses by  $\delta T$ . This technique is used in modified

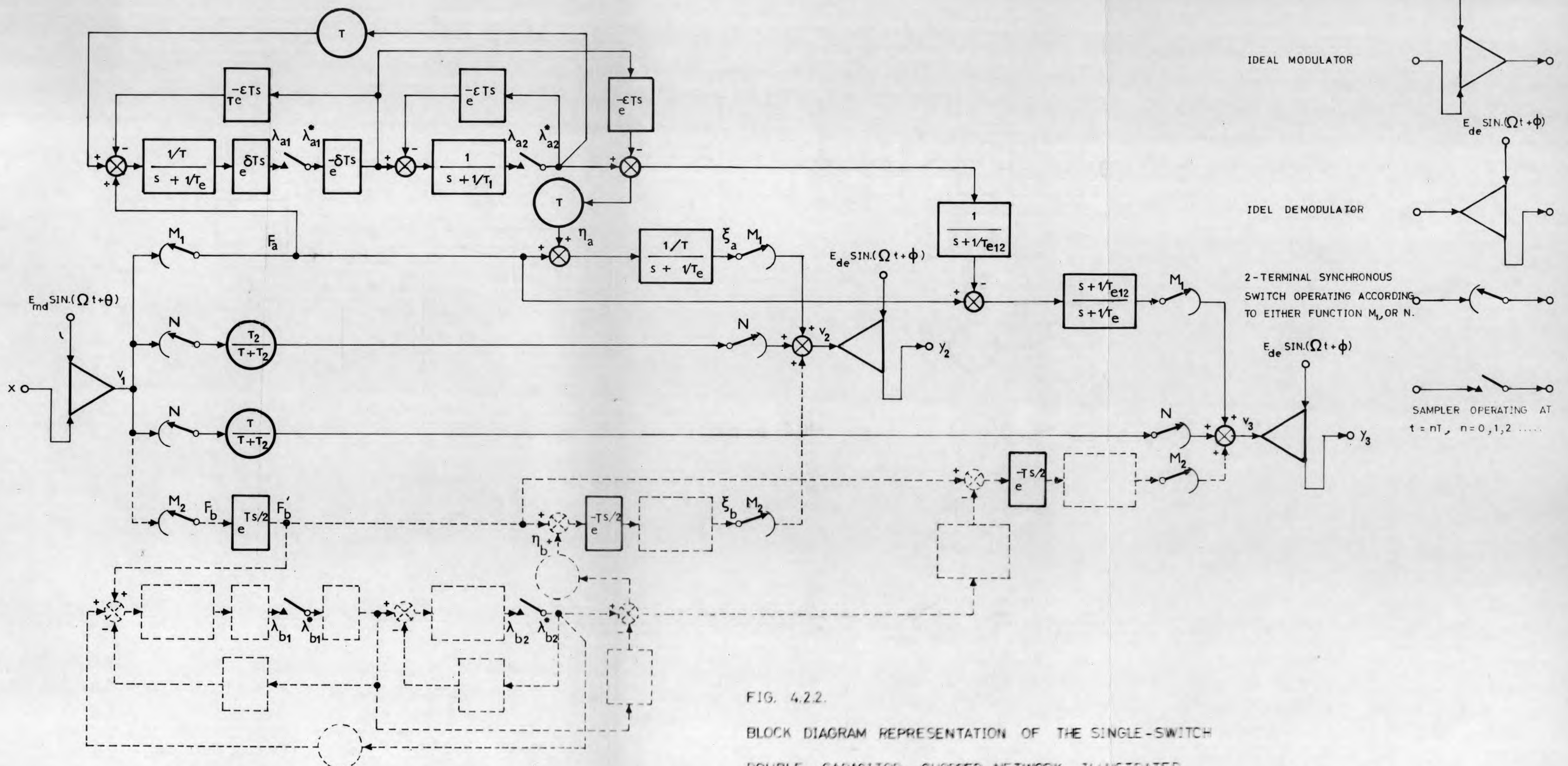


FIG. 4.22.  
 BLOCK DIAGRAM REPRESENTATION OF THE SINGLE-SWITCH  
 DOUBLE-CAPACITOR CHOPPER NETWORK ILLUSTRATED  
 IN FIG. 4.13-a.

Z-transforms.<sup>125,126</sup> Having computed  $\lambda_{a1}^*(s)$ , it is first delayed by  $\delta T$ , then fed back through the block with transfer function  $\tau e^{-\epsilon TS}$  to fulfil step "c" (where  $\epsilon > 0$  is an infinitesimal).

During the period  $(n+\delta)T \leq t < (n+1)T$ , the capacitor of branch a discharges through the resistance  $1/G_1$ . The voltage across the capacitor is therefore

$$\lambda_{a2}(s) = (\lambda_{a1}^*(s) e^{-\delta TS}) G_1(s) \quad 4.2.13$$

where

$$G_1(s) = \frac{1}{s + 1/\tau_1} \quad 4.2.14$$

wherein

$$\tau_1 = c/G_1 \quad 4.2.15$$

In order to compute the voltage at the instants  $nT$ , a sampler may be introduced which operates at  $t = nT$ . The undesired transient that would otherwise appear at the output of the block with transfer function  $G_1(s)$  in Fig. 4.2.2 is eliminated by the feedback of the impulse function  $\lambda_{a2}^*(s)$  through the block with transfer function  $e^{-\epsilon TS}$  (this corresponds to step "c" above). To provide the effect stated in step "b",  $\lambda_{a2}^*(s)$  is fed back through a gain of  $\tau$  as illustrated by the outer feedback path.

- ii) For  $(n+\delta)T \leq t < (n+\frac{1}{2})T$  and for  $(n+\frac{1}{2}+\delta)T \leq t < (n+1)T$ , the voltage  $v_2(t)$  can be easily derived from  $v_1(t)$  by the simple relation

$$v_2(t) = \frac{\tau_2}{\tau + \tau_2} v_1(t) \quad 4.2.16$$



where  $\tau_2 = c/G_2$  4.2.17-a

To show that Eqn. 4.2.16 is only valid during the period specified above, a function  $N(t)$  is introduced such that

$$v_2(t) = \frac{\tau_2}{\tau + \tau_2} v_1(t) N(t) \quad 4.2.17$$

where

$$N(t) = \sum_{n=0}^{n=\infty} \left[ U_{-1} \left\{ t - (n+\delta)T \right\} - U_{-1} \left\{ t - (n+\frac{1}{2})T \right\} \right] \quad 4.2.18$$

which is illustrated in Fig. 4.2.1.

The operation described by Eqn. 4.2.17 is represented in Fig. 4.2.2 where an ON-OFF switch functioning according to  $N(t)$  is introduced.

iii) For  $(n+\frac{1}{2})T \leq t < (n+\frac{1}{2}+\delta)T$ , the voltage  $v_2(t)$  is identical to the voltage appearing across the capacitor of branch "b". From the symmetry between branches a and b, a similar procedure to that outlined in (i) above may be pursued provided that the following changes are made:

a) To account for the delay of  $T/2$  between the identical operations of the 2-terminal switches associated with branches b and a, the function  $F_a(t)$  is replaced by  $F_b(t)$  such that

$$F_b(t) = v_1(t) \cdot M_2(t) \quad 4.2.19$$

where  $M_2(t)$  is defined as

$$M_2(t) = \sum_{n=0}^{n=\infty} \left[ U_{-1} \left\{ t - \left( n + \frac{1}{2} \right) T \right\} - U_{-1} \left\{ t - \left( n + \frac{1}{2} + \delta \right) T \right\} \right]$$

..4.2.20

which is illustrated in Fig. 4.2.1.

- b) Subscript a associated with various variables is replaced by subscript b.
- c) The portion of the block diagram, which includes the sampled-data system particularly employed for the computation of  $\lambda_{b1}^*(s)$  and  $\lambda_{b2}^*(s)$ , is made exactly similar to that used for branch a by means of advancing the signal  $F_b(s)$  by  $T/2$ , sampling at  $t = nT$ , and then retarding the signals  $\lambda_{b1}^*(s)$  and  $\lambda_{b2}^*(s)$  by  $T/2$ . This portion of the block diagram is shown in dotted line in Fig. 4.2.2.

On the basis of the above discussion, the complete response  $v_2(t)$  can be obtained as the sum of three components which correspond to the periods

$$nT \leq t < (n+\delta)T,$$

$$(n+\delta)T \leq t < \left( n + \frac{1}{2} \right) T \quad \text{and} \quad \left( n + \frac{1}{2} + \delta \right) T \leq t < (n+1)T,$$

and  $\left( n + \frac{1}{2} \right) T \leq t < \left( n + \frac{1}{2} + \delta \right) T$ .

To make sure that these three output components are taken only during their assigned periods, three ON-OFF switches are introduced which operate according to the functions  $M_1(t)$ ,

$N(t)$  and  $M_2(t)$  respectively.

Finally, the voltage  $y_2(t)$  is derived from  $v_2(t)$  by the demodulation process

$$y_2(t) = E_{de} \sin(\omega t + \phi) \cdot v_2(t) \quad 4.2.21$$

On similar basis, the complete response  $v_3(t)$  may be considered as the sum of three components corresponding to the periods mentioned above. In this case, two blocks representing the transfer functions

$$G_2(s) = 1/(s + 1/\tau_{e12}) \quad 4.2.22$$

$$\text{and} \quad G_3(s) = (s + 1/\tau_{e12})/(s + 1/\tau_e) \quad 4.2.23$$

$$\text{where} \quad \tau_{e12} = c/(G_1 + G_2) \quad 4.2.24$$

are introduced, as shown in Fig. 4.2.2, so that the signals  $F_a(s)$  and  $F_b(s)$  are impressed on a linear network with transfer function  $G_3(s)$ , whereas  $-\lambda_{a1}^*(s) \cdot Z_1^{-1} e^{(1-\delta)TS}$ ,  $-\lambda_{b1}^*(s) \cdot Z_1^{-1} e^{(1-\delta)TS}$ ,  $\lambda_{a2}^*(s)$ , and  $\lambda_{b2}^*(s)$  are impressed on a linear network with transfer function  $G_2(s) \cdot G_3(s)$  which is equal to  $\tau \cdot G(s)$ .

Block diagram representations of the double-dwitch single-capacitor and of the cascaded inverted double-switch double-capacitor chopper networks, shown in Fig. 4.1.3, can be developed by pursuing similar techniques as outlined above. These block diagrams are shown in Figs. 4.2.3 and 4.2.4 respectively, where

$$M(t) = M_1(t) - M_2(t) \quad , \quad 4.2.25$$



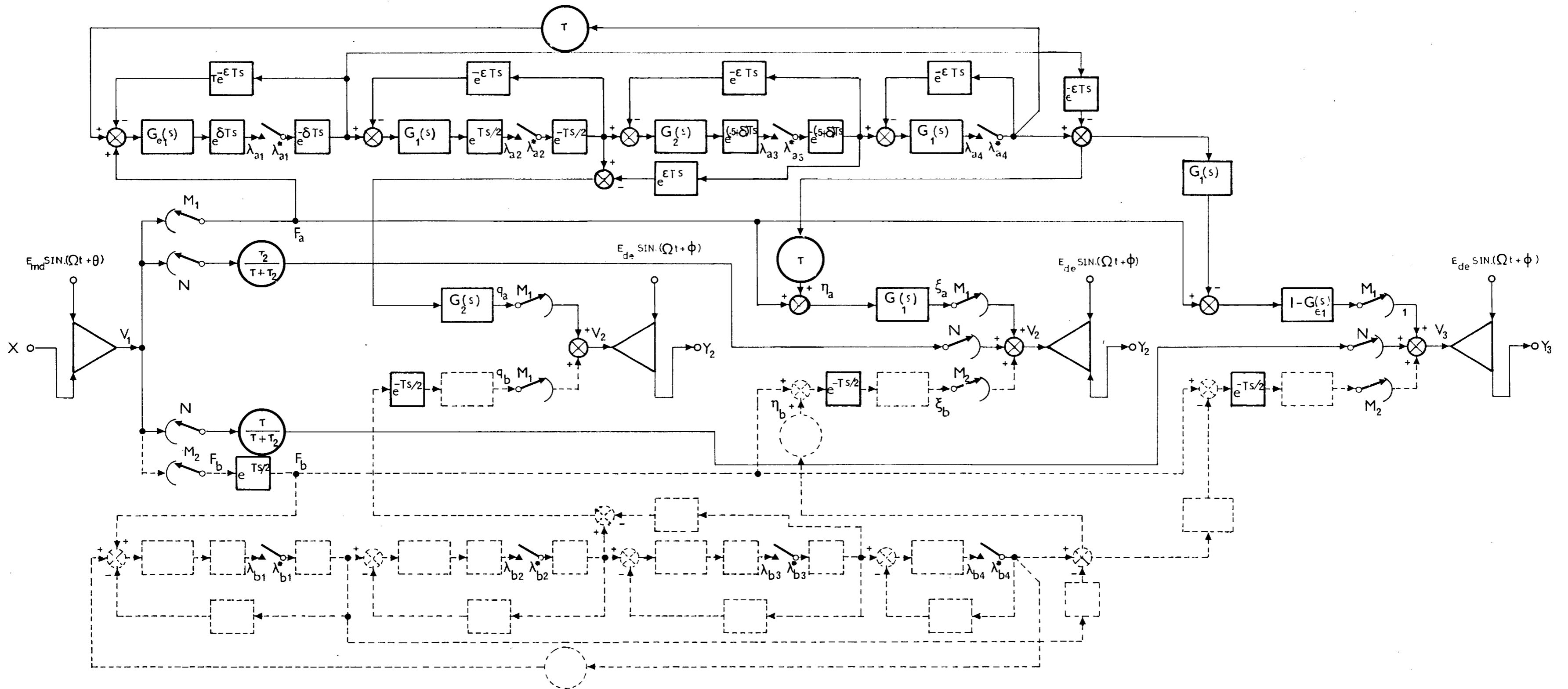


FIG. 4.2.4.

BLOCK DIAGRAM REPRESENTATION OF THE CASCADED INVENTED DOUBLE-SWITCH DOUBLE-CAPACITOR CHOPPER NETWORK ILLUSTRATED IN FIG. 4.1.3-c.

$$G_{e1}(s) = \frac{1/\tau}{s + 1/\tau_{e1}} \quad 4.2.26$$

wherein

$$\tau_{e1} = c/(G + G_1) \quad 4.2.27$$

#### 4.2.2 Derivation of the Z-transform of the voltage appearing across the capacitor

Attention is confined only to Fig. 4.2.2.

i) For branch a:

Establishing the signal relationship around the first sampler, yields

$$\left[ \left\{ F_a(s) + \tau \lambda_{a2}^*(s) - \tau Z_1^{-1} e^{(1-\delta-\epsilon)TS} \lambda_{a1}^*(s) \right\} e^{\delta TS} G(s) \right]^* = \lambda_{a1}^*(s) \quad \dots 4.2.28$$

$$\text{where} \quad Z_1^{-1} = e^{-TS} \quad 4.2.29$$

Similarly, the signal relationship around the second sampler can be set up resulting in

$$\left[ \left\{ Z_1^{-1} e^{(1-\delta)TS} \lambda_{a1}^*(s) - Z_1^{-1} e^{(1-\epsilon)TS} \lambda_{a2}^*(s) \right\} G_1(s) \right]^* = \lambda_{a2}^*(s) \quad \dots 4.2.30$$

Since,

$$\left[ G_1(s) \right]^* = \frac{1}{1 - Z_1^{-1} e^{-T/\tau_1}} \quad 4.2.31$$

Eqn. 4.2.30 can thus be solved and the result may be rearranged to give

$$\lambda_{a2}^*(s) = e^{-(1-\delta)T/\tau_1} Z_1^{-1} \lambda_{a1}^*(s) \quad 4.2.32$$

Substituting Eqn. 4.2.32 into Eqn. 4.2.28, results in

$$\frac{1 - Z_1^{-1} r}{1 - Z_1^{-1} e^{-T/\tau_e}} \cdot \lambda_{a1}^*(s) = \left[ F_a(s) e^{\delta TS} G(s) \right]^* \quad 4.2.33$$

where

$$r = \exp \left\{ -T \left( \frac{1}{\tau_1} + \frac{\delta}{\tau_{e2}} \right) \right\} \quad 4.2.34$$

From the definition<sup>125,126</sup> of Z-transform, the R.H.S. of Eqn. 4.2.33 may be expressed by an infinite summation as written below

$$\left[ F_a(s) e^{\delta TS} G(s) \right]^* = \frac{1}{T} \sum_{L=-\infty}^{L=\infty} F_a(s - j\Omega L) e^{\delta T(s - j\Omega L)} G(s - j\Omega L) \quad 4.2.35$$

To determine the Z-transform of the voltage appearing across the capacitor  $\lambda_{a2}^*(nT)$ ,  $n = 0, 1, 2, \dots$ , Eqns. 4.2.33 and 4.2.35 are substituted in Eqn. 4.2.32, resulting in

$$\lambda_{a2}^*(s) = \frac{e^{-(1-\delta)T/\tau_1} Z_1^{-1} (1 - Z_1^{-1} e^{-T/\tau_e})}{(1 - Z_1^{-1} r)} \cdot \frac{1}{T} \sum_{L=-\infty}^{L=\infty} \left[ F_a(s - j\Omega L) e^{\delta T(s - j\Omega L)} \cdot G(s - j\Omega L) \right] \quad 4.2.36$$

ii) For branch b:

By using an analogous approach as outlined above in connection with branch a, the following relationships can be easily derived:

$$\lambda_{b2}^*(s) = e^{-(1-\delta)T/\tau_1} z_1^{-1} \lambda_{a1}^*(s), \quad 4.2.37$$

$$\frac{1 - z_1^{-1} r}{1 - z_1^{-1} e^{-T/\tau_1}} \cdot \lambda_{b1}^*(s) = \left[ F_b'(s) e^{\delta TS} G(s) \right]^* \quad 4.2.38$$

$$\text{and} \quad \lambda_{b2}^*(s) = \frac{e^{-(1-\delta)T/\tau_1} z_1^{-1} (1 - z_1^{-1} e^{-T/\tau_1})}{(1 - z_1^{-1} r)} \cdot \frac{1}{T} \sum_{L=-\infty}^{L=\infty} \left[ F_b'(s - j\Omega L) \cdot e^{\delta T(s - j\Omega L)} G(s - j\Omega L) \right] \quad 4.2.39$$

where

$$F_b'(s) = e^{TS/2} \cdot F_b(s) \quad 4.2.40$$

The corresponding formulae for Figs. 4.2.3 and 4.2.4 are given in Appendices B.1.1 and C.1.1 respectively.

#### 4.2.3 Determination of the output voltage

Fig. 4.2.2 shows that two possible outputs can be obtained from such system termed as  $y_2$  and  $y_3$ . Determination of either of them may be considerably simplified by considering the contribution of various signals during the periods

$$nT \leq t < (n+\delta)T,$$

$$(n+\frac{1}{2})T \leq t < (n+\frac{1}{2}+\delta)T;$$

$$\text{and} \quad (n+\delta)T \leq t < (n+\frac{1}{2})T \quad \text{and} \quad (n+\frac{1}{2}+\delta)T \leq t < (n+1)T$$



then superposing the three contributions.

Focussing the attention to the output  $y_2$ , then:

4.2.3.1 Contribution during the periods  
 $nT \leq t < (n+\delta)T$  :

The contribution due to channel a is given by  $\zeta_a(s)$  which may be expressed as

$$\zeta_a(s) = \tau \left[ \lambda_{a2}^*(s) - e^{(1-\delta-\varepsilon)TS} Z_1^{-1} \lambda_{a1}^*(s) \right] \quad \dots 4.2.41$$

According to the block diagram of Fig. 4.2.2, the signal  $\zeta_a(s)$  adds to  $F_a(s)$  before being impressed on the block with transfer function  $G(s)$  resulting in

$$\xi_a(s) = \left[ F_a(s) + \zeta_a(s) \right] G(s) \quad 4.2.42$$

Thus, the contribution to the output may be obtained, in the time domain, as follows

$$y_{21}(t) = \xi_a(t) \cdot M_1(t) \cdot E_{de} \sin(\Omega t + \theta) \quad \dots 4.2.43$$

Since the form of  $y_{21}(t)$  is similar to that of  $F_a(t)$ , the procedure used in Appendix D.1 is thus readily applicable to obtain the transform of  $y_{21}(t)$ . This gives

$$y_{21}(s) = E_{de} \sum_{n=-\infty}^{n=\infty} R_2(\theta, n) \xi_a(s - j\Omega n) \quad \dots 4.2.44$$

where  $R_2(\theta, n)$  may be deduced from Eqn. D.1.10 provided the following changes are made

$$\begin{array}{l} \theta \text{ is replaced by } \emptyset \\ m \text{ " " " " } n \end{array} \quad 4.2.45$$

On substitution of Eqns. 4.2.32, 4.2.36, 4.2.41, 4.2.42, and D.1.12 into Eqn. 4.2.44 and rearranging the result, yields

$$\begin{aligned} y_{21}(s) &= E_{md} E_{de} \sum_{n=-\infty}^{n=\infty} \sum_{m=-\infty}^{m=\infty} R_2(\emptyset, n) R_2(\theta, m) G(s-j\Omega n) x\{s-j\Omega(n+m)\} \\ &+ E_{md} E_{de} \frac{\tau}{T} \frac{Z_1^{-1} (1-Z_1^{-1} e^{-T/\tau})}{(1-Z_1^{-1} r)} \sum_{n=-\infty}^{n=\infty} \sum_{L=-\infty}^{L=\infty} \sum_{m=-\infty}^{m=\infty} R_2(\emptyset, n) \\ R_2(\theta, m) G(s-j\Omega n) &\left[ e^{-\frac{(1-\delta)T}{\tau_1}} e^{(1-\delta)T(s-j\Omega n)} \right] G\{s-j\Omega(L+n)\} \\ &e^{\delta T} \{s-j\Omega(L+n)\} x\{s-j\Omega(n+m+L)\} \end{aligned} \quad 4.2.46$$

#### 4.2.3.2 Contribution during the periods $(n+1/2)T \leq t < (n+1/2+\delta)T$ .

The contribution to the output may be formulated from the block diagram of Fig. 4.2.2 on similar basis as outlined in Sub-section 4.2.3.1 above. This may be written in the time domain as

$$y_{22}(t) = \xi_b(t) \cdot M_2(t) \cdot E_{de} \sin(\Omega t + \emptyset) \quad 4.2.47$$

$$\text{where } \xi_b(s) = \left[ F_b(s) + \zeta_b(s) e^{-TS/2} \right] G(s) \quad 4.2.48$$

wherein

$$\zeta_b(s) = \tau \left[ \lambda_{b2}^*(s) - e^{(1-\delta-\epsilon)TS} Z_1^{-1} \lambda_{a1}^*(s) \right] \quad \dots 4.2.49$$

Employing similar techniques as outlined in Appendix D.2, Eqn. 4.2.47 may be transformed to give the expression

$$y_{22}(s) = -E_{de} \sum_{n=-\infty}^{n=\infty} R_2(\emptyset, n) e^{-j\pi n} \xi_b(s-j\Omega n) \quad 4.2.50$$

Eqn. 4.2.50 may be expanded, using the results of Eqns. 4.2.37, 4.2.39, 4.2.40, 4.2.48, 4.2.49 and D.2.4, to give

$$\begin{aligned} y_{22}(s) = & E_{md} E_{de} \sum_{n=-\infty}^{n=\infty} \sum_{m=-\infty}^{m=\infty} R_2(\emptyset, n) R_2(\emptyset, m) G(s-j\Omega n) \times \left\{ s-j\Omega(n+m) \right\} \\ & e^{j\pi(n+m)} \\ & + E_{md} E_{de} \frac{\tau}{T} \frac{Z_1^{-1} (1-Z_1^{-1} e^{-T/\tau})}{(1-Z_1^{-1} r)} \sum_{n=-\infty}^{n=\infty} \sum_{L=-\infty}^{L=\infty} \sum_{m=-\infty}^{m=\infty} R_2(\emptyset, n) R_2(\emptyset, m) \\ & G(s-j\Omega n) \left[ e^{-(1-\delta)T/\tau_1} - e^{(1-\delta)T(s-j\Omega n)} \right] G\left\{ s-j\Omega(L+n) \right\} \\ & e^{\delta T\left\{ s-j\Omega(L+n) \right\}} \times \left\{ s-j\Omega(n+m+L) \right\} e^{-j\pi(n+m+L)} \quad 4.2.51 \end{aligned}$$

4.2.3.3 Contribution during the periods  
 $(n+\delta)T \leq t < (n+1/2)T$  and  
 $(n+1/2+\delta)T \leq t < (n+1)T$ :

In the time domain, it can be deduced from the block diagram of Fig. 4.2.2 and thus

$$y_{23}(t) = x(t) \cdot E_{md} \sin(\Omega t + \theta) \cdot N(t) \cdot \frac{\tau_2}{\tau + \tau_2} \cdot E_{de} \sin(\Omega t + \phi) \quad \dots 4.2.52$$

This can be rearranged to give

$$y_{23}(t) = \frac{E_{md} E_{de}}{2} \cdot \frac{\tau_2}{\tau + \tau_2} x(t) \cdot [\cos(\theta - \phi) - \cos(2\Omega t + \theta + \phi)] \cdot N(t) \quad \dots 4.2.53$$

which yields on transformation

$$y_{23}(s) = \frac{E_{md} E_{de}}{2} \cdot \frac{\tau_2}{\tau + \tau_2} \left[ x(s) * \left\{ \frac{\cos(\theta - \phi)}{s} - \frac{e^{j(\theta + \phi)}}{2(s - j2\Omega)} - \frac{e^{-j(\theta + \phi)}}{2(s + j2\Omega)} \right\} \right] * N(s) \quad \dots 4.2.54$$

where

$$N(s) = \int_0^{\infty} N(t) e^{-sT} dt = \frac{e^{-\delta TS}}{s} \left[ \frac{1 - e^{-\frac{1}{2}TS}}{1 - e^{-TS/2}} \right] \quad 4.2.55$$

The first convolution may be written as

$$x'(s) = \frac{1}{2\pi j} \int_{c_1 - \infty}^{c_1 + \infty} x(s-p) \left\{ \frac{\cos(\theta - \phi)}{p} - \frac{e^{j(\theta + \phi)}}{2(p - j2\Omega)} - \frac{e^{-j(\theta + \phi)}}{2(p + j2\Omega)} \right\} dp \quad \dots 4.2.56$$

where  $c_1 < [\Re s]$  is greater than the abscisse of the

absolute convergence of

$$\frac{\cos(\theta - \phi)}{p} = \frac{e^{j(\theta + \phi)}}{2(p - j2\Omega)} + \frac{e^{-j(\theta + \phi)}}{2(p + j2\Omega)} \quad 4.2.57$$

Applying the method of residues to solve the convolution integral, expressed by Eqn. 4.5.56, would yield

$$x'(s) = \cos(\theta - \phi) \cdot x(s) - \frac{1}{2} \left[ e^{j(\theta + \phi)} x(s - j2\Omega) + e^{-j(\theta + \phi)} x(s + j2\Omega) \right] \quad \dots 4.2.58$$

Substituting Eqn. 4.2.58 into Eqn. 4.2.54 and rearranging, then

$$y_{23}(s) = \frac{E_{md} E_{de}}{2} \cdot \frac{\tau_2}{\tau_1 + \tau_2} \cdot \frac{1}{2\pi j} \int_{c_1 - j\infty}^{c_1 + j\infty} x'(s-p) \cdot N(p) dp \quad \dots 4.2.59$$

Applying the method of residue once more where the poles of  $N(p)$  lie at the solution

$$p = j2\Omega m \quad 4.2.60$$

where  $m$  is an integer that can take all possible values lying between  $-\infty$  to  $\infty$ . The corresponding residues can be evaluated from  $N(p)$  as follows

$$R_3(m) = \frac{e^{-\delta T p} (1 - e^{-(\frac{1}{2} - \delta) T p})}{\frac{d}{dp} [1 - e^{-T p / 2}]} \Bigg|_{\text{at } p = j2\Omega m}$$

$$= \frac{1}{2\pi jm} \left[ e^{-j4\pi\delta m} - e^{-j2\pi m} \right] \quad 4.2.61$$

which may be rearranged into the suitable form

$$R_3(m) = -2\delta e^{-j2\pi\delta m} \frac{\sin 2\pi\delta m}{2\pi\delta m} \quad 4.2.62$$

this is valid for all values of  $m$  except for  $m = 0$  at which the residue may be evaluated by taking the limiting value of Eqn. 4.2.61 as  $m$  tends to zero, i.e.

$$R_3(0) = \lim_{m \rightarrow 0} R_3(m) = \frac{1}{2\pi j} \left. \frac{\frac{d}{dm} [e^{-j4\pi\delta m} - e^{-j2\pi m}]}{\frac{d}{dm} (m)} \right|_{\text{at } m = 0}$$

$$= 1 - 2\delta \quad 4.2.63$$

On substitution of Eqns. 4.2.61 and 4.2.58 into Eqn. 4.2.59, gives

$$y_{23}(s) = \frac{E_{md} E_{de}}{2} \cdot \frac{\tau_2}{\tau_1 + \tau_2} \sum_{m=-\infty}^{m=\infty} R_3(m) \left[ \cos(\theta - \phi) \cdot x(s - j2\omega m) \right. \\ \left. - \frac{e^{j(\theta + \phi)}}{2} x\{s - j(m+1)2\omega\} - \frac{e^{-j(\theta + \phi)}}{2} x\{s - j(m-1)2\omega\} \right]$$

..4.2.64

From the results of Eqns. 4.2.46, 4.2.51 and 4.2.64, an expression for the output  $y_2(s)$  can be obtained according to the relationship

$$y_2(s) = y_{21}(s) + y_{22}(s) + y_{23}(s) \quad 4.2.65$$

With an analogous procedure, the output  $y_3(s)$  can be determined. This may be written in the form

$$y_3(s) = y_{31}(s) + y_{32}(s) + y_{33}(s) \quad 4.2.66$$

where the three constituent terms can be deduced as given by the expressions below

$$y_{31}(s) = E_{md} E_{de} \sum_{n=-\infty}^{m=\infty} \sum_{m=-\infty}^{m=\infty} \left[ R_2(\emptyset, n) R_2(\emptyset, m) \times \left\{ s - j\Omega(n+m) \right\} \right] - y_{21}(s) \quad 4.2.67$$

$$y_{32}(s) = E_{md} E_{de} \sum_{n=-\infty}^{n=\infty} \sum_{m=-\infty}^{m=\infty} \left[ R_2(\emptyset, n) R_2(\emptyset, m) \times \left\{ s - j\Omega(n+m) \right\} e^{-j\pi(n+m)} \right] - y_{22}(s) \quad 4.2.68$$

and

$$y_{33}(s) = \frac{\tau}{\tau_2} y_{23}(s) \quad 4.2.69$$

#### 4.2.4 Derivation of the multiplicative modulation transfer function

Inspecting the details of Eqns. 4.2.65 and 4.2.66 shows that the output signals yield not only the input signal but also an infinite series of carrier harmonics. The coefficients of the harmonic, however, diminish very rapidly as the order of the harmonic increases. Therefore, if all the high harmonic components are neglected, a linear

relationship between the output and input signal transforms can be established which may be referred to as the multiplicative modulation transfer function  $G_{mm}(s)$ . In mathematical terms,  $G_{mm}(s)$  can be defined as follows for the case of the output  $y_2(s)$

$$G_{mm2}(s) = \frac{y_2(s) \left[ \text{neglecting harmonic terms} \right]}{x(s)} \cdot \frac{1}{\left( \frac{E_{md} E_{de}}{2} \right)}$$

..4.2.70

where the division factor  $\left( \frac{E_{md} E_{de}}{2} \right)$  is introduced for the same reason explained earlier in Sub-section 3.3.2.

Collecting the terms containing only  $x(s)$  of Eqns. 4.2.46, 4.2.51 and 4.2.64 and substituting the results into Eqn. 4.2.70, thus

$$\begin{aligned} G_{mm2}(s) = & 4 \sum_{n=-\infty}^{n=\infty} R_2(\phi, n) R_2(\theta, -n) G(s-j\Omega n) \\ & + \frac{4\tau}{T} \cdot \frac{Z_1^{-1} (1-Z_1^{-1} e^{-T/\tau_1})}{(1-Z_1^{-1} r)} \left[ \sum_{n=-\infty}^{n=\infty} R_2(\phi, n) G(s-j\Omega n) \right. \\ & \left. \left\{ e^{-\frac{(1-\delta)T}{\tau_1} - e^{(1-\delta)T(s-j\Omega n)}} \right\} \left[ \sum_{m=-\infty}^{m=\infty} R_2(\theta, m) G(s+j\Omega m) \right] \right. \\ & \left. e^{\delta T(s+j\Omega m)} \right] \\ & + \frac{\tau_2}{\tau+\tau_2} \left[ (1-2\delta) \cos(\theta-\phi) + \frac{1}{\pi} \sin(2\pi\delta) \cos(2\pi\delta+\theta+\phi) \right] \end{aligned}$$

..4.2.71



Similarly, for the output  $y_3(s)$ , the multiplicative modulation transfer function may be written as

$$\begin{aligned}
 G_{mm3}(s) &= \frac{y_3(s) \left[ \text{neglecting harmonic terms} \right]}{x(s)} \cdot \frac{1}{(E_{md} E_{de}/2)} \\
 &= 4 \sum_{n=-\infty}^{n=\infty} R_2(\phi, n) R_2(\theta, -n) \\
 &= 4 \sum_{n=-\infty}^{n=\infty} R_2(\phi, n) R_2(\theta, -n) G(s - j\Omega n) \\
 &= \frac{4\tau}{T} \frac{Z_1^{-1} (1 - Z_1^{-1} e^{-T/\tau_1})}{(1 - Z_1^{-1} r)} \left[ \sum_{n=-\infty}^{n=\infty} R_2(\phi, n) G(s - j\Omega n) \right. \\
 &\quad \left. \left\{ e^{-(1-\delta)T/\tau_1} - e^{(1-\delta)T(s - j\Omega n)} \right\} \left[ \sum_{m=-\infty}^{m=\infty} R_2(\theta, m) G(s + j\Omega m) \right] \right. \\
 &\quad \left. \left. e^{\delta T(s + j\Omega m)} \right] \right. \\
 &+ \frac{\tau}{\tau + \tau_2} \left[ (1 - 2\delta) \cos(\theta - \phi) + \frac{1}{\pi} \sin(2\pi\delta) \cos(2\pi\delta + \theta + \phi) \right]
 \end{aligned}$$

..4.2.72

#### 4.2.5 Closed form for the multiplicative modulation transfer function.

The multiplicative modulation transfer functions derived in the previous Sub-section are of infinite series form. This renders it very difficult to compute accurately

their frequency loci. It is, therefore, desirable to obtain the alternative closed forms for such functions.

It is evident from Eqns. 4.2.71 and 4.2.72 that both  $G_{mm2}(s)$  and  $G_{mm3}(s)$  contain common infinite series terms. Economising the effort can therefore be achieved by analysing each infinite series separately as outlined below:

$$4.2.5.1. \quad I_1 = 4 \sum_{n=-\infty}^{m=\infty} R_2(\theta, n) R_2(\theta, -n) \quad 4.2.73$$

Multiplying and dividing by the  $Z$ -transform of a unit step function,  $I_1$  becomes

$$I_1 = 4(1-Z_1^{-1}) \sum_{n=-\infty}^{n=\infty} R_2(\theta, n) R_2(\theta, -n) \frac{1}{1 - e^{-T(s-jn\Omega)}} \quad \dots 4.2.74$$

The resulting infinite series in Eqn. 4.2.74 can be proved to be equivalent to a contour integral, thus Eqn. 4.2.74 may be rewritten as

$$I_1 = 4(1-Z_1^{-1}) \cdot \frac{1}{2\pi j} \int_{c_1-j\infty}^{c_1+j\infty} \frac{1}{1-e^{-Tp}} \cdot Q_1(s-p) dp \quad 4.2.75$$

where

$$Q_1(s) = \frac{1}{4T} \cdot \frac{1}{1-e^{-Ts}} \left[ e^{j\theta} \frac{\{1-e^{-\delta T(s-j\Omega)}\}}{(s-j\Omega)} - e^{-j\theta} \frac{\{1-e^{-\delta T(s+j\Omega)}\}}{(s+j\Omega)} \right] \\ \left[ e^{j\theta} \frac{\{1-e^{\delta T(s+j\Omega)}\}}{(s+j\Omega)} - e^{-j\theta} \frac{\{1-e^{\delta T(s-j\Omega)}\}}{(s-j\Omega)} \right] \quad 4.2.76$$

From the definition of Z-transform, the contour integral included in Eqn. 4.2.75 is seen to be equivalent to the Z-transform of  $Q_1(s)$ , therefore Eqn. 4.2.75 may be rewritten as

$$I_1 = 4 (1 - Z_1^{-1}) \cdot Q_1^*(s) \quad 4.2.77$$

Expression for  $Q_1^*(s)$  is obtained in Appendix D.3. Substituting this expression, described by Eqn. D.3.3, into Eqn. 4.2.77, results in

$$I_1 = 2\delta \cos(\theta - \theta) - \frac{1}{\pi} \sin 2\pi\delta \cos(2\pi\delta + \theta + \theta) \quad 4.2.78$$

$$4.2.5.2. \quad I_2 = \sum_{n=-\infty}^{n=\infty} R_2(\theta, n) G(s - j\Omega n) \left\{ e^{-(1-\delta)T/\tau_1} - e^{(1-\delta)T(s - j\Omega n)} \right\} \quad \dots 4.2.79$$

By inspection, Eqn. 4.2.79 can be replaced by an equivalent contour integral as given below:

$$I_2 = \frac{1}{2\pi j} \int_{c_1 - j\infty}^{c_1 + j\infty} G(p) \left\{ e^{-(1-\delta)T/\tau_1} - e^{(1-\delta)Tp} \right\} \cdot Q_2(s-p) dp \quad \dots 4.2.80$$

where

$$Q_2(s) = \frac{1}{2j} \cdot \frac{1}{1 - e^{-Ts}} \left[ e^{j\theta} \frac{\{1 - e^{-\delta T(\delta - j\Omega)}\}}{(s - j\Omega)} - j\theta \frac{\{1 - e^{-\delta T(\delta + j\Omega)}\}}{(s + j\Omega)} \right] \quad \dots 4.2.81$$

In effecting the contour integration of Eqn. 4.2.80, one can enclose the poles of  $Q_2(s-p)$  in the right half of the  $p$ -plane as shown in Fig. 4.2.5, or alternatively, one may enclose the left half plane as shown in Fig. 4.2.6 provided the integral is zero along the infinite semi-circle in both the right and left half-planes<sup>125,126</sup>.

From the above it follows that Eqn. 4.2.80 can be written in either one of two ways as demonstrated below

$$I_2 = \frac{1}{2\pi j} \oint G(p) \left\{ e^{-(1-\delta)T/\tau_1} - e^{(1-\delta)Tp} \right\} \cdot Q_2(s-p) dp$$

..4.2.82

$$\text{or} = \frac{1}{2\pi j} \oint G(p) \left\{ e^{-(1-\delta)T/\tau_1} - e^{(1-\delta)Tp} \right\} \cdot Q_2(s-p) dp$$

..4.2.83

It is noticed that the line integral expressed by Eqn. 4.2.82 is equivalent to integration in the negative sense along the closed integral in the right half of the  $p$ -plane, since the integral is zero along the infinite semi-circle. Likewise, the line integral expressed by Eqn. 4.2.83 is equivalent to integration in a positive sense along the closed contour formed by the line and the infinite semi-circle in the left half-plane of complex frequency  $p$ . Thus Cauchy's integral formula which gives the value of the integral can be applied as follows

$$\frac{1}{2\pi j} \oint G(p) \left\{ e^{-(1-\delta)T/\tau_1} - e^{(1-\delta)Tp} \right\} \cdot Q_2(s-p) dp$$

= - (sum of the residues of the integrand  
at the poles enclosed) 4.2.84

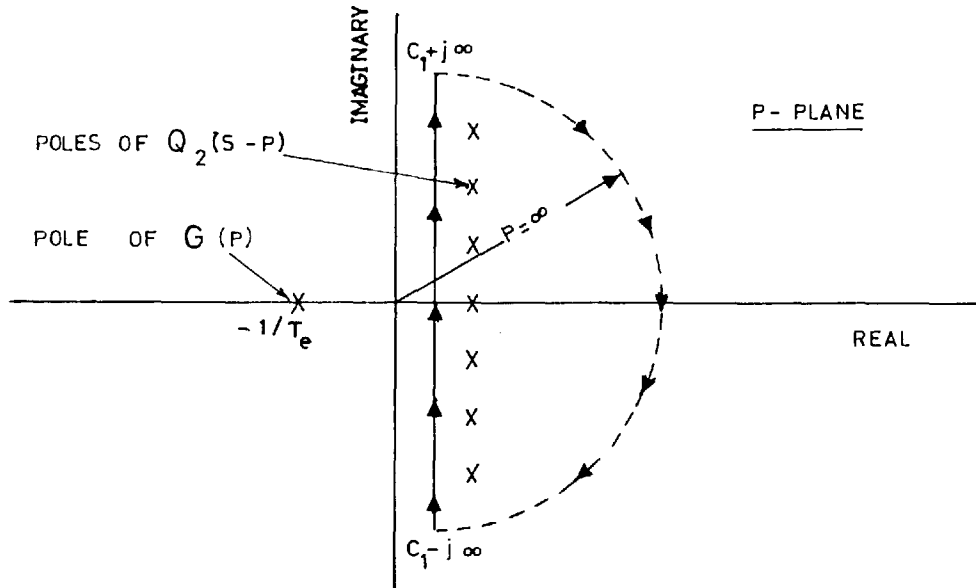


FIG. 4.2.5.

PATHS OF INTEGRATIONS ALONG THE LINE  $C-j\infty$  TO  $C+j\infty$  AND IN THE RIGHT HALF OF THE P- PLANE

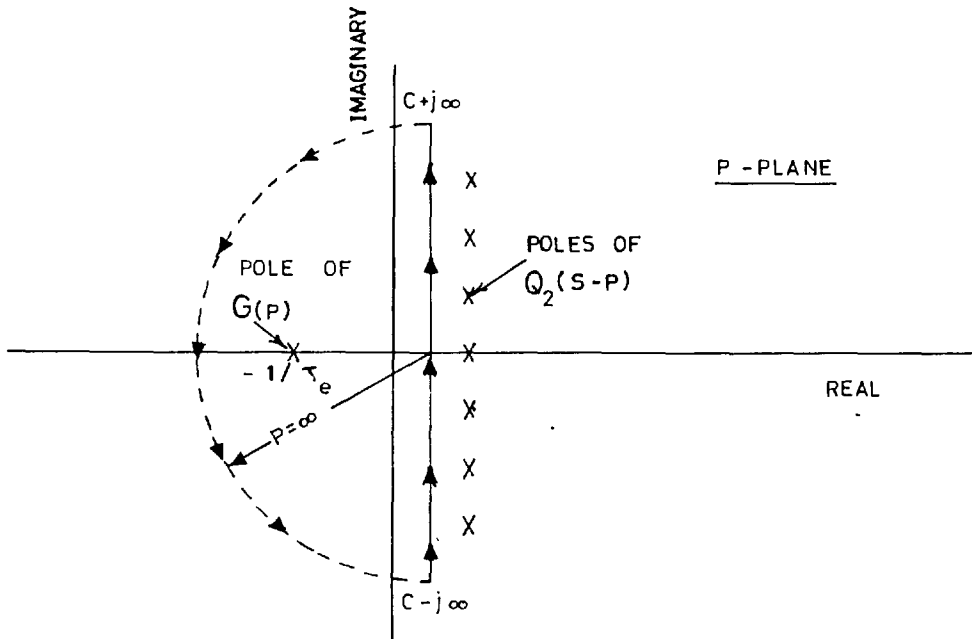


FIG. 4.2.6.

PATH OF INTEGRATION IN THE LEFT HALF OF THE P- PLANE

$$\text{and } \frac{1}{2\pi j} \oint G(p) \left\{ e^{-(1-\delta)T/\tau_1} - e^{(1-\delta)Tp} \right\} \cdot Q_2(s-p) dp$$

$$= (\text{sum of the residues of the integrand at the poles enclosed}) \quad 4.2.85$$

In effecting the contour integration by applying Eqn. 4.2.84, the infinite series expressed by Eqn. 4.2.79 would result; because of the infinite number of poles enclosed. Alternatively, if Eqn. 4.2.85 is applied, only one pole is enclosed which lies at

$$p = -1/\tau_e \quad 4.2.86$$

and the corresponding residue is

$$\frac{1}{\tau} \left\{ e^{-(1-\delta)T/\tau_1} - e^{-(1-\delta)T/\tau_e} \right\} \quad 4.2.87$$

Substituting Eqns. 4.2.86 and 4.2.87 into Eqn. 4.2.80, a closed form for the infinite series can be obtained as expressed below

$$I_2 = \frac{1}{\tau} \left[ \left\{ e^{-(1-\delta)T/\tau_1} - e^{-(1-\delta)T/\tau_e} \right\} / \left\{ 1 - e^{-T(s+1/\tau_e)} \right\} (s+1/\tau_e)^2 + \Omega^2 \right]$$

$$\left[ \left\{ \Omega \cos\phi + (s+1/\tau_e) \sin\phi \right\} - e^{-\delta T(s+1/\tau_e)} \left\{ \Omega \cos(2\pi\delta + \phi) + (s+1/\tau_e) \sin(2\pi\delta + \phi) \right\} \right] \quad 4.2.88$$

$$4.2.5.3. \quad I_3 = \sum_{m=-\infty}^{m=\infty} R_2 \left( \begin{matrix} \theta \\ \uparrow \\ m \end{matrix} \right) G(s+j\Omega m) e^{\delta T(s+j\Omega m)} \quad \dots 4.2.89$$

This can be replaced by the equivalent contour integral

$$I_3 = \frac{1}{2\pi j} \int_{c_1 - \infty}^{c_1 + \infty} G(p) e^{\delta T p} Q_3(s-p) dp \quad 4.2.90$$

where

$$Q_3(s) = \frac{-1}{2j} \cdot \frac{1}{1 - e^{-Ts}} \left[ e^{j\theta} \left\{ \frac{1 - e^{\delta T(s+j\Omega)}}{(s+j\Omega)} \right\} - e^{-j\theta} \left\{ \frac{1 - e^{\delta T(s-j\Omega)}}{(s-j\Omega)} \right\} \right] \quad \dots 4.2.91$$

On similar lines as in Sub-section 4.2.5.2 above, the contour integration may be effected in the left half of the  $p$ -plane, where  $G(p)$  contains only one enclosed pole at  $p = -1/\tau_e$ , in order that a closed form may be obtained. The residue at this pole is  $(e^{-\delta T/\tau_e}/\tau)$ . Thus

$$I_3 = \frac{e^{-\delta T/\tau}}{\tau} e \left[ \left\{ \Omega \cos \theta - (s+1/\tau_e) \sin \theta \right\} - e^{\delta T(s+1/\tau_e)} \left\{ \Omega \cos(2\pi\delta + \theta) - (s+1/\tau_e) \sin(2\pi\delta + \theta) \right\} \right] \\ \hline \left[ 1 - e^{-T(s+1/\tau_e)} \right] \left[ (s+1/\tau_e)^2 + \Omega^2 \right] \quad \dots 4.2.92$$

$$4.2.5.4. \quad I_4 = \sum_{n=-\infty}^{n=\infty} R_2(\emptyset, n), R_2(\theta, -n) G(s-j\Omega n) \quad \dots 4.2.93$$

This again may be replaced by the equivalent contour integral

$$I_4 = \frac{1}{2\pi j} \int_{c_1 - j\infty}^{c_1 + j\infty} G(p) \cdot Q_1(s-p) dp \quad 4.2.94$$

where  $Q_1(s)$  is expressed by Eqn. 4.2.76.

On the basis of the above treatment, the contour integral may be evaluated in the left half of the p-plane where only one enclosed pole at  $-1/\tau_e$  and the corresponding residue is  $1/\tau$ . Thus

$$\begin{aligned}
 I_4 = & \left[ \frac{1}{\tau T} / \left\{ 1 - e^{-T(s+1/\tau_e)} \right\} \left\{ (s+1/\tau_e)^2 + \Omega^2 \right\}^2 \right] \\
 & \left[ \left\{ \Omega \cos \phi + (s+1/\tau_e) \sin \phi \right\} - e^{-\delta T(s+1/\tau_e)} \left\{ \Omega \cos(2\pi\delta + \phi) \right. \right. \\
 & \quad \left. \left. + (s+1/\tau_e) \sin(2\pi\delta + \phi) \right\} \right] \\
 & \left[ \left\{ \Omega \cos \theta - (s+1/\tau_e) \sin \theta \right\} - e^{\delta T(s+1/\tau_e)} \left\{ \Omega \cos(2\pi\delta + \theta) \right. \right. \\
 & \quad \left. \left. - (s+1/\tau_e) \sin(2\pi\delta + \theta) \right\} \right] \quad 4.2.95
 \end{aligned}$$

Substituting the results of Eqns. 4.2.78, 4.2.88, 4.2.92 and 4.2.95 into Eqns. 4.2.71 and 4.2.72, closed forms for  $G_{mm2}(s)$  and  $G_{mm3}(s)$  can be obtained

$$\begin{aligned}
 G_{mm2}(s) = & \frac{\tau_2}{\tau + \tau_2} \left\{ (1-2\delta) \cos(\phi - \theta) + \frac{1}{\pi} \sin(2\pi\delta) \cos(2\pi\delta + \theta + \phi) \right\} \\
 & + 4 I_4 \left[ \frac{1 - Z_1^{-1} e^{-T/\tau_e}}{1 - Z_1^{-1} r} \right] \quad 4.2.96
 \end{aligned}$$

and

$$G_{mm3}(s) = \cos(\phi - \theta) - G_{mm2}(s) \quad 4.2.97$$



#### 4.2.6 Derivation of the rotary modulation transfer function

In this case, consideration should be given to the diagram shown in Fig. 4.1.2 where the chopper network is subject to rotary modulated signal  $v_1(t)$ . This signal is derived from the modulating signal  $x(t)$  according to the relationship

$$v_1(t) = p \left[ x(t) \cdot E_{md} \sin(\Omega t + \theta) \right] \quad 4.2.98$$

which is accomplished by the rotary modulator illustrated in Fig. 4.2.7-a. Evaluating the differentiation, the signal  $v_1(t)$  can be considered as the sum of two signals

$$v_1(t) = v_{11}(t) + v_{12}(t) \quad 4.2.99$$

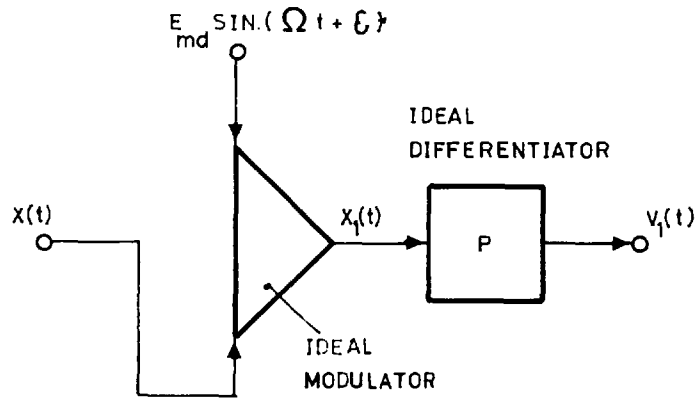
where

$$v_{11}(t) = \Omega x(t) \cdot E_{md} \cos(\Omega t + \theta) \quad 4.2.100$$

and

$$v_{12}(t) = x^*(t) \cdot E_{md} \sin(\Omega t + \theta) \quad 4.2.101$$

This implies that the rotary modulated signal  $v_1(t)$  can be resolved into two terms of multiplicative modulated signals  $v_{11}(t)$  and  $v_{12}(t)$  as represented by the equivalent arrangement shown in Fig. 4.2.7-b. In this way, the techniques used in the previous Sub-sections 4.2.2 to 4.2.5 are readily applicable to each signal separately. However, by combining the effects of the two signals, a rotary modulation transfer function can be easily obtained.



a) ROTARY MODULATOR

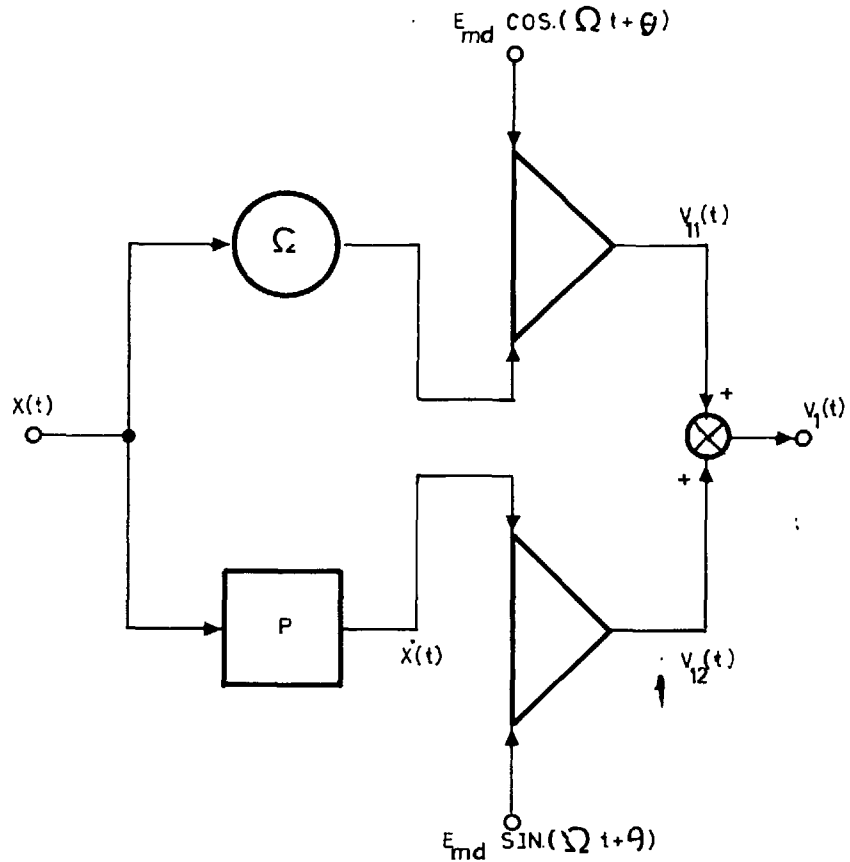
b) EQUIVALENT ARRANGEMENT FOR PRODUCING  
ROTARY MODULATION

FIG. 4.2.7.

#### 4.2.7 Noise study.

Because of the switching mechanism involved in the chopper networks as well as the modulation and demodulation processes included in the system shown in Fig. 4.1.1, high harmonic components are generated which appear in the output voltage expression at double carrier frequency (see Eqns. 4.2.46, 4.2.51 and 4.2.64). In a.c. servo-mechanisms, such noise components, fortunately, have negligible effects on the system dynamic performance due to the filtering action of the 2-phase servomotor. However, they result in heating up the control coil of the 2-phase servo-motor. This may force the designer to use a bigger size motor which is very undesirable in some applications such as in air-borne equipment. Therefore, a thorough study of the chopper network noise content with the aim of minimising them is evidently quite useful. Furthermore, the noise content may be used as a criterion for selecting the most suitable type of chopper network.

The effect of the noise generated by chopper networks may be appropriately assessed on the basis of the power-density spectrum. This is related to the voltage according to its definition, as equal to the mean square voltage spectrum. It follows, therefore, that the determination of the voltage spectrum would be of great value to the noise study. In this Sub-section, only the voltage spectrum of the output signal will be considered.

On the basis of the results of Eqns. 4.2.46, 4.2.51 and 4.2.64, it is possible to regroup terms of each carrier frequency component so that the output signal may take the suitable form

$$y(s) = G_{0\text{mm}}(s) \cdot x(s) + G_{-2\text{mm}}(s) \cdot x(s-j2\Omega) + G_{2\text{mm}}(s) \cdot x(s+j2\Omega) \\ + G_{-4\text{mm}}(s) \cdot x(s-j4\Omega) + \dots \text{ etc.} \quad 4.2.102$$

where the presubscripts associated with the various modulation transfer functions are employed to denote the order of the corresponding carrier harmonic components.  $G_{0\text{mm}}(s)$  has already been derived in Sub-sections 4.2.4 and 4.2.5 as expressed by either Eqn. 4.2.96 or Eqn. 4.2.97 depending on the output under consideration. Following similar procedure as outlined in these sub-sections, corresponding expressions for the modulation transfer functions associated with the various carrier harmonic components can be obtained. Thus, their characteristics can be studied.

In the light of Eqn. 4.2.102, the output signal may conveniently be re-written in the compact form

$$y(s) = \sum_{n=-\infty}^{n=\infty} G_{2n\text{mm}}(s) \cdot x(s+j2n\Omega) \quad 4.2.103$$

For real frequency,  $s$  is simply replaced by  $j\omega$ , thus

$$y(j\omega) = \sum_{n=-\infty}^{n=\infty} G_{2n\text{mm}}(j\omega) \cdot x\{j(\omega+2\Omega n)\} \quad 4.2.104$$

Under this condition, it is noticed that only the zero term of the above infinite series is linearly related to the input signal excluding the values of  $\omega$  which satisfy the equation

$$\omega = m\Omega, \quad m = \text{integer} \neq 0 \quad 4.2.105$$

Under the above condition, the negative  $m^{\text{th}}$  term becomes also, in addition to the zero term, linearly related to the input signal. 4.2.106

#### 4.3. Application of the Approximate Analytical Approach

##### 4.3.1 Derivation of the voltage appearing across the capacitor at the switching instants.

This voltage has already been obtained in Sub-section 4.2.2, for the single-switch double-capacitor chopper network in the Z-domain, as  $\lambda_{a2}^*(s)$  and  $\lambda_{b2}^*(s)$  for the capacitors in branches a and b respectively. Therefore, to obtain this voltage as a discrete time function, the inverse Z-transform has to be applied to Eqns. 4.2.36 and 4.2.39. Before doing so, considerable simplification of these equations may first be obtained through the use of the assumption that the modulating signal  $x(t)$  is a unit step function, i.e.

$$x(t) = U_{-1}(t) \quad 4.3.1$$

On this basis, the expressions for  $F_a(s)$  and  $F_b(s)$ , derived in Appendices D.1 and D.2, become

$$F_a(s) = E_{md} \cdot F_{a1}(s) \quad 4.3.2$$

and

$$F_b(s) = -e^{-Ts/2} \cdot F_a(s) \quad 4.3.3$$

where  $F_{a1}(s)$  is expressed by Eqn. D.1.7.

Substituting Eqn. 4.3.2 into Eqn. 4.2.35 and solving, gives

$$\left[ F_a(s) e^{\delta Ts} G(s) \right]^* = E_{md} \cdot \frac{\tau_e}{\tau} \cdot \frac{1}{1 + \tau_e^2 \Omega^2} \cdot \frac{\left[ \alpha e^{-\delta T/\tau_e} - \beta \right]}{(1 - Z_1^{-1})(1 - Z_1^{-1} e^{-T/\tau_e})} \quad \dots 4.3.4$$

$$\text{where } \alpha = \tau_e \Omega \cos \theta - \sin \theta \quad 4.3.5$$

$$\text{and } \beta = \tau_e \Omega \cos(2\pi\delta + \theta) - \sin(2\pi\delta + \theta) \quad 4.3.6$$

Substituting the result of Eqn. 4.3.4 into Eqn. 4.2.36, gives

$$\lambda_{a2}^*(s) = E_{md} \cdot \Delta \cdot \frac{Z_1^{-1}}{(1 - Z_1^{-1})(1 - Z_1^{-1} r)} \quad 4.3.7$$

$$\text{where } \Delta = \frac{\tau_e}{\tau} \cdot \frac{e^{-(1-\delta)T/\tau_1}}{1 + \tau_e^2 \Omega^2} \left[ \alpha e^{-\delta T/\tau_e} - \beta \right] \quad \dots 4.3.8$$

Expanding  $\lambda_{a2}^*(s)$  in partial fractions, yields

$$\lambda_{a2}^*(s) = E_{md} \cdot \frac{\Delta}{1-r} \left[ \frac{1}{1 - Z_1^{-1}} - \frac{1}{1 - Z_1^{-1} r} \right] \quad \dots 4.3.9$$

The inverse Z-transform of Eqn. 4.3.9 can thus be easily obtained as

$$\lambda_{a2}^*(t) = E_{md} \cdot \frac{\Delta}{1-r} \sum_{n=0}^{n=\infty} (1-r^n) U_o(t-nT) \quad 4.3.10$$

Similarly, it can be proved that the voltage across the capacitor in branch b is

$$\lambda_{b2} \left\{ \left( n + \frac{1}{2} \right) T \right\} = - \lambda_{a2}(nT) \quad 4.3.11$$

#### 4.3.2 Derivation of the chopper network response

Details of the derivation of the response from first principles are outlined in Sub-section II.4.1. Table II.4.2 gives the final expressions of the response in Laplacian form applicable during various intervals of the carrier cycle. At that stage, however, the initial conditions, although are accounted for, were left as undefined constants. In this sub-section, the complete response in the time domain is going to be considered; firstly, by defining the initial conditions with the help of the results of the previous sub-section, and secondly, by applying the inverse Laplace transform.

During the period  $nT \leq t < (n+1)T$ , the response  $v_2(s)$  may be rewritten from Table II.4.2, thus

$$v_2(s) = \left[ {}_n v_1(s) + \tau \cdot {}_n V_a \right] \cdot G(s) \quad 4.3.12$$

where

- i)  $V_a$  is the initial value of the voltage appearing across the capacitor in branch a at the instant indicated by its presubscript as a multiple of the period T.
- ii) presubscripts when multiplied by the carrier period T;

the result defines the instant at which the Laplace transform is taken.

From the above definition

$${}_n v_1(s) = \int v_1(t+nT) \quad 4.3.13$$

But according to Eqns. 4.2.12 and 4.3.1

$$v_1(t) = E_{md} \sin(\Omega t + \theta) \cdot U_{-1}(t) \quad 4.3.14$$

Then

$${}_n v_1(s) = E_{md} \frac{\Omega \cos \theta + s \sin \theta}{s^2 + \Omega^2} \quad 4.3.15$$

Also from the above definition of  ${}_n V_a$ ,

$${}_n V_a = \lambda_{e2}(nT)$$

which on substitution in Eqn. 4.3.10, yields

$${}_n V_a = E_{md} \cdot \Delta \cdot \frac{1-r^n}{1-r} \quad 5.3.16$$

Substituting Eqns. 4.3.15 and 4.3.16 into Eqn. 4.3.12, and then applying the inverse Laplace transform to the result, gives

$$\begin{aligned} v_2\{(n+\mu)T\} &= E_{md} \cdot \Delta \cdot \frac{1-r^n}{1-r} e^{-\mu T/\tau_e} \\ &+ E_{md} \cdot \frac{\tau_e}{\tau} \cdot \frac{1}{1+\tau_e^2 \Omega^2} \left[ \alpha e^{-\mu T/\tau_e} - \left\{ \tau_e \Omega \cos(2\pi\mu+\theta) \right. \right. \\ &\quad \left. \left. - \sin(2\pi\mu+\theta) \right\} \right] \quad 4.3.17 \end{aligned}$$

$$\text{where} \quad 0 \leq \mu < \delta \quad 4.3.18$$



During the period  $(n+\delta)T \leq t < (n+\frac{1}{2})T$ , the response  $v_2(s)$  again can be obtained from Table II.4.2, which may be directly written in the time domain as

$$v_2 \left\{ (n+\delta+\mu)T \right\} = \frac{\tau_2}{\tau+\tau_2} \cdot E_{md} \cdot \sin \left\{ 2\pi(\mu+\delta)+\theta \right\} \quad 4.3.19$$

where

$$0 \leq \mu < \left( \frac{1}{2} - \delta \right) \quad 4.3.20$$

During the period  $(n+\frac{1}{2})T \leq t < (n+\frac{1}{2}+\delta)T$ , one can easily prove that (it may also be directly deduced from the symmetry of the branches a and b of the chopper network),

$$v_2 \left\{ \left( n+\frac{1}{2}+\mu \right) T \right\} = - v_2 \left\{ (n+\mu)T \right\} \quad 4.3.21$$

Likewise, during the period  $(n+\frac{1}{2}+\delta)T \leq t < (n+1)T$ , it is easy to prove that

$$v_2 \left\{ \left( n+\frac{1}{2}+\delta+\mu \right) T \right\} = - v_2 \left\{ (n+\delta+\mu)T \right\} \quad 4.3.22$$

For the response  $v_3(t)$ , it is easy to deduce its forms during the various intervals by substituting the proper time in the following relation

$$v_3(t) = v_1(t) - v_2(t) \quad 4.3.33$$

#### 4.3.3. Determination of equivalent time-invariant passive electric network

##### 4.3.3.1. Phase-lag aspect

Since the output of the chopper network is applied to a demodulator (in a.c. servomechanisms ,

the output is employed to drive a 2-phase servomotor where demodulation process is effected), which is excited by the reference carrier-frequency sinusoid  $E_{de} \sin(\Omega t + \phi)$ , only the sinusoidal component at carrier frequency and in phase with the reference excitation is the useful portion of this output. Thus, if the envelope of  $v_2(t)$  changes slowly relative to the carrier by assuming the condition

$$\tau_e \gg T/2 \quad 4.3.34$$

is satisfied, the approximate magnitude of the fundamental component, in phase with the demodulation reference, during the  $n^{\text{th}}$  switching period can be obtained by quasi-stationary Fourier analysis as given below:

$$\begin{aligned} nV_2 &= \frac{2}{\pi} \int_0^{2\pi\delta} v_2 \left\{ \left( n + \frac{h}{2\pi} \right) T \right\} \cdot \sin(h + \phi) \, dh \\ &+ \frac{2}{\pi} \int_{2\pi\delta}^{\pi} v_2 \left\{ \left( n + \delta + \frac{h}{2\pi} \right) T \right\} \cdot \sin(h + \phi) \, dh \end{aligned} \quad 4.3.35$$

where

$$h = 2\pi\mu \quad 4.3.36$$

Solving the integrations gives

$$nV_2 = E_{md} \cdot M \left[ A_1 + B_1 (1 - r^n) \right] \quad 4.3.37$$

where

$$M = \frac{2}{\pi} \frac{\tau_e}{1 + \tau_e^2 \Omega^2} \quad 4.3.38$$

$$A_1 = \frac{k_1}{\tau\Omega} - \frac{\tau_c}{\tau} k_2 + \frac{1}{\tau\Omega} \alpha k_3 + \frac{2}{\pi} \cdot \frac{1}{M} \frac{\tau_2}{\tau + \tau_2} k_4$$

and

$$B_1 = \frac{2}{\pi} \cdot \frac{1}{M} \cdot \Delta \cdot \frac{k_3}{1-r} \quad 4.3.40$$

wherein

$$\begin{aligned} k_1 &= \int_0^{2\pi\delta} \sin(h+\theta) \cdot \sin(h+\phi) \, dh \\ &= \pi\delta \cos(\phi-\theta) + \frac{1}{4} \cdot \sin(\phi+\theta) - \frac{1}{4} \sin(4\pi\delta+\phi+\theta) \end{aligned}$$

$$k_2 = \int_0^{2\pi\delta} \cos(h+\theta) \cdot \sin(h+\phi) \, dh \quad \dots 4.3.41$$

$$= \pi\delta \sin(\phi-\theta) + \frac{1}{4} \cdot \cos(\phi-\theta) - \frac{1}{4} \cos(4\pi\delta+\phi+\theta) \quad \dots 4.3.42$$

$$\begin{aligned} k_3 &= \int_0^{2\pi\delta} e^{-h/\tau_e} \cdot \sin(h+\phi) \, dh \\ &= \frac{\tau_e \Omega}{1+\tau_e^2 \Omega^2} \left[ \left\{ \tau_e \Omega \cos\phi + \sin\phi \right\} e^{-\delta T/\tau_e} \left\{ \tau_e \Omega \cos(2\pi\delta+\phi) \right. \right. \\ &\quad \left. \left. + \sin(2\pi\delta+\phi) \right\} \right] \quad 4.3.43 \end{aligned}$$

and

$$\begin{aligned} k_4 &= \int_{2\pi\delta}^{\pi} \sin(h+2\pi\delta+\theta) \cdot \sin(h+\phi) \, dh \\ &= \frac{\pi}{2} (1-2\delta) \cos(\phi-\theta-2\pi\delta) - \frac{1}{4} \sin(2\pi\delta+\phi+\theta) \\ &\quad + \frac{1}{4} \sin(6\pi\delta+\phi+\theta) \quad 4.3.44 \end{aligned}$$

It is noticed that the form of the R.H.S. of Eqn. 4.3.35 is similar to the responses of both the phase-lag passive electric networks a and b illustrated in solid line in Fig. 4.3.1 when a step function of magnitude  $E_{md}$  is applied at  $t=0$  to their input terminals and with the assumption of zero initial charges on their associated capacitors. Such responses can be easily obtained in terms of the network's parameters and are given by

$$y_{2a}(t) = E_{md} \cdot k_a \left[ 1 - (1-k'_a) e^{-t/\tau_a} \right] \quad 4.3.45$$

and

$$y_{2b}(t) = E_{md} \left[ \left\{ 1 - k_b (1 - k'_b) \right\} - (1 - k_b)(1 - k'_b) e^{-t/\tau_b k_b} \right] \quad 4.3.46$$

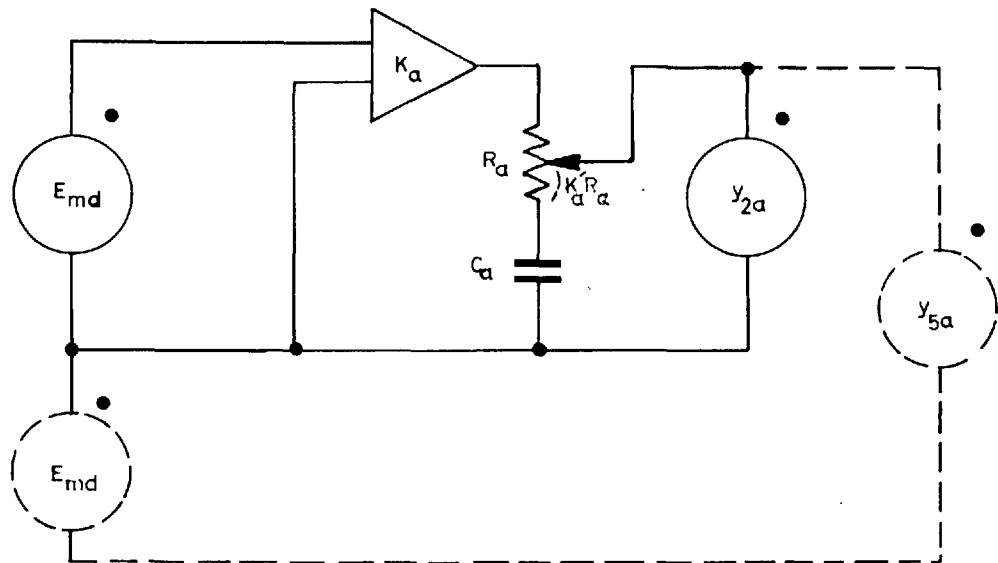
for networks a and b respectively, where

$$\left. \begin{aligned} \tau_a &= R_a C_a \\ k_a &= \text{amplifier gain} \\ k'_a &= \text{a proportion of resistor } R_a \end{aligned} \right\} 4.3.47$$

and

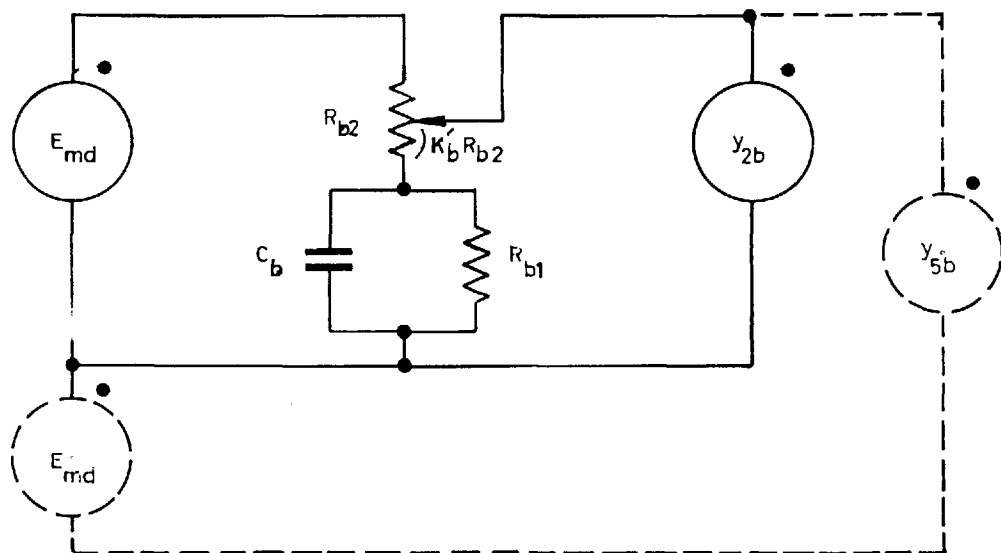
$$\left. \begin{aligned} \tau_b &= R_{b1} C_b \\ k_b &= R_{b2} / (R_{b1} + R_{b2}) \\ k'_b &= \text{a proportion of resistor } R_{b2} \end{aligned} \right\} 4.3.48$$

An equivalence between the d.c. networks of Fig. 4.3.1 and the system shown in Fig. 4.1.1 can now be established by equating Eqn. 4.3.37, in turn, to Eqns. 4.3.45 and 4.3.46 at the instants at which the peaks of the demodulation



(a)

WITH BUFFER AMPLIFIER



(b)

WITHOUT BUFFER AMPLIFIER

FIG. 4.3.1.

CIRCUIT DIAGRAMS OF THE EQUIVALENT PHASE - LAG  
TIME - INVARIANT PASSIVE ELECTRIC NETWORKS

reference carrier occur (see Fig. 4.3.3). Thus the following relationships are obtained

$$M \left[ A_1 + B_1 (1-r^n) \right] = k_a \left[ 1 - (1-k'_a) e^{-(n+\sigma)T/\tau_a} \right] \quad 4.3.49$$

$$= \left\{ 1 - k_b (1-k'_b) \right\} - (1-k_b)(1-k'_b) e^{-(n+\sigma)T/\tau_b k_b}$$

..4.3.50

where  $\sigma = \frac{1}{4} - \frac{\phi}{2\pi}$  4.3.51

Each side of Eqns. 4.3.49 and 4.3.50 is a function of  $n$ . If the slopes of the curves represented by the two sides of each equation are to be equal as desired, the following conditions must be satisfied.

$$\frac{1}{\tau_a} = \frac{1}{\tau_1} + \frac{\delta}{\tau_{e2}} \quad 4.3.52$$

and

$$\frac{1}{\tau_b k_b} = \frac{1}{\tau_1} - \frac{\delta}{\tau_{e2}} \quad 4.3.53$$

Substituting Eqn. 4.3.52 into Eqn. 4.3.49 and Eqn. 4.3.53 into Eqn. 4.3.50, one can obtain the equivalent d.c. network parameters in terms of the chopper network parameters by simple comparison, thus

i) For d.c. network a (Fig. 4.3.1)

$$k_a = M(A_1 + B_1) \quad 4.3.54$$

$$k'_a = 1 - \frac{B_1}{A_1 + B_1} \cdot H \quad 4.3.55$$

where

$$H = e^{\left\{ (\pi - 2\phi) \left( \frac{1}{\tau_1} + \frac{\delta}{\tau_e \omega} \right) / 2\omega \right\}} \quad 4.3.56$$

ii) For d.c. network b (Fig. 4.3.1)

$$k_b = \frac{1 - M(A_1 + B_1)}{1 - M[A_1 + B_1 - B_1 H]} \quad 4.3.57$$

and

$$k'_b = M [A_1 + B_1 - B_1 H] \quad 4.3.58$$

#### 4.3.3.2. Phase-lead aspect

Following similar reasoning as above, the fundamental component of  $v_3(t)$ , in phase with the demodulation reference, during the  $n^{\text{th}}$  switching period can be obtained and is given by

$${}_n V_3 = E_{\text{md}} \cdot M [A_2 - B_1 (1 - r^n)] \quad 4.3.59$$

where  $M$  and  $B_1$  are as defined above

$$\begin{aligned} \text{and } A_2 = & \left( \tau_e \omega + \frac{1}{\tau_{e12} \omega} \right) k_1 + \frac{\tau_e}{\tau} k_2 - \frac{1}{\tau \omega} \alpha k_3 \\ & + \frac{2}{\pi} \cdot \frac{1}{M} \cdot \frac{\tau}{\tau + \tau_2} k_4 \end{aligned} \quad 4.3.60$$

The responses of the d.c. networks a and b illustrated in Fig. 4.3.2 to a step input of magnitude  $E_{md}$  can be easily derived in terms of their parameters as given below

$$y_{3a}(t) = E_{md} k_c \left[ k_c' + (1-k_c') e^{-t/\tau_c k_c'} \right] \quad 4.3.61$$

and

$$y_{3b}(t) = E_{md} k_d \left[ k_d' + (1-k_d') e^{-t/\tau_d k_d'} \right] \quad 4.3.62$$

where

$$\tau_c = R_{c1} C_c$$

$$k_c = \text{amplifier gain} \quad 4.3.63$$

$$k_c' = R_{c2} / (R_{c1} + R_{c2})$$

and

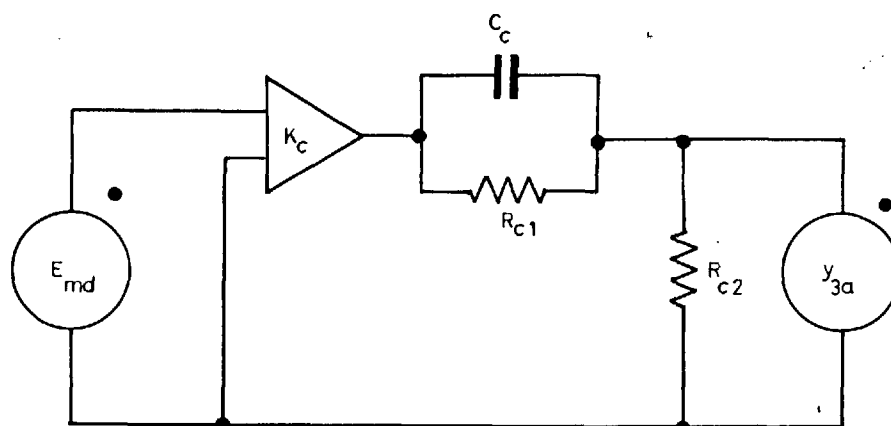
$$\tau_d = R_{d1} C_d$$

$$k_d = \text{a proportion of } R_{d2} \quad 4.3.64$$

$$k_d' = R_{d2} / (R_{d1} + R_{d2})$$

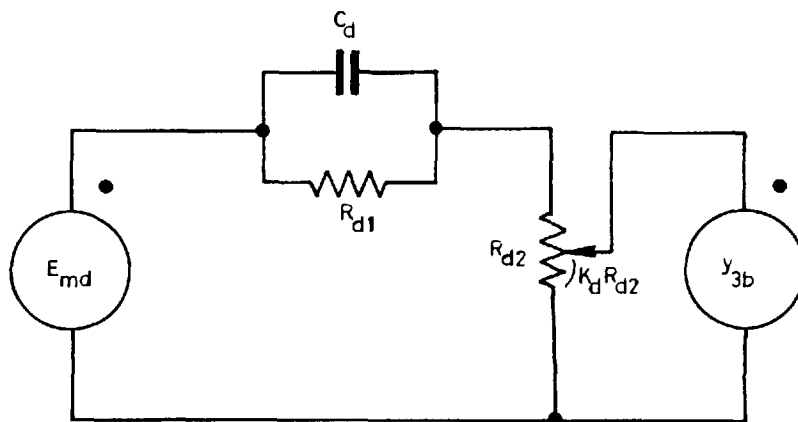
Because of the similarity in the forms of Eqns. 4.3.60, 4.3.61 and 4.3.62, each of the d.c. networks shown in solid line in Fig. 4.3.2 can be considered as equivalent to the system shown in Fig. 4.1.1 in its phase-lead aspect. By comparing each of the Eqns. 4.3.61 and 4.3.62, in turn, with Eqn. 4.3.60 at the instants at which the peaks of the demodulation reference carrier occur, it is possible to determine the d.c. network parameters in terms of the chopper network parameters. The following relations are deduced from the comparison:





(a)

WITH BUFFER AMPLIFIER



(b)

WITHOUT BUFFER AMPLIFIER

FIG. 4.3.2.

CIRCUIT DIAGRAMS OF EQUIVALENT PHASE-LEAD  
TIME - INVARIANT PASSIVE ELECTRIC NETWORKS

i) For d.c. network a (Fig. 4.3.2)

$$\frac{1}{\tau_c k_c'} = \frac{1}{\tau_1} + \frac{\delta}{\tau_{e2}} \quad 4.3.65$$

$$k_c' = \frac{A_2 - B_1}{A_2 - B_1 [1-H]} \quad 4.3.66$$

$$k_c = M [A_2 - B_1 (1-H)] \quad 4.3.67$$

ii) For d.c. network b (Fig. 4.3.2)

Equations 4.3.65 to 4.3.67 are also applicable here provided that the subscript c is replaced by d.

#### 4.3.4. Derivation of the multiplicative modulation transfer function

##### 4.3.4.1. Phase-lag aspect

On the basis of the work outlined in the previous Sub-section, it can be stated that the multiplicative modulation transfer function of the single-switch double-capacitor chopper network is approximately identical to the transfer function of either the equivalent d.c. network a or b of Fig. 4.3.1, i.e.,

$$G_{mm2}(s) = G_a(s) \quad 4.3.68$$

$$= G_b(s) \quad 4.3.69$$

Derivation of the transfer functions for the equivalent d.c. networks can be easily carried out and the result is the following general form

$$G_{mm2}(s) = G_a(s) = G_b(s) = k_o \frac{1 + \frac{k_\infty}{k_o} \tau_n s}{1 + \tau s} \quad 4.3.70$$

where

$$k_o = \text{d.c. gain}$$

$$k_\infty = \text{infinite frequency gain}$$

$$1/\tau_n = \text{network frequency, in radians/second} \\ (\text{see Fig. 4.3.4})$$

These parameters can be defined in terms of the parameters of the equivalent d.c. networks as given below

- i) In terms of the parameters of the d.c. phase-lag network a (Fig. 4.3.1)

$$\tau_n = \tau_a \quad 4.3.71$$

$$k_o = k_a \quad 4.3.72$$

and

$$k_\infty = k_a k_a' \quad 4.3.73$$

- ii) In terms of the parameters of the d.c. phase-lag network b (Fig. 4.3.1)

$$\tau_n = \tau_b k_b \quad 4.3.74$$

$$k_o = \frac{R_{b1} + k_b' R_{b2}}{R_{b1} + R_{b2}} \quad 4.3.75$$

$$k_\infty = \frac{R_{b2}}{R_{b1} + R_{b2}} \cdot \frac{k_b'}{k_b} \quad 4.3.76$$

On the basis of Eqn. 4.3.70, the frequency response of the equivalent d.c. networks, which also represents the

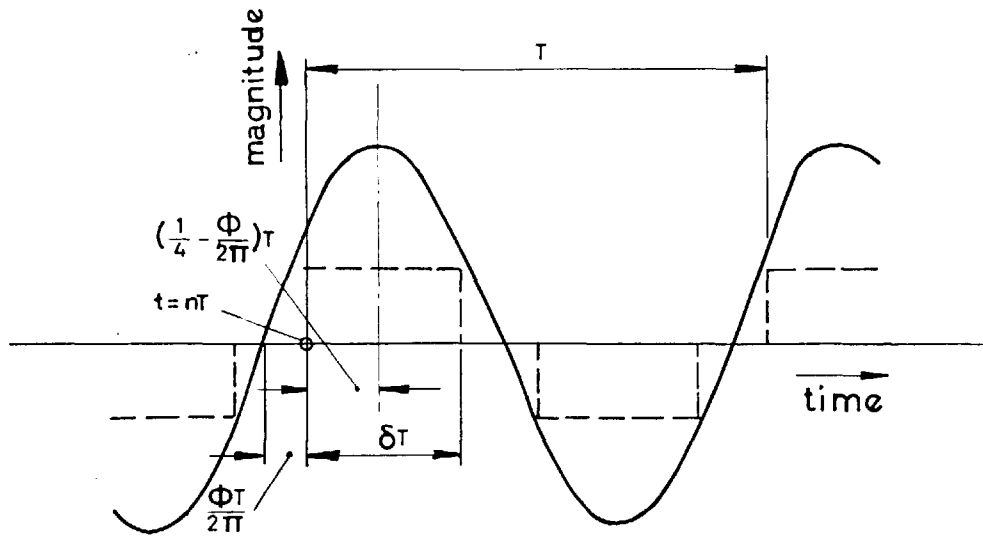


FIG. 4.3.3.  
 DIAGRAM ILLUSTRATING THE INSTANT AT WHICH THE PEAK OF THE DEMODULATION REFERENCE CARRIER OCCURS RELATIVE TO THE SWITCHING INSTANT

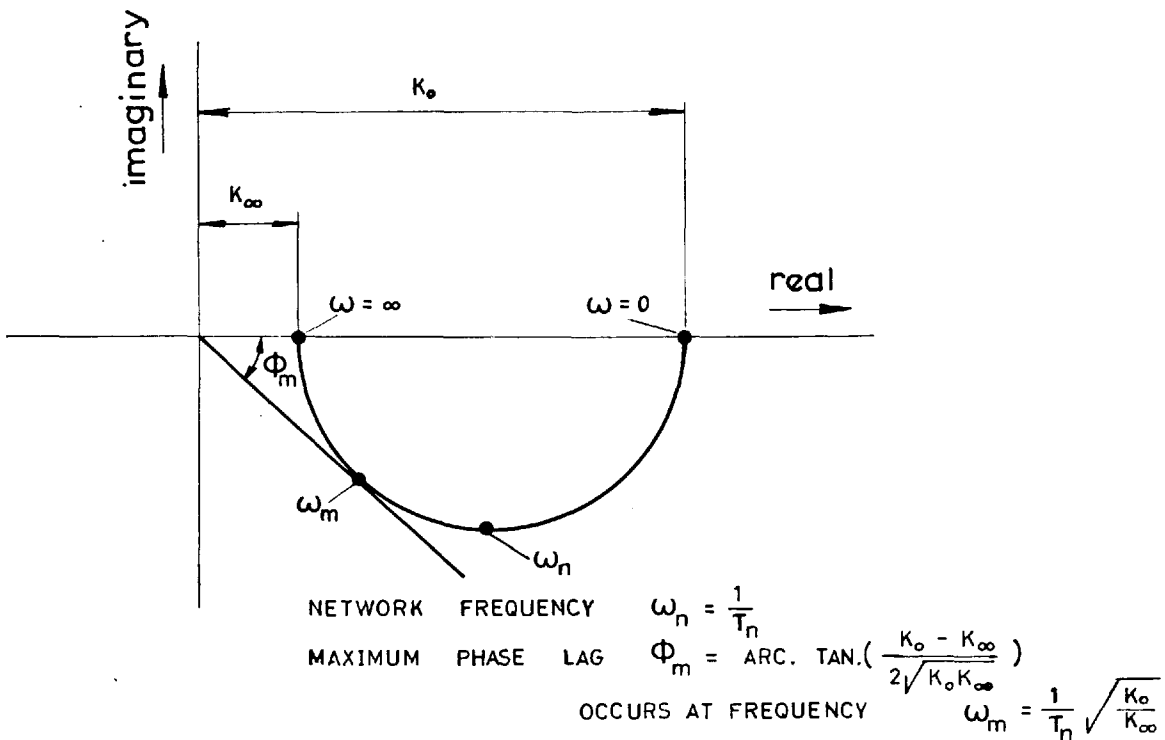


FIG. 4.3.4.  
 FREQUENCY RESPONSE LOCUS OF THE EQUIVALENT DC NETWORKS SHOWN IN FIG. 4.3.1.

NETWORK FREQUENCY

$$\omega_n = \frac{1}{T_n} \frac{K_\infty}{K_o}$$

MAXIMUM PHASE LEAD

$$\Phi_m = \text{ARC TAN.} \left( \frac{K_\infty - K_o}{2 \sqrt{K_o K_\infty}} \right)$$

OCCURS AT FREQUENCY

$$\omega_m = \frac{1}{T_n} \sqrt{\frac{K_o}{K_\infty}}$$

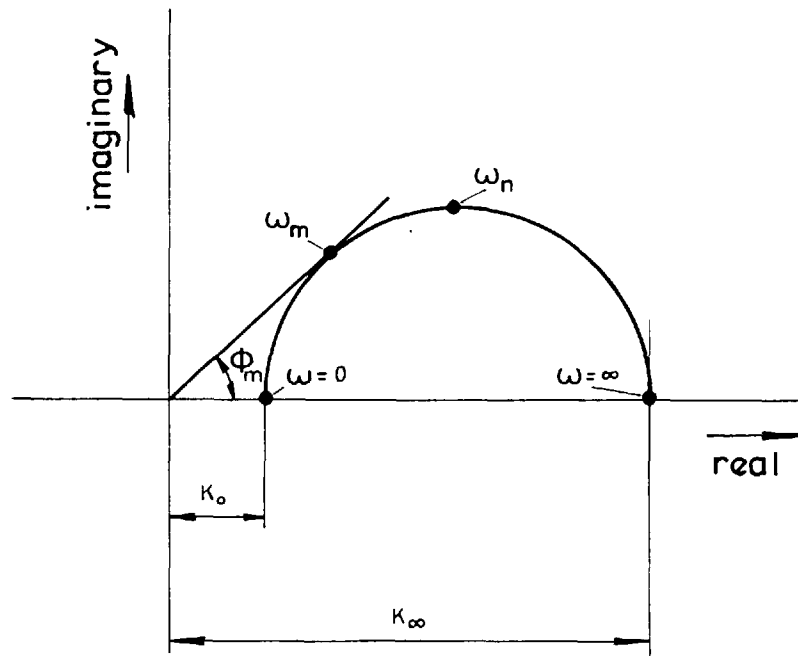


FIG. 4.3.5.

FREQUENCY RESPONSE LOCUS OF THE EQUIVALENT

DC NETWORKS SHOWN IN FIG. 4.3.2.

approximate multiplicative modulation frequency response of the chopper network in its phase-lag aspect, can be easily sketched as a semi-circle locus as shown in Fig. 4.3.4.

#### 4.3.4.2. Phase-lead aspect

Similarly, as above, from the equivalence established between the d.c. networks illustrated in Fig. 4.3.2 and the system shown in Fig. 4.1.1, in its phase-lead aspect, it is deduced that the common transfer function of the former also represents the multiplicative modulation transfer function of the latter. Thus

$$G_{mm3}(s) = G_c(s) \quad 4.3.77$$

$$G_d(s) \quad 4.3.78$$

where  $G_c(s)$  and  $G_d(s)$  can be easily derived and are given by the general form

$$G_c(s) = G_d(s) = k_o \frac{1 + \tau_n s}{1 + \frac{k_o}{k_\infty} \tau_n s} \quad 4.3.79$$

where the parameters  $\tau$ ,  $k_o$  and  $k_\infty$  may be defined in terms of those pertinent to the equivalent d.c. networks as given below

- i) In terms of the parameters of the d.c. phase-lead network a (Fig. 4.3.2)

$$\tau_n = \tau_c \quad 4.3.80$$

$$k_o = k_c \cdot k_c' \quad 4.3.81$$

and

$$k_{\infty} = k_c \quad 4.3.82$$

ii) In terms of the parameters of the d.c. phase-lead network b (Fig. 4.3.2).

Eqns. 4.3.80 to 4.3.82 are also applicable here provided that the subscript c is replaced by d.

## CHAPTER 5

### MODULATION FREQUENCY RESPONSES OF CHOPPER NETWORKS

#### 5.1. General

In the previous Chapter, chopper networks have been analysed by two different methods; exact and approximate. The significance of these analyses lies in the fact that they provide the designer with the necessary knowledge to synthesise the suitable compensating chopper network once the required modulation transfer function and type of modulation (multiplicative or rotary) are specified.

Before applying these theoretical analysis to the practical problems, their validity should first be verified. The limitations and amount of approximation involved in the approximate method must be assessed.

To achieve these objectives, extensive practical studies have been conducted on a selected number of chopper networks under various operating conditions. The experimental results obtained were then compared with the theoretical computed by both the exact and approximate methods.

In performing the various practical investigations on the chopper network's modulation characteristics, it was possible to study different types of problems which arise in many practical applications of a.c. servo-mechanisms, such as the effects of large variations in carrier frequency and phase variations of the modulation and demodulation references on the performance of the compensating device.

This Chapter outlines the various studies performed.



## 5.2. Experimental Investigations.

### 5.2.1. Tests performed

Modulation frequency response test was considered to be most suitable since it reveals most of the modulation characteristics information to be studied. This test was therefore conducted on a number of chopper networks, and repeated under different operating conditions to permit the study of the effects of various factors as will be given in Section 5.3.

The rest of this Section is devoted to the techniques of measurement adopted, their limitations and accuracy.

### 5.2.2. Apparatus used for measuring the modulation frequency response

Fig. 5.2.1 shows a test arrangement designed for measuring the modulation frequency responses of chopper networks. The required test signal, in the form of suppressed-carrier amplitude modulated-wave, is produced by a sinusoidal modulator whose operational details are given in Ref. 127. The carrier signal is supplied from a variable a.c. supply so that studies under carrier frequency deviations can be performed. A description of this variable a.c. supply will be given later in this Section. The modulation signal is supplied from a low-frequency oscillator<sup>128</sup> in the form of a balanced signal.

The chopper network incorporates synchronous switches whose detailed design is given in Section I.4. A driving circuit capable of controlling the operation of the synchronous switches in the positive and negative fly-time regions is also incorporated (see description in Section I.5).

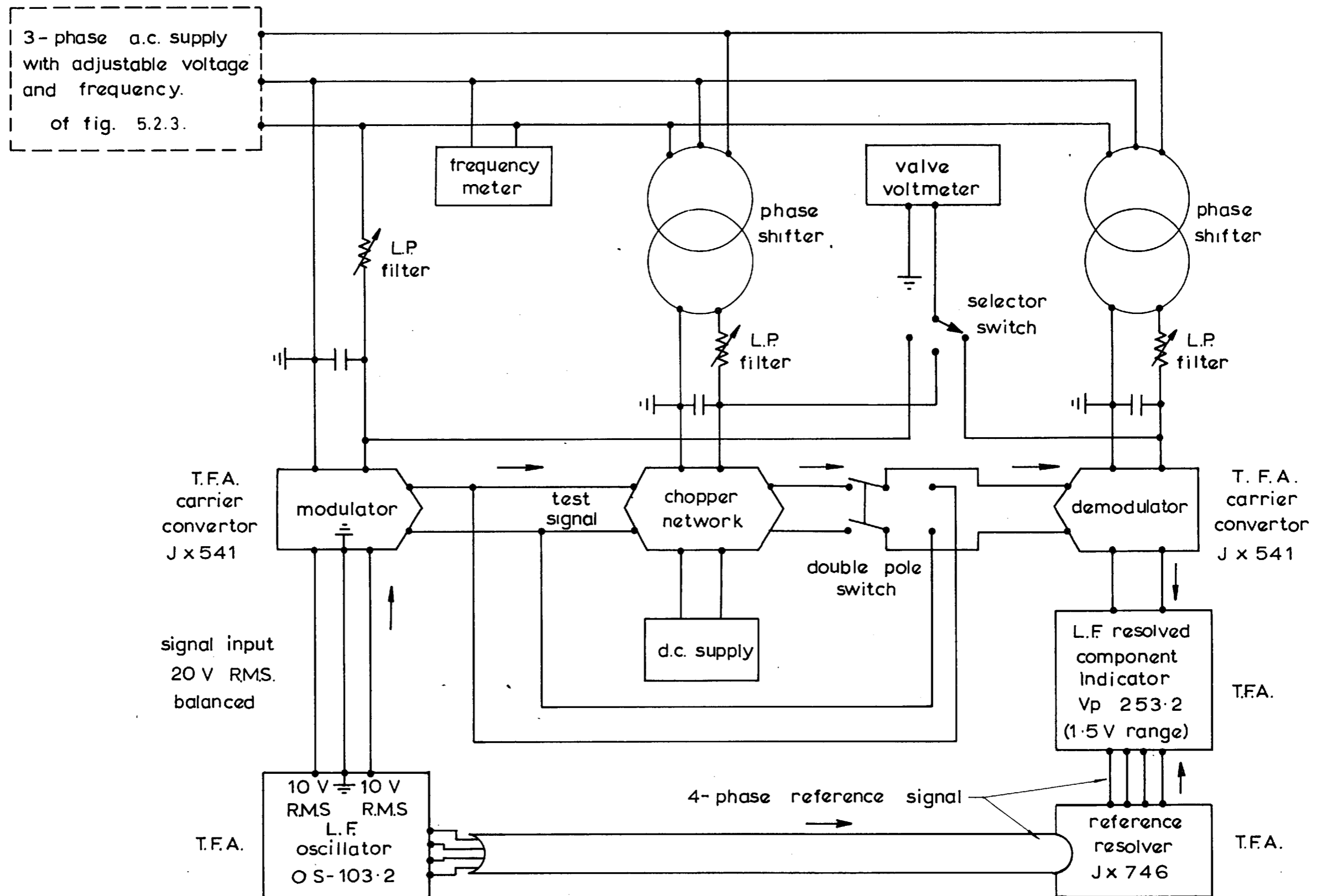


FIG. 5.2.1.

EQUIPMENT SET-UP FOR MEASURING THE MODULATION FREQUENCY RESPONSES OF CHOPPER NETWORKS

The carrier signal applied to this driving circuit is supplied through a phase-shifter in order to control the switching instant relative to the carrier-wave. A stabilized d.c. supply is provided to give the required bias on the various transistors of the synchronous switches and its driving circuit. The passive electric elements of the chopper networks as well as the synchronous switches are constructed as plugin units to suit a standard sockets so that changes can be easily made (see plate E.4.2.)

The output from the chopper network is demodulated by a sinusoidal demodulator in order to recover the low frequency envelope. Again, a phase-shifter is employed to adjust the phase of the demodulation carrier reference relative to that pertaining to the modulator.

The recovered envelope is then measured by means of the low-frequency Resolved Component Indicator type VP 2.5.3.2.<sup>129</sup> which displays the measured signal in the form of two resolved voltage components referred to the reference source. The low frequency Resolved Component Indicator requires a constant amplitude 4-phase reference signal, which is provided by the low frequency Decade Oscillator, since it employs the wattmeter principle for phase resolution. Consequently, it achieves the greatly desired characteristic that the measurements obtained are unaffected by the presence of harmonics or unrelated frequencies.

Since the indicated components of the recovered envelope of the chopper network output are in phase and in quadrature with respect to the modulating reference signal, their plot on cartesian co-ordinates would uniquely define the modulating signal in amplitude and phase. By taking a series of measurements at different frequencies, it is

possible to obtain the information required to plot the modulation frequency response locus.

To obtain the modulation response information in the form of a signal amplitude and a phase shift suitable for polar plotting, the Reference Resolver<sup>130</sup> is inserted in the 4-phase reference connection between the reference source and the Resolved Component Indicator. This instrument gives an identical and controlled phase shift to each of the four reference phases. Thus the reference phase can be shifted to give an output signal indication in the in-phase quadrant of the reference meter only.

In conducting this experiment, particularly at low modulating frequencies, it has been observed that the output from the L.F. Decade Oscillator was drifting. This made it very difficult to obtain accurate results from the L.F. Resolved Component Indicator for it derives its reference signal, which should have a stabilized amplitude of 10 v. R.M.S. per phase, from that drifting oscillator. To overcome this problem, a double pole switch is introduced between the chopper network and the demodulator. The purpose of this switch is to enable two successive readings at each modulating frequency to be taken; the first reading corresponds to the input signal to the chopper network and the second reading corresponds to the output signal from the chopper network. By calculating the relative magnitude and phase difference of the two readings gives the required result. To obtain the best accuracy by this method, the two readings should be taken at a very rapid succession as compared to the drifting speed so that the magnitude of the reference signal may be assumed constant during the two readings. Furthermore, this method effectively calibrates the modulator and demodulator at every modulating frequency

and the results obtained are thus free from any likely magnitude or phase errors introduced by them.

However, when the modulation frequency exceeds the usually specified maximum limit of 10% of carrier frequency, the performance characteristics of the modulator and demodulator become unsatisfactory and errors might be introduced. Although a scheme has been developed to overcome this problem which is presented in Chapter 8, its practical realization was not yet ready at the time this experiment was conducted. Therefore, the accuracy of the results obtained at modulating frequencies above that specified maximum limit should be assessed in the light of the work done in Chapter 8.

At d.c. modulating signal, the measuring arrangement shown in Fig. 5.2.1 cannot be used because the L.F. Decade Oscillator does not generate d.c. signal. However, a simple equipment set-up for measuring the d.c. transference may be employed as illustrated in Fig. 5.2.2. Because a carrier modulated by a d.c. signal produces again the same carrier-wave, the modulator is dispensed with and the carrier voltage is directly applied to the chopper network terminals. Similarly, instead of demodulating the output from the chopper network in order to recover the envelope signal which is at same frequency as the modulating signal, i.e., d.c., a simple alternative method is used in which the demodulator is completely discarded. This method depends on measuring the magnitude and phase of the fundamental component of the output voltage. The d.c. modulation transference can thus be deduced from the simple relation

$$\text{d.c. modulation transference} = \frac{1}{2} \cdot \frac{V_o}{V_i} \cos(\theta_o - \theta_i) \quad 5.2.1.$$

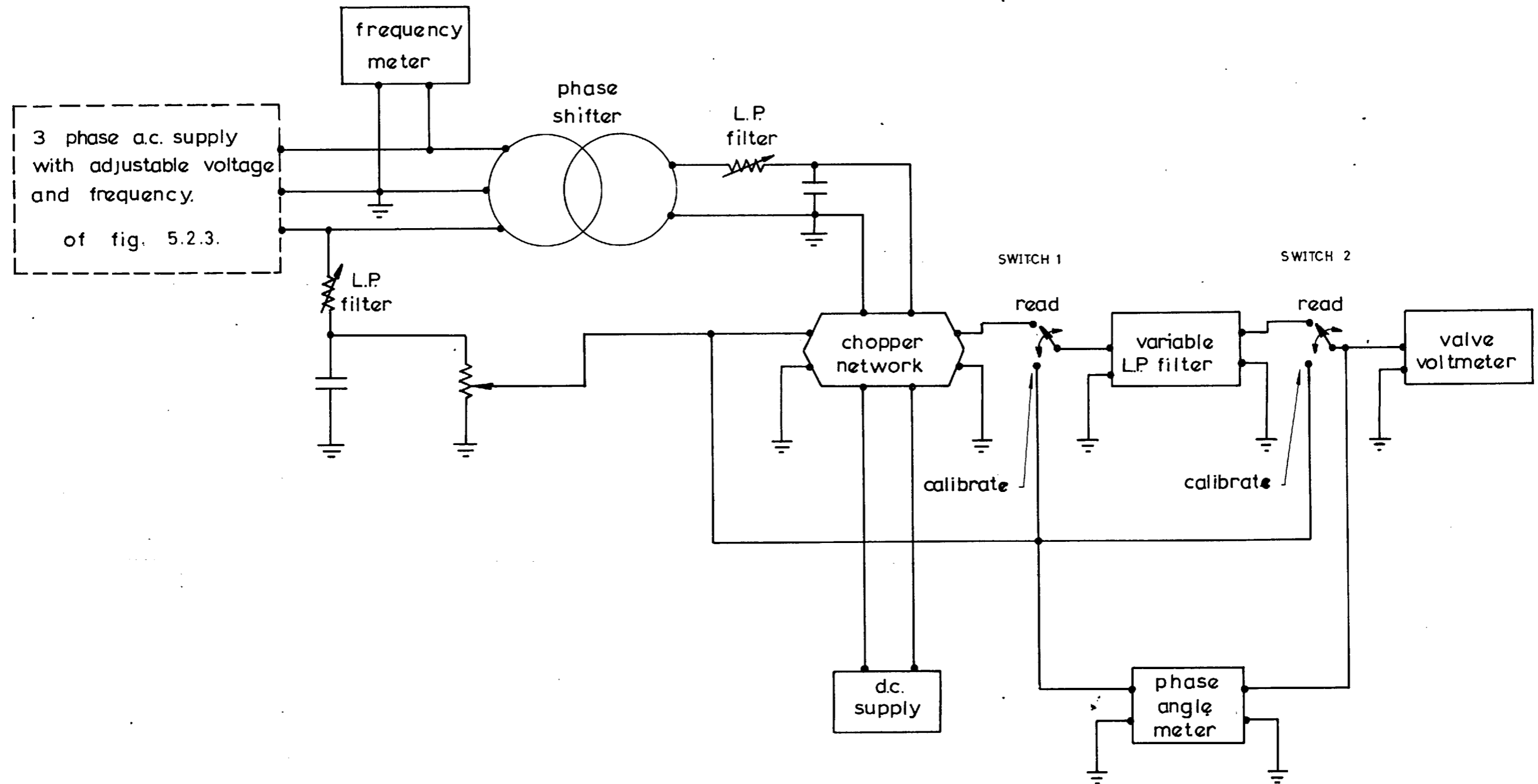


FIG. 5.22.

EQUIPMENT SET-UP FOR MEASURING THE DC MODULATION TRANSFERENCE

where

$V_i$  is the R.M.S. input carrier,  
 $V_o$  " " " of the fundamental output,  
 $\theta_o$  " " phase of the input carrier relative to  
 a certain reference,  
 $\theta_o$  is the phase of the fundamental output relative  
 to the same reference

and the factor 0.5 is introduced to make the d.c. modulation transference unity when the chopper network is replaced by a unity transfer function block.

A low-pass filter with sharp cut-off frequency was used to remove the noise components in the chopper network output. The filter employed is electronic type Model 315A (see details of performance characteristics in Ref.131) whose gain is approximately unity in the pass bands and drops outside the pass bands at the rate of 24 db per octave. It incorporates input and output buffer stages and thus provides a high impedance input and a low impedance output. Furthermore, it has the facility of adjusting the cut-off frequency which allows the experiment to be conducted at different carrier frequencies.

The magnitudes of the voltage signals are measured by a valve voltmeter and the phases by a phase angle meter.<sup>132</sup> In order to account for the gain and phase shift introduced by the filter, both the input and the output signals are first passed through the filter before their magnitudes and phases are measured. Therefore, by evaluating the relative magnitudes and the phase difference, the effect of the filter is cancelled out and does not appear in the expression of Eqn. 5.2.1. The double pole switches 1 and 2 were introduced to enable both the input and output signals to be passed through the filter and then be measured. An easier alternative

way could have been employed if another identical filter were available in order to be continuously connected to the input signal. In this case, switches 1 and 2 would have been removed and the measurements become a continuous process.

### 5.2.3. Variable frequency supply.

In order to perform experimental studies on the effect of carrier frequency variations on the modulation responses of various chopper networks, an adjustable frequency supply was required. Although, an electronic oscillator seems to be the simplest and most convenient means, nevertheless, it was not possible to be used because the required ranges of voltage, current and power were much higher than the corresponding ratings of the available oscillators.

Therefore, a system, whose principle of operation is based on changing the frequency of the available 3-phase 50 c/s supply, has been employed in the Laboratory. A schematic diagram of this system is illustrated in Fig. 5.2.3. In this connection, a 3-phase slip-ring induction motor is employed as a frequency changer. Its 3-phase stator winding is energised by the 50 c/s supply whose voltage magnitude is controlled by means of a 3-phase variac. By driving its motor at different speeds, the frequency of the pick-up voltage in the rotor 3-phase winding can be varied. In order to provide a means of fine and wide speed control, a d.c. machine with both field and armature controls is used to drive the frequency changer. The direction of rotation of the set was kept constant and therefore to obtain frequency values higher as well as lower than 50 c/s, provision of phase-sequence reversal of the 3-phase input should be included. This has been easily accomplished by interchanging



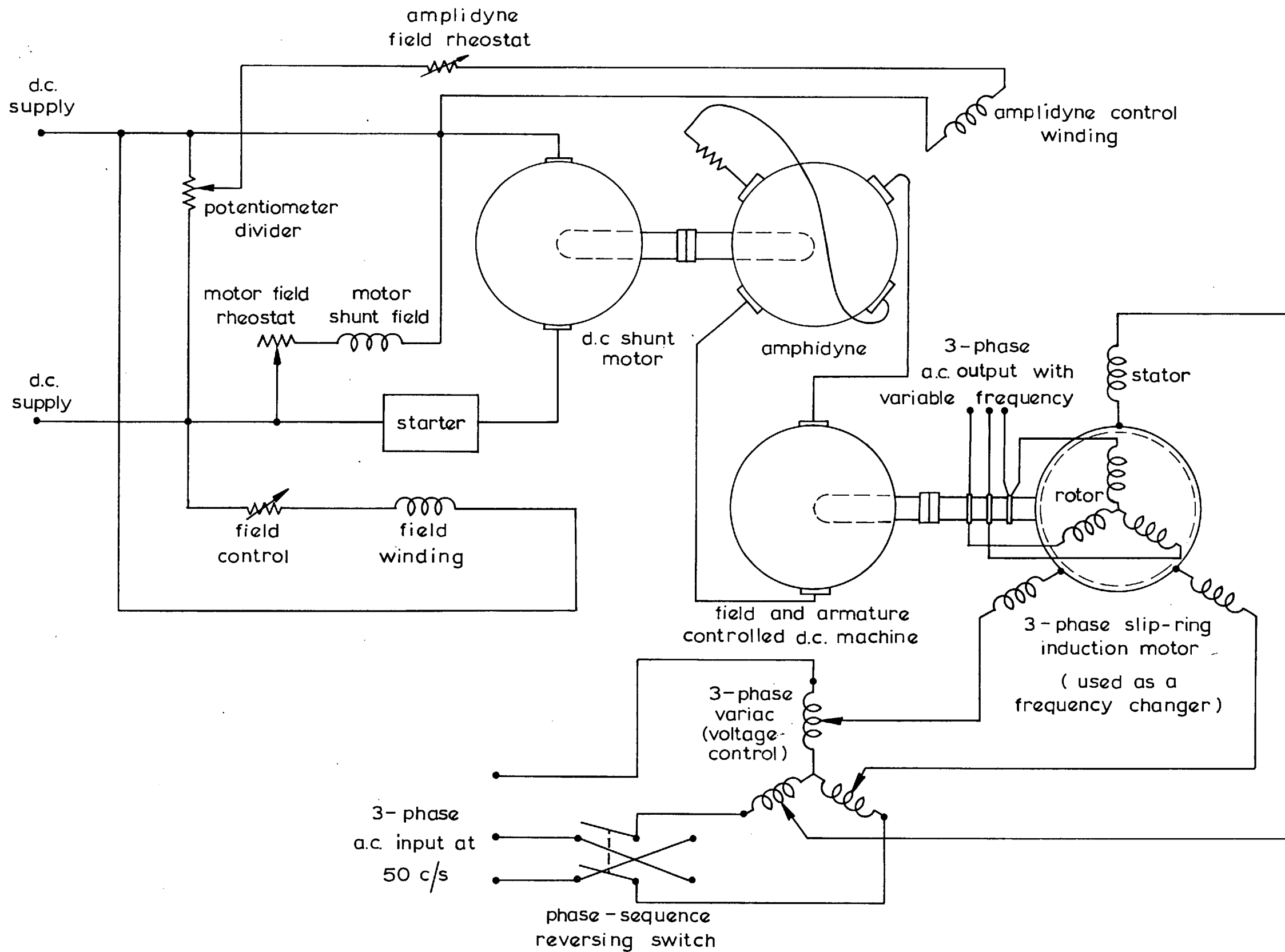


FIG. 5.2.3.  
SCHEMATIC DIAGRAM OF A SYSTEM FOR CHANGING FREQUENCY

any two phases by means of a reversing switch.

An amplidyne, driven by a d.c. shunt motor, was used to control the armature current of the d.c. machine and hence its speed. A rheostat in the field circuit provided the other means of speed control. The former and latter types of speed control may be considered as fine and course control respectively.

This system, being an open-loop control system, does not provide a highly stable frequency output. However, the variation of the output frequency has been found to be within  $\pm 0.1$  c/s which will have a negligible effect on the accuracy of the various experiments conducted.

This system, besides providing the required levels of voltages, currents and powers, allows the use of transformer type phase-shifters equipped with dials which directly indicate the phase angles.

### 5.3. Effects of the Various Factors on the Modulation Frequency Response.

To study the effects of various parameters, modes of operation and conditions of the modulating input voltages on the modulation frequency responses of chopper networks, a large number of experiments have been performed. These experiments, however, can only be considered representative and not exhaustive. To keep the number of the experiments to the minimum without affecting the maximum possible variety of useful information, the following passive electric elements incorporated in the various chopper networks under investigation were kept constant all throughout at the value

$$G_1 = G_2 = 0$$

5.3.1.

except in one case when dealing with the chopper network of Fig. 4.3.1-c.

In the present work, the modulation frequency responses are studied with two types of modulating input voltages, viz., multiplicative modulation and rotary modulation. The former type is used in various experiments included in Sub-sections 5.3.1 to 5.3.6 and the latter type is included in the remaining Sub-section.

The various studies carried out are outlined below.

#### 5.3.1. Variations of the passive electric elements.

Under the condition expressed by Eqn. 5.3.1, the modulation frequency response can be varied with only one degree of freedom. This is the time constant  $\tau$ . Changing the value of this time constant can be attained by changing either C or G. The latter was adopted for it was practically simpler.

Figs. 5.3.1 to 5.3.3 show the effects of varying the time constant  $\tau$  on the multiplicative modulation transfer functions of the chopper network configurations illustrated in Fig. 4.1.3. Other data and operating conditions under which the experiments were conducted are given under each figure.

A study of the figures shows that although the shapes of the various loci are maintained virtually as semicircles, the d.c. modulation transferences and the distribution of the modulation frequencies along the loci vary as  $\tau$  changes.

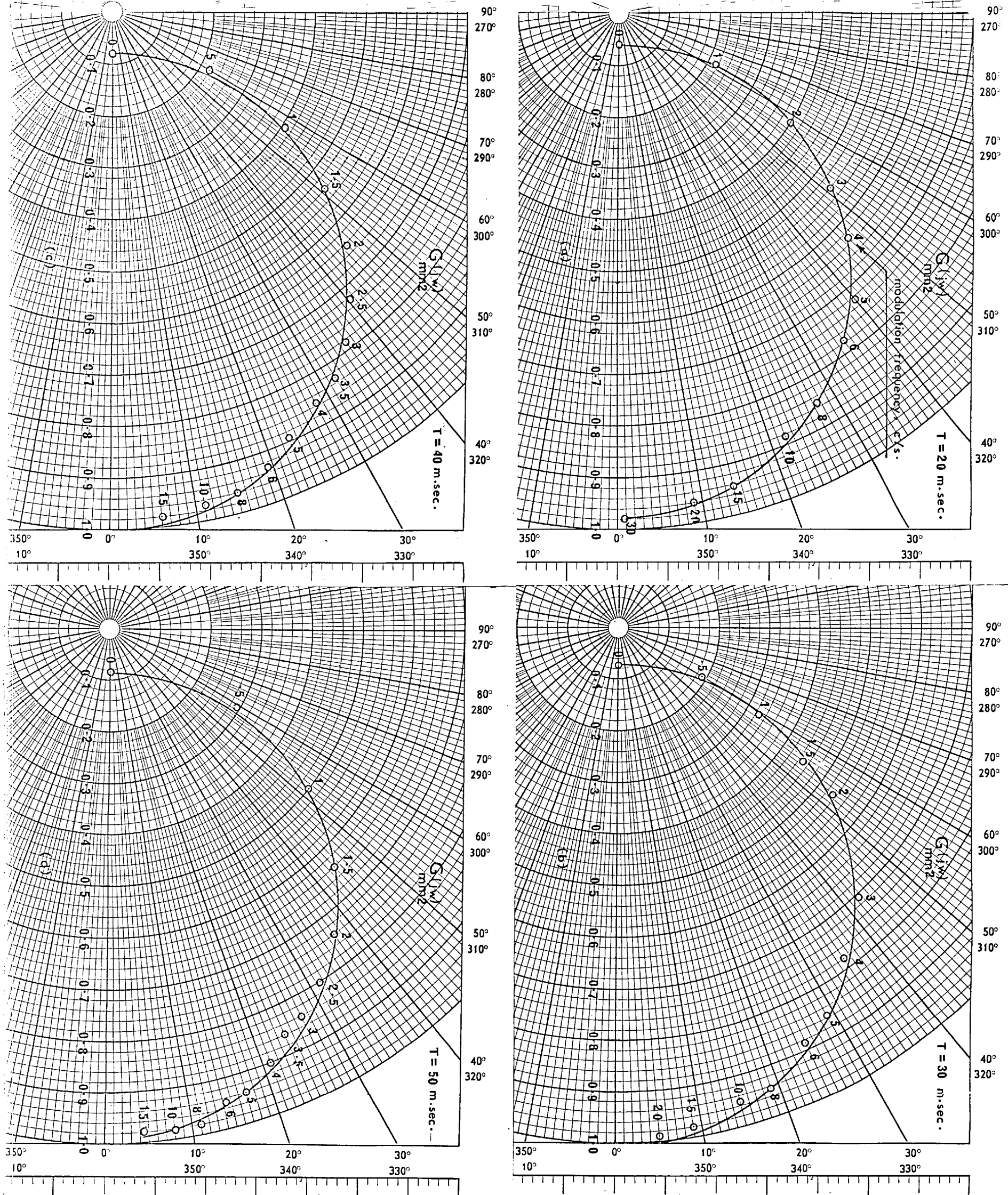


FIG. 5.3.1.  
 MULTIPLICATIVE MODULATION FREQUENCY RESPONSE LOCI OF SINGLE - SWITCH  
 DOUBLE - CAPACITOR CHOPPER NETWORK

DATA :

$$\Omega = 314 \text{ RAD. / SEC.}$$

$$\delta = 0.5$$

$$\theta = 0^\circ$$

$$\phi = 0^\circ$$

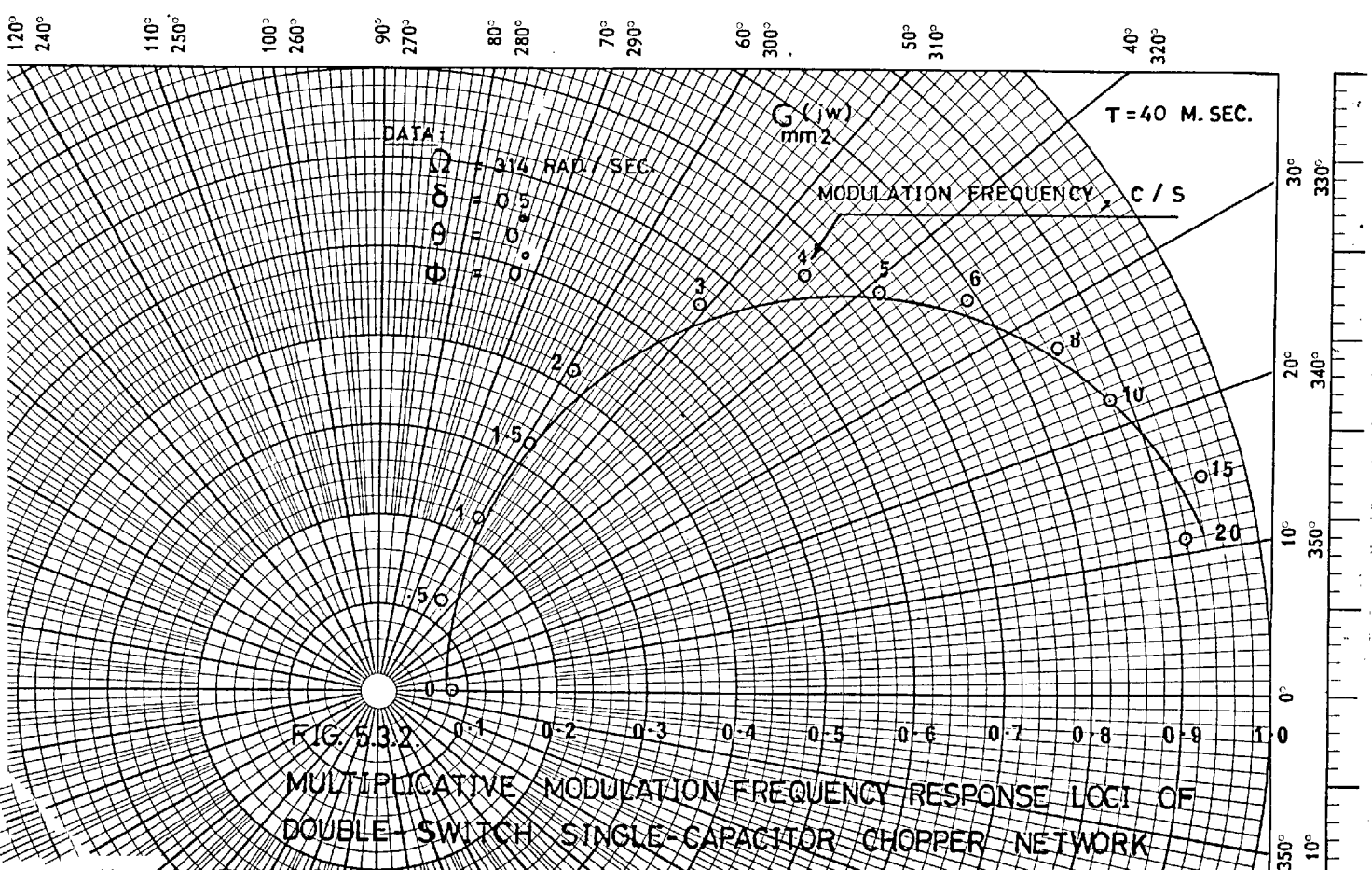
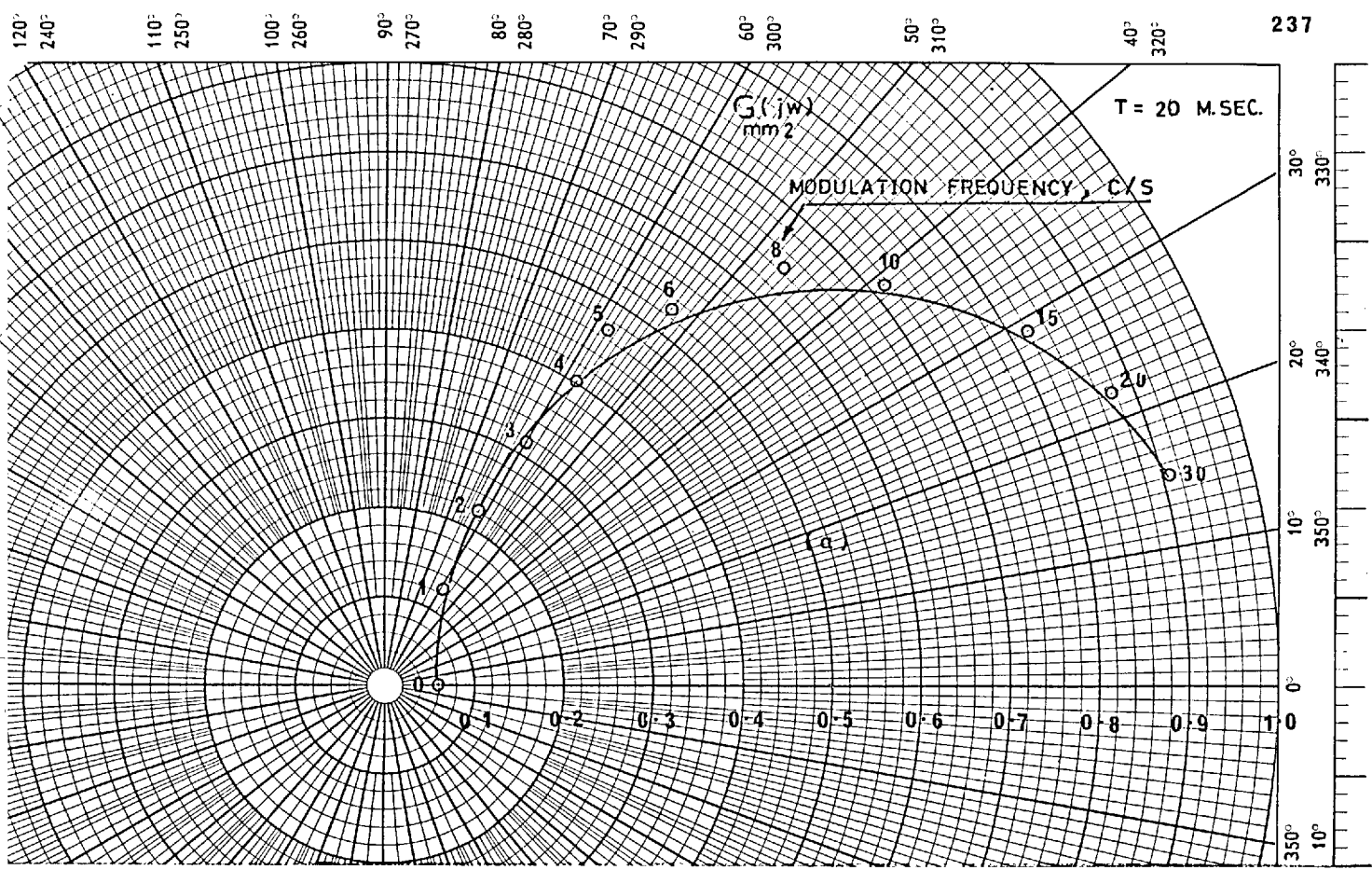
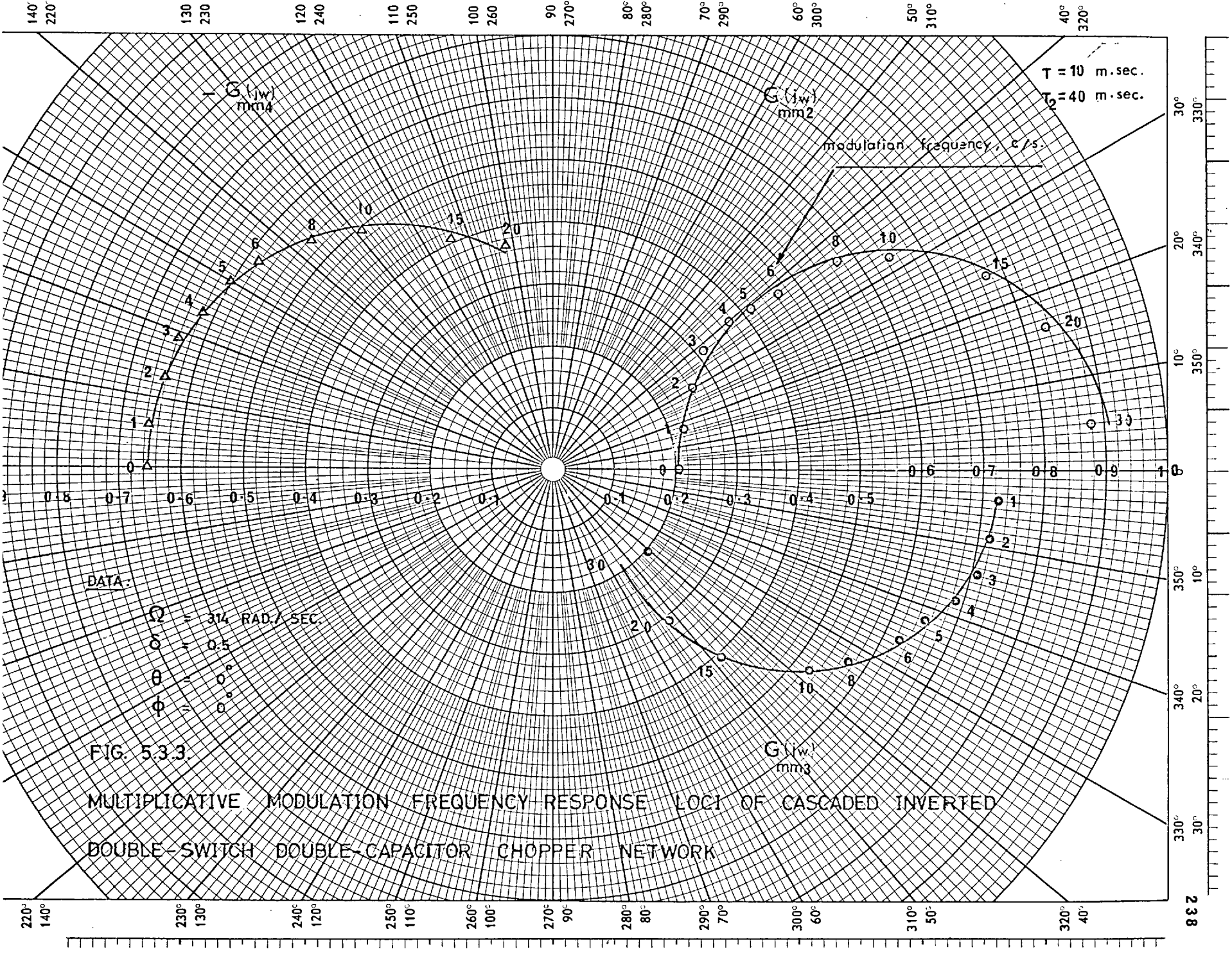


FIG. 5.3.2  
MULTIPLICATIVE MODULATION FREQUENCY RESPONSE LOGI OF  
DOUBLE-SWITCH SINGLE-CAPACITOR CHOPPER NETWORK



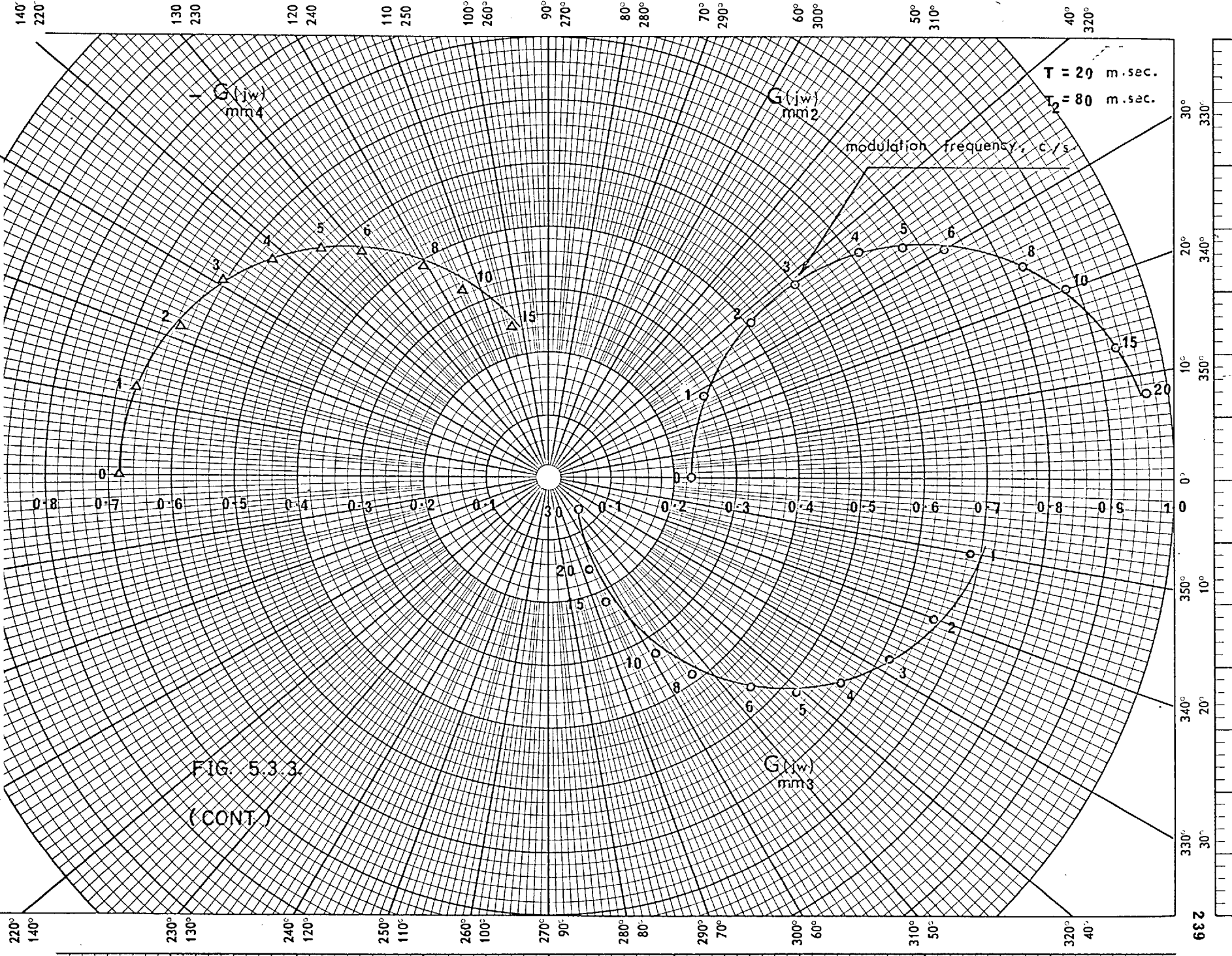


FIG. 5.3.3  
 (CONT.)

To show these effects even much more clearly, the d.c. modulation transference and the normalized equivalent d.c. network frequency  $\omega_n/\Omega$  (see definition in Section 4.3.4) have been plotted against the normalized time constant  $\tau/T$  for the single-switch double-capacitor chopper network as shown in Figs. 5.3.4 and 5.3.5 respectively. In addition, curves showing the dependence of the maximum phase-lead introduced by the chopper network under investigation and the frequency occurring at this maximum phase-lead, on a normalized basis, upon the normalized time constant  $\tau/T$  are illustrated in Figs. 5.3.6 and 5.3.7 respectively.

### 5.3.2. Fly-time of the synchronous switches

To study the effect of the fly-time of the synchronous switches incorporated in the chopper networks, on their responses a series of experiments were conducted on the single-switch double-capacitor chopper network as an example. The fly-time was varied in steps from zero to 0.2 and the corresponding multiplicative modulation frequency responses were measured, keeping other parameters and operating conditions constant. Fig. 5.3.8 shows the plots of the loci of these responses for both the phase-lead and phase-lag modes of operation. The semi-circular shape of the various loci does not seem to be significantly affected. However, a slight change in the modulation frequency distribution along the loci is observed. On the other hand, the fly-time shows a marked effect on the d.c. modulation transference as further displayed in Fig. 5.3.9. The significance of this effect lies not only in the amount of change in the d.c. transference but also in the change of its sign. Because, as the d.c. transference changes its sign, the behaviour of the chopper network becomes such that the instability of the a.c. servo-mechanism is aggravated, and the chopper



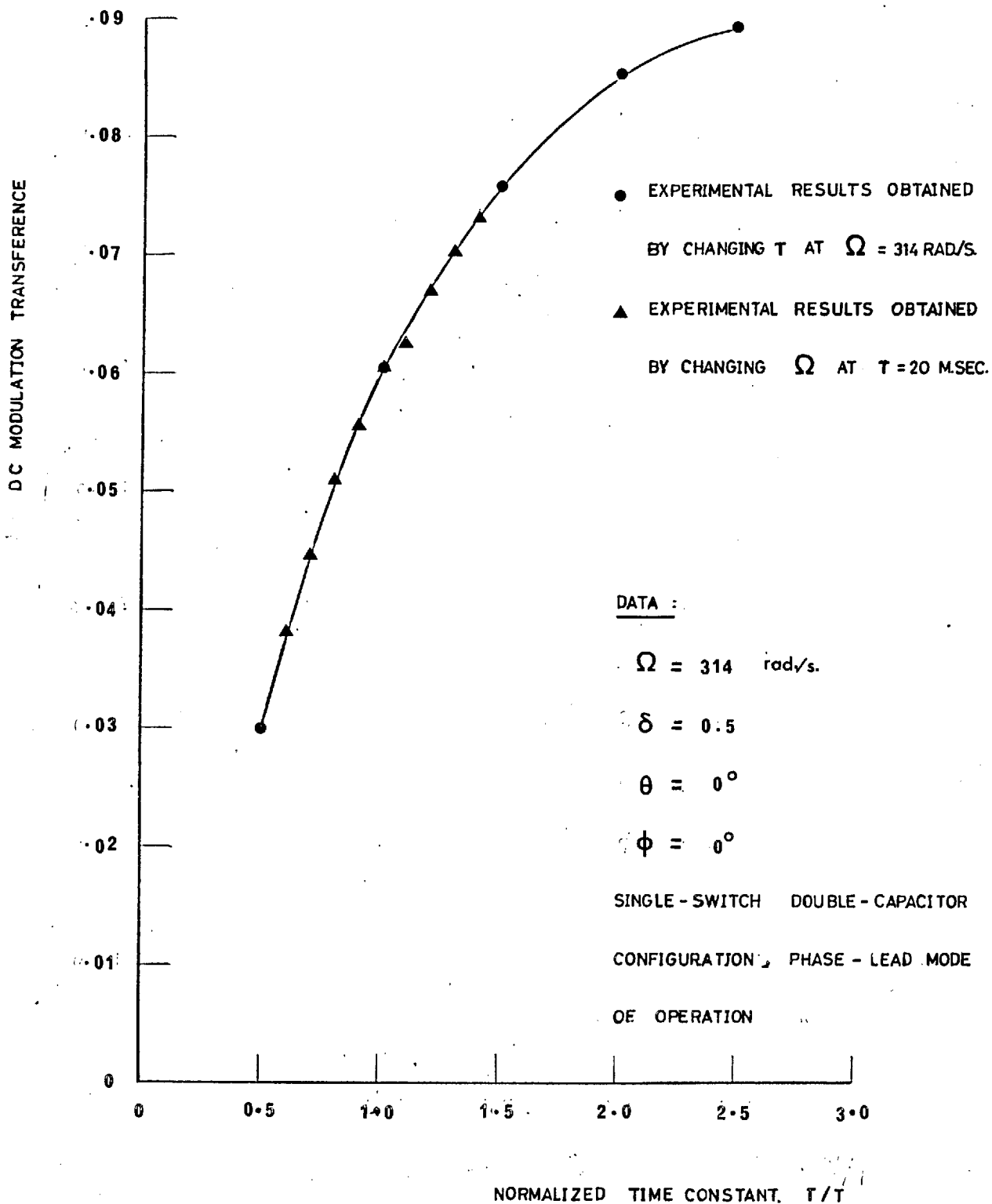


FIG. 5.3.4.

VARIATION OF DC MODULATION TRANSFERENCE WITH THE NORMALIZED TIME CONSTANT  $T/T$

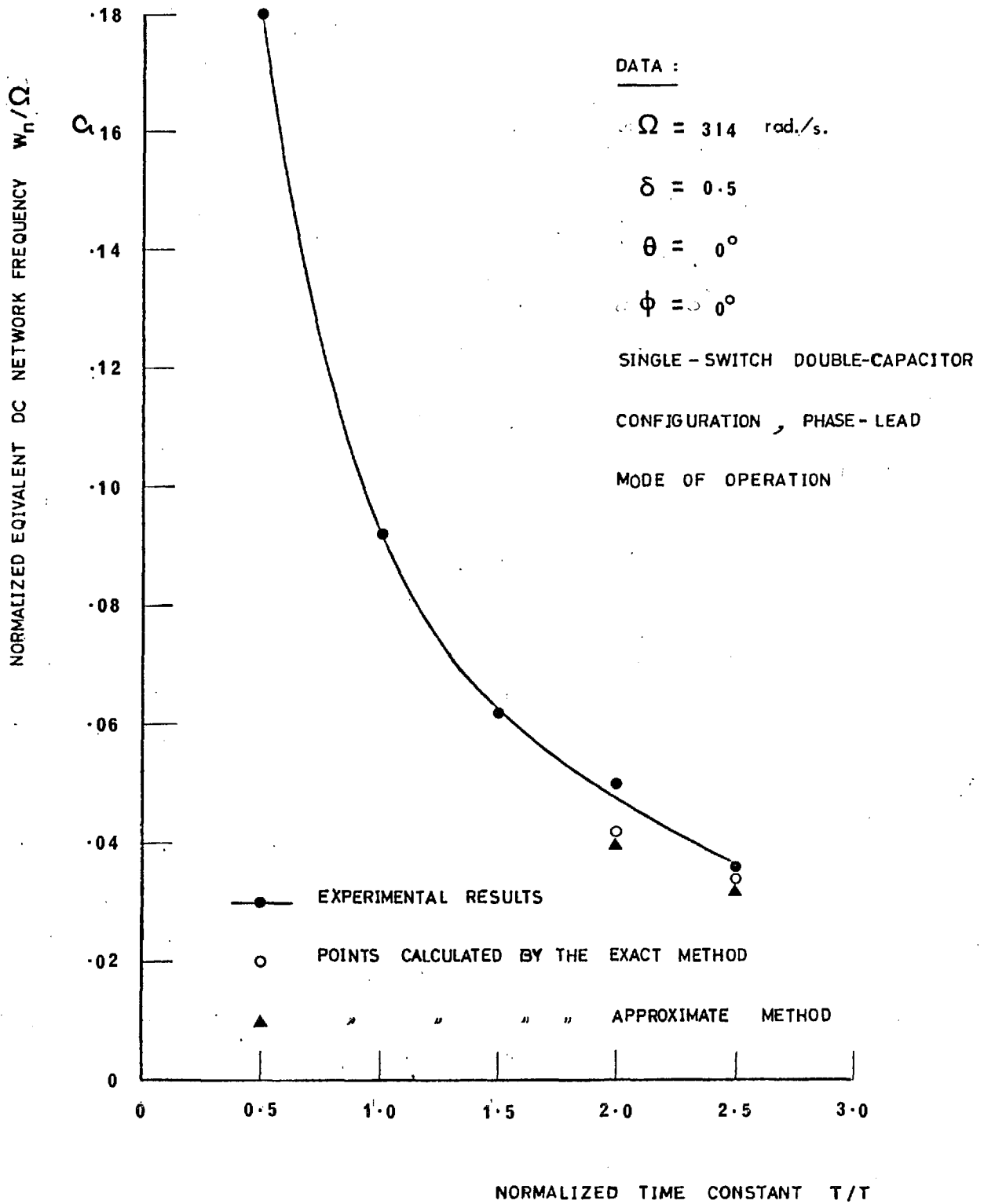


FIG. 5.3.5.

VARIATION OF THE NORMALIZED EQUIVALENT DC NETWORK FREQUENCY  $\omega_n/\Omega$  WITH THE NORMALIZED TIME CONSTANT  $\tau/T$

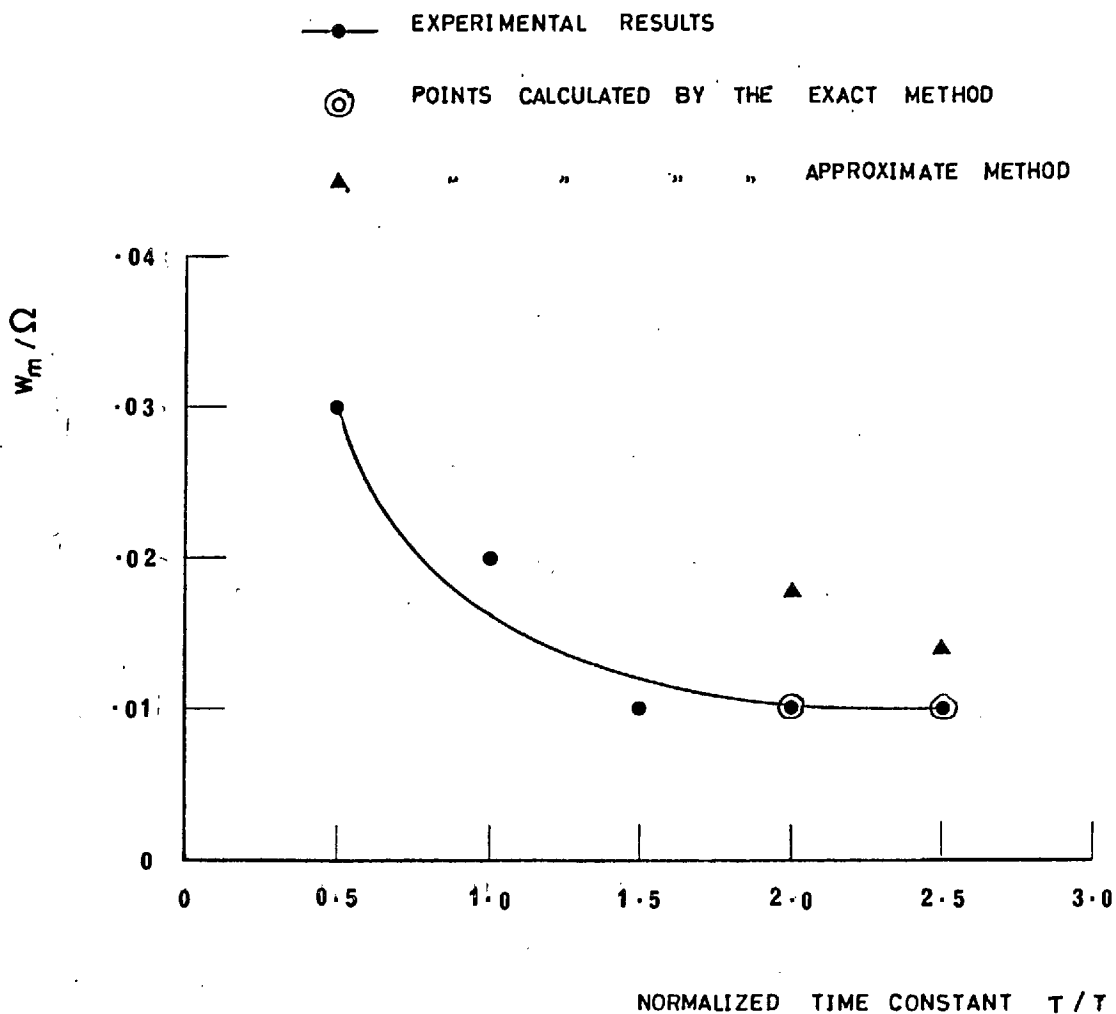


FIG. 5.3.6.

THE DEPENDENCE OF THE NORMALIZED FREQUENCY  $W_m/\Omega$   
ON THE NORMALIZED TIME CONSTANT  $\tau/T$

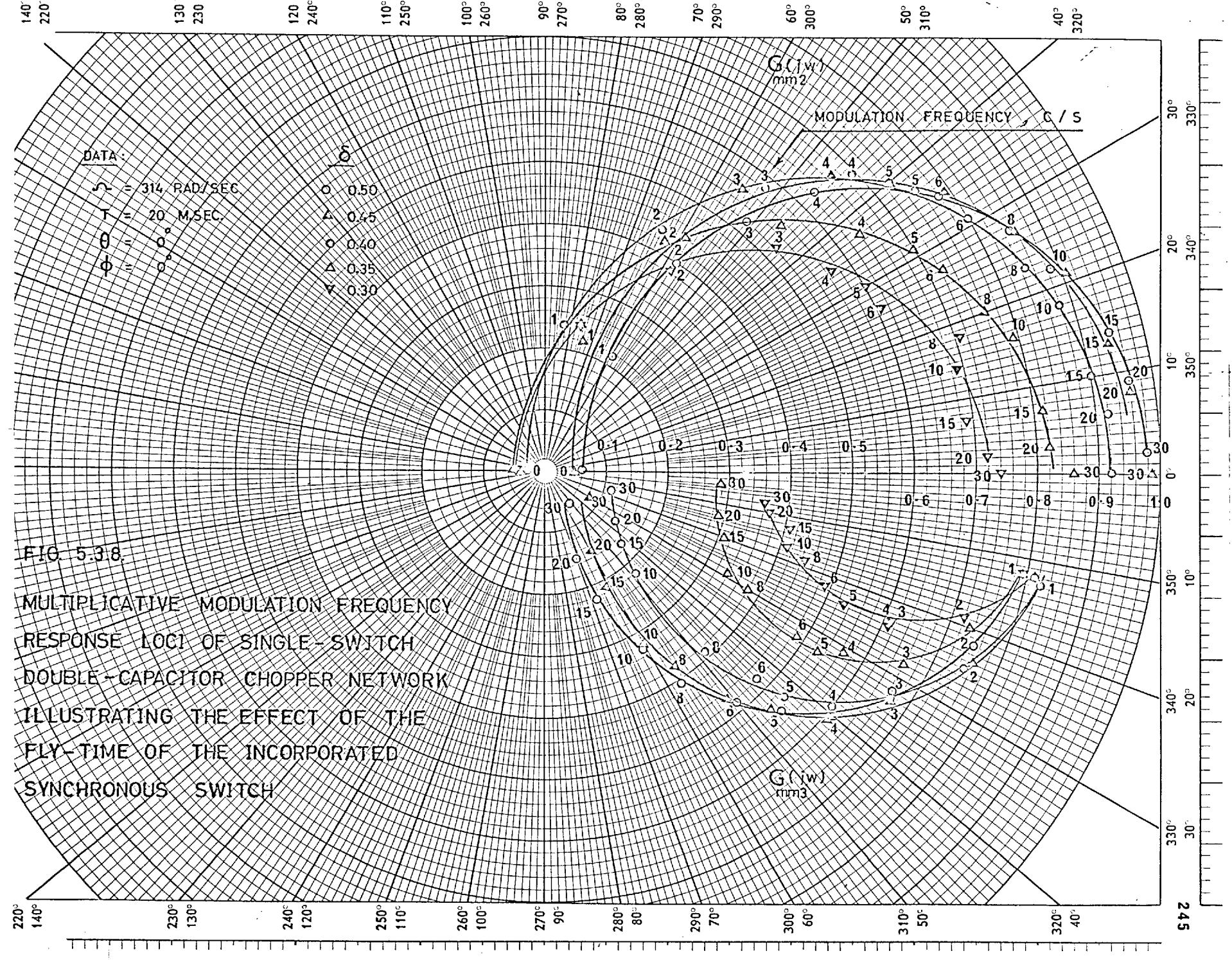
( SINGLE - SWITCH DOUBLE - CAPACITOR CONFIGURATION , PHASE - LEAD  
MODE OF OPERATION )

DATA :

$$\Omega = 314 \text{ rad/s.} \quad \theta = 0^\circ$$

$$\delta = 0.5 \quad \phi = 0^\circ$$





DATA :

SEE DATA OF FIG. 5.3.8.

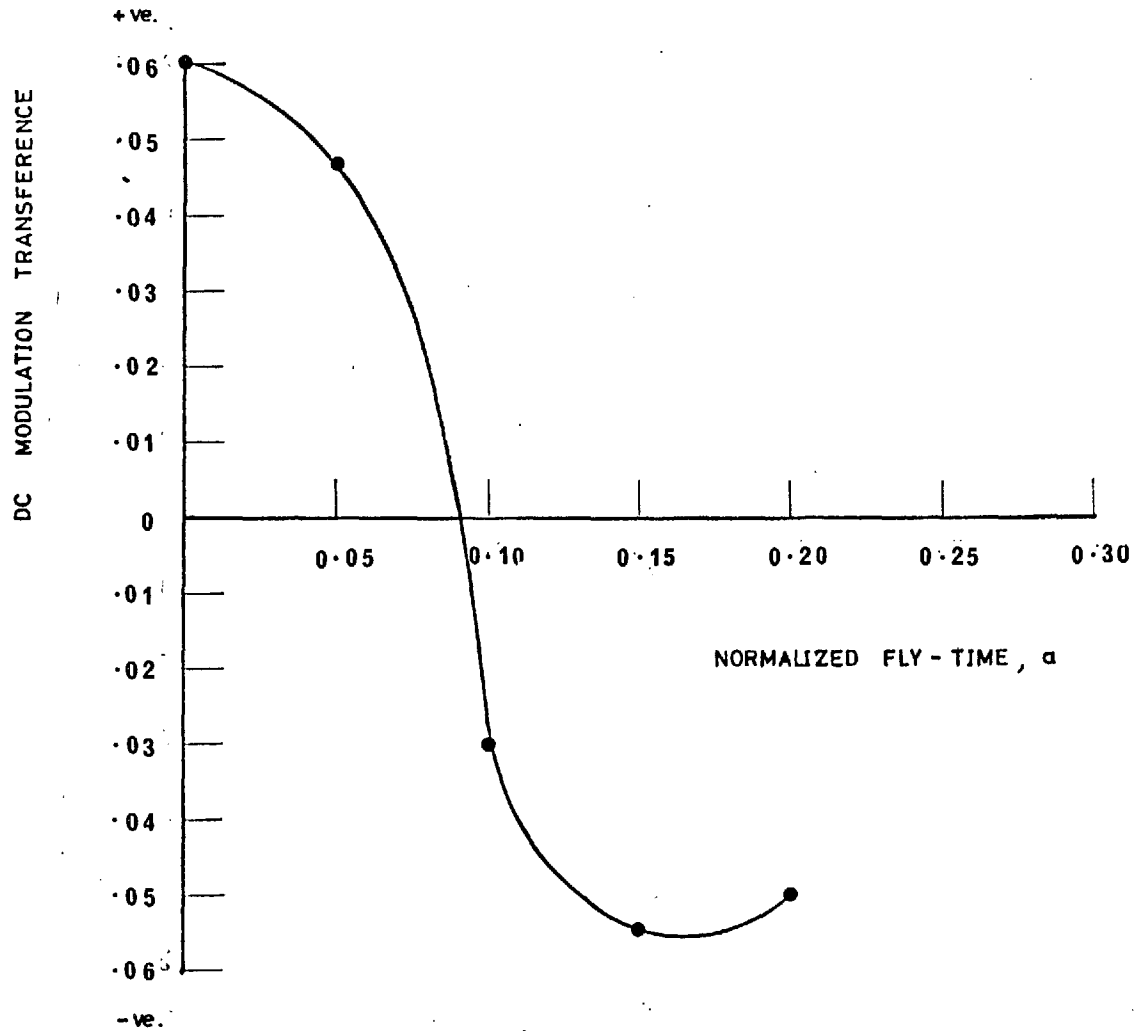


FIG. 5.3.9.

VARIATION OF DC MODULATION TRANSFERENCE WITH THE  
NORMALIZED FLY-TIME OF THE SYNCHRONOUS SWITCH

(SINGLE-SWITCH DOUBLE-CAPACITOR CONFIGURATION, PHASE-LEAD

MODE OF OPERATION)

network will therefore no longer be suitable as a compensating device.

For example, the single-switch double-capacitor chopper network, according to Fig. 5.3.9, will cease to be a suitable phase-lead compensator to a.c. servo-mechanisms over the region of the synchronous switch fly-time lying above 0.09, provided that the values of the various parameters and conditions of operation are as enlisted on the figure.

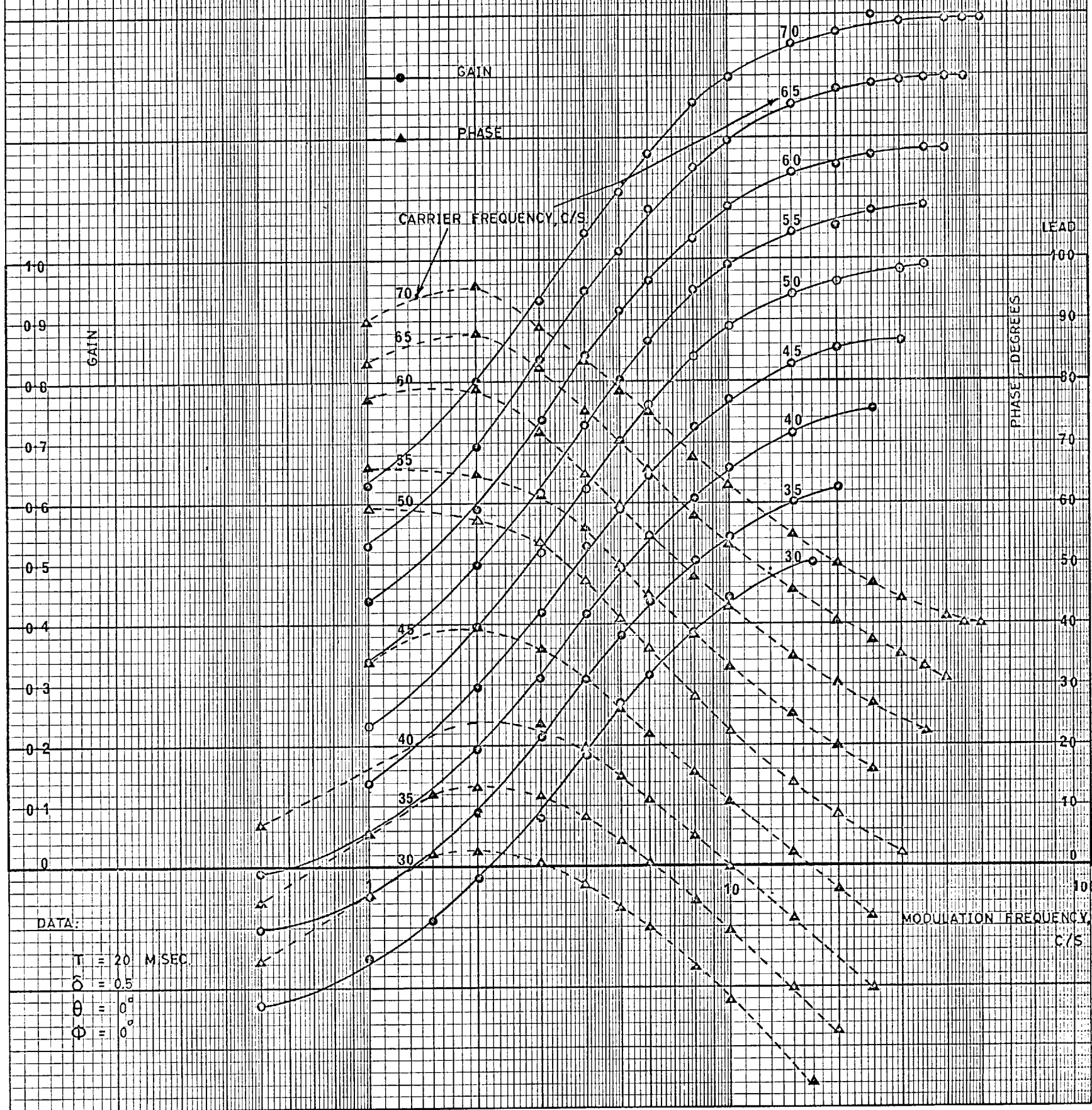
It may be worthwhile mentioning that the conclusions drawn above are even much more important particularly when mechanical synchronous switches are employed in view of the unavoidable physical fly-time associated with them.

### 5.3.3. Carrier frequency deviation.

As mentioned earlier in this thesis, the carrier frequency deviation is a common problem in air-borne equipment. It is therefore important to examine its effects on the chopper network's performance.

The carrier frequency was varied in steps from 30 c/s to 70 c/s (i.e. in the range of  $\pm 40\%$  of the nominal carrier frequency of 50 c/s), without changing any other parameter, and the multiplicative modulation frequency gain and phase responses of single-phase double-capacitor chopper network were measured. These experimental results are plotted versus the modulation frequency as shown in Fig. 5.3.10, where the gain and phase axes are associated with the curves at 50 c/s carrier frequency. The curves at other carrier frequencies are shifted vertically by constant equal distances to allow for a better comparison.

FIG. 5.3.10.  
 MULTIPLICATIVE MODULATION FREQUENCY GAIN AND PHASE RESPONSES OF  
 SINGLE-SWITCH DOUBLE-CAPACITOR CHOPPER NETWORK UNDER DIFFERENT  
 VALUES OF CARRIER FREQUENCY



DATA:  
 $T = 20$  M/SEC.  
 $\phi = 0.5$   
 $\theta = 0^\circ$   
 $\alpha = 0^\circ$



A thorough examination of these curves reveals that by changing the carrier frequency between the limits 0.6 to 1.4 times the nominal value of 50 c/s, a negligible effect results in both the modulation gain and phase particularly for high modulation frequency values. In the very low modulation frequency region, however, small changes were observed in both the modulation gain and phase responses. To bring out the effect on the former even more clearly, d.c. modulation transference is plotted against  $\tau/T$  as shown in Fig. 5.3.4.

#### 5.3.4. Phase variations of the demodulation carrier reference.

In a.c. servo-mechanisms utilizing 2-phase servomotors, phase shift is introduced into the carrier excitation reference mainly by the stator impedance as it has been shown in Chapter 2. If chopper networks are to be inserted in the carrier channels of such systems, knowledge of the changes in their dynamic performances which may be caused by the change in the phase of the demodulation reference will be of profound importance to the designer.

A representative set of experimental curves showing the effect of varying the phase of the demodulation reference on the multiplicative modulation transfer function response loci of single-switch double-capacitor chopper network is illustrated in Fig. 5.3.11. Further data and information on the modes of operation are given in the figure.

A study of these loci shows that the phase of the demodulation reference has a pronounced effect on both the shape and magnitude of the modulation response. The effect is even much more significant in the low modulation frequency

region. It was also found that the d.c. modulation transference varies sinusoidally with the phase of the demodulation reference as shown in Fig. 5.3.14.

For the phase-lead mode of operation, the maximum modulation phase shift increases (which is desirable in some applications) as the phase of the demodulation reference advances. Meanwhile, the whole modulation locus shrinks. On the other hand, as the phase of the demodulation reference retards, considerable deterioration in the shaping quality of the chopper network takes place in terms of decrease in the maximum modulation phase shift and shrink in the modulation locus. Also, if the d.c. modulation transference changes sign (see Fig. 5.3.14), the chopper network might contribute to destabilizing the a.c. system in which it is incorporated which is contrary to its prime function.

In view of the above discussion, a conclusion may be drawn that the unavoidable phase shift of the demodulation reference effected in the 2-phase servo-motor can give rise to considerable deterioration in the shaping characteristics of the compensating chopper network. Furthermore, by deliberately adjusting the phase of the demodulation reference, a useful control of the chopper networks modulation responses can be achieved but at the expense of introducing further attenuation.

#### 5.3.5. Phase variations of the modulation carrier reference.

In practice, a large percentage of a.c. servo-mechanisms employ machine type error-detectors such as synchros, magslips, selsyns and similar devices. These devices, apart from producing rotary modulated signals,

introduce phase shifts into the carrier excitation reference due to their winding's impedances. It is therefore desirable to study the effects of this phase shift on the chopper networks modulation characteristics.

Fig. 5.3.12 shows a representative set of multiplicative modulation frequency loci of single-switch double-capacitor chopper network plotted at different values of the phase of the modulation carrier reference. These loci clearly show the pronounced effects on the shape, attenuation, and maximum phase shift of the modulation response. In addition, considerable change in the d.c. modulation transference is also observed. Since its value varies sinusoidally with the phase of the demodulation carrier reference  $\phi$ , only its peak value and the corresponding value of  $\phi$  at which it occurs were plotted against the phase of the modulation carrier reference  $\theta$  as shown in Fig. 5.3.15.

In this connection, it is important to mention that in deducing the d.c. modulation transference from the measured quantities, the formula expressed by Eqn. 5.2.1. should be modified to account for the phase misalignment between the modulation and demodulation carrier references. This can be done by adding the phase misalignment  $(\phi - \theta)$  to the angle difference  $(\theta_o - \theta_i)$  appearing in the formula. The same modification is also applicable to the case given in the previous Sub-section.

On the basis of both Figs. 5.3.12 and 5.3.15, it may be concluded that serious changes in the modulation responses of chopper networks can result from the phase shifts of the modulation carrier reference. However, by studying these changes thoroughly, it is possible to use the adjustment of the phase of modulation reference as a means of controlling

the modulation responses of chopper networks as well as for compensating the effects due to the unavoidable phase shifts taking place in the machine type error-detectors. In doing so, attenuation may take place and therefore a compromise would be required.

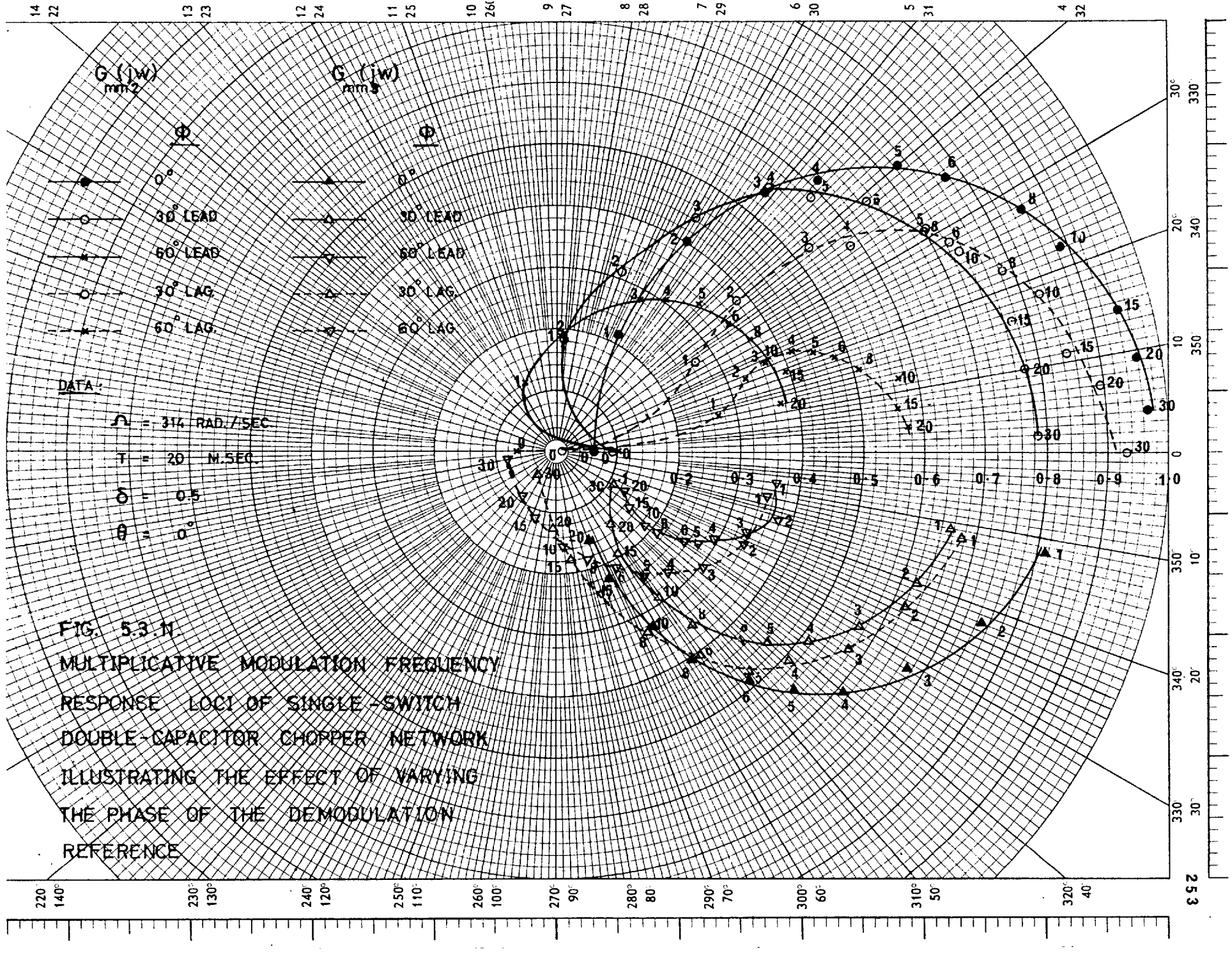
### 5.3.6. Combined effect of changing simultaneously the modulation and demodulation carrier references.

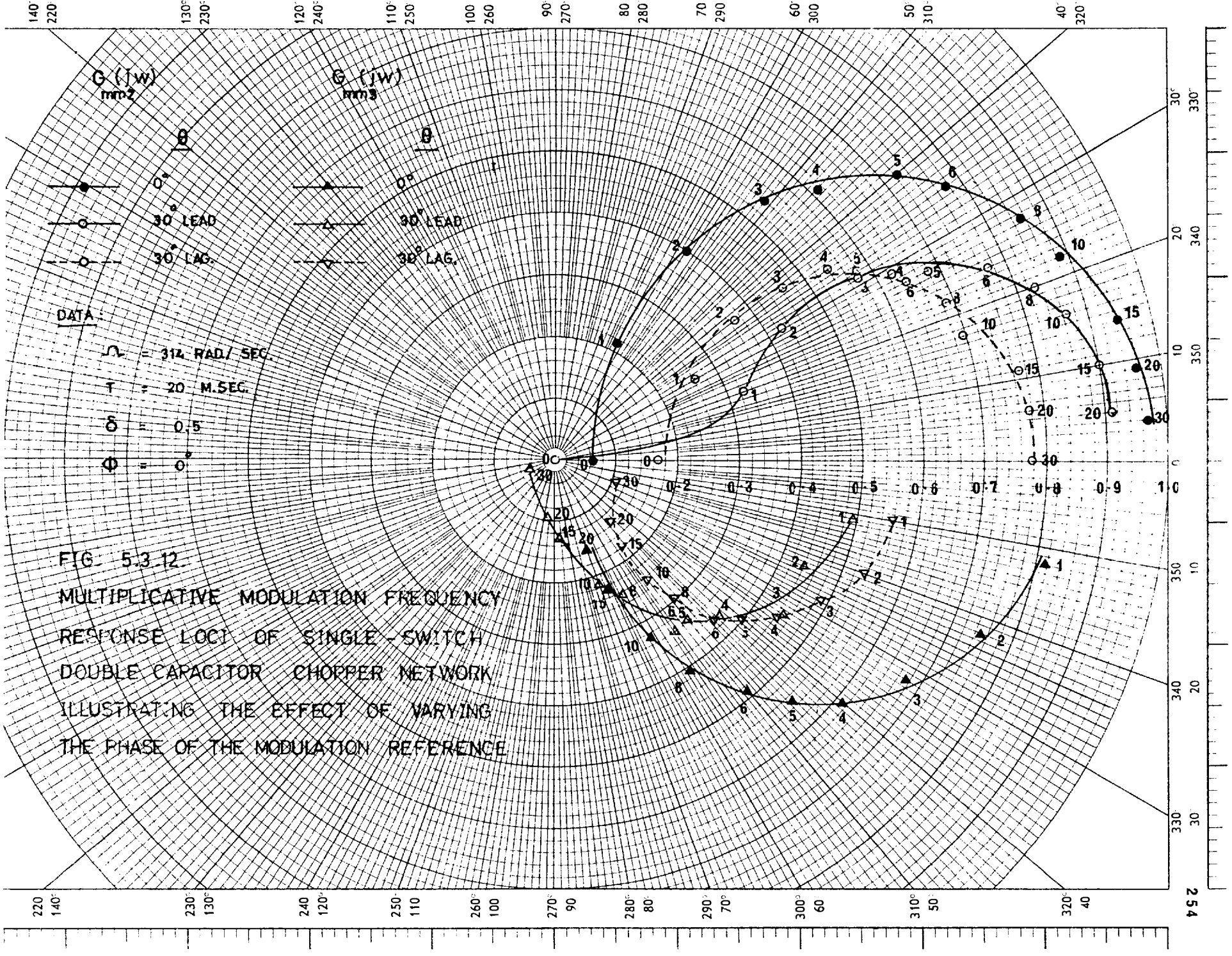
To give an idea about such combined effect on the modulation responses of chopper networks, a few representative multiplicative modulation frequency response loci are illustrated in Fig. 5.3.13. Curves similar to those shown in Figs. 5.3.14 and 5.3.15 can serve to provide the knowledge of how the d.c. modulation transference would change under this condition of operation.

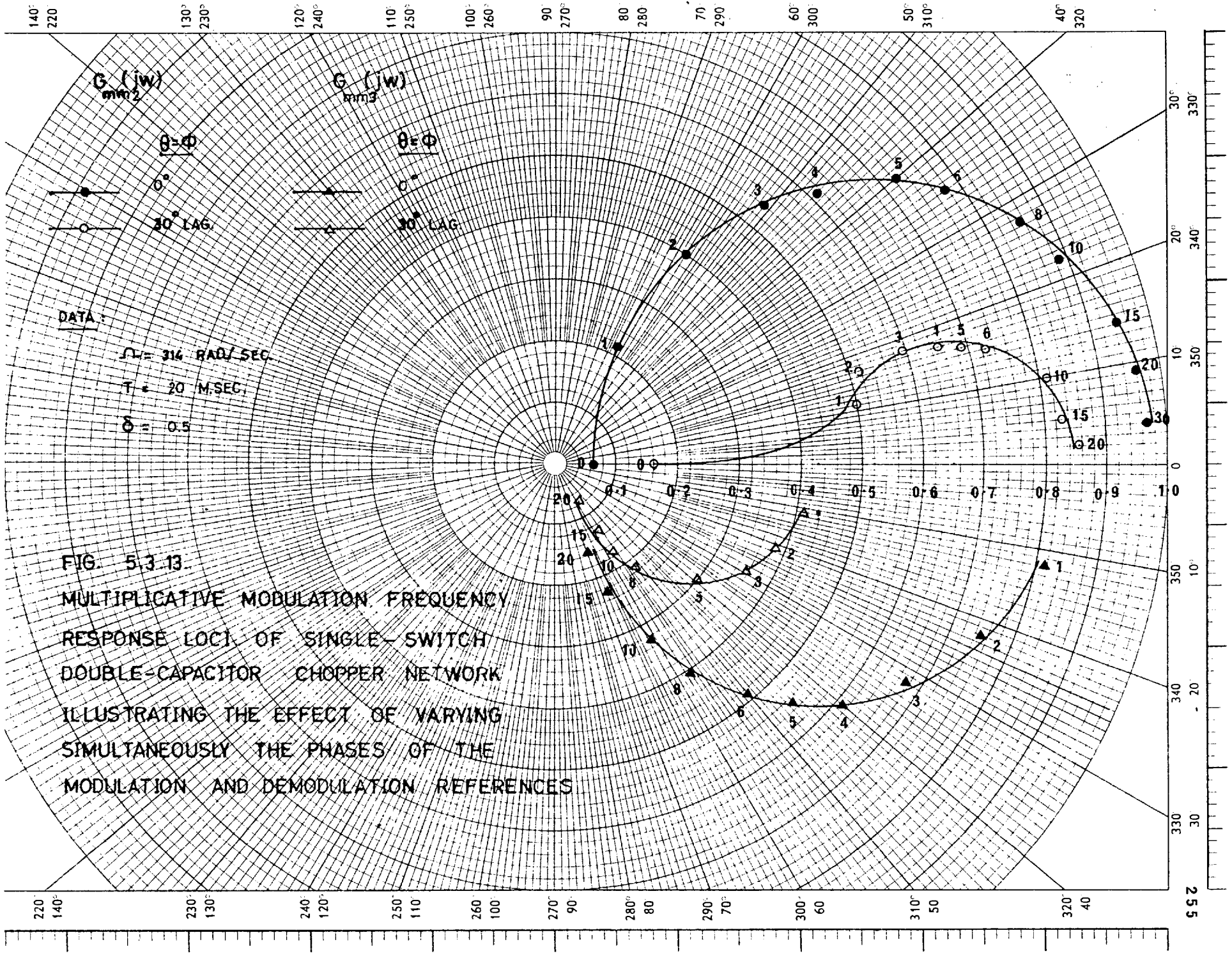
### 5.3.7. Rotary modulation.

As mentioned earlier, error-detectors in the form of synchros, magslips, selsyns and similar devices are characterized by producing rotary modulated signals. If chopper networks are employed to compensate a.c. servo-mechanisms incorporating such devices, their rotary modulated responses should then be considered. To do so, a simple means of generating a rotary modulated signal to be used as a test signal should be examined in the first place.

In the analysis presented in Chapter 2, the rotary modulated signal was correlated to suppressed-carrier amplitude-modulated (S.C.A.M.) wave as its rate of change with respect to time. In practice, this can be simulated by inserting a differentiator after an electronic modulator. The practical differentiating circuit<sup>133</sup> shown in Fig. 5.3.16







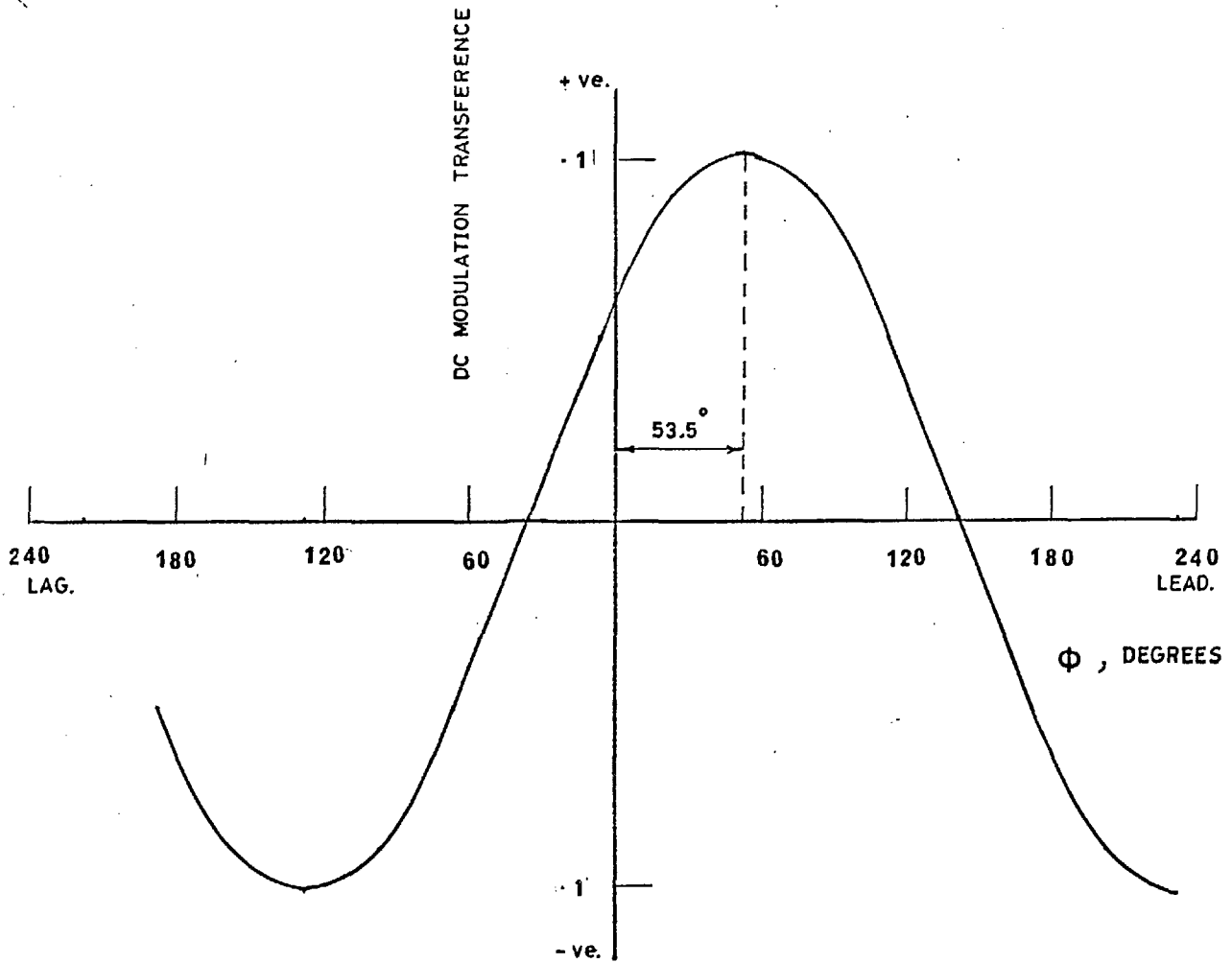


FIG. 5.3.14.

PLOT OF THE DC MODULATION TRANSFERENCE AS A FUNCTION OF THE PHASE OF THE DEMODULATION REFERENCE

DATA :

SEE DATA OF FIG. 5.3.11.



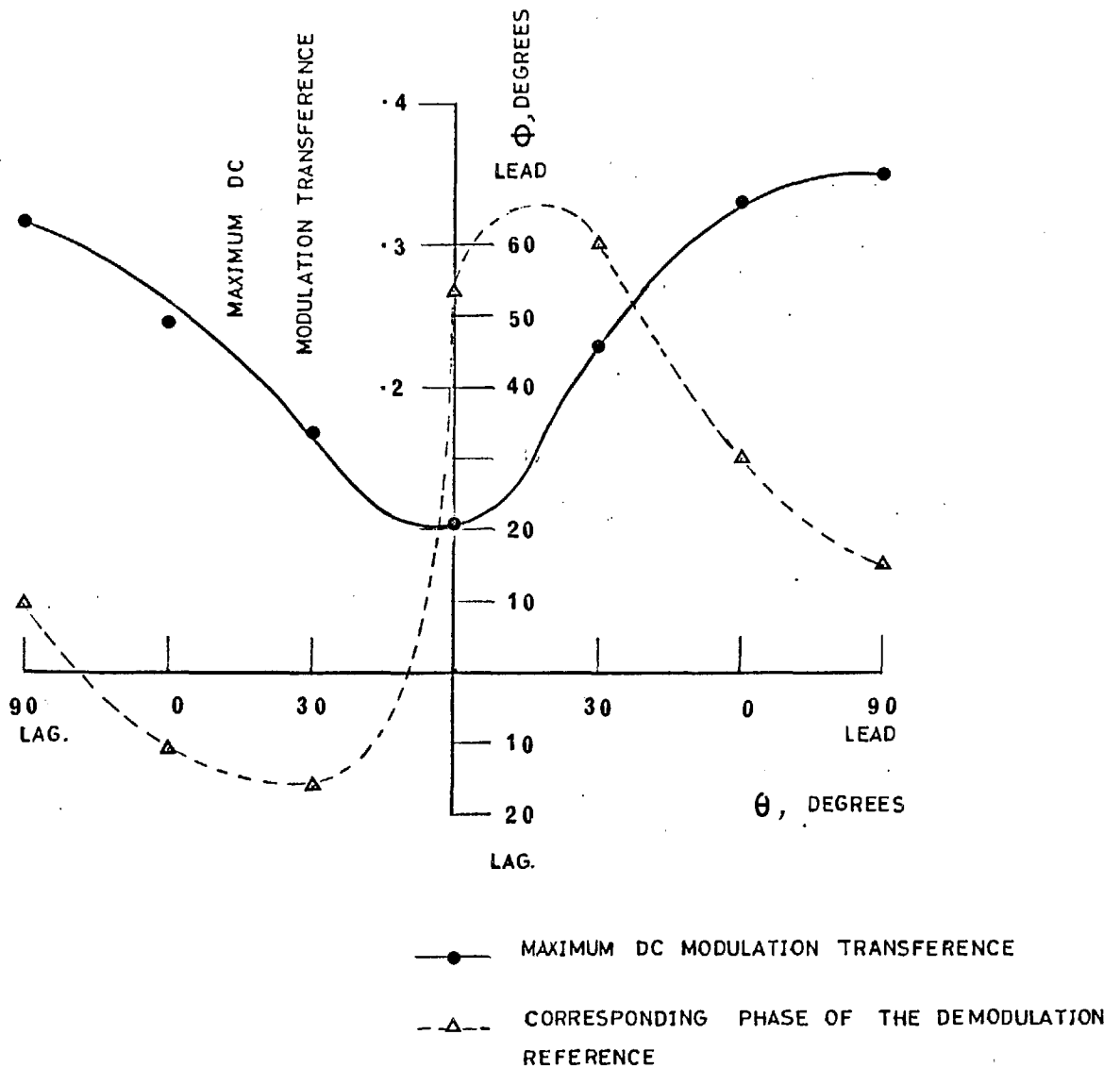


FIG. 5.3.15.

DEPENDENCE OF THE MAXIMUM DC MODULATION TRANSFERENCE  
 AND THE CORRESPONDING PHASE OF THE DEMODULATION REFERENCE  
 UPON THE PHASE OF THE MODULATION REFERENCE

DATA:

$$\omega = 314 \text{ RAD./SEC.}$$

$$T = 20 \text{ M. SEC.}$$

$$\delta = 0.5$$

SINGLE-SWITCH DOUBLE-CAPACITOR CONFIGURATION, PHASE-LEAD MODE OF OPERATION

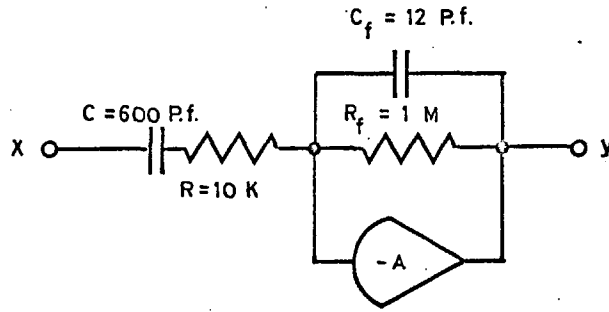


FIG 5.3.16.

A PRACTICAL DIFFERENTIATING CIRCUIT

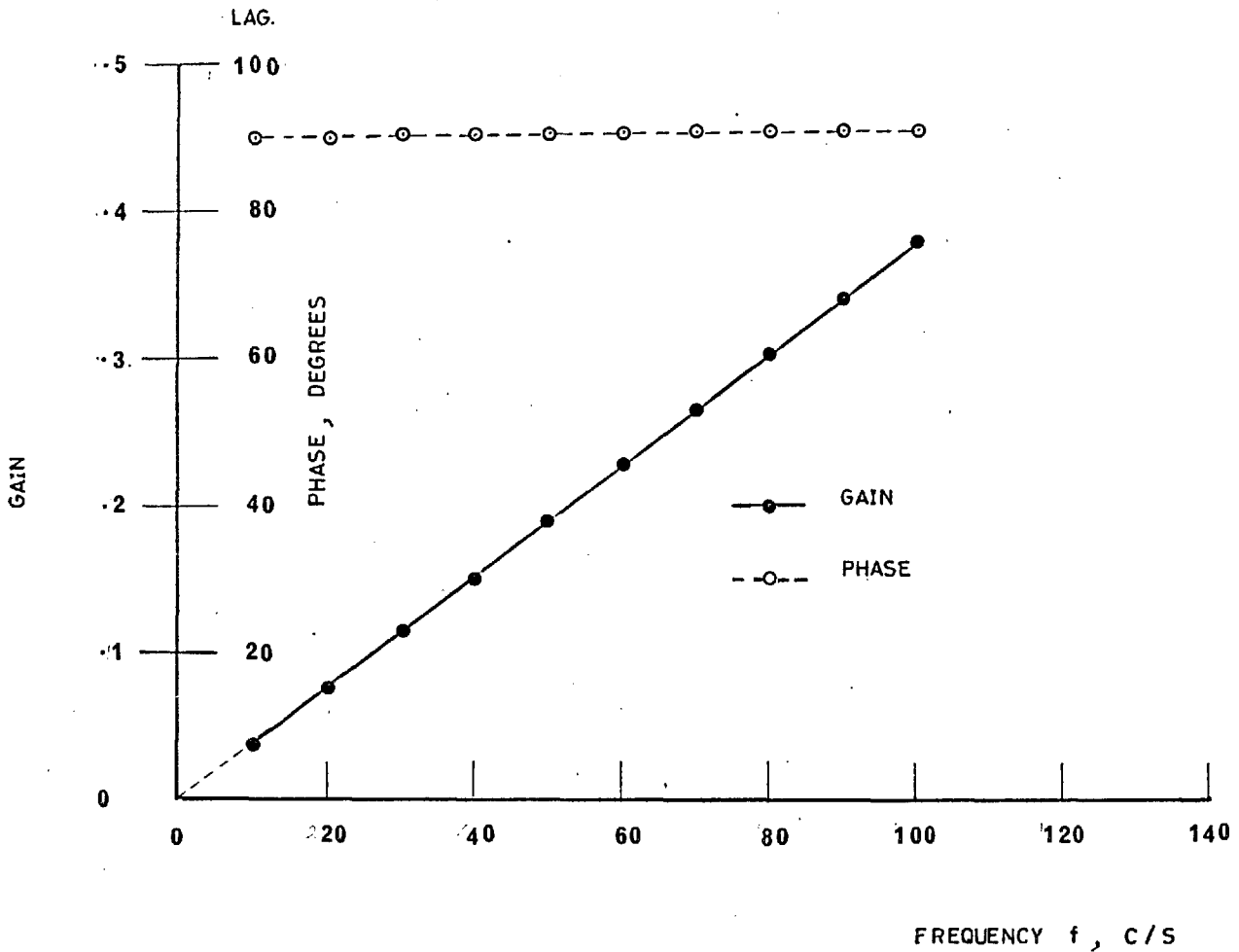


FIG. 5.3.17.

FREQUENCY RESPONSE OF THE DIFFERENTIATING CIRCUIT SHOWN IN FIG. 5.3.16.

was used in the Laboratory. This circuit was then incorporated in the test arrangement of Fig. 5.2.2 to enable rotary modulation responses of chopper networks to be measured. The frequency response of this circuit with a resistance load of 10 k was first tested and the results are shown in Fig. 5.3.17 in terms of gain and phase characteristics. Over the frequency range 20 to 100 c/s, the phase deviation from the  $90^\circ$ , expected from the ideal differentiator, is only one degree which can be considered negligible. The gain characteristics, on the other hand, is a good straight line which would pass through the origin when extended.

In testing the rotary modulation characteristics of chopper networks, both the phase reversal and the attenuation introduced by the differentiating circuit were taken into account. Such attenuation can either be deduced from the gain characteristics as the slope of the line or be calculated from the transfer function as given below

$$\text{transfer function } \frac{Y}{X} = - \frac{R_f C p}{(RC p + 1)(R_f C_f p + 1)} \quad 5.3.1.$$

where the approximate attenuation is  $R_f C$ .

Representative rotary modulated loci of single-switch double-capacitor chopper network are illustrated in Fig. 5.3.18. These loci were obtained at different values of the phase of demodulation reference ranging from  $90^\circ$  lag to  $90^\circ$  lead, whereas other parameters and conditions of operation were kept constant as indicated by the data given in the figure. The shape of locus changes considerably from almost a semi-circle at  $\phi = 90^\circ$  lead to a vertical line at  $\phi = 0^\circ$  then back again to almost a semi-circle at  $\phi = 90^\circ$  lag. A

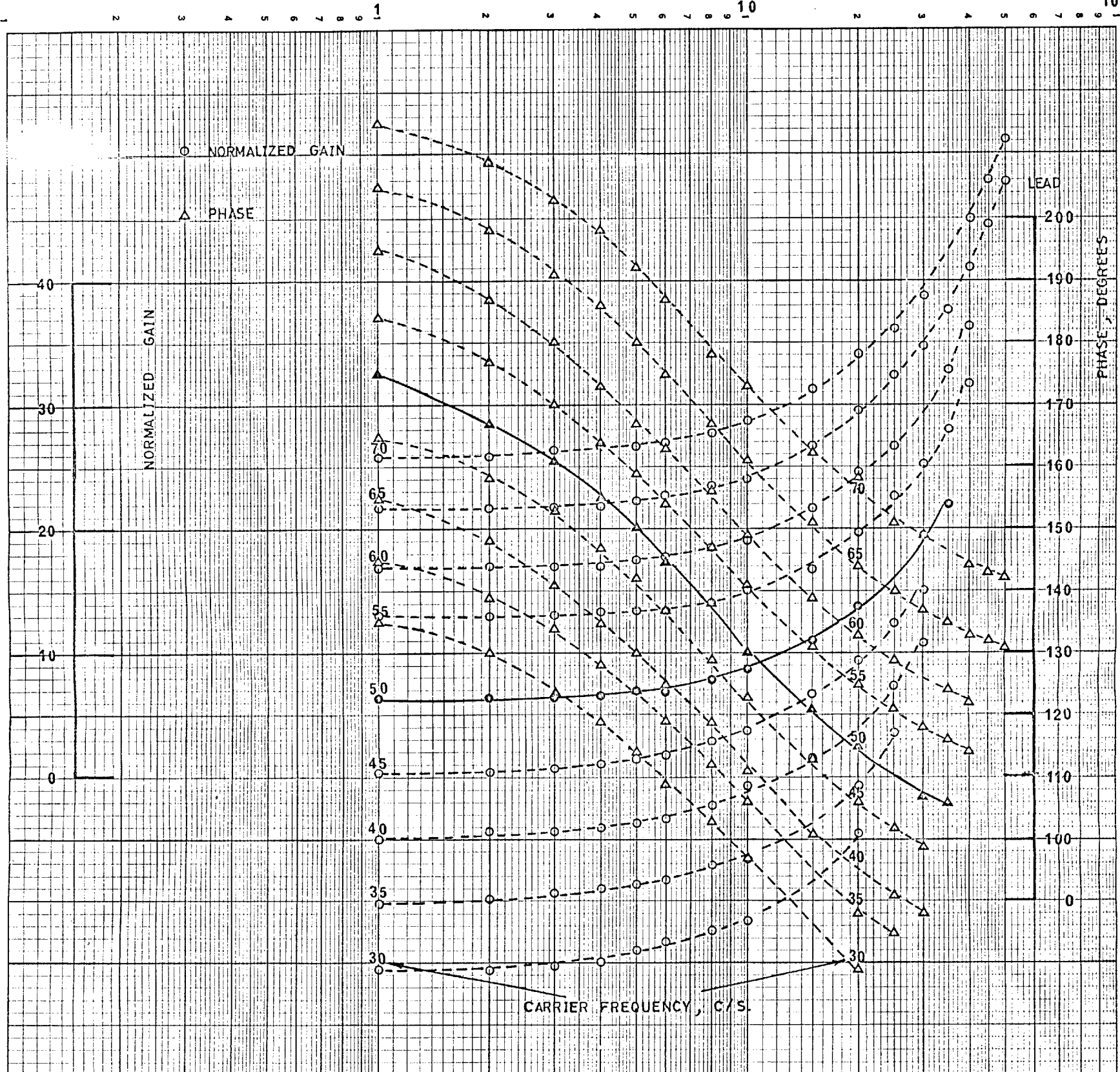


marked variation in the phase shift at various modulation frequencies is also observed.

In addition, experiments were conducted to determine the rotary modulation response under different values of carrier frequency. The results of these experiments are plotted in Fig. 5.3.19 in terms of rotary modulation gain and phase responses against modulation frequency. The gain and phase axes are associated with the curves at 50 c/s carrier frequency, whereas curves at other carrier frequencies are shifted by constant equal distances to allow for a better comparison. The good parallelism between these curves shows clearly that rotary modulation response of the chopper network under investigation is insensitive to carrier frequency variations over the range 0.6 to 1.4 times the nominal value of 50 c/s.

#### 5.4. Comparison of Results.

In the previous chapter, two analytical approaches to the analysis of chopper networks have been considered, viz., exact method and approximate method. To check the validity of the first method and to assess the approximation of the second method, comparison with experimental results was called for. In addition, comparison between the two theoretical methods, from the viewpoint of their applicability under different conditions of chopper network's operations, would supplement useful information. It was found convenient to conduct the various comparisons in three steps as outlined below.



CARRIER FREQUENCY, C/S.

DATA:

- T = 20 MSEC.
- $\delta$  = 0.5
- $\theta$  = 0°
- $\phi$  = 0°

FIG. 5.3.19.

ROTARY MODULATION FREQUENCY GAIN AND PHASE RESPONSES OF SINGLE-SWITCH DOUBLE-CAPACITOR CHOPPER NETWORK UNDER DIFFERENT VALUES OF CARRIER FREQUENCY

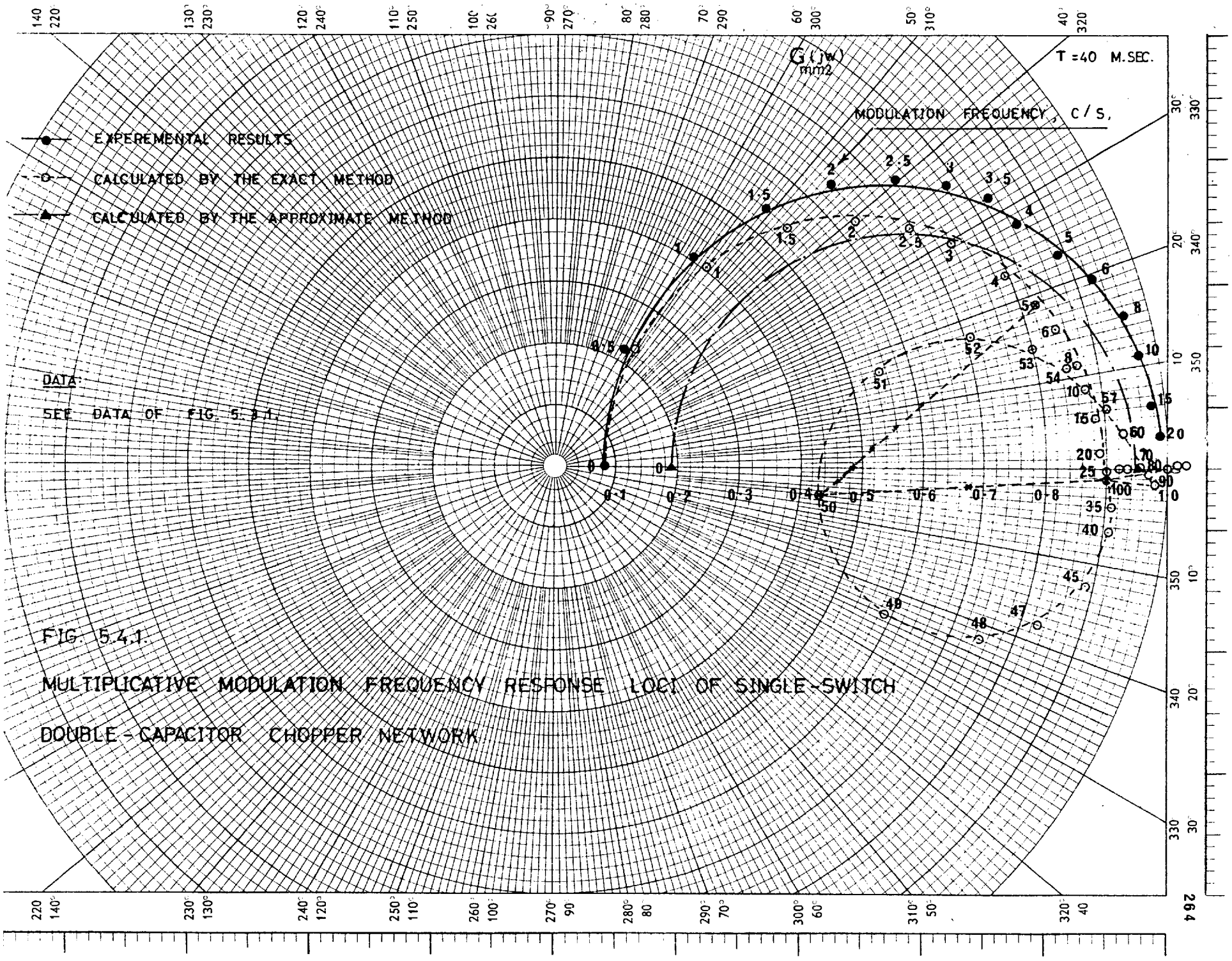
5.4.1. Experimental results versus theoretical calculations by the exact method.

Representative results showing the multiplicative modulation frequency response loci of two configuration types of chopper networks are shown in Figs. 5.4.1 to 5.4.3. The theoretical loci pertinent to the single-switch double-capacitor chopper network appear as if they are composed of three segments:

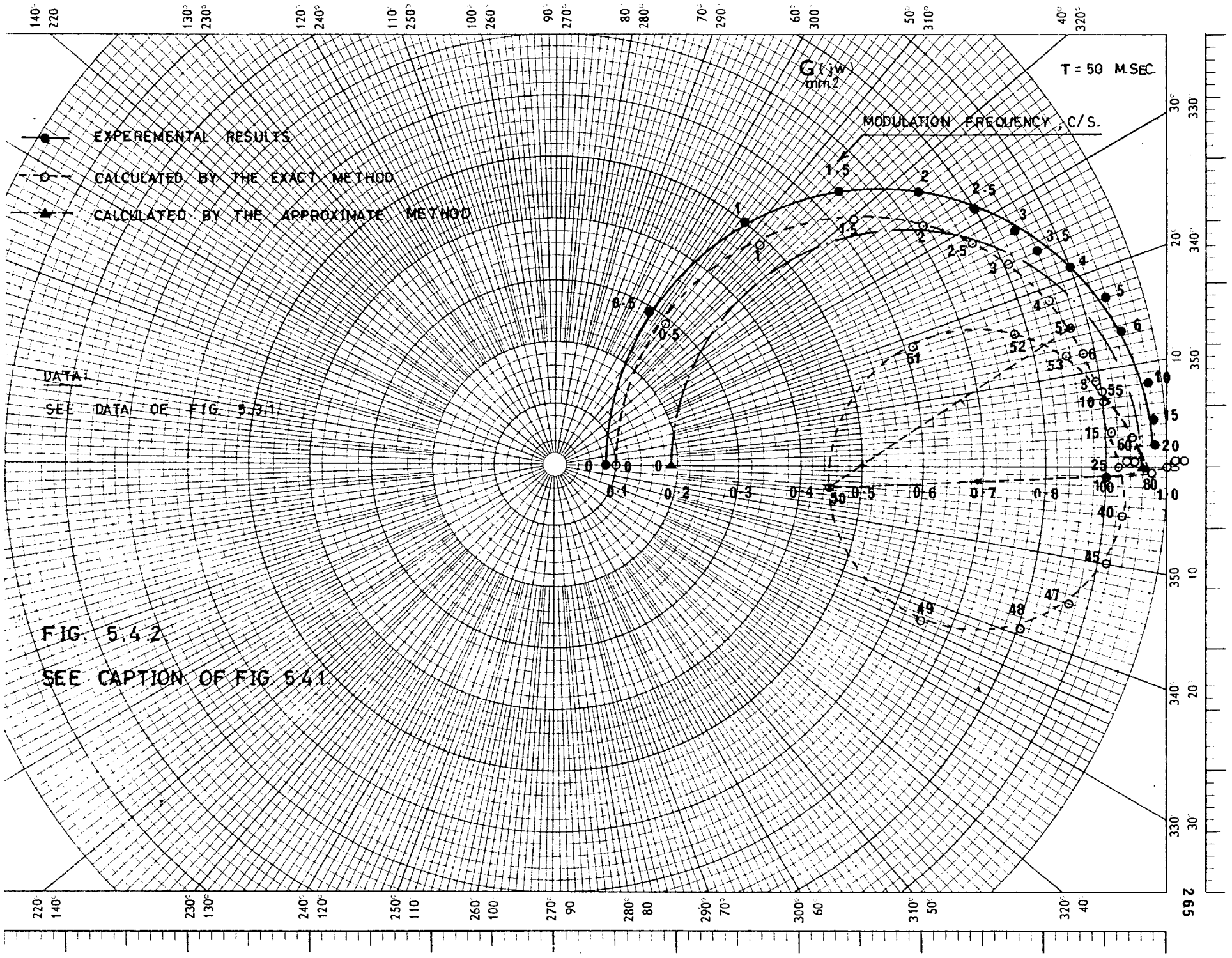
- i) the first segment includes the modulation frequencies lying between zero and half the carrier frequency and has the shape of almost perfect semi-circle.
- ii) the second segment includes the modulation frequencies lying between 25 c/s and 55 c/s and has the shape of a circle (slightly incomplete).
- iii) the third segment includes modulation frequencies lying above 55 c/s whose shape is a more general curve which ends at the point 1 on the real axis. A discontinuity appears at the modulation frequency of double the carrier frequency. This, however, is expected as the formula used (expressed by Eqn. 4.2.96) is not valid at modulation frequencies equal to multiples of the carrier frequency as explained in Sub-section 4.2.7.

Other geometrical features which have been observed are that: the centre of the semi-circle lies on the line joining the modulation frequencies at 5 c/s and the carrier frequency 50 c/s, and the centre of the circle lies on the line joining the modulation frequencies at 50 c/s and 100 c/s.

On the other hand, the theoretical locus pertinent to the double-switch single-capacitor chopper network appears to be







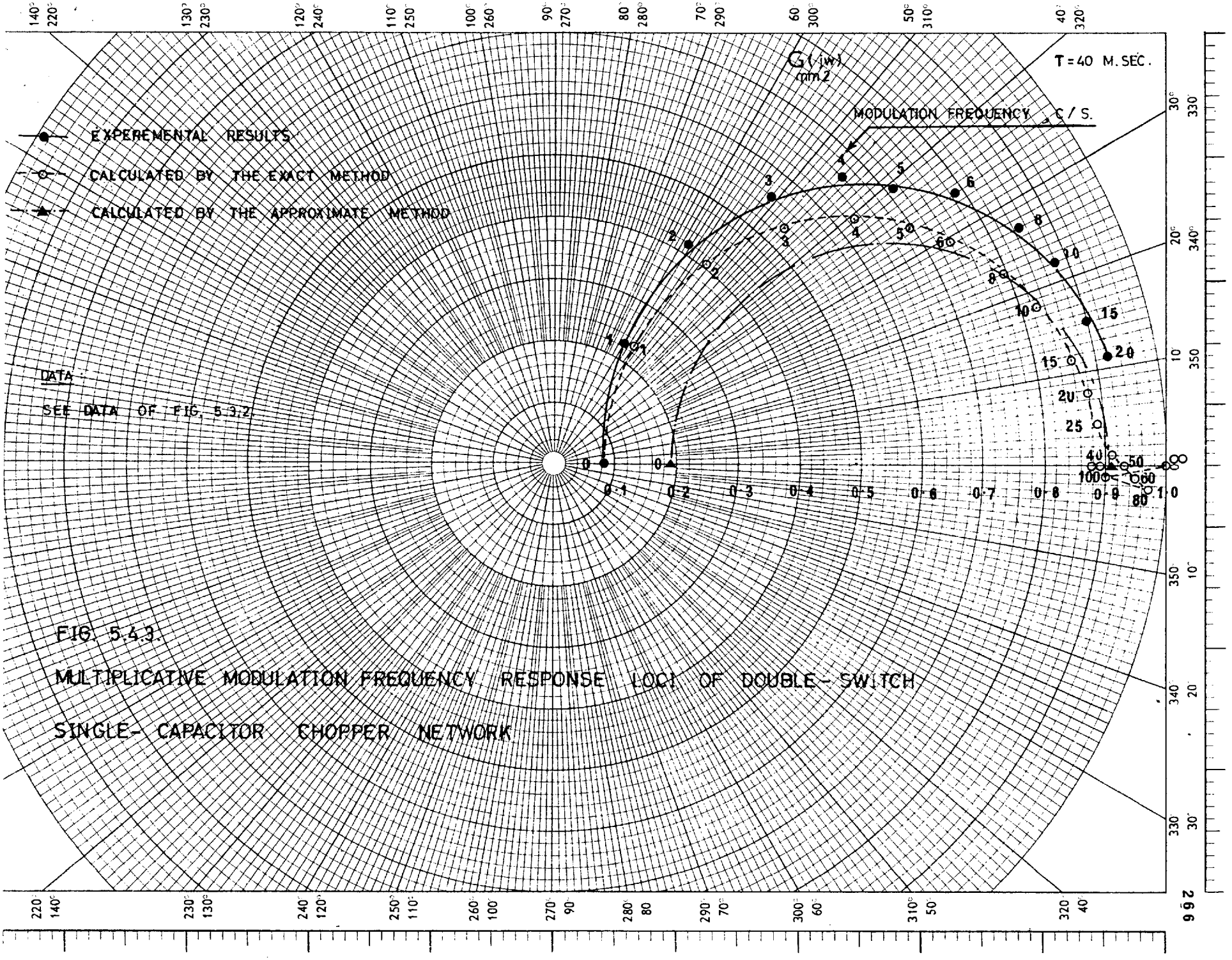


FIG 5.43.

MULTIPLICATIVE MODULATION FREQUENCY RESPONSE LOCUS OF DOUBLE-SWITCH SINGLE-CAPACITOR CHOPPER NETWORK

composed of only two segments: the first includes the modulation frequencies that lie between zero and 25 c/s (half the carrier frequency) and has the shape of slightly incomplete semi-circle, the second includes modulation frequencies lying above 25 c/s and has a shape of a more general curve that ends at the point 1 on the real axis. Again, a discontinuity at the modulation frequency equal to double the carrier frequency is observed which can be explained along the lines outlined in Sub-section 4.2.7.

The various loci given in these figures clearly show a very close agreement between the experimental results and the theoretical results obtained by the exact method particularly at the low modulation frequency region. The agreement between the results is, however, not perfect at the high modulation frequency region. This partly might be attributed to the errors introduced by some of the testing apparatus, namely the modulator and demodulator, when the modulation frequency exceeds their practical limit as will be explained in detail in Chapter 8.

Figs. 5.4.4 and 5.3.5 to 5.3.7 also show experimental curves and calculated points computed from the formula of Eqn. 4.2.96 for the variations of d.c. modulation transference, normalized equivalent d.c. network frequency, normalized frequency at which maximum phase shift occurs and the peak phase shift with the normalized time constant  $\tau/T$ . On the whole, the agreement can be considered as good.

On the basis of the above comparison of the results, the exact method of analysis can be considered as sufficiently accurate and reliable method to predict the chopper network's responses. Furthermore, the perfect agreement between the experimental results, obtained by changing the time constant  $\tau$

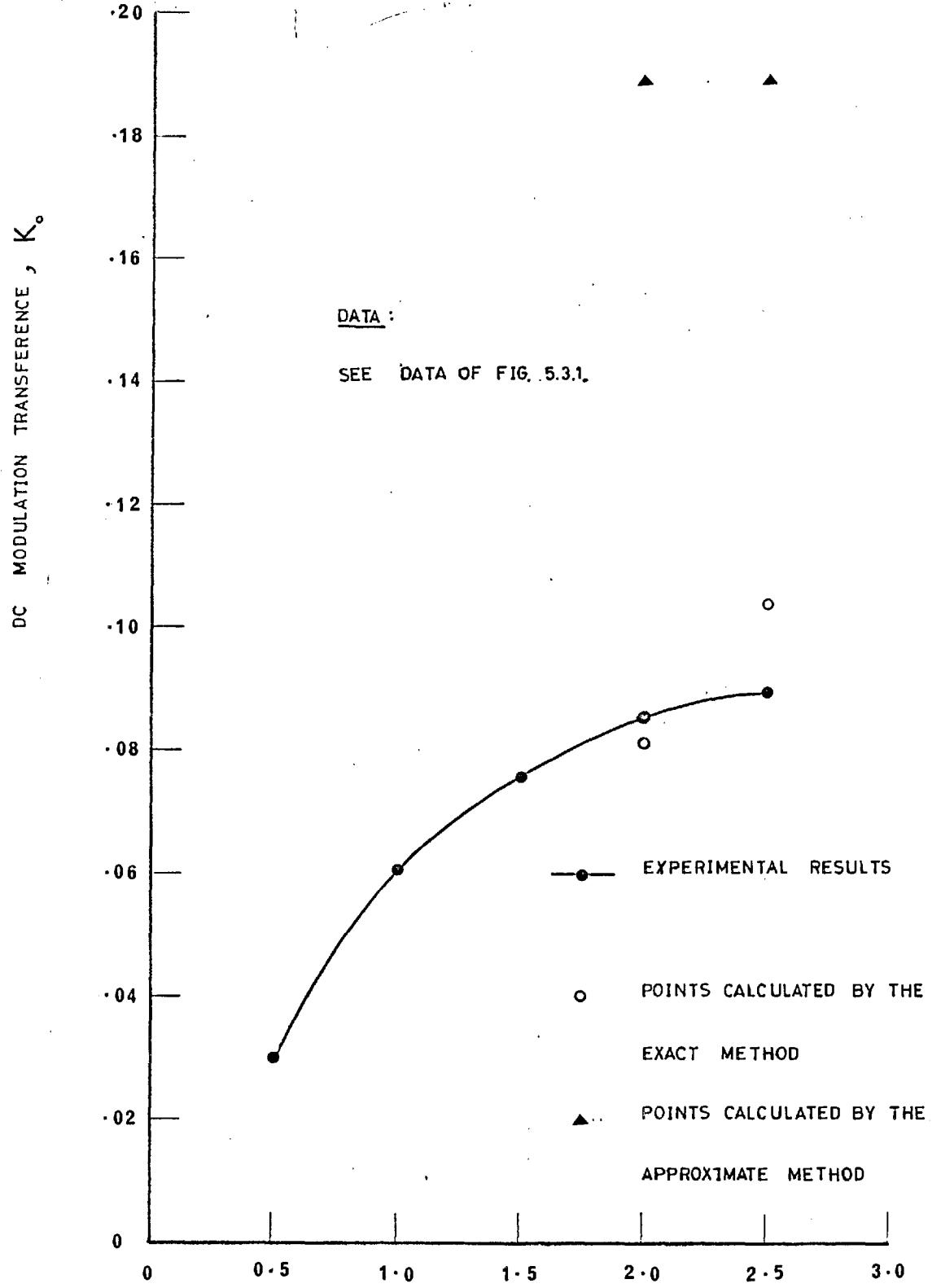


FIG. 5.4.4. VARIATION OF THE DC MODULATION TRANSFERENCE WITH THE NORMALIZED TIME CONSTANT  $T/T$

keeping the carrier frequency constant, with the experimental results obtained by changing the latter keeping the former constant as illustrated in Fig. 5.3.4, confirms, in an indirect way, the validity of the formulæ derived by the exact method. This is because both the experimental results and the theoretical exact formula (see Eqn. 4.2.96) agree with each other on that the d.c. modulation transference is a function of  $\tau/T$ .

#### 5.4.2. Experimental results versus theoretical calculations by the approximate method.

Figs. 5.4.1 to 5.4.3 show representative number of the multiplicative modulation frequency response loci of two types of chopper networks obtained both experimentally and theoretically employing the approximate formulæ. By comparing the results, it is shown that although the approximate theoretical method predicts the semi-circular shape of the loci, appreciable discrepancies exist between them and their corresponding experimentally determined loci throughout the modulation frequency range. This divergence increases as the modulation frequency increases. Figs. 5.4.4 and 5.3.5 to 5.3.7 show even much clearer the significant difference between the experimental results and the results obtained by this theoretical method for a selected representative conditions of operation of single-switch double-capacitor chopper network.

On the basis of the above comparison of the results, it is evident that the approximate method of the chopper network analysis cannot be relied upon to give sufficiently accurate results particularly in the low modulation frequency region, which is normally the area of interest for the design purposes.

#### 5.4.3. Exact theoretical method versus approximate theoretical method.

By examining the various curves and loci shown in the Figs. 5.3.5 to 5.3.7 and 5.4.1 to 5.4.4, it may be concluded that the results, particularly at low modulation frequencies, obtained by the exact analytical method are more accurate and closer to the practical values than those obtained by the approximate analytical method, which is based on a number of assumptions. At high modulation frequency, however, the two analytical methods give almost the same degree of agreement with the experimental results.

Furthermore, the formulae derived by the approximate analytical method (see Section 4.3) predict that the shape of the multiplicative modulation frequency response loci of the chopper networks under consideration are maintained as semi-circles regardless of any change in the various parameters. The experimental results illustrated in Figs. 5.3.11 to 5.3.13 clearly show that this prediction is unrealistic and incorrect. In addition, the basis upon which the approximate solution was derived neither permits the extension of its application for determining the rotary modulation transfer functions of chopper networks nor renders it possible to evaluate the noise contents of the chopper network's responses.

On the other hand, the formulae derived by the exact analytical method (see Section 4.2), besides being accurate and reliable as verified by the various experimental results mentioned above, they are valid under any change in the various parameters and under any mode of chopper network's operations. Also, this method is adaptable, by minor modifications, to extend its application for deriving the

chopper network's responses when subject to rotary modulated signals as it has been shown in Sub-section 4.2.6. Furthermore, with this method, accurate evaluation of the noise generated by chopper networks is possible according to the work outlined in Sub-section 4.2.7.

On the basis of the above discussion, the numerous merits of the exact analytical approach over the approximate method warrant its use despite the fact that it is much more complicated in comparison with the latter method.

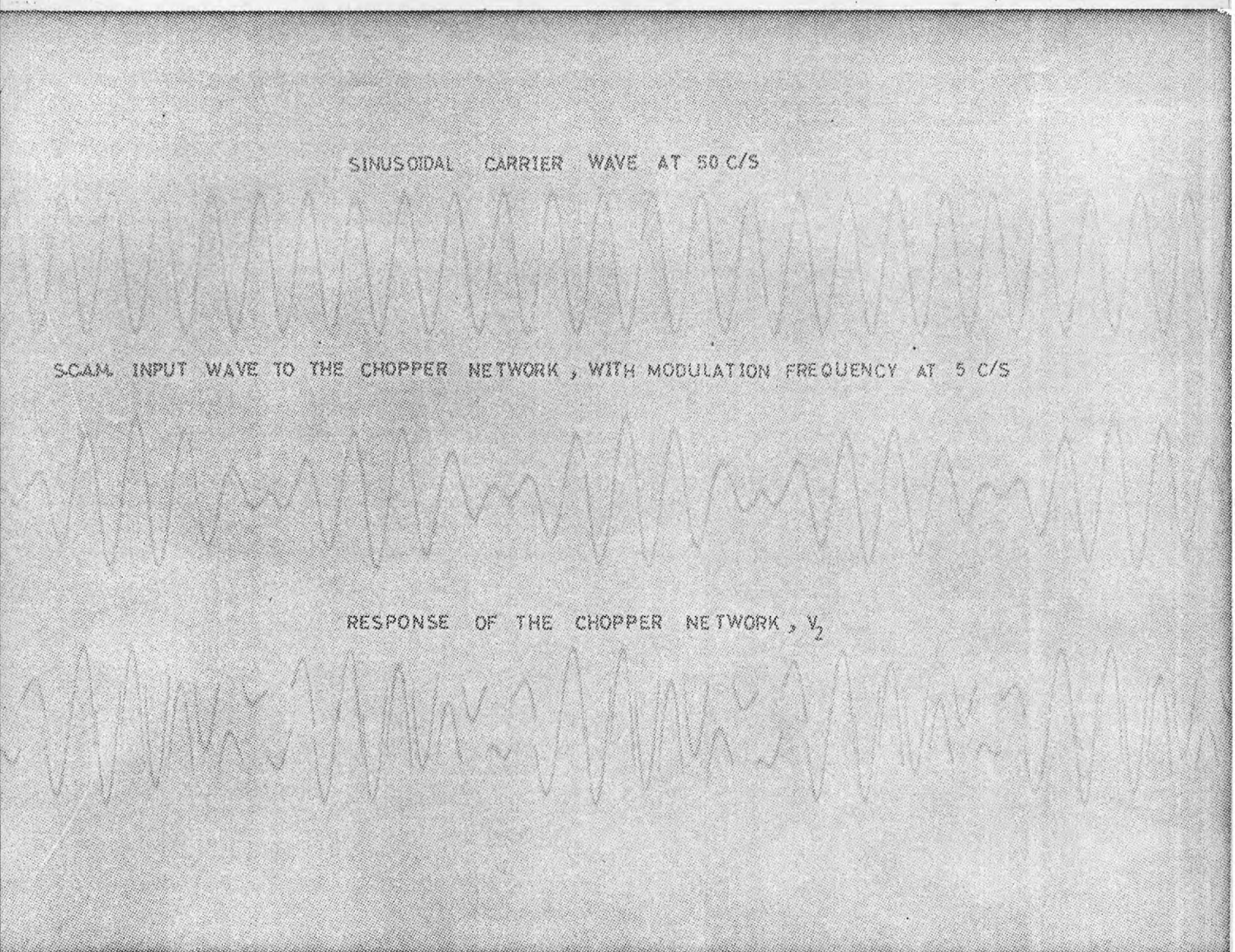
#### 5.5. Records of Wave Forms.

In order to visualize the shaping effect of chopper networks on various types of input modulated signals and to provide a qualitative idea about the noise associated with their responses, a representative number of records, using Ultra Violet Recorder, have been obtained for the single-switch double-capacitor chopper network under a variety of operating conditions.

Figs. 5.5.1 and 5.5.2 show records of the steady state response wave forms when the chopper network is subject to suppressed-carrier amplitude-modulated wave. The two records were taken under similar conditions except the fly-time of the synchronous switch which was changed from zero to 0.1. In doing so, the response wave form became much more rough in view of the sudden disappearance and reappearance of the response at the beginning and end of the synchronous switch fly-time, with the implication of more noise contact.

Figs. 5.5.3 to 5.5.6 show records of the steady state response wave forms when the chopper network is impressed

SINUSOIDAL CARRIER WAVE AT 50 C/S



S.C.A.M. INPUT WAVE TO THE CHOPPER NETWORK, WITH MODULATION FREQUENCY AT 5 C/S

RESPONSE OF THE CHOPPER NETWORK,  $V_2$

FIG. 5.51.


STEADY STATE RESPONSE OF SINGLE-SWITCH DOUBLE-CAPACITOR  
CHOPPER NETWORK SUBJECT TO SUPPRESSED-CARRIER AMPLITUDE-  
MODULATED WAVE (S.C.A.M.)

DATA:


$\tau = 20$  m.sec. ,  $\delta = 0.5$  ,  $\theta = 0^\circ$



SINUSOIDAL CARRIER WAVE AT 50 C/S



S.C.A.M. INPUT WAVE TO THE CHOPPER NETWORK, WITH MODULATION FREQUENCY AT 5 C/S



RESPONSE OF THE CHOPPER NETWORK,  $V_2$




FIG. 5.5.2.

SEE CAPTION OF FIG.5.5.1

DATA:

$\tau = 20$  m.sec. ,  $\delta = 0.4$  ,  $\theta = 0^\circ$

S.C.A.M. WAVE SUPPLIED TO THE DIFFERENTIATOR WITH  
CARRIER FREQUENCY AT 50 C/S AND MODULATION FREQUENCY AT 5 C/S



R.M.W. INPUT TO THE CHOPPER NETWORK



RESPONSE OF THE CHOPPER NETWORK,  $V_2$



FIG.5.5.3

STEADY STATE RESPONSE OF SINGLE-SWITCH DOUBLE-CAPACITOR  
CHOPPER NETWORK SUBJECT TO ROTARY MODULATED WAVE (R.M.W.)

DATA:

$$\tau = 20 \text{ m.sec.} \quad , \quad \delta = 0.5 \quad , \quad \theta = 0^\circ$$

S.C.A.M. WAVE SUPPLIED TO THE DIFFERENTIATOR WITH  
CARRIER FREQUENCY AT 50 C/S AND MODULATION FREQUENCY AT 5 C/S



R.M.W. INPUT TO THE CHOPPER NETWORK



RESPONSE OF THE CHOPPER NETWORK,  $\frac{1}{2}$



FIG. 5.5.4

SEE CAPTION OF FIG. 5.5.3

DATA:

$\tau = 20$  m.sec. ,  $\delta = 0.5$  ,  $\theta = 30^\circ$  lag

S.C.A.M. WAVE SUPPLIED TO THE DIFFERENTIATOR WITH  
CARRIER FREQUENCY AT 50 C/S AND MODULATION FREQUENCY AT 5 C/S

R.M.W. INPUT TO THE CHOPPER NETWORK

RESPONSE OF THE CHOPPER NETWORK,  $V_2$

FIG. 5.55

SEE CAPTION OF FIG.5.5.3

DATA:

$$\tau = 20 \text{ m sec} , \delta = 0.5 , \theta = 60^\circ \text{ lag}$$

S.C.A.M. WAVE SUPPLIED TO THE DIFFERENTIATOR WITH  
CARRIER FREQUENCY AT 50 C/S AND MODULATION FREQUENCY AT 5 C/S



R.M.W. INPUT TO THE CHOPPER NETWORK



RESPONSE OF THE CHOPPER NETWORK,  $V_2$



FIG.5.56

SEE CAPTION OF FIG.5.53

DATA:

$$\tau = 20 \text{ m.sec.}, \quad \delta = 0.5, \quad \theta = 90^\circ \text{ lag}$$

upon by a rotary modulated wave. In taking this record, the phase of the modulation reference wave was changed keeping other conditions constant. By examining the records, it is noted that at zero phase of the modulation reference, the response wave is relatively smooth and almost free of the sudden jumps at the switching instants. These sudden breaks in the response wave form, taking place at the switching instants, start to appear with increasing degree as the phase of the modulation reference increases from zero to  $90^{\circ}$ . This implies that the noise content associated with the response is minimum at zero phase of the demodulation reference and increases to a maximum value when that phase reaches  $90^{\circ}$ .

CHAPTER 6BREADBOARD MODEL OF A POSITIONAL CONTROL A.C.  
SERVO-MECHANISM - (SPECIFICATIONS, CONSTRUCTION,  
AND PRELIMINARY STUDIES)6.1. Introduction

In the previous Chapter, extensive investigations have been carried out on the performance characteristics of chopper networks when subject to carrier modulated signals. In these studies, rotary modulation and phase shift as those effected in machine type error-detectors (such as synchros, magslips, selsyns and similar devices) were completely simulated. On the other hand, however, demodulation of the type effected in 2-phase servo-motors (see Chapter 2) was simplified by an ideal demodulator. Although the phase shift of the carrier excitation was possible to simulate, the actual case which may be encountered in many practical a.c. servo-mechanisms employing 2-phase induction motors was not accurately represented.

Therefore, to establish beyond any doubt the stabilizing capability of chopper networks and to demonstrate their effectiveness in improving the performance of practical a.c. servo-mechanisms, it was considered desirable to simulate some actual tests. For this purpose, a breadboard model of a positional control a.c. servo-mechanism, whose block diagram is based on that shown in Fig. 1.2.1, was designed and assembled in the Laboratory. Plate E.4.1 shows a photograph of the model assembly.

The purpose of this Chapter is to give directly the specifications of the various components employed in the

model without much design details since they can easily be found in many a.c. servo-mechanisms text books. More attention was given to the description and design of a suitable transistor servo-amplifier. To provide useful information necessary in conducting the various tests on the model, preliminary studies were performed on the magslip-system. In general, the present Chapter serves to pave the way to the next Chapter which deals with the practical investigations on the model.

## 6.2. Component's specifications

### 6.2.1. Load

In the present application in which a rotational mechanical load is controlled, the load characteristics are describable in terms of polar moment of inertia, coefficient of viscous friction, and the coulomb or static friction forces present. To simulate this kind of load as realistically as possible, an unenergized 3" control magslip was employed whose relevant data is given in Appendix E.1.

At the shaft of the servo-motor, however, the moment of inertia of the motor rotor and the reflected inertia effects of gearing, error-detector and the driven load should be considered. Similarly, in considering the effect of the net viscous friction and net coulomb friction at the motor shaft, one should add those due to the motor to the corresponding ones reflected due to gearing, error-detector and the driven load.

### 6.2.2. Servo-motor

Since there were no high load power requirements nor high rotational rates and accelerations needed, geared



type 2-phase induction motor was employed. To compute the required motor size and the gearing, the maximum load velocity and acceleration must be known, and therefore had to be assumed in the present case. Their selected values are given below

$$\dot{\gamma}_{L(\max)} = 20 \text{ r.p.m.}$$

and

$$\ddot{\gamma}_{L(\max)} = 20 \text{ rad./sec.}^2$$

The total power required to drive the load is the sum of

- i) Power required to overcome coulomb friction
- ii) " " " " unbalanced forces
- iii) " " " accelerate the load
- iv) " " " overcome velocity losses.

These factors may be expressed mathematically as<sup>134</sup>

$$P_{\text{total}} = (T_{cf} + T_v) \dot{\gamma}_L + \left( J_L + \frac{n_L^2}{n_m^2} J_m \right) \ddot{\gamma}_L \dot{\gamma}_L + \left( F_L + \frac{n_L^2}{n_m^2} F_m \right) \dot{\gamma}_L^2 \quad 6.2.1.$$

Since the viscous friction is usually negligible, its contribution may be ignored and Eqn. 6.2.1. may be reduced to

$$P_{\text{total}} = (T_{cf} + T_v) \dot{\gamma}_L + \left( J_L + \frac{n_L^2}{n_m^2} J_m \right) \ddot{\gamma}_L \dot{\gamma}_L \quad 6.2.2.$$

Since the gear-train and motor have not yet been selected, it is necessary to estimate  $\frac{n_L^2}{n_m^2} J_m$ . Based on experience,

a conservative estimate is

$$J_L = \frac{n_L^2}{n_m^2} J_m \quad 6.2.3.$$

As maximum velocity and maximum acceleration seldom occur simultaneously, it is also conservative to use both maximum values for  $\dot{\gamma}_L$  and  $\ddot{\gamma}_L$  in the equation. Thus

$$P_{\text{total}} = \left[ (43+86)(9.8)10^{-5} + (2 \times 970)(20)10^{-7} \right] \frac{(2\pi)(20)}{60}$$

$$= 0.0346 \text{ watts} \quad 6.2.4$$

This estimate neglects friction effects and uses a guess for the reflected inertia of the motor. At a later point, after selection of the gear-train and motor, it would be appropriate to re-compute as a check. The computed maximum power requirement was increased by a safety factor to the value of 0.1 watt in order to allow for the mechanical loading of the error-detector when coupled to the system, and also for the effect of environmental factors such as ambient temperature, cooling conditions, etc.

Because of the availability of the 50 c/s power supply facilities, the working ranges of the various instruments, and the availability of 50 c/s magslips that can be suitably used as error-detectors it was decided to employ 50 c/s servomotor. From the list of acceptable motors, one was selected whose characteristics are given in Appendix E.2.

### 6.2.3. Error-detector

Fifty c/s, 2" control magslips were available

in the Laboratory and it was decided to employ two control magslips arranged as transmitter and coincidence-transmitter. In addition, another type of error-detector in the form of a potentiometer-bridge was also used in order to enable a wider variety of investigations to be performed.

To eliminate the possible hunting problems associated with the common wire-wound potentiometers (which result from the finite resolution corresponding to the displacement between adjacent wires), helically wound potentiometers were employed. Also, to increase the travel or the angular rotation, multiple-turn potentiometers were preferred.

Appendix E.3 gives the detailed characteristics of both types of error-detector.

#### 6.2.4. Gear-train.

At this stage, it is possible to select the proper gear ratios by plotting two curves:

- i) Required power versus gear ratio
- ii) Power available from motor versus gear ratio.

A reasonable choice of the various gear ratios is given below

$$n_m/n_L = 80 \quad , \quad 6.2.5.$$

$$n_m/n_S = 100 \quad , \quad 6.2.6$$

and

$$n_m/n_P = 50 \quad . \quad 6.2.7$$

To check, the basic torque equation for torque equilibrium can be used, verifying that sufficient torque

will be available at the maximum specified speed to accelerate the load at 20 rad./sec.<sup>2</sup> (the specified maximum load acceleration).

$$\frac{n_L}{n_m} T_m - (T_{cf} + T_v) > \left[ J_L + n_L^2 \left( \frac{J_m}{n_m^2} + \frac{J_s}{n_s^2} + \frac{J_p}{n_p^2} \right) \right] \ddot{\gamma}_L + \left[ F_L + n_L^2 \left( \frac{F_m}{n_m^2} + \frac{F_s}{n_s^2} + \frac{F_p}{n_p^2} \right) \right] \dot{\gamma}_L$$

..6.2.8

where  $T_m$  is the motor torque at speed corresponding to maximum load speed, and which can be obtained from the torque-speed characteristics plotted in Fig. E.2.1.

The gear-train employed consists of a gearhead unit size 11 of ratio 20:1 (for performance details and curves see Technical Data, Vactric Control Equipment Limited), fitted to the motor shaft. Minimum gear combinations were then added to obtain the required reducing speed ratios with minimum additional backlash.

### 6.3. Servo-Amplifier.

#### 6.3.1. General design considerations.

To be capable of accepting the modulated signal form provided by the mag-slip error-detector and to provide at its output a signal of the proper type to operate the 2-phase servo-motor, a.c. amplifier was evidently the suitable type to be chosen. The servo-amplifier

design should provide sufficient flexibility to handle compensation and gain adjustment requirements. Special attention should be given to the distribution of gains within the amplifier. At each junction input signals tend to introduce noise, and the noise spectrum can cause difficulties by producing various types of saturation in different elements, such as excessive power dissipation, loss of gain, and reduction in the effectiveness of compensators. Both the gain distribution in the amplifier and the location of the compensation device are affected by the non-linear action resulting from very large input signals.

The servo-amplifier should cause a minimum electrical loading effect on the error-detector as possible so that the overall system performance is kept unaffected. It must also have ample power-output capacity, and must be able to drive the servo-motor in accordance with the expected velocities and accelerations.

Finally, the simplicity of the design is very desirable since complexity usually impairs reliability of operation, ease of maintenance, cost of manufacture, and cost of repair.

#### 6.3.2. Design requirements and specifications.

Since the main goal of setting up the a.c. servo-mechanism breadboard model was to carry out investigations on the overall system performance, the servo-amplifier performance therefore should not introduce any serious effect that may impair the essential features of the servo under study. In order to ensure this, the following requirements ideally must be met in the design

- i) The frequency response of the amplifier (gain and

phase versus frequency) must be flat over the frequency range of  $(\Omega + \omega_{\max})$  to  $(\Omega - \omega_{\max})$ , where  $\Omega$  is the carrier frequency and  $\omega_{\max}$  is the highest modulation frequency the servo will permit.

- ii) There should be no change in the phase shift with the level of the input signal within its working range. Also, linear relationship between the gain and the input signal should be maintained throughout that zone.
- iii) The amplifier should have a low output impedance to minimize its effect on the performance of the servo-motor. If the output impedance is high, the servo-motor may become unstable.
- iv) The amplifier input impedance should be very high to provide minimum electrical loading effect on either the error-detector or the compensating device. Otherwise, changes in their performances may take place.
- v) The amplifier should have a low noise characteristic.

In view of the advantages to be gained in employing transistors, in terms of improved reliability, higher efficiency, less size and weight, by comparison with thermionic valves, it was decided that the servo-amplifier would be completely transistorized. Before starting the design, specifications (based on so many factors not included here) were put forward. These are summarized as follows:

- i) Gain: the maximum gain should be 2000 volts/volt  $\pm 5\%$  with system load and power supply.
- ii) Phase: the phase shift of the amplifier shall be  $0 \pm 3$  degrees with system loading and power supply.

- iii) Response: the gain of the amplifier shall not change more than 3 db over the frequency range of 20 to 80 c/s.
- iv) Stability: with  $\pm 10\%$  change in power, the amplifier gain shall not change more than  $\pm 5\%$ .
- v) Noise: with system power and input shorted to ground, the output shall be less than 0.5 volts.
- vi) Maximum output: 25 volts (r.m.s.)
- vii) Load: 2-phase induction motor type 11 MG 72, see Appendix E.2 for further details.
- viii) Linearity: the gain shall remain within  $\pm 5\%$  up to 20 volts (r.m.s.) output.
- ix) Power supply: -60 and -24 volts d.c.
- x) Input impedance: 6 k minimum.

### 6.3.3. Amplifier transistor circuit design

In designing the amplifier, it was considered convenient to divide the amplifier stages into three groups, viz.,

- i) Low signal (1st stage and possibly 2nd)
- ii) Medium signal (middle stage or stages)
- iii) Large signal (output stage, and possibly the driver).

Direct interstage coupling was used throughout to extend the frequency response particularly at low frequencies. In addition, as will be seen in a later stage, a single negative feedback loop was employed which further extends the frequency response and reduces internal non-linearity distortion.

The subsequent subsections are devoted primarily to the design of the various amplifier stages.

### 6.3.3.1. List of principal symbols

The symbols enlisted below are mainly used in this section concerning the transistor circuit design for the amplifier. To refer to the various transistor stages, subscripts indicating the stage number will be employed in conjunction with the various symbols.

$E_c$	: d.c. supply voltage
$V_{CE}$	: break-down voltage between collector and emitter with base open circuit
$V_{be}$	: voltage between base and emitter
$V_c, V_e, V_b$	: d.c. voltage bias at collector, emitter, and base of a transistor
$I_c, I_e, I_b$	: current bias of collector, emitter, and base of transistor
$v_c, v_e, v_b$	: peak voltage swing at collector, emitter, and base of transistor
$i_c, i_e, i_b$	: peak current excursion in collector, emitter, and base of transistor
$P_{out}$	: output power
$P_d$	: power dissipation in each transistor
$\beta$	: static forward current gain in common-emitter connection
$A_i$	: current gain
$A_v$	: voltage gain



### 6.3.3.2. Output stage

The split control winding of the 2-phase servo-motor represents the load of this stage. To obtain the characteristics of such load, the following tests were conducted on the servo-motor at the nominal carrier frequency (50 c/s),

- i) Blocked rotor open-circuit characteristics, with reference winding unexcited
- ii) No-load characteristics, with reference winding excited by a constant voltage of 35 volts at phase quadrature with the testing voltage applied to the control winding.

The results of the first test are shown in Fig. 6.3.1 in terms of open-circuit voltage and power of the control winding plotted against its current. From these results, the control winding impedance, reactance, and resistance were deduced and their dependence on the control current is illustrated in Fig. 6.3.2.

The results of the second test plotted against the control current are shown in Fig. 6.3.3. In this figure, the variations of both the control winding and the reference winding impedances with the control current are illustrated.

Since under normal operating conditions the motor velocity varies from zero to a certain maximum value (usually lower than the no-load speed), the above two tests effectively represent the two extreme conditions. Consequently, the values of the impedances continuously vary between their limits corresponding to these two extreme conditions.

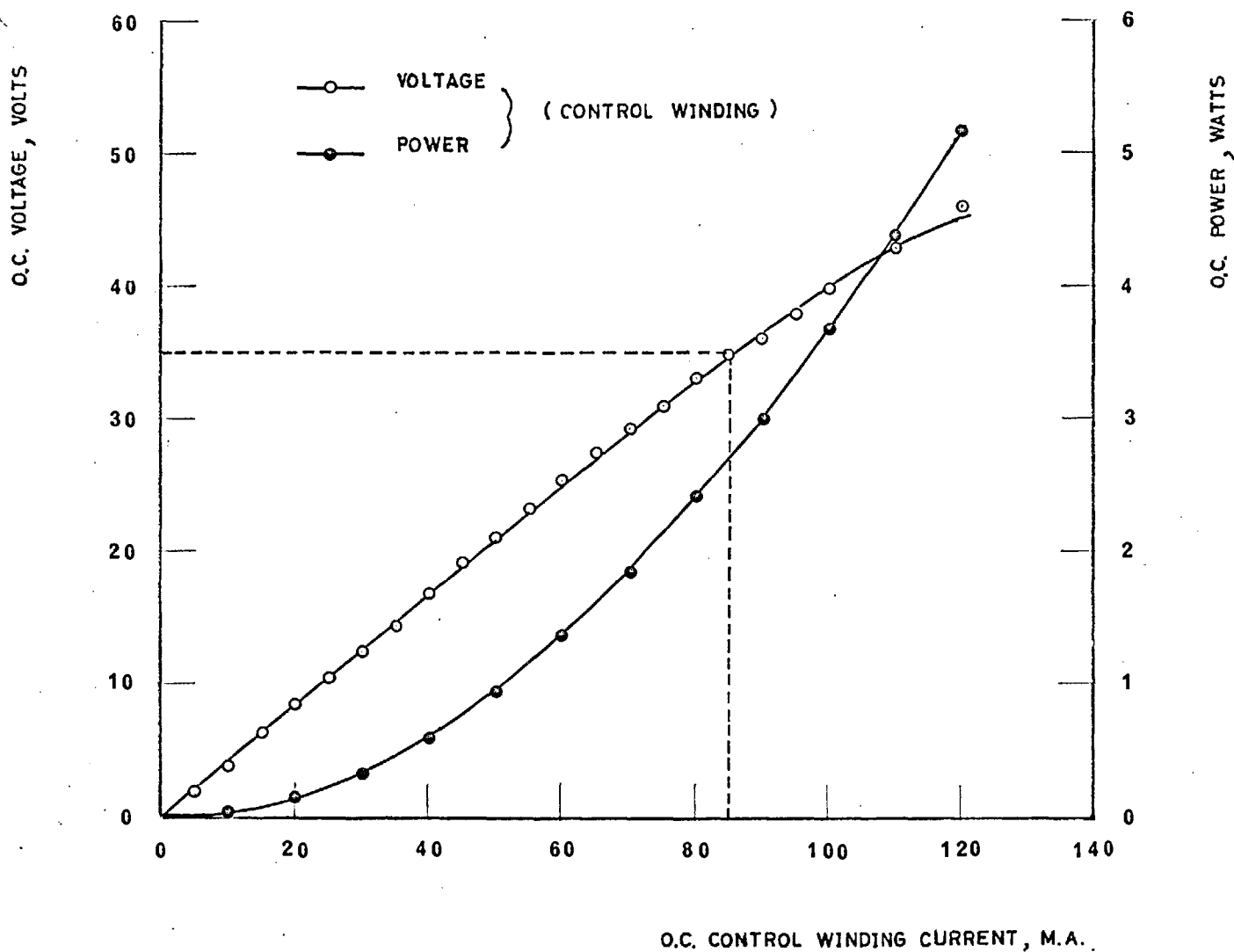


FIG. 6.3.1.

BLOCKED ROTOR OPEN CIRCUIT CHARACTERISTICS OF  
THE SERVOMOTOR

(REFERENCE WINDING UNEXCITED)

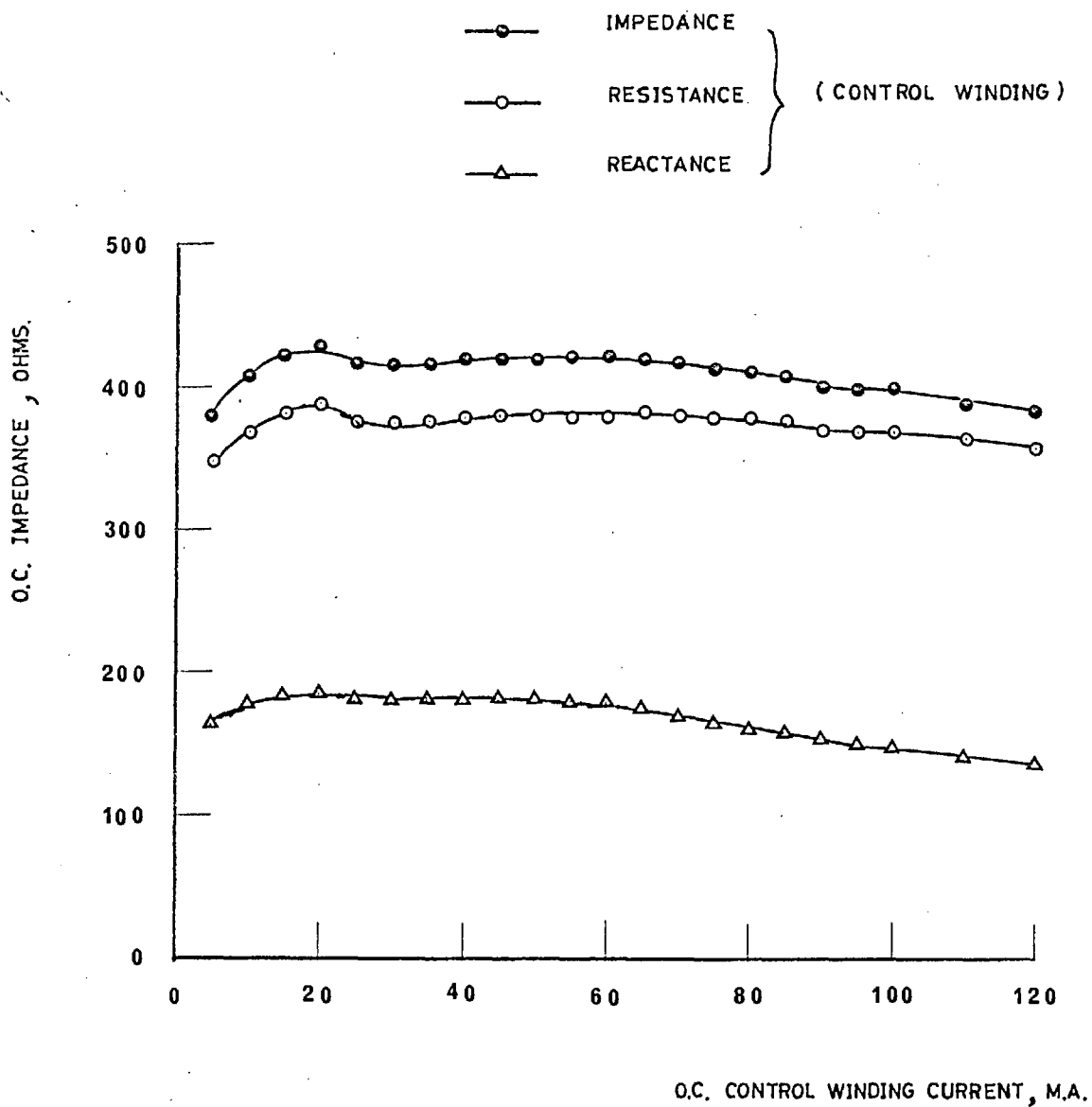


FIG. 6.3.2.

OPEN CIRCUIT IMPEDANCE CHARACTERISTICS OF  
THE SERVOMOTOR

(REFERENCE WINDING UNEXCITED, BLOCKED ROTOR)

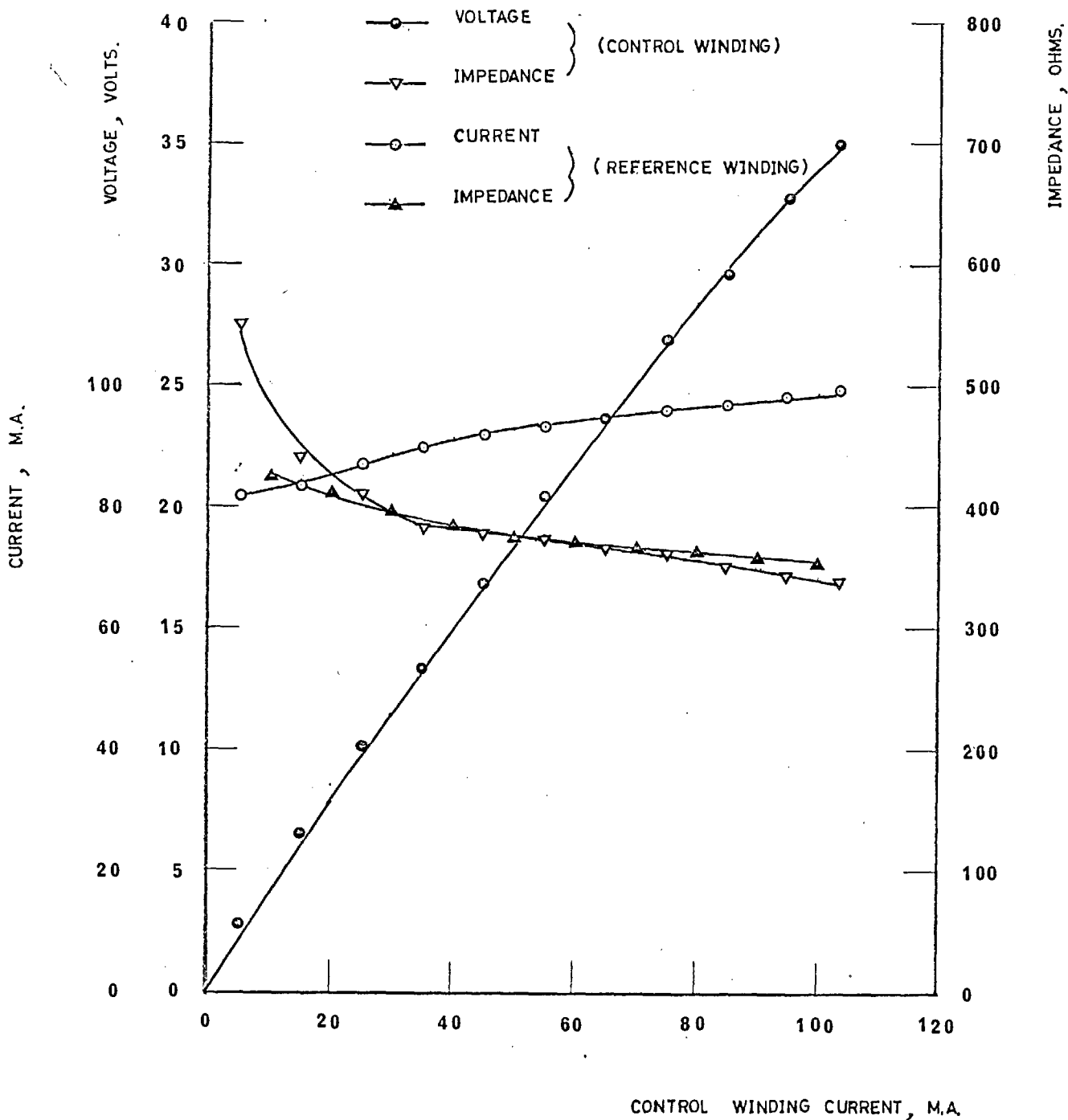


FIG. 6.3.3.

NO-LOAD CHARACTERISTICS OF THE SERVO MOTOR

(REFERENCE WINDING EXCITED BY A CONSTANT VOLTAGE OF 35 VOLTS)

On the basis of the above discussions, the control winding impedance and the ratio inductance/resistance depend on the following factors:

- i) Motor speed and the mutual coupling between the reference and control windings.
- ii) Magnitude of the control current (or control voltage).
- iii) Degree of saturation of the magnetic circuit.

The loading effect of such impedance on the amplifier response represents a significant problem in the design particularly when it results into oscillation at high frequencies. In such case, however, phase-lag feedback stabilization may be used.

Having studied the load characteristics of the output stage, its design consideration was the next step. Fig. 6.3.4. shows the complete circuit of the servo-amplifier in which transistors  $N_5$  and  $N_6$  represent the output stage. These output transistors were arranged to operate in class A push-pull because low distortion is a requirement. A matched pair of OC 28<sup>135</sup> transistors have been chosen for their high cut-off frequency and the good linearity of the  $V_c/I_c$  characteristics.  $E_c$  was chosen as -60 volts to satisfy the specified maximum output with still a reasonable margin below the transistor breakdown voltage  $V_{CE}$ .

To determine the suitable quiescent collector current, the two extreme load resistances may be represented in the usual way by two load lines down across the output characteristics for OC28 common emitter. The effect of the inductance is to change the load line to an ellipse whose centre coincides with the quiescent point and one of

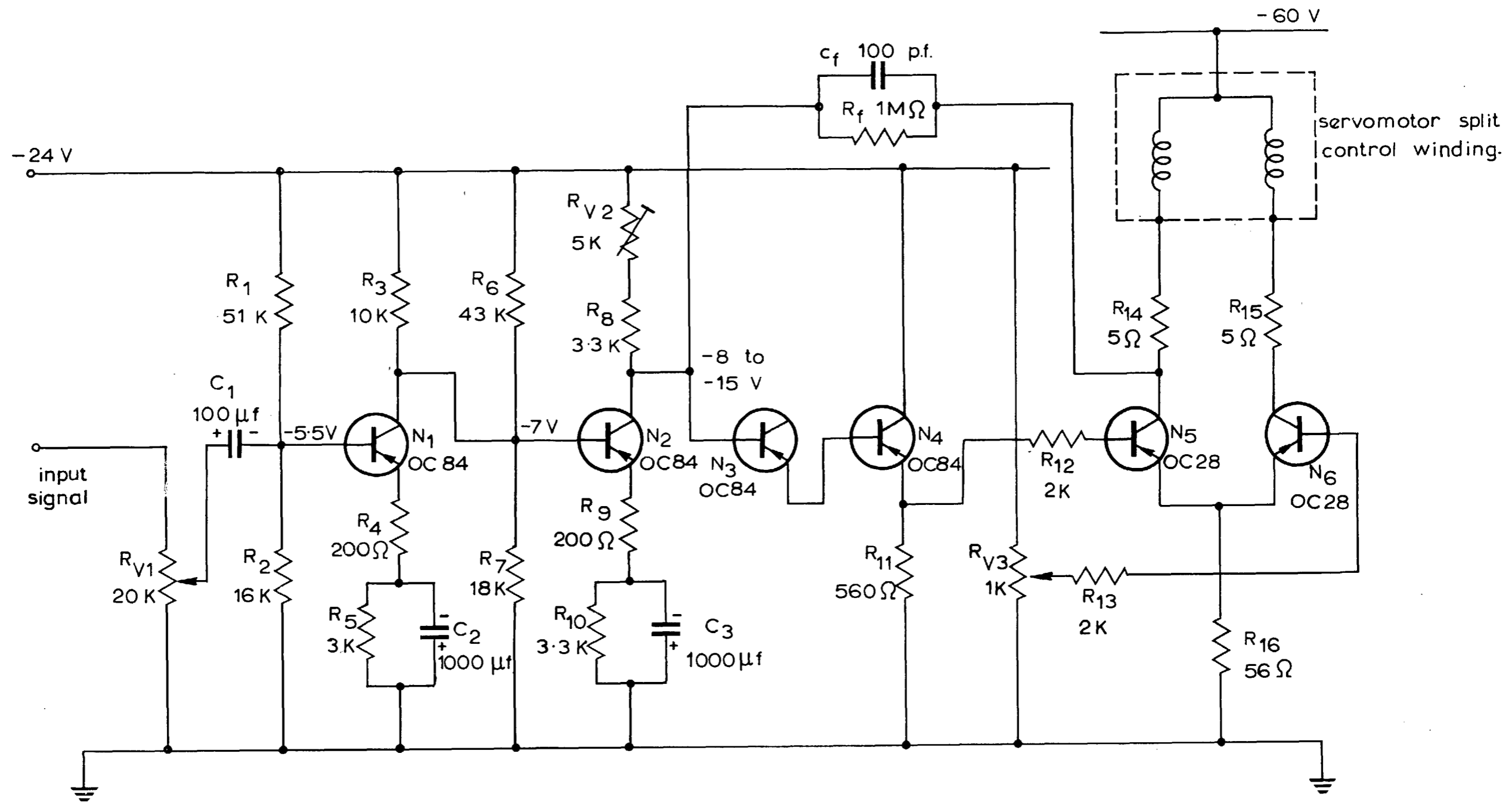


FIG. 6.3.4.

A TRANSISTOR CIRCUIT FOR THE SERVOAMPLIFIER

its axes lies along the load line. The deduction of this ellipse from an eccentric ellipse, with its axes parallel to the cartesian coordinates and the magnitude ratio of its vertical axis/horizontal axis is equivalent to the load reactance/resistance ratio, is well known technique. By drawing the two load ellipses corresponding to the two limiting values at the maximum working frequency (say, 100 c/s), and maximum allowable output voltage excursion (bearing in mind that the minimum allowable collector voltage is slightly greater than the knee voltage), it was possible to fix the quiescent point as

$$I_q = 90 \text{ m.A.} \quad 6.3.1.$$

and

$$V_q = -42 \text{ volts.} \quad 6.3.2.$$

The maximum output power from the two output transistors may therefore be calculated as below

$$P_{\text{out max}} = 2 \frac{|E_c - V_q|}{\sqrt{2}} \cdot \frac{I_q}{\sqrt{2}} = 1.62 \text{ watts} \quad 6.3.3.$$

The maximum power dissipation per transistor is approximately given by

$$P_d = |V_q \cdot I_q| = 3.78 \text{ watts} \quad 6.3.4.$$

In the light of the maximum dissipation value, heat sink design <sup>136</sup> (not included here) was considered. Temperature stabilization is effected by the emitter resistance  $R_{16}$ , being common to both emitters of the output transistors.

The output transistor  $N_5$  is driven by the double emitter follower stage  $N_3$  and  $N_4$ , while the transistor

$N_6$  is driven by the feedback introduced by the common emitter resistance  $R_{16}$ . The base voltage of the stage  $N_3$ , and therefore the base bias of the output transistor  $N_5$  are driven through resistances  $R_8$  and  $R_{v2}$ . On the other hand, the base bias of  $N_6$  is driven from a potential divider  $R_{v3}$ .

The maximum and minimum base bias current required by the output stage (transistor  $N_5$  or  $N_6$ ), having maximum and minimum values of  $\beta$  as 20 and 55 respectively, are given below

$$I_{b \text{ max}(5 \text{ or } 6)} = \frac{I_q}{\beta_{\min}} = 4.5 \text{ m.A.} \quad 6.3.5.$$

and

$$I_{b \text{ min}(5 \text{ or } 6)} = \frac{I_q}{\beta_{\min}} = 1.64 \text{ m.A.} \quad 6.3.6.$$

Hence, the corresponding base bias voltages of the output stage are

$$\begin{aligned} V_{b \text{ max}(5 \text{ or } 6)} &= -(I_q + I_{b \text{ max}}) R_{16} + V_{be} \\ &= -6.1 \text{ volts} \quad 6.3.7. \end{aligned}$$

and

$$\begin{aligned} V_{b \text{ min}(5 \text{ or } 6)} &= -(I_q + I_{b \text{ min}}) R_{16} + V_{be} \\ &= -5.93 \text{ volts} \quad 6.3.8. \end{aligned}$$

The maximum required base-current excursion is

$$i_{b \text{ max}(5 \text{ or } 6)} = \frac{I_q}{\beta_{\min}} = 4.5 \text{ m.A. peak} \quad 6.3.9.$$



The preceding stage must be able to provide this peak drive current.

In order to provide a means of measuring the output current response, two identical resistors  $R_{14}$  and  $R_{15}$  were inserted in series with the two branches of the motor control winding which are connected to the collectors of  $N_5$  and  $N_6$ . The voltage drops across these resistors, being proportional to the currents flowing through them, can be easily measured. The value of each resistance was selected as low as 5 Ohms in order not to influence the amplifier characteristics.

#### 6.3.3.3. Middle stages.

These include the double emitter follower formed by the transistors  $N_3$  and  $N_4$  as shown in Fig. 6.3.4. This configuration although does not contribute to voltage amplification, it provides substantial current amplification and hence power amplification which are needed by the output stage. Furthermore, by offering a high input impedance and low output impedance, the interaction problem between the high power output stage and the highly sensitive input stage is considerably reduced.

The main requirement from these stages is to ensure adequate drive to the base of the output stage. With the assumption of matched output transistors, their base voltages would remain virtually constant during normal operation, since any current variation in the common emitter resistor  $R_{16}$  due to one of the transistors will be counterbalanced by an equal and opposite current variation due to the second transistor. Therefore, base resistors  $R_{12}$  and  $R_{13}$  should be employed in order to convert voltage swing at the emitter

of transistor  $N_4$  (caused by the transmitted information) into base drive current swing for the output stage. In designing these base resistances, two situations arise:

- i) With low values of the base resistance, high gain can be obtained from the output stage but on the expense of linearity since the non-linearity associated with the input characteristics ( $I_b$  versus  $V_{be}$ ) becomes more predominant.
- ii) With high values of the base resistance, improved linearity is obtained but on the expense of the output stage gain which may require additional amplifying stages to meet the overall gain requirements.

Studying the above situations and with the knowledge of the gain and linearity requirements, a compromise design can be reached. On this basis

$$R_{12} = R_{13} = 2 \text{ k. Ohms} \quad 6.3.10$$

Therefore, to be able to provide the required maximum base-current excursion (calculated by Eqn. 6.3.9), the available maximum emitter voltage excursion of transistor  $N_4$  must be

$$v_{e4 \text{ max}} = i_{b5 \text{ max}} R_{12} = 9 \text{ volts peak} \quad 6.3.11$$

The bias provided by resistors  $R_{v2}$  and  $R_g$  must be capable of adjusting the emitter voltage of transistor  $N_4$  between the limits

$$V_{e4 \text{ max}} = V_{b5 \text{ max}} - I_{b5 \text{ max}} R_{12} = -15.1 \text{ volts} \quad 6.3.12$$

and

$$V_{e4 \text{ min}} = V_{b5 \text{ min}} - I_{b5 \text{ min}} R_{12} = -9.2 \text{ volts} \quad 6.3.13$$

In the light of the above operating conditions, transistors type OC 84<sup>137</sup> were found suitable for stages 3 and 4. Depending on the absolute maximum ratings of the selected transistors and on the required operating conditions, a suitable value for the supply voltage was selected

$$E_c = -24 \text{ volts d.c.} \quad 6.3.14$$

According to experience, the emitter resistance  $R_{11}$  was chosen to be in the order of  $R_{12}/4$ , thus

$$R_{11} = 560 \text{ Ohms} \quad 6.3.15$$

At this stage, both the emitter quiescent current limits  $I_{e4 \text{ max}}$  and  $I_{e4 \text{ min}}$ , and the maximum current excursion  $i_{e4 \text{ max}}$  can be calculated as given below

$$I_{e4 \text{ max}} = \frac{|V_{e4 \text{ max}}|}{R_{11}} + I_{b5 \text{ max}} = 31.45 \text{ m.A.} \quad 6.3.16$$

$$I_{e4 \text{ min}} = \frac{|V_{e4 \text{ min}}|}{R_{11}} + I_{b5 \text{ min}} = 18.05 \text{ m.A.} \quad 6.3.17$$

and

$$i_{e4 \text{ max}} = \frac{v_{e4 \text{ max}}}{R_{11}} + i_{b5 \text{ max}} = 20.57 \text{ m.A. peak}$$

..6.3.18

With typical production spreads of transistors OC 84 according to their characteristics given in Ref.137,

$$\beta_{\max} = 200, \quad \beta_{\min} = 60 \quad 6.3.19$$

and

$$V_{be \max} = -0.75 \text{ volts}, \quad V_{be \min} = 0 \text{ volts} \quad \dots 6.3.20$$

Consequently, the limiting values of the base bias current and voltage of transistor  $N_3$  may be calculated as follows

$$I_{b3 \max} = \frac{I_{e4 \max}}{(\beta_{\min} + 1)^2} = 8.45 \mu\text{A.} \quad 6.3.21$$

$$I_{b3 \min} = \frac{I_{e4 \min}}{(\beta_{\max} + 1)^2} = 0.446 \mu\text{A.} \quad 6.3.22$$

$$V_{b3 \max} = V_{e4 \max} + 2 V_{be \max} = -16.6 \text{ volts} \quad 6.3.23$$

and

$$V_{b3 \min} = V_{e4 \min} + 2 V_{be \min} = -9.2 \text{ volts} \quad 6.3.24$$

Whereas, the maximum base current and voltage excursions are  
 $i_{b3 \max} = i_{e4 \max} / (\beta_{\min} + 1)^2 = 5.55 \mu\text{A. Peak } 6.3.25$   
 $V_{b3 \max} = V_{e3 \max} = V_{b4 \max} = V_{e4 \max} = 9 \text{ volts, peak } 6.3.26$   
 Hence, the minimum input impedance (mainly resistive)

of stage  $N_3$  can be determined as

$$R_{in3 \min} = (\beta_{\min} + 1)^2 \frac{R_{11} \cdot R_{12}}{R_{11} + R_{12}} = V_{b3 \max} / i_{b3 \max} \\ = 1.63 \text{ M. Ohms} \quad 6.3.27$$

By calculating the maximum power dissipation in the transistors  $N_3$  and  $N_4$  (not included here), and hence the maximum expected temperature under worst conditions of ambient temperature, it was found that the transistors will operate satisfactorily without any need of heat sink. However, for extra safety, transistor  $N_4$  was fitted with a cooling clip type b (see Ref.137).

After designing these stages, their construction followed. In order to have a preliminary check on the design figures obtained for the completed portion, tests were carried out to determine the actual required base bias voltage of transistor  $N_3$ , and the actual maximum voltage swing at its base. The results of these tests are given below

$$V_{b3} = -11.5 \text{ volts} \quad 6.3.28$$

$$v_{b3 \text{ max}} = 3.5 \text{ volts peak} \quad 6.3.29$$

voltage amplification of the built stages at 50 c/s

$$= \frac{25 \sqrt{2}}{3.5} = 10.1 \text{ volts/volt} \quad 6.3.30$$

On the basis of the above result and with the help of the required maximum overall voltage gain, the voltage amplification required by the input stage (or stages) can be determined as

$$\frac{2000}{10.1} \sim 200 \text{ volts/volt} \quad 6.3.31$$

To obtain such amount of amplification, the input stages must contain at least two stages.

#### 6.3.3.4. Input stages.

These include the first two transistors  $N_1$  and  $N_2$  as shown in Fig. 6.3.4. Common-emitter connection was used for both stages because of the high power gain obtainable in this configuration. The biasing arrangement, by means of a potential divider in conjunction with an emitter resistance, was employed as it provides best control over d.c. stabilization. Insufficient d.c. stabilization can give rise to the following effects:

- i) Widespread in input and output impedances<sup>n</sup>
- ii) Risk of overloading (bottoming) at high ambient temperatures
- iii) Possibility of thermal runaway (this effect is normally important only in high-voltage and/or high power stages).

The emitter resistance introduces negative d.c. feedback. The higher its value, the better the stabilization. Therefore to increase the emitter resistance without affecting the a.c. signal conditions, the emitter resistance is divided into two parts with the larger part shunted by means of a large capacitance which provides a very low impedance path to the a.c. signal. The unbypassed part will provide negative feedback for the a.c. signal, thereby distortion and noise are minimized and the cut-off frequency is increased. In addition, it increases the stage input impedance which is very desirable. The value of the emitter resistance has, however, a maximum limit depending on how much of the d.c.

supply voltage can be dropped across it.

The feedback also depends on how constant the base potential can be maintained during changes in base current; low values of the potential divider resistance parts improve the stabilization. However, there is a minimum limit to their values dictated by the current which the potential divider can be allowed to bleed from the d.c. supply, and/or by the shunting of the incoming a.c. signal.

Choice of transistor type OC 84 was appropriate not only in providing suitable characteristics for the stages  $N_1$  and  $N_2$ , but also in minimising the types of transistors used in the servo-amplifier as usually desirable.

Proceeding with the design of stage  $N_2$ , the minimum peak collector voltage required to drive the next stage is

$$v_{c2 \text{ max}} = v_{b3 \text{ max}} = 3.5 \text{ volts peak} \quad 6.3.32$$

Consequently, the collector-emitter voltage  $V_{ce2}$  should be chosen slightly higher than this maximum peak value in order to avoid the knee voltage for satisfactory transistor action. A reasonable choice is

$$V_{ce2} = -4.5 \text{ volts} \quad 6.3.33$$

Since the collector voltage in the absence of a.c. signal is

$$V_{c2} = V_{b3} = -11.5 \text{ volts} \quad 6.3.34$$

then the corresponding emitter voltage is

$$V_{e2} = V_{c2} - V_{ce2} = -7 \text{ volts} \quad 6.3.35$$

The value of the quiescent collector current was then chosen much higher than the base bias current drawn by transistors  $N_3$ , and thereby ensuring d.c. stability. In addition, the choice of this current was also governed by other factors such as its relative value in comparison with the maximum current swing, and how satisfactory will the various characteristics of the transistor OC 84 when operating with such current value. Hence

$$I_{c2} = 2 \text{ m.A.} \quad 6.3.36$$

The collector resistance can thus be evaluated

$$R_8 + R_{v2} = \frac{|E_c - V_{c2}|}{I_{c2}} = 6.25 \text{ k.Ohms} \quad 6.3.37$$

This resistance was split into two resistances, a fixed resistance  $R_8$  of 3.3 k and an adjustable resistance  $R_{v2}$  of 5 k. The value of the adjustable resistance was selected higher than suggested by the calculations in order to allow flexibility in adjusting the required bias for the stages  $N_3$ ,  $N_4$  and  $N_5$ , and hence to cope with the variations in the biasing conditions which might arise from changes in temperature, the introduction of the multistage negative feedback (from the collector of  $N_5$  to the base of  $N_3$ ), and/or from the tolerances of the various resistors and transistors.

With a typical value of  $\beta = 90$ , the quiescent emitter and base currents may be evaluated, thus



$$I_{e2} = I_{c2} \cdot \frac{\beta+1}{\beta} \approx 2 \text{ m.A} \quad 6.3.38$$

and

$$I_{b2} = I_{c2}/\beta = 22.2 \mu\text{.A.} \quad 6.3.39$$

Hence, the emitter resistance is given by

$$R_4 + R_5 = \frac{|V_{e2}|}{I_{e2}} = 3.5 \text{ K.Ohms} \quad 6.3.40$$

This again was split into an unbypassed resistor  $R_4$  of 200 Ohms and a bypassed resistor  $R_5$  of 3.3 K.

The maximum collector current excursion is therefore

$$i_{c2 \text{ max}} = \frac{v_{c2 \text{ max}}}{R_8 + R_{v2}} = 0.56 \text{ m.A. peak} \quad 6.3.41$$

In order to evaluate the current gain, the voltage gain, and the input impedance of this stage, the complete small-signal circuit model is constructed as shown in Fig. 6.3.5. However, before proceeding further, considerable simplification for this model can be achieved since the working frequency range is relatively low (less than 20 k.c.). The simplified model is shown in Fig. 6.3.6. From this model, the following expressions can easily be worked out

$$A_{i2} = \frac{g_m r_{\pi} r_o - R_9}{R_4 + r_o + R_{L2}} = 80 \quad 6.3.42$$

$$A_{v2} = \frac{A_{i2} R_{L2}}{(r_x + r_{\pi}) + R_9 (1 + A_{i2})} = 30.7 \quad 6.3.43$$

and

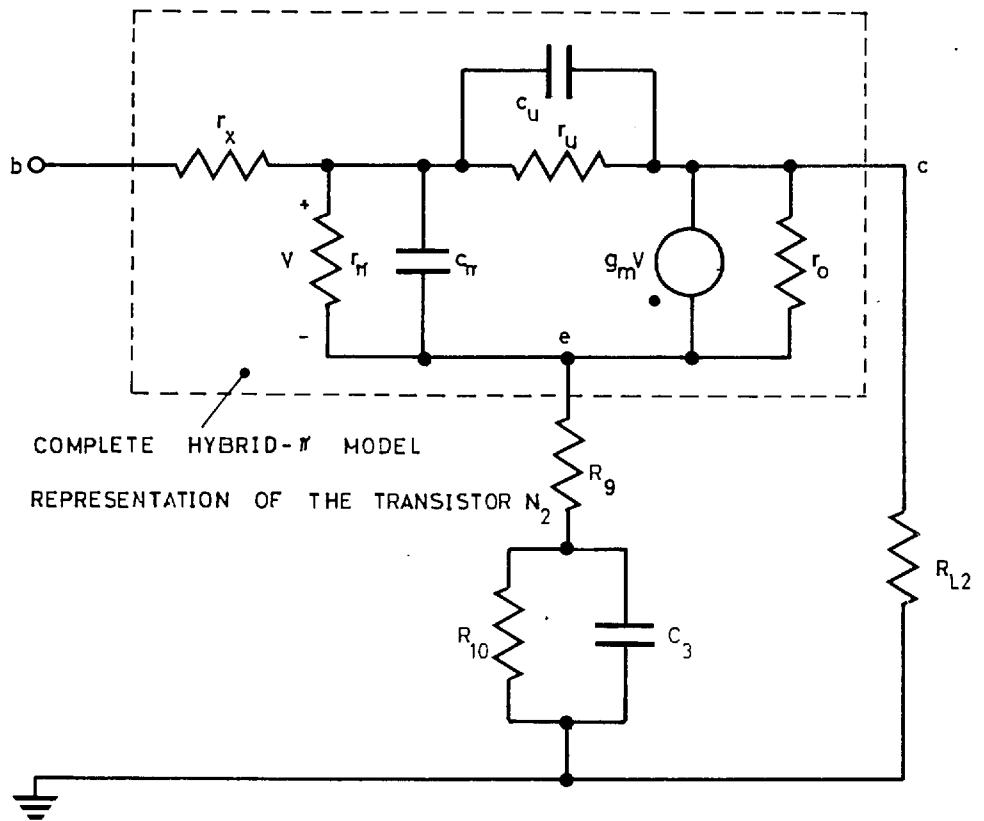


FIG. 6.35  
COMPLETE SMALL-SIGNAL CIRCUIT MODEL FOR THE STAGE 2  
OF THE SERVO-AMPLIFIER

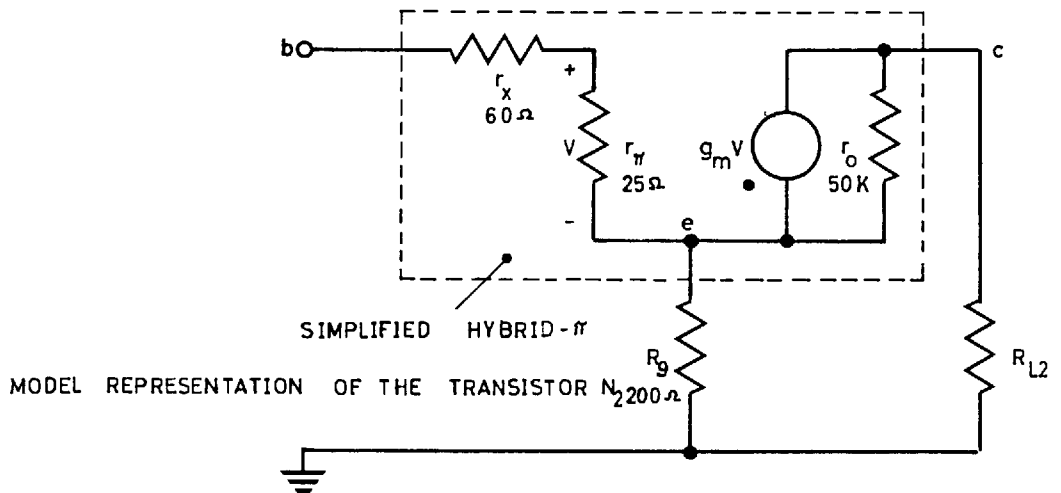


FIG. 6.36  
SIMPLIFIED LOW-FREQUENCY CIRCUIT MODEL FOR THE  
STAGE 2 OF THE SERVO-AMPLIFIER (VALID UP TO 20 KC)

$$R_{in2} = r_x + r_\pi + R_9(1+A_{i2}) = 16.285 \text{ K. Ohms} \quad 6.3.44$$

where

$$\frac{1}{R_{L2}} = \frac{1}{(R_8 + R_{v2})} + \frac{1}{R_{in3}} \quad 16 \text{ m.Mhos} \quad 6.3.45$$

(The values of the parameters  $r_x$ ,  $r_\pi$ ,  $r_o$  and  $g_m$  are given in the published data of transistor OC 84.)

With the knowledge of the current and voltage gains, the calculation of the maximum base current and voltage excursions becomes easy, thus

$$i_{b2 \text{ max}} = \frac{i_{c2 \text{ max}}}{A_{i2}} = 7 \mu\text{.A. peak} \quad 6.3.46$$

and

$$v_{b2 \text{ max}} = \frac{v_{c2 \text{ max}}}{A_{v2}} = 0.114 \text{ volts peak} \quad 6.3.47$$

Now, the design of the potential divider  $R_6$ ,  $R_7$  is to be considered. By allowing about 20 times the base bias current to flow through the potential divider to ensure d.c. stability, thus

$$R_6 + R_7 \approx \frac{|E_c|}{20 I_{b2}} \quad 6.3.48$$

Also, since the base bias voltage is

$$V_{b2} = V_{e2} + V_{be2} \approx -7 \text{ volts} \quad 6.3.49$$

thus it will be useful in the following relation

$$\frac{R_7}{R_6 + R_7} \approx \frac{V_{b2}}{E_c} \quad 6.3.50$$

Solving the simultaneous Eqns. 6.3.48 and 6.3.50, it is possible to obtain values for  $R_6$  and  $R_7$  as given below

$$R_6 = 43 \text{ K. Ohms} \quad 6.3.51$$

and

$$R_7 = 18 \text{ K. Ohms} \quad 6.3.52$$

Pursuing a similar design procedure as above, it is possible to evaluate the various resistances and potential dividers, and to determine the biasing conditions required for the first stage  $N_1$ . The various design values are given in Fig. 6.3.4. Therefore, only the current gain, voltage gain, and the input impedance are going to be calculated here because of their significance in the subsequent discussion.

The expressions given by Eqns. 6.3.42 to 6.3.44 are applicable to this stage provided that the following modifications are made:

$$R_9 \text{ is replaced by } R_4 \quad 6.3.53$$

$$R_{L2} \text{ is replaced by } R_{L1} \quad 6.3.54$$

$$\text{and subscript 2 is replaced by subscript 1} \quad 6.3.55$$

It therefore follows that

$$A_{i1} = 83 \quad 6.3.56$$

$$A_{v1} = 20.5 \quad 6.3.57$$

and

$$R_{in1} = 16.885 \text{ K. Ohms} \quad 6.3.58$$

where

$$\frac{1}{R_{L4}} = \frac{1}{R_3} + \frac{1}{R_6} + \frac{1}{R_7} + \frac{1}{R_{in2}} = 0.24 \text{ m.Mhos}$$

..6.3.59

Neglecting the effect of the d.c. blocking capacitor  $c_1$ , the amplifier input impedance before fitted with the gain control attenuator  $R_{v1}$  is

$$R_{in} = \frac{1}{\frac{1}{R_1} + \frac{1}{R_2} + \frac{1}{R_{in1}}} = 7.1 \text{ k.Ohms} \quad 6.3.60$$

which meets the specified requirement.

The maximum available overall voltage gain can be estimated from Eqns. 6.3.30, 6.3.43 and 6.3.57, thus

$$A_v = 6350 \quad 6.3.61$$

which is even higher than the specified figure.

### 6.3.3.5. Negative feedback loop

After completing the design of the remaining stages of the amplifier, they were constructed. To simplify the wiring while keeping the compactness, the various stages of the amplifier were built on two veroboard sheets made as plug-in units to suit standard plugs. Plate E.4.2 shows a photograph of the built servo-amplifier, together with electronic synchronous switches and their driving circuits to be incorporated in chopper network compensators.

By testing the completed amplifier over the frequency range 5 to 1000 c/s, and with different settings of the gain control, the performance was quite satisfactory so long as the amplifier output stage was not driven to saturation. However, when the input signal level was increased to cause saturation in the output stage, the amplifier started to oscillate at a high frequency (about 5 k.c.). This is obviously undesirable in the present application.

To stabilize the amplifier under such operating condition, phase-lag negative feedback technique was employed. The negative feedback is taken over the last three stages; from the collector of  $N_5$  to the base of  $N_3$  as shown in Fig. 6.3.4. As a result, the overall amplifier gain was reduced, but still satisfies the requirements.

The design procedure for determining the parameters of the phase-lag network in the feedback loop is extremely involved as explained in Ref. 138. Although the procedure was applied to the present problem, the intention was not to include it here since it is remotely concerned with the present work of this thesis. The results of the designed phase-lag network, however, are given in the figure.

#### 6.3.4. Amplifier overall performance

To check the overall performance characteristics of the constructed amplifier with respect to the design specifications, frequency response tests were carried out over the frequency range 5 to 1000 c/s and at different settings of the gain control.

The T.F.A. oscillator was employed to excite the

amplifier by a variable frequency sinusoidal wave. The collectors of the output transistors  $N_5$  and  $N_6$  were then connected to the balanced input terminals of the T.F.A. Resolved Component Indicator with which, and in conjunction with the T.F.A. Reference Resolver, the amplitude and phase of the output voltage were measured. Because the output balanced signal is superimposed on a d.c. voltage due to the bias of the output transistors, the T.F.A. Resolved Component Indicator may yield inaccurate results in view of the saturation of its various amplifiers and electronic circuits. To overcome this problem, two floated (isolated) d.c. power supplies may be inserted, in the proper sense, between the collectors of  $N_5$  and  $N_6$  and the input terminals of the T.F.A. Resolved Component Indicator. By adjusting the voltages of these power supplies, it is possible to completely neutralise the effect of the d.c. voltage component. The internal impedances of these power supplies are considerably smaller in comparison with the input impedance of the T.F.A. Resolved Component Indicator, therefore they will introduce a negligible effect on the accuracy of the measurements. The interconnections between the various T.F.A. instruments have been described in detail in the previous Chapter.

Fig. 6.3.7 illustrates the amplifier frequency response obtained experimentally in terms of voltage gain and phase. To be able to check the linearity of the voltage gain, the frequency response test was repeated with different settings of the gain control. Correspondingly a set of voltage gain response curves was plotted. While only the average phase response curve was plotted with vertical lines at the various test frequencies whose magnitudes indicate the limits of the phase variation with the gain control settings.

In examining the voltage gain response curves, it is

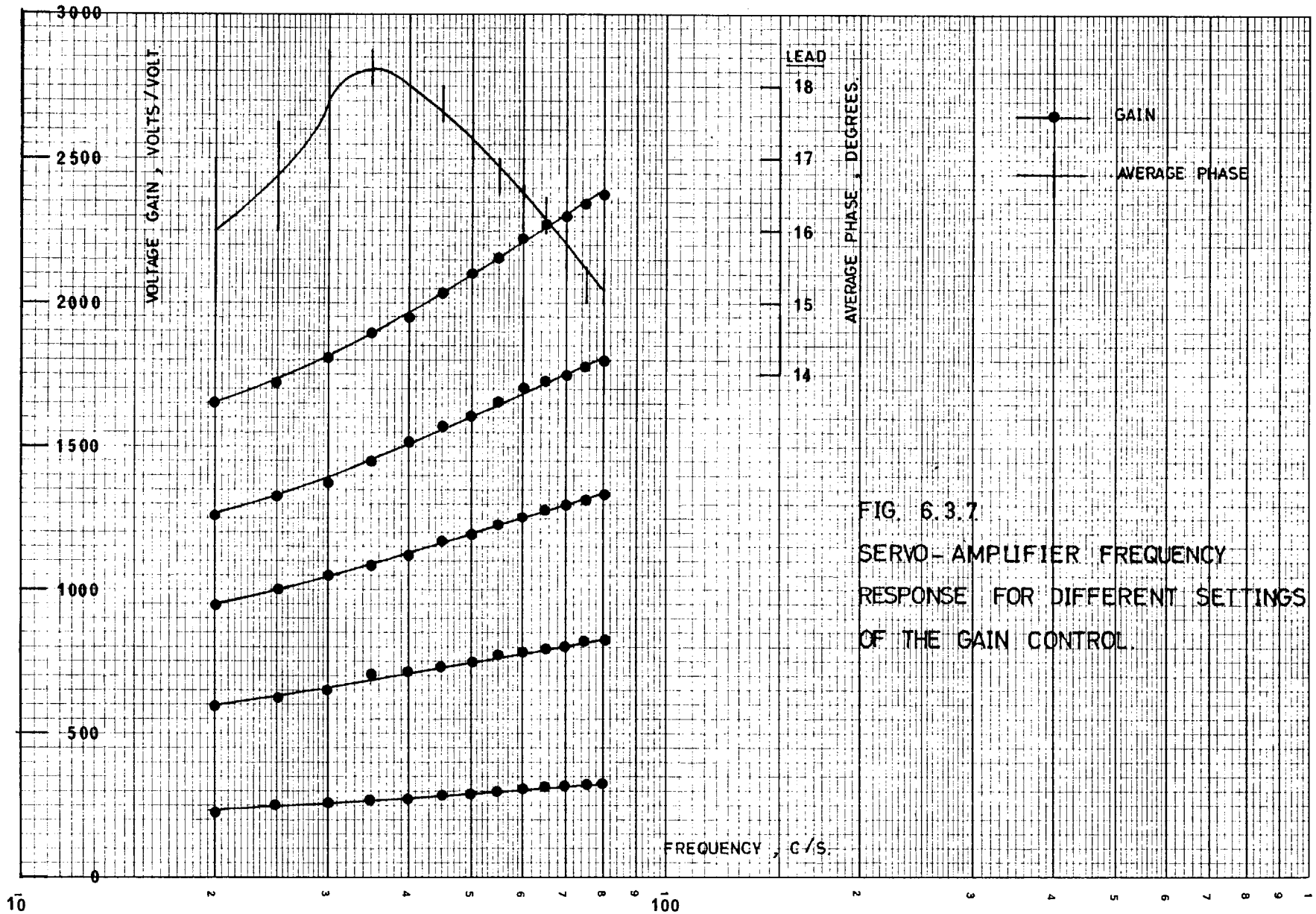


FIG. 6.3.7  
SERVO-AMPLIFIER FREQUENCY  
RESPONSE FOR DIFFERENT SETTINGS  
OF THE GAIN CONTROL.



noticed that the gain rises by almost 3 db as the frequency changes from 20 to 80 c/s, but is virtually independent of the gain control setting. Also, the gain remains within  $\pm 2\%$  up to full output voltage of 20 volts r.m.s. measured at a test frequency of 50 c/s. A study of the phase response reveals that the phase deviates from a mean value of 16.5 degrees by  $\pm 1.5$  degrees maximum as the frequency changes from 20 to 80 c/s. Further, by varying the gain control setting, a maximum phase deviation of 2 degrees occurs at frequency of 20 c/s.

At this point, it is important to mention that when this servo-amplifier is used in conjunction with the a.c. servo-mechanism breadboard model, a constant phase misalignment of 16.5 degrees between the carrier excitations of the servo-motor and the error-detector should be intentionally made in order to compensate for the mean phase response of the amplifier. In so doing, only small phase deviation of  $\pm 1.5$  degrees maximum still exists. It, however, may be considered of negligible effect on the overall response of the servo-system.

Although the above frequency response has yielded most of the amplifier performance characteristics, another test was conducted to reveal more performance information. In this test, the current response was measured instead of the voltage response. For this purpose, two identical resistors  $R_{14}$  and  $R_{15}$  of 5 Ohms each were inserted in series with the two branches of the motor control winding which are connected to the collectors of the output transistors  $N_5$  and  $N_6$ . Therefore, by measuring the magnitude and phase of the voltage drops across these resistors, using the same measuring techniques as described above, it is possible to deduce from them the corresponding magnitude and phase

of the output current; being linearly related. On the other hand, since the amplifier input impedance is virtually resistive, the input voltage was measured rather than the input current which is difficult to measure with enough accuracy. By dividing the output current by the input voltage, the amplifier transfer admittance characteristics were thus obtained. The magnitude and phase of this transfer admittance are plotted as functions of frequency for different settings of the gain control as shown in Fig. 6.3.8.

Inspecting the curves of this figure, it is observed that the transfer admittance drops by approximately 8% as the frequency varies from 20 to 80 c/s, and this figure is virtually independent of the gain control setting. At the test frequency of 50 c/s, the magnitude of the transfer admittance remains within 1% up to full output current.

By examining the phase of the transfer admittance, it can be seen that it deviates from a mean value of 4 degrees by  $\pm 3$  degrees maximum over the frequency range 20 to 80 c/s. Also, it varies with the gain control setting reaching a maximum deviation of one degree at frequency of 70 c/s.

By comparing the overall performance characteristics obtained experimentally with those desired as specified in Sub-section 6.3.2, it may be concluded that the servo-amplifier designed and constructed on the above basis is quite satisfactory.

#### 6.4. Practical Determination of the Relevant Parameters of the Transmitter-Coincidence Transmitter Magslip-System

In Chapter 2, a complete analysis of such system has been presented. An examination to the mathematical model

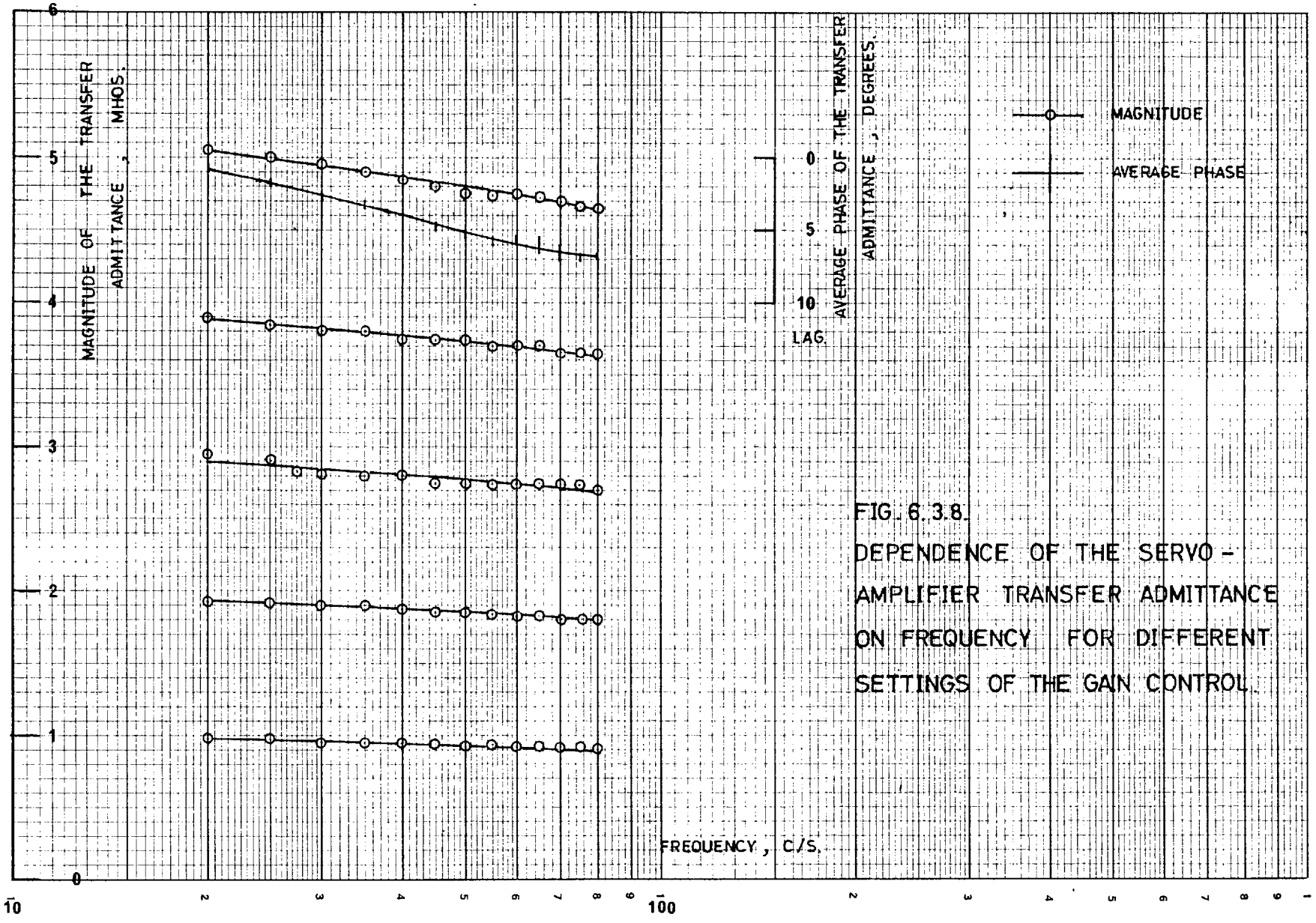


FIG. 6.3.8.  
 DEPENDENCE OF THE SERVO -  
 AMPLIFIER TRANSFER ADMITTANCE  
 ON FREQUENCY FOR DIFFERENT  
 SETTINGS OF THE GAIN CONTROL.

and the complex frequency block diagram representations developed in Sub-sections 2.3.3 and 2.3.4 shows that only two parameters are involved  $k_s$  and  $\mu_s$ . Depending on the knowledge of the values of these parameters, the behaviour of the magstrip-system can be completely defined. It is therefore necessary to evaluate these parameters.

The formulae for  $k_s$  and  $\mu_s$  given by Eqns. 2.3.36 and 2.3.34 respectively express these parameters in terms of the physical parameters of the magstrip-system. Evaluation of such parameters is therefore possible by substituting the values of the various physical parameters in their respective formulae. An alternative method, however, is to measure these parameters directly by a simple static test. The following Sub-section is devoted to this test.

#### 6.4.1. Static test

The most appropriate way of introducing this test is first to discuss the various logical steps which have led to its formalisation.

The relationship between the output voltage of the coincidence-transmitter rotor and the angular misalignment between the rotor's positions of the transmitter and coincidence-transmitter has been derived in Sub-section 2.3.3, and its expression in the time domain is reproduced here below

$$e_{b2} = -k_s p \left[ \sin \gamma_s \sin(\Omega t + \theta - \mu_s) \right] \quad 6.4.1$$

where  $\gamma_s$  is the angular difference between the rotor's positions ( $\gamma_{s1} - \gamma_{s2}$ ) of the transmitter and coincidence-transmitter, which is in general a function of time under

normal operating conditions. However, by keeping the two rotors stationary,  $\gamma_s$  becomes a constant, and hence the above expression can be re-written as

$$e_{b2} = k_s \Omega \sin \gamma_s \sin(\Omega t + \theta + \frac{\pi}{2} - \mu_s) \quad 6.4.2$$

which is a simple sinusoidal wave with

$$\text{amplitude } E_{b2} = k_s \Omega \sin \gamma_s \quad 6.4.3$$

and

$$\text{phase } \alpha = \theta + \frac{\pi}{2} - \mu_s \quad 6.4.4$$

which are easily measurable.

Therefore, under such static condition, by measuring the amplitude and phase of both the exciting input voltage to the transmitter rotor winding and the induced voltage in the coincidence-transmitter rotor winding for a certain value of the angular misalignment between their rotor's positions, it is possible to deduce the values of  $k_s$  and  $\mu_s$ .

To measure the angular misalignment between the mag-slips shafts, the two rotors were first aligned. This was done in the Laboratory by energising the transmitter rotor winding by a 50 c/s signal and the induced voltage in the coincidence-transmitter rotor winding was observed on the screen of an oscilloscope. Then, the transmitter rotor was slowly rotated manually, while the coincidence-transmitter rotor kept stationary, until a minimum induced voltage was observed (ideally or for zero resolution, the minimum induced voltage is expected to be zero). At this position, the two rotors are considered to be aligned, i.e.,  $\gamma_s = 0$ , although

the windings in the two rotors are actually at 90 degrees apart. Throughout the experiment, the rotor position of the coincidence-transmitter was kept fixed while the required angular misalignment was obtained by rotating the transmitter rotor. This rotation was amplified by means of a gear system of ratio 1:5 to a shaft on which a graduated protractor was mounted for measuring the angular displacement with ample sensitivity.

The amplitude and phase of the input and output signals were measured by means of a valve voltmeter and a phase angle meter respectively. A variable low pass filter is also used to eliminate any possible errors arising from saturation. The techniques of measurement are based on the method used in measuring the d.c. modulation transference of chopper networks outlined in Sub-section 5.2.2.

To be able to conduct tests at different carrier frequencies the variable frequency supply system shown in Fig. 5.2.3. (see description in Sub-section 5.2.3) was employed to energise the transmitter rotor winding. Such frequencies were measured by means of an electronic digital frequency meter.

On the basis of the static test described above, a number of tests were carried out under a variety of conditions not only to enable to study the dependence of the parameters  $k_s$  and  $\mu_s$  on these conditions, but also to assess the validity of the theoretical analysis derived in Section 2.3. The results of the various tests accompanied by discussions are outlined in the subsequent Sub-sections.

6.4.2. Dependence of the parameters  $k_s$  and  $\mu_s$  on the angular misalignment  $\gamma_s$  and the magnetic flux density in the transmitter.

The results were obtained by the static test described above. To study the influence of the magnetic flux density in the transmitter on the determined parameters, the test was repeated for three representative values of the energising voltage of the transmitter rotor winding, while the frequency was maintained constant at 50 c/s. If the resistive drop is negligible, the ratio  $e_{a1}/f_c$  may be considered to be proportional to the flux density. On this basis, when the value of this ratio is 1 volts/cycles/sec., it corresponds to the full-load (rated) flux density, as the voltage and frequency ratings of the transmitter under investigation are 50 volts and 50 c/s respectively (see specifications in Appendix E.3.1).

The results obtained are plotted in Fig. 6.4.1. In studying the various curves, it is evident that the average curves for  $k_s$  and  $\mu_s$ , are virtually horizontal lines which imply that they are independent of  $\gamma_s$ . This supports the theoretical formulae of  $k_s$  and  $\mu_s$ , given by Eqns. 2.3.36 and 2.3.34 respectively, which predict the same property. It is observed, however, that some departure exists between the experimental results of  $k_s$  and the drawn mean curves. This departure is particularly predominant at small values of  $\gamma_s$  with a maximum offset of 5%. This may be attributed to the measuring error for  $\gamma_s$  which increases as  $\gamma_s$  decreases.

With the increase of the transmitter magnetic flux density from 60% to 100% of the full-load value, the average value of  $k_s$  drops by 1.5%, and the average value

$\mu_s$	$e_{a1}/f_c$	$K_s/E_s$	$e_{a1}/f_c$	TRANSMITTER MAGNETIC FLUX DENSITY
—○—	0.6	—△—	0.6 VOLTS/CYCLES/SEC.	60 %
—○—	0.8	—△—	0.8 " " "	80 %
—○—	1.0	—▽—	1.0 " " "	100 %

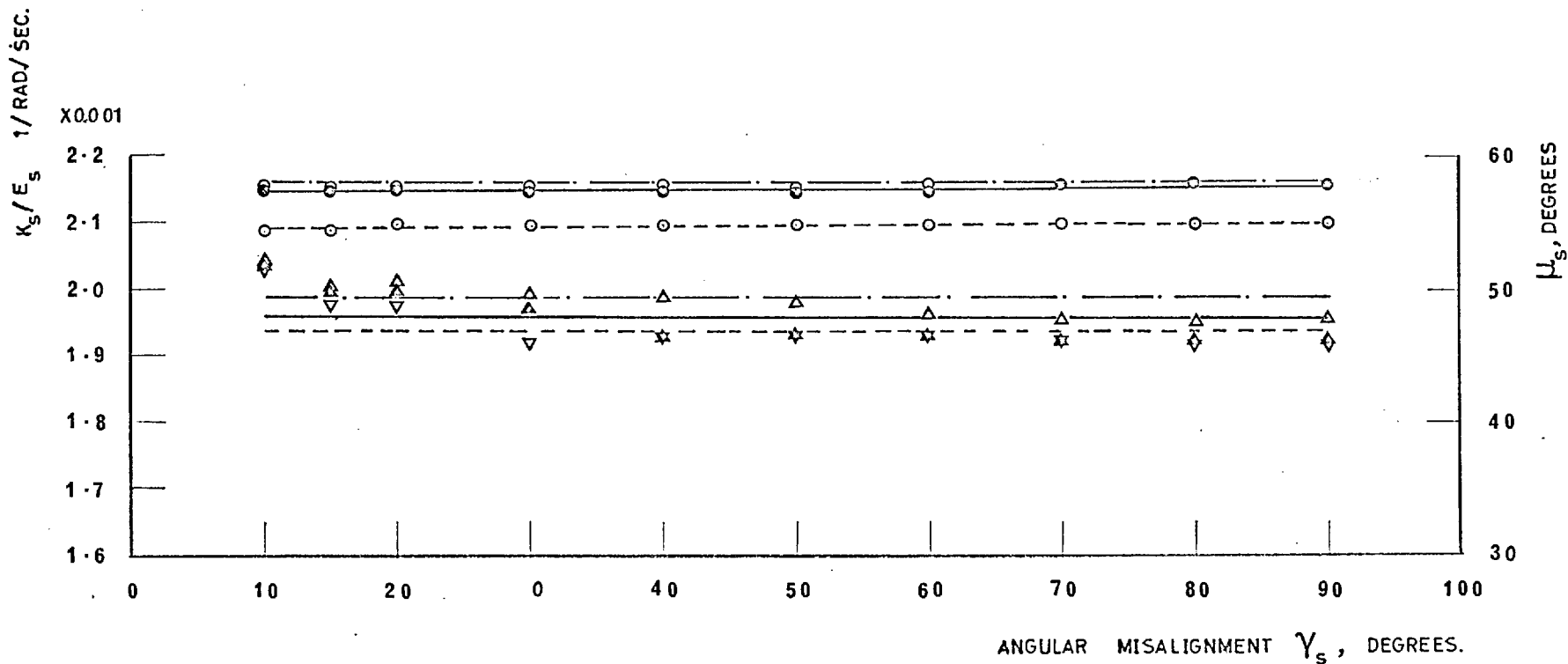


FIG. 6.4.1.

DEPENDENCE OF THE PARAMETERS  $K_s$  AND  $\mu_s$  ON THE ANGULAR MISALIGNMENT  $\gamma_s$  FOR DIFFERENT VALUES OF THE TRANSMITTER MAGNETIC FLUX DENSITY



of  $\mu_s$  drops by 3 degrees (or by 5.2%). The theoretical expressions of  $k_s$  and  $\mu_s$  do not show such dependence because their derivations have been based on idealised magnetic assumptions (see Section 2.1). However, since the percentage changes in the values of  $k_s$  and  $\mu_s$  are approximately of the same order as the errors that may be obtained from the measuring instruments, the theoretical expressions can still be considered reliable and reasonably accurate.

#### 6.4.3. Effect of the carrier frequency variation on the average values of the parameters $k_s$ and $\mu_s$ .

In some practical applications, a.c. servo-mechanisms are energised by a carrier source with poor frequency regulation. This can cause serious effects on the performance characteristics of the individual components as well as of the overall servo-systems. A study of the carrier frequency deviation on the parameters  $k_s$  and  $\mu_s$  is therefore considered very desirable, since it will enable to assess its effect on the mag-slip-system performance. As a secondary result of conducting such experimental studies under different carrier frequencies, it was possible to check the validity of the theoretical expressions of  $k_s$  and  $\mu_s$  as will be seen later in this Sub-section.

Fig. 6.4.2 shows the experimental results of the parameters  $k_{s\text{ av}}$  and  $\mu_{s\text{ av}}$  as functions of carrier frequency for two representative values of transmitter magnetic flux density; 50% and 100% ( $k_{s\text{ av}}$  and  $\mu_{s\text{ av}}$  are the average values of  $k_s$  and  $\mu_s$  evaluated over different values of  $\gamma_s$ ).

Examination of the curves shows that  $k_{s\text{ av}}$  drops with a decreasing rate as the carrier frequency increases. At

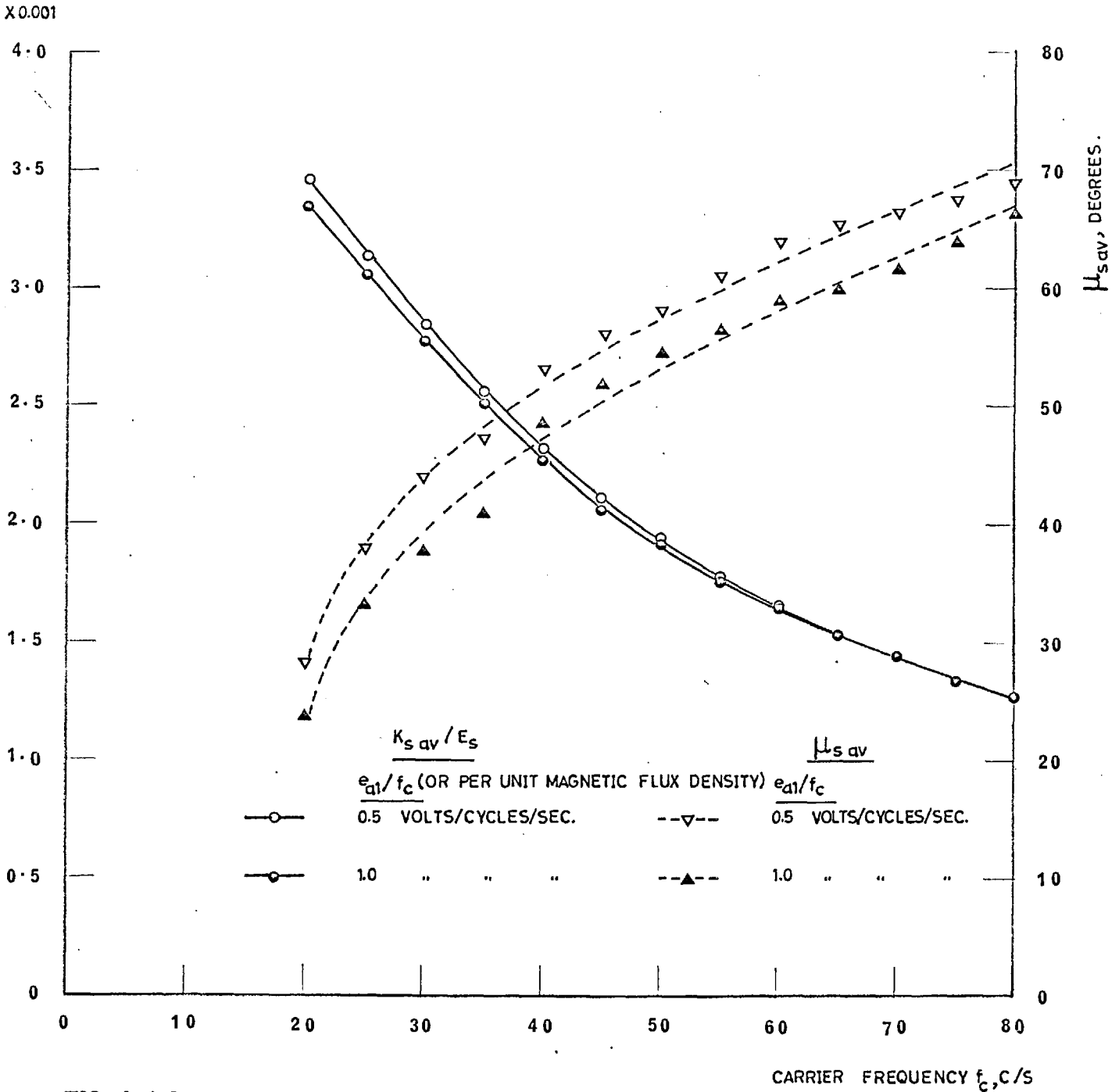


FIG. 6.4.2.

DEPENDENCE OF THE PARAMETES  $K_{sav}$  AND  $\mu_{sav}$  ON THE ENERGISATION CARRIER FREQUENCY FOR TWO VALUES OF THE TRANSMITTER MAGNETIC FLUX DENSITY.

high carrier frequency, the two curves of  $k_{s \text{ av}}$  at 50% and 100% transmitter magnetic flux density coincide. However, they start to diverge from each other at approximately 55 c/s, and the divergence increases as the carrier frequency decreases to reach a percentage value of 3% at 20 c/s. On the other hand,  $\mu_{s \text{ av}}$  increases with the carrier frequency with a decreasing rate. Its curves at 50% and 100% transmitter magnetic flux density depart from each other, and this departure ranges from 5 to 3 degrees as the carrier frequency changes from 20 to 80 c/s.

By comparing the experimental results given in Fig. 6.4.2 with the theoretical expressions of  $k_s$  and  $\mu_s$ , two conclusions can be drawn:

- i) For the same carrier frequency, the drop detected in  $\mu_{s \text{ av}}$  suggests that the ratio  $L_{rs}/R_{rs}$  decreases with the increase of the transmitter magnetic flux density.
- ii) For the same carrier frequency, the drop detected in  $k_{s \text{ av}}$  suggests that the quantity

$$R_{rs} \sqrt{1 + \Omega^2 \frac{L_{rs}^2}{R_{rs}^2}}$$

increases with the increase of the transmitter magnetic flux density.

From the above two conclusions, it is easy to deduce that  $R_{rs}$  increases with the magnetic flux density of the transmitter.

The increase in the effective value of  $R_{rs}$  (may be denoted as  $R_{\text{eff}}$ ) may be explained in terms of the iron losses (eddy and hysteresis losses) which are usually represented

by an additional fictitious resistance. On this basis, the ratio  $L_{rs}/R_{rs}$  decreases, although there may be an additional contribution if magnetic saturation occurs at the high flux density resulting in a decrease in  $L_{rs}$ .

By re-arranging Eqn. 6.4.2 in the vector form, with the help of Eqns. 2.3.12, 2.3.34 and 2.3.36, thus

$$\begin{aligned} \frac{e_{b2}}{e_{a1}} \cdot \frac{1}{\Omega \sin \gamma_s} &= \frac{n_L}{n_s} \cdot \frac{M_s^2}{2 L_{Ds}} \cdot \frac{1}{R_{rs} + j \Omega L_{rs}} \\ &= \bar{K}_s / E_s \end{aligned} \quad 6.4.5$$

It is clear from the above equation that as the carrier frequency  $\Omega$  varies, the head of the vector  $\bar{K}_s / E_s$  traces out a semi-circular locus in the fourth quadrant of the complex plane. To check this by the experimental results obtained above, three transfer loci, corresponding to transmitter magnetic flux density of 50%, 80% and 100%, were plotted on the complex plane with  $k_{s \text{ av}} / E_s$  and  $M_{s \text{ av}}$  representing the vector magnitude and phase for varying  $\Omega$ . By fitting the best curves, semi-circular loci extending from the origin were obtained as shown in Figs. 6.4.3 to 6.4.5. This conforms with the result of Eqn. 6.4.5 which is derived from the theoretical analysis given in Section 2.3. The validity of this analysis is therefore confirmed.

In this respect, although the theoretical analysis was based on idealised magnetic conditions, it is feasible to extend its application to practical magnetic conditions by introducing simple modifications to  $R_{rs}$  and  $L_{rs}$ , such as

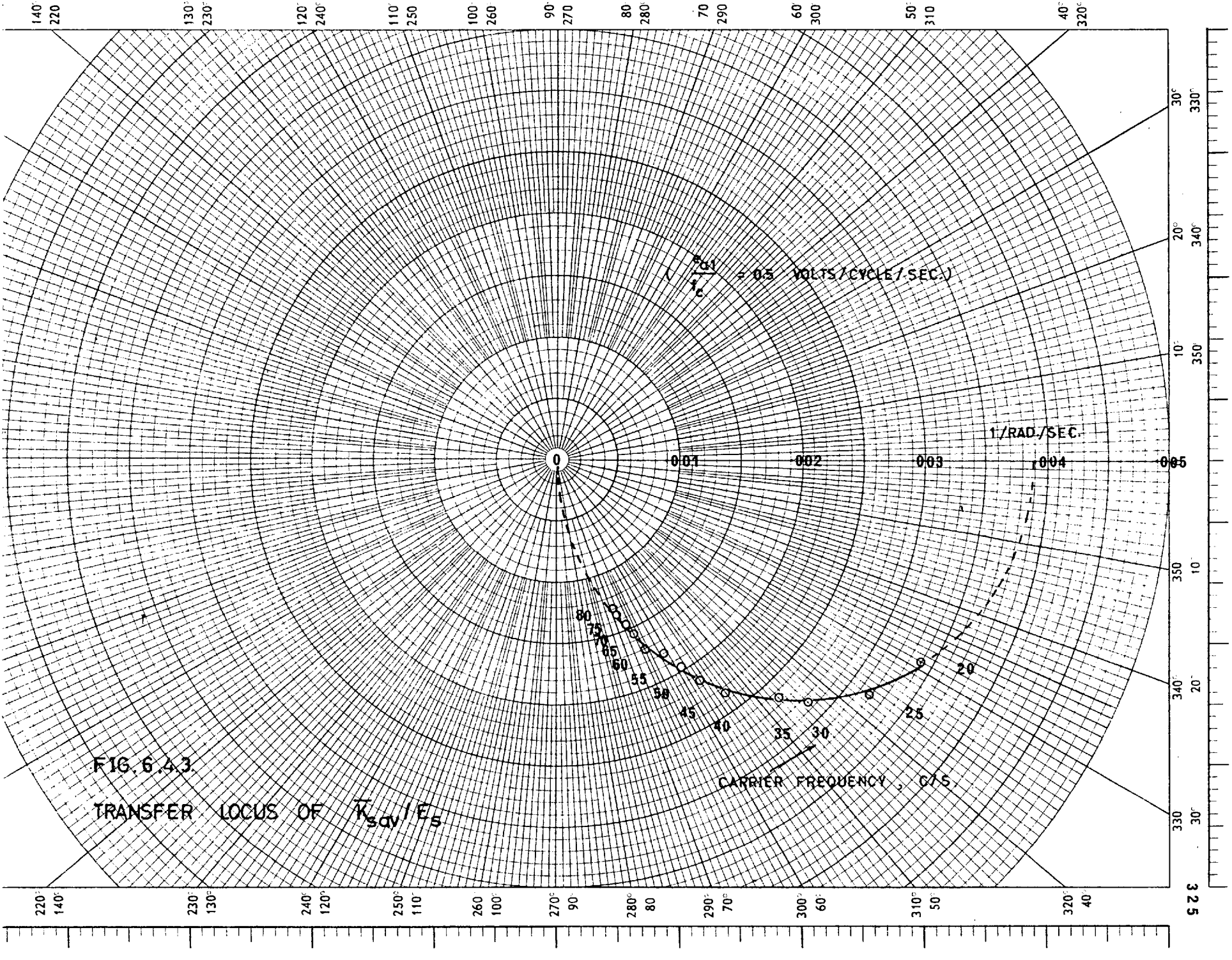
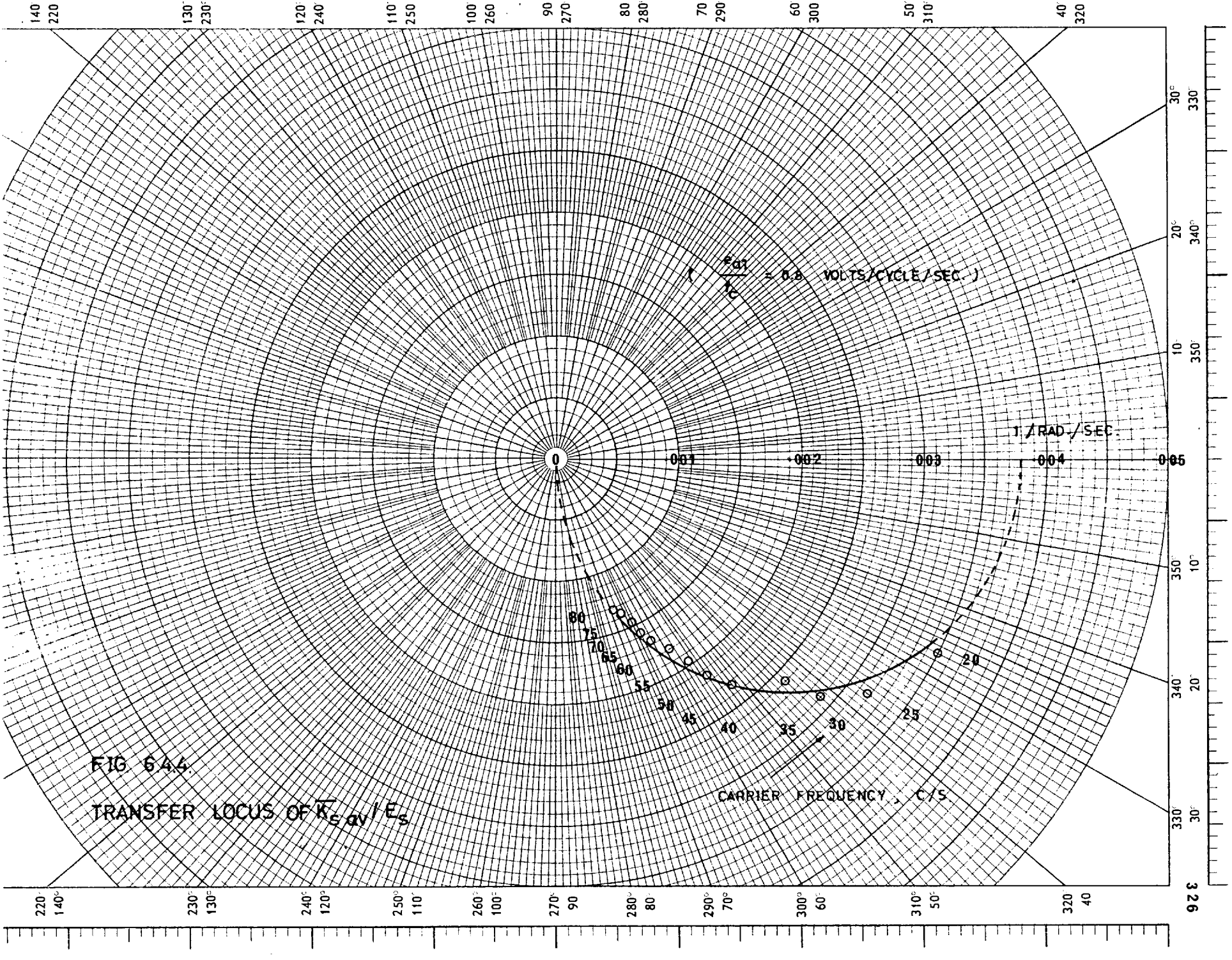


FIG. 6.4.3  
 TRANSFER LOCUS OF  $K_{sav}/E_s$

$\frac{E_{s1}}{E_c} = 0.5$  VOLTS/CYCLE/SEC.

1/RAD/SEC.

CARRIER FREQUENCY, GHz



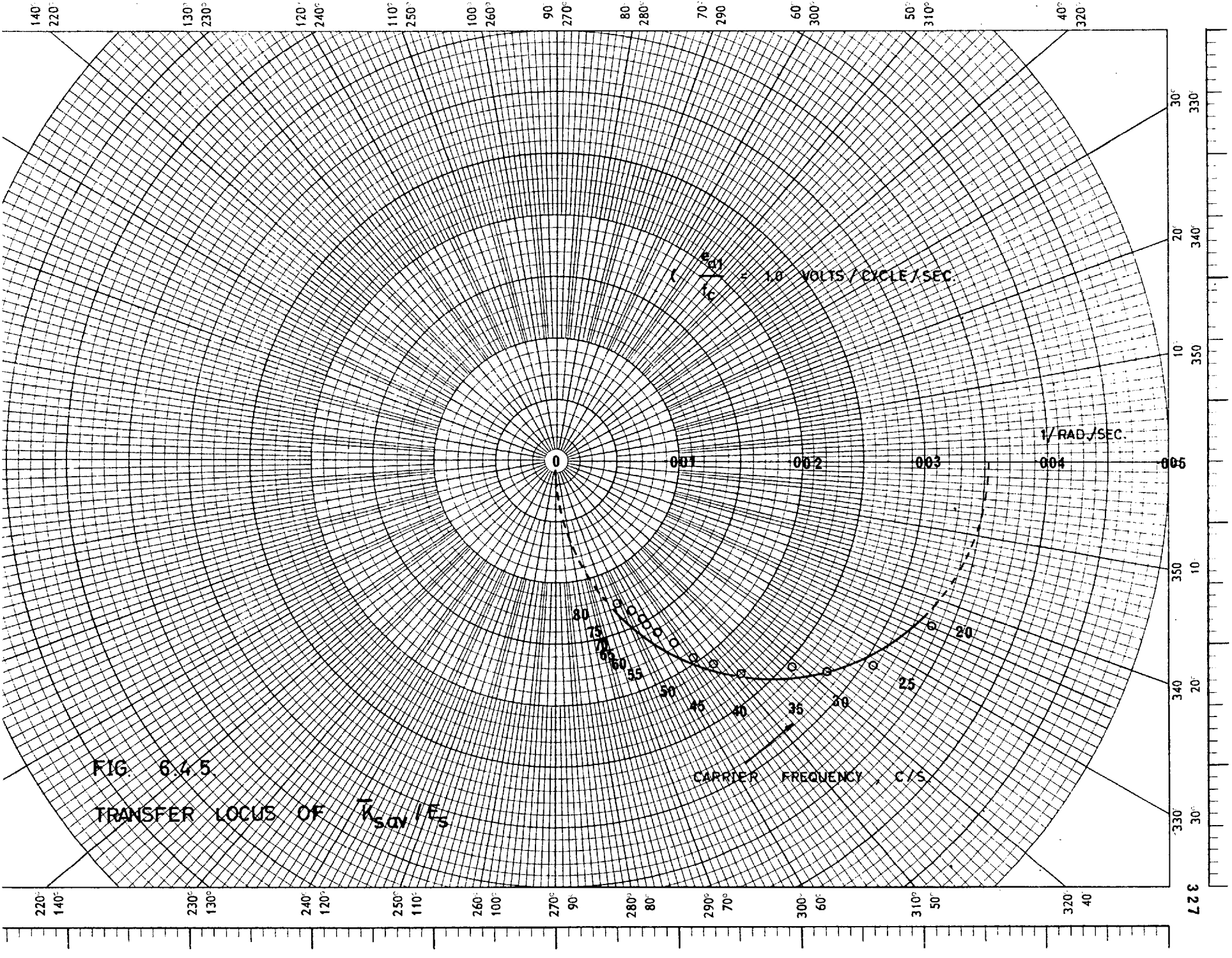


FIG. 6.45

TRANSFER LOCUS OF  $T_{s_{av}}/E_s$

$$\frac{E_s}{1c} = 1.0 \text{ VOLTS/CYCLE/SEC}$$

CARRIER FREQUENCY, C/S

1/RAD/SEC

adding terms as functions of the magnetic flux density.

To obtain a quantitative idea about the change in  $R_{\text{eff}}$  corresponding to change in the transmitter magnetic flux density, the diameters of the semi-circular transfer loci of Figs. 6.4.3 to 6.4.5 can be taken as inversely proportional to  $R_{\text{eff}}$ . This is deduced from Eqn. 6.4.5 by substituting  $\Omega = 0$ . On this basis, the percentage increase in  $R_{\text{eff}}$  as the flux density increases from 50% to 100% is approximately 10%.

In this connection, it may be worthwhile pointing out that the present static test with different carrier frequency can provide a simple means of evaluating  $R_{\text{eff}}$  and  $L_{\text{eff}}$ . Evaluation of  $R_{\text{eff}}$ , as mentioned earlier, can be obtained from the diameter of the transfer locus  $\bar{k}_s/E_s$  which corresponds to frequency  $\Omega = 0$  in the expression given by Eqn. 6.4.5. Then, on substituting the value of  $R_{\text{eff}}$  in Eqn. 2.3.34,  $L_{\text{eff}}$  can be determined, where the values of  $\mu_{s \text{ av}}$  and  $\Omega$  appearing in the equation may be chosen from the various experimental points.

#### 6.4.4. Effect of the transmitter magnetic flux density on the average values of the parameters $k_s$ and $\mu_s$

Although such effect has been examined in the previous two Sub-sections, the examination was limited to only few representative values of the flux density. Therefore, to allow for wider investigations, the static test was repeated over a large range of the flux density. The measured parameters  $k_{s \text{ av}}$  and  $\mu_{s \text{ av}}$  were then plotted against the per unit magnetic flux density in the transmitter for different values of carrier frequency as illustrated in Fig. 6.4.6.



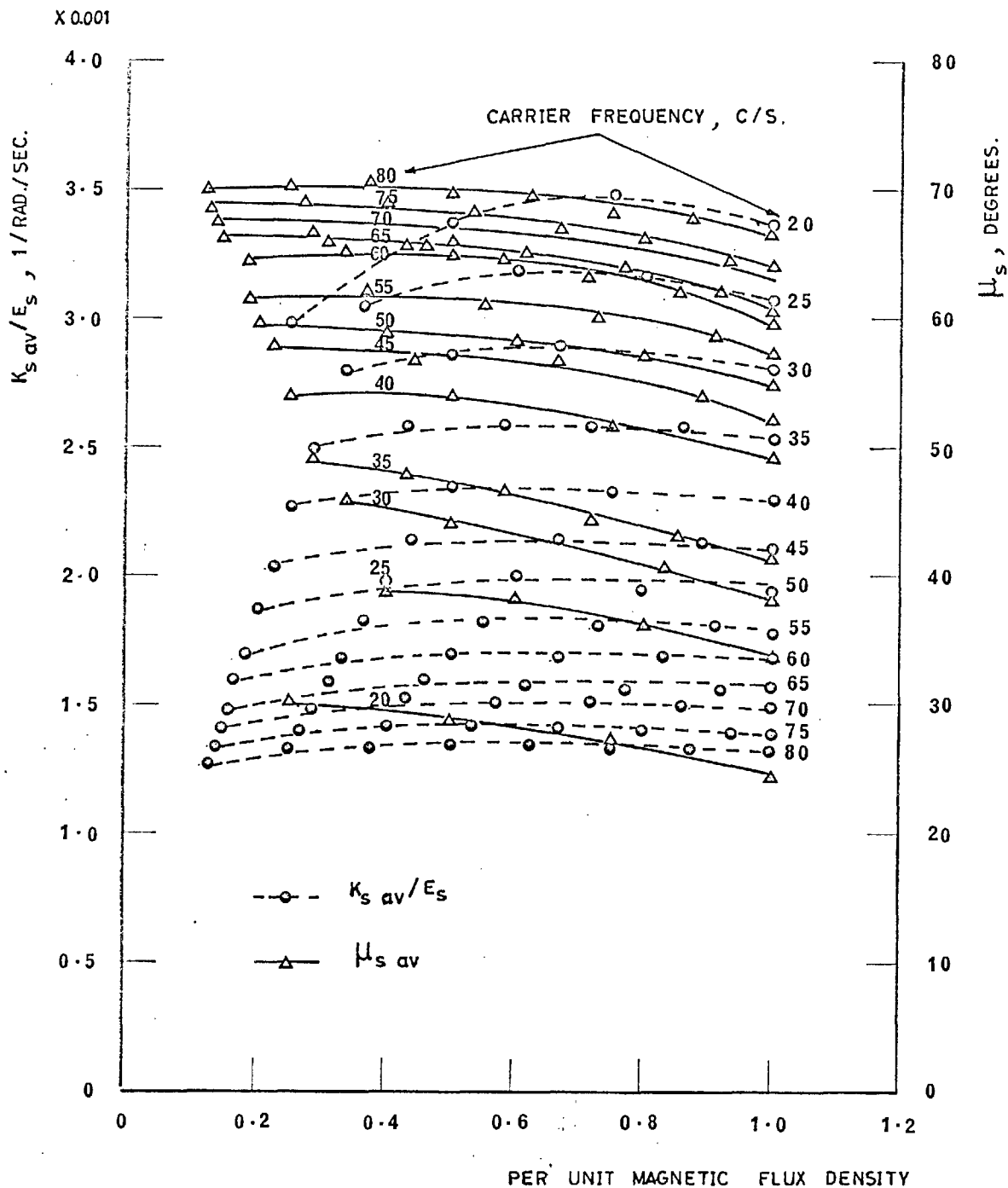


FIG. 6.4.6.

VARIATION OF THE PARAMETERS  $K_{s \text{ av}}$  AND  $\mu_{s \text{ av}}$  WITH THE PER UNIT TRANSMITTER MAGNETIC FLUX DENSITY FOR DIFFERENT VALUES OF THE ENERGISING CARRIER FREQUENCY.

A study of the  $k_{s \text{ av}}$  curves shows that as the carrier frequency increases the curvature decreases and the curves become more straight and horizontal; indicating less dependence on the magnetic flux density.

In inspecting  $\mu_{s \text{ av}}$  curves, it is noticed that their portions lying in the region below 90% flux density can be considered reasonably linear with a slope decreasing with the carrier frequency increase. Again, this implies that  $\mu_{s \text{ av}}$  becomes more independent of the flux density as the carrier frequency rises.

Furthermore, both the sets of curves pertaining to  $k_{s \text{ av}}$  and  $\mu_{s \text{ av}}$  are seen to become more crowded and parallel with the increase of the carrier frequency.

On the basis of Fig. 6.4.6, both  $k_{s \text{ av}}$  and  $\mu_{s \text{ av}}$  can be considered (for the magslip-system under consideration) independent of the flux density in the region lying above 40 c/s carrier frequency and below 90% flux density. In this region, therefore, the theoretical formulae of  $k_s$  and  $\mu_s$  given by Eqns. 2.3.36 and 2.3.34 respectively can give accurate predictions without a need of modification to include the effect of the magnetic flux density as suggested in the previous Sub-section.

#### 6.4.5. Input characteristics of the static transmitter-coincidence transmitter magslip-system for different values of the energising carrier frequency

In the various investigations performed above, it has been found that an increase in the transmitter magnetic flux density resulted in an increase in the effective value of  $R_{rs}$  and a decrease in the ratio  $L_{rs}/R_{rs}$ . A tentative

explanation has been also given in terms of the changes in the iron losses and possible magnetic saturation. To be able to study the variations of these quantities with the magnetic flux density, the present test was conducted.

In this test, the transmitter input voltage  $e_{a1}$ , current  $i_{a1}$ , and phase difference between their fundamental components  $\lambda_{a1}$  were measured at different values of the carrier frequency. The power input to the stationary mag-slip system was then calculated from the measured quantities according to the well known relationship

$$P_{a1} = e_{a1} \cdot i_{a1} \cdot \cos \lambda_{a1} \quad 6.4.6$$

The results of this test are plotted in Fig. 6.4.7 in terms of three sets of curves illustrating the relationships

$$\begin{aligned} & e_{a1}/f_c \text{ (or per unit magnetic flux density) versus } \lambda_{a1}, \\ & e_{a1}/f_c \text{ ( " " " " " " ) " } i_{a1}, \\ \text{and} \\ & P_{a1} \text{ " } i_{a1}. \end{aligned}$$

It is noticed that the curves in each set become more closer to each other as the carrier frequency increases. The curves  $e_{a1}/f_c$  versus  $i_{a1}$  start as straight lines then show slight saturation for values of  $e_{a1}/f_c$  (also may be considered as the per unit magnetic flux density if the resistive drop in the transmitter rotor winding is negligible) lying above 0.9 volts/cycles/sec. The slope of the linear portion decreases with the increase of the carrier frequency. Since the slope is a function of the inductance  $L_{rs}$ , it may be concluded that  $L_{rs}$  decreases with the carrier frequency.

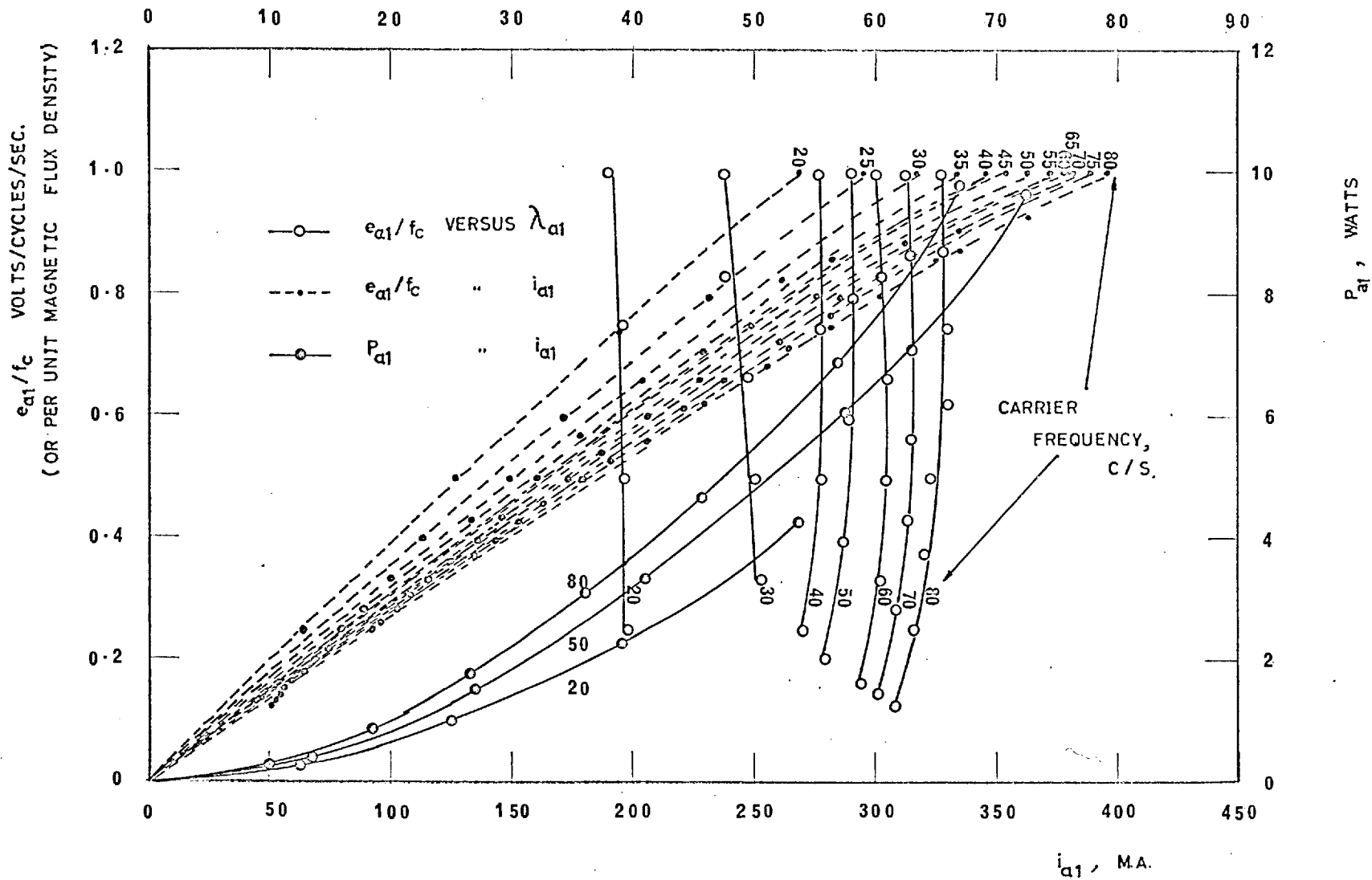


FIG. 6.4.7.

INPUT CHARACTERISTICS OF THE STATIC TRANSMITTER - COINCIDENCE  
 TRANSMITTER MAGSLIP - SYSTEM FOR DIFFERENT VALUES OF THE  
 ENERGISING CARRIER FREQUENCY.

In examining the curves relating the power input  $P_{a1}$  and the input current  $i_{a1}$ , it is observed that for the same value of  $i_{a1}$ ,  $P_{a1}$  increases with the carrier frequency. The power input  $P_{a1}$  effectively represents the sum of the iron and copper losses. But, since the latter is usually negligible in comparison with the former (under the present test conditions),  $P_{a1}$  may be taken as the iron losses without committing a serious error. These iron losses may be represented by a copper loss in a fictitious resistance which may be added to the real resistance of the transmitter rotor winding resulting in an effective resistance  $R_{eff}$ . On this basis and in view of the above observations derived from  $P_{a1} - i_{a1}$  curves, it may be concluded that  $R_{eff}$  increases with the carrier frequency.

Finally, it may be added that the conclusions drawn from the present test are in conformity with those obtained in Sub-section 6.4.3 although derived by a different approach. This gives confidence in the work presented above.

CHAPTER 7POSITIONAL CONTROL A.C. SERVOMECHANISM -  
PRACTICAL INVESTIGATIONS7.1. General

In this chapter, performance studies for the positional control a.c. servomechanism breadboard model, whose detailed design and construction have been outlined in Chapter 6, are going to be performed with the aim of demonstrating the stabilizing effect of chopper networks when cascaded in the main transmission channel of a practical a.c. servomechanism.

The performance characteristics data of the a.c. servomechanism were experimentally obtained in the form of modulation frequency response and transient response (since they augment each other) for both the uncompensated and compensated system. Inspection of the open-loop and closed-loop response plots would then determine much of the basic required information such as stability, modulation frequency, bandwidth, etc., whereas a study of records of the system time response to a step-function would still reveal more performance information such as maximum overshoot, rise time, etc.

In performing the above various tests, the effects of two important factors on the overall system performance were also investigated. These factors are:

- i) Variations in the carrier frequency.
- ii) Misalignment between the phases of the modulation and demodulation reference excitations.

To increase the scope of the investigations, the various

tests were repeated for the two types of error-sensing devices, viz. potentiometer-bridge and transmitter-coincidence transmitter mag-slip-system.

In practical servosystems, it is widely recognized that the existence of non-linearities can introduce significant effects on the over-all performance and the stability of the system. The most predominant sources of non-linearities associated with the practical servomechanisms are listed below.

- i) Coulomb friction.
- ii) Gear-train backlash.
- iii) Component saturation (mainly in the servo-amplifier).

A study of the system performance under non-linear conditions produced by the above sources, although may be of profound importance for the design purposes, has not been the object of the present investigations. The presence of these non-linearities, however, may impair the accuracy of the intended investigations. Means of minimising the unavoidable coulomb friction and backlash in the gear-train, therefore, have been applied while setting up the breadboard model by careful alignment in installation and by good gear matching (there are special techniques to eliminate the effects of the backlash, but they were not adopted however on the grounds that they would either raise the friction level or introduce undue complexity to the present model). Further reduction of their effects on the accuracy of the experimental results was obtained by choosing the level of the testing signal such that the angular displacements of the shafts of the servo-motor, error-detector, and the mechanical load are sufficiently large. By properly adjusting the servo-amplifier gain, it was possible to ensure that the level of the testing signal appearing at its input will not drive it to the saturation zone.

The gain adjustment is, in addition, governed by two important factors which set up an upper and a lower limit to its value. The lower gain setting is such that the resulting system loop-gain is sufficient to overcome the static friction and accelerate the system with a reasonable acceleration to enable accurate measurements to be obtained. The upper gain limit, on the other hand, depends on the system stability and the required modulation frequency bandwidth to be tested.

To perform the modulation frequency response test on the a.c. system under consideration, a sinusoidal disturbance (representing the modulation signal reference) of known amplitude and frequency may be applied to the system input. The resulting output signal is then either directly measured (if it is of simple frequency form) or demodulated then measured (if it is of modulated wave form), and then compared with the input disturbance. In the present system, both the input and output signals are of simple frequency mechanical form since they represent the angular displacements of the shafts of the transmitter and coincidence-transmitter magnslips (or the shafts of the input and output potentiometers), respectively. To produce this kind of mechanical disturbance is practically very difficult, and an alternative electrical method must be employed. Also, the output mechanical angular position should first be transformed into an electrical signal before measured. These considerations are dealt with in the next Section.

## 7.2. Techniques of Measuring the Modulation Frequency Response of the A.C. System.

### 7.2.1. Error-detector in the form of a potentiometer-bridge

In Fig. 1.5.1, if the shaft angular position of the reference potentiometer 1 follows a simple sinusoidal



disturbance as described mathematically by

$$\gamma_{p1} = E_1 \sin \omega t \quad 7.2.1.$$

thus the voltage picked up by its sliding contact is given by

$$e_{p1} = \frac{E_p E_1}{\Gamma} \sin(\omega t) \sin(\Omega t + \theta) \quad 7.2.2.$$

where  $\Gamma$ ,  $\Omega$  and  $\theta$  are defined in Sub-section 1.5.1.

This equation represents a suppressed carrier amplitude modulated wave (S.C.A.M.) which can be easily generated electronically by means of an oscillator (to supply the modulation signal  $E_1 \sin(\omega t)$ ) followed by a sinusoidal modulator (energized by the carrier signal  $\frac{E_p}{\Gamma} \sin(\Omega t + \theta)$ ) similar to the setup described in Sub-section 5.2.2. On this basis, the shaft of the reference potentiometer 1 may be kept stationary, while a S.C.A.M. wave  $e_{ip}$  may be injected in the manner shown in Fig. 7.2.1. to simulate the effect of the required reference shaft rotation, such that

$$e_{ip} = e_{p1} \quad 7.2.3.$$

The shaft angular position of the potentiometer 2, being coupled to the servo-motor shaft, appears as the envelope of a modulated signal picked up at its sliding contact

$$e_{p2} = \frac{E_p}{\Gamma} \gamma_{p2} \sin(\Omega t + \theta) \quad 7.2.4.$$

This signal therefore must be demodulated in order to recover the envelope, which is proportional to the output shaft position. By measuring the magnitude and phase of

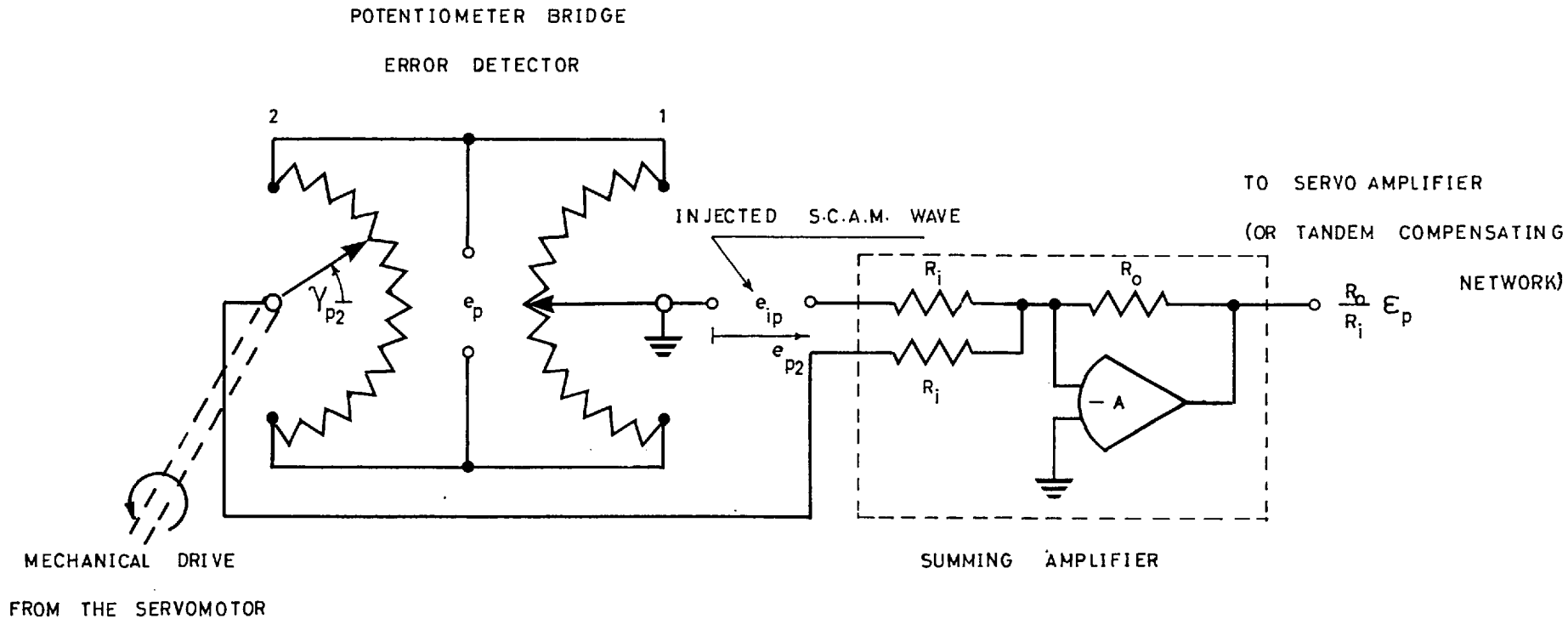


FIG. 7.2.1

SIMULATION OF THE SINUSOIDAL ANGULAR-DISPLACEMENT DISTURBANCE OF THE REFERENCE POTENTIOMETER SHAFT BY MEANS OF AN INJECTED S.C.A.M. WAVE

this envelope, and then comparing them with those pertinent to the reference modulation signal (taking into account the factor of proportionality), the closed-loop modulation frequency response  $G_{cp}(j\omega)$  is obtained. The demodulation process, and the magnitude and phase measurements have been obtained by a similar instruments set-up as that described in Sub-section 5.2.2. and illustrated in Fig. 5.2.1.

The summing amplifier shown in Fig. 7.2.1. was employed not only to subtract the signals  $e_{p1}$  and  $e_{p2}$  (which contain the reference and output information) to obtain the actuating signal (containing the error information), but also to introduce an earth point since the servo-amplifier was designed to accept an earthed signal. A check conducted on the frequency response of the summing amplifier showed that it is virtually flat over a wide frequency range covering the frequency bandwidth under investigation. Therefore, the effect introduced by this summer on the system response was only an extra gain of  $\frac{R_o}{R_i}$ .

The output from the summer can be easily worked out with the help of Eq. 1.5.2.

$$\frac{R_o}{R_i} \epsilon_p = \frac{R_o}{R_i} k_p \epsilon \sin(\omega t + \theta) \quad 7.2.5.$$

where  $\epsilon$  and  $k_p$  are as defined by Eqns. 1.5.3 and 1.5.4 respectively.

The above expression shows that the error appears as the envelope of a modulated signal. Therefore, by demodulating the summer output signal, a signal proportional to the error signal can be recovered. On comparing its magnitude and

phase with those of the reference modulation signal, the result is

$$1 - G_{cp}(j\omega) \quad 7.2.6.$$

from which the closed-loop modulation frequency response can be easily deduced. This may be used as a check on the value obtained earlier by comparing the output and reference signals.

The open-loop modulation frequency response  $G_{op}(j\omega)$  can be deduced either by comparing the measured magnitudes and phases of the error and output signals, or from the closed-loop modulation frequency response according to the relationship

$$G_{op}(j\omega) = G_{cp}(j\omega) / [1 - G_{cp}(j\omega)] \quad 7.2.7.$$

#### 7.2.2. Error-detector in the form of a transmitter - coincidence transmitter mag slip-system

On the basis of the analysis of the synchro-system outlined in Sub-section 2.3.2, the output of the coincidence-transmitter rotor winding as a time function can be deduced from Eqn. 2.3.32 by making use of Eqn. 2.3.23, thus

$$e_{b2} = k_s \frac{n_s}{n_L} p \left[ \sin(\gamma_{s1} - \gamma_{s2}) \sin(\omega t + \theta - \mu_s) \right] \quad 7.2.8.$$

which on expansion gives

$$e_{b2} = k_s \frac{n_s}{n_L} p \left[ \sin \gamma_{s1} \cos \gamma_{s2} \sin(\omega t + \theta - \mu_s) \right. \\ \left. - k_s \frac{n_s}{n_L} p \left[ \sin \gamma_{s2} \cos \gamma_{s1} \sin(\omega t + \theta - \mu_s) \right] \right] \quad 7.2.9.$$

If the values of  $\gamma_{s1}$  and  $\gamma_{s2}$  are small enough to permit the adoption of the approximations

$$\sin \gamma_{s1} \simeq \gamma_{s1}, \quad 7.2.10$$

$$\sin \gamma_{s2} \simeq \gamma_{s2}, \quad 7.2.11$$

and

$$\cos \gamma_{s1} = \cos \gamma_{s2} \simeq 0 \quad 7.2.12$$

then Eqn. 7.2.9 is simplified to

$$\begin{aligned} e_{b2} &= k_s \frac{n_s}{n_L} p \left[ \gamma_{s1} \sin(\omega t + \theta - \mu_s) \right] \\ &- k_s \frac{n_s}{n_L} p \left[ \gamma_{s2} \sin(\omega t + \theta - \mu_s) \right] \end{aligned} \quad 7.2.13$$

Now, if the transmitter shaft is kept stationary at  $\gamma_{s1} = 0$ , the output of the coincidence-transmitter rotor winding becomes

$$e'_{b2} = -k_s \frac{n_s}{n_L} p \left[ \gamma_{s2} \sin(\omega t + \theta - \mu_s) \right] \quad 7.2.14$$

In order to compensate for the effect of keeping the transmitter shaft stationary, a voltage  $e_{is}$  may be injected in series with the output  $e'_{b2}$  in the manner shown in Fig. 7.2.2. The expression of this voltage can be deduced from Eqns. 7.2.13 and 7.2.14, and is given by

$$e_{is} = k_s \frac{n_s}{n_L} p \left[ \gamma_{s1} \sin(\omega t + \theta - \mu_s) \right] \quad 7.2.15$$

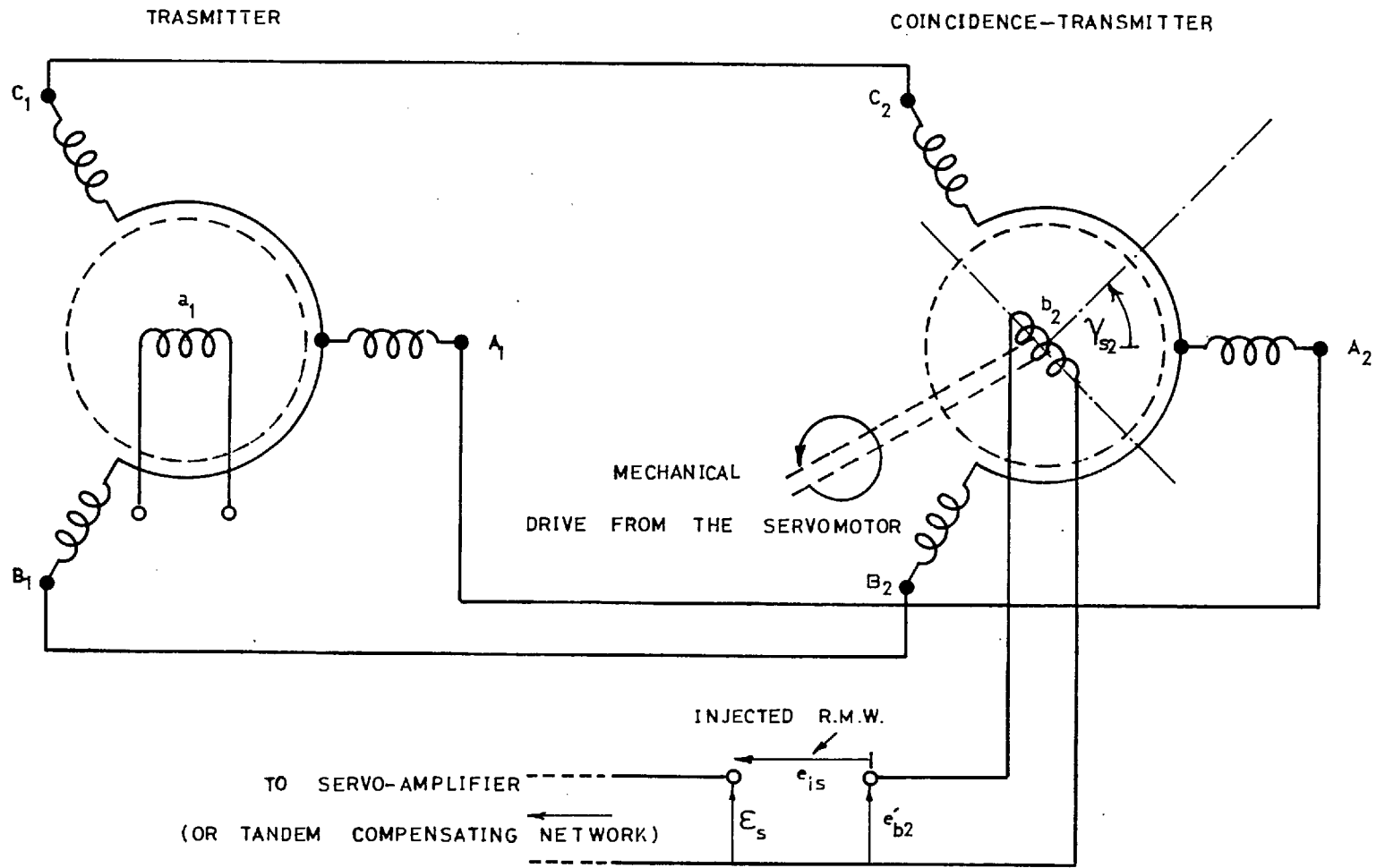


FIG. 7.2.2  
 SIMULATION OF THE SINUSOIDAL ANGULAR - DISPLACEMENT  
 DISTURBANCE OF THE TRANSMITTER MAGSLIP SHAFT BY  
 MEANS OF AN INJECTED R.M.W.

Adding  $e'_{b2}$  and  $e_{is}$  results in the actuating signal  $\xi_s$ ,

$$\xi_s = k_s \frac{n_s}{n_L} p \left[ (\gamma_{s1} - \gamma_{s2}) \sin(\omega t + \theta - \mu_s) \right] \quad 7.2.16$$

Examination of Eqns. 7.2.14, 7.2.15 and 7.2.16 shows that the signals  $e'_{b2}$ ,  $e_{is}$  and  $\xi_s$  contain the output, input, and the error informations in the form of rotary modulation waves (R.M.W.). In generating the injected signal  $e_{is}$ , an oscillator was used to generate a sinusoidal wave to simulate the angular displacement disturbance of the transmitter shaft

$$\gamma_{s1} = E_1 \sin(\omega t) \quad 7.2.17$$

This signal was then applied to a sinusoidal modulator to produce S.C.A.M. wave, and finally a differentiating circuit was employed to transform the S.C.A.M. into the required R.M.W. The details of these processes and the equipment used are described in Sub-section 5.3.7.

To enable the measurements of the magnitudes and phases of the output and error signals, the signals  $e_{b2}$  and  $\xi_s$  may first be integrated and then demodulated before being applied to the T.F.A. Resolved Component Indicator and the Reference Resolver. An alternative method for obtaining the output information directly is to use a potentiometer with its shaft coupled to that of the coincidence-transmitter. By energising this additional potentiometer by a stabilized d.c. voltage, the voltage picked up by its sliding contact is thus proportional to the output, which again may be measured by the same T.F.A. instruments.

The closed-loop and open-loop modulation frequency response  $G_{cs}(j\omega)$ ,  $G_{os}(j\omega)$  can be deduced from the

measured quantities by pursuing a similar procedure as in the previous Sub-section. The corresponding relationships are

$$G_{cs}(j\omega) = \gamma_{s2}(j\omega) / \gamma_{s1}(j\omega) \quad 7.2.18$$

and

$$G_{os}(j\omega) = G_{cs}(j\omega) / [1 - G_{cs}(j\omega)] \quad 7.2.19$$

The major drawback of this method stems from the fact that it is only valid for small values of  $\gamma_{s1}$  and  $\gamma_{s2}$  where the approximations expressed by Eqns. 7.2.10 to 7.2.12 hold. As a consequence, the effects of the nonlinearities, introduced by the coulomb friction and gear-train backlash, may therefore become predominant in the measured quantities leading to unrepresentative results for the system performance. For this reason, it is important to seek for an alternative method which may permit the use of large values of  $\gamma_{s1}$  and  $\gamma_{s2}$  without introducing errors. This is deferred to the next Sub-section.

### 7.2.3. Simulation of the mag-slip-system by means of a potentiometer-bridge in cascade with a differentiator.

If the servomechanism under consideration is behaving satisfactorily, the error  $(\gamma_{s1} - \gamma_{s2})$  is very small. On this basis, the following approximation

$$\sin(\gamma_{s1} - \gamma_{s2}) \approx (\gamma_{s1} - \gamma_{s2}) \quad 7.2.20$$

becomes valid irrespective of the separate values of  $\gamma_{s1}$  and  $\gamma_{s2}$ . With this approximation, Eqn. 7.2.8 reduces to

$$e_{b2} = k_s \frac{n_s}{n_L} p \left[ (\gamma_{s1} - \gamma_{s2}) \sin(\omega t + \theta - \mu_s) \right] \quad 7.2.21$$



In the potentiometer-bridge arrangement of Fig. 7.2.1, if the phase of the carrier excitations to the potentiometer-bridge and the modulator is delayed by the angle  $\mu_s$ , i.e.,

$$e_p = E_p \sin(\omega t + \theta - \mu_s) \quad 7.2.22$$

and

$$e_{ip} = \frac{E_p}{\Gamma} \gamma_{p1} \sin(\omega t + \theta - \mu_s) \quad 7.2.23$$

hence the output of the summer can be written as

$$\frac{R_o}{R_i} \mathcal{E}_p = \frac{R_o}{R_i} \cdot \frac{E_p}{\Gamma} (\gamma_{p1} - \gamma_{p2}) \sin(\omega t + \theta - \mu_s) \quad 7.2.24$$

By differentiating this signal with respect to time, the result is proportional to the expression of Eqn. 7.2.21. In practical terms, if the potentiometer-bridge and summer arrangement of Fig. 7.2.1 is cascaded by a differentiating circuit similar to the one shown in Fig. 5.3.16, the combination becomes equivalent to the mag-slip arrangement of Fig. 7.2.2, provided that the phase of the carrier excitations is shifted by  $\mu_s$  and the gain is adjusted to the value  $k_s \frac{n_s}{n_L}$ .

In this equivalent arrangement, no restriction is imposed on the separate values of  $\gamma_{p1}$  and  $\gamma_{p2}$ , though their difference (which depends on the overall performance of the servomechanism under test) should be adequately small to satisfy Eqn. 7.2.20. Therefore, the results obtained by this method is expected to be reliable and accurate in comparison with the results obtained by the method described in the previous Sub-section.

Setting up the present arrangement, however, depends on a knowledge of the values of the parameters  $\mu_s$  and  $k_s$ .

205

These parameters can either be evaluated by substituting the values of the various physical parameters of the mag-slip system into Eqns. 2.3.34 and 2.3.36 respectively, or be measured by means of a static test as described in Section 6.4.

Measurements of the magnitudes and phases of the output and error signals follow the same pattern of steps outlined in Sub-section 7.2.1, using the same T.F.A. instruments set-up. The results obtained may be substituted in Eqns. 7.2.18 and 7.2.19 to determine the closed-loop and open-loop modulation frequency responses of the servo-system under a condition similar to the case of employing a mag-slip-system as an error-detector.

### 7.3. Experimental Results of the Uncompensated System Modulation Frequency Responses.

#### 7.3.1. System with a potentiometer-bridge error-detector

With reduced amplifier gain of 48 db, a large number of modulation frequency response tests have been conducted on the positional control a.c. servomechanism breadboard model (whose details are outlined in Chapter 6) under different values of excitation carrier frequency and different phases of the 2-phase servo-motor excitation reference. The techniques of measurements were based on Sub-section 7.2.1. Since it is very difficult to include all the results obtained in this thesis, only a representative selection is given.

Fig. 7.3.1. shows the open-loop modulation frequency response of the uncompensated system plotted on a Nichols-chart in dashed line at three different values of carrier frequency, viz. 40, 50 and 60 c/s. By inspection of the plots, it is apparent that the system is stable. However,

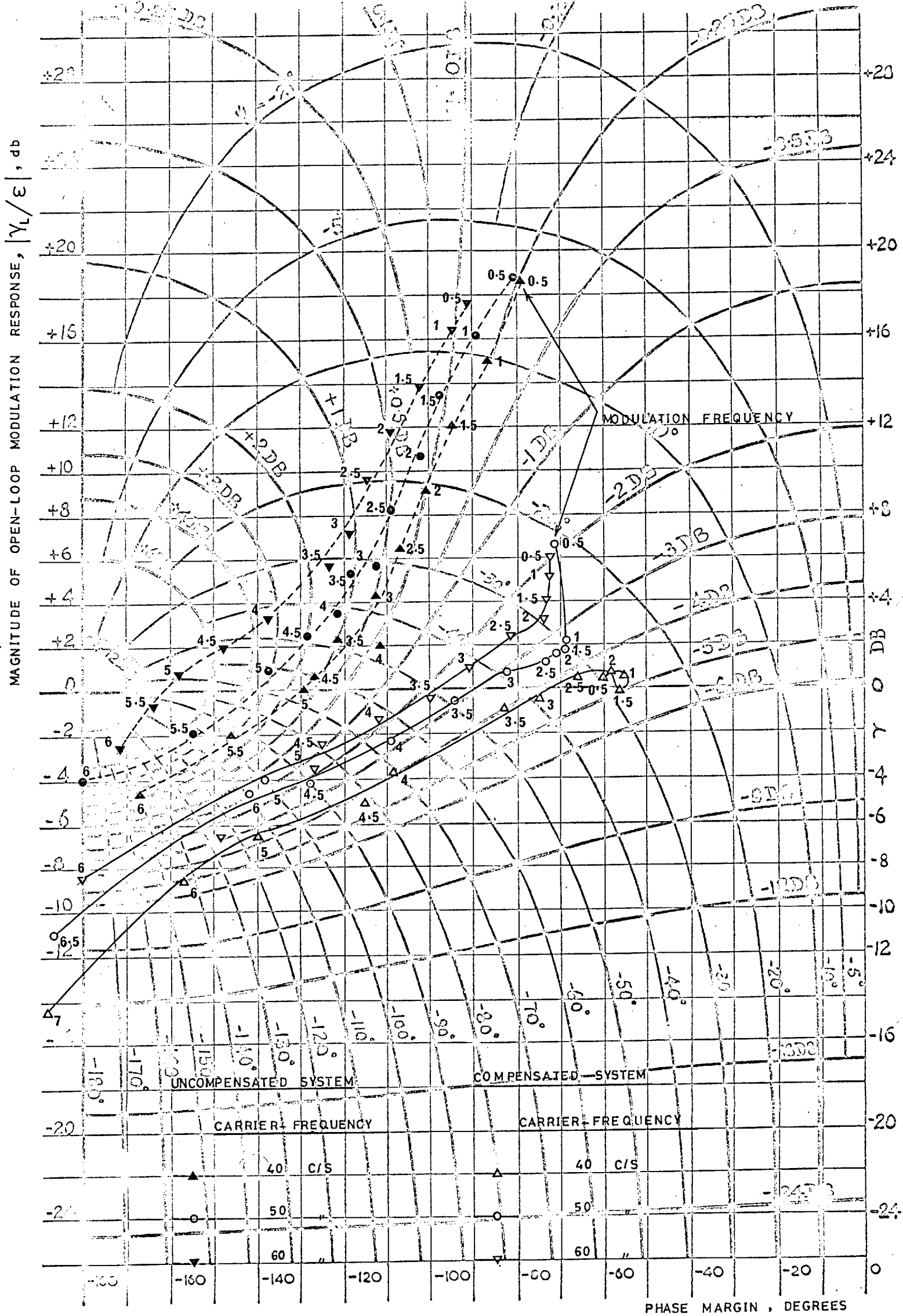


FIG. 7.3.1  
 NICHOLS DIAGRAM FOR THE SYSTEM UNDER DIFFERENT CARRIER-FREQUENCY OF ENERGISATION

DATA: (SYSTEM WITH A POTENTIOMETER-BRIDGE ERROR-DETECTOR)

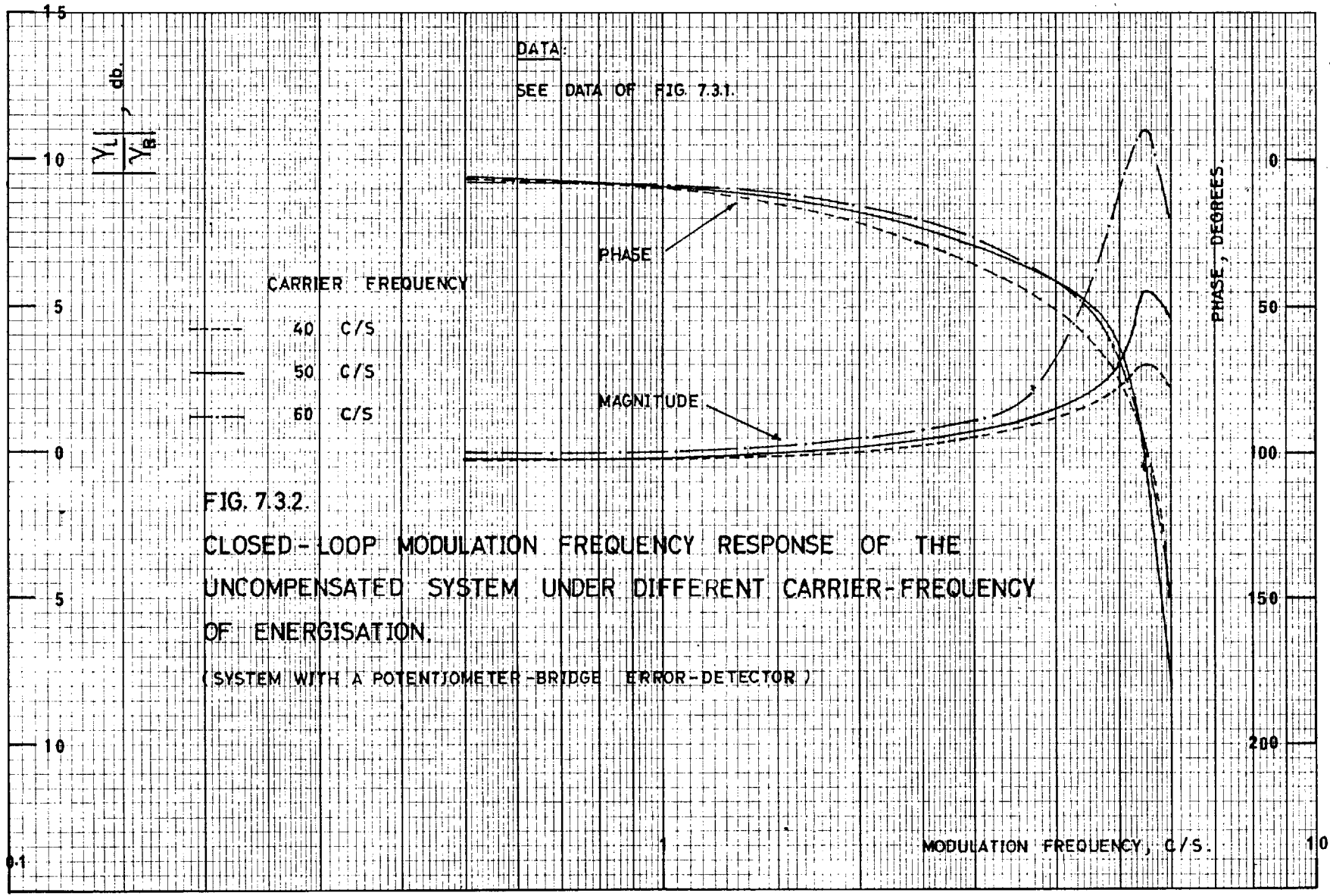
- $\theta = 0$  DEG.
- $\varphi = 90$  "
- $A = 48$  db

the decrease in the phase margin and increase in the gain margin clearly show that the degree of this stability decreases significantly as the carrier frequency increases. Similarly, if the loop-gain is increased, the phase margin decreases and the gain margin increases. Consequently, a useful conclusion may be drawn that the effect of carrier frequency variations on the system performance, to some extent, is similar to that caused by loop-gain variations.

To check the modulation frequency bandwidth and the response peak, the closed-loop modulation frequency response curves may be constructed from the Nichols diagram since the system is unity feedback (see Sub-section 2.4.2.). This closed-loop modulation frequency response can be directly read from the intersections of the Nichols diagram with the M (constant magnitude ratio  $\frac{Y_L}{Y_R}$ ) and N (constant phase) contours. The results were then plotted in Fig. 7.3.2.

In this figure, the curves show that the resonance frequency is approximately 5.5 c/s and is almost independent of the carrier frequency variations (in the range of 40 to 60 c/s). The resonance peak, however, is markedly dependent on the carrier frequency. It takes the values 3, 5.5 and 11 db corresponding to the carrier frequencies 40, 50 and 60 c/s respectively.

In changing the phase of the excitation reference of the 2-phase servo-motor from 90 to 60 deg. lag, the phase margin reduces from 37 to 26 deg., while the gain margin maintains constant at -4 db as shown in solid line in Fig. 7.3.3. This implies that the system becomes less damped. The closed-loop modulation frequency response of Fig. 7.3.4. confirms this in terms of an increase in the resonance peak from 5.5 to 10 db. This is accompanied by a reduction in the resonance frequency from 5.5 to 5 c/s.





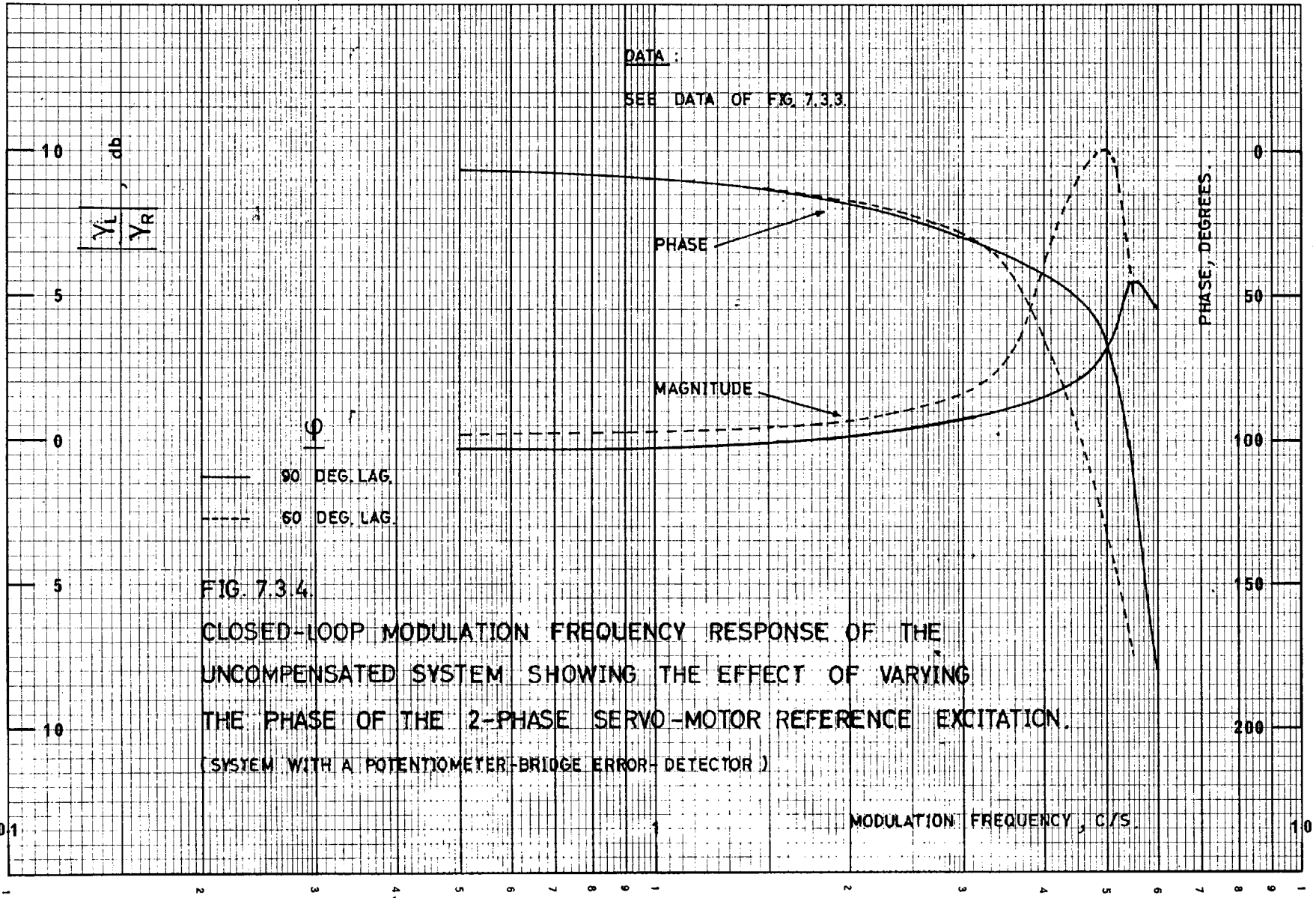


FIG. 7.3.4.

CLOSED-LOOP MODULATION FREQUENCY RESPONSE OF THE UNCOMPENSATED SYSTEM SHOWING THE EFFECT OF VARYING THE PHASE OF THE 2-PHASE SERVO-MOTOR REFERENCE EXCITATION. (SYSTEM WITH A POTENTIOMETER-BRIDGE ERROR DETECTOR)

### 7.3.2. System with a mag-slip-system error-detector

In this case, the system modulation frequency response tests were carried out on the basis of the techniques outlined in Sub-section 7.2.3 due to the advantages mentioned. The mag-slips, although were not directly involved in the test measurements, have been kept mechanically coupled to the system in order to account for their mechanical loading. During the test, the amplifier gain was properly reduced to 54 db to avoid any possible instability of the system.

The dashed-line curves of Fig. 7.3.5 illustrates the Nichols plots of the open-loop modulation frequency response for the uncompensated system for three values of the energization carrier frequency selected at 80%, 100% and 120% of the nominal carrier frequency (50 c/s). It is noted that the system is stable with the phase margin decreasing (with a decreasing rate) as the carrier frequency increases. This indicates that the damping of the system tends to decrease with the increase of the carrier frequency.

The closed-loop modulation frequency response for the uncompensated system is shown in Fig. 7.3.6, as computed from the Nichols diagram of Fig. 7.3.5. A study of the curves shows that the system is overdamped at carrier frequency 80%. At carrier frequencies of 100% and 120%, the system exhibits small resonance peaks of 1.5 and 1 db occurring at the resonance frequencies of approximately 3.5 and 4 c/s respectively.

Fig. 7.3.7 (dashed-line curves) shows the effect of varying the phase misalignment between the reference excitation of the error-detector and the 2-phase servo-motor on the open-loop modulation frequency response of the system. Only two situations were considered:



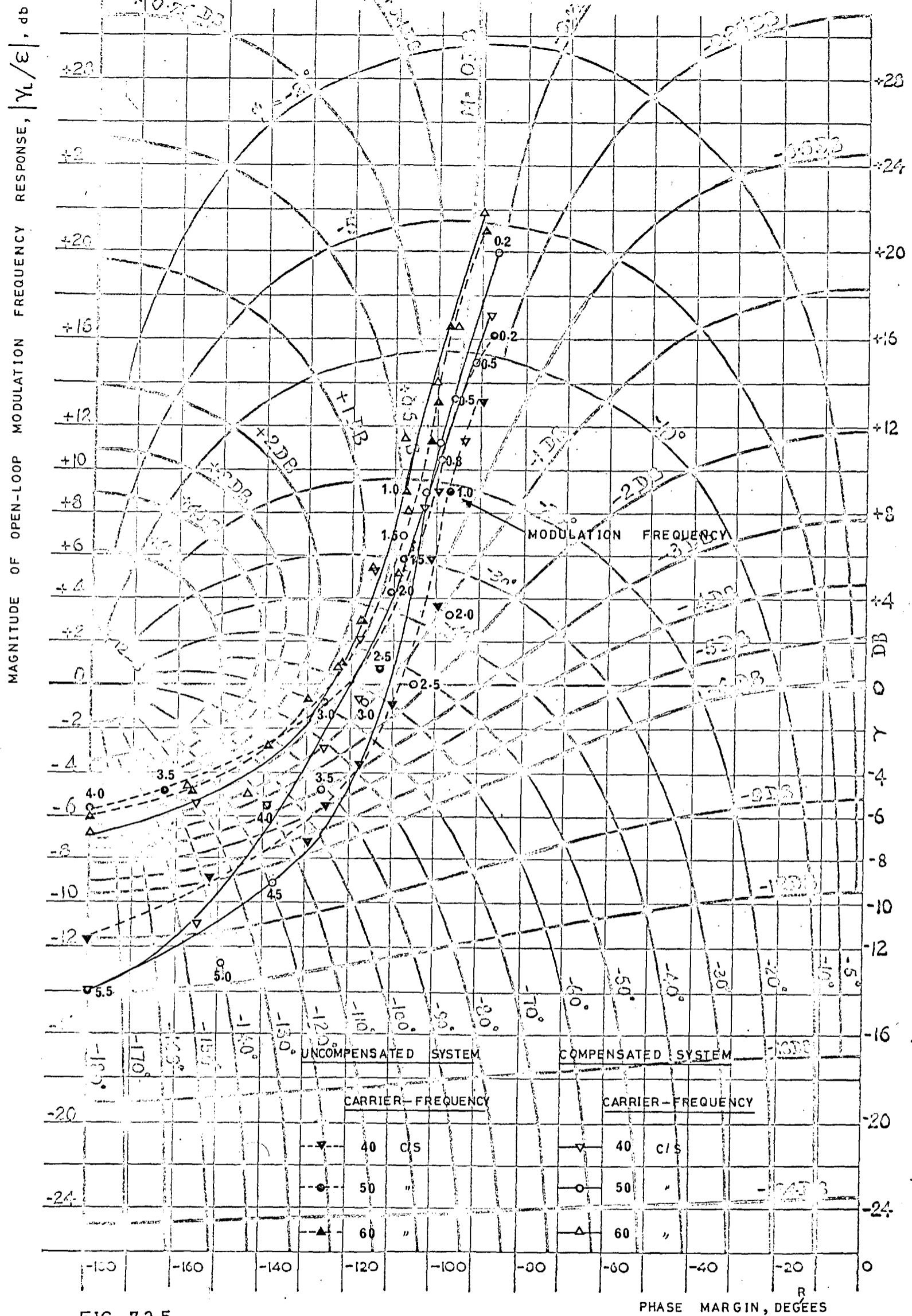
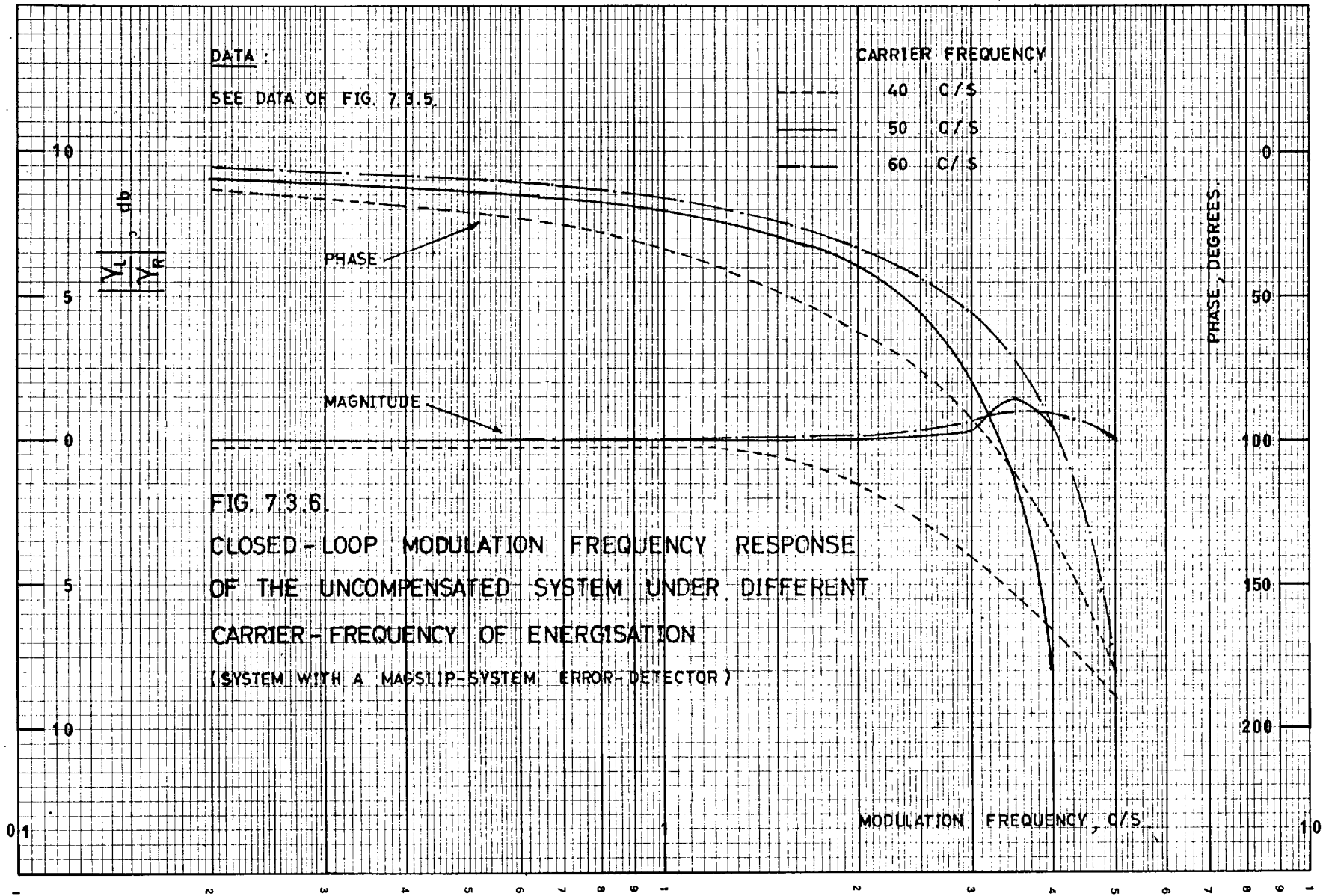


FIG. 7.3.5

NICHOLS DIAGRAM FOR THE SYSTEM SHOWING THE EFFECT OF VARYING THE ENERGISATION CARRIER-FREQUENCY (SYSTEM WITH A MAGSLIP-SYSTEM ERROR-DETECTOR)

DATA:

$\theta = 0$  DEG.       $\phi = 0$  DEG.       $A = 54$  db



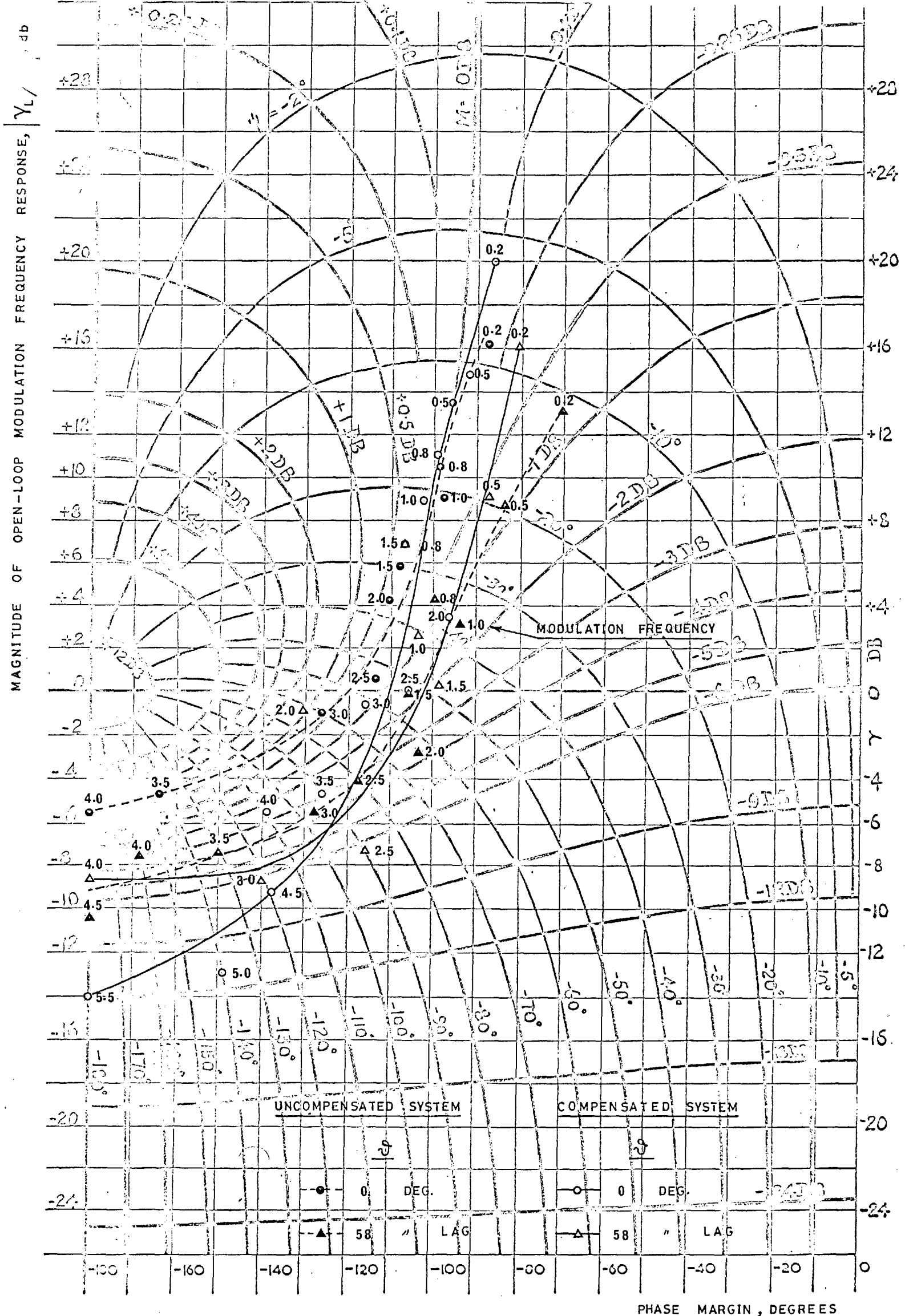


FIG. 7.3.7

NICHOLS DIAGRAM FOR THE SYSTEM SHOWING THE EFFECT OF THE PHASE VARIATIONS OF THE ERROR-DETECTOR REFERENCE EXCITATION (SYSTEM WITH A MAGSLIP-SYSTEM ERROR-DETECTOR)

DATA:

$\Omega = 314$  RAD./SEC.       $\varphi = 0$  DEG.       $A = 54$  db

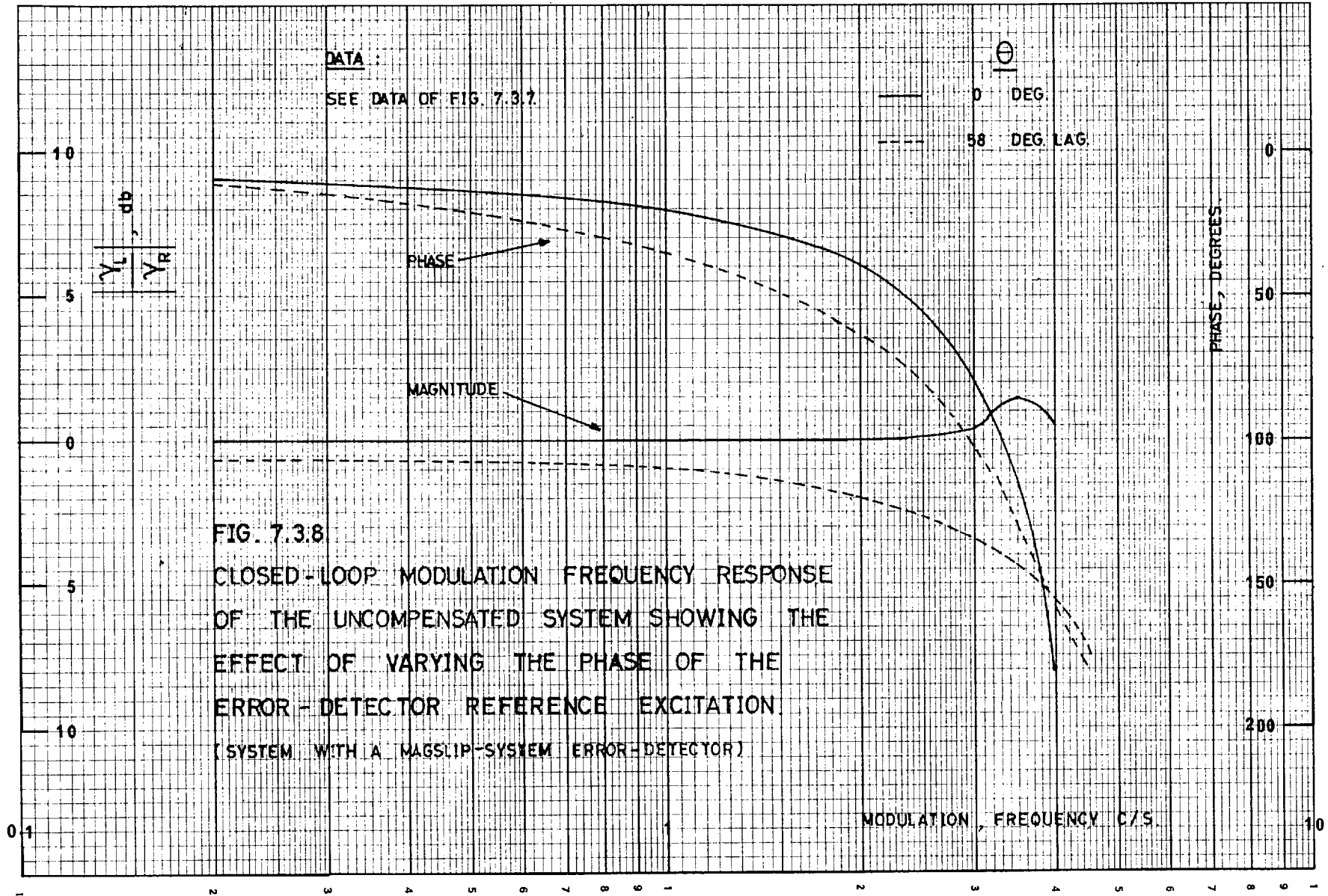
(i) First case:

Zero phase misalignment which can be simulated, on the basis of the work in Sub-section 7.2.3, by delaying the phase of the excitation to the potentiometer-bridge (which is used in conjunction with a differentiator to simulate the action of the mag-slip-system) by an angle equal to  $\mu_s$ . Under the test conditions of excitation voltage and frequency intended for supplying the mag-slip-system, the value of  $\mu_s$  can be obtained from Fig. 6.4.6, and was found to be 58 deg.

(ii) Second case:

A misalignment equivalent to complete compensation of the phase shift of the excitation reference effected in the mag-slip-system. On the basis of Sub-section 7.2.3, this is equivalent to zero phase misalignment between the reference excitations of the 2-phase servo-motor and the potentiometer-bridge.

Examining the curves of Fig. 7.3.7 shows that by compensating the phase shift of the excitation effected in the mag-slip-system, the phase margin decreases from 77 to 60 deg., and the gain margin increases from -9 to -5.5 db, which indicates a general decrease in the system damping. This is even further confirmed by the closed-loop modulation frequency response shown in Fig. 7.3.8. which indicates that the system condition changes from an over-damped to a slightly oscillatory with a small resonance peak of 1.5 db occurring at the resonance frequency of 3.5 c/s.



#### 7.4. Experimental Results of the Compensated System Modulation Frequency Responses.

##### 7.4.1. System with a potentiometer-bridge error-detector

From the open-loop and closed-loop modulation frequency responses of the uncompensated system under different operating conditions (see Figs. 7.3.1 to 7.3.4), it may be concluded that, on the whole, the system is under-damped though stable. To increase the system damping, a reduction in the loop-gain is required. Since the loop-gain was already reduced to enable the tests to be conducted, the steady-state performance, the static accuracy, the rise time, and the settling time are expected to be unsatisfactory. This, on the other hand, requires an increase in the loop-gain for improvement. It is therefore apparent that a compensation technique should be employed since the gain adjustment does not appear to offer the best possibility of meeting performance requirements.

On studying the open-loop and closed-loop modulation frequency responses of the uncompensated system, it was decided to employ a single-switch double-capacitor chopper network, operating as a phase-lead compensator (see Fig. 4.1.3), cascaded in the forward path of the system between the error-detector and the servo-amplifier. The selected passive electric elements and the fly-time of the synchronous switch incorporated into the chopper network are:

$$G_1 = G_2 = 0$$

$$1/G = 20.9 \text{ K. Ohms (it represents the input resistance of the servo-amplifier)}$$

$$c = 1 \mu\text{.f.}$$

$$a = 0 .$$

With this type of compensation and amplifier gain of 48 db, the system modulation frequency response tests were again performed under different energization carrier frequencies and different phases of the 2-phase servo-motor excitation reference. Figs. 7.3.1 and 7.3.3 show (in solid-line and dashed-line respectively) Nichols diagrams of the compensated system under various operating conditions. Inspection of these compensated plots reveals an effective increase in the phase margin and a decrease in the gain margin, indicating a decrease in the system damping.

As the carrier frequency varies from 80% to 120%, the difference between the compensated and uncompensated open-loop modulation frequency responses is observed to be virtually the same except in the very low modulation frequency region where a slight variation is noticed. This clearly suggests that the modulation transfer function of the chopper network, under such practical conditions, is rather insensitive to carrier frequency deviation of  $\pm 20\%$ . This agrees with the results given in Sub-section 5.3.3 where the chopper network was tested under ideal conditions.

However, in changing the phase of the excitation reference of the 2-phase servo-motor, the difference between the compensated and uncompensated open-loop modulation frequency responses varies particularly in the low modulation frequency region. This implies that the modulation transfer function of the chopper network is dependent on the phase of the servo-motor excitation reference, which is in conformance with the results of Sub-section 5.3.4.

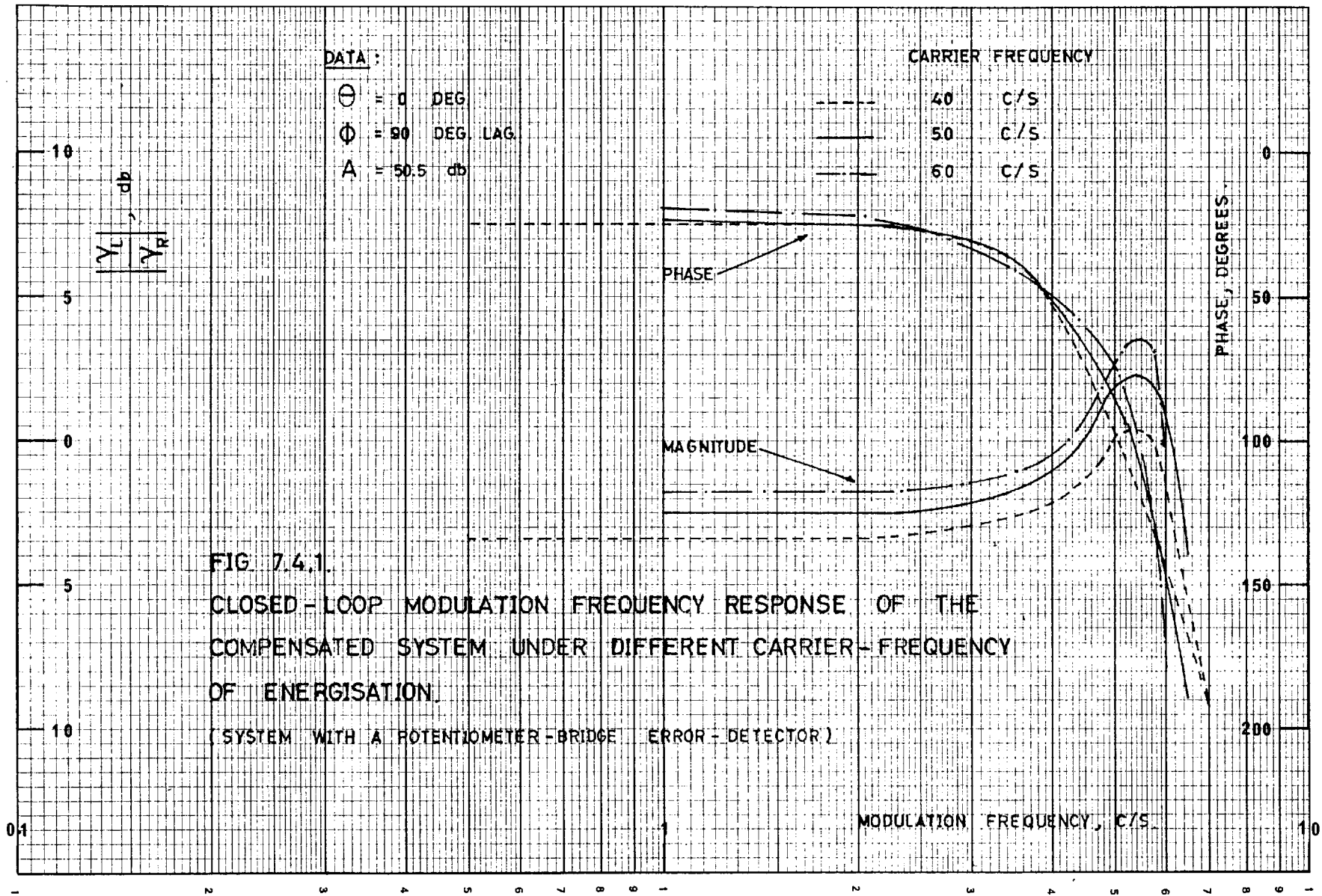
In constructing the compensated closed-loop modulation frequency response utilizing the Nichols diagrams of Figs. 7.3.1 and 7.3.3, the loop-gain was first adjusted such

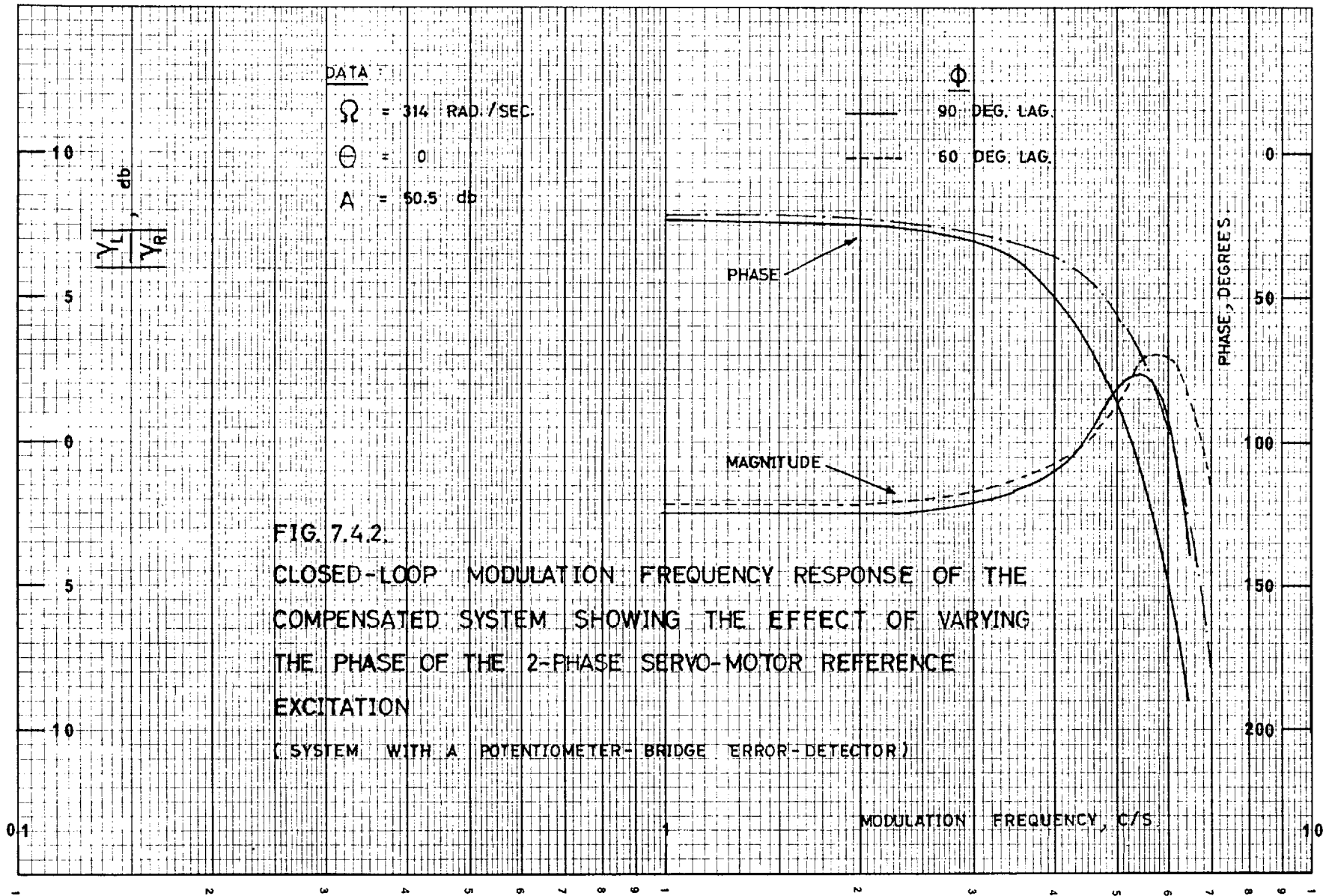
that the compensated open-loop modulation frequency response at the nominal carrier frequency and with  $\theta = \emptyset = 0$  becomes tangential to the M contour of 2.5 db, thereby setting the resonance peak amplitude to 2.5 db which is generally acceptable for good system performance. For this reason, an extra loop-gain of 2.5 db was required which may be supplied by the servo-amplifier as it offers the simplest means of accomplishing it. On this basis, the compensated closed-loop modulation frequency response were deduced and plotted in Figs. 7.4.1 and 7.4.2, illustrating the effects of carrier frequency deviations and phase variations of the excitation reference of the 2-phase servo-motor respectively.

Examining the curves of Fig. 7.4.1 shows definite improvements to the dynamic performance of the compensated system in terms of reduction in the resonance peak. Where the amplitudes of these resonance peaks are 0.5, 2.5 and 3.5 db corresponding to the carrier frequencies 80%, 100% and 120% respectively, though they occur approximately at the same resonance frequency of 5.5 c/s. In essence, such variation of the resonance peak with the carrier frequency reflects the change in the degree of the system damping.

Fig. 7.4.2 shows still another example of the chopper network compensating qualities. Despite the loop-gain increase of 2.5 db, the resonance peaks decrease by applying the chopper network compensation from 5.5 to 2.5 db and from 10 to 3 db for the phases of 90 and 60 deg. lag of the excitation reference of the servo-motor. It is also observed that for  $\emptyset = 90$  deg. lag, the resonance frequency remains approximately the same at 5.5 c/s after applying the compensation, while for  $\emptyset = 60$  deg. lag, it increases from 5 to 6 c/s.







#### 7.4.2. System with a mag-slip-system error-detector.

A study of the open-loop and closed-loop modulation frequency responses of the uncompensated system under different operating conditions (see Figs. 7.3.5 to 7.3.8) shows that despite the system is stable throughout, neither the static or the dynamic performances can be considered satisfactory. A loop-gain increase seems to be capable of providing adequate improvements to the system performance without a need for compensation. However, to check the effectiveness of the chopper networks as suitable compensators for carrier systems, it was decided to attempt one type as a representative example. Single-switch double-capacitor chopper network (see Fig. 4.13) operating as phase-lead was selected for this purpose. The passive electric elements and fly-time of the synchronous switch pertinent to the chopper network employed were suitably chosen as given below

$$\begin{aligned}
 G_1 &= G_2 = 0 \\
 1/G &= 12.5 \text{ K. Ohms (which also represents the} \\
 &\quad \text{input resistance of the servo-amplifier)} \\
 c &= 0.9 \mu\text{f.} \\
 a &= 0 .
 \end{aligned}$$

The compensated system was then tested under different operating conditions, but with the same amplifier gain of 54 db. Figs. 7.3.5 and 7.3.7 show (in solid-line) Nichols diagrams of the compensated system for different energization carrier frequencies, and different phase misalignments between the reference excitations of the error-detector and the servo-motor, respectively. It is observed that there is a significant decrease in the gain margin, but only slight variation in the phase margin. The net effect of

compensation is, however, an increase in the system damping.

In examining the effects of the carrier frequency variations, it is noted that the difference between the compensated and uncompensated open-loop modulation frequency responses is independent of the carrier frequency deviation only in the low modulation frequency region. As the modulation frequency increases, however, this difference becomes more dependent on the carrier frequency deviation. This implies that the rotary modulation transfer function of the chopper network under such practical conditions varies with the carrier frequency. This result is in disagreement with that obtained in Sub-section 5.3.7 when the chopper network was tested under ideal conditions. The reason of the discrepancy may, however, be explained by the phase shift of the excitation reference effected in the 2-phase servo-motor. Such phase shift is obviously a function of carrier frequency. Since the rotary modulation transfer function of the chopper network is pronouncely sensitive to this phase shift (see Fig. 5.3.18), it becomes indirectly dependent on the carrier frequency variations. This, however, does not mean that, in the absence of the excitation phase shift, the rotary modulation transfer function of the chopper network is directly dependent on the carrier frequency deviations.

The compensated closed-loop modulation frequency responses are shown in Figs. 7.4.3 and 7.4.4. They were deduced from the Nichols diagrams of Figs. 7.3.5 and 7.3.7 after adjusting the loop-gain, such that the resonance peak of the compensated closed-loop modulation frequency response at the nominal carrier frequency and with  $\theta = \phi = 0$  is 2.8 db.

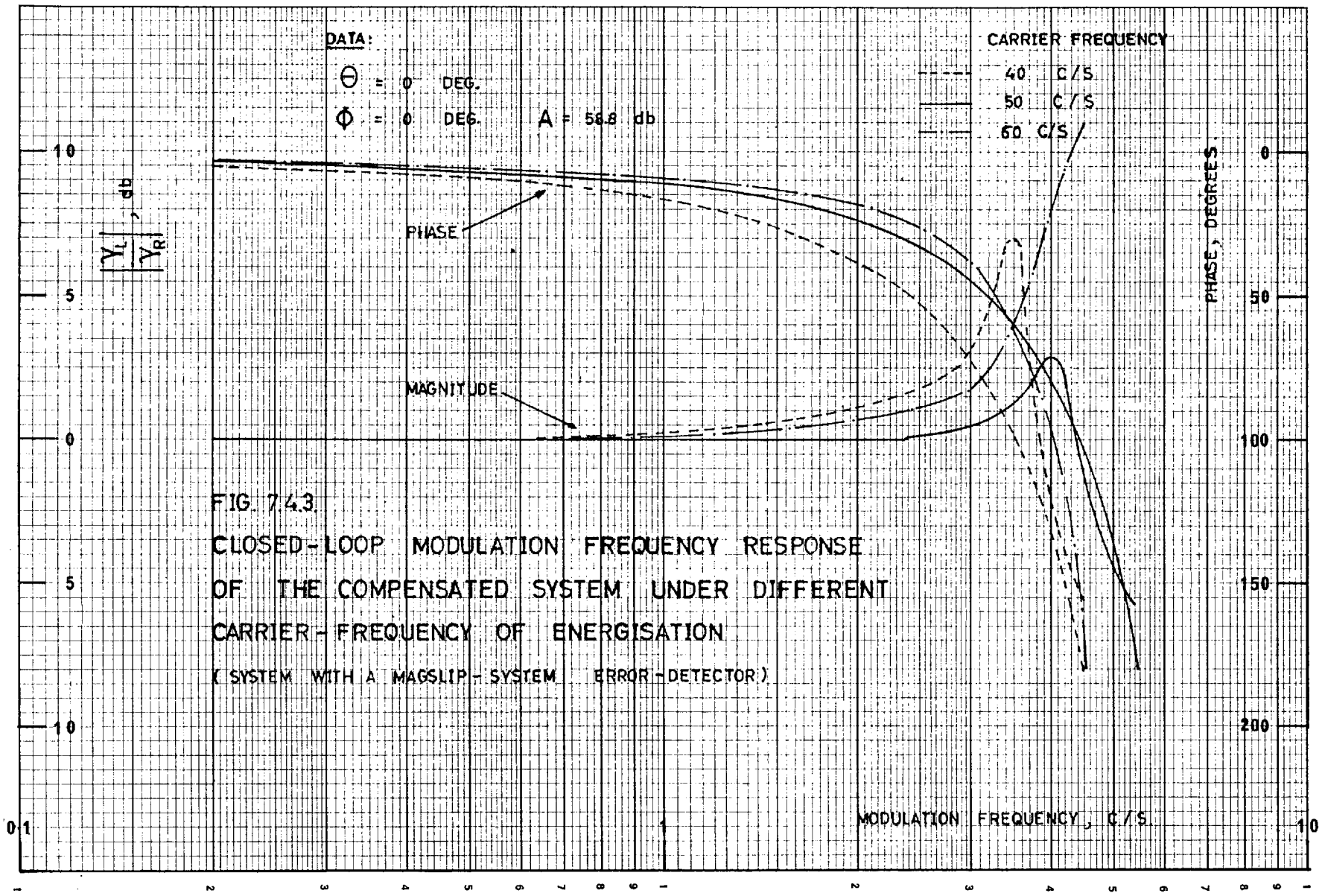
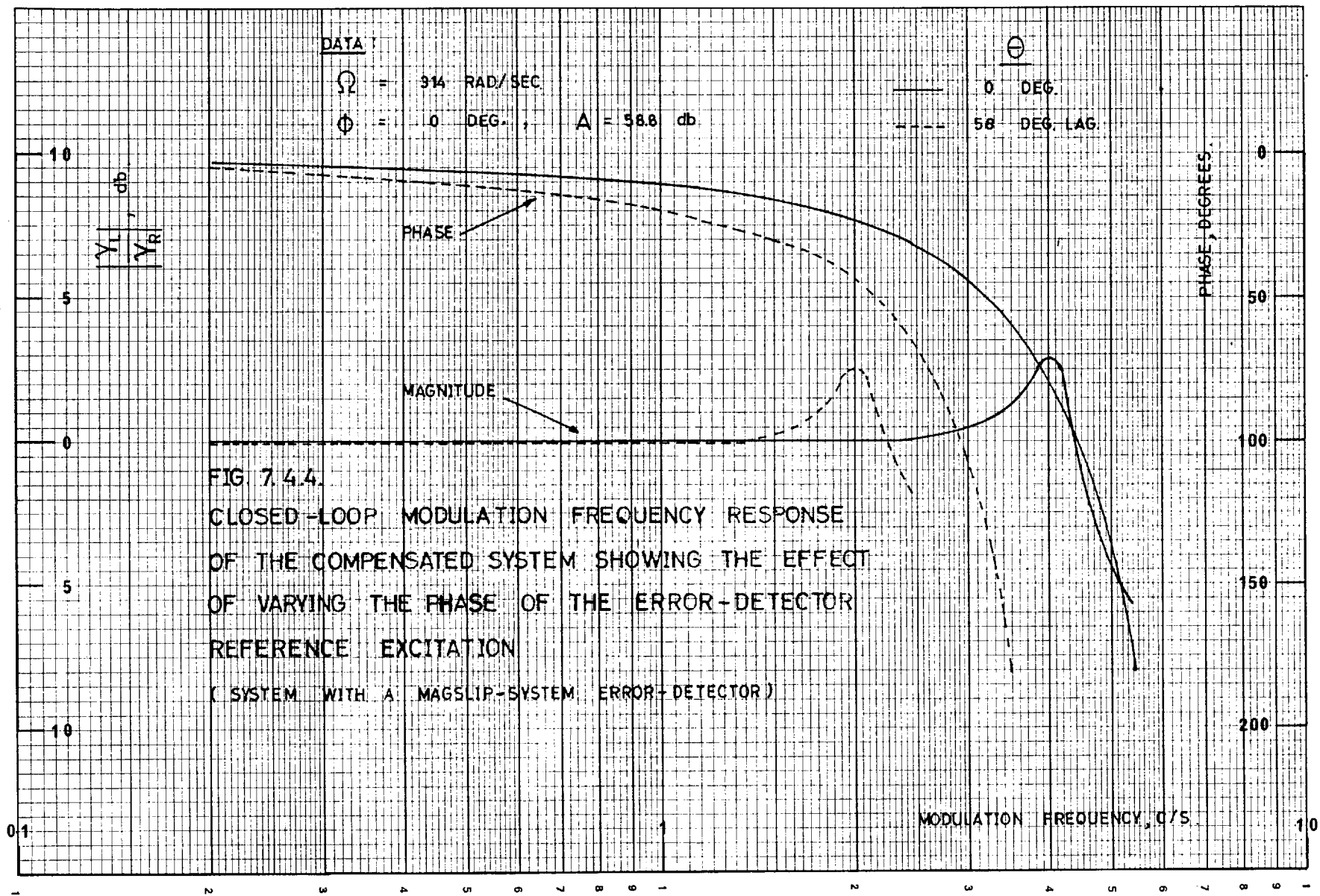


FIG. 7.4.3.  
 CLOSED-LOOP MODULATION FREQUENCY RESPONSE  
 OF THE COMPENSATED SYSTEM UNDER DIFFERENT  
 CARRIER-FREQUENCY OF ENERGISATION  
 (SYSTEM WITH A MAGSLIP-SYSTEM ERROR-DETECTOR)



Under the above conditions, it is seen from Fig. 7.4.3 that the resonance peaks are approximately 7, 2.8 and 11 db corresponding to the carrier frequencies 80%, 100% and 120% respectively. The corresponding resonance frequencies are approximately 3.5, 4 and 4.5 c/s. Although the compensated system at the nominal carrier frequency is expected to perform satisfactorily, it does not appear to be adequately damped at both carrier frequencies 80% and 120%. This does not only show that the chopper network parameters were not optimally chosen, but also bring out to our notice the significant effects of the carrier frequency deviations on the uncompensated system performance characteristics. In particular, the effect on the phase shifts of the reference excitations effected in both the error-detector and the 2-phase servo-motor which may be considered the major responsible factor in deteriorating the rotary modulation transfer function of the compensating chopper network (see Fig. 5.3.18). In view of all these problems, an optimum design to the compensating chopper network seems to be extremely difficult and possibly unpractical. It is therefore very desirable to minimize the dependence of the uncompensated system performance on the carrier frequency variations.

To achieve this aim, a means of compensation for the loop-gain increase with the carrier frequency (refer to the studies performed in Section 7.3) should be added. Although there are many methods which can be adopted, the simplest means envisaged is to insert suitable phase-lag passive electric networks in the paths of the reference carrier excitations to the error-detector and the servo-motor. The simplest form of these phase-lag networks may be just series inductances whose impedances increase with the carrier frequency, thereby decreasing the excitation voltages applied to the error-detector and servo-motor.

This, in turn, brings the loop-gain down. Also, by carefully designing these phase-lag networks, it is possible to compensate for the effective phase shifts of these reference excitations, and thus avoiding any possible deterioration to the chopper network performance characteristics.

Fig. 7.4.4 shows the effect of varying the phase misalignment between the reference excitations of the error-detector and the servo-motor on the compensated closed-loop modulation frequency response. A study of the curves shows a significant effect on the resonance frequency, while the resonance peak is slightly affected. This result may suggest the use of a deliberate phase misalignment between the reference excitations as an effective means of controlling the modulation frequency bandwidth of the system provided that it does not introduce serious deterioration to the compensating chopper network performance characteristics.

#### 7.5. Transient Response Test Considerations.

In general, there are two types of transient tests in common use depending on the form of the command signal, whether as a step-displacement or a step-velocity (i.e., ramp-displacement). Different applications place emphasis on various aspects of the transient response. With regard to the present positional control a.c. system model, however, most of the significant transient characteristics information can be obtained by a step-angular displacement test.

In applying the step-angular displacement test, the closed-loop of the system was electrically interrupted by means of a switch inserted in the error signal path between the error-detector and the servo-amplifier. This has prevented the system from responding while adjusting the



input-angular displacement. By closing the switch instantly, the system will thus behave in a way as if a step-angular displacement has been applied.

The transient response of the system can be measured at the output of the error-detector. With a potentiometer-bridge as error-sensor, the signal appearing just after the switch (see Fig. 7.5.1) carries the error information as the envelope of a modulated wave, and therefore was directly recorded by an Ultra-Violet Recorder. With a mag-slip-system as error-detector, however, the signal appearing at its output carries the error information in the form of a rotary modulated wave. It was therefore necessary to integrate this signal, thereby transforming it into S.C.A.M. wave, before applying it to the recorder. In order to obtain accurate records for the transient response, galvanometers with flat response over a wide frequency bandwidth (5000 c/s) were employed.

With a potentiometer-bridge as error-detector, it was undesirable to leave the summing amplifier in the system (see Fig. 7.2.1) under transient test, since it may introduce some distortion to the high frequencies. An alternative summing arrangement using two resistors was therefore employed as shown in Fig. 7.5.1. Where  $Z_i$  represents the input impedance of either the servo-amplifier or the compensating chopper network depending on whether the system is uncompensated or compensated. In this arrangement, the excitation  $e_p$  must be of balanced type. This was provided in the Laboratory by a transformer with a centre-tapped secondary winding. Hence, by earthing the centre-tap point, the central points of the potentiometers windings were automatically set to the earth potential.

The transfer function of the summing circuit can be

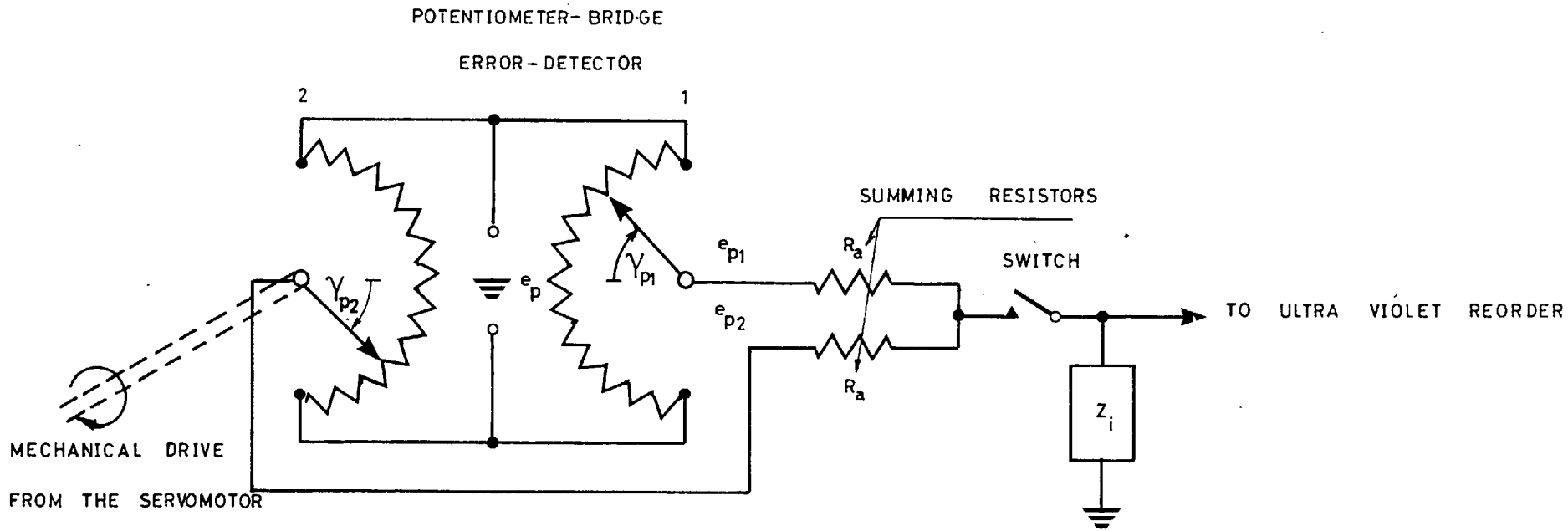


FIG. 7.5.1

CIRCUIT ARRANGEMENT SUITABLE FOR THE TRANSIENT RESPONSE  
TEST OF THE SERVOMECHANISM WITH POTENTIOMETER-BRIDGE  
AS ERROR-DETECTOR

easily derived from the figure and is given by

$$\frac{v_i}{(e_{p1} + e_{p2})} = \left[ R_a + \frac{R_{p2} e_{p1} + R_{p1} e_{p2}}{e_{p1} + e_{p2}} \right] \frac{Z_i}{(R_a + R_{p1})(R_a + R_{p2}) + Z_i(2R_a + R_{p1} + R_{p2})}$$

..7.5.1.

where  $R_{p1}$  and  $R_{p2}$  are the internal resistances formed by the parts of the potentiometers windings 1 and 2 between their centre points and the sliding contacts.

To eliminate the variation of the transfer function with the electrical loading, the value of  $R_a$  should be chosen very high compared to the maximum expected values of  $R_{p1}$  and  $R_{p2}$ . In mathematical terms, this condition may be written as

$$R_a \gg R_{p1 \text{ max}} \quad 7.5.2.$$

and

$$R_a \gg R_{p2 \text{ max}} \quad 7.5.3.$$

If the above conditions are satisfied, Eqn. 7.5.1 becomes

$$\frac{v_i}{(e_{p1} + e_{p2})} = \frac{Z_i}{R_a + 2Z_i} \quad 7.5.4.$$

On the basis of the above equation, if  $Z_i$  represents the amplifier input impedance, then the transfer function of the summing circuit becomes a constant as  $Z_i$  in this case is virtually a constant resistance. If  $Z_i$  represents the input impedance of the compensating chopper network, however,

the transfer function becomes a function of the transmitted signal frequency. This is obviously undesirable because it will affect the overall system performance. Therefore, to minimise such frequency dependence to an acceptable level (depending on the required accuracy), the minimum expected value of  $Z_i$  should be very high compared to  $R_a$ , i.e.,

$$Z_{i \text{ min}} \gg R_a \quad 7.5.5.$$

If this condition is satisfied, the transfer function of the summing circuit expressed by Eqn. 7.5.4 becomes

$$\frac{v_i}{(e_{p1} + e_{p2})} = 0.5 \quad 7.5.6.$$

i.e., independent of the transmitted signal frequency.

In the present work,  $Z_{i \text{ min}}$  was expected to be approximately 12 K.Ohms, while  $R_{p1 \text{ max}}$  and  $R_{p2 \text{ max}}$  were calculated from the expected maximum angular displacements  $\gamma_{p1}$  and  $\gamma_{p2}$  of 20 deg. each, which resulted in 27.8 Ohms each. To satisfy the conditions expressed by Eqns. 7.5.2, 7.5.3 and 7.5.5, the value of  $R_a$  was suitably chosen as 500 Ohms.

## 7.6. Step-Function Response Test Results for the A.C. System with a Potentiometer-Bridge as Error-Detector.

### 7.6.1. System uncompensated.

To study the transient response characteristics of the uncompensated system under different operating conditions, a large number of step-function response tests have

been performed. A representative record of one of these tests is shown in Fig. 7.6.1.

The transient performance characteristics of the system can be interpreted in terms of the following quantities:

- i) Maximum overshoot,
- ii) Response or rise time,
- iii) Settling time (is taken approximately as equivalent to four times the time constant of the envelope of the damped oscillations),
- iv) Damped oscillation frequency.

These quantities can be easily deduced from the step-function response test records similar to the one given in Fig. 7.6.1. The system transient characteristics obtained in terms of these quantities are given in tables 7.6.1 to 7.6.3 which enable the effects of the various factors given below to be studied.

- i) Servo-amplifier saturation,
- ii) Phase variations of the excitation reference of the 2-phase servo-motor,
- iii) Carrier frequency deviation.

Throughout the various transient tests performed, the following quantities were maintained constant

$$A = 2022 \quad , \quad v_m = 30 \text{ volts (r.m.s.)}$$

$$\theta = 0 \text{ deg.} \quad , \quad v_p = 20 \quad " \quad "$$

In table 7.6.1, the servo-amplifier was operated under saturation condition with increasing degree as  $\gamma_{p1}$  changes

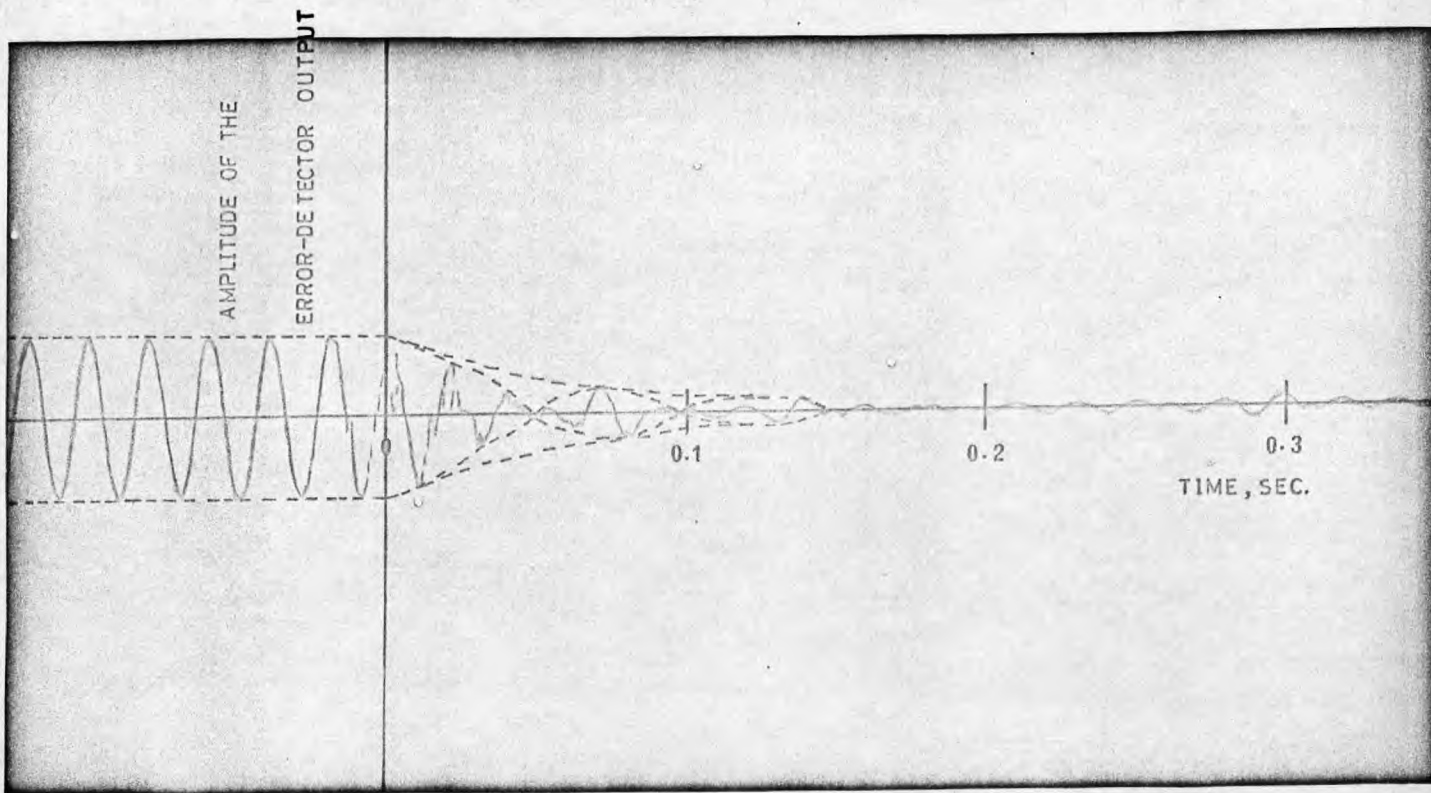


FIG. 7.61

STEP-FUNCTION RESPONSE OF THE UNCOMPENSATED SYSTEM  
(SYSTEM WITH A POTENTIOMETER-BRIDGE AS ERROR-DETECTOR)

DATA:

$$\Omega = 314 \text{ RAD./SEC.}$$

$$\gamma_{P1} = 4 \text{ DEG.}$$

$$\varphi = 90 \text{ " LAG}$$

SEE SUBSEC. 7.6.1 FOR FURTHER DATA

from 8 to 20 deg. In this region, the damped oscillation frequency was noticed to be a function of time (increasing with time) and its value is therefore not given in the table.

Table 7.6.1.

Effect of the servo-amplifier saturation on the transient response characteristics of the uncompensated system

Data:  $\Omega = 314$  rad./sec.,  $\phi = 90$  deg. lag.

Step-input angular displacement $\gamma_{p1}$ , deg.	Maximum Overshoot, %	Response time, m.sec.	Settling time, sec.	Damped oscillation frequency, c/s
4	33	48	0.324	10.4
8	26.4	60	0.342	-
12	17.2	63.8	0.352	-
16	15.4	84	0.400	-
20	11.5	108	0.433	-

Table 7.6.2.

Effect of varying the phase of the excitation reference of the servo-motor on the transient response characteristics of the uncompensated system

Data:  $\Omega = 314$  rad./sec.,  $\gamma_{p1} = 4$  deg.

$\phi$ , deg. lag	Maximum overshoot, %	Response time, m.sec.	Settling time, sec.	Damped oscillation frequency, c/s
90	33	48	0.324	10.4
60	25.7	46.3	0.274	11.9
30	23.9	57.5	0.304	8.8

Table 7.6.3

Effect of carrier frequency deviation on the transient response characteristics of the uncompensated system

Data:  $\gamma_{p1} = 4 \text{ deg.}$  ,  $\phi = 90 \text{ deg. lag}$

Carrier frequency $\Omega$ , c/s	Maximum overshoot, %	Response time, m.sec.	Settling time, sec.	Damped oscillation, frequency, c/s
40	20.3	64.5	0.344	11.5
50	33	48	0.324	10.4
60	32.3	49	0.304	11.5

#### 7.6.2. System compensated.

A single-switch double-capacitor chopper network (see Fig. 4.1.3) was suitably selected as a phase-lead compensator. The values of the various parameters of the chopper network are given below

$$G_1 = G_2 = 0$$

$$1/G \quad (\text{which is also the input resistance of the servo-amplifier}) = 14.3 \text{ K. Ohms}$$

$$c = 1.4 \mu\text{f.}$$

$$a = 0$$

Tables 7.6.4 and 7.6.5 give the transient performance characteristics of the compensated system under phase variations of the excitation reference of the 2-phase servomotor, and carrier frequency deviation respectively. These transient characteristics were calculated from the records of step-function response tests similar to the representative records shown in Fig. 7.6.2.



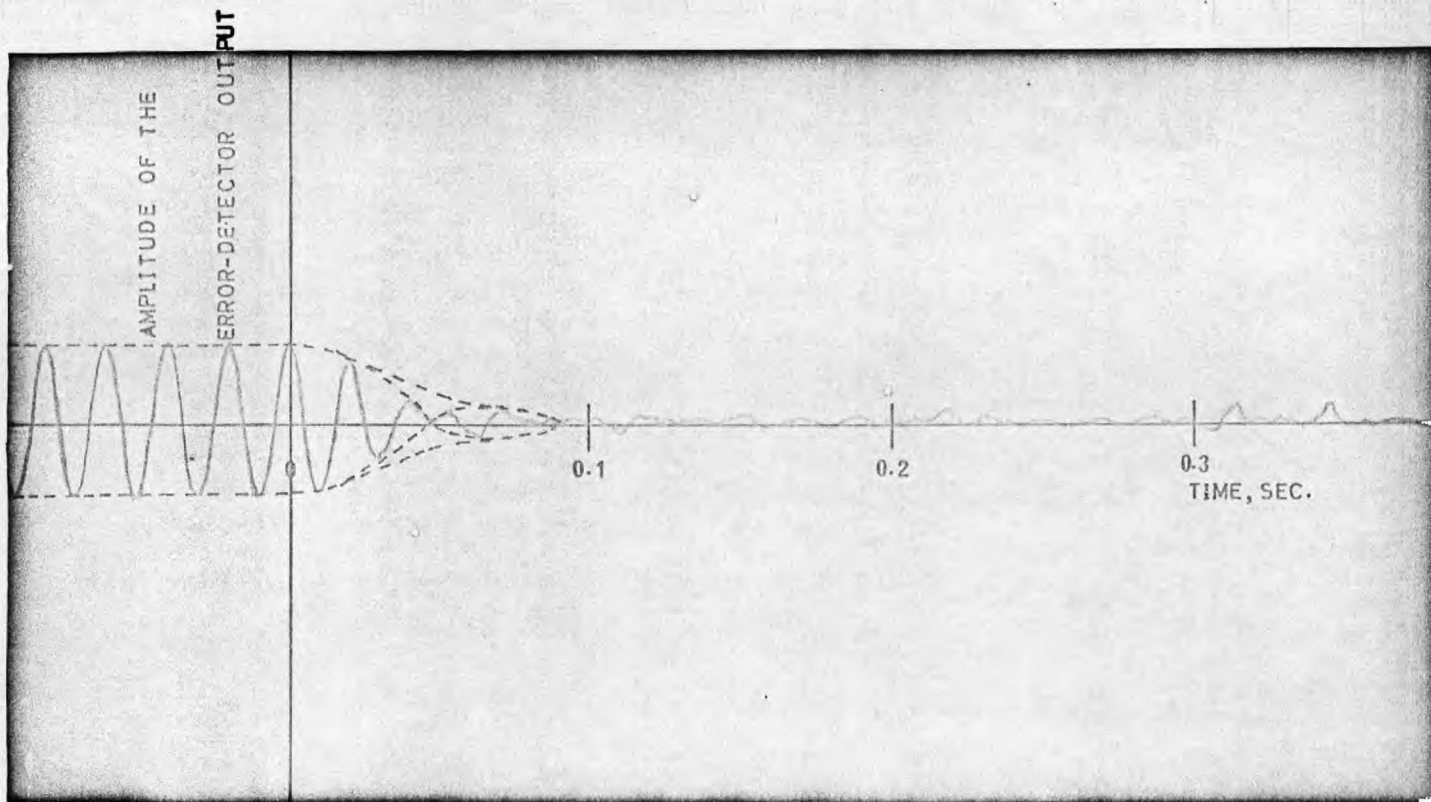


FIG. 7.62

## STEP-FUNCTION RESPONSE OF THE COMPENSATED SYSTEM

(SYSTEM WITH A POTENTIOMETER-BRIDGE AS ERROR-DETECTOR)

DATA:

$$\Omega = 314 \text{ RAD./SEC.}$$

$$\gamma_{PI} = 4 \text{ DEG.}$$

$$\psi = 90 \text{ " LAG}$$

SEE SUBSEC. 7.62 FOR FURTHER DATA

Throughout the transient tests performed on the compensated system, the values of the quantities  $v_m$ ,  $v_p$  and  $\theta$  were kept the same as given in the previous Sub-section, while the gain of the amplifier A was raised to 2730.

Table 7.6.4

Effect of varying the phase of the excitation reference of the 2-phase servo-motor on the transient response characteristics of the compensated system

Data:  $\omega = 314$  rad./sec. ,  $\gamma_{p1} = 4$  deg.

$\phi$ , deg.lag.	Maximum overshoot, %	Response time, m.sec.	Settling time, sec.	Damped oscillation frequency, c/s
90	19.6	43	0.264	11.05
60	16.7	54.2	0.276	12.9
30	22.6	59.2	0.258	11.9

Table 7.6.5

Effect of carrier frequency deviation on the transient response characteristics of the compensated system

Data:  $\gamma_{p1} = 4$  deg. ,  $\phi = 90$  deg.lag

Carrier frequency $\omega$ , c/s	Maximum overshoot, %	Response time, m.sec.	Settling time, sec.	Damped osci- llation frequency, c/s
40	System is almost critically damped with a time constant of 70 m.sec.			
50	19.6	43	0.264	11.05
60	14.5	49.5	0.224	13

7.7. Step-Function Response Test Results for the A.C. System with a Magslip-System as Error-detector.

7.7.1. System uncompensated.

Step-function response tests have been performed to study the effects of the servo-amplifier saturation, variations of the phase of the excitation reference of the servo-motor, and carrier frequency deviation on the transient performance characteristics of the uncompensated system. The results obtained are in the form of records of the time-integral of the magslip-system output signal. Fig. 7.7.1 shows a representative record.

The system transient characteristics, in terms of maximum overshoot, response time, settling time, and damped oscillation frequency, were then deduced from the records obtained and tabulated in the tables 7.7.1 to 7.7.3 for various operating conditions. It has been noticed that operation under saturation condition of the servo-amplifier results in a damped oscillation frequency varying with time. For this reason, its value is not given in table 7.7.1 for values of  $\gamma_{s1}$  above 6 deg.

In conducting the various transient tests, the following quantities were kept constant

$$A = 72.6 \quad , \quad v_m = 30 \text{ volts (r.m.s.)}$$

$$\theta = 0 \text{ deg.} \quad , \quad v_s = 33 \quad " \quad "$$

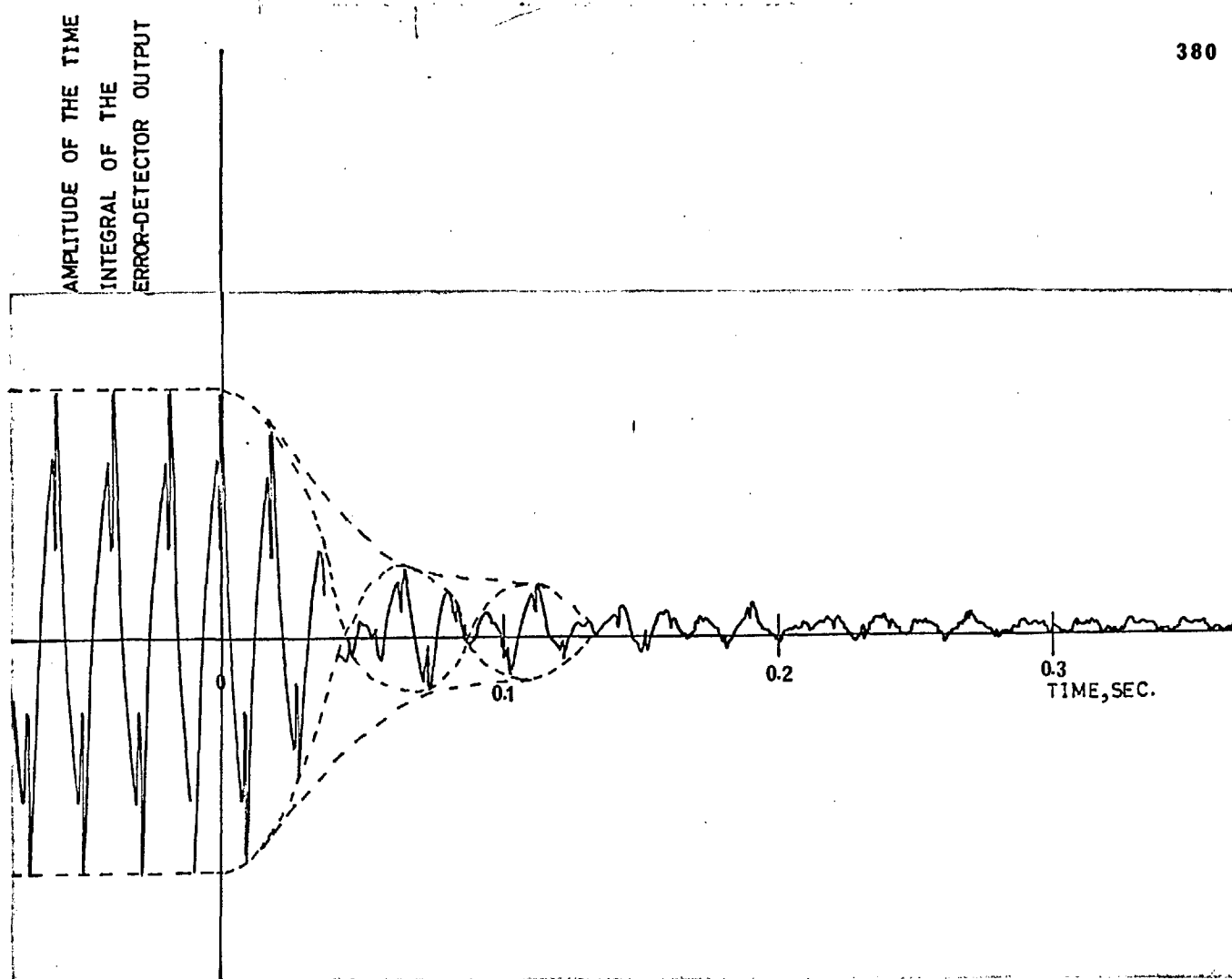


FIG. 7.7.1

## STEP-FUNCTION RESPONSE OF THE UNCOMPENSATED SYSTEM

(SYSTEM WITH A SYNCHRO-SYSTEM AS ERROR-DETECTOR)

DATA:

$$\Omega = 314 \quad \text{RAD. / SEC.}$$

$$\gamma_{s1} = 4 \quad \text{DEG.}$$

$$\psi = 0$$

SEE SUBSEC. 7.7.1 FOR FURTHER DATA

Table 7.7.1

Effect of the servo-amplifier saturation on the transient response characteristics of the uncompensated system

Data:  $\Omega = 314$  rad./sec. ,  $\phi = 0$  deg.

Step input angular displacement $\gamma_{s1}$ , deg.	Maximum overshoot, %	Response time, m.sec.	Settling time, sec.	Damped oscillation frequency, c/s.
4	25.8	42.5	0.328	11.5
6	16.7	58.5	0.29	10.5
8	14.2	77.5	0.387	-
10	12.7	82.5	0.374	-

Table 7.7.2

Effect of varying the phase of the excitation reference of the servo-motor on the transient response characteristics of the uncompensated system

Data:  $\Omega = 314$  rad./sec. ,  $\gamma_{s1} = 4$  deg.

$\phi$ , deg.	Maximum overshoot, %	Response time, m.sec.	Settling time, sec.	Damped oscillation frequency, c/s.
0	25.8	42.5	0.328	11.5
30 lead	21	63.8	0.319	10.5
60 "	System is overdamped with a time constant of 160 m.sec.			
30 lag.	19.7	55	0.284	11.6
60 "	17.7	64.5	0.311	9

Table 7.7.3

Effect of carrier frequency deviation on the transient response characteristics of the uncompensated system

Data:  $\gamma_{s1} = 4 \text{ deg.}$  ,  $\phi = 0 \text{ deg.}$

Carrier frequency $\Omega$ , c/s	Maximum overshoot, %	Response time, m.sec.	Settling time, sec.	Damped oscillation frequency, c/s
40	17	65	0.326	10.2
50	25.8	42.5	0.328	11.5
60	31.3	41.5	0.285	10.5

#### 7.7.2. System compensated.

Phase-lead compensation using a single-switch double-capacitor chopper network was employed. The selected values of the various parameters of the chopper network are given below

$$G_1 = G_2 = 0$$

$$1/G \text{ (which also represents the input resistance of the servo-amplifier)} = 17.2 \text{ K.Ohms}$$

$$c = 1.2 \mu\text{.f.}$$

$$a = 0$$

Step-function response tests have been conducted on the compensated system with the excitations  $v_m$  and  $v_s$  kept at the same values as those given in the previous Sub-section, while the gain of the servo-amplifier A raised to 110.

Fig. 7.7.2 shows a representative record for one of these tests. Tables 7.7.4 to 7.7.6 give the results of the transient performance characteristics of the compensated system under phase variations of the excitation references of the servo-motor and the mag-slip-system, and finally under carrier frequency deviations.

Table 7.7.4

Effect of the phase variations of the excitation reference of the servo-motor on the transient response characteristics of the compensated system

Data:  $\Omega = 314$  rad./sec. ,  $\gamma_{s1} = 4$  deg.,  $\theta = 0$  deg.

$\phi$ , deg.	Maximum overshoot, %	Response time, m.sec.	Settling time, sec.	Damped oscillation frequency, c/s
0	22.6	49.5	0.275	12.4
30 lead	17.4	56.5	0.261	9.6
60 "	19.2	45.2	0.219	13.8
30 lag	System is overdamped with a time constant of 121.5 m.sec.			
60 "	24.6	42	0.348	10.2

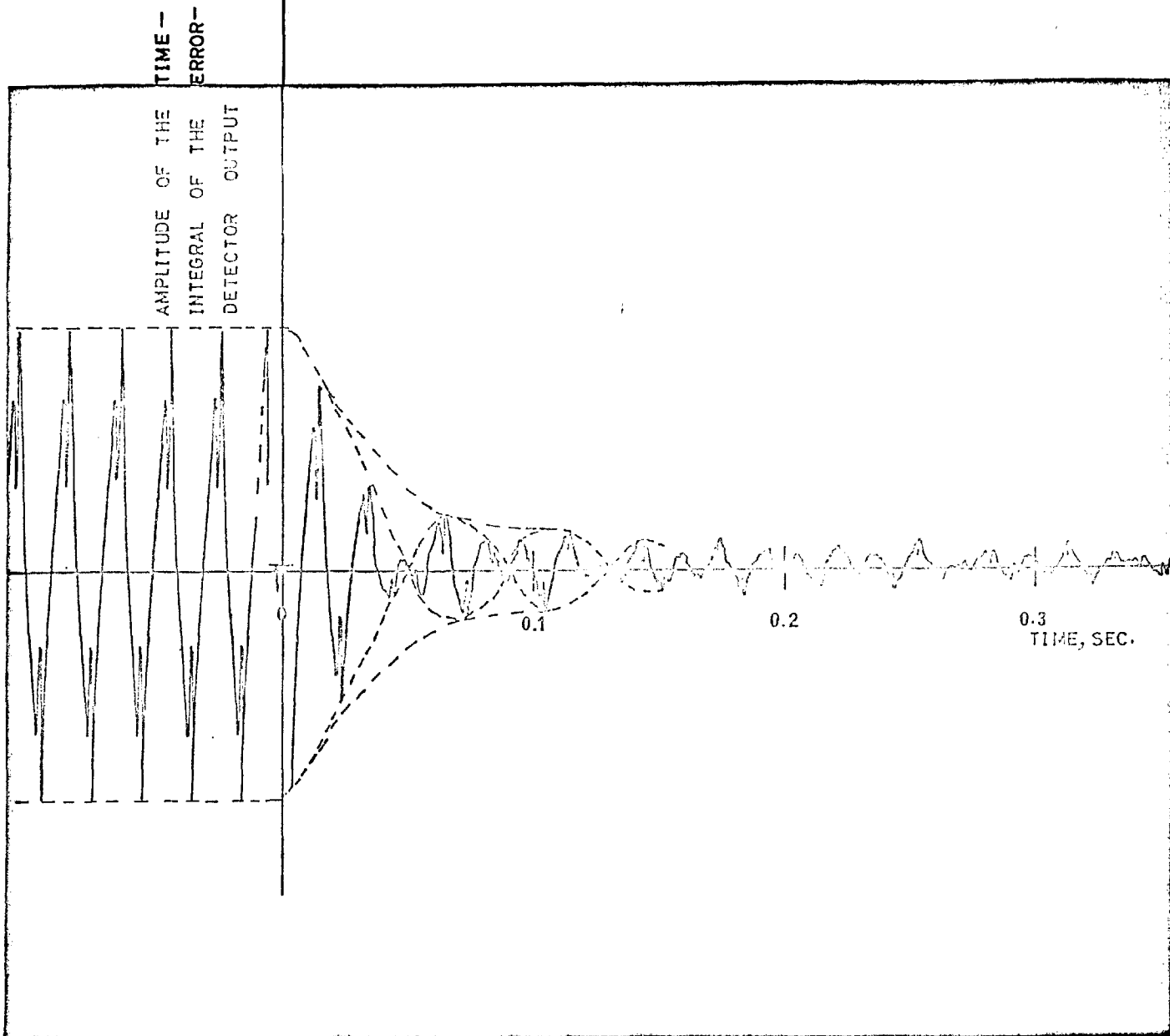


FIG. 7.7.2

## STEP-FUNCTION RESPONSE OF THE COMPENSATED SYSTEM

(SYSTEM WITH A SYNCHRO-SYSTEM AS ERROR-DETECTOR)

DATA :

$$\Omega = 314 \text{ RAD./SEC.} \quad \psi = 0 \text{ DEG.}$$

$$\gamma_{s1} = 4 \text{ DEG.} \quad \delta = 0$$

SEE SUBSEC. 7.7.2 FOR FURTHER DATA



Table 7.7.5

Effect of the phase variations of the excitation reference of the mag-slip-system on the transient response characteristics of the compensated system

Data:  $\Omega = 314$  rad./sec.,  $\gamma_{s1} = 4$  deg.,  $\phi = 0$  deg.

$\theta$ , deg.	Maximum overshoot, %	Response time, m.sec.	Settling time, sec.	Damped oscillation frequency, c/s
0	22.6	49.5	0.275	12.4
30 lag.	28.2	43	0.284	9.8
60 "	17.5	82	0.344	8.8
30 lead	11.6	55.3	0.238	11.8
60 "	System is almost critically damped with a time constant of 86 m.sec.			

Table 7.7.6

Effect of carrier frequency deviation on the transient response characteristics of the compensated system

Data:  $\gamma_{s1} = 4$  deg.,  $\phi = 0$  deg.

Carrier frequency $\Omega$ , c/s	Maximum overshoot, %	Response time, m.sec.	Settling time, sec.	Damped oscill- ation frequency c/s
40	System is almost critically damped with a time constant of 59. m.sec.			
50	22.6	49.5	0.275	12.4
60	27.8	44.5	0.267	12

CHAPTER 8SCHEME FOR EXTENDING THE PRACTICAL RANGE OF  
OPERATION OF COMMERCIAL ELECTRONIC MODULATORS  
AND DEMODULATORS8.1 General

At some stage during the course of designing a.c. servo-mechanisms, it is generally required to have experimental information on the performance characteristics of the prototype model. This permits the designer to find out whether the performance meets the specified requirements, and helps to observe any anomalies in the performance so that the design may be modified. Furthermore, the need for gain refinement and for compensation may be checked, and quantitative data obtained. Where Bode-diagram and Nichols-chart techniques of design are to be used, the design information has to be of a modulation frequency response nature.

In the previous practical investigations presented in Chapters 5 and 7, it has been shown that modulators and demodulators play a significant role in the process of measuring modulation frequency responses of a.c. or carrier systems. The purpose of the modulator is essentially to produce a signal in the form of suppressed-carrier amplitude-modulated wave to act as a test signal for the system under consideration. Whereas, the demodulator is employed to recover the low-frequency envelope of the output signal of the system. The phase and attenuation of the recovered envelope of the output may thus be compared with those pertinent to the reference modulating signal which determine a point location on the modulation frequency locus. Repeating this test for different modulating frequencies, which lie within the frequency band under study, would enable a portion of the modulation frequency response to be plotted.

The usefulness of the modulation frequency response test lies in the degree to which its results can be relied upon and in the extent of the frequency range over which the results can possibly be obtained. These basically depend upon the capability and practical limitations of the measuring instruments. The most serious limitations exist particularly in commercial electronic modulators and demodulators. Although these limitations have received a widespread recognition, it seems that there is still no successful attempt to overcome them. In this chapter, a scheme is developed whereby commercial electronic modulators and demodulators can extend their working range. Before introducing the theory of that scheme, it would be appropriate to explain the possible causes of these practical limitations.

## 8.2 Practical limitations

In general, the performance characteristics of commercial electronic modulators are satisfactory provided that they operate with modulating frequencies not exceeding the usually specified maximum limit of 10% of carrier frequency. On this basis, experimental determination of the modulation frequency responses of carrier systems can be obtained over only a small range if accuracy is to be maintained. This may not give sufficient information for the design purposes, particularly for high speed response a.c. servomechanisms where the modulating frequencies approach the same order of magnitude as the carrier frequency. Furthermore, with this limitation, investigations into carrier-systems which may operate with modulating frequencies greater than the carrier frequency are practically impossible. As a result, the scope of the development and expansion in the field of carrier-systems is seriously restricted.

The operational limitations of commercial electronic modulators and demodulators, mentioned above, may be explained in simple physical terms by considering problems which may arise due to the

transmission of suppressed-carrier amplitude modulated waves through them. In this regard, to make the explanation more comprehensive, and consistent, a brief description of the principles of operation, demonstrated by block diagrams, of typical modulators and demodulators used in practice may be appropriate to be outlined, at the outset, as below.

### 8.2.1 A practical modulator

The block diagram of a typical commercial electronic modulator is shown in Fig. 8.2.1<sup>127</sup>. The double balanced modulator, basically, consists of four simple modulators arranged as two balanced modulators. The output from these two balanced modulators contain side bands and modulating signal frequencies, but with the carrier suppressed. These two outputs are combined in such a way that the modulating signal component is cancelled. The output then consists of lower side bands and higher side bands only in the ideal case.

In practice, however, complete suppression of the unwanted products of modulation is not achieved; the small amount of residual must then be removed by other means.

The output from the double balanced modulator, which is mainly side bands, is amplified by the first side band amplifier and passes through the modulator filter. The purpose of this filter is to transmit the two side bands with minimum phase shift, and to reject the unwanted products of the modulation process. The output from the filter is amplified by the second side band amplifier. From the second side band amplifier, the amplified side bands are fed into the power output stage via a potentiometer for level adjustments. The power output stage is a Class A push-pull amplifier with transformer output, employing negative feedback.

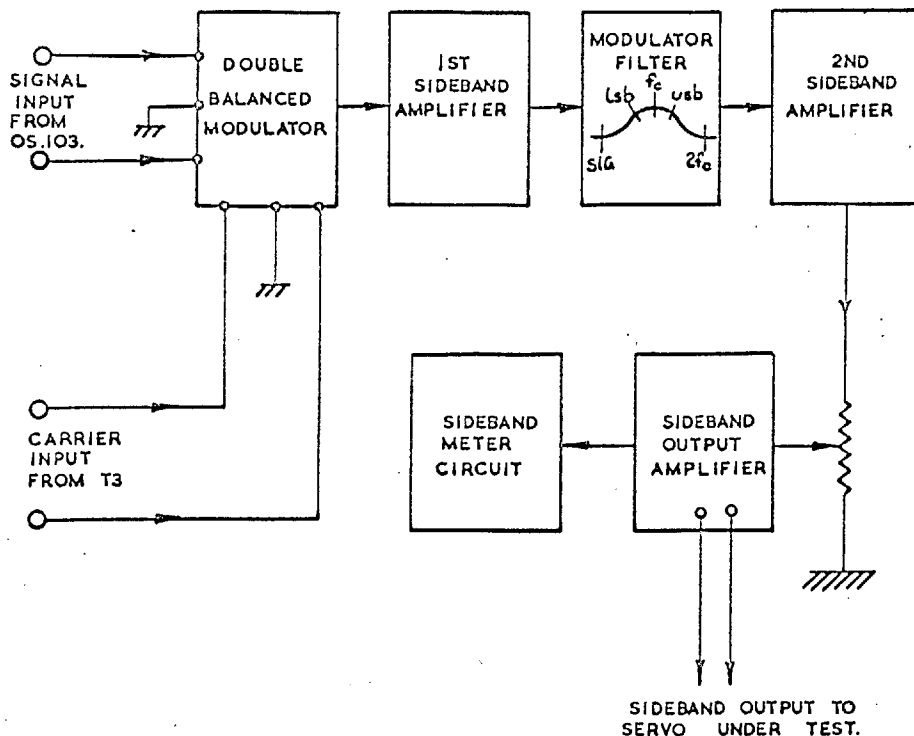


FIG. 8.2.1.  
 BLOCK DIAGRAM OF A PRACTICAL ELECTRONIC MODULATOR  
 (REPRODUCTION FROM REF. 127 )

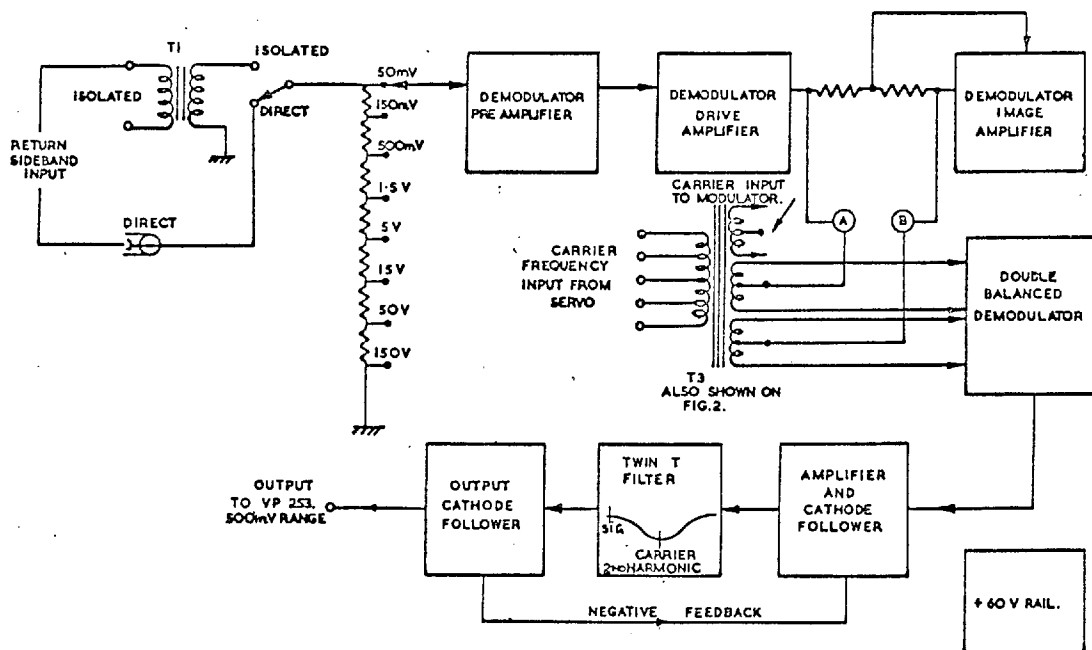


FIG. 8.2.2.  
 BLOCK DIAGRAM OF A PRACTICAL ELECTRONIC DEMODULATOR  
 (REPRODUCTION FROM REF. 127 )

In order to ensure minimum distortion to the suppressed-carrier amplitude-modulated wave, the two side bands should ideally undergo zero phase shift and constant attenuation over the whole range of frequency down to d.c. Such conditions require that various stages placed after the double balanced modulator, which are primarily amplifiers should have frequency-independent transmission characteristics. In practice, however, amplifiers with output transformers and interstage capacitor or transformer couplings, which are frequency dependent, can be designed to give almost a flat response, but over only a limited range of frequency. To extend that frequency band, considerably complicated design would be required particularly if the extension is in the lower frequency direction. Therefore the lower side band may be considered as the deciding factor in setting up the maximum limit on the proportion of modulating frequency to carrier frequency.

### 8.2.2 A practical demodulator

Fig. 8.2.2<sup>127</sup> shows a block diagram of a typical commercial electronic demodulator. The drive and image amplifiers together produce a push-pull side band output, which is fed into the double balanced demodulator where the carrier is re-introduced and demodulation takes place. This action is the reverse of that described for the double balanced modulator.

The demodulator output is then passed through a combined amplifier and filter. This filter rejects the unwanted components of demodulation, and passes the signal frequency with minimum phase shift.

The return side bands or the output from the servo under test have to pass through the transformer or capacitor input pre-amplifier, drive amplifier and image amplifier before being demodulated. Therefore, zero or very small phase shift and constant attenuation over the working frequency range, are the

required characteristics for these amplifiers if accurate and reliable results are to be obtained. Again, in view of the design difficulties to meet these requirements specially in the low frequency region, a practical limit on the lower side band seems to be inevitable.

### 8.3 Principle of operation of a proposed scheme for overcoming the practical limitations

In the previous Section, it has been shown that the operational limitation imposed on the maximum ratio of modulating frequency to carrier frequency in electronic modulators and demodulators used in practice may simply be explained in terms of the phase and magnitude distortions, which take place in transmitting modulated signals through the incorporated amplifiers. This explanation has effectively paved the way to the development of the present scheme.

The principle of operation of the proposed scheme is primarily based on the idea of shifting the frequency of the side bands to a sufficiently high frequency level, so that the non-flat portion of the frequency characteristics of the various incorporated circuits and amplifiers may be avoided. This can easily be realised using an auxiliary amplitude modulation process onto a second carrier whose frequency is higher than that of the principal carrier. The resulting double-modulated signal after being transmitted through the various circuits and amplifiers, its high frequency level then has to be shifted back to its original level to be ready for use. To accomplish this, an auxiliary demodulation process by the same high frequency carrier may be adopted.

Having established the broad line basis on which the proposed scheme should work, it would be appropriate to consider the details of operation and the governing criteria on theoretical basis to provide the background for the physical realisation of such scheme.

The subsequent Subsections, therefore, are devoted to the formulation of these theoretical basis.

### 8.3.1 Theory of the scheme's operation

In order to differentiate between the carrier used in the electronic modulators and demodulators under consideration and the carrier employed in the auxiliary modulation and demodulation involved in the proposed scheme, subscripts  $p$  and  $a$ , which signify the meanings principal and auxiliary, are used respectively.

Considering the practical modulator shown in Fig. 8.2.1., the operation taking place in the double balanced modulator is essentially a multiplication of the signal  $x_1(t)$  by a sinusoidal carrier. Ideally, this may be interpreted mathematically as follows:

$$y_1(t) = x_1(t) \cdot \sin(\omega_p t + \theta) \quad 8.3.1$$

where  $y_1(t)$  is the output of the double balanced modulator.

Now, suppose the modulated signal  $y_1(t)$  is operated upon twice by a function  $M(t)$  in the way described below,

$$y'_1(t) = y_1(t) \cdot M(t) \cdot M(t) \quad 8.3.2$$

Then, in order to obtain the same function after this double operation, i.e.  $y'_1(t) = y_1(t)$ , the function  $M(t)$  must be of some form so as to fulfil the condition

$$M^2(t) = 1 \quad 8.3.3$$

On this basis, square-wave can be considered as the simplest possible form of the function  $M(t)$ , provided that the trivial solution  $M(t) = 1$  is discarded. In the light of this, the double operation expressed by Equation 8.3.2 may be described in simple



physical terms as a modulation and a demodulation processes carried out by a square-wave carrier. By splitting the application of the square-wave modulation and demodulation, so that the former process is applied first to form a double modulated signal,

$$f_1(t) = y_1(t) \cdot M(t) \quad 8.3.4$$

passing the resulting signal through the various amplifiers existing after the double balanced modulator, then at last applying the square-wave demodulation to the output of the side-band output amplifier, will completely simulate the required operation of the proposed scheme.

Similarly, in regarding the practical demodulator shown in Fig. 8.2.2, the signal normally fed into its either input capacitor or isolated transformer is in the form of amplitude modulated wave, which may generally be written as

$$y_2(t) = x_2(t) \cdot \sin(\Omega_p t + \phi) \quad 8.3.5$$

To avoid the transmission problems associated with the amplifiers existing before the double balanced demodulator, the signal  $y_2(t)$  may first be employed to modulate a square-wave carrier before being applied to the input terminals of the practical demodulator. The new input signal is thus in the form of double-modulation as given below

$$f_2(t) = x_2(t) \cdot \sin(\Omega_p t + \phi) \cdot M(t) \quad ..8.3.6$$

After passing the above signal through the amplifiers, demodulation by the square-wave carrier has to be applied either just before or after the double balanced demodulator in order to neutralise the effect of the earlier square-wave modulation.

It is important to mention that the modulator filter can no longer be used when the present scheme is applied. This is because

the filter was originally intended for filtering out the by-products of the principal modulation and thus tuned to the principal carrier frequency with symmetrical characteristics around it so that the two side bands will be treated identically. With the present scheme, however, the signal appears in the filter region as double modulation; once by the sinusoidal principal carrier, and the other by the square-wave auxiliary carrier, which may be decomposed into infinite number of side bands. As a consequence, the tuned filter with its notch characteristics will give rise to distortion, and thus should be removed. On the other hand, the demodulator tuned filter may still be used because it is placed in the region where the demodulated signal appears, and thus the above problem does not exist.

### 8.3.2 Criteria for the calculation of the auxiliary carrier frequency

In reviewing the principle of operation of the proposed scheme described above, it can be observed that the auxiliary carrier only appears in the section where the signal form has been transformed from simple amplitude modulation, by the principal carrier, to double amplitude modulation using the square-wave auxiliary carrier in the second modulation process. It is, therefore, important to examine closely the transmission characteristics of such signal when passing through the amplifiers existing in its path in order to determine the effect of the various factors on the choice of the auxiliary carrier frequency. To do so, the double-modulated signal  $f_1(t)$  expressed by Equation 8.3.4 may be rearranged in a more suitable form by expressing the function  $M(t)$  in terms of its Fourier series, thus

$$f_1(t) = x_1(t) \cdot \sin \left( \frac{\omega_p}{p} t + \theta \right) \cdot \frac{4}{\pi} \sum_{n=0}^{n=\infty} \left[ \left\{ \sin(1+2n)\pi a t \right\} / (1+2n) \right] \quad 8.3.6$$

where  $n$  is an integer number.

If the signal  $x_1(t)$  is a simple harmonic voltage with frequency  $\omega$ , thence the double modulated signal described by Equation 8.3.6 can easily be expanded in the form of a summation of infinite simple harmonic components. The frequency of the general term of these components may be written as

$$(1+2n)\omega_a \pm \omega_p \pm \omega \quad 8.3.7$$

To ensure that minimum or even no transmission distortion will take place to the double modulated signal, the frequency spectrum of its components should only lie in the region of the flat frequency characteristics of the pertinent amplifiers. This seems practically impossible for the frequency spectrum of these components, according to Equation 8.3.7, is extended to infinity. Fortunately, however, the components' magnitude decreases rapidly (by the factor  $1/(1+2n)$ ) as the frequency increases. Therefore, with reasonably designed amplifiers, distortion would only occur to the very high frequency components which are negligible. In the low frequency region, however, a limit is set up by the amplifiers' flat frequency characteristics which cannot further be extended without adopting very complicated or impractical designs. Consequently, the lowest frequency component of the double modulated signal should be of higher frequency than that limit otherwise serious distortion would occur. This condition may be written in mathematical terms, after deducing the minimum value of the expression 8.3.7 as follows

$$\omega_a(\text{min}) - \omega_p + \omega_{\text{max}} \geq \omega_{Cl} \quad 8.3.8$$

Where  $\omega_{Cl}$  is the lower frequency limit of the flat frequency characteristics of the amplifiers <sup>and</sup>  $\omega_{\text{max}}$  is the maximum modulating frequency.

By rearranging the above expression, a simple criterion for calculating the minimum value of the auxiliary carrier frequency can be deduced,

$$\omega_a (\text{min}) = \omega_p + \omega_{\text{max}} + \omega_{C_1} \quad 8.3.9$$

From the criterion derived above, three factors establish the basis on which a suitable value of the auxiliary carrier frequency could be calculated, viz:

- 1) the principal carrier frequency,
- 2) the maximum modulating frequency, and
- 3) the lower frequency limit of the amplifiers flat frequency response.

#### 8.4 Practical realization of the scheme

On the basis of the theory of operation of the proposed scheme introduced above, a square-wave modulator and demodulator are essentially required to be used in conjunction with either the electronic commercial modulator or demodulator to improve their working frequency range. The design of these square-wave modulators and demodulators depends on so many factors among which are the characteristics of the circuits just preceding and succeeding them. It is, therefore, appropriate to consider their possible positions before attempting the detailed design.

##### 8.4.1 Possible positions of the square-wave modulators and demodulators

With regard to the practical modulator shown in Fig. 8.2.1 the square-wave modulator can be inserted somewhere before the 1st sideband amplifier. By re-writing Equation 8.3.4 in the various possible arrangements

$$f_1(t) = \left[ x_1(t) \cdot \sin(\omega_p t + \theta) \right] \cdot M(t) \quad 8.4.1$$

$$f_1(t) = \left[ x_1(t) \cdot M(t) \right] \cdot \sin(\omega_p t + \theta) \quad 8.4.2$$

$$f_1(t) = \left[ \sin(\omega_p t + \theta) \cdot M(t) \right] \cdot x_1(t) \quad 8.4.3$$

three possible positions may be suggested, viz:-

- i) after the double balanced modulator so that the signal input would first modulate the sinusoidal principal carrier, and then the resulting signal would modulate the square-wave auxiliary carrier.
- ii) before the double balanced modulator and in the path of the signal input so that a square-wave modulation by the auxiliary carrier would first take place and then a sinusoidal modulation by the principal carrier would follow.
- iii) before the double balanced modulator and in the path of the principal carrier so that the principal carrier would first modulate the square-wave auxiliary carrier and the resulting signal would then be used as a complex carrier for the second modulation by the simple frequency input signal.

With regard to the square-wave demodulator, however, there is only one position to be inserted in, which is that after the sideband output amplifier.

In the case of the practical demodulator, it looks in a way as if the reverse is taking place. Just before either the input isolating transformer or input capacitor can be considered as the only possible position for the square-wave modulator. For the square-wave demodulator, however, there are three possible positions which can be deduced in a manner similar to that used in obtaining positions of the square-wave modulator associated with the practical modulator. These three positions are:

- i) after the double balanced demodulator. In this way, the output signal from the demodulator drive and image amplifiers, which is in the form of double modulated signal as expressed by Equation 8.3.5, is first demodulated by the sinusoidal principal carrier, then demodulated by the square-wave auxiliary carrier.
- ii) before the double balanced demodulator and in the path of the output signal from the demodulator drive and image amplifiers. In this way, the double modulated signal is first demodulated by the square-wave auxiliary carrier, then demodulated by the sinusoidal principal carrier.
- iii) before the double balanced demodulator and in the path of the principal carrier. In this way, the square-wave auxiliary carrier is first modulated by the sinusoidal principal carrier to form a complex carrier by which the double modulated signal is demodulated.

#### 8.4.2 Design and construction of a transistor square-wave modulator and/or demodulator

Because the square-wave modulation and demodulation are basically identical operations, the same circuit may be used for both the modulator and demodulator. It would henceforth be more convenient to confine the attention to only one of them - the modulator.

Instead of looking at the square-wave modulation as the operation of multiplying the signal by a square-wave carrier, an alternative look, as the action of reversing the polarity of the signal at carrier frequency, may be adopted to provide the basis of the practical realisation. With the later interpretation, it is feasible to realise the square-wave modulation by means of two 3-terminal switches operating in synchronism with the carrier under zero fly-time condition (see Section I.2.0). The two fixed contacts of one switch are connected to the opposite ones of the other switch,

so that the common fixed contacts would form the input signal terminals, whereas the two moving contacts would form the output terminals of the built up modulator. Because of the symmetry of the modulator construction, the input and output terminals can be interchanged.

A transistor circuit for the square-wave modulator, based on the 3-terminal synchronous switch circuit of Fig. I.5, is shown in Fig. 8.4.1. The zero fly-time operation of the switches permits the use of one pulse-transformer, with four identical secondary windings. The primary winding of the pulse-transformer is fed with square-wave carrier by an appropriate driving circuit similar to that shown in Fig. I.16. The four secondary windings of the pulse-transformer are connected in such a way that the net direct current always remains zero provided that the transistors are matched. Because of this, and also of the symmetrical operation of the four 2-terminal switches, Zener diodes could be dispensed with.

The design procedure for the square-wave modulator shown in Fig. 8.4.1 basically depends on that developed for the transistor 3-terminal synchronous switch which is outlined in detail in Chapter I. As the modulator operates, the two 2-terminal switches a and b conducts for a half carrier cycle during which the switches c and d are under OFF condition, and the reverse takes place during the other half of the cycle. According to this, one pair of the windings of the pulse transformer secondary would carry identical currents flowing through their corresponding transistors bases of the conducting switches, while the other pair of the secondary windings would be carrying almost zero current (the leakage currents of the OFF transistors bases will be flowing which may be considered very negligible). Such action occurs during one half of carrier cycle and then the two pairs of windings interchange their operating conditions during the second half of the cycle. As a consequence, considerable simplification could be obtained by visualizing the pulse-transformer as if it only contains two of its secondary

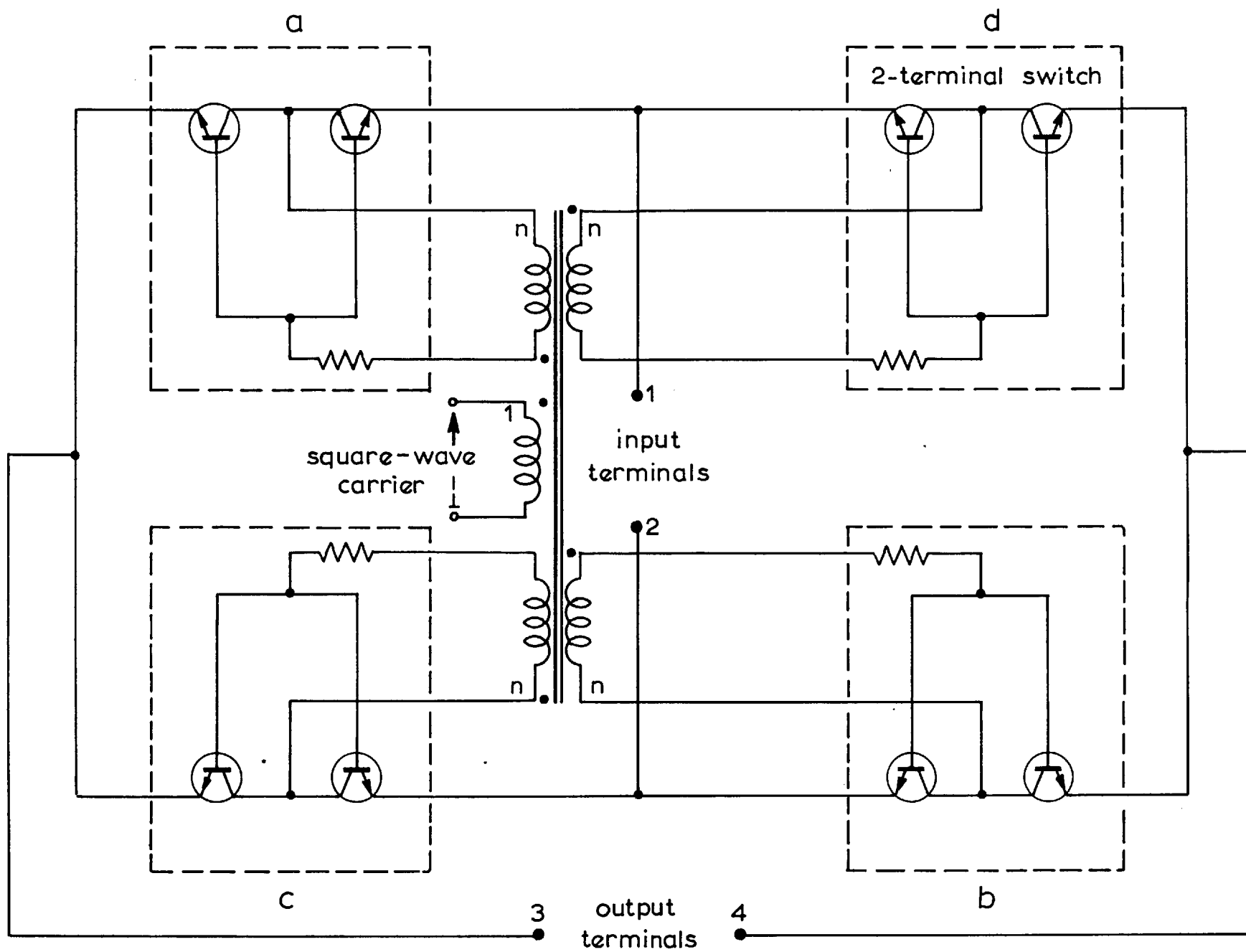


FIG. 8.4.1.

A TRANSISTOR SQUARE-WAVE MODULATOR OR DEMODULATOR



windings connected in series (as the same current would be flowing through them due to their assumed matched loads), and feeding a resistance of double the value of the base resistance. In this way, the same formulae and various design steps for calculating the principal parameters of the pulse-transformer given in Subsection I.4.3.3 can be adopted without any modification. One should, however, bear in mind that the parameters obtained by this method for the secondary side are pertinent to one pair of the secondary windings, and therefore their values should be divided by two to render them per single secondary winding.

Square-wave modulators and demodulators have been constructed in the Laboratory using the transistor circuit of Fig. 8.4.1, for the purpose of checking experimentally the validity of the scheme theory, as will be discussed in Section 8.5. Because the design procedure for the modulators and demodulators is essentially based on that presented in Chapter I, no details will be given here. Only the specified requirements and the values of the calculated parameters will be given below.

#### 8.4.2.1 The specified requirements

- i) The auxiliary carrier frequency = 400 c/s.
- ii) The maximum current passing through the switches = 5 m.A.
- iii) The incorporated 3-terminal synchronous switches should operate with zero fly-time.
- iv) The maximum tilt of the pulse flat top appearing in the output of the pulse-transformer = 0.2.
- v) The maximum transformer primary current that can be supplied by the driving circuit = 10 m.A.
- vi) The pulse height of the input voltage of the pulse-transformer = 12 volts.

#### 8.4.2.2 Selected components and the values of the designed parameters

- i) The selected transistors are of the type 2 N 1302, whose characteristics are given in Appendix I.9.2.
- ii) The pulse-transformer calculated parameters:
  - a) Resistance of the primary winding = 1 k
  - b) Resistance of a single secondary winding including the base resistance = 1.2 k
  - c) The effective shunt inductance referred to the primary side = 2.1 Henries.
  - d) The turns ratio = 1/1-1-1-1
- iii) The driving circuit for the pulse-transformer is similar to that shown in Fig. I.16 which is capable to provide simultaneously adequate drive to two pulse-transformers. It is therefore suitable to be used as a common drive to the pulse-transformers incorporated in a modulator and a demodulator. In this way, the switching instances in both the modulator and demodulator can be adjusted to be aligned, thereby satisfying the operation requirements of the scheme.

#### 8.4.3 General discussion

In general, the auxiliary modulation and demodulation processes included in the proposed scheme may be carried out employing either a sinusoidal or a square-wave carrier. Choosing or rejecting either method entirely depends on their relative merits and demerits.

The following points outline the reasons for favouring the use of the square-wave modulation and demodulation for this particular type of application.

- i) Square-wave modulators and demodulators can be physically realised by very simple circuits (see Fig. 8.4.1).

- ii) Sinusoidal modulation followed by sinusoidal demodulation will produce noise components at double the carrier frequency. Such noise does not appear when the corresponding square-wave processes are employed.
- iii) The square-wave modulator or demodulator shown in Fig. 8.4.1. does not include frequency dependent elements, such as capacitors, inductors or transformers, in the signal path. Therefore, no signal distortion will take place.
- iv) The square-wave modulation and demodulation do not cause signal attenuation and therefore no amplifying stages are needed to be employed after the modulators nor the demodulators.

#### 8.5. Practical investigations into the performance of the scheme.

On the basis of the above work, the feasibility of building up a scheme comprising a square-wave modulator and a demodulator, which can be incorporated into any commercial electronic modulator or demodulator to extend their working frequency range has been established. However, to test the effectiveness of the scheme when applied in actual practice, the overall transmission characteristics of a system consisting of a standard electronic modulator and demodulator may experimentally be determined with and without the scheme, and the results obtained may then be compared. The several steps outlined below are designed for this purpose.

##### 8.5.1. General test arrangement

The T.F.A. Carrier Converter<sup>127</sup>, which consists of the electronic modulator and demodulator described in the

Sub-sections 8.2.1 and 8.2.2 above, and which is primarily designed to be used in conjunction with the Solartron Transfer Function Analyser for testing a.c. or carrier systems, was employed as a test-specimen for testing the performance of the proposed scheme.

The first experiment was designed to obtain the transmission characteristics of the Carrier Converter alone. The test signal is obtained from the L.F. decade oscillator<sup>128</sup> which feeds the modulator section of the Carrier Converter. The side-band output from the modulator is directly connected to the side-band input of the demodulator. The output from the demodulator is then fed to the Resolved Component Indicator<sup>129</sup> which is capable of displaying the in-phase and quadrature components of only the fundamental with respect to the reference test signal. The Reference Resolver is inserted in the four-phase reference connection between the reference source and the Resolved Component Indicator thereby giving an identical and controlled phase shift to each of the four reference phases. Thus, the reference phase can be shifted to give an output test signal indication in the in-phase quadrant of the reference meter only. The response information is then available in the form of a signal amplitude and a phase shift. By varying the frequency of the test signal and taking the readings from the Reference Resolver and the Resolved Component Indicator, the response diagram can easily be plotted.

The second experiment was designed to obtain the transmission characteristics of the Carrier Converter when compensated by the proposed scheme. Fig. 8.5.1 shows the method of inter-connection of the instruments for measuring the overall response, under this condition of operation, in terms of the phase shift and attenuation of the modulating signal. It was observed that the incorporation of the scheme has

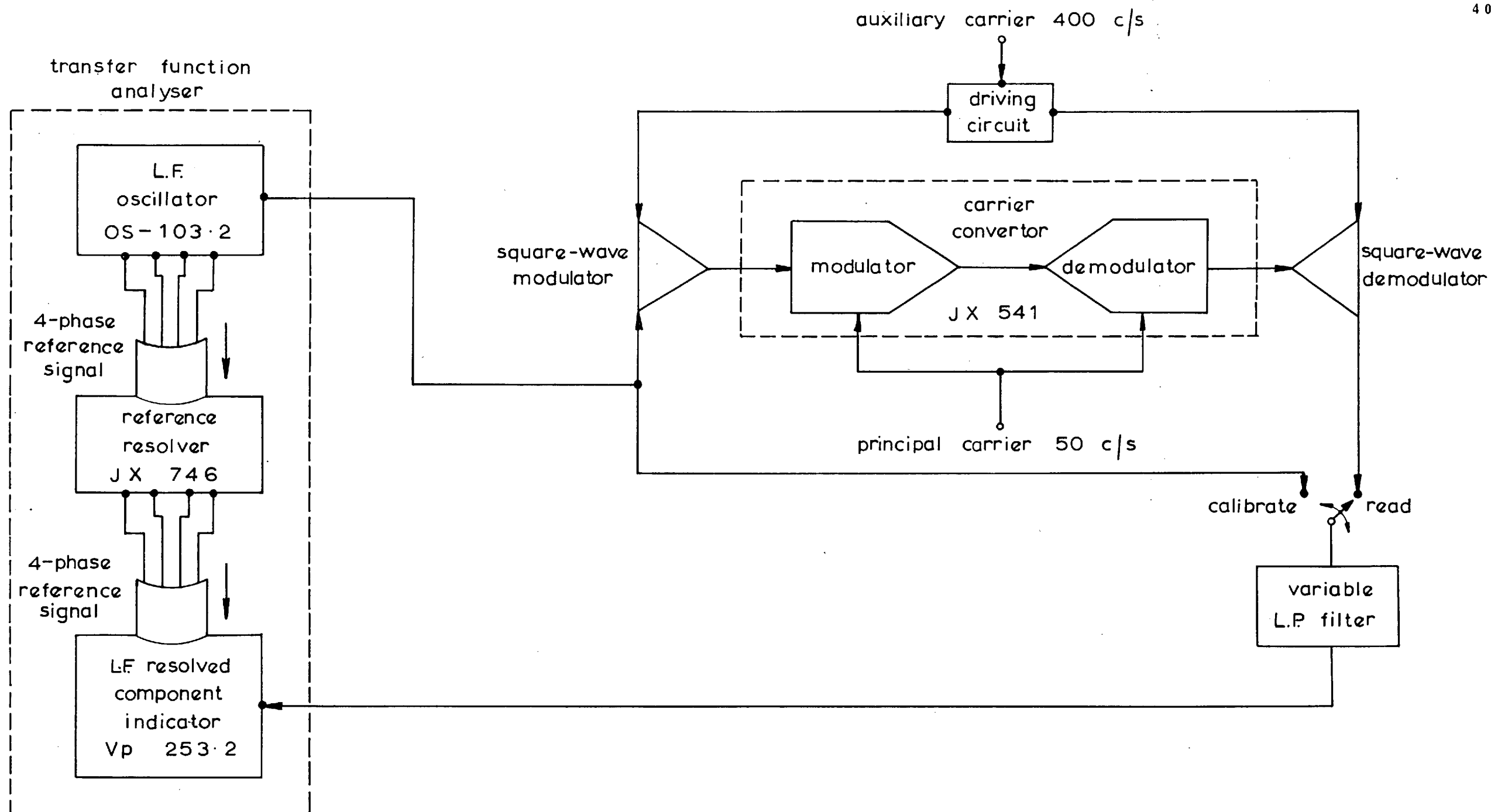


FIG. 8.5.1.

TEST ARRANGEMENT FOR MEASURING THE CARRIER CONVERTOR RESPONSE WHEN COMPENSATED  
BY THE PROPOSED SCHEME

resulted in an increased noise level of the output signal. This has raised two problems:

- i) The excess noise of the output signal might cause overloading and subsequent damage of the delicate thermocouple elements associated with the meters of the Resolved Component Indicator.
- ii) The various signal amplifiers, preceding the bridge connected thermocouple meters of the Resolved Component Indicator, might be driven to saturation by the high noise components of the signal giving rise to distortion and inaccurate results.

To provide a solution to the above problems, it was necessary to insert a variable low-pass filter just before the Resolved Component Indicator. However, to compensate for the attenuation and phase shift of the signal fundamental introduced by the filter presence, identical filters should be incorporated in each reference channel. An alternative way, which was used in the laboratory, is to measure the effect of the filter at every test signal frequency by setting the switch on the "Calibrate" position so that the test signal may directly be applied to the filter and its attenuation and phase shift with respect to the reference are thus recorded. Setting the switch on the "Read" position will enable the overall attenuation and phase shift of the signal including those due to the filter to be measured. In this way, the phase shift and attenuation of only the work under test can be easily deduced from the results of the two successive tests by merely subtracting the phase shifts and calculating the relative magnitude.

According to the proposed scheme, each of the commercial electronic modulator and demodulator would require to incorporate a square-wave modulator and a demodulator. In

the above test, however, the square-wave demodulator associated with the commercial modulator and the square-wave modulator associated with the commercial demodulator would be directly connected in tandem. As the transference of the square-wave demodulator and modulator connected in this manner is unity, they have been dispensed with.

### 8.5.2 Comparison of the results.

The above tests were carried out with a principal carrier frequency of 50 c/s and an auxiliary carrier frequency of 400 c/s. The results obtained are so arranged to give normalised gain and phase shift. These are conveniently plotted versus normalised frequency, with  $\Omega_p$  as the base frequency, as shown in Figs. 8.5.2 and 8.5.3 respectively.

From the normalised gain curves of Fig. 8.5.2, it is observed that when the compensating scheme is not incorporated amplitude attenuation occurs in the frequency band lying between the frequencies  $0.8 \Omega_p$  and  $1.2 \Omega_p$ . The attenuation curve is almost symmetrical around the principal carrier frequency and it changes in such a way that the closer the frequency to the principal carrier frequency the larger is the attenuation. To give a quantitative idea, the attenuations corresponding to the frequencies  $0.96 \Omega_p$  and  $1.04 \Omega_p$  are 12% and 33% respectively. By incorporating the compensating scheme, however, there is almost no change in the gain except in a very narrow frequency band of about  $0.1 \Omega_p$  width lying just below the principal carrier frequency where a slight attenuation has been detected. The maximum attenuation in this region is only 3%.

Referring to the carrier convertor phase response shown in Fig. 8.5.3, if the compensating scheme is not employed, phase shift would take place throughout the frequency range lying above the frequency  $0.15 \Omega_p$ . In the frequency region

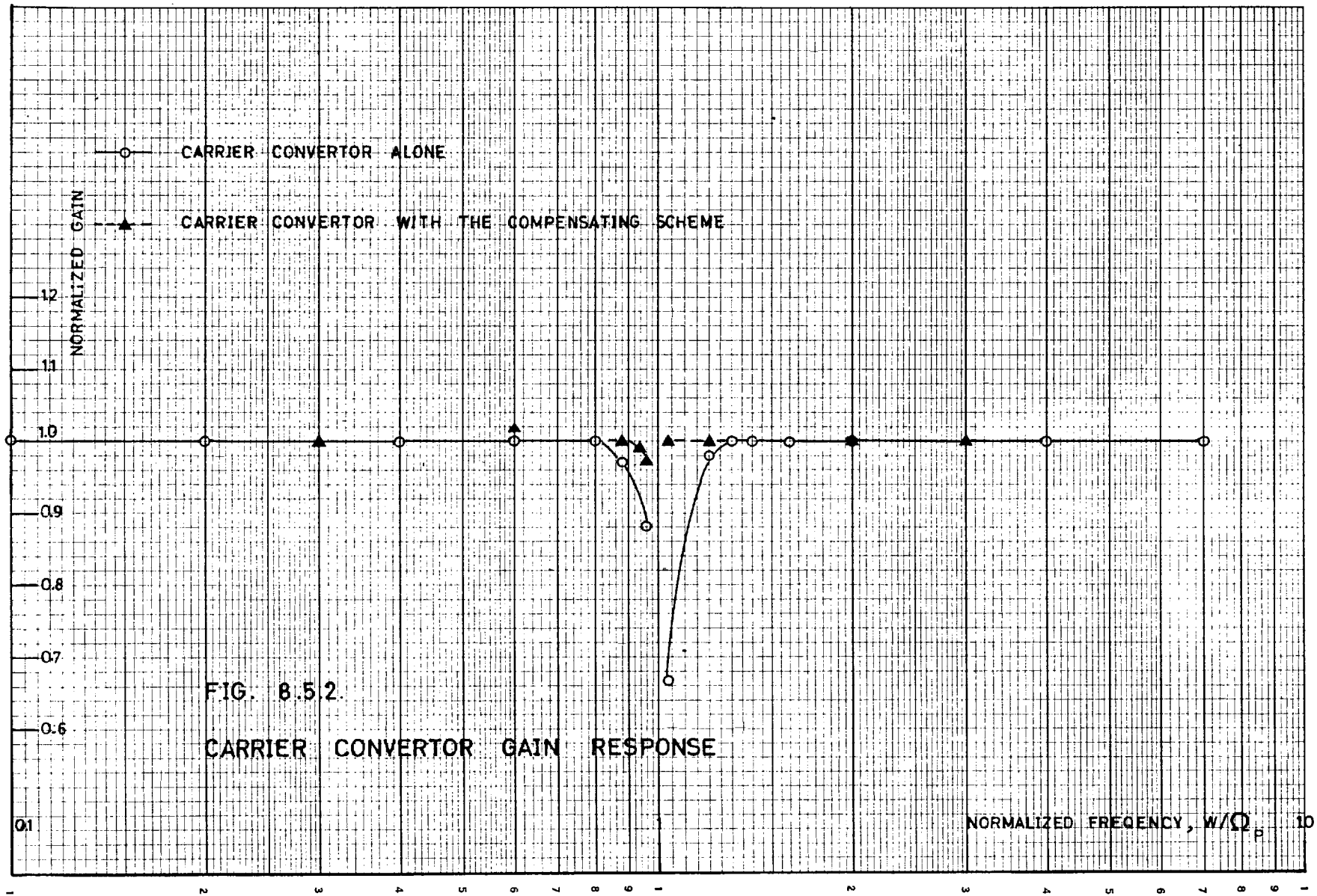
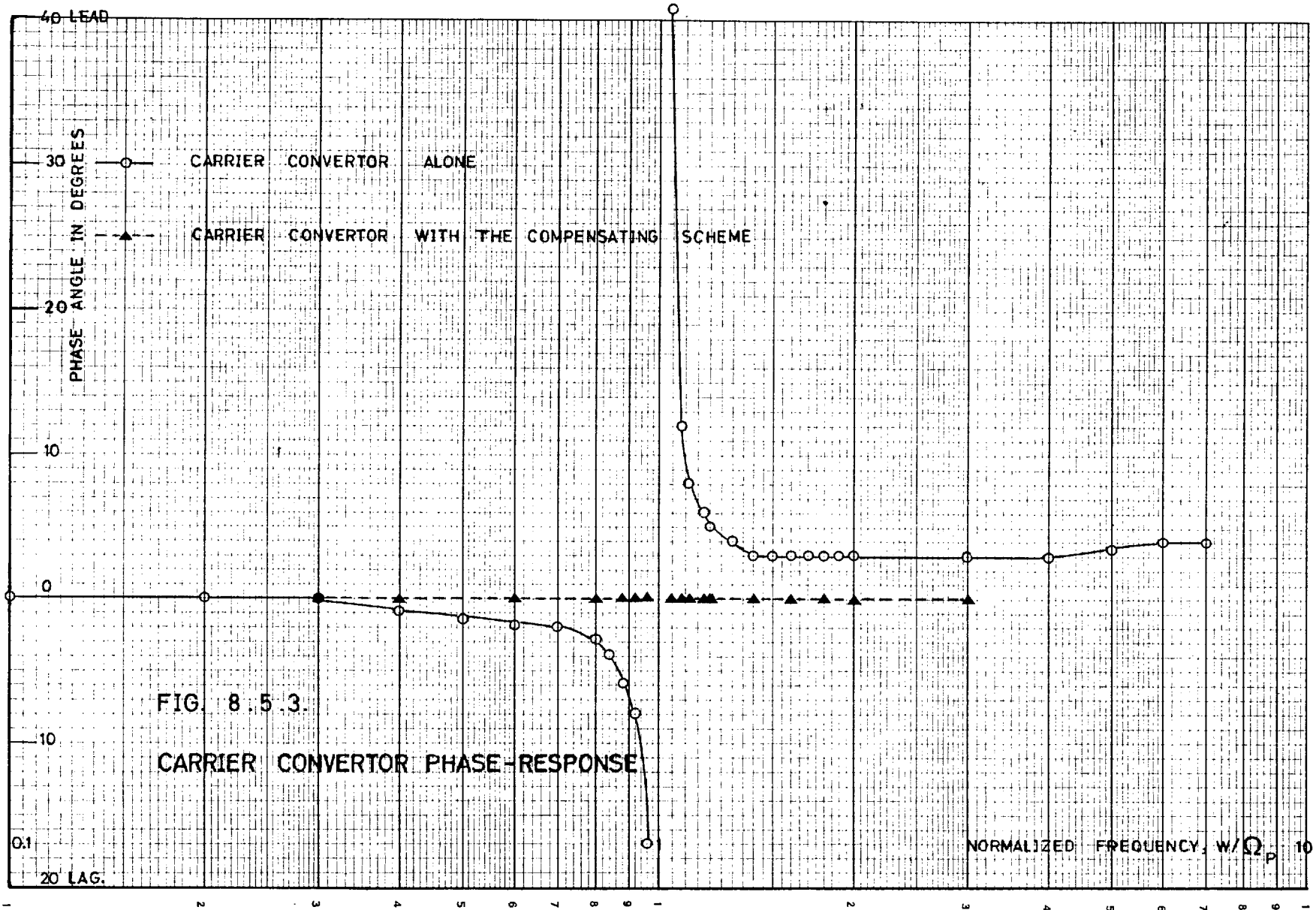


FIG. 8.5.2  
CARRIER CONVERTOR GAIN RESPONSE





lying between  $0.15\Omega_p$  and  $\Omega_p$ , the phase shift first increases slowly with frequency to reach the value of 2 degrees lag at the frequency  $0.7\Omega_p$ , then it increases more rapidly to reach the value of 14 degrees lag at the frequency  $0.96\Omega_p$ . In the frequency region lying immediately above the principal carrier, the phase shift starts with a very high value of 41 degrees lead at the frequency  $1.04\Omega_p$  and it drops sharply to about 3 degrees lead at the frequency  $1.5\Omega_p$  beyond which it remains almost constant.

On applying the compensating scheme, however, no phase shift is observed throughout the investigated frequency band of  $3\Omega_p$  which has been chosen to be conveniently lower than the employed auxiliary carrier frequency.

Although the above results show clearly and decisively the practicability of the proposed scheme, it still remains the problem of reducing the excessive noise generated when such a scheme is incorporated into the carrier converter. A thorough study of this problem is therefore proposed as a further work. However, the following points are hoped to throw some light on the future lines of thought:

- i) There is a possibility that the switching transistors employed in the square-wave modulators and demodulators are not fast enough giving rise to such noise. If this is the case, replacement of these transistors by a faster type would provide the required solution.
- ii) The switching instances in the square-wave modulator and demodulator may be deliberately misaligned to counteract any possible phase shift which may take place in the various circuits incorporated in the commercial modulator (or demodulator). This misalignment can be easily adjusted by the driving circuit of the synchronous switches (see Section I.5).

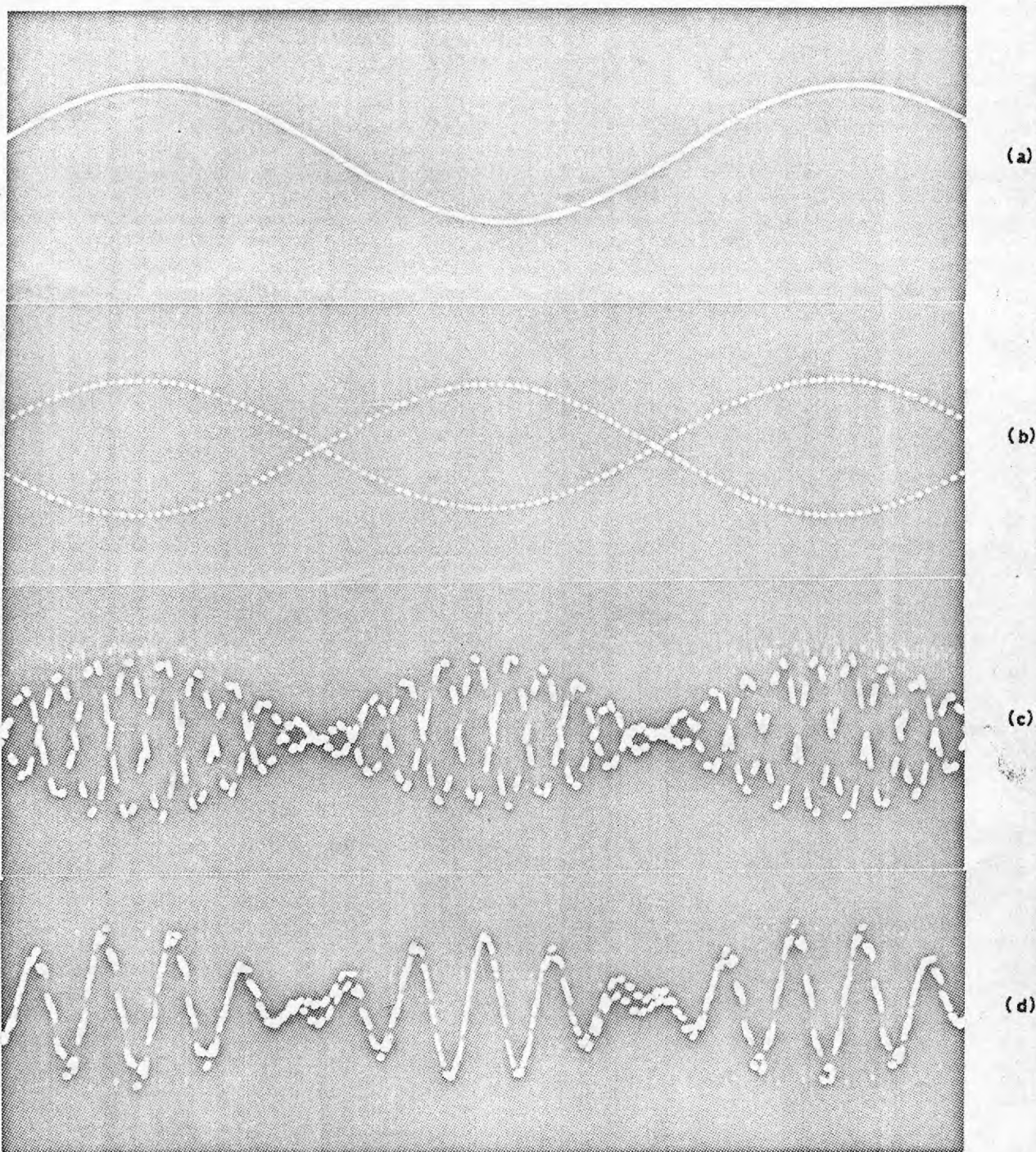
iii) Although, according to Sub-section 8.4.1, there are several possible positions where the square-wave modulators and demodulators can be incorporated into the commercial modulators and demodulators, only one position was attempted during the above test due to lack of time. It is, therefore, worthwhile to attempt the other positions to see which one provides the minimum noise.

### 8.5.3 Oscillograms illustrating the principle of operation of the scheme

In order to visualise even more the operation of the scheme, oscillograms of the signal at various points of a commercial modulator compensated by such a scheme have been obtained. These oscillograms are reproduced in Fig. 8.5.4 where:

- i) oscillogram "a" shows a sinusoidal input signal at a frequency of 5 c/s.
- ii) oscillogram "b" shows the signal after being modulated upon an auxiliary square-wave carrier whose frequency is 400 c/s.
- iii) oscillogram "c" shows the signal after being modulated, for the second time, on to a sinusoidal principal carrier of 50 c/s to form a double modulated signal.
- iv) oscillogram "d" shows, apart from the high noise components which may be attributed to the switching action in the square-wave modulator and demodulator, a suppressed carrier amplitude modulated wave with the 5 c/s as the envelope of a 50 c/s carrier.

b) SIGNAL (a) MODULATED ONTO A SQUARE-WAVE CARRIER OF 400 C/S



c) SIGNAL (b) MODULATED ONTO A SINUSOIDAL CARRIER OF 50 C/S

d) SIGNAL (c) DEMODULATED BY THE SQUARE-WAVE CARRIER (400 C/S), RESULTING INTO A SCAM. WAVE WITH ENVELOPE AT 5 C/S, CARRIED ON THE SINUSOIDAL CARRIER OF 50 C/S

FIG. 8.5.4. WAVE-FORM OSCILLOGRAMS OF SIGNALS APPEARING AT VARIOUS POINTS ALONG AN ELECTRONIC MODULATOR COMPENSATED BY THE PROPOSED SCHEME

## CHAPTER 9

### CONCLUSIONS

#### 9.1. Review and summary of work done

1. Despite the numerous advantages of a.c. servomechanisms over the d.c. servomechanisms, the scope of their development has been so far much limited in contrast with that of the d.c. systems. This has been mainly due to the presence of certain problems associated with the a.c. systems, which made the application of more refined and systematic methods to their design to retard behind similar applications to d.c. systems.

In Chapter 1, the various salient problems associated with the a.c. servomechanisms were formulated, which may be summarised in the following points:

- i) The lack of accurate and simple description to the performance characteristics of the basic a.c. systems components,
- ii) Difficulties associated with the realization of appropriate a.c. compensation designed to operate on the envelope of a modulated signal,
- iii) The presence of practical limitations in some of the available equipment employed to test the modulation frequency response of a.c. control systems.

An historical review provided the background on which basis improved solutions to the aforementioned problems have been propounded in the present thesis. It has also helped.

in determining the areas where further development is demanded, to which the present work has contributed by exploiting new concepts, and by amplifying and expanding the application of well known principles. All these factors have provided sufficiently powerful incentives to the present studies underlying the modulation transfer functions of a.c. servo-mechanism components.

2. The behaviours of 2-phase servomotors and synchro systems have been analysed by a number of investigators in the past. Most of this previous work is based on so many simplifying assumptions, which resulted in approximate and unrealistic representations with very limited value to the servo designer.

In Chapter 2, rigorous analysis has been attempted for these basic components based on the application of the 2-axis general theory of machines with more realistic assumptions. Simple but accurate block diagram representations for both the 2-phase servomotor and synchro-pair were then developed, the construction of which can be done easily and systematically without the need of going into the details of the elaborate mathematical operations. These block diagrams are particularly useful to the servo designer, not only because they provide accurate and simple descriptions to the behaviour of the basic a.c. system components, but also because they allow the available techniques of block diagram manipulation to be applied, and enable both the analogue and digital computers to be exploited in performing various studies.

It has been emphasised that the basic a.c. system components, in which either a modulation (as in the case of the synchro-pair error-detector) or a demodulation process

(as in the case of 2-phase motor) takes place, cannot be represented individually by explicit open-loop transfer functions because of the fact that the associated input and output signals are of different form. It has been shown, however, that by combining these components together to form the closed-loop system, it is possible to obtain an overall open-loop and closed-loop modulation transfer functions, in which the contributions of the various components are in implicit form, provided that the effect of the generated noise is neglected.

One of the major advantages of the system of equations derived and the block diagrams developed for representing the 2-phase servomotor and the synchro-pair error-detector stems from the fact that they are adaptable, such that, the effects of other associated components, such as compensating devices, can be easily included. Furthermore, they are presented in such form that permits investigation into the effects of variations in the carrier-frequency, carrier-phase, electrical parameters, and mechanical parameters on the system performance to be easily carried out.

The analysis outlined is based on linearized conditions realised by generally accepted simplifying assumptions. However, it provides a basis on which extensions and modifications could be made to account for the non-linearities resulting from the gear backlash and coulomb friction, and to include the effects of the high harmonic components generated by the modulation-demodulation process.

3. Compensation techniques play an important role in the design of servomechanisms as a means of modifying the systems performance characteristics either for the stability purposes or for improvement of the overall static and

dynamic performances to meet specified requirements. Each of these techniques has its advantages as well as its limitations, which appear with different proportions depending on the type of application. It is necessary for the servo designer to acquire a thorough knowledge of all the available compensating methods in order to have a wider freedom of choice, and thus be able to apply the most suitable method to his particular application. The main object of the work presented in Chapter 3 was to eliminate or reduce the limitations associated with a.c. tachometers and tandem linear networks as two types of a.c. compensation.

The space and weight restrictions of a.c. tachometers are of profound importance particularly in air-borne applications, but are not the immediate concern of the present work. Even of comparable importance is the need of provision of accurate description to their behaviour particularly when they are employed to compensate instrument and analogue computers servos. A rigorous analysis has, therefore, been attempted using the 2-axis general theory of machines. From the analysis, comprehensive and accurate block diagram representation for the a.c. tachometer was deduced, which can be easily integrated with the corresponding block diagrams of the 2-phase servomotor and synchro-pair error-detector to form the overall block diagram representing the compensated a.c. system.

In some applications of the a.c. servomechanisms, such as instrument servos, where the carrier frequency is sufficiently stable, linear electrical networks can be considered the most superior type of compensation almost in every aspect. The available synthesis techniques<sup>46-62</sup> for such networks, however, when operating on modulated signals, do not seem to form a systematic general approach, and still



depend largely on experience and intuition of the designer. This has led to a slow progress in this field. A novel synthesis method has, therefore, been developed in Chapter 3, based on the derivation of the transfer function from the specified modulation transfer function and then applying the conventional linear network synthesis techniques to the resulting transfer function. The processes of obtaining the transfer function from a specified modulation transfer function and vice versa have been explained in simple terms by means of time-domain mathematical models and complex-frequency-domain block diagrams, and the two processes have been shown to be reversible if the high harmonic components were neglected. Similar processes have been developed for rotary modulated systems which enabled the synthesis method, with small modifications, to be applicable to such systems. The synthesis method presented is apparently more general and flexible than those previously attempted with no limitations more than those inherent in the conventional theories of linear network synthesis.

4. In some applications of a.c. servomechanisms, particularly common in air-borne control systems, where the need to keep the physical weight and size of the system to minimum prevents the use of suitable frequency regulating equipment; the carrier frequency fluctuates considerably. Under such condition of operation, chopper networks have recently emerged as most superior type of compensation. The author had a considerable interest in this type of network and a proportional part of this thesis was thus devoted to the promotion of previous ideas and propounding new developments in its various aspects with the object of securing a wider scope of application and new exploitations.

In this respect, Chapter I has established the feasibility of constructing widely controlled fly-time 3-terminal synchronous switches which form basic elements in chopper networks structures. It has been shown that switches capable of operation with positive fly-time and negative fly-time are physically realizable. A superior circuit employing switching transistors driven by pulse-transformer has been described and its dynamic behaviour has been analysed. Design criteria, which determine the limits of validity of various parameters, have been laid down. A simple design procedure for 3-terminal synchronous switch and an appropriate driving circuit has been outlined and demonstrated by an illustrative example.

The physical realizability of synchronous switches with such wide operational capabilities can only lead to new developments. Some of these possibilities have been expounded in the conclusions of Chapter I.

5. In Chapter II, it has been shown that, by breaking the 3-terminal synchronous switch into its most elementary form of 2-terminal switch, applying the duality concept, then reconstructing into a new 3-terminal switch, the positive fly-time switch is the dual of the negative fly-time switch. This result has led to the development of systematic techniques whereby the dual of chopper networks of complicated configurations can be easily constructed.

It has been shown that, by applying the duality concept, Thevenin's and Norton's theorems, derivation of physically dissimilar chopper networks with identical responses can be realized. This can result in substantial economy in computational effort since the analysis of only one chopper

network gives the behaviour of its equivalent ones. Freedom in selecting either voltage or current forms for excitation and response signals of various chopper networks is envisaged to lead to increased flexibility in many applications. Although the analysis presented was limited to chopper networks comprising only two electrical passive elements RC or RL, however, it lays down the foundation for further development of more elaborate configurations involving the three passive elements RLC.

It has also been shown that modified responses of various chopper networks can be realized not only by varying the values of the incorporated passive elements but also by:

- i) modifying the structure of the chopper network by utilizing additional number of synchronous switches which may be connected in different ways.
- ii) varying the fly-time of the incorporated synchronous switches over its positive range as well as its negative range.
- iii) making use of operational amplifiers and transformers for adding or subtracting proportional quantities of the input and any particular output of the chopper network.

The work described in Chapter II was originally suggested by Professor D.G.O. Morris, D.Sc., F.I.E.E., to whom the author is deeply grateful.

6. All previous attempts<sup>88-111</sup> to analyse chopper networks have virtually resulted into approximate methods. The application of these approximate analysis were usually

confined to a few number of chopper networks with very simple configurations which are, in turn, treated under restricted operating conditions. In some cases<sup>89,90,94,97,98,108,110</sup>, few experimental results were given for very special cases which neither provide sufficient assessment to the approximations involved nor determine their limits of validity under various modes of operation.

A portion of Chapter 4, has, therefore, been devoted to reformulation of an approximate method of analysis developed in the past<sup>97-99</sup> in order to extend its application to more general and complex configurations of chopper networks. The analysis is based on determining an equivalent time-invariant passive network whose transmission characteristics with respect to the unmodulated data is approximately similar to the transmission characteristics of the chopper network with respect to the carrier-modulated data. Consequently, the modulation transfer function of the chopper network can be obtained simply as the transfer function of the equivalent d.c. network.

In the same Chapter, an exact analytical approach has been also presented free from all the aforementioned limitations. The method makes use of the Z-transform and the modified Z-transform techniques in order to automatically compute the voltage appearing across the switched capacitors which, in turn, enables the initial conditions to be accounted for at each switching instant. The mathematical processes have been explained in simple terms and accompanied by comprehensive block diagrams. Although the expression obtained for the modulation transfer function is in the form of complicated infinite series, a mathematical method has been developed whereby a closed form expression

can be derived. It has been shown that this method of analysis provides the means for evaluating the noise components generated within the chopper network which cannot be done by the approximate method. Furthermore, by minor modifications, it has been shown feasible to extend the application of the exact analysis to cover the case of chopper networks subject to rotary modulation signals. No similar modifications seem to be possible to be applied to the approximate analysis.

The applications of both the exact and approximate analysis have been demonstrated on three types of RC chopper networks:

- i) Single-switch double-capacitor,
- ii) Double-switch single-capacitor,
- iii) Cascaded inverted double-switch double-capacitor.

where the analysis for networks (ii) and (iii) are given in Appendices B and C respectively.

7. In Chapter 5, extensive practical studies have been performed on a representative selection of chopper networks under various modes of operation, which helped in checking the validity of the theoretical methods of analysis, and in determining the limitations associated with the approximate analytical approach. The investigations performed have been primarily concerned with the determination of the effects of the various parameters and modes of operation on the modulation frequency responses of the chopper networks when excited: firstly, by a suppressed-carrier amplitude-modulated (S.C.A.M.) wave, and secondly, by a rotary modulated (R.M.) wave. The various studies carried out are enumerated below:-

- a) Chopper network excited by S.C.A.M. wave
  - i) Variation of the passive electric elements
  - ii) Variation of the fly-time of the synchronous switches
  - iii) Deviation of carrier frequency
  - iv) Variation of the phase of the demodulation carrier reference
  - v) Variation of the phase of the modulation carrier reference
  - vi) Simultaneous change in the phases of modulation and demodulation carrier references.
- b) Chopper network excited by R.M. wave
  - i) Variation of the phase of the demodulation carrier reference
  - ii) Change in carrier frequency.

Comparing the experimental results with the theoretical predictions calculated by both the exact and approximate methods has shown that, on the whole, the former method is more accurate and reliable than the latter method. The divergence of the results of the approximate method from those obtained experimentally has been found to become even more predominant under the modes of operation assigned above by (iv), (v), and (vi). Further limitations associated with the approximate analysis lie in the fact that it cannot be modified to calculate either the rotary modulation response or the noise components of the chopper networks as it is possible with the exact analysis. All these findings have led to the conclusion that the numerous advantages of the propounded exact analysis over its approximate counterpart convincingly outweigh its relative complexity.

8. To enable the study of the stabilizing properties of chopper networks when cascaded in the forward path of a practical a.c. servomechanism employing 2-phase servomotor under various modes of operation, a breadboard model of a positional control a.c. system was designed and constructed in the Laboratory. Chapter 6 outlines a brief account of the design details of the various components with greater emphasis placed on the description of a suitable servo-amplifier employing transistors. In the same chapter, preliminary tests have been carried out on the transmitter-coincidence transmitter mag-slip error-detector to determine the relevant parameters whose knowledge is necessary in conducting the various full-scale tests on the complete a.c. model. As a byproduct, the results from these tests have, within certain limits, verified the validity of the theoretical expressions derived earlier in Section 2.3.

9. Extensive studies have been carried out on the positional control a.c. system model to investigate its performance characteristics for both with and without chopper network compensation, and to study the effects on these characteristics brought out by the following factors:

- a.) variations in the carrier frequency,
- b.) misalignment between the phases of the modulation and demodulation reference carrier excitations.

The tests conducted are in the form of modulation frequency response and transient response, whose techniques have been discussed in detail in Chapter 7. Inferences based on the studies performed on the a.c. system model are summarised below.

- i) The effects of carrier frequency variations on the

uncompensated system performance have been found to be, to a certain extent, similar to those which can be caused by loop-gain variations; since the increase of any of them would result in phase-margin reduction and in gain-margin increase, and vice versa. Therefore, to compensate for such effects, it was proposed to insert a low-pass filter in the reference carrier excitation circuit of either the 2-phase servomotor or the error-detector. Such filter, being sensitive to the carrier frequency, will automatically reduce the exciting reference voltage as the carrier frequency increases, and vice versa.

- ii) Deliberate adjustment of the phase misalignment between the reference carrier excitations to the 2-phase servomotor and the error-detector can be used to advantage.
- iii) The effectiveness of the chopper networks as good stabilizers to practical a.c. systems has been assessed, and the characteristics obtained are in conformance with the results presented in Chapter 5 where the chopper networks were tested under ideal conditions.
- iv) Because of the phase shifts taking place in the reference windings of the 2-phase servomotor and the error-detector, a phase misalignment may occur between the modulation and demodulation carrier references, even though the carrier excitations to the servomotor and error-detector were phase aligned. Such phase misalignment has a considerable influence on the chopper networks modulation characteristics, and can cause serious deterioration



to their stabilizing properties when it exceeds a certain value depending on many factors. If this phase misalignment is constant, it is possible to compensate for it by a fixed phase misalignment between the carrier excitations to the servomotor and error-detector. However, such phase misalignment is expected to be varying in the event of employing unstabilized carrier frequency source; since the phase shifts effected in the 2-phase motor and the error-detector are frequency dependent. Under this condition, automatic control for the phase misalignment between the carrier excitations to the servomotor and error-detector is necessary in order to obtain continuous compensation. Auxiliary control systems may be employed for this purpose. However, the simplest means envisaged is to insert two low-pass filters in the carrier excitation circuits of the servomotor and error-detector. Designing these filters properly would provide automatic compensation not only for the phase misalignment between the modulation and demodulation carrier references, but also for the change in the performance characteristics of the uncompensated system (as mentioned in (i) above) due to fluctuations in the carrier frequency.

10. Electronic modulators and demodulators play a significant role in testing the modulation frequency responses of a.c. control systems. However, for practical reasons, accurate and reliable results obtained by the available commercial types of these equipment are only guaranteed for modulating frequencies not exceeding 10% of the carrier frequency. This limits the range of the modulation frequency

response obtainable experimentally to only a small value, which may, in some cases, provide insufficient information for the design purposes.

In Chapter 8, these operational limitations have been explained in terms of the distortions which may occur in transmitting modulated signals through the incorporated circuits and amplifiers with non-flat frequency characteristics. On this basis, a simple scheme has been developed to extend the modulating frequency range of conventional electronic modulators and demodulators, which can be easily integrated into them without any modification to their basic circuitry. The principle of operation of the proposed scheme is based on shifting the frequency of the sidebands of the modulated signal to a sufficiently high level to avoid the non-flat portion of the frequency characteristics of the various circuits and amplifiers. After passing through these circuits without distortion, the frequency level of the sidebands is then shifted back to its original value. Such operations have been accomplished by modulating the sidebands on to an auxiliary carrier (whose value is higher than the principal carrier), passing through the various circuits and amplifiers, then demodulation by the auxiliary carrier to recover the original sidebands. Useful criteria have been laid down whereby the suitable value of the auxiliary frequency can be determined.

Square-wave modulator and demodulator have been designed and constructed in the Laboratory in order to realize the required operations of the scheme. They were then incorporated into a Laboratory electronic modulator-demodulator unit to test the practicality of the scheme. The results obtained have shown a marked improvement to the working range of the modulation frequency of the unit under

test. Oscillograms illustrating the principle of operation of the scheme have been also presented.

It was stressed, however, that the proposed scheme still suffers from the disadvantage of generating noise; and some proposals have been put forward to reduce its level.

## 9.2. Suggestions for further work

1. The mathematical models and block diagrams representations describing the behaviour of the basic a.c. servomechanism components, developed in Chapter 2, should provide the servo designer with the basis upon which more refined and systematic design procedures could be applied to a.c. control systems in parallel with those already available for d.c. systems. Although the validity of the theoretical analysis presented is adequately convincing, some practical check is still demanded, and careful assessment of the involved simplifying assumptions is still lacking. Further work would, therefore, be mainly concerned with filling these two gaps.

A comparison could be made, in terms of the modulation frequency response and transient response of an a.c. control system, between results obtained from a breadboard model (as outlined in Chapter 7) and results obtained from either analogue or digital computer on which the mathematical models and block diagrams representations are simulated. The various principal parameters associated with these mathematical models and block diagrams can be easily measured by appropriate laboratory tests on the breadboard model components.

2. In the present work, the analysis of only one

structure of synchros, arranged as transmitter-coincidence transmitter synchro-pair, based on the 2-axis general theory of machines, has been outlined. However, it lays down the foundation for similar analysis to be attempted, whereby the performance characteristics of other configurations and arrangements of synchro or magslip systems can be accurately described and easily represented. Some of the magslip systems where such analytical approach should be deployed are enumerated below:

- i) Magslip hunter system: particularly suitable for hydraulic servo systems. Arranged in the form of transmitter, resetting transmitter, and hunter.
- ii) Follow-through magslip system: suitable for summation of mechanical movements. Arranged in the form of transmitter, follow-through transmitter, and receiver.

3. A general synthesis procedure for realizing specified multiplicative and rotary modulation transfer functions by linear networks has been developed in Chapter 3. The practical application of this method, however, has not been attempted, and is thus suggested for future work. To systematize its application, realizability criteria should be first established. Also the practical limitations associated with the propounded synthesis method still remain to be determined.

4. By establishing the duality between positive and negative fly-time 3-terminal synchronous switches, it was possible to extend the application of the duality concept to chopper networks as has been shown in Chapter II. Applying the duality concept in conjunction with Thevenin's

and Norton's theorems then enabled the derivation of physically dissimilar chopper networks but with equivalent response. The ideas involved should be suitable for developing general techniques for synthesising RLC chopper networks comprising a combination of positive fly-time and negative fly-time synchronous switches; thereby realizing a wide variety of modulation response which would considerably increase the scope of chopper networks applications.

5. The superiority of chopper networks over other types of a.c. compensation, in terms of insensitivity to carrier frequency, physical size, weight and cost, are now widely recognised. However, due to the switching mechanism involved, chopper networks generate noise which would cause undesirable heating to the control windings of the 2-phase servomotors. A thorough study of the noise content is therefore needed in order to find the ways of minimising it. In Section 4.2.7, suitable formulae have been derived for evaluating the noise content. Such an assessment of the noise is envisaged to be very useful in establishing one of the important criteria for selecting the suitable type of chopper network.

6. In the studies performed on the breadboard a.c. servomechanism model (Chapter 7), the effects of carrier frequency variations on the performance characteristics of the uncompensated system have been shown to be similar to those due to loop-gain variations. It has been proposed that by inserting a low-pass filter in the reference carrier excitation circuit of either the 2-phase servomotor or the error-detector, automatic compensation for such effects could be achieved. It would be worthwhile to pursue studies along these lines.

It has been also shown that fluctuations in carrier frequency would result in phase misalignment between the modulation and demodulation carrier references, which may lead to some detrimental effects on the stabilizing capabilities of chopper networks. Insertion of two low-pass filters in the carrier excitation circuits of the servomotor and the error-detector has been suggested as a possible means of automatic compensation not only for the phase misalignment but also for the change in the performance characteristics of the uncompensated system. The feasibility and practical limitations of such compensating scheme require further study.

7. Because of the practical limitations associated with the available electronic modulators and demodulators, a suitable scheme has been described in Chapter 8, which, on being incorporated into these electronic modulators and demodulators, are capable of extending their working range of the modulation frequency. Although the practicability of the scheme has been established, more work is still needed to reduce the level of the noise introduced. Section 8.5.2 outlines some possible modifications to the scheme which may be considered as helpful guidance to future work in this field.

BIBLIOGRAPHY

1. MORRIS, D.G.O. "A Theoretical and Experimental Method of Modulation Analysis for the Design of A.C. Servo-Systems". Automatic & Manual Control, Editor, A.Tustin, Butterworths Scientific Publications, 1952.
2. SMITH, O.J.M. "Feedback Control Systems", (book), McGraw-Hill, 1958.
3. BJOMSON, George, M. "Network Synthesis by Graphical Methods for A.C. Servomechanisms". Trans. A.I.E.E., Vol. 70, Pt. 1, pp.619-625, 1951.
4. STANLEY, H.C. "An Analysis of the Induction Motor", Trans. A.I.E.E., 57, p.751, 1938.
5. KOOPMAN, R.J.W. "Operating Characteristics of 2-phase Servo-Motors", A.I.E.E., Vol. 68, Pt.I, p.319, 1949.
6. BOND, C.G. "The Two-Phase Servo-Motor". Control, Vol. 4, No. 37, p.91, 1961.
7. BROWN, G.S., and CAMPBELL, D.P. "Principles of Servomechanisms". (book), Wiley, 1950.
8. BROWN, Lloyd, O. "Transfer Function of the Two-Phase Servo Induction Motor". A.I.E.E., Vol. 70, Pt.II, p.1890, 1951.
9. HOPKIN, A.M. "Transient Response of Small Two-Phase Motors". A.I.E.E., Vol.70, Pt.I, p.881, 1951.
10. CHANG, S.S.L. "Transient Analysis of A.C. Servomechanisms". A.I.E.E., Pt.II, Vol.74, p.30, 1955.
11. MIKHAIL, S.L., and FETT, G.H. "Transfer Function of a Two-Phase Servo-Motor". A.I.E.E., Vol.77, Pt.II, p.97, 1958.

12. KUTVINOV, V.G. "On the Transfer Function of an Asynchronous Two-Phase Motor", Automatic & Remote Control, Vol. 20, No. 7, 1959.
13. CONNELLY, D. "The Two-Phase Induction Motor Used as a Servo-Motor". Proc. I.E.E., Vol. 107A, p.366, 1960.
14. HESMONDHALGH, D.E., and LAITHWAITE, E.R. "Method of Analysing the Properties of Two-Phase Servo-Motor". Proc.I.E.E., Vol. 110, No.11, p.2039, 1963.
15. LHOPE, F. "Generalized Transfer Function of a 2-phase Asynchronous Servo-Motor". C.R. Acad.Sci., 258 (5), pp.1444-1446, 1964.
16. WEST, J.C., et.al. "Analysis of Dynamic Performance of Induction Motors in Control Systems". Proc. I.E.E., Vol. 111, No. 8, Aug. 1964.
17. HUGHES, F.M., and ALDRED, A.S., "Transient Characteristics and Simulation of Induction Motors", Proc. I.E.E., Vol. 111, No. 12, December 1964.
18. LAW, J., and SCHMITZ, N.L. "Transient Response Characteristics of an A.C. Servo-Motor Excited Non-Sinusoidally and through Non-linear Source Impedance". I.E.E.E., Trans. Power Appar. & Sys., 83 (6), pp.584-588, June 1964.
19. WILSON, D.R. "A.C. Servo-Systems with Particular Reference to Chopper Network Stabilization". A Thesis presented to the Victoria University of Manchester, 1964.
20. ROGERS, G.J. "Linearised Analysis of Induction-Motor Transients". Proc. I.E.E., Vol. 112, No.10, October 1965.



21. HESMONDHALGH, D.E., and DRIVER, K.L. "Design of the A.C. Servo-Motor". Proc.I.E.E., Vol. 113, No. 10, October 1966.
22. TRUXAL, J.G. "Control Engineers Handbook". McGraw-Hill, 1958.
23. IVEY, Keith,A. "A.C. Carrier Control Systems", (book), John Wiley & Sons, Inc., 1964.
24. McDONALD, D. "Electromechanical Lead Networks for A.C. Servomechanisms". Review of Scientific Instruments, Vol. 20, pp.775-779, November 1949.
25. McDONALD, D. "Improvements in the Characteristics of A.C. Lead Networks for Servomechanisms", Trans. A.I.E.E., Vol. 69, Pt.1, pp.293-300, 1950.
26. COSGRIFF, R.L. "Integral Controller for use in Carrier-Type Servomechanisms". Trans. A.I.E.E., Vol. 69, Pt. 2, pp.1379-1385, 1950.
27. TRUXAL, R.J. "Automatic Feedback Control System Synthesis". McGraw-Hill Book Co., Inc., 1955.
28. HALL, A.C. "Damper Stabilized Instrument Servomechanisms". Trans. A.I.E.E., Vol. 68, Pt.I, pp.299-306, 1949.
29. FRAZIER, R.H. "Analysis of Drag-Cup A.C. Tachometer by means of Two-Phase Symmetrical Component". Trans. A.I.E.E., Vol. 70, Pt.I, pp.1894, 1951.
30. FRAZIER, R.H. "Drag-Cup A.C. Tachometer with Constant Current Excitation". Trans. A.I.E.E., Vol. 72, Pt. II, pp.150, 1953.
31. KNOX, L.A. "Approximate Analysis of the Drag-Cup A.C. Tachometer". Trans. A.I.E.E., Vol. 77, Pt.II, pp.202, 1958.

32. KAZARYAN, S.T. "Induction Tachometer as an Angular Acceleration Transducer". Automatic and Remote Control, Vol. 20, No.5, May 1959.
33. TRICKEY, P.H. "Performance Calculations on Phase Converters, Single-Phase A.C. Drag-Cup Tachometer Generators and Single-Phase Brakes". Trans. A.I.E.E., Vol. 80, Pt.III, p.444, 1961.
34. LAW, J., and NOVOTNY, D.W. "The Two-Phase Accelerometer". Elect.Eng., September 1963.
35. DOUCE, J.L., and EDWARDS, K.H. "Envelope Frequency Response of Networks Subjected to a Suppressed Carrier Modulated Input Wave". Electronics Letters, Vol. 1, p.12, March, 1965.
36. MORRIS, D.G.O. "Modulation Analysis of A.C. Servo-Systems". Electronics Letters, Vol. 1, p.63, May 1965.
37. MORRIS, D.G.O. "The Analysis of A.C. Servo-Systems". Unpublished Manuscript.
38. MORRIS, D.G.O. "The Frequency Calibration of Second Order Loci". International Journal of Electrical Engineering Education, Vol. 4, No. 2, p.201, April, 1966.
39. SABEZYK, A. "Stabilisation of Carrier Frequency Servo-mechanisms". Franklin Inst., Journal, Vol. 246, 1948.
40. CHANG, S.S.L. "On the Seperability of Laplace Transform Variables and its Application in Carrier Systems". I.R.E., Convention Record, Pt.2, p.27, 1955.
41. CANDY, C.J.N. "A Vector Method for Amplitude Modulated Signals". Proc. I.E.E., 103B, p.410, 1956.

42. TOU, J. "Analysis of Feedback Control Systems Containing Carrier Frequency Elements". N.E.C., pp.1012-1016, 1955.
43. PANZER, M. "Envelope Transfer Function Analysis in A.C. Servo Systems". Trans. A.I.E.E., Vol. 75, Pt.II, p.274, 1956.
44. LEVENSTEIN, H. "On the Design of A.C. Networks for Servo Compensators". I.R.E., P.G.A.C., Vol. 1, No.1, 1957.
45. CANDY, C.J.N. "Bifid Operators". Mathematical Gazette, Vol. 38, p.270, 1954.
46. BLANTON, H.E. "Carrier Compensation for Servomechanisms". Franklin Inst.Journal, Vol. 250, No. 5, p.391, and No. 6, p.525, 1950.
47. AIGRAIN, P.R., et.al. "Generalised Theory of the Band-Pass Low-Pass Analogy". Proc.I.E.E., Vol. 37, p.1152, 1959.
48. GRAHAM, R.E. "Modulated Control Systems". I.R.E. Convention Record, Vol. 4, Pt.2, p.18, 1956.
49. MAYNE, D.Q. "Transient Response of Band-Pass Filters to Modulated Signals". Proc. I.E.E., Vol. 106C, p.144, 1959.
50. COWLESS, L.G. "Parallel T - R.C. Networks". Proc. I.R.E., Vol. 40, p.1712, 1952.
51. SAVANT, C.J. "How to Design Notch Networks". Electronics, p.188, May 1963.
52. SAVANT, C.J., and BOLIE, V.W. "Notch Network Design". Electronics, Vol. 28, No. 9, p.172, 1955.
53. OONO, Y. "Design of Parallel T Resistance Capacitance Networks". Proc.I.R.E., Vol. 43, No. 4, p.617, 1955.

54. WHITE, G. "Design and Use of R.C. Parallel T. Networks". N.E.C., Vol. 15, p.92, 1959.
55. WEISS, G. "On the Design of A.C. Servo Lead Networks". Trans. A.I.E.E., Vol. 80, Pt.II, p.152, 1961.
56. COCQUYT, G. "Evaluating Bridge T Networks for A.C. Systems". Control Eng., Vol. 10, p.77, 1963.
57. RIPS, A. et.al. "Selection of Correcting Networks Parameters for A.C. Control Systems". Elektrichestvo, No. 8, 1964.
58. CARLSON, R.S., and TRUXAL, J.G. "Synthesis of Compensation Networks for Carrier Frequency Servomechanisms". N.E.C., Vol. 8, p.37, 1952.
59. GRONNER, A.D. "A.C. Stabilising Networks". Control Eng., Vol. 1, No. 1, 1954.
60. HELLERMAN, H. "Transfer Function for Amplitude Modulated Signals". Trans. A.I.E.E., Vol. 74, Pt. I, p.729, 1955.
61. WEISS, G. "A Network Theory for Carrier Suppressed Modulated Systems". I.R.E., P.G. A.C., No. 6, p.54, 1961.
62. SAPFIROV, S.G. "Following System with Ideal Modulator and Phase Detector". Elektromekhanika, No.10, pp.1156-1162, 1965.
63. DIPROSE, K.V., Discussion to Reference 1, pp.536-537.
64. SCORGIE, D.G. "Lead Network Utilizing A Saturable Core Memory". Trans. A.I.E.E., Vol. 71, Pt. II, p.297, 1952.
65. CLEGG, J.C. "A Time Dependent Non-linear Compensating Network". Trans. A.I.E.E., Vol. 73, Pt.II, p.306, 1956.

66. SALLEN, R.P., and KEY, E.L. "A Practical Method of Designing R.C. Active Filters". Trans. I.R.E., P.G. C.T., Vol. CT-2, p.74, 1955.
67. IVEY, K.A. "Active Compensating Networks". Control Eng., Vol. 10, p.111, November 1963.
68. LOONEY, C.H. "An Equalising Network for Carrier Type Feedback Control Systems". Proc. I.R.E., Vol. 43, p.20, 1955.
69. PYERSON, J.L. "Imaginary Axis Translation of Transfer Functions". I.R.E. Convention Record, Vol. 6, Pt. 4, p.236, 1958.
70. PRABHAKOV, A. "An A.C. Integrator". Electronic Engineering, p.444, 1963.
71. CANDY, C.J.N. "The Specification of the Properties of the Thermister as a Circuit Element in Very-Low Frequency Systems". Proc. I.E.E., Vol. 103, Pt.8, p.398, 1956.
72. SALBRAKEN, A. "Use of Thermistors for Error Integration in Carrier Type Servos". Instrument Practice, Vol. II, No. 6, 1960.
73. LEVINSON, E. "Gain and Phase Relations of Non-Linear Circuit". I.R.E., National Convention Record, Vol. 6, Pt. 4, p.141, 1958.
74. TUSTIN, A. "Problems to be solved in the Development of Control Systems". Trans. Soc. of Inst. Tech., Vol. 2, No. 2, 1950.
75. VOLZ, C. "The Magnetic Modulator in A.C. Servo Corrective Networks". N.E.C., Vol. 9, p.209, 1953.
76. NOTTHOFF, A.P. "Phase Lead for A.C. Servo Systems with Compensation for Carrier Frequency Changes". Journal A.I.E.E. Transactions, Pt. I, Vol. 69, p.285, 1950.

77. ATTURA, G.M. "Effects of Carrier Drift on Derivative Networks for A.C. Servomechanisms". Trans. A.I.E.E., Vol. 70, p.612, 1951
78. NASHMAN, L. et.al. "Effects of Carrier Frequency Drift on Performance on Notch Networks in A.C. Servo Systems". Aero.Eng.Rev., Vol. 14, No. 2, p.61, 1955.
79. MEHLICH, E.W., and MURPHY, G.J. "Effects of Variation in Carrier Frequency on the Performance of Carrier Control Systems Utilizing Two-Phase Servo-Motors". N.E.C., Vol. 14, p.506, 1958.
80. WEISS, G. "Carrier Frequency Networks", Research Report R-701-58, PIB-629, Microwave Research Institute, Systems and Controls Group, Polytechnic Institute of Brooklyn, 1959.
81. NAGRATH, I.J., and ARYA, V.K. "Design of Lead Networks for A.C. Servos with Carrier Frequency Drift". Trans. A.I.E.E., Vol. 81, Pt.II, p.291, 1962.
82. WILLIAMS, A.J., and PAYNE, J.F. "A.C. Null Type Recorder with Balancing Amplifier, which Provides Damping and Suppresses the Quadrature Component". Trans. A.I.E.E., Vol. 72, Pt.I, p.611, 1953.
83. HUTCHEON, I.C., and HARRISON, D.N. "A Transistor Quadrature Suppressor for A.C. Servo Systems". Proc. I.E.E., Vol. 107-B, p.73, 1960.
84. CONSTABLE, G.E.P. "Removing the Quadrature Signal from a Synchro Output". Electronic Eng. Vol. 33, p.716, November 1961.

85. SCHURR, K. "Stabilisation of Variable Carrier Frequency Servomechanisms", Proc. N.E.C., Vol. 7, p.14, 1951.
86. DOUCE, J.L., and EDWARDS, K.H. "Compensation of A.C. Control Systems Subjected to Carrier Frequency Fluctuations". Proc.I.E.E., Vol. 112, No. 1, Jan. 1965.
87. DOUCE, J.L., and EDWARDS, K.H. "A Simple Null Filter with Variable Notch Frequency". Elect.Eng., Vol. 36, p.478, 1964.
88. BOLIE, V.W., "Analysis of a Special Purpose R.C. Filter Incorporating a Periodically Conducting Bilinear Element". Proc.I.R.E., Vol. 42, No.9, p.1435, 1954.
89. MURPHY, G.J., and EGAN, J.F. "The Analysis of Compensating Detectors for A.C. Control Systems". N.E.C., Vol. 15, p.1056, 1959.
90. MURPHY, G.J., and EGAN, J.F. "The Analysis of Demodulating Compensating Networks". I.R.E., P.G.A.C., Vol.A.C.4, No. 3, December 1959.
91. GOSTER, V.I. "Method of Analysing Correcting R.C. Circuits with Circuit Breakers for Carrier Operated Automatic Control Systems". Izv. Akad. Nauk., Tekhn. Kibern., (6), pp.78-88, 1963.
92. BOHN, E.V. "Demodulator Lead Networks". I.R.E., P.G.C.T., Vol. C.T.7, p.56, 1960.
93. TUSTIN, A. "Automatic and Manual Control". R.V. Diporse, Butterworth's Scientific Publications, Eng. p.536, 1952.
94. LYONS, L.F. "Wide Band A.C. Rate Networks". I.R.E., Convention Record, Vol. 3, Pt.10, p.173, 1955.

95. BOHN, E.V. "A Simple Method for the Analysis of Demodulator Compensating Networks". I.R.E., P.G.C.T., Vol. C.T.8, p.306, September 1961.
96. WHITELEY, A.L. "British Patent 620028, 1944.
97. KNOX, A., and MURPHY, G.J. "A Method for the Design of Phase-lead Demodulating Compensators for Use in Carrier Control Systems". I.E.E.E., Vol. A.C.8, No. 4, 1963.
98. MURPHY, G.J., and KNOX, A. "A Method for the Design of a Phase-lag Demodulating Compensator for Use in Carrier Control Systems". I.E.E.E., Trans. Applic., Industry, No. 73, pp.252-7, July 1964.
99. NAGRATH, I.J., and RISHI PRATAP. "Analysis and Design of a Synchronously Switched Lag Compensator for A.C. Control Systems". Proc. of the 3rd International Congress of I.F.A.C., Electric Logic and Control Elements, June 1966, Paper 47D.
100. WEISS, G. "Synchronous Networks". Trans.I.R.E., P.G.A.C., Vol. A.C.7, No. 2, pp.45-55, March 1962.
101. OLIVER, B.M. "Wave Transmission Network". U.S. Patent 2,521,125, September 1950, (Application 769,853, August 1947).
102. LOW, S., and HAMMERSTEIN, H. "Demodulator Lead Network". American Bosch Arma Corp., Garden City, N.Y., Laboratory Report 28A, (File 1108), November 1952.
103. DONOVAN, A.C. "Alternating Current Rate Circuit". M.I.T. Instrumentation Laboratory Report E-110, Sept., 1951, (A.S.T.I.A. 88092).
104. SLOAN, G. "Design of A-C Filter Network Using Choppers". M.I.T. Instrumentation Laboratory Report E-470, July 1955.



105. WALKER, F., and WILSON, D.R. "The Analysis of an RC Chopper Network". Electronics Eng., p.300, 1963.
106. WILSON, D.R. "Transfer Function of an Active A.C. Phase-Advance Network". Electronics Letters, p.162, Pt.1, 1965.
107. WILSON, D.R., and WALKER, F. "Design of Switched Networks for A.C. Servo-Compensation". Control, Vol. 10, Pt.1, pp.299-301, June 1966.
108. WILSON, D.R., and WALKER, F. "Design of Switched Networks for A.C. Compensation". ibid., Vol. 10, Pt.2, pp.370-371, 1966.
109. WILSON, D.R. "Note on Whiteley's A.C. Compensating Network". Proc. I.E.E., Vol. 114, No. 1, 1967.
110. WILSON, D.R. "An Exact Modulation Model for a Demodulating Compensating Network". Proc. of the 3rd International Congress of I.F.A.C., Electric Logic and Control Elements, June 1966, Paper 47C.
111. SCHLESINGER, E.R. "Choppers Compensate A.C. Servos". Control Eng., 11 (9), pp.113-114, Sept. 1964.
112. VLASOV, N.P. "A Method for Obtaining Transfer Functions of Automatic Control Systems Operating on Alternating Current". Automatic and Remote Control, Vol. 21, No. 6, pp.538-543, 1960.
113. VLASOV, N.P. "A.C. Servo Systems in which the Signal Depends on the Error and its Derivative". Automatic and Remote Control, Vol. 20, No. 10, p.1327, 1960.
114. VLASOV, N.P. "A Servomechanism with Two-Phase Asynchronous Motor Whose Control Winding is Powered by a Current Generator". Automatic and Remote Control, Vol.22, No. 5, pp.539-543, 1961.

115. L'VOV, E.L. "The Transfer Function of an Automatic Control System with a Modulator and a Halfwave Demodulator". Automatic and Remote Control, Vol. 22, No. 3, pp.291-300, 1961.
116. STEIN, W.A., and THALER, G.J. "Evaluating the Effect of a Non-linearity in a 2-Phase Servomotor". Trans.A.I.E.E., Vol. 73, Pt.II, p.518, 1954.
117. STEIN, W.A., and THALER, J.G. "Obtaining the Frequency Response Characteristics of a Non-linear Servo from an Amplitude and Frequency Sensitive Describing Function". Trans. A.I.E.E., Vol.77, Pt.II, pp.91-96, 1958.
118. STEIN, W.A. "Analyzing the Transient Response of a Non-linear Servo System by the Phase-plane Method". Trans. A.I.E.E., Vol. 79, Pt.II, pp.287-292, 1960.
119. BAILEY, K.V., and ZINIUK, M.A. "Design of High Performance Instrument Servos for General Purpose Computation". I.R.E., P.G.I.E., Vol. 9, 1959.
120. COX, F.B., and JOHANNESSEN, P.R. "Application of Switching Transistors and Saturable Reactors in a High Performance Servo". Trans. A.I.E.E., Vol. 78, Pt.II, pp.466-474, 1960.
121. IVEY, K.A. "A General Classification of Amplitude-Modulated Carrier Control Systems". I.E.E.E., Vol. A.C.8, No. 3, pp.264-266, 1963.
122. ADKINS, B. "The General Theory of Electrical Machines". (book), Chapman & Hall, 1959.
123. GUILLEMIN, E.A. "The Mathematics of Circuit Analysis". (book), Chapter 2, John Wiley & Sons, Inc., 1959.
124. WEBER, E. "Complex Convolution Applied to Non-linear Problems". Proc. Symposium on Non-linear Circuit Analysis, Polytechnic Institute of Brooklyn, p.409, 1956.

125. RAGAZZINI, J.R., and FRANKLIN, G.F. "Sampled-Data Control Systems". McGraw Hill Book Co., Inc., New York, N.Y., 1958.
126. JURY, E.I. "Sampled-Data Control Systems". John Wiley & Sons, Inc., New York, N.Y., 1958.
127. "Instruction Manual for T.F.A. Carrier Converters Types JX 541/641". Solartron Laboratory Instruments Limited.
128. "Instruction Manual for T.F.A. Low Frequency Decade Oscillator Type Os 103.2". Solartron Laboratory Instruments Limited.
129. "Instruction Manual for T.F.A. LF Resolved Component Indicator Type VP 253.2". Solartron Laboratory Instruments Limited.
130. "Instruction Manual for T.F.A. Reference Resolver Type JX 746". Solartron Laboratory Instruments Ltd.
131. "Band-Pass, Band-Reject, and High-Pass Variable Electronic Filter Model 315-A". Krohn-Hite Corporation, Bulletin 315, June 1961.
132. PASSIAC, N.J. "Type 405L Precision Phase Meter". AD-YU Electronics Laboratory, Inc.
133. KRON, G.A., and KRON, T.M. "Electronic Analog and Hybrid Computers". (book), Chapter 1.16, McGraw Hill Company, 1964.
134. THALER, B.E., and BROWN, R.G. "Analysis and Design of Feedback Control Systems". McGraw-Hill Book Company, Inc., New York, N.Y., 1960.
135. "Mullard Data Sheets for the Junction Transistors OC28, OC29, OC35 and OC36".
136. "Mullard Reference Manual of Transistor Circuits". Mullard Limited, 1961.

137. "Mullard Data Sheets for the Junction Transistor OC84".
138. SEARLE, C.L., et.al. "Multistage Transistor Circuits". S.E.E.C. Notes 2, John Wiley & Sons, Inc.

APPENDIX A

Analytical Reduction of Various Expressions

A.1. Approximate expression for matrix  $\Delta_1$

Based on the assumption described by Eqn. 2.2.22, the various elements of the matrix  $\alpha_{12} \alpha_{22}^{-1} \alpha_{21}$  expressed by Eqn. 2.2.20 can be reduced as described below:

$$\begin{aligned} & \cos \gamma_m \frac{p}{Z_d} \cos \gamma_m + \sin \gamma_m \frac{p}{Z_d} \sin \gamma_m \approx \\ & \frac{1}{R_d} \left[ \cos^2 \gamma_m p - \cos \gamma_m \sin(\gamma_m) \gamma_m + \sin^2 \gamma_m p + \sin \gamma_m \cos(\gamma_m) \gamma_m \right] \\ & = \frac{1}{R_d} p \end{aligned} \quad \text{A.1.1}$$

Similarly, it is easy to prove that:

$$\begin{aligned} & \cos(\gamma_m) \frac{p}{Z_d} \sin \gamma_m - \sin(\gamma_m) \frac{p}{Z_d} \cos \gamma_m \approx 0 \\ & \dots \text{A.1.2} \end{aligned}$$

Substituting Eqns. A.1.1 and A.1.2 in Eqn. 2.2.20, yields

$$\begin{aligned} \Delta_1 &= Z_D \begin{bmatrix} 1 & \\ & 1 \end{bmatrix} - \frac{M^2}{R_d} p^2 \begin{bmatrix} 1 & \\ & 1 \end{bmatrix} \\ &= \left( Z_D - \frac{M^2}{R_d} p^2 \right) \begin{bmatrix} 1 & \\ & 1 \end{bmatrix} \end{aligned} \quad \text{A.1.3}$$

A.2. Approximate expression for matrix  $\Delta_2$

Following a similar procedure as outlined above in A.1, the simple expression for  $\Delta_2$  can be directly written as below:

$$\Delta_2 \cong \left( Z_d - \frac{M^2}{R_D} p^2 \right) \begin{array}{|c|c|} \hline 1 & \\ \hline & 1 \\ \hline \end{array} \quad \text{A.2.1}$$

A.3. Approximate expression for  $e_{a1}$

Breaking Eqn. 2.3.35 into simple elements and then considering these elements separately, thus

$$\begin{aligned} \cos(\gamma_{s1}) \cdot \frac{p}{Z_{DS}} \cdot \cos(\gamma_{s1}) i_{a1} &= \frac{1}{L_{DS}} \left[ \cos^2 \gamma_{s1} - \right. \\ &\quad \left. \cos(\gamma_{s1}) \frac{R_{DS}}{Z_{DS}} \cos \gamma_{s1} \right] i_{a1} \end{aligned} \quad \dots \text{A.3.1}$$

Similarly,

$$\begin{aligned} \sin(\gamma_{s1}) \cdot \frac{p}{Z_{DS}} \cdot \sin(\gamma_{s1}) i_{a1} &= \frac{1}{L_{DS}} \left[ \sin^2 \gamma_{s1} - \sin(\gamma_{s1}) \right. \\ &\quad \left. \frac{R_{DS}}{Z_{DS}} \sin \gamma_{s1} \right] i_{a1} \end{aligned} \quad \dots \text{A.3.2}$$

Adding Eqns. A.3.1 and A.3.2 and then differentiating the result w.r.t time, gives

$$\begin{aligned}
& p \left[ \cos(\gamma_{s1}) \cdot \frac{p}{Z_{DS}} \cos \gamma_{s1} + \sin(\gamma_{s1}) \cdot \frac{p}{Z_{DS}} \sin \gamma_{s1} \right] i_{a1} = \\
& \frac{1}{L_{DS}} \left[ p - \frac{R_{DS}}{L_{DS}} \left\{ 1 - R_{DS} \left( \cos(\gamma_{s1}) \frac{1}{Z_{DS}} \cos \gamma_{s1} + \sin(\gamma_{s1}) \frac{1}{Z_{DS}} \sin \gamma_{s1} \right) \right. \right. \\
& \left. \left. + L_{DS} \gamma_{s1} \left( \cos(\gamma_{s1}) \cdot \frac{1}{Z_{DS}} \sin \gamma_{s1} - \sin(\gamma_{s1}) \frac{1}{Z_{DS}} \cos \gamma_{s1} \right) \right\} \right] i_{a1}
\end{aligned}$$

..A.3.3

With the assumption expressed by Eqn. 2.3.27, the first two terms in Eqn. A.3.3 predominate the rest of the terms. Substituting this result into Eqn. 2.3.25, it simplifies to

$$e_{a1} \approx \left[ Z_{ds} - \frac{M_s^2}{2L_{DS}} \cdot p + \frac{M_s^2 R_{DS}}{2 L_{DS}^2} \right] i_{a1} \quad \text{A.3.4}$$

APPENDIX B

Analysis of the double-switch single-capacitor chopper network  
shown in Figure 4.1.3-b

Since the analysis and method of deriving various relations are rather similar to those outlined in Chapter 4, the details of the analysis are omitted and only the final expressions and important relations are directly given.

B.1. Application of the exact analytical approach

B.1.1. Derivation of the Z-transform of the voltage appearing across the capacitor

With the help of the block diagram shown in Fig. 4.2.3, the following expressions can be easily deduced by setting up the signal relationships around the two samplers;

$$\lambda_2^*(s) = e^{-(1-2\delta)T/2\tau_1} \cdot z_2^{-1} \cdot \lambda_1^*(s) \quad \text{B.1.1}$$

$$\frac{1 - z_2^{-1} r}{1 - z_2^{-1} e^{-T/2\tau_1}} \cdot \lambda_1^*(s) = \left[ F(s) e^{\delta TS} G(s) \right]^* \quad \text{B.1.2}$$

and

$$\lambda_2^*(s) = e^{-(1-2\delta)T/2\tau_1} \frac{z_2^{-1} (1 - z_2^{-1} e^{-T/2\tau_2})}{(1 - z_2^{-1} r)} \cdot \frac{z}{T} \sum_{L=-\infty}^{L=\infty} \left[ F(s - j2\Omega L) e^{\delta T(s - j2\Omega L)} \cdot G(s - j2\Omega L) \right] \quad \text{B.1.3}$$



where the sampling period is  $\frac{T}{2}$ , B.1.4

$$Z_2^{-1} = e^{-TS/2},$$

$$r = \exp \left\{ -T \left( \frac{1}{2\tau_1} - \frac{\delta}{\tau_{e2}} \right) \right\} \quad \text{B.1.5}$$

and

$$F(s) = \int x(t) \cdot E_{md} \sin(\Omega t + \theta) \cdot M(t) \quad \text{B.1.6}$$

wherein

$$M(t) = M_1(t) - M_2(t)$$

$$= \sum_{n=-\infty}^{n=\infty} \left[ U_{-1} \left\{ t - nT \right\} - U_{-1} \left\{ t - (n+\delta)T \right\} \right] - \left[ U_{-1} \left\{ t - \left( n + \frac{1}{2} \right) T \right\} \right. \\ \left. - U_{-1} \left\{ t - \left( n + \frac{1}{2} + \delta \right) T \right\} \right] \quad \text{B.1.7}$$

which is illustrated in Fig. 4.2.1.

### B.1.2. Determination of the output voltage

From Fig. 4.2.3, it is evident that  $y_2$  and  $y_3$  are the useful outputs. Determination of either can be obtained by considering the contribution of various signals during two periods as outlined below for the output  $y_2$ .

#### B.1.2.1. Contribution during the periods $nT \leq t < (n+\delta)T$ and $(n+1/2)T \leq t < (n+1/2+\delta)T$ :

This is given in the time-domain, according to Fig. 4.2.3, by

$$y_{21}(t) = \int x(t) \cdot M(t) \cdot E_{de} \sin(\Omega t + \theta) \quad \text{B.1.8}$$

where

$$\xi(s) = [F(s) + \zeta(s)] \cdot G(s) \quad \text{B.1.9}$$

wherein

$$\zeta(s) = \tau \left[ \lambda_2^*(s) - e^{(1-2\delta-\epsilon)Ts/2} z_2^{-1} \lambda_1^*(s) \right]$$

..B.1.10

Transformation of Eqn. B.1.8 into the complex frequency domain can be effected by using twice the complex convolution, in a similar manner as presented in Appendix D.1. This would yield

$$y_{21}(s) = E_{de} \sum_{n=-\infty}^{n=\infty} R(\phi, n) \xi(s - j2\omega n) \quad \text{E.1.11}$$

where  $R(\phi, n)$  can be obtained by using the result of Eqns. D.1.10 according to the relation

$$R(\phi, n) = R_2(\phi, n) \left[ 1 + e^{-j\pi n} \right] \quad \text{B.1.12}$$

which reduces to

$$R(\phi, n) = \frac{-1}{\pi} \cdot \frac{1}{(4n^2 - 1)} \left[ \left\{ \cos\phi + j2n \sin\phi \right\} e^{-j4\pi\delta n} \right. \\ \left. \left\{ \cos(2\pi\delta + \phi) + j2n \sin(2\pi\delta + \phi) \right\} \right] \quad \text{B.1.13}$$

since the form of  $F(t)$  is similar to that of  $y_{12}(t)$ , the transform of the former can thus be written as

$$F(s) = E_{md} \sum_{m=-\infty}^{m=\infty} R(\theta, m) x(s - j2\omega m) \quad \text{B.1.14}$$

where  $R(\theta, m)$  can be directly deduced from Eqn. B.1.13 by simply replacing  $\phi$  by  $\theta$  and  $n$  by  $m$ .

Substituting the results of Eqns. B.1.1, B.1.3, B.1.9, B.1.10 and B.1.14 and rearranging the result, gives

$$\begin{aligned}
 y_{21}(s) = & E_{md} E_{de} \sum_{n=-\infty}^{n=\infty} \sum_{m=-\infty}^{m=\infty} R(\phi, n) R(\theta, m) G(s - j2n\Omega) \\
 & \times \left\{ s - j2\Omega L(n+m) \right\} \\
 + E_{md} E_{de} \frac{2\tau}{T} & \frac{Z^{-1} (1 - Z^{-1} e^{-T/2\tau_2})}{(1 - Z_2^{-1} r)} \sum_{n=-\infty}^{n=\infty} \sum_{L=-\infty}^{L=\infty} \sum_{m=-\infty}^{m=\infty} R(\phi, n) R(\theta, m) \\
 & G(s - j2\Omega n) \left[ \begin{array}{cc} -(1-2\delta)T/2\tau_1 & (1-2\delta)(s - j2\Omega n)T/2 \\ e & -e \end{array} \right] \\
 G\{s - j2\Omega(L+n)\} & e^{\delta T} \{s - j2\Omega(L+n)\} \times \{s - j2\Omega(n+m+L)\} \quad \text{B.1.15}
 \end{aligned}$$

B.1.2.2. Contribution during the periods  
 $(n+\delta)T \leq t < (n+1/2)T$  and  $(n+1/2+\delta)T \leq t < (n+1)T$ :

According to Sub-section 4.2.3.2, the contribution can be directly given in the complex frequency domain by Eqn. 4.2.64. Combining this and the above contribution, the output  $y_2(s)$  can thus be obtained as written below

$$y_2(s) = y_{21}(s) + y_{22}(s) \quad \text{B.1.16}$$

Pursuing similar steps as outlined above, the output  $y_3(s)$  can be easily determined as given below

$$y_3(s) = y_{31}(s) + y_{32}(s) \quad \text{B.1.17}$$

where

$$y_{31}(s) = E_{md} E_{de} \sum_{n=-\infty}^{n=\infty} \sum_{m=-\infty}^{m=\infty} \left[ R(\phi, n) R(\theta, m) \times \left\{ s - j2\alpha(n+m) \right\} \right] - y_{21}(s) \quad \text{B.1.18}$$

and

$$y_{32}(s) = \frac{\tau}{\tau_2} y_{31}(s) \quad \text{B.1.19}$$

### B.1.3. Derivation of the multiplicative modulation transfer function

On the basis of the definition given in Sub-section 4.2.4, the modulation transfer functions  $G_{mm2}(s)$  and  $G_{mm3}(s)$  can be deduced from Eqns. B.1.16 and B.1.17 respectively. This would yield the following expressions

$$G_{mm2}(s) = 2 \sum_{n=-\infty}^{n=\infty} R(\phi, n) R(\theta, n) G(s - j2\alpha n) + \frac{4\tau}{T} Z_2^{-1} \frac{(1 - Z_2^{-1} e^{-T/2\tau_2})}{(1 - Z_2^{-1} r)} \left[ \sum_{n=-\infty}^{n=\infty} R(\phi, n) G(s - j2\alpha n) \left\{ e^{-((1-2\delta)T/2\tau_1 - e^{(1-2\delta)(s-j2\alpha n) T/2})} \left[ \sum_{m=-\infty}^{m=\infty} R(\theta, m) G(s + j2\alpha m) e^{\delta t(s + j2\alpha m)} \right] \right\} \right] + \frac{\tau_2}{\tau + \tau_2} \left[ (1-2\delta) \cos(\phi - \theta) + \frac{1}{\pi} \sin(2\pi\delta) \cos(2\pi\delta + \phi + \theta) \right]$$

and

$$\begin{aligned}
 G_{mm3}(s) &= 2 \sum_{n=-\infty}^{n=\infty} R(\phi, n) R(\theta, n) \\
 &+ (1-2\delta) \cos(\phi-\theta) + \frac{1}{\pi} \sin(2\pi\delta) \cos(2\pi\delta+\phi+\theta) \\
 &- G_{mm2}(s) \qquad \dots B.1.21
 \end{aligned}$$

B.1.4. Closed form for the multiplicative modulation transfer function

On the basis of the method adopted in Sub-section 4.2.5, each infinite series appearing in Eqns. B.1.20 and B.1.21 may first be attempted to be replaced by a convolution of two functions of the complex frequency  $s$  with at least one of these functions should obviously be possessing infinite poles, then the evaluation of the convolution integral may be effected by choosing the contour which encloses these limited number of poles. In doing so, a closed form may be obtained for each infinite series. Since this process has been explained in detail in Sub-section 4.2.5, only the results of the mathematical manipulations are given below

$$\begin{aligned}
 B.1.4.1. \quad I_1 &= 2 \sum_{n=-\infty}^{n=\infty} R(\phi, n) R(\theta, n) \\
 &= 2\delta \cos(\phi-\theta) - \frac{1}{\pi} \sin(2\pi\delta) \cos(2\pi\delta+\phi+\theta)
 \end{aligned}$$

..B.1.22

B.1.4.2.

$$I_2 = \sum_{n=-\infty}^{n=\infty} R(\vartheta, n) G(s-j2\Omega n) \left\{ e^{-(1-2\delta)T/2} \tau_1 \right. \\ \left. - e^{(1-2\delta)(s-j2\Omega n)T/2} \right\}$$

$$= \frac{1}{\tau} \left[ \left\{ e^{-(1-2\delta)T/2} \tau_1 - e^{-(1-2\delta)T/2} \tau_e \right\} / \left\{ 1 - e^{-(s+1/\tau_e)T/2} \right\} \right. \\ \left. \left\{ (s+1/\tau_e)^2 + \Omega^2 \right\} \right]$$

$$\left[ \left\{ \Omega \cos \vartheta + (s+1/\tau_e) \sin \vartheta \right\} - e^{-\delta T(s+1/\tau_e)} \left\{ \Omega \cos(2\pi\delta + \vartheta) \right. \right. \\ \left. \left. + (s+1/\tau_e) \sin(2\pi\delta + \vartheta) \right\} \right]$$

..B.1.23

B.1.4.3.  $I_3 = \sum_{m=-\infty}^{m=\infty} R(\theta, -n) G(s+j2\Omega m) e^{\delta T/s+j2\Omega m}$

$$= \frac{e^{-\delta T/\tau_e}}{\tau} \left[ \left\{ \Omega \cos \theta - (s+1/\tau_e) \sin \theta \right\} - e^{\delta T(s+1/\tau_e)} \right. \\ \left. \left\{ \Omega \cos(2\pi\delta + \theta) - (s+1/\tau_e) \sin(2\pi\delta + \theta) \right\} \right]$$

$$\frac{\left[ 1 - e^{-(s+1/\tau_e)T/2} \right] \left[ (s+1/\tau_e)^2 + \Omega^2 \right]}{\left[ 1 - e^{-(s+1/\tau_e)T/2} \right] \left[ (s+1/\tau_e)^2 + \Omega^2 \right]}$$

..B.1.24

$$\begin{aligned}
 \text{B.1.4.4. } I_4 &= \sum_{n=-\infty}^{n=\infty} R(\emptyset, n) R(\theta, -n) G(s-j2\pi n) \\
 &= 2 \frac{\tau}{T} \frac{\left[ 1 - e^{-(s+1/\tau_e)T/2} \right]}{e^{-\delta T/\tau} \left[ e^{-(1-2\delta)T/2\tau_1} - e^{-(1-2\delta)T/2\tau} \right]} I_2 \cdot I_3 \\
 &\quad \dots \text{B.1.25}
 \end{aligned}$$

Substituting the results of Eqns. B.1.22 to B.1.25 into Eqns. B.1.20 and B.1.21, closed forms for the multiplicative modulation transfer functions can be obtained as given below

$$\begin{aligned}
 G_{\text{mm}2}(s) &= \frac{\tau_2}{\tau + \tau_2} \left[ (1-2\delta)\cos(\emptyset-\theta) + \frac{1}{\pi} \sin(2\pi\delta)\cos(2\pi\delta+\emptyset+\theta) \right] \\
 &+ 2 I_4 \frac{1 - Z_2^{-1} e^{-T/2\tau}}{1 - Z_2^{-1} r} \quad \text{B.1.26}
 \end{aligned}$$

and

$$G_{\text{mm}3}(s) = \cos(\emptyset-\theta) - G_{\text{mm}2}(s) \quad \text{B.1.27}$$

## B.2. Application of the approximate analytical approach

### B.2.1. Derivation of the voltage appearing across the capacitor at the switching instants.

This voltage has already been obtained in the Z-domain as  $\lambda_2^*(s)$  in Sub-section B.1.1. If the input modulating signal  $x(t)$  is a unit step function, then

$$\left[ F(s) e^{\delta T S} G(s) \right]^* = E_{\text{md}} \cdot \frac{\tau_e}{\tau} \cdot \frac{1}{1 + \tau_e^2 \Omega^2} \frac{\left[ \alpha e^{-\delta T/\tau} - \beta \right]}{(1 - Z_2^{-1})(1 - Z_2^{-1} e^{-T/2\tau_e})}$$

..B.2.1

where  $\alpha$  and  $\beta$  are as defined by Eqns. 4.3.4 and 4.3.5 respectively.

Substituting the result of Eqn. B.2.1 into Eqn. B.1.3, yields

$$\lambda_2^*(s) = E_{md} \cdot \Delta \cdot \frac{z_2^{-1}}{(1-z_2^{-1})(1-z_2^{-1}r)} \quad \text{B.2.2}$$

where

$$\Delta = \frac{\tau_2}{\tau} \cdot \frac{e^{-(1-2\delta)T/2\tau_1}}{1 + \tau_e^2 \Omega^2} \left[ \alpha e^{-\delta T/\tau_e} - \beta \right] \quad \dots \text{B.2.3}$$

Expanding Eqn. B.2.2 in partial fractions,

$$\lambda_2^*(s) = E_{md} \cdot \frac{\Delta}{1-r} \left[ \frac{1}{1-z_2^{-1}} - \frac{1}{1-z_2^{-1}r} \right] \quad \text{B.2.4}$$

On taking its inverse Z-transform, gives

$$\lambda_2^*(t) = E_{md} \cdot \frac{\Delta}{1-r} \sum_{m=0}^{m=\infty} (1-r^m) U_0(t - m\frac{T}{2}) \quad \text{B.2.5}$$

### B.2.2. Derivation of the chopper network response

Table II.4.3 gives the response in Laplacian form applicable during the various intervals of the carrier cycle.

Rewriting the response  $v_2(s)$  during the period  $nT \leq t < (n+\delta)T$



$$v_2(s) = \left[ {}_n v_1(s) + \tau \cdot {}_n V \right] \cdot G(s) \quad \text{B.2.6}$$

where

${}_n v_1(s)$  is as defined by Eqn. 4.3.15,

and

$${}_n V = \lambda_2(nT) \quad \text{B.2.7}$$

which on substitution in Eqn. B.2.5, gives

$${}_n V = E_{md} \cdot \Delta \cdot \frac{1-r^{2n}}{1-r} \quad \text{B.2.8}$$

Substituting Eqns. 4.3.15 and B.2.8 into Eqn. B.2.6 and then applying the inverse Laplace transform to the result, gives

$$\begin{aligned} v_2 \left\{ (n+\mu)T \right\} &= E_{md} \cdot \Delta \cdot \frac{1-r^{2n}}{1-r} e^{-\mu T/\tau} e \\ &+ E_{md} \cdot \frac{\tau_e}{\tau} \cdot \frac{1}{1+\tau_e^2 \Omega^2} \left[ \alpha e^{-\mu T/\tau} e - \left\{ \tau_e \Omega \cos(2\pi\mu+\theta) \right. \right. \\ &\quad \left. \left. - \sin(2\pi\mu+\theta) \right\} \right] \quad \text{B.2.9} \end{aligned}$$

where

$$0 \leq \mu < \delta \quad \text{B.2.10}$$

During the periods  $(n+\delta)T \leq t < (n+\frac{1}{2})T$  and  $(n+\frac{1}{2}+\delta)T \leq t < (n+1)T$ , the response, again, can be obtained from Table II.4.3 and may be expressed in the time domain by Eqns. 4.3.19 and 4.3.22 respectively.

Also, during the period  $(n+\frac{1}{2})T \leq t < (n+\frac{1}{2}+\delta)T$ , the corresponding response may be deduced in a similar manner as above and is given by

$$\begin{aligned}
v_2 \left\{ \left( n + \frac{1}{2} + \mu \right) T \right\} &= -E_{md} \cdot \Delta \cdot \frac{1-r^{(2n+1)}}{1-r} e^{-T/\tau_e} \\
&- E_{md} \cdot \frac{\tau_e}{\tau} \cdot \frac{1}{1+\tau_e^2 \Omega^2} \left[ \alpha e^{-\mu T/\tau_e} - \left\{ \tau_e \Omega \cos(2\pi\mu + \theta) \right. \right. \\
&\quad \left. \left. - \sin(2\pi\mu + \theta) \right\} \right] \quad \text{B.2.11}
\end{aligned}$$

By applying the simple relation expressed by Eqn. 4.3.33, the response  $v_3(t)$  can be obtained during the various intervals of the carrier cycle.

### B.2.3. Determination of equivalent time-invariant passive electric network

#### B.2.3.1. Phase-lag aspect

On the basis of the assumption expressed by Eqn. 4.3.34, the output voltage envelope will vary slowly as compared to the carrier frequency. Under this condition, the approximate amplitude of the fundamental component, in phase with the demodulation reference, during the  $n^{\text{th}}$  switching can be found by quasi-stationary Fourier analysis and is given for the output  $v_2$  as

$$\begin{aligned}
{}_n v_2 &= \frac{1}{\pi} \int_0^{2\pi\delta} v_2 \left\{ \left( n + \frac{h}{2\pi} \right) T \right\} \cdot \sin(h + \phi) dh \\
&+ \frac{1}{\pi} \int_0^{2\pi\delta} v_2 \left\{ \left( n + \frac{1}{2} + \frac{h}{2\pi} \right) T \right\} \cdot \sin(h + \pi + \phi) dh \\
&+ \frac{2}{\pi} \int_{2\pi\delta}^{\pi} v_2 \left\{ \left( n + \delta + \frac{h}{2\pi} \right) T \right\} \cdot \sin(h + \phi) dh \quad \text{B.2.12}
\end{aligned}$$

where  $h$  is as defined by Eqn. 4.3.36.

Solving the integrations, gives

$${}_n V_2 = E_{md} \cdot M \left[ A_1 + B_1 \left\{ 1 + \frac{(r+1)}{2} r^{2n} \right\} \right] \quad \text{B.2.13}$$

where  $M$ ,  $A_1$  and  $B_1$  are as defined by Eqns. 4.3.38, 4.3.39 and 4.3.40 respectively.

If a step function of magnitude  $E_{md}$  is applied at  $t = 0$  to the input terminals of both the phase-lag d.c. networks  $a$  and  $b$  illustrated in solid line in Fig. 4.3.1, their responses can be shown, as given by Eqns. 4.3.45 and 4.3.46 respectively, to have a similar form as the R.H.S. of Eqn. B.2.13. This is only valid if the initial charges on their respective capacitors are zero. Under this condition, these d.c. networks can therefore be considered as equivalent to the system shown in Fig. 4.1.1 in its phase-lag aspect. In order to obtain the parameters of the equivalent d.c. networks in terms of those pertinent to the chopper network under consideration, Eqns. 4.3.45 and 4.3.46 may be compared, in turn, with Eqn. B.2.13 at the instants at which the peaks of the demodulation reference carrier occur (see Fig. 4.3.3). The results of the comparison are given below

i) For d.c. network  $a$  (Fig. 4.3.1)

$$\frac{1}{\tau_a} = \frac{1}{\tau_1} + \frac{2\delta}{\tau_{e2}} \quad \text{B.2.14}$$

$$K_a \text{ is as defined by Eqn. 4.3.54} \quad \text{B.2.15}$$

$$\text{and } K'_a = 1 - \left(\frac{1+r}{2}\right) \frac{B_1}{A_1 + B_1} H \quad \text{B.2.16}$$

$$\text{where } H = e^{\left\{(\pi-2\theta)\left(\frac{1}{\tau_1} + \frac{2\delta}{\tau_{e2}}\right) / 2\Omega\right\}} \quad \text{B.2.17}$$

ii) For d.c. network b (Fig. 4.3.1)

$$\frac{1}{\tau_b K_b} = \frac{1}{\tau_1} + \frac{2\delta}{\tau_{e2}} \quad \text{B.2.18}$$

$$K'_b = \left[ M \frac{A_1 + B_1}{A_1 + B_1} - \left(\frac{1+r}{2}\right) \frac{B_1}{A_1 + B_1} H \right] \quad \text{B.2.19}$$

$$\text{and } K_b = \frac{1 - M \frac{(A_1 + B_1)}{A_1 + B_1}}{1 - M \left[ \frac{A_1 + B_1}{A_1 + B_1} - \left(\frac{1+r}{2}\right) \frac{B_1}{A_1 + B_1} H \right]} \quad \text{B.2.20}$$

### B.2.3.2. Phase-lead aspect

Following similar pattern of steps as above, the fundamental component of  $v_3(t)$ , in phase with the demodulation reference, during the  $n^{\text{th}}$  switching period can be obtained and is given by

$${}_n V_3 = E_{md} \cdot M \left[ A_2 - B_1 \left\{ 1 - \left(\frac{1+r}{2}\right) r^{2n} \right\} \right] \quad \text{B.2.21}$$

where  $A_2$  is as defined by Eqn. 4.3.60.

The responses of the d.c. networks a and b illustrated in Fig. 4.3.2 to a step input of magnitude  $E_{md}$  are given by Eqns. 4.3.61 and 4.3.62 respectively. It is evident that the form of each of these responses is similar to the R.H.S. of Eqn. B.2.2.1. Consequently, they can be considered equivalent to the system of Fig. 4.1.1 in its

phase-lead aspect. Therefore, by comparing Eqns. 4.3.61 and 4.3.62, in turn, with Eqn. B.2.21 at the instants at which the peaks of the demodulation reference carrier occur, it is possible to determine the d.c. network parameters in terms of those pertinent to the chopper network under consideration. The following relations are deduced from the comparison

i) For d.c. network a (Fig. 4.3.2)

$$\frac{1}{\tau_c K_c'} = \frac{1}{\tau_1} + \frac{2b}{\tau_{e2}} \quad \text{B.2.22}$$

$$K_c' = \frac{A_2 - B_1}{A_2 - B_1 \left[ 1 - \frac{(1+r)}{2} H \right]} \quad \text{B.2.23}$$

and

$$K_c = M \left[ A_2 - B_1 \left\{ 1 - \frac{(1+r)}{2} H \right\} \right] \quad \text{B.2.24}$$

ii) For d.c. network b (Fig. 4.3.2)

Eqns. B.2.22 to B.2.24 are also applicable here provided that the subscript c is replaced by d.

#### B.2.4. Derivation of the multiplicative modulation transfer function

From the equivalence established in the previous sub-section, the multiplicative modulation transfer function of the chopper network under consideration may be obtained as the transfer function of its equivalent d.c. networks. On this basis, the expressions given by Eqns. 4.3.70 and 4.3.79 can be considered as the phase-lag and phase-lead multiplicative modulation transfer functions provided that the various parameters are substituted in terms of those obtained in this Appendix.

APPENDIX C

Analysis of the cascaded inverted double-switch  
double-capacitor chopper network shown in Fig. 4.1.3-c.

Since the analysis and techniques of deriving various relations are analogous to those outlined in Chapter 4, the details of the analysis are omitted and only the final expressions and useful relations are directly given.

C.1. Application of the exact analytical approach

C.1.1. Derivation of the Z-transform of the voltage  
appearing across the capacitor

Formulating the signal relationships around the samplers with the help of Fig. 4.2.4 would lead to the following results

i) For branch a:

$$\lambda_{a4}^*(s) = e^{-(\frac{1}{2} - \delta) T/\tau_1} \cdot Z_1^{-1} \lambda_{a3}^*(s) \quad \text{C.1.1.}$$

$$\lambda_{a3}^*(s) = e^{-\delta T/\tau_1} e^{1/2} \cdot \lambda_{a2}^*(s) \quad \text{C.1.2}$$

$$\lambda_{a2}^*(s) = e^{-(\frac{1}{2} - \delta)T/\tau_1} \cdot \lambda_{a1}^*(s) \quad \text{C.1.3}$$

and

$$\lambda_{a1}^*(s) = \frac{1 - Z_1^{-1} e^{-T/\tau_1}}{1 - Z_1^{-1} r} \left[ F_a(s) e^{\delta Ts} G_{e1}(s) \right]^* \quad \text{C.1.4}$$

where  $\tau_{e12}$ ,  $\tau_{e1}$ ,  $G_{e1}(s)$  are defined by Eqns. 4.2.24, 4.2.27 and 4.2.26 respectively

$$\text{and} \quad r = \exp \left\{ -T \left( \frac{1}{\tau_1} + \frac{\delta}{\tau_{e2}} \right) \right\} \quad \text{C.1.5}$$

$$\text{wherein} \quad \tau_{e2} = C/(G + G_2) \quad \text{C.1.6}$$

ii) For branch b:

By comparison with branch a, Eqns. C.1.1 to C.1.6 are also applicable here provided that the following changes are made

subscript a is replaced by b C.1.7

function  $F_a(s)$  is replaced by function  $F_b(s)$  C.1.8

#### C.1.2. Determination of the output voltage

Fig. 4.2.4 shows that four output voltages are possible. Because the output  $y_5$  does not appear to be of much use, only the other three outputs are going to be considered. Again, the procedure of obtaining the output expressions depends on that outlined in Sub-section 4.2.3 and which is given below without much detail.

Focusing the attention to the output  $y_2$ , then

##### C.1.2.1. Contribution during the periods $nT \leq t < (n+\delta)T$

This is given in the time domain, according to Fig. 4.2.4, by Eqn. 4.2.43 where

$$\xi_a(t) = \mathcal{L}^{-1} \left[ F_a(s) + \zeta_a(s) \right] G_{e1}(s) \quad \text{C.1.9}$$

wherein

$$\zeta_a(s) = \tau \left[ \lambda_{a4}^*(s) - e^{(1-\delta-\epsilon)T} Z_1^{-1} \cdot \lambda_{a1}^*(s) \right]$$

..C.1.10

Transforming  $y_{21}(s)$  into the complex frequency domain, using the complex convolution method twice as explained in Appendix D.1, thus

$$y_{21}(s) = E_{de} \sum_{n=-\infty}^{n=\infty} R_2(\emptyset, n) \xi_a(s-j\Omega n) \quad \text{C.1.11}$$

where  $R_2(\emptyset, n)$  may be deduced from Eqn. D.1.10 by replacing  $\emptyset$  by  $\emptyset$  and  $m$  by  $n$ .

Substituting the results of Eqns. C.1.1 to C.1.4, C.1.9 and C.1.10 into Eqn. C.1.11 and rearranging gives

$$\begin{aligned} y_{21}(s) &= E_{md} E_{de} \sum_{n=-\infty}^{n=\infty} \sum_{m=-\infty}^{m=\infty} R_2(\emptyset, n) R_2(\emptyset, m) G_{e1}(s-j\Omega n) x \{s-j\Omega(n+m)\} \\ &+ E_{md} E_{de} \frac{\tau}{T} Z_1^{-1} \frac{(1-Z_1^{-1} e^{-T/\tau} e^1)}{(1-Z_1^{-1} r)} \sum_{n=-\infty}^{n=\infty} \sum_{L=-\infty}^{L=\infty} \sum_{m=-\infty}^{m=\infty} R_2(\emptyset, n) \\ &G_{e1}(s-j\Omega n) \left[ e^{-\delta T/\tau_2} e^{-(1-\delta)T/\tau_1} - e^{(1-\delta)T(s-j\Omega n)} \right] R_2(\emptyset, m) \\ &G_{e1} \{s-j\Omega(L+n)\} e^{\delta T} \{s-j\Omega(L+n)\} x \{s-j\Omega(n+m+L)\} \quad \text{C.1.12} \end{aligned}$$



C.1.2.2. Contribution during the period  
 $(n+1/2)T \leq t < (n+1/2+\delta)T$

By comparison with C.1.2.1 above and with the guidance of Sub-section 4.2.3.2, the contribution can be written directly as

$$\begin{aligned}
 y_{22}(s) = & E_{md} E_{de} \sum_{n=-\infty}^{n=\infty} \sum_{m=-\infty}^{m=\infty} R_2(\emptyset, n) R_2(\theta, m) G_{e1}(s-j\alpha n) \\
 & \times \{s-j\alpha(n+m)\} e^{-j\pi(n+m)} \\
 & + E_{md} E_{de} \frac{\tau}{T} Z_1^{-1} \frac{(1 - Z_1^{-1} e^{-T/\tau} e_1)}{(1 - Z_1^{-1} r)} \sum_{n=-\infty}^{n=\infty} \sum_{L=-\infty}^{L=\infty} \sum_{m=-\infty}^{m=\infty} R_2(\emptyset, n) \\
 & R_2(\theta, m) G_{e1}(s-j\alpha n) \left[ e^{-\delta T/\tau_2} e^{-(1-\delta)T/\tau_1} e^{(1-\delta)T(s-j\alpha n)} \right] e^{-j\pi(n+m+L)} \\
 & G_{e1} \{s-j\alpha(L+n)\} e^{\delta T \{s-j\alpha(L+n)\}} \times \{s-j\alpha(n+m+L)\} \quad \text{C.1.13}
 \end{aligned}$$

C.1.2.3. Contribution during the periods  
 $(n+\delta)T \leq t < (n+1/2)T$  and  $(n+1/2+\delta)T \leq t < (n+1)T$

According to Sub-section 4.2.3.3, the contribution is given by Eqn. 4.2.64.

Combining the three contributions

$$y_2(s) = y_{21}(s) + y_{22}(s) + y_{23}(s) \quad \text{C.1.14}$$

Following similar steps as presented above, the output  $y_3(s)$  can be easily obtained and is

$$y_3(s) = y_{31}(s) + y_{32}(s) + y_{33}(s) \quad \text{C.1.15}$$

where  $y_{31}(s)$ ,  $y_{32}(s)$  and  $y_{33}(s)$  are defined by Eqns. 4.2.67, 4.2.68 and 4.2.69 respectively.

For the output  $y_4$ , one may proceed as follows.

C.1.2.4. Contribution during the periods  
 $nT \leq t < (n+\delta)T$

With the help of Fig. 4.2.4, the contribution in the time domain is

$$y_{41}(t) = q_a(t) \cdot M_1(t) \cdot E_{de} \sin(\omega t + \phi) \quad \text{C.1.16}$$

which on transformation, using similar techniques as those presented in Appendix D.1, yields

$$y_{41}(s) = E_{de} \sum_{n=-\infty}^{n=\infty} R_2(\phi, n) q_a(s - j\omega n) \quad \text{C.1.17}$$

where

$$q_a(s) = \left[ e^{-Ts/2} \cdot \lambda_{a2}^*(s) - e^{\left(\frac{1}{2} - \delta - \ell\right)TS} \cdot Z_1^{-1} \lambda_{a3}^*(s) \right] G_2(s)$$

..C.1.18

Substituting the results of Eqns. C.1.3, C.1.4 and C.1.18 into Eqn. C.1.17, gives

$$y_{41}(s) = E_{md} E_{de} \frac{e^{-\left(\frac{1}{2} - \delta\right)T/\tau_1}}{T} \cdot \frac{Z_1^{-1} (1 - Z_1^{-1})^{-1} e^{-T/\tau_1}}{(1 - Z_1^{-1})^r}$$

$$\sum_{n=-\infty}^{n=\infty} \sum_{L=-\infty}^{L=\infty} \sum_{m=-\infty}^{m=\infty} R_2(\theta, n)$$

$$R_2(\theta, m) G_2(s - j\omega n) e^{(s - j\omega n)T/2} \left[ 1 - Z_1^{-1} e^{(1-\delta)T(s - j\omega n)} e^{-\delta T/\tau_1} \right]$$

$$G_{e1} \{s - j\omega(L+n)\} e^{\delta T \{s - j\omega(L+n)\}} \times \{s - j\omega(n+m+L)\} \quad \text{C.1.18}$$

C.1.2.5. Contribution during the periods  
 $(n+1/2)T \leq t < (n+1/2+\delta)T$

By comparison with C.1.2.4 above and with the guidance of Sub-section 4.2.3.2, the contribution during this period can be directly written as

$$y_{42}(s) = y_{41}(s) e^{-j\pi(n+m+L)} \quad \text{C.1.19}$$

Since the contribution during the remaining periods is zero, the output  $y_4$  may thus be written

$$y_4(s) = y_{41}(s) + y_{42}(s) \quad \text{C.1.20}$$

C.1.3. Derivation of the multiplicative modulation transfer function

On the basis of the definition given in Sub-section 4.2.4, the modulation transfer functions  $G_{mm2}(s)$ :

$G_{mm3}(s)$  and  $G_{mm4}(s)$  can be deduced from Eqns. C.1.14, C.1.15 and C.1.20 respectively. Their expressions are

$$\begin{aligned}
 G_{mm2}(s) &= 4 \sum_{n=-\infty}^{n=\infty} R_2(\phi, n) R_2(\phi, -n) G_{e1}(s-j\omega n) \\
 &+ \frac{4\tau}{T} Z_1^{-1} \frac{(1-Z_1^{-1} e^{-T/\tau} e_1)}{(1-Z_1^{-1} r)} \left[ \sum_{n=-\infty}^{n=\infty} R_2(\phi, n) G_{e1}(s-j\omega n) \right. \\
 &\left. \left\{ e^{-\delta T/\tau_2} e^{-(1-\delta)T/\tau_1} e^{(1-\delta)T(s-j\omega n)} \right\} \right] \left[ \sum_{m=-\infty}^{m=\infty} R_2(\theta, m) \right. \\
 &\left. G_{e1}(s+j\omega m) e^{\delta T(s+j\omega m)} \right] \\
 &+ \frac{\tau_2}{\tau+\tau_2} \left[ (1-2\delta) \cos(\phi-\theta) + \frac{1}{\pi} \sin(2\pi\delta) \cos(2\pi\delta+\phi+\theta) \right] \\
 &\dots C.1.21
 \end{aligned}$$

$$\begin{aligned}
 G_{mm3}(s) &= 4 \sum_{n=-\infty}^{n=\infty} R_2(\phi, n) R_2(\theta, -n) \\
 &+ (1-2\delta) \cos(\phi-\theta) + \frac{1}{\pi} \sin(2\pi\delta) \cos(2\pi\delta+\phi+\theta) \\
 &- G_{mm}(s) \dots C.1.22
 \end{aligned}$$

and

$$G_{mm4}(z) = \frac{4}{T} e^{-\left(\frac{1}{2}-\delta\right)T/\tau_1} z_1^{-1} \frac{(1-z_1^{-1} e^{-T/\tau_1})}{1-z_1^{-1} r} \left[ \sum_{n=-\infty}^{n=\infty} R_2(\theta, n) \right. \\ \left. G_2(s-j\omega n) e^{(s-j\omega n)T/2} \left\{ 1 - e^{-\delta T(s-j\omega n)} e^{-\delta T/\tau_1} \right\} \right] \\ \left[ \sum_{m=-\infty}^{m=\infty} R_2(\theta, m) G_{e1}(s+j\omega m) e^{\delta T/s+j\omega m} \right] \quad C.1.23$$

#### C.1.4. Closed form for the multiplicative modulation transfer function

In Sub-section 4.2.5 bounded forms for the various infinite series associated with the multiplicative modulation transfer functions were derived. Because the forms of these infinite series are similar to those associated with Eqns. C.1.21 to C.1.23, the closed forms of the latter can thus be directly deduced from the corresponding ones pertinent to the former. In this way, the closed forms for  $G_{mm2}(s)$ ,  $G_{mm3}(s)$  and  $G_{mm4}(s)$  may be written as below

$$G_{mm2}(s) = \frac{\tau_2}{\tau+\tau_2} \left[ (1-2\delta) \cos(\theta-\theta) + \frac{1}{\pi} \sin(2\pi\delta) \cos(2\pi\delta+\theta+\theta) \right] \\ + \frac{4}{\tau T} I_1 \frac{1-z_1^{-1} e^{-T/\tau_1}}{1-z_1^{-1} r} \quad C.1.24$$

$$G_{mm3}(s) = \cos(\theta-\theta) - G_{mm2}(s) \quad C.1.25$$

and

$$G_{mm4}(s) = \frac{4}{\tau T} e^{-\left(\frac{1}{2}-\delta\right)T/\tau_1} z_1 \frac{(1-z_1^{-1} e^{-T/\tau_1})}{1-z_1^{-1} r} I_2 \cdot I_3$$

where

$$I_1 = \frac{1}{\left\{1 - e^{-T(s+1/\tau_{e1})}\right\} \left\{(s+1/\tau_{e1})^2 + \Omega^2\right\}^2} \left[ \left\{ \Omega \cos \theta + (s+1/\tau_{e1}) \sin \theta \right\} \right. \\ \left. - e^{-\delta T(s+1/\tau_{e1})} \left\{ \Omega \cos(2\pi\delta + \theta) + (s+1/\tau_{e1}) \sin(2\pi\delta + \theta) \right\} \right] \\ \left[ \left\{ \Omega \cos \theta - (s+1/\tau_{e1}) \sin \theta \right\} - e^{\delta T(s+1/\tau_{e1})} \left\{ \Omega \cos(2\pi\delta + \theta) \right. \right. \\ \left. \left. - \sin(2\pi\delta + \theta) \right\} \right] \quad \text{C.1.27}$$

$$I_2 = \frac{e^{-T/2\tau_{e12}}}{\left\{(s+1/\tau_{e12})^2 + \Omega^2\right\}} \left[ \left\{ \Omega \cos \theta + (s+1/\tau_{e12}) \sin \theta \right\} - e^{-\delta T(s+1/\tau_{e12})} \right. \\ \left. \left\{ \Omega \cos(2\pi\delta + \theta) + (s+1/\tau_{e12}) \sin(2\pi\delta + \theta) \right\} \right] \quad \text{C.1.28}$$

and

$$I_3 = \frac{e^{-\delta T/\tau_{e1}}}{\left\{1 - Z_1^{-1} e^{-T/\tau_{e1}}\right\} \left\{(s+1/\tau_{e1})^2 + \Omega^2\right\}} \left[ \left\{ \Omega \cos \theta - (s+1/\tau_{e1}) \right. \right. \\ \left. \left. \sin \theta \right\} - e^{\delta T/(s+1/\tau_{e1})} \left\{ \Omega \cos(2\pi\delta + \theta) - (s+1/\tau_{e1}) \sin(2\pi\delta + \theta) \right\} \right]$$

..C.1.29

## C.2. Application of the Approximate Analytical Approach

### C.2.1. Derivation of the voltage appearing across the capacitor at the switching instants.

This voltage has already been obtained in the Z-domain in Sub-section C.1.1 as  $\lambda_{a4}^*(s)$  and  $\lambda_{b4}^*(s)$  for the capacitors in branches a and b respectively. If the input modulating signal  $x(t)$  is a unit step function, thus

$$\left[ F_a(s) e^{\delta T S} G_{e1}(s) \right]^* = E_{md} \cdot \frac{\tau_{e1}}{\tau} \cdot \frac{1}{1 + \tau_{e1}^2 \Omega^2} \frac{[\alpha e^{-\delta T/\tau} e_1 - \beta]}{(1 - Z_1^{-1})(1 - Z_1^{-1} e^{-T/\tau} e_1)}$$

..C.2.1.

where  $\alpha$  and  $\beta$  are as defined by Eqns. 4.3.4 and 4.3.5 respectively provided that  $\tau_e$  is replaced by  $\tau_{e1}$ .

Substituting the results of Eqns. C.1.1 to C.1.4 and C.2.1 into Eqn. C.1.1, results in

$$\lambda_{a4}^*(s) = E_{md} \cdot \Delta \cdot \frac{Z_1^{-1}}{(1 - Z_1^{-1})(1 - Z_1^{-1} r)} \quad \text{C.2.2}$$

where

$$\Delta = \frac{\tau_{e1}}{\tau} \cdot \frac{e^{-\delta T/\tau_2} e^{-(1-\delta)T/\tau_1}}{1 + \tau_{e1}^2 \Omega^2} \left[ \alpha e^{-\delta T/\tau} e_1 - \beta \right]$$

..C.2.3

Expanding Eqn. C.2.2 in partial fractions and then applying the inverse Z-transform to the result, gives

$$\lambda_{a4}^*(t) = E_{md} \cdot \frac{\Delta}{1-r} \sum_{n=0}^{n=\infty} (1-r^n) U_o(t-nT) \quad \text{C.2.4}$$

Either by following a similar procedure as above or by simple deduction from the symmetry of the chopper network, it can be shown that

$$\lambda_{b4}(nT) = -\lambda_{a4}(nT) \quad C.2.5$$

### C.2.2. Derivation of the chopper network response

Table II.5.2 gives the response in Laplacian form applicable during the various intervals of the carrier cycle. Re-writing the response  $v_2(s)$  during the interval  $nT \leq t < (n+\delta)T$

$$v_2(s) = [{}_n v_1(s) + \tau \cdot {}_n V_a] \cdot G_{e1}(s) \quad C.2.6$$

where  ${}_n v_1(s)$  is as defined by Eqn. 4.3.15

$$\text{and } {}_n V_a = \lambda_{a4}(nT) \quad C.2.7$$

which on substitution into Eqn. C.2.4, gives

$${}_n V_a = E_{md} \cdot \Delta \cdot \frac{1-r^n}{1-r} \quad C.2.8$$

Substituting Eqns. 4.3.15 and C.2.8 into Eqn. C.2.6 and then applying the inverse Laplace transform to the result, gives

$$v_2 \left\{ (n+\mu)T \right\} = E_{md} \cdot \Delta \cdot \frac{1-r^n}{1-r} e^{-\mu T/\tau} e_1$$

$$+ E_{md} \cdot \frac{\tau e_1}{\tau} \cdot \frac{1}{1 + \tau_{e1}^2 \Omega^2} \left[ \alpha e^{-\mu T/\tau} e_1 - \left\{ \tau_{e1} \Omega \cos(2\pi\mu + \theta) - \sin(2\pi\mu + \theta) \right\} \right] \quad C.2.9$$

where

$$0 \leq \mu < \delta$$

C.2.10



During the interval  $(n+\delta)T \leq t < (n+\frac{1}{2})T$ , the response, again, can be obtained from Table II.5.2 and may be expressed in the time domain by Eqn. 4.3.19.

From the symmetry of the branches a and b of the chopper network, Eqns. 4.3.21 and 4.3.22 can be proved to be valid.

By applying the simple relationship expressed by Eqn. 4.3.33, the response  $v_3(t)$  can be obtained during the various intervals of the carrier cycle. To obtain the response  $v_4(t)$ , however, one has to adopt a similar procedure as the one used in obtaining the response  $v_2(t)$  above. This response, in the S-domain, can be obtained from Table II.5.2 as rewritten below for the interval  $nT \leq t < (n+\delta)T$

$$v_4(s) = {}_n V_b G_2(s) \quad \text{C.2.11}$$

But

$${}_n V_b = \lambda_{b2}(nT) \quad \text{C.2.12}$$

which gives due to the symmetry

$${}_n V_b = -\lambda_{a2}(nT) \quad \text{C.2.13}$$

which gives on using the results of Eqns. C.1.3, C.1.4 and C.2.1 and by applying the inverse Z-transform

$${}_n V_b = -E_{md} e^{\delta T/\tau} e^{12} e^{(1-2\delta)T/2\tau_1} \cdot \Delta \cdot \frac{1-r^{(n-1)}}{1-r} \quad \text{..C.2.14}$$

Substituting this into Eqn. C.2.11 and transforming the result into the time domain, gives

$$v_4 \left\{ (n+\mu)T \right\} = - E_{md} \cdot e^{\delta T/\tau} e^{12} e^{(1-2\delta)T/2\tau} \cdot \Delta \frac{1-r^{(n-1)}}{1-r} e^{-\mu T/\tau} e^{12}$$

..C.2.15

Similarly, it is possible to obtain the response during the interval  $(n + \frac{1}{2}) \leq t < (n + \frac{1}{2} + \delta)T$  which is found to be related to the above as

$$v_4 \left\{ (n + \frac{1}{2} + \mu)T \right\} = - v_4 \left\{ (n+\mu)T \right\} \quad \text{C.2.16}$$

Finally, as it is evident from the synchronous switches positions, the response remains zero during the remaining parts of the carrier cycle. In regarding the response  $v_5(t)$ , its expressions during the various intervals can be easily deduced from the following relation provided that the proper time is substituted

$$v_5(t) = v_1(t) - v_4(t) \quad \text{C.2.17}$$

### C.2.3. Determination of equivalent time-invariant passive electric network

#### C.2.3.1. Phase-lag aspect

Under the condition expressed by Eqn. 4.3.34, the output voltage envelope will vary slowly as compared to the carrier frequency. Consequently, the approximate amplitude of the fundamental component, in phase with the demodulation reference, during the  $n^{\text{th}}$  switching can be found by quasi-stationary Fourier analysis and is given for the outputs  $v_2$  and  $v_4$  as

$${}_n V_2 = E_{md} \cdot M_1 \left[ A_1 + B_1 (1-r^n) \right] \quad \text{C.2.18}$$

and

$$-{}_n V_4 = E_{md} \cdot M_2 \left[ 1 - r^{(n-1)} \right] \quad \text{C.2.19}$$

where  $M_1$ ,  $A_1$  and  $B_1$  are as defined by Eqns. 4.3.38, 4.3.39 and 4.3.40 respectively provided that  $\tau_e$  is replaced by  $\tau_{e1}$ , and

$$M_2 = \frac{2}{\pi} \cdot \Delta \cdot e^{\mathbb{T} \left\{ \frac{1}{2\tau_1} + \frac{\delta}{\tau_2} \right\}} \cdot \frac{K_5}{1-r} \quad \text{C.2.20}$$

wherein  $K_5$  can be defined by Eqn. 4.3.43 provided that  $\tau_e$  is replaced by  $\tau_{e12}$ .

Both the expressions of  ${}_n V_2$  and  $-{}_n V_4$  obtained above have a similar form to the responses of the initially quiescent phase-lag d.c. networks a and b, illustrated in solid line in Fig. 4.3.1, to a step function of magnitude  $E_{md}$ . Therefore, they can be considered as equivalent to the system of Fig. 4.1.1 in its phase-lag aspect. In order to obtain the parameters of the equivalent d.c. networks in terms of those pertinent to the chopper network under consideration, Eqns. 4.3.45 and 4.3.46 may be compared, in turn, with Eqns. C.2.18 and C.2.19 respectively, at the instants at which the peaks of the demodulation reference carrier occur (see Fig. 4.3.3). The results of the comparison are given below

a) For the output  $v_2$

i) d.c. network a (Fig. 4.3.1)

Eqns. 4.3.52, 4.3.54 to 4.3.56 are also applicable here provided that  $M$  is replaced by  $M_1$ .

ii) d.c. network b (Fig. 4.3.1)

Eqns. 4.3.53, 4.3.57 and 4.3.58 are also applicable here provided that  $M$  is replaced by  $M_1$ .

b) For the output  $-v_4$

i) d.c. network a (Fig. 4.3.1)

$\frac{1}{\tau_a}$  is as defined by Eqn. 4.3.52

$$k_a = M_2 \quad \text{C.2.21}$$

and  $k_a' = 1 - \frac{H}{r} \quad \text{C.2.22}$

where  $H$  is as defined by Eqn. 4.3.56.

ii) d.c. network b (Fig. 4.3.1)

$\frac{1}{\tau_b k_b}$  is as defined by Eqn. 4.3.53

$$k_b' = M_2 \left[ 1 - \frac{H}{r} \right] \quad \text{C.2.23}$$

and  $k_b = \frac{1 - M_2}{1 - M_2 \left\{ 1 - \frac{H}{r} \right\}} \quad \text{C.2.24}$

### C.2.3.2. Phase-lead aspect

Pursuing similar pattern of steps as above, the fundamental component of  $v_3(t)$ , in phase with the demodulation reference, during the  $n^{\text{th}}$  switching period can be obtained and is given by

$${}_n V_3 = E_{md} \cdot M_1 \left[ A_2 - B_1 (1-r^n) \right] \quad \text{C.2.25}$$

The responses of the d.c. phase-lead networks a and b illustrated in Fig. 4.3.2 to a step input of magnitude

$E_{md}$  are given by Eqns. 4.3.61 and 4.3.62 respectively. It is obvious that the form of these responses is similar to that of  $nV_3$  expressed above. As a result these d.c. networks can be considered as equivalent to the system of Fig. 4.1.1 in its phase-less aspect. Therefore, by comparing Eqns. 4.3.61 and 4.3.62 in turn with Eqn. C.2.25 at the instants at which the peaks of the demodulation reference carrier occur, it is possible to determine the parameters of the equivalent d.c. networks in terms of those pertinent to the chopper network under consideration. The following relations result from the comparison

i) For d.c. network a (Fig. 4.3.2)

Eqns. 4.3.65 to 4.3.67 are also applicable here provided that  $M$  is replaced by  $M_1$ .

ii) For d.c. network b (Fig. 4.3.2)

Eqns. 4.3.65 to 4.3.67 are also applicable here provided that  $M$  is replaced by  $M_1$  and subscript  $c$  is replaced by  $d$ .

With regard to the output  $v_5(t)$ , following a similar steps as above, thus

$$nV_5 = E_{md} \cdot M_2 \left[ A_3 - 1 - r^{(n-1)} \right] \quad C.2.26$$

where

$$A_3 = \frac{2}{\pi} \cdot \frac{1}{M_2} \left[ k_1 + k_4 \right] \quad C.2.27$$

wherein  $k_1$  and  $k_4$  are as defined by Eqns. 4.3.41 and 4.3.44 respectively.

$nV_5$  can be shown to be similar to the responses  $y_{5a}$

and  $y_{5b}$  of the d.c. phase-lag networks a and b illustrated in Fig. 4.3.1 in solid and dotted lines. It is apparent that such response is not of much practical use and therefore further derivations for this particular case will not be carried out.

#### C.2.4. Derivation of the multiplicative modulation transfer function

From the equivalence established in the previous Sub-section, the multiplicative modulation transfer function of the chopper network under consideration may be obtained as the transfer function of its equivalent d.c. networks. On this basis, the expressions given by Eqns. 4.3.70 and 4.3.79 can be considered as the phase-lag and phase-lead multiplicative modulation transfer functions provided that the various parameters are substituted in terms of those obtained in this Appendix.

APPENDIX D

Solution of equations associated with the  
analysis of chopper networks

D.1. Solution for function  $F_a(s)$ 

According to Eqns. 4.2.4 and 4.2.12, the function  $F_a$  may be expressed in the time domain as the multiplication of three functions of time,

$$F_a(t) = x(t) \cdot \left[ E_{md} \sin(\omega t + \theta) \cdot M_1(t) \right] \quad \text{D.1.1.}$$

and hence its transform would involve two successive complex convolution <sup>124,126</sup> as given below

$$F_a(s) = E_{md} x(s) * \left[ \frac{1}{2j} \left\{ \frac{e^{j\theta}}{(s-j\omega)} - \frac{e^{-j\theta}}{(s+j\omega)} \right\} * M_1(s) \right] \quad \text{..D.1.2}$$

where  $M_1(s)$  can be easily obtained with the help of the translated time function's theorem <sup>125,126</sup> which may be written as

$$M_1(s) = \frac{1}{s} \cdot \frac{1 - e^{-\delta T s}}{1 - e^{-T s}} \quad \text{D.1.3}$$

Consequently, the first complex convolution of Eqn. D.1.2 may be re-written as

$$F_{a1}(s) = \frac{1}{2\pi j} \int_{c_1 - j\infty}^{c_1 + j\infty} \frac{1}{2j} \left\{ \frac{e^{j\theta}}{p-j\omega} - \frac{e^{-j\theta}}{p+j\omega} \right\} \cdot M_1(s-p) dp \quad \text{..D.1.4}$$

where  $c_1 < [\mathcal{R}(s)]$  is greater than the abscissa of the absolute convergence of

$$\frac{1}{2j} \left\{ \frac{e^{j\theta}}{p-j\Omega} - \frac{e^{-j\theta}}{p+j\Omega} \right\} .$$

This convolution integral may be evaluated by the method of residues, and thus the poles of the first function lie at the solution

$$p = \pm j\Omega \quad \text{D.1.5}$$

with the corresponding residues of

$$R_1 = \pm \frac{e^{\pm j\theta}}{2j} \quad \text{D.1.6}$$

Hence, the convolution integral expressed by Eqn. D.1.4 may be re-written as

$$\begin{aligned} F_{a1}(s) &= \frac{1}{2j} \left[ e^{j\theta} M_1(s-j\Omega) - e^{-j\theta} M_1(s+j\Omega) \right] \\ &= \frac{1}{2j} \cdot \frac{1}{1 - e^{-TS}} \left[ e^{j\theta} \left\{ \frac{1 - e^{-\delta T(s-j\Omega)}}{s-j\Omega} \right\} \right. \\ &\quad \left. - e^{-j\theta} \left\{ \frac{1 - e^{-\delta T(s+j\Omega)}}{s+j\Omega} \right\} \right] \quad \text{D.1.7} \end{aligned}$$

Substituting Eqn. D.1.7 into Eqn. D.1.2, results into one convolution integral

$$F_a(s) = \frac{E_{md}}{2\pi j} \int_{c-\infty}^{c+\infty} F_{a1}(p) \cdot x(s-p) dp \quad \text{D.1.8}$$



Applying again the method of residues, the poles of  $F_{a1}(p)$  can be proved to lie at the solution

$$p = j\Omega m \quad \text{D.1.9}$$

where  $m$  is an integer that can take any value between  $-\infty$  and  $+\infty$ . The corresponding residues can be evaluated from  $F_{a1}(p)$  as follows

$$\begin{aligned} R_2(\theta, m) &= \frac{1}{2j} \frac{1}{\frac{d}{dp} (1 - e^{-Tp})} \left[ e^{j\theta} \left\{ \frac{1 - e^{-\delta T(p-j\Omega)}}{p - j\Omega} \right\} \right. \\ &\quad \left. - e^{-j\theta} \left\{ \frac{1 - e^{-\delta T(p+j\Omega)}}{p + j\Omega} \right\} \right] \Bigg|_{\text{at } p = j\Omega m} \\ &= \frac{-1}{2\pi(m^2 - 1)} \left[ \left\{ \cos \theta + jm \sin \theta \right\} - e^{-j2\pi\delta m} \right. \\ &\quad \left. \left\{ \cos(2\pi\delta + \theta) + jm \sin(2\pi\delta + \theta) \right\} \right] \quad \text{D.1.10} \end{aligned}$$

where the values at the particular roots  $p = \pm j\Omega$  may be obtained in the following manner

$$\begin{aligned} R_2(\theta, \pm 1) &= \lim_{m \rightarrow \pm 1} \left\{ R_2(\theta, \pm m) \right\} \\ &= \mp \frac{j}{4\pi} \left[ 2\pi\delta e^{\pm j\theta} + \sin \theta - e^{\mp j2\pi\delta} \sin(2\pi\delta + \theta) \right] \\ &\quad \dots \text{D.1.11} \end{aligned}$$

With the help of Eqns. D.1.8 to D.1.10, the function  $F_a(s)$  may be expressed as

$$F_a(s) = R_{md} \sum_{m=-\infty}^{m=\infty} R_2(\theta, m) x(s-j\Omega m) \quad D.1.12$$

### D.2. Solution for function $F_b(s)$

On the basis of Eqns. 4.2.12 and 4.2.19, the function  $F_b$  may be expressed in the time domain as the multiplication of three functions of time

$$F_b(t) = x(t) \cdot \left[ E_{md} \sin(\Omega t + \theta) \cdot M_2(t) \right] \quad D.2.1$$

and its transform would therefore involve two successive complex convolution as given below

$$F_b(s) = E_{md} x(s) * \left[ \frac{1}{2j} \left\{ \frac{e^{j\theta}}{s-j\Omega} - \frac{e^{-j\theta}}{s+j\Omega} \right\} * M_2(s) \right] \quad \dots D.2.2$$

where  $M_2(s)$  can be obtained in the same way as  $M_1(s)$ , thus it may be directly written as

$$M_2(s) = \frac{e^{-TS/2}}{s} \cdot \frac{1 - e^{-\delta Ts}}{1 - e^{-TS}} \quad D.2.3$$

The method of the evaluation of the function  $F_b(s)$  is basically similar to that used in Appendix D.1 with which one can easily arrive at the following expression:

$$F_b(s) = -E_{md} \sum_{m=-\infty}^{m=\infty} R_2(\theta, m) e^{-j\pi m} x(s-j\Omega m) \quad D.2.4$$

D.3. Z-Transform of function  $Q_1(s)$

The function  $Q_1(s)$  expressed by Eqn. 4.2.76 may be re-arranged into the suitable form

$$\begin{aligned}
 Q_1(s) = \frac{1}{4T} \cdot \frac{1}{1 - Z_1^{-1}} & \left[ \frac{e^{j(\phi+\theta)} \left\{ 1 - Z_1^{-1} e^{(1-\delta)Ts} e^{j\delta T\Omega} \right\} \left\{ \frac{1 - e^{\delta T(s+j\Omega)}}{(s+j\Omega)} \right\}}{(s - j\Omega)} \right. \\
 & + \frac{e^{-j(\phi+\theta)} \left\{ 1 - Z_1^{-1} e^{(1-\delta)Ts} e^{-j\delta T\Omega} \right\} \left\{ \frac{1 - e^{\delta T(s-j\Omega)}}{(s - j\Omega)} \right\}}{(s + j\Omega)} \\
 & - \frac{e^{j(\phi-\theta)} \left\{ 1 - Z_1^{-1} e^{(1-\delta)Ts} e^{j\delta T\Omega} \right\} \left\{ \frac{1 - e^{\delta T(s-j\Omega)}}{(s - j\Omega)} \right\}}{s - j\Omega} \\
 & \left. - \frac{e^{-j(\phi-\theta)} \left\{ 1 - Z_1^{-1} e^{(1-\delta)Ts} e^{-j\delta T\Omega} \right\} \left\{ \frac{1 - e^{\delta T(s+j\Omega)}}{(s + j\Omega)} \right\}}{(s + j\Omega)} \right]
 \end{aligned}$$

..D.3.1

Applying the Z-transform to each term separately, thus

$$\begin{aligned}
 Q_1^*(s) = \frac{1}{4T} \cdot \frac{1}{1 - Z_1^{-1}} & \left[ e^{j(\phi+\theta)} \left( \frac{1 - e^{j4\pi\delta}}{2j\Omega} \right) - e^{-j(\phi+\theta)} \left( \frac{1 - e^{-j4\pi\delta}}{2j\Omega} \right) \right. \\
 & \left. + \delta T \left\{ e^{j(\phi-\theta)} + e^{-j(\phi-\theta)} \right\} \right]
 \end{aligned}
 \tag{D.3.2}$$

This may be rearranged to yield

$$Q_1^*(s) = \frac{1}{4} \cdot \frac{1}{1 - Z_1^{-1}} \left[ 2\delta \cos(\phi-\theta) - \frac{1}{\pi} \sin(2\pi\delta) \cos(2\pi\delta + \theta + \phi) \right]$$

..D.3.2

APPENDIX EData of the breadboard model componentsE.1. Mechanical load

Simulated by an unenergised 3" mag slip whose relevant data is given below

<u>Quantities</u>		<u>Units</u>
Rotor inertia	= 970	gm. cm <sup>2</sup>
Bearing friction	= 43	gm. cm
Brush friction	= 86	gm. cm

E.2. Servomotor

Size 11 a.c. motor, type 11 MG72, number 420586.F.

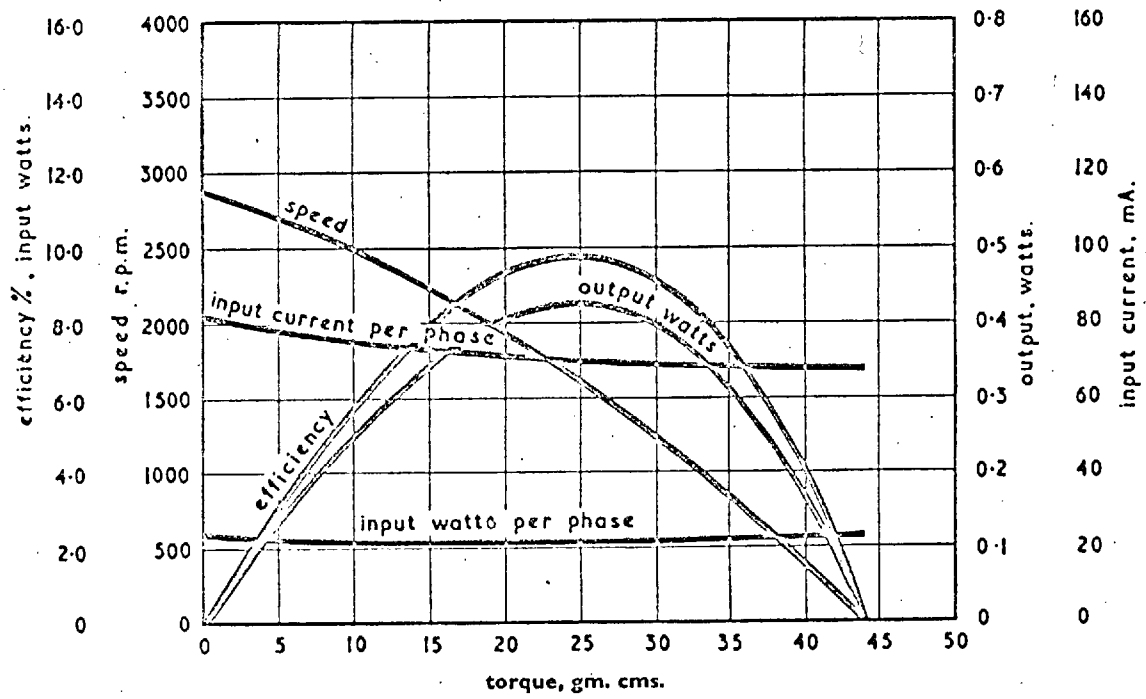
Characteristics

Frequency	= 50 c/s
No. of phases	= 2
No-load speed	= 2500 r.p.m. min.
Stall torque	= 40 gm.cm <sup>2</sup>
Moment of inertia	= 1 gm.cm <sup>2</sup>
Stall input power	= 3.5 watts/phase
Standard Voltage	= 35 volts/phase
Impedance Z	= 425 ± 10% ohms
R	= 403 ± 10% ohms
X	= 136 ± 10% ohms
Weight	= 110 grams.

Fig. E.2.1 shows average performance curves.

For description, mounting facilities and further performance details, see the Technical Data, Vactric Control Equipment Limited.

FIG. E.21. Average performance curve for 35v winding



E.3. Error-detectorE.3.1. Transmitter and coincidence-transmitter magslips

2" control magslips working at 50 c/s.

Characteristics

<u>Element</u>	<u>Transmitter</u>	<u>Coincidence transmitter</u>
British services Nos.	6550 614A	10682 1677A
<u>Primary winding</u>	<u>Rotor</u>	<u>Stator</u>
Number of phases	1	3
Voltage, Volts	50	50
Current, Amps	0.25	0.11
Power, Watts	3.5	2.1
Resistance A.C., Ohms	55	170
Reactance, Ohms	200	450
Impedance, Ohms	208	480
Resistance, D.C., Ohms	35	80
<u>Secondary Winding</u>	<u>Stator</u>	<u>Rotor</u>
Number of phases	3	1
Voltage at maximum coupling, volts	60	30
Voltage gradient, volts per Deg.	-	0.5
Output impedance, Ohms	115	79
Resistance D.C., Ohms	80	50
<u>Mechanical Data</u>		
Weight, kg	0.9	0.9
Rotor inertia, gm. cm <sup>2</sup>	220	220
Bearing friction, gm.cm	29	29
Brush friction, gm. cm	79	79

<u>Performance</u>	<u>Stator</u>	<u>Rotor</u>
Maximum stator error, Degrees	$\pm 0.15$	$\pm 0.15$
" rotor " , "	-	-

Drawing and other details see Muirhead Magslip  
Data Sheet, Muirhead & Company, Limited.

### E.3.2. Potentiometer-bridge

Use two identical miniature precision helical potentiometers with international synchro frame size 11 fixing dimensions.

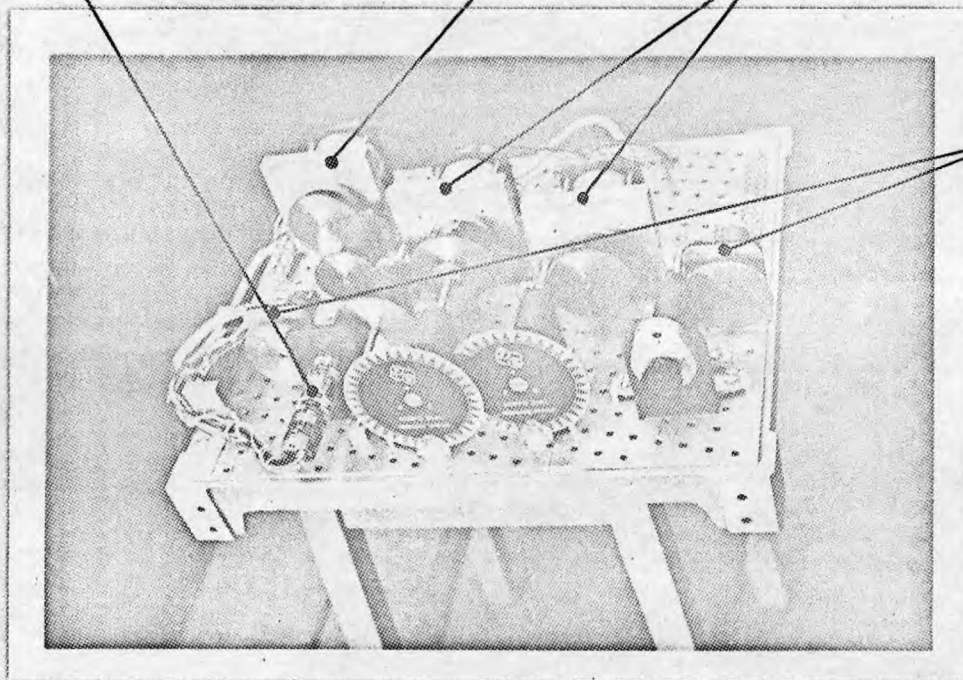
Type C M T.11

### Specifications

<u>Quantities</u>		<u>Units</u>
Temperature range	- 40° to 70°	C
Rating at 40°C	2	watts
Resistance	5	k.Ohms
Resistance tolerance-standard	$\pm 5\%$	
" " -best practical	$\pm 2\%$	
Terminal linearity - standard	$\pm 0.5\%$	
" " - best practical	$\pm 0.2\%$	
Maximum working volts spindle/track	750	volts d.c.
Effective resistance angle	$3600^\circ \pm 2^\circ$	
Maximum starting torque	1	C /in
Number of turns	10	turn

For further mechanical details, see Technical Data on Colvern Helical Potentiometers, Colvern Limited.

### E.4. Photographs for the breadboard model components assembly and the measuring instruments.



POTENTIOMETER  
BRIDGE

### PLATE E.4.1

BREADBOARD MODEL ASSEMBLY OF THE POSITIONAL  
CONTROL AC SERVOMECHANISM

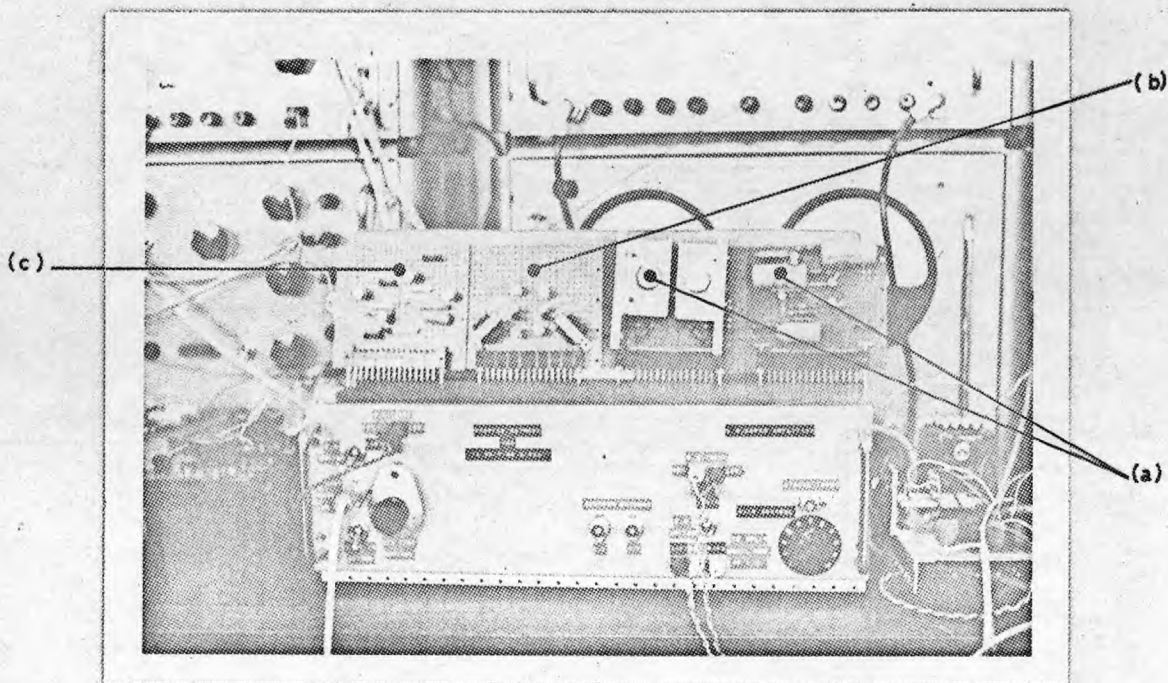


### PLATE E.4.2

a) SERVO-AMPLIFIER TRANSISTOR CIRCUIT

b) 3-TERMINAL SYNCHRONOUS SWITCH (TO BE INCORPORATED IN THE COMPENSATING  
CHOPPER NETWORK)

c) DRIVING CIRCUIT FOR THE SYNCHRONOUS SWITCH



T.F.A. L F OSCILLATOR

T.F.A. CARRIER CONVERTER

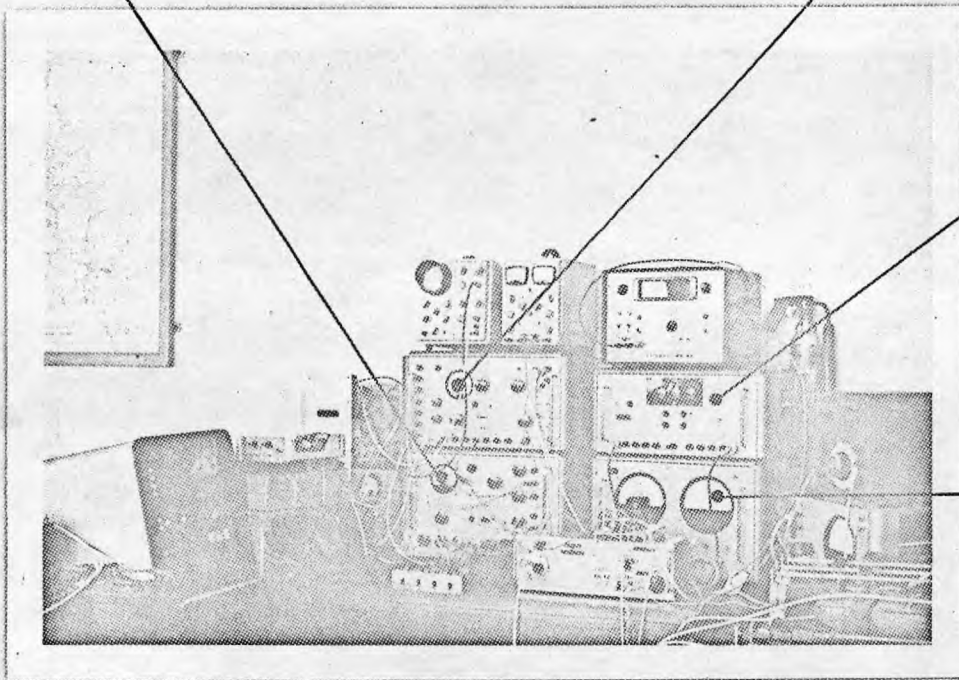
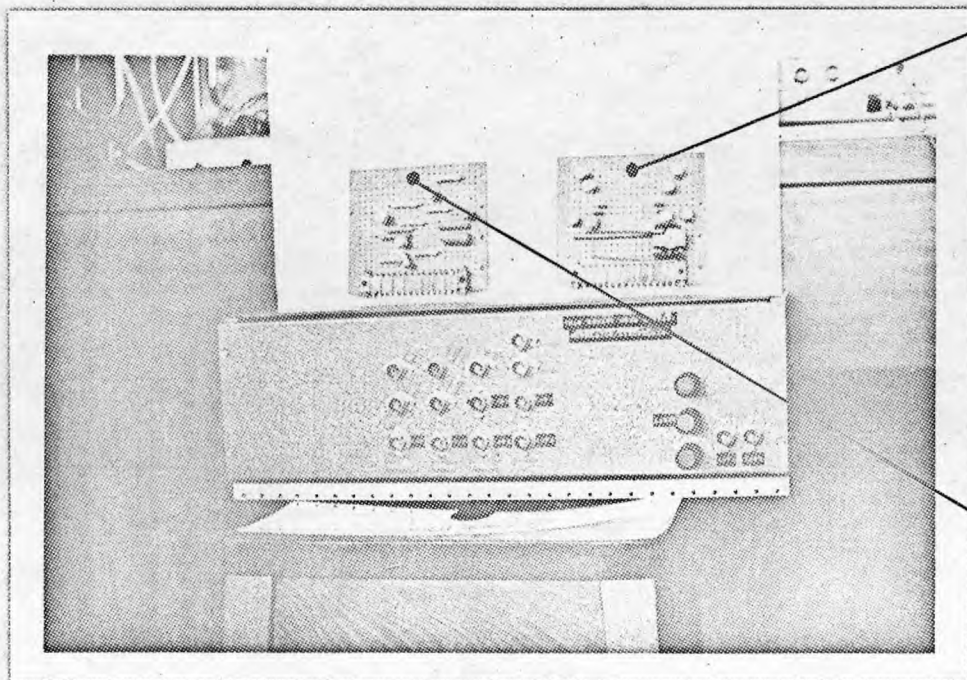
T.F.A. REFERENCE  
RESOLVERT.F.A. RESOLVED  
COMPONENT  
INDICATOR

PLATE E.4.3

EQUIPMENT SET-UP FOR MEASURING THE MODULATION  
FREQUENCY RESPONSE OF CHOPPER NETWORKA SQUARE-WAVE  
MODULATOR OR  
DEMODULATOR

DRIVING CIRCUIT

PLATE E.4.4

SQUARE-WAVE MODULATORS AND DEMODULATORS REQUIRED  
TO REALIZE THE PRINCIPLE OF OPERATION OF THE  
SCHEME PROPOSED IN CHAPTER 8



CHAPTER I

IMPERIAL COLLEGE OF SCIENCE AND TECHNOLOGY

---Department of Electrical Engineering---

Power Systems Laboratory Report No. 67

DESIGN OF A TRANSISTOR 3-TERMINAL SYNCHRONOUS SWITCH  
\*\*\*\*\*

AND ITS DRIVING CIRCUIT  
\*\*\*\*\*

**F.B. Khalafalla**

May, 1967

SYNOPSIS

The paper establishes the practical feasibility of constructing a 3-terminal synchronous switch which is capable of operating with positive and negative fly-time. The 3-terminal switch consists of two symmetrical 2-terminal switches, operating in synchronism with carrier signal. ON-OFF periods of these 2-terminal switches are correlated in such a way as to give the desired overall response.

Design criteria have been developed for a high quality switch employing transistors driven by pulse-transformer. Formulae are given to help in the estimation of different parameters under various operating conditions. An illustrative example, on the use of the developed design procedure, has been presented.

An appropriate driving circuit, capable of controlling the switch fly-time over its positive and negative ranges, has been described and its practical design has been briefly outlined.

CONTENTS

Synopsis

Contents

List of Principal Symbols

- 1.0 Introduction
- 2.0 Principle of Operation
- 3.0 Practical Circuits
  - 3.1 Single diode-bridge
  - 3.2 Double diode-bridge
  - 3.3 Transistor switch
- 4.0 Transistor 3-Terminal Synchronous Switch
  - 4.1 Description
  - 4.2 Switch analysis
    - 4.2.1 Requirements and specifications
    - 4.2.2 Derivation of switch formulae
    - 4.2.3 Principal and secondary parameters of pulse-transformer
    - 4.2.4 Pulse-transformer response equations
    - 4.2.5 Transformer formulae directly involved in the design
  - 4.3 Survey of design procedure
    - 4.3.1 Criteria for selecting the switching transistors
    - 4.3.2 Limits of validity of pulse-transformer principal parameters
    - 4.3.3 Method of calculating the principal parameters of the pulse transformer
    - 4.3.4 Refinements to the prototype design of the pulse-transformer.
    - 4.3.5 Factors influencing Zener diode selection
  - 4.4 Illustrative example

- 5.0 Switch Driving Circuit
  - 5.1 Requirements
  - 5.2 Description
- 6.0 Conclusions
- 7.0 Acknowledgments
- 8.0 References
- 9.0 Appendixes
  - 9.1 Equivalent Circuits of Pulse-Transformer
  - 9.2 Characteristics of Alloy-Junction Germanium Transistor  
Type 2N1302 (N-P-N)

LIST OF PRINCIPAL SYMBOLS

$t$	: time (independent variable)
$S$	: Laplace complex frequency variable
$T$	: period of carrier wave, in seconds
$\omega$	: carrier frequency, in radians/second
$\delta$	: proportion of conducting period of a switch to carrier period
$a$	: proportion of fly-time of a switch to carrier period
$m$	: mark/space ratio of square-wave
$\epsilon$	: infinitesimal quantity
$\theta$	: tilt of pulse flat-top
$n$	: turns ratio of pulse-transformer
$\alpha_n$	: common-base emitter-to-collector current transfer ratio, or normal alpha of transistor
$\alpha_i$	: common-base collector-to-emitter current transfer ratio (for a transistor working on the reverse mode), or inverted alpha
$V_p$	: pulse height
$v_s$	: transformer secondary open-circuit voltage
$I$	: current required to be switched
$I_b, I_c, I_e$	: base, collector and emitter currents of a transistor
$i_p$	: primary current of pulse transformer
$I_{d.c.}$	: direct current in the primary winding of pulse-transformer
$r$	: base resistor
$R_1$	: sum of source and transformer primary winding resistances
$R_2$	: sum of base and transformer secondary winding resistances
$R_c$	: equivalent core-loss (shunt) resistance referred to primary
$L$	: effective shunt inductance referred to primary

$l$  : leakage inductance referred to primary  
 $c_e$  : effective interwinding (shunt) capacitance referred  
to primary



## 1.0 INTRODUCTION

Synchronous switches have significant applications in many fields such as instrumentation, computers and control systems. They form basic units in various chopper-stabilization schemes used to minimize d.c. amplifier drift. They are also employed in constructing choppers suitable for analog-to-digital conversion, for sampled-data-type d.c. measurements, and for electronic analog multiplier-divider required for use in process-control schemes. Chopper networks, comprising passive elements interconnected by one or more 3-terminal synchronous switches, have recently been used as superior type of compensators to carrier control systems.<sup>(1)</sup> Physical realization of a 3-terminal synchronous switch, capable of operating with positive and negative fly-time, was required for use in constructing and developing modified types of chopper networks.<sup>(1)</sup> This establishes the fundamental motive of this paper.

Construction of simple synchronous switches has been physically realized either electromechanically or electronically (employing thermionic valves or solid-state devices.<sup>(2-8)</sup> In view of the numerous advantages of faster response, negligible phase shift (up to about 10 kc/s), higher efficiency, more reliability, longer life, less weight and size, and freedom of problems such as wear, fatigue and contact pitting, electronic switches are much preferred to the electromechanical. In addition, it is simpler, as will be shown in this paper, to control the fly-time of electronic switches over a wide range including zero fly-time which cannot be achieved with electromechanical switches.

On the other hand, solid-state switches are superior, in comparison with the thermionic valve switches, in terms of size, weight, efficiency, reliability and capability of operating under sever conditions of shock and vibration. However, not even a solid-state device acts as a perfect switch due to the reason that

during ON period the resistance between its terminals is not zero, and during OFF period it is not infinity. In addition, the perfect switch has no spurious current or voltage offsets and opens and closes instantaneously. Nevertheless, these imperfections are usually tolerated in many applications and there are some circuit arrangements and additions useful in minimizing them. (4,5,6)

On the basis of the above survey, synchronous switches employing solid-state devices are going to be discussed.

## 2.0 PRINCIPLE OF OPERATION.

Principle of operation of 3-terminal synchronous switch is basically to connect point 3, successively and periodically, to points 1 and 2, as shown in Fig. (1), each for a period of  $\delta T$ . Where the value of  $\delta$  may be adjusted to lie between the limits

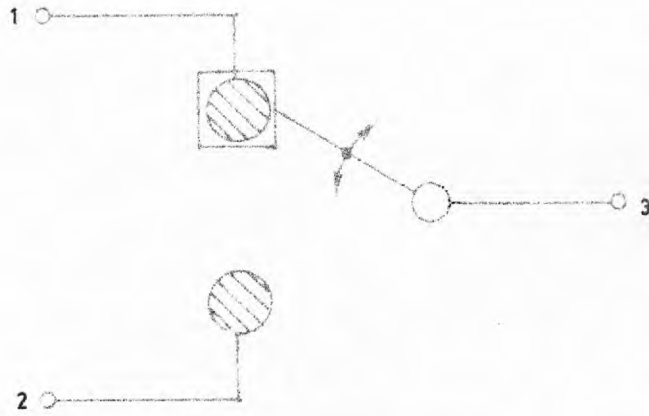
$$0 < \delta < 1 \quad (2.1)$$

Fig. (1) illustrates a simple representation which describes the switch operation, in terms of points 1 and 2 as fixed contacts and a moving contact represented as head of link hinged to point 3. The hinged link swings around point 3 with a fixed angle of travel at carrier frequency  $\omega$ , where

$$\omega = \frac{2\pi}{T} \quad (2.2)$$

The time required for the moving contact to bridge the distance between the two fixed contacts 1 and 2 may conveniently be termed as "Fly-Time". This fly-time can be expressed by the simple relation

$$aT = \left(\frac{1}{2} - \delta\right)T \quad (2.3)$$



**Fig.1**  
**Representation of a 3-terminal synchronous switch**

On the basis of Eqns. (2.1) and (2.3), two modes of switch operation may be possible; operation with positive fly-time (P.F.T), and operation with negative fly-time (N.F.T.). Where P.F.T. and N.F.T. correspond to positive and negative values of  $a$ , respectively. It is evident that operation with zero fly-time (Z.F.T.) can be considered as a common limiting case of P.F.T. and N.F.T. The range of values of  $a$  and  $\delta$ , corresponding to different switch modes of operation, may be written as follows

$$\text{For P.F.T. , } \frac{1}{2} > a \geq 0 \quad , \quad 0 < \delta \leq \frac{1}{2} \quad (2.4a) \quad (2.4)$$

$$\text{For N.F.T. , } 0 \geq a > -\frac{1}{2} \quad , \quad \frac{1}{2} \leq \delta < 1 \quad (2.4b)$$

Due to the fact that most electronic switches are essentially single-throw (ON or OFF) switches, it is appropriate to seek for an alternative arrangement, employing only 2-terminal switches, as an equivalent to that shown in Fig. (1). This can be easily achieved by splitting point 3 into two connected ones, as shown in Fig. (2.a). However, in order to obtain the same overall switch response, it is necessary to introduce a delay period of  $T/2$  between identical operating conditions of the 2-terminal switches.

In this case, it is evident that operation with P.F.T. and N.F.T. is feasible provided that the ratio ON/OFF ( $m$ ), which is related to  $\delta$  and  $a$  as given below,

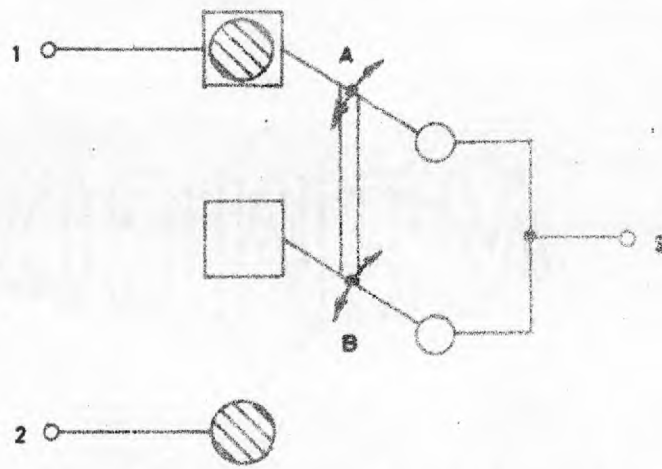
$$m = \frac{\delta}{1-\delta} \quad (2.5a) \quad (2.5)$$

$$= \frac{1-2a}{1+2a} \quad (2.5b)$$

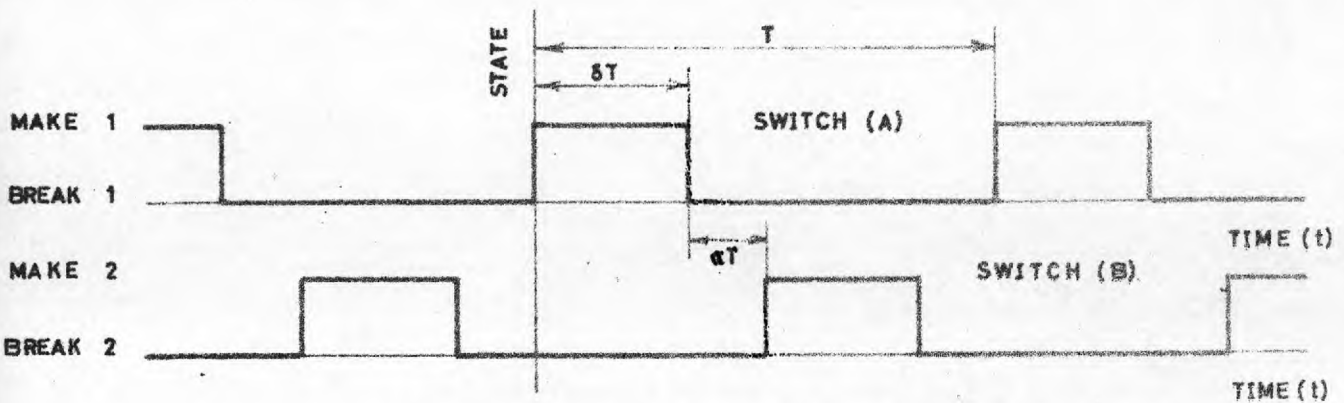
can possibly be adjusted to any value within the ranges specified below

$$\text{For P.F.T. , } 0 < m \leq 1 \quad (2.6a) \quad (2.6)$$

$$\text{For N.F.T. , } 1 \leq m < \infty \quad (2.6b)$$

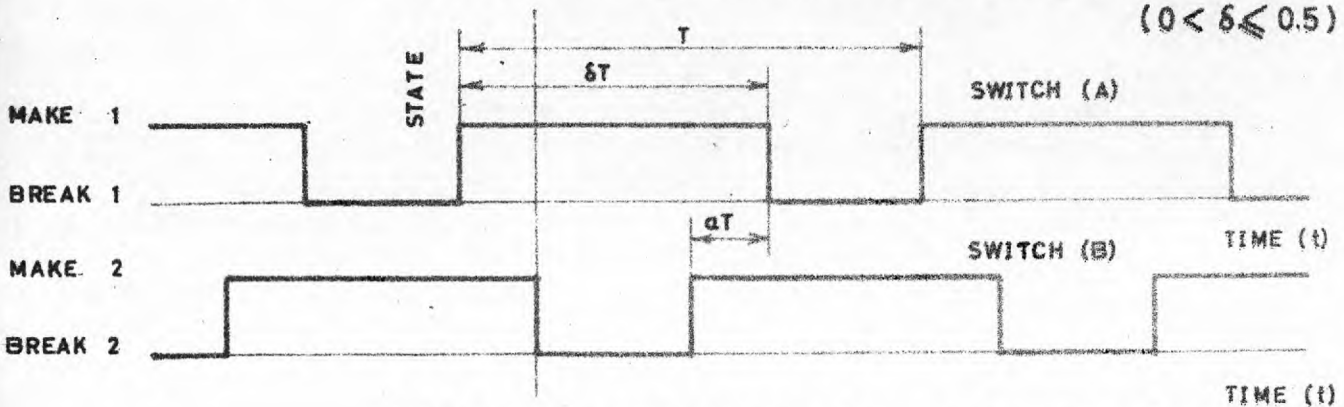


(a) Equivalent arrangement of 2-terminal switches



(b) State/time relationship for P.F.T. mode of operation

$$(0 < \delta \leq 0.5)$$



(c) State/time relationship for N.F.T. mode of operation

$$(0.5 \leq \delta < 1)$$

Fig.2

Alternative representation of 3-terminal synchronous switch and its state/time relationship

Figs. (2.b) and (2.c) illustrate state/time relationship of the 2-terminal switches A and B for P.F.T., and N.F.T. modes of operation.

### 3.0. PRACTICAL CIRCUITS.

There are many practical circuits which can possibly fulfil the 3-terminal synchronous switch operational requirements outlined in the previous section. Only three circuits, employing either diodes or transistors, are going to be described. Emphasis is placed on minimizing various imperfections associated with semiconductor switches by selecting proper designs. For fast switching and minimum interference between control and signal voltages, control voltages for diode and transistor switches are best obtained from low-impedance sources floating with respect to signal ground, such as pulse-transformer windings.

#### 3.1. Single Diode-Bridge

Fig. (3) illustrates a single diode-bridge circuit which simulates the operation of a 3-terminal synchronous switch in a manner similar to that of the arrangement shown in Fig. (1). This type of switch is intended only for operating with Z.F.T. and the control signal is therefore a square-wave carrier with 1/1 mark-space ratio, fed in through a coupling transformer with centre-tapped secondary winding. Two equal resistors are symmetrically inserted in series with the transformer secondary winding to standardize the ON control current flowing through the diodes. The presence of these current limiting resistors combined with that of the transformer secondary resistance and leakage inductance, in the signal path, establishes a major drawback.

#### 3.2. Double Diode-Bridge.

Another possible circuit, using two symmetrical diode-bridges,

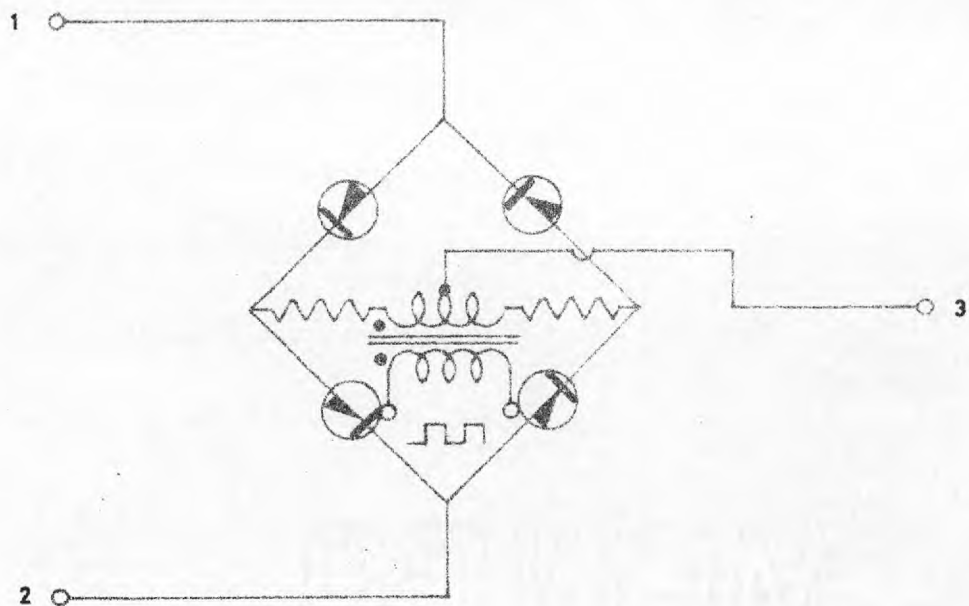


**Fig.3**

Single diode-bridge circuit operating as a Z.F.T.  
3-terminal synchronous switch

is shown in Fig. (4), Each diode-bridge operates as a 2-terminal switch and the combination operates on the same principle as that of the arrangement shown in Fig. (2.a).

To provide a delay period of  $T/2$  between the identical operating conditions of the two diode-bridges, the carrier signal is split into two square-wave control voltage signals,  $v_{p1}$  and  $v_{p2}$ , at  $180^\circ$  phase difference. The two control signals are fed in through two coupling transformers. This type of switch is capable of operating with almost full range of P.F.T. and N.F.T. by means of proper adjustment of the mark/space ratio of the control signals.

Substantial improvement of switching performance is expected due to the removal of the current limiting resistors and the transformer secondary winding from the signal path.

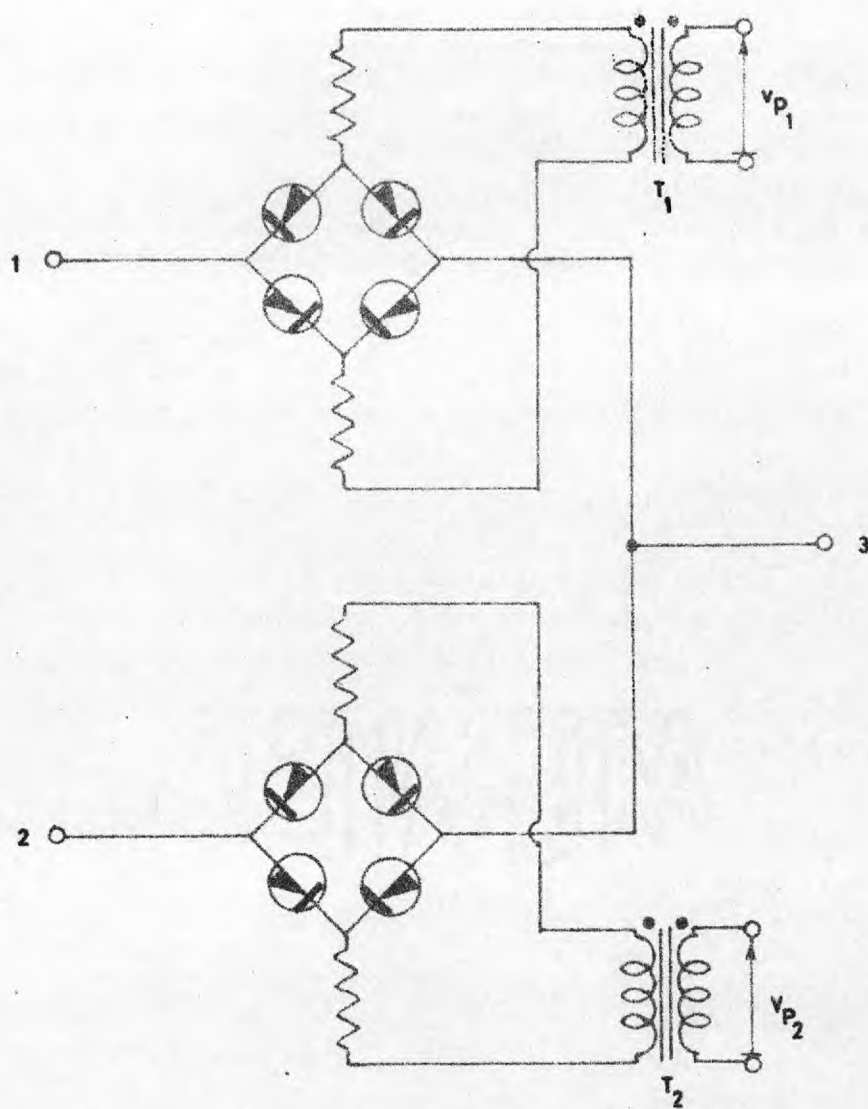
### 3.3. Transistor Switch

Fig. (5) illustrates a transistor switch circuit whose principle of operation and control signal requirements are exactly the same as those of the double diode-bridge switch. This type is also capable of operating with almost full range of P.F.T. and N.F.T.

The circuit comprises two symmetrical 2-terminal switches, each employs a matched pair of inverted transistor switches for partial offset cancellation.<sup>(3,5,6,7)</sup> The matched transistors have a common collector-base structure which accounts for improved thermal matching, reduction in number of thermoelectric junctions, and minimization of interference between control and signal currents.<sup>(7)</sup> For all these reasons, this circuit provides high quality switching of low-level signals.

Due to the superiority of this circuit, its detailed design is going to be discussed in the next section.





**Fig.4**

**Double diode-bridge circuit capable of operating as a P.F.T. and/or N.F.T. 3-terminal synchronous switch**

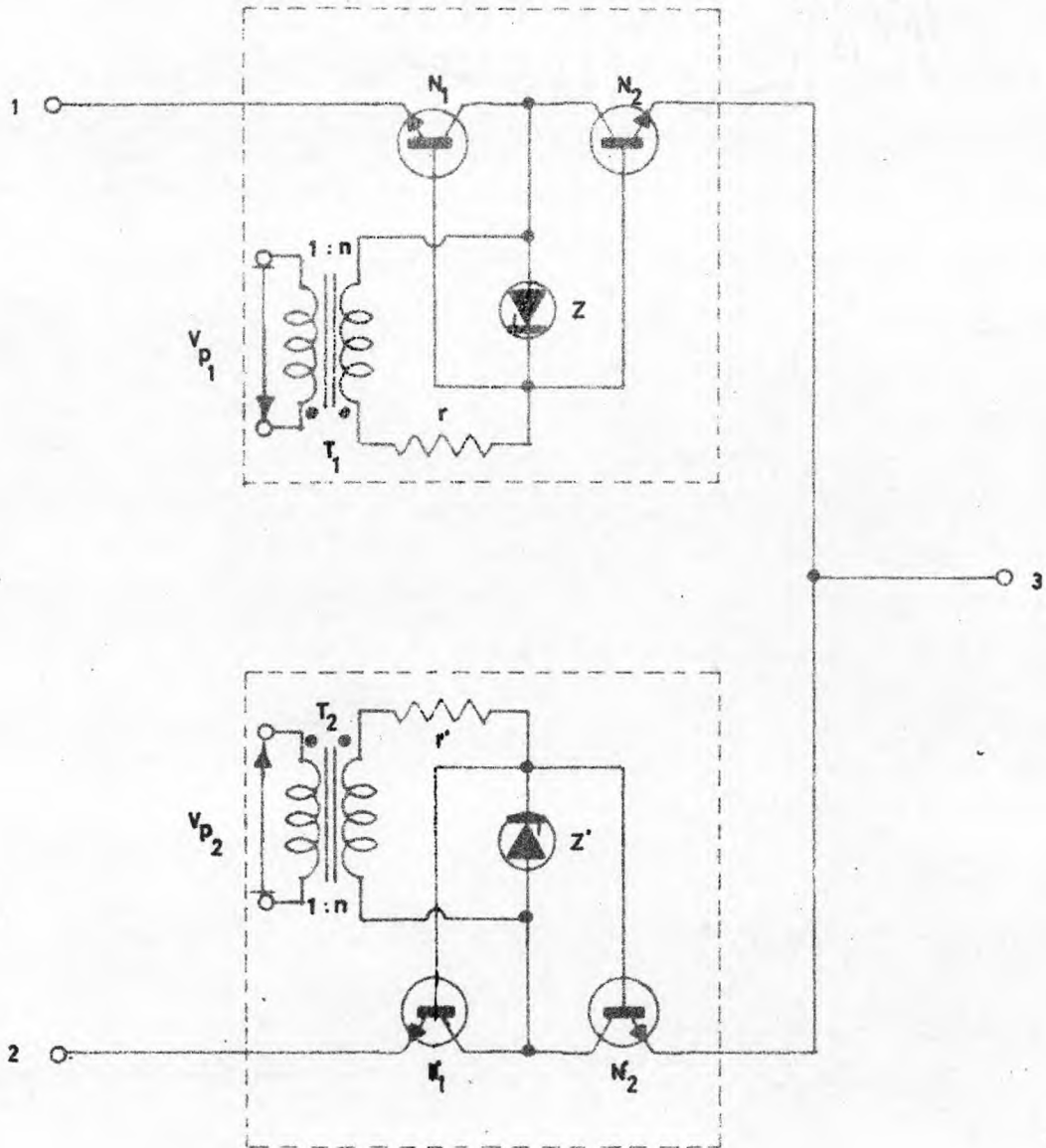


Fig.5

Transistor switch circuit capable of operating as a P.F.T. and/or N.F.T. 3-terminal synchronous switch

#### 4.0. TRANSISTOR 3-TERMINAL SYNCHRONOUS SWITCH.

##### 4.1. Description.

Due to the symmetry of the circuit, shown in Fig. (5), description, analysis, and design can be considerably simplified by confining attention to only one half of the circuit, i.e., a 2-terminal synchronous switch as redrawn in Fig. (6).

Square-wave carrier, with adjustable mark/space ratio, is used as a base drive. For proper operation, isolated driving voltage is required. This can be achieved using a pulse-transformer  $T_1$ . The square-wave control signal is derived from the carrier by means of an appropriate circuit which is designed to provide, in addition, adequate drive to the pulse-transformers, and mark/space ratio control facility, as will be discussed in Section 5.0.

$r$  is base resistor necessary for standardizing the ON control currents flowing through the transistor bases. It also limits the current flowing through the Zener diode  $Z$  during the OFF period. Due to the possibility of high voltage spikes being generated at the front and trailing edges of the transformer output wave-form, an appropriate Zener diode limiter may be used to protect both transistors and pulse-transformer. It also, in conjunction with  $r$ , protects the base-collector common junction of transistors against excessive reverse bias during the OFF period. Furthermore, without the Zener diode, current will flow through the transformer secondary winding during only such periods as the control voltage polarity is as shown in Fig. (6). Negligible current will flow during the reverse polarity, thereby resulting in a net direct current in the transformer secondary winding. Depending on the magnitude of this current, the transformer may become saturated, which imposes further constraint on its design. Whereas, by inserting the Zener diode, in the sense shown in the figure, current will flow through the transformer

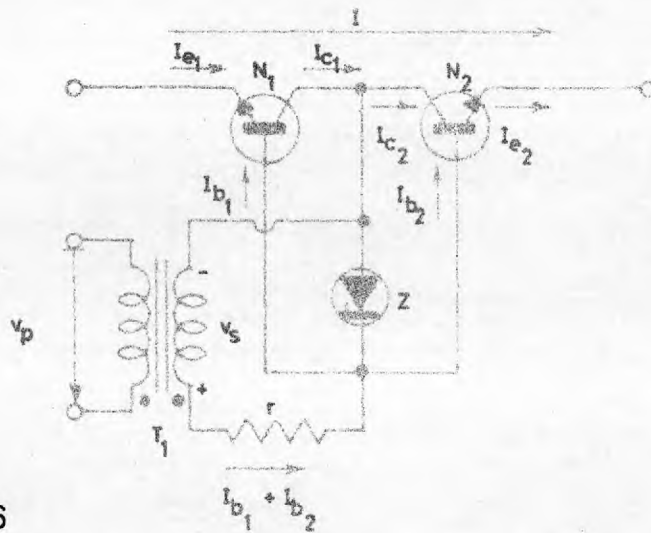
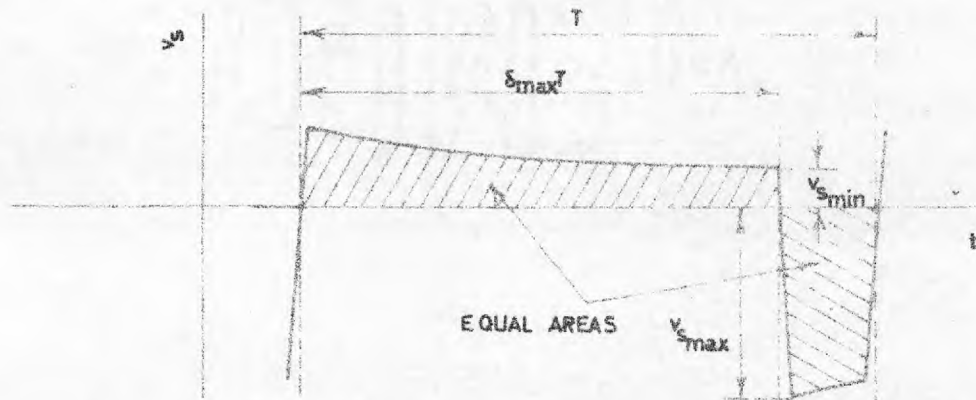
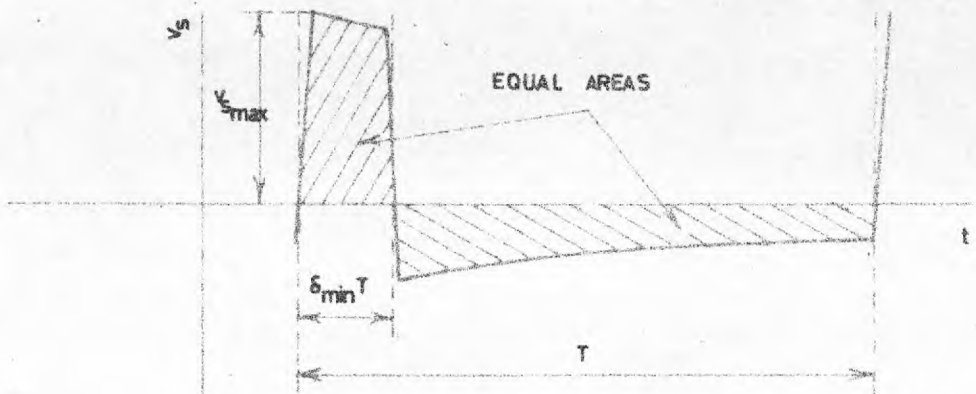


Fig.6  
Transistor 2-terminal synchronous switch



(a) Maximum ON/OFF period ratio ( $m_{max}$ )



(b) Minimum ON/OFF period ratio ( $m_{min}$ )

Fig.7  
Steady-state response of pulse-transformer to rectangular-waves for the conditions of maximum and minimum ON/OFF period ratios

secondary winding in both directions with negligible net direct current. Any such current results only from the possible mismatch between the characteristics of the Zener diode and the parallel combination of the base-collector junction of the transistors.

#### 4.2. Switch Analysis

##### 4.2.1. Requirements and specifications.

The basic requirement is that a current  $I$ , which is a general function of time, can be switched in either direction. The maximum value of that current may be specified according to the given application, knowing the source signal and type of load. In general, the current  $I$  may be conveniently expressed as

$$I_{\max} \geq I \geq -I_{\max} \quad (4.1)$$

The carrier frequency  $\Omega$  and the required range of fly-time (or ON/OFF ratio  $m$ ), must be specified. The magnitude of the square-wave input voltage  $V_p$  and the maximum driving current  $i_{p\max}$ , which are applied to the pulse-transformer primary, and can be determined according to the driving circuit design, should be given.

Other data needed include specifications such as size, weight, power-supply requirements, and design limits on temperature, humidity, shock, .. etc.

##### 4.2.2. Derivation of switch formulae.

Current and voltage polarities, for the switch ON condition, are shown in Fig. (6). Applying Kirchhoff's current law, at each transistor, the following relations can be easily formulated

$$I = I_{e1} = I_{c1} - I_{b1} = \frac{I_{b1}}{(1/\alpha_1 - 1)} \quad (4.2)$$

and

$$I = I_{e2} = I_{c2} + I_{b2} = \frac{I_{b2}}{1 - \alpha_n} \quad (4.3)$$

Where  $I_{b1}$ ,  $I_{c1}$ ,  $I_{e1}$  and  $I_{b2}$ ,  $I_{c2}$ ,  $I_{e2}$  are base, collector, and emitter currents of transistors  $N_1$  and  $N_2$ , respectively. Neglecting the voltage drop across the transformer secondary leakage inductance (justification of this assumption will be explained in subsection 4.2.3.), and applying Kirchhoff's voltage law, it can be easily shown that

$$v_s - v_{cb(ON)} = R_2 (I_{b1} + I_{b2}) \quad (4.4)$$

Where

$v_s$  is the transformer secondary open-circuit voltage,  
 $v_{cb(ON)}$  is the common forward base-collector voltage drop.  
 and  $R_2$  is the series combination of  $r$  and the transformer secondary resistance.

Substituting the values of  $I_{b1}$  and  $I_{b2}$  from Eqns. (4.2) and (4.3), respectively, and rearranging, Eqn. (4.4) reduces to

$$R_2 = \frac{v_s - v_{cb(ON)}}{I \left( \frac{1 - \alpha_i \alpha_n}{\alpha_i} \right)} \quad (4.5)$$

The voltage  $v_s$  is a periodic time function of the form as shown in Fig. (7), for the conditions of maximum and minimum ON/OFF period ratios. In addition, the values of  $\alpha_n$ ,  $\alpha_i$ , and  $v_{cb(ON)}$  vary according to their limits of tolerance. Consequently,  $R_2$ , which is expressed by Eqn. (4.5), has a range of values whose limits vary periodically with time. The proper overall limiting values of  $R_2$  should, then, be calculated to fulfil the requirements under the worst conditions. Expression for the maximum value of  $R_2$  may be obtained from Eqn. (4.5) by substituting the proper

limiting values of various parameters, as

$$R_{2.\max} = \frac{v_{s.\min} - v_{cb(ON)\max}}{I_{\max} \left\{ \frac{1 - \alpha_{i.\min} \alpha_{n.\min}}{\alpha_{i.\min}} \right\}} \quad (4.6)$$

Where  $v_{s.\min}$  occurs at the end of the ON period for condition of maximum ON/OFF ratio, i.e. when  $\delta = \delta_{\max}$ .

The minimum value of  $R_2$  may be determined from eqn. (4.4) such that the resulting value of the sum ( $I_{b1} + I_{b2}$ ) must not exceed roughly twice the maximum rated base-current of the transistor used, under the worst condition. Accordingly, eqn. (4.4) may be rewritten as

$$R_{2.\min} \cong \frac{v_{s.\max} - v_{cb(ON)\min}}{2 I_{b.\max}} \quad (4.7)$$

Where  $v_{s.\max}$  occurs at the beginning of the ON period for the condition of minimum ON/OFF ratio, i.e. when  $\delta = \delta_{\min}$ .

Considering  $v_{cb(ON)\min}$  to be equal to zero for the worst condition, eqn. (4.7) may be rewritten as

$$R_{2.\min} = \frac{v_{s.\max}}{2 I_{b.\max}} \quad (4.8)$$

For a successful design, the ratio  $R_{2.\max}/R_{2.\min}$  must be equal to or greater than unity. This constraint of realizability may be written as

$$\Delta = R_{2.\max}/R_{2.\min} = \frac{2\alpha_{i.\min}}{1 - \alpha_{i.\min} \alpha_{n.\min}} \cdot \frac{I_{b.\max}}{I_{\max}} \cdot \left\{ \frac{v_{s.\min}}{v_{s.\max}} - \frac{v_{cb(ON)\max}}{v_{s.\max}} \right\} \gg 1 \quad (4.9)$$

It is convenient to introduce the dimensionless parameters

$$\beta = \frac{2 \alpha_{i.min}}{1 - \alpha_{i.min} \alpha_{n.min}} \quad 4.10a$$

$$\gamma = I_{b.max} / I_{max} \quad 4.10b \quad (4.10)$$

$$e = v_{s.min} / v_{s.max} \quad 4.10c$$

Eqn. (4.9) may then be rewritten as

$$\Delta = \beta \gamma \left\{ e - v_{cb} / v_{s.max} \right\} \quad (4.11)$$

$$\text{where } v_{cb} = v_{cb(ON)max} \quad (4.12)$$

The proper value of  $R_2$  may be conveniently taken as the average value of  $R_{2.max}$  and  $R_{2.min}$ , thus

$$R_2 = \frac{1}{2} (R_{2.max} + R_{2.min}) = \frac{1}{2} R_{2.min} (1 + \Delta) \quad (4.13)$$

Substituting the results of eqns. (4.8) and (4.11) in eqn. (4.13), it is easy to obtain

$$R_2 = \frac{r_1 \beta \gamma}{4} \frac{(1 + \Delta)}{(\beta \gamma e - \Delta)} \quad (4.14)$$

$$\text{where } r_1 = v_{cb} / I_{b.max} \quad (4.15)$$



#### 4.2.3. Principal and Secondary Parameters of Pulse-Transformer.

In the process of designing a pulse-transformer, a large number of factors are involved. Initially, specifications should be put forward according to the requirements. For this particular application, the specifications may be summarized as: the pulse input voltage  $V_p$ , maximum primary current  $i_{p.max}$ , carrier frequency  $\omega$ , range of fly-time  $a$  or ON/OFF ratio  $m$ , the allowable rise-time and overshoot on the leading edge of the pulse, the allowable tilt  $\delta$  of the pulse-top, the allowable back swing at the pulse termination, the generator impedance, and the load impedance.

On the basis of the above specifications, it is possible to determine the value of some transformer parameters such as  $R_1$ ,  $R_2$ ,  $L$ ,  $n$ , and  $I_{d.c.max}$ , as will be shown in subsection (4.3.3). Since the knowledge of value of these parameters is essential for constructing the transformer, it is therefore convenient to give them the term "Principal Parameters".

After selecting the core material, computing the transformer geometry and number of turns of each coil, the leakage inductance  $\ell$  and the core loss, which may be represented by a shunting resistance  $R_c$ , can be calculated.<sup>(9-13)</sup> Also, interturn and interwinding capacitances can be calculated from the knowledge of the dielectric constant of the insulation and transformer structure<sup>(13)</sup>. These capacitances can be approximated by an equivalent shunt lumped capacitance  $C$ . Since, determination of values of the three parameters  $\ell$ ,  $R_c$ , and  $C$  depends entirely on a prior knowledge of the transformer structure, in which they have not participated as a direct means, the term "Secondary Parameters" may conveniently be given to them. However, the calculated secondary parameters help in checking as to whether the predicted dynamic response of the tentative transformer design

will meet the specified requirements, and according to the results, design alterations may be suggested.

#### 4.2.4. Pulse-Transformer Response Equations.

A clearer picture of the pulse-transformer load may be visualized from the simple representation shown in Fig. (8). Where diode D is introduced to represent the behaviour of the parallel combination of base-collector junctions of transistors  $N_1$  and  $N_2$ , as viewed by the transformer.

According to Appendix (9.1), three sets of differential equations may be formulated whose solution describes the transformer behaviour, under conditions of square-wave input signal, at the three regions; front edge, flat top, and termination of the input pulses. Figs. (9.2) to (9.4) show three approximate equivalent circuits which may be used to obtain responses at the three regions. It is evident that rise-time and decay-time responses involve the secondary parameters  $\ell$  and  $C$ . However, the rise and fall times may, in general, be neglected with respect to the flat-top time and remaining part of the decay-time without imposing serious errors. Therefore, transformer response, corresponding to only these portions, is going to be obtained.

Derivation of various equations is based on the following reasonable assumptions:

- i) Leakage inductance  $\ell$  and shunt capacitance  $C$  are neglected.
- ii) Inductance  $L$  is assumed constant which is valid as long as the iron is not saturated.
- iii) Negligible core loss.
- iv) Negligible voltage drop across the parallel combination of diodes  $Z$  and  $D$ , shown in Fig. (8).
- v) Negligible generator impedance.

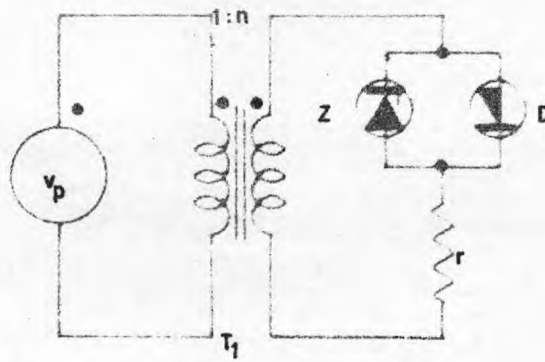


Fig.8

Representation of the 2-terminal synchronous switch shown in Fig.6

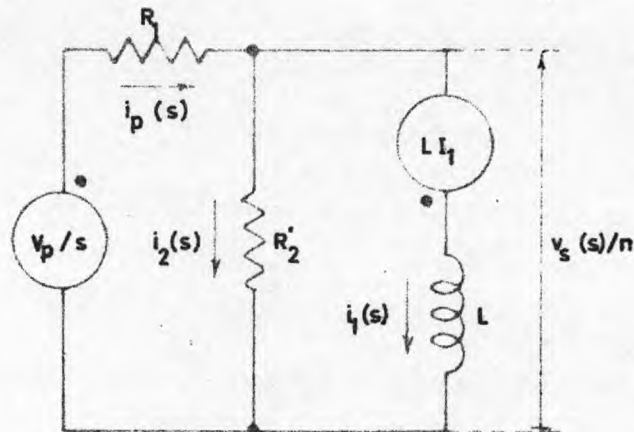


Fig.9

Circuit used to set up the pulse-transformer response equations during ON period of the switch

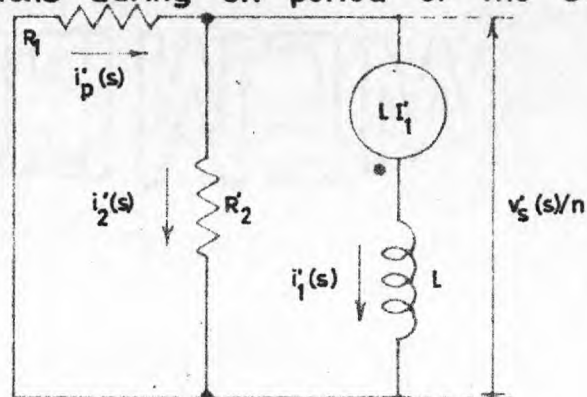


Fig.10

Circuit used to set up the pulse-transformer response equations during OFF period of the switch

#### 4.2.4.1. During ON Period.

On the basis of the discussion and assumptions presented above, Fig. (9) may be derived from Figs. (8) and (9.2) to represent the transformer equivalent circuit and its load during the ON condition of the switch. Assuming that time origin is coinciding with the starting instant of the ON period, and taking into account the proper initial value of the inductor current, the input voltage can then be considered as a step function of magnitude  $V_P$  which is applied at  $t = 0$ . Consequently, current  $i_p$  can be easily obtained, by help of Fig. (9), and be expressed in the Laplacian form as follows

$$i_p(s) = \frac{V_P}{s} \frac{1}{R_1 + R_2'} \left( \frac{s + 1/\tau_2}{s + 1/\tau_1} \right) + I_1 \frac{R_2'}{R_1 + R_2'} \left( \frac{1}{s + 1/\tau_1} \right) \quad (4.16)$$

Where  $\tau_2 = L/R_2'$  , (4.17a)

$$\tau_1 = L / \left( \frac{R_1}{R_1 + R_2'} \right) , \quad (4.17b)$$

and  $I_1$  is the initial condition value of the current in the inductor at time  $t = 0$  (4.18)

Applying Kirchhoff voltage and current laws for the circuit shown in Fig. (9), the following relations can be easily derived

$$\frac{v_s(s)}{n} = R_2' i_2(s) = sL i_1(s) - L I_1 \quad (4.19)$$

and

$$i_p(s) = i_1(s) + i_2(s) \quad (4.20)$$

Solving for  $i_1(s)$  and  $v_s(s)$  using the simultaneous eqns. (4.19) and (4.20), hence

$$i_1(s) = \frac{i_p(s) + \tau_2 I_1}{1 + \tau_2 s} \quad (4.21)$$

and

$$\frac{v_s(s)}{n} = L \frac{s i_p(s) - I_1}{1 + \tau_2 s} \quad (4.22)$$

In order to obtain time-domain solution for  $i_p$ ,  $i_1$ , and  $v_s$ , the inverse Laplace has to be taken for eqns. (4.16), (4.21) and (4.22), respectively. This yields the following expressions

$$i_p(t) = \frac{V_p}{R_1} \left\{ 1 - \frac{R_2'}{R_1 + R_2'} e^{-t/\tau_1} \right\} + I_1 \frac{R_2'}{R_1 + R_2'} e^{-t/\tau_1} \quad (4.23)$$

$$i_1(t) = \frac{V_p}{R_1} \left\{ 1 - e^{-t/\tau_1} \right\} + I_1 e^{-t/\tau_1} \quad (4.24)$$

and

$$\frac{v_s(t)}{n} = V_p \frac{R_2'}{R_1 + R_2'} e^{-t/\tau_1} - I_1 \frac{R_1 R_2'}{R_1 + R_2'} e^{-t/\tau_1} \quad (4.25)$$

#### 4.2.4.2. During OFF Period.

Using Figs. (8) and (9.4b), it is possible to derive the circuit shown in Fig. (10) to represent the transformer equivalent circuit and its load during the OFF condition of the switch. Under this condition it is evident that both the circuit diagram and various expressions can be easily derived from their corresponding ones obtained under the CN condition, provided that the following modifications are made

$$V_p \quad \text{to be replaced by} \quad 0 \quad (4.2.6a)$$

$$I_1 \quad \text{" " " " } I_1' \quad (4.2.6b) \quad (4.26)$$

$$\text{Time origin assumed to be at } t = \delta T \quad (4.2.6c)$$

On the basis of the above modifications, time-domain expressions for  $i'_p$ ,  $i'_1$  and  $\frac{v'_s}{n}$  can be directly written from eqns. (4.23) to (4.25), as

$$i'_p(t) = I_1 \frac{R'_2}{R_1 + R'_2} e^{-t/\tau_1} \quad (4.27)$$

$$i'_1(t) = I'_1 e^{-t/\tau_1} \quad (4.28)$$

and

$$\frac{v'_s(t)}{n} = -I'_1 \frac{R_1 R'_2}{R_1 + R'_2} e^{-t/\tau_1} \quad (4.29)$$

#### 4.2.4.3. Steady-State Boundary Conditions.

As the synchronous switch starts to function, two different types of transients are encountered; "Initial Transient", which occurs as a result of the initial sudden application of electric signal to start the switching mechanism, and "Cyclic Transient", which occurs twice per carrier cycle corresponding to the infinitesimal transitional periods during which the switch changes its state from ON to OFF or vice versa, which coincide with the input square-wave discontinuities.

In order to avoid unnecessary complications, the boundary conditions are going to be examined after a sufficiently long period to justify the assumption that initial transient has reached its steady state. On this basis, the average transformer secondary voltage, during a complete carrier cycle, must be zero. This may be expressed as

$$\int_{\xi \rightarrow 0}^{(\delta T - \xi)} v_s(t) dt + \int_{\xi \rightarrow 0}^{\{(1-\delta)T - \xi\}} v'_s(t) dt = 0 \quad (4.30)$$

But,  $v_s(t)$  and  $v'_s(t)$  can be expressed in terms of  $i_1(t)$  and  $i'_1(t)$ , respectively, as follows

$$v_s(t) = nL \frac{di_1(t)}{dt} \quad (4.31a)$$

and

$$v'_s(t) = nL \frac{di'_1(t)}{dt} \quad (4.31b)$$

Substituting the results of eqn. (4.31) in eqn. (4.30) and solving the integration, the following can be easily obtained

$$i_1(\delta T - \xi) - I'_1 \Big|_{\xi \rightarrow 0} = I_1 - i'_1 \Big|_{\xi \rightarrow 0} \left\{ (1-\delta) T - \xi \right\} \quad (4.32)$$

It is conceivable that under any transient condition, the current in the inductor does not undergo abrupt change. Consequently, an equation can be set up to relate the inductor currents before and after the infinitesimal transitional period starting at the instant  $t = \delta T$ , thus

$$i_1(\delta T - \xi) = I'_1 \quad (4.33)$$

$$\xi \rightarrow 0$$

From eqns. (4.32) and (4.33), the following may be deduced

$$i'_1 \left\{ (1-\delta) T - \xi \right\} = I_1 \quad (4.34)$$

$$\xi \rightarrow 0$$

Using the solutions expressed by eqns. (4.24) and (4.28), eqns. (4.33) and (4.34) may be rewritten as

$$I_1' = \frac{V_p}{R_1} \left\{ 1 - e^{-\delta T/\tau_1} \right\} + I_1 e^{-\delta T/\tau_1} \quad (4.35)$$

and

$$I_1 = I_1' e^{-(1-\delta)T/\tau_1} \quad (4.36)$$

Solving the two simultaneous eqns. (4.35) and (4.36),  $I_1$  and  $I_1'$  may be expressed as

$$I_1 = \frac{V_p}{R_1} \frac{1 - e^{-\delta T/\tau_1}}{1 - e^{-T/\tau_1}} e^{-(1-\delta)T/\tau_1} \quad (4.37)$$

and

$$I_1' = \frac{V_p}{R_1} \frac{1 - e^{-\delta T/\tau_1}}{1 - e^{-T/\tau_1}} \quad (4.38)$$

#### 4.2.5. Transformer Formulae Directly Involved in the Design

In this subsection, it is intended to relate various transformer principal parameters and design constraints in a condensed number of formulae which are arranged in such a form to be useful for the design procedure.

- i) The tilt of the transformer output voltage  $v_s$ , for a particular value of  $\delta$ , may be defined as

$$\sigma = 1 - v_{s.min}/v_{s.max} \quad (4.39)$$

Where  $v_{s.min}$  and  $v_{s.max}$  may be deduced from eqn. (4.25), as

$$v_{s.max} = v_s(\xi t) \quad (4.40a)$$

and  $\xi \rightarrow 0 \quad (4.40)$

$$v_{s.min} = v_s(\delta T - \xi) \quad (4.40b)$$

$$\xi \rightarrow 0$$

Substituting eqn. (4.40) into eqn. (4.39), and using the



result of eqn. (4.25), then

$$\sigma = 1 - e^{-\delta T/\tau_1} \quad (4.41)$$

Since, the maximum allowable tilt plays a predominant part in the design, therefore an expression for it may be directly deduced from eqn. (4.41) and written as

$$\sigma_{\max} = 1 - e^{-\delta_{\max} T/\tau_1} \quad (4.42)$$

ii) Another important constraint is the maximum transformer primary current  $i_{p.\max}$ , whose value may be specified according to the driving circuit capability. An expression for  $i_{p.\max}$  can be easily obtained from eqns. (4.23) and (4.37), as given below

$$\begin{aligned} i_{p.\max} &= i_p(\delta_{\max} T - \xi) \\ &\quad \xi \rightarrow 0 \\ &= \frac{V_p}{R_1} \left\{ 1 - \frac{R_2'}{R_1 + R_2'} \frac{1 - e^{-(1-\delta_{\max})T/\tau_1}}{1 - e^{-T/\tau_1}} e^{-\delta_{\max} T/\tau_1} \right\} \end{aligned} \quad \dots(4.43)$$

iii) Since,  $R_2$  depends on the maximum and minimum value of the transformer output voltage  $v_{s.\max}$ ,  $v_{s.\min}$ , it will be convenient to derive expressions for them. This is given below using results of eqns. (4.25) and (4.37)

$$\begin{aligned} \frac{v_{s.\max}}{n} &= \frac{v_s(\xi t)}{n} \Bigg|_{\substack{\xi \rightarrow 0 \\ \delta = \delta_{\min}}} \\ &= V_p \frac{R_2'}{R_1 + R_2'} \frac{1 - e^{-(1-\delta_{\min})T/\tau_1}}{1 - e^{-T/\tau_1}} \quad (4.44) \end{aligned}$$

and

$$\frac{v_{s.min}}{n} = \frac{v_s (\delta_{max} T - \xi)}{n} \Big|_{\substack{\xi \rightarrow 0 \\ \delta = \delta_{max}}} = V_p \frac{R'_2}{R_1 + R'_2} \left\{ \frac{1 - e^{-(1-\delta_{max})T/\tau_1}}{1 - e^{-T/\tau_1}} \right\} e^{-\delta_{max} T/\tau_1}$$

$$= V_p - R_1 i_{p.max} \quad (4.45)$$

The ratio  $v_{s.min}/v_{s.max}$  can then be written as

$$e = \frac{1 - e^{-(1-\delta_{max})T/\tau_1}}{1 - e^{-(1-\delta_{min})T/\tau_1}} e^{-\delta_{max} T/\tau_1} \quad (4.46)$$

- iv) The knowledge of the maximum direct current  $I_{d.c.max}$ , flowing through the transformer primary winding, is essential to check the degree of iron saturation and to compute the proper air-gap dimensions if required.  $I_{d.c.}$  can be calculated as the average of  $i_p$  over one carrier cycle, thus

$$I_{d.c.} = \frac{1}{T} \left\{ \int_0^{\delta T - \xi} i_p(t) dt + \int_0^{\{(1-\delta)T - \xi\}} i'_p(t) dt \right\}_{\xi \rightarrow 0} \quad ..(4.47)$$

From eqns. (4.23), (4.37) and (4.27), (4.38),  $i_p(t)$  and  $i'_p(t)$  may be rewritten, respectively as

$$i_p(t) = \frac{V_p}{R_1} \left\{ 1 - \frac{R'_2}{R_1 + R'_2} \frac{1 - e^{-(1-\delta)T/\tau_1}}{1 - e^{-T/\tau_1}} e^{-t/\tau_1} \right\} \quad (4.48)$$

and

$$i'_p(t) = \frac{V_p}{R_1} \left\{ \frac{R'_2}{R_1 + R'_2} \frac{1 - e^{-\delta T/\tau_1}}{1 - e^{-T/\tau_1}} e^{-t/\tau_1} \right\} \quad (4.49)$$

Substituting the expressions of  $i_p(t)$  and  $i'_p(t)$  in eqn. (4.47), and solving the integration, then

$$I_{d.c.} = \frac{V_p}{R_1} \delta \quad (4.50)$$

Eqn. (4.50) shows that  $I_{d.c.}$  is directly proportional to  $\delta$ , therefore

$$I_{d.c.max} = \frac{V_p}{R_1} \delta_{max} \quad (4.51)$$

### 4.3. Survey of Design Procedure

#### 4.3.1. Criteria for Selecting the Switching Transistors.

Having specified the parameters  $\sigma_{max}$ ,  $\delta_{max}$  and  $T$ , the value of  $\tau_1$  can then be calculated from eqn. (4.42). As a result, the value of  $\rho$  can be determined since it is a function of  $\tau_1$ , as given by eqn. (4.46) where  $\delta_{min}$  is again a specified quantity.

For any particular transistor,  $I_{b.max}$ ,  $V_{cb}$ ,  $\alpha_{n.min}$ , and  $\alpha_{i.min}$  may be regarded as specified parameters. It is possible then, to evaluate  $\beta$ ,  $\gamma$ , and  $r_1$  using eqns. (4.10a), (4.10b) and (4.15).

On this basis,  $R_2$  varies only with  $\Delta$  in a manner as described by eqn. (4.14). This function can be easily plotted whose form is as shown in Fig. (11). Since  $R_2$  represents a positive real physical quantity, only the portion of the curve lying above  $\Delta$ -axis should be considered for practical solution. A vertical line, passing through the lower limit value of  $\Delta$  ( $\Delta = 1$ ), is drawn to represent a boundary for the zone of feasible solution. Another boundary may be set up at  $\Delta = \beta \gamma \epsilon$ . Therefore, a feasible solution for  $R_2$  exists only when

$$\beta \gamma \epsilon \geq 1 \quad (4.52)$$

Substituting back various parameters, eqn. (4.52) may be conveniently rewritten as

$$\frac{2 \alpha_{i.min}}{1 - \alpha_{i.min} \alpha_{n.min}} I_{b.max} \geq \frac{1 - e^{-(1 - \delta_{min})T/\tau_1}}{1 - e^{-(1 - \delta_{max})T/\tau_1}} \frac{I_{max}}{e^{-\delta_{max}T/\tau_1}} \quad (4.53)$$

Where 
$$\tau_1 = \delta_{max} T / \log\left(\frac{1}{1 - \delta_{max}}\right) \quad (4.54)$$

Eqn. (4.53) establishes a simple realization criteria, relating transistor parameters to the required switch specifications, which must be satisfied by the selected transistor.

Other factors, which govern the choice of transistor, may be summarized in the following points:

- i) The total transistor switching time  $t_t$  (see Appendix (9.2)) must be very small compared to the minimum switch conducting period  $\delta_{min} T$ .

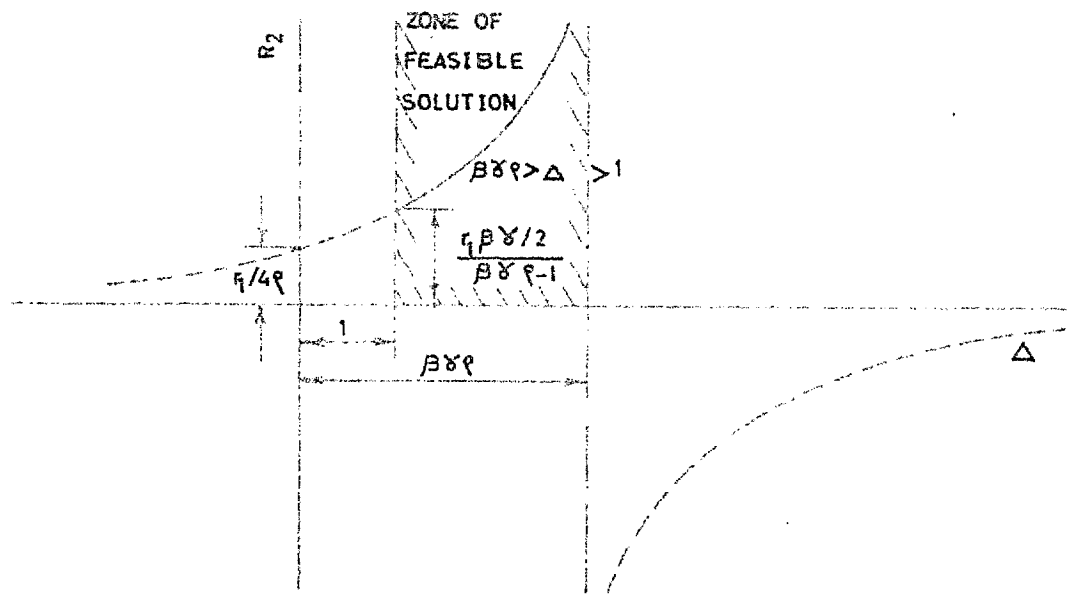


Fig.11

Variation of  $R_2$  with  $\Delta$ , as given by Eq.4.14

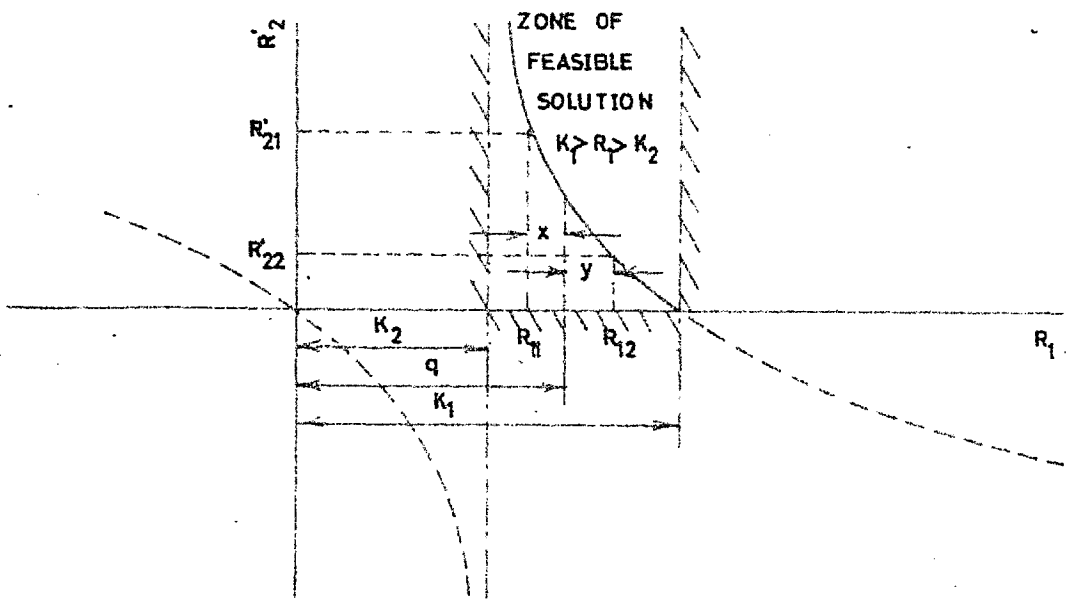


Fig.12

Variation of  $R'_2$  with  $R_1$ , as given by Eq.4.55

- ii)  $I_{\max}$  must not exceed the maximum rated collector current.
- iii) The maximum signal voltage, required to be switched ON and OFF with either polarity, must be less than the transistor breakdown voltage.

In general, alloy-junction or epitaxial-planer type of transistors may be employed for they combine low saturation resistance with relatively small junctions for high switching speed.<sup>(8)</sup>

#### 4.3.2. Limits of Validity of Pulse-Transformer Principal Parameters.

Having selected the proper switching transistor, values of its various parameters  $\alpha_n$ ,  $\alpha_i$ ,  $I_{b.\max}$ , and  $V_{cb}$  may be obtained either from supplied data or by simple test and thus will be considered constant throughout subsequent treatment. Other parameters, which will also be treated as constants, are those which are specified such as  $\omega_{\max}$ ,  $\delta_{\max}$ ,  $\delta_{\min}$ ,  $T$ ,  $V_p$ ,  $I_{\max}$ , and  $i_{p.\max}$ . As a result, it is easy to prove that  $\beta$ ,  $\gamma$ ,  $r_1$ ,  $\tau_1$ , and  $\epsilon$  can be evaluated and hence will be considered fixed quantities.

Eqn. (4.43) expresses the relationship between  $R_1$  and  $R_2'$  in an implicit form. Solving for  $R_2'$  in terms of  $R_1$ , thus

$$R_2' = R_1 \left( \frac{K_1 - R_1}{R_1 - K_2} \right) \quad (4.55)$$

Where 
$$K_1 = V_p / i_{p.\max} \quad (4.56)$$

and 
$$K_2 = \frac{V_p}{i_{p.\max}} \left\{ 1 - \frac{1 - e^{-(1-\delta_{\max})T/\tau_1}}{1 - e^{-T/\tau_1}} e^{-\delta_{\max} T/\tau_1} \right\} \quad \dots(4.57)$$

This function can be easily plotted whose form is as shown in Fig. (12). Since both  $R_1$  and  $R_2'$  represent positive real physical quantities, then the practical solution exists only in the zone lying between the limits

$$K_2 < R_1 < K_1 \quad (4.58)$$

Solving the simultaneous eqns. (4.45) and (4.55), and using the relations  $\frac{R_2}{n^2} = R_2'$ , it is easy to deduce an expression for  $R_1$  in terms of  $\Delta$  as given below

$$R_1^2 - (K_1 + K_2 - Q_1) R_1 + K_1 K_2 = 0 \quad (4.59)$$

where

$$\begin{aligned} Q_1 &= \left( \frac{v_{s.min}}{i_{p.max}} \right)^2 \frac{1}{R_2} \\ &= \frac{(2 r_2 e)^2 \beta \gamma}{r_1} \frac{1}{(\beta \gamma e - \Delta)(1 + \Delta)} \end{aligned} \quad (4.60)$$

Wherein  $r_2 = V_{cb}/i_{p,max}$  (4.61)

This implies that for every value of  $\Delta$ , there are two corresponding values for  $R_1$ , which are the roots of eqn. (4.59). Assuming that these roots are  $R_{11}$  and  $R_{12}$ , then

$$R_{11} \cdot R_{12} = K_1 K_2 \quad (4.62)$$

$$R_{11} + R_{12} = K_1 + K_2 - Q_1 \quad (4.63)$$

From eqn. (4.62), it follows that  $R_{11} \cdot R_{12}$  is a positive

constant quantity  $K_1 K_2$ , from which the extreme values of the roots.

$$K_{11} = K_2 \quad \text{and} \quad R_{12} = K_1 \quad (4.64)$$

may be set up to comply with condition (4.58).

In general, the roots may be written as

$$R_{11} = q - x \quad (4.65)$$

$$R_{12} = q + y \quad (4.66)$$

Where  $q = \sqrt{K_1 K_2} \quad (4.67a)$

$$q - K_2 \gg x \gg 0 \quad (4.67b) \quad (4.67)$$

and  $K_1 - q \gg y \gg 0 \quad (4.67c)$

Substituting eqns. (4.65) and (4.66) into eqns. (4.62) and (4.63), the following relations can be deduced

$$y = \frac{q x}{q - x} \quad (4.68)$$

$$Q_2 = K_1 + K_2 - 2q - \frac{x^2}{q - x} \quad (4.69)$$

Where  $Q_2 = Q_1 \quad (4.70)$

Plotting  $Q_2$  as a function of  $x$  and  $Q_1$  as a function of  $\Delta$ , whose form are as shown in Figs. (13) and (14), respectively, it is easy to derive conditions for existence of feasible solution according to the relative position of the minimum value of  $Q_1$  (which occurs at  $\Delta = \frac{\beta \gamma - 1}{2}$ ) with respect to the lower limiting



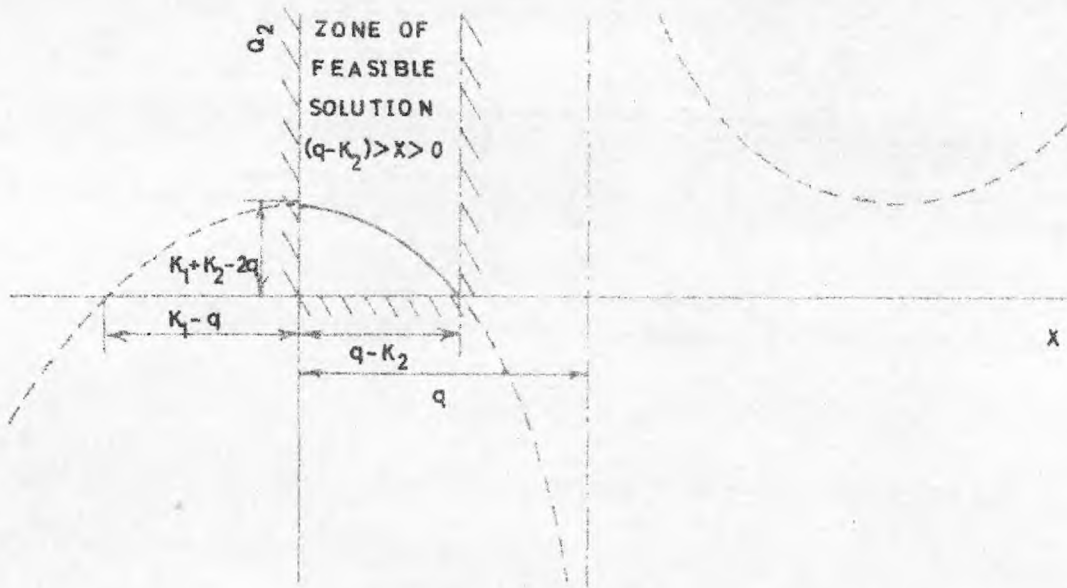


Fig.13

Variation of  $Q_2$  with  $X$ , as given by Eq.4.69

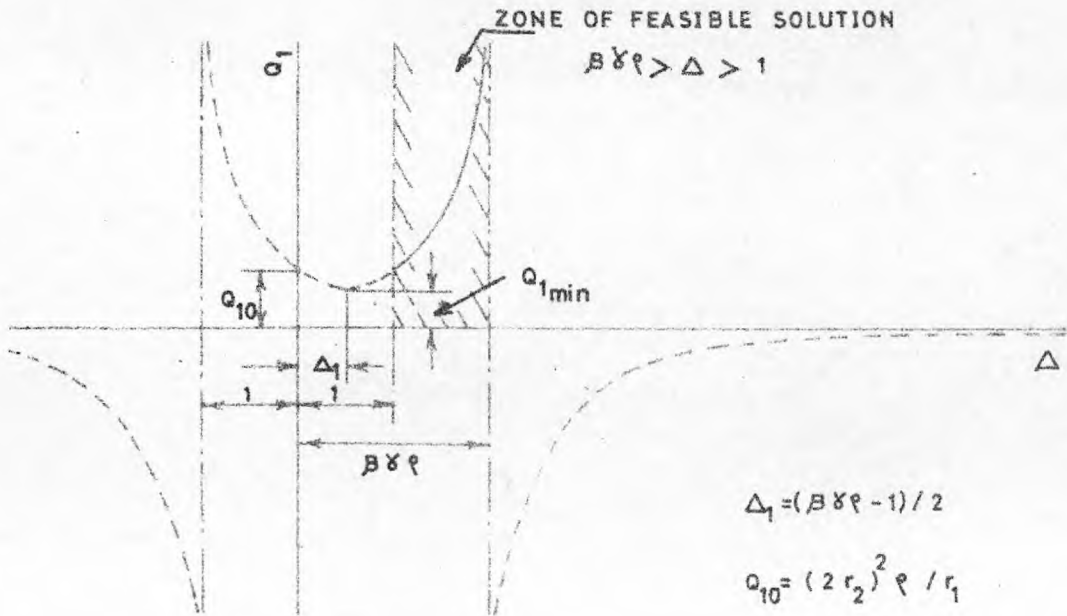


Fig.14

Variation of  $Q_1$  with  $\Delta$ , as given by Eq.4.60

value of  $\Delta$  ( $\Delta = 1$ ). Consequently, one of the two following situations may arise:

$$\text{i) If } \frac{\beta \gamma \epsilon - 1}{2} > 1 \quad (4.71)$$

Then, to obtain feasible solution, the following condition must be satisfied

$$Q_{1.\min} \leq Q_{2.\max}$$

$$\text{i.e. } \frac{(2 r_2 \epsilon)^2 \beta \gamma}{r_1} \left\{ \frac{1}{\left( \frac{\beta \gamma \epsilon - 1}{2} \right)^2} \right\} \leq K_1 + K_2 - 2q \quad (4.72)$$

which may be rewritten as

$$\beta \gamma \epsilon + 1 \geq \frac{4 r_2 \epsilon}{(\sqrt{K_1} - \sqrt{K_2})} \sqrt{\frac{\beta \gamma}{r_1}} \quad (4.73)$$

$$\text{(ii) If } \frac{\beta \gamma \epsilon - 1}{2} \leq 1 \quad (4.74)$$

Then, to obtain feasible solution, the following condition must be satisfied

$$Q_1 \Big|_{\text{at } \Delta=1} \leq Q_{2.\max}$$

$$\text{i.e. } \frac{(2 r_2 \epsilon)^2 \beta \gamma}{r_1} \frac{1}{2 (\beta \gamma \epsilon - 1)} \leq K_1 + K_2 - 2q \quad (4.75)$$

which may be re-written as

$$\beta \gamma R - 1 \geq \left\{ \frac{2 r_2 R}{\sqrt{K_1} - \sqrt{K_2}} \right\}^2 \frac{\beta \gamma}{2r_1} \quad (4.76)$$

Checking the validity of either condition (4.73) or (4.76), is very useful in predicting as to whether practical solution exists, before attempting any design calculation for various transformer parameters. In case these conditions are not satisfied, either the switching transistors may be changed or slight modification to the various specified parameters may be adopted.

Eqn. (4.51) shows that the maximum direct current  $I_{d.c.max}$  is inversely proportional to  $R_1$ . Therefore, in order to reduce  $I_{d.c.max}$ , which is desirable to obtain better transformer design, the maximum possible value of  $R_1$  may be adopted.

### 4.3.3. Method of Calculating the Principal Parameters of the Pulse-Transformer.

- (i) Calculate the quantity  $\frac{\beta \gamma e - 1}{2}$  and according to whether its value is greater, equal or less than unity, either condition (4.73) or (4.76) may be checked.
- (ii) Assuming that the above condition is satisfied, select a set of values for  $\Delta$  that lies between the limits 1 and  $\beta \gamma e$ . Substitute these values in eqns. (4.9), (4.10c) and (4.14) to obtain the corresponding values for  $v_{s.min}$  and  $R_2$ .  $Q_1$  may be also calculated from eqn. (4.60).
- (iii) For each value of  $\Delta$ , inspect the condition for real roots of eqn. (4.59), that is

$$(K_1 + K_2 - Q_1)^2 \geq 4 K_1 K_2 \quad (4.77)$$

then calculate the roots  $R_{11}$  and  $R_{12}$  of eqn. (4.59) only for the range of values of  $\Delta$  which satisfy eqn. (4.77).

- (iv) From eqns. (4.45) and (4.55), calculate the values of  $n_1$ ,  $n_2$  and  $R'_{21}$ ,  $R'_{22}$ , which correspond to the two roots  $R_{11}$  and  $R_{12}$ , respectively.  $n_1$  and  $n_2$  may also be calculated from the relation  $n^2 = R_2/R'_2$  which may be used as a check for the calculation.

- (v)  $L_1$ ,  $L_2$  and  $I_{d.c.max_1}$ ,  $I_{d.c.max_2}$  may be calculated from eqns. (4.17b) and (4.51), respectively, where the subscripts correspond to the use of calculated parameters having the same subscripts.

- (vi) Plot the various calculated parameters against  $\Delta$ .

Due to various conflicting factors, it is hardly possible to attain simultaneous optimum value for all these parameters.

Nevertheless, a good compromise which may depend on experience, can be easily judged from that plot, as will be shown in the illustrative example.

#### 4.3.4. Refinements to the Prototype Design of the Pulse-Transformer.

Knowledge of values of principal parameters, together with weight and size requirements, will enable one to select the core material and compute the geometry of the prototype transformer. These, in turn, will enable one to evaluate the secondary parameters  $\ell$  and  $c$ . Consequently, the rise and fall-time responses can be easily determined, using Figs. (9.2) and (9.4a), respectively, which is beyond the scope of the present paper.

Inspection of these responses determines whether modification to the prototype design is required. However, with the aid of various criteria developed and with the establishment of limits of validity of principal parameters, it is possible to decide which parameter may be altered and in which direction.

#### 4.3.5. Factors Influencing Zener Diode Selection.

(i) In order to minimize the net direct current in the transformer secondary winding, the Zener diode forward characteristics should match, closely as possible, those of the parallel combination of the base-collector junctions of the switching transistors.

(ii) The average forward current, flowing through the Zener diode, may be written for a particular value of  $\delta$  as

$$i_{f.av} = \frac{1}{T} \int_0^{(1-\delta)T} \frac{v_s'(t)}{R_2} dt \quad (4.78)$$

Using results of eqns. (4.29) and (4.38), and neglecting the negative sign, eqn. (4.78) may be reduced to

$$i_{f_{av}} = \frac{n V_p}{T} \frac{L}{R_1 R_2} \frac{(1 - e^{-\delta T/\tau_1})(1 - e^{-(1-\delta)T/\tau_1})}{1 - e^{-T/\tau_1}} \quad (4.79)$$

In order to obtain the maximum value of  $i_{f_{av}}$ , one may proceed by putting

$$\frac{d i_{f_{av}}}{d \delta} = 0 \quad (4.80)$$

which results in

$$\delta = \frac{1}{2} \quad (4.81)$$

then

$$(i_{f_{av}})_{\max} = \frac{n V_p}{T} \frac{L}{R_1 R_2} \frac{(1 - e^{-T/2\tau_1})}{(1 + e^{-T/2\tau_1})} \quad (4.82)$$

The calculated value of  $(i_{f_{av}})_{\max}$  must not exceed the rated average forward current of the selected Zener diode.

(iii) The peak forward current may be calculated from the fall-time response of the pulse-transformer. However, if the full-time response is critical or over-damped, that current may be easily calculated from the flat-top response, as follows

$$(i_f)_{\text{peak}} = \left. \frac{v'_s(0)}{R_2} \right|_{\text{when } \delta = \delta_{\max}} \\ = -n V_p \frac{1}{n^2 R_1 + R_2} \frac{(1 - e^{-\delta_{\max} T/\tau_1})}{(1 - e^{-T/\tau_1})} \quad (4.83)$$

where the negative sign is immaterial as it merely indicates the flowing direction of the current.

The calculated value of  $(i_f)_{\text{peak}}$  must not exceed the corresponding rated value of the selected Zener diode.

(iv) The Zener voltage must be well below the break-down voltage of base-collector junction of the switching transistor.

(v) The maximum Zener current, which may be calculated from the rise-time response of the pulse-transformer, must not exceed the corresponding rated value.

#### 4.4. Illustrative Example.

The use of the design procedure is illustrated in the following example.

Given required switch specifications are:

$$T = 20 \text{ m.sec.}, \quad \delta_{\text{max}} = 0.9, \quad \delta_{\text{min}} = 0.1, \quad I_{\text{max}} = 2 \text{ mA}, \\ i_{p.\text{max}} = 20 \text{ m.A.}, \quad V_p = 12 \text{ volts}, \quad \sigma = 0.2.$$

$\tau_1$  and  $\rho$  can then be calculated from eqns. (4.42) and (4.46), respectively,

$$\tau_1 = 80.6 \text{ m.sec.}, \quad \rho = 0.098.$$

Transistor type 2N1302, whose characteristics are given in Appendix (9.2), was selected according to subsection (4.3.1). Consequently, the following parameters can be calculated

$$\beta = 12.4, \quad \gamma = 10, \quad r_1 = 10 \Omega, \quad r_2 = 10 \Omega,$$

$$K_1 = 600 \Omega, \quad K_2 = .546 \Omega$$

from which

$\beta \gamma \rho = 12.15 > 1$  ; hence, condition (4.52) is satisfied.

As  $\frac{\beta \gamma \rho - 1}{2} = 5.575 > 1$  , then, validity of condition (4.73) should be investigated for existence of practical solution,

L.H.S. of eqn. (4.73) is  $\beta \gamma \rho + 1 = 13.15$

R.H.S. " " " "  $\frac{4 r_2 \rho}{(\sqrt{K_1} - \sqrt{K_2})} \sqrt{\frac{\beta \gamma}{r_1}} = 12$

Therefore, condition (4.73) is satisfied.

Table (4.1) indicates the results of calculation of the transformer principal parameters following the steps outlined in subsection (4.3.3.). These results are plotted in Fig. (15) to illustrate the variation of various parameters, within their limits of validity, corresponding to change in  $\Delta$  .

A reasonable choice of parameters values, for the prototype transformer, may be taken at  $\Delta = 5.575$ , where

$$\begin{aligned} R_2 &= 310 \text{ ohms} \\ R_1 &= R_{12} = 583.51 \text{ ohms} \\ n &= n_2 = 1.121 \\ L &= L_2 = 14.35 \text{ henries} \\ I_{d.c.max} &= I_{d.c.max2} = 18.5 \text{ m.A.} \end{aligned}$$

The subsequent design steps may then be easily applied to complete the switch design following similar steps as those outlined in subsections (4.3.4) and (4.3.5).



Results of calculation of pulse-transformer principal parameters.

TABLE (4.1)

$\Delta$	$Q_1$ Ohms.	Nature of roots of eqn. (4.59)	$R_{11}$ ohms	$R_{12}$ ohms	$v_s$ min volts	$R_2$ ohms	$n_1$	$n_2$	$R'_{21}$ ohms	$R'_{22}$ ohms	$L_1$ hen- ries	$L_2$ hen- ries	$I_{d.c.}$ max. mA <sub>1</sub>	$I_{d.c.}$ max. mA <sub>2</sub>
1	2.13	Imaginary roots												
2	1.56													
3	1.3													
4	1.169	Real roots	565.89	581.29	0.298	190	0.437	0.796	970	305	29	16.1	19.1	18.58
5	1.109		563.86	583.26	0.340	260	0.470	1.015	1140	262	30.4	14.6	19.17	18.52
5.575	1.1		563.59	583.51	0.370	310	0.509	1.121	1167	256.2	30.6	14.35	19.19	18.50
6	1.105		563.7	583.40	0.395	353	0.544	1.19	1156	250	30.5	14.50	19.18	18.51
7	1.154		565.33	581.83	0.472	482	0.680	1.30	1015	290	20.25	15.60	19.10	18.57
8	1.273	Imaginary roots												
9	1.51													
10	2.012													
11	3.445													
12	24.4													

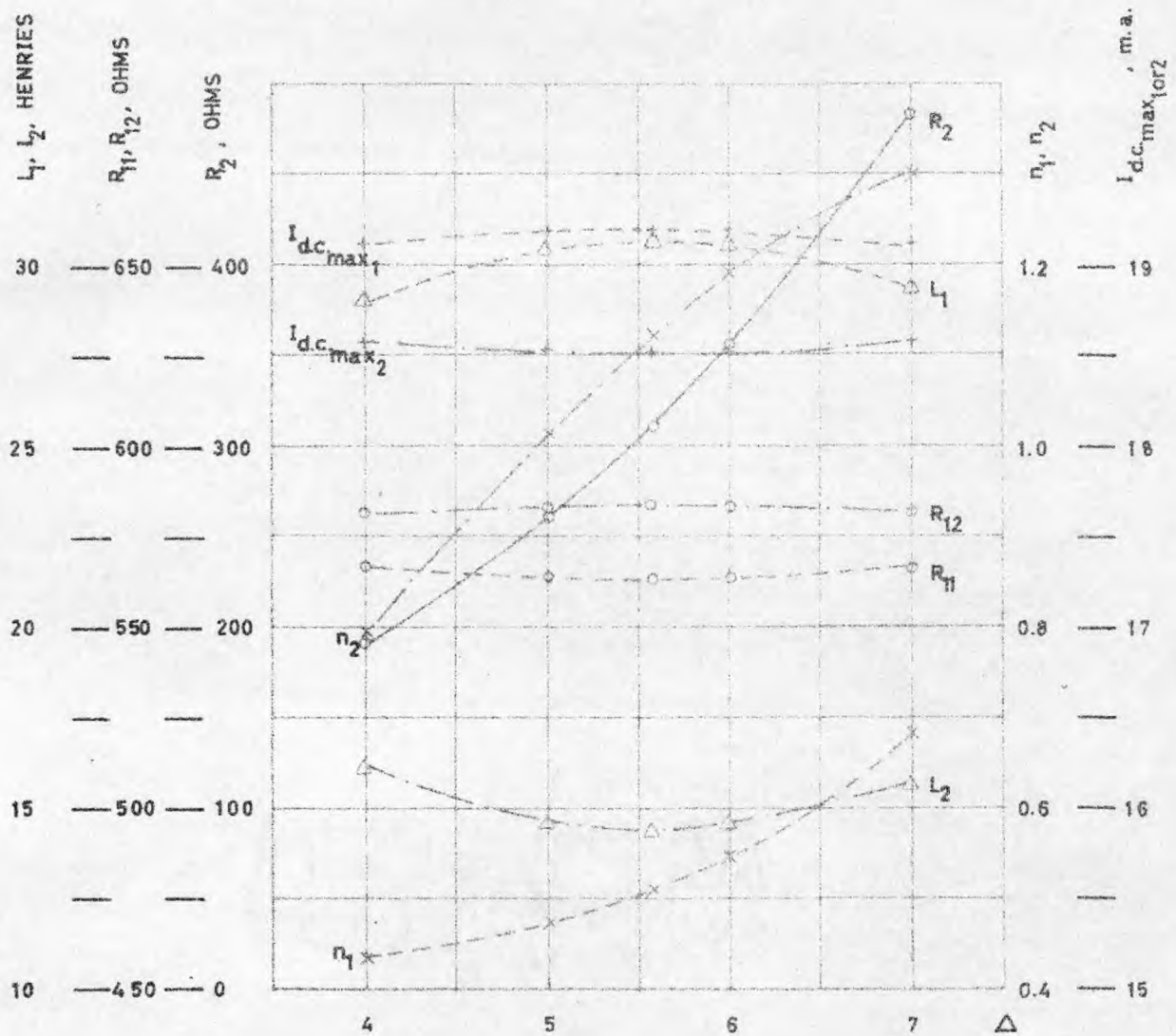


Fig.15

Plot of the calculated values of various pulse-transformer parameters with respect to  $\Delta$

## 5.0. SWITCH DRIVING CIRCUIT

### 5.1. Requirements.

The driving circuit's main purpose is to provide an adequate drive to the pulse-transformer in the form of two similar square-waves carrier at  $180^\circ$  phase difference. It should also include a means of control for the mark/space ratio ( $m$ ), such that, its value may be adjusted to any magnitude that lies within specified limits  $m_{\min} < m \leq m_{\max}$ .

### 5.2. Description.

A possible practical circuit is shown in Fig. (16). It consists of two symmetrical channels fed from a centre-tapped transformer  $T_1$ , which provides  $180^\circ$  phase-shift between their inputs. The transformer primary winding is excited by a sinusoidal carrier-signal.

Each channel consists of four transistors. Transistors  $N_1$  and  $N_2$  are limiting amplifiers operating as square-wave generators. Transistor  $N_3$  is an emitter-follower stage which operates the last amplifier stage  $N_4$ . This last stage transmits the necessary square-wave drive to the pulse-transformer  $T_2$  whose secondary winding is connected to the common base-collector junction of the switch transistors.

The mark/space ratio can be varied by applying a d.c. bias to the centre-tapped point of transformer  $T_1$ . This causes a variation in the instantaneous input voltage level at which the input transistors  $N_1$  and  $N_1'$  commence conducting.

A model, based on Fig. (16), has been constructed which is capable of controlling the mark/space ratio between the limits 1/20 and 20/1. A brief account of the components employed and design values of various elements are given in the diagram.

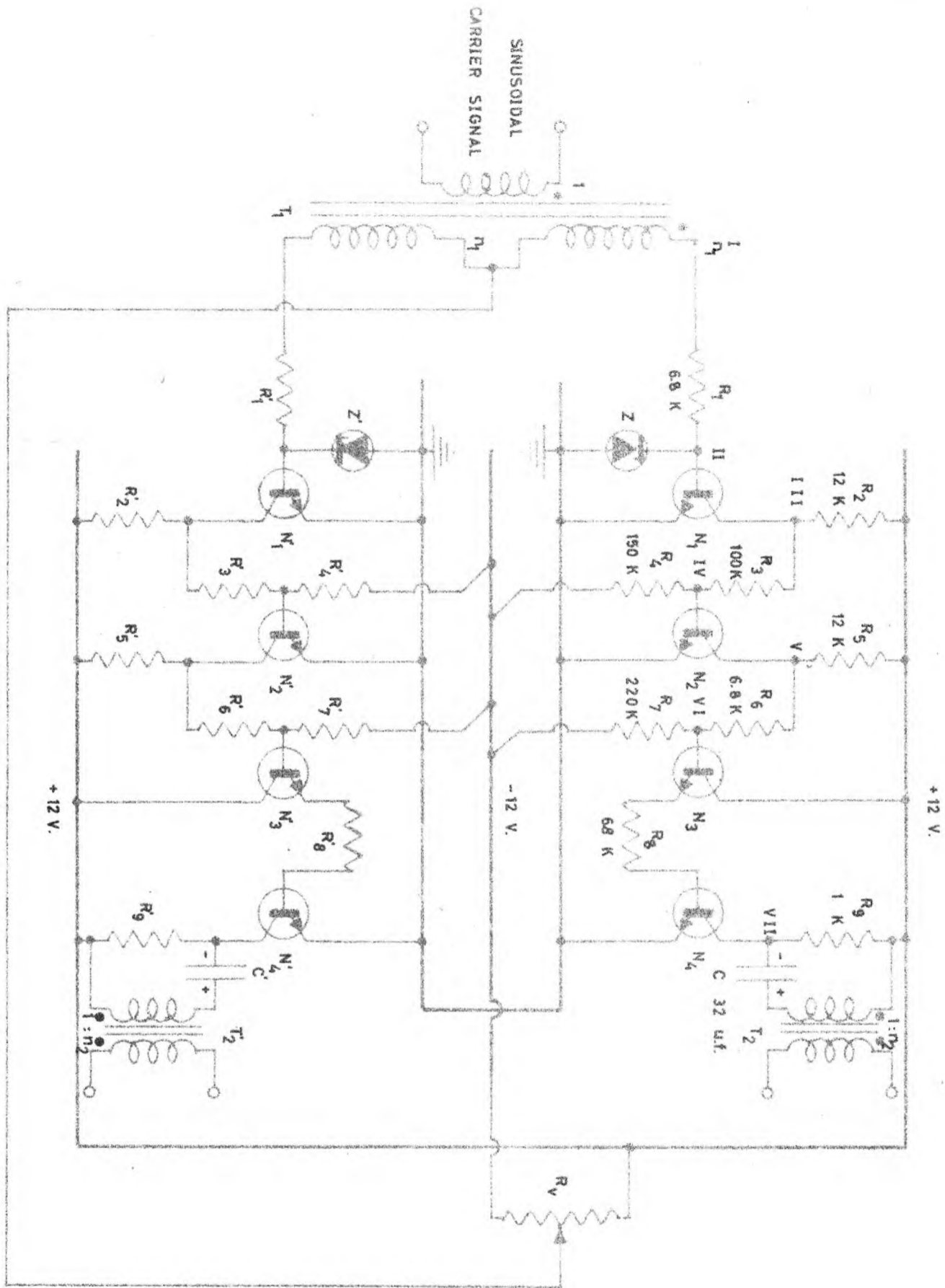


Fig.16

A transistor driving circuit for 3-terminal synchronous switch

$R_v$  : Miniature helical potentiometer, 10 K, 10 turns, type CLR 2402/22

$N_1, N_2, N_3, N_4$  : Alloy-junction Germanium transistors, N.P.N., type 2N1302

Z : Zener diode, type 0AZ 213

Fig. (17) illustrates wave-forms at various points of the driving circuit for conditions of  $\delta < 1$ ,  $\delta = 1$  and  $\delta > 1$ , which correspond to negative, zero, and positive d.c. bias, respectively. Potentiometer  $R_v$ , fed from +12 and -12 volt supply, is adjustable to give the required d.c. bias. The input transistor  $N_1$  is unbiased and does not conduct when its input voltage is negative. It conducts and its collector voltage falls almost to zero if its base current exceeds 50  $\mu$ A., which occurs if its base voltage becomes more positive than 0.3 volts. Resistor  $R_1$  is designed to satisfy the two extreme conditions :

- (i) To limit the base current to a safe value in case of applying maximum input voltage, which occurs when maximum positive d.c. bias is applied to the transformer centre-tapped point.
- (ii) To allow the flow of adequate base current to saturate the transistor in case of applying minimum input voltage, which occurs when maximum negative d.c. bias is applied.

The Zener diode  $Z$  is employed to protect transistor  $N_1$  by diverting excessive positive base current, and limiting excessive negative base voltage.

The output of transistor  $N_1$  consists of pulses, the rise-time of which is determined by the frequency and amplitude of the input voltage. The pulses are amplified and inverted by transistor  $N_2$ , which is overdriven by transistor  $N_1$  so that pulse rise-time is considerably diminished. Resistors  $R_2$ ,  $R_3$  and  $R_4$  are designed to provide proper biasing for transistor  $N_2$ .

The signal at the collector of transistor  $N_2$  consists of square-waves which are applied to the base of transistor  $N_3$ . Transistor  $N_3$ , which is properly biased by resistors  $R_5$ ,  $R_6$  and  $R_7$ , operates as a buffer stage. The last stage  $N_4$  operates as an amplifier whose load is the pulse-transformer  $T_2$ . The signal

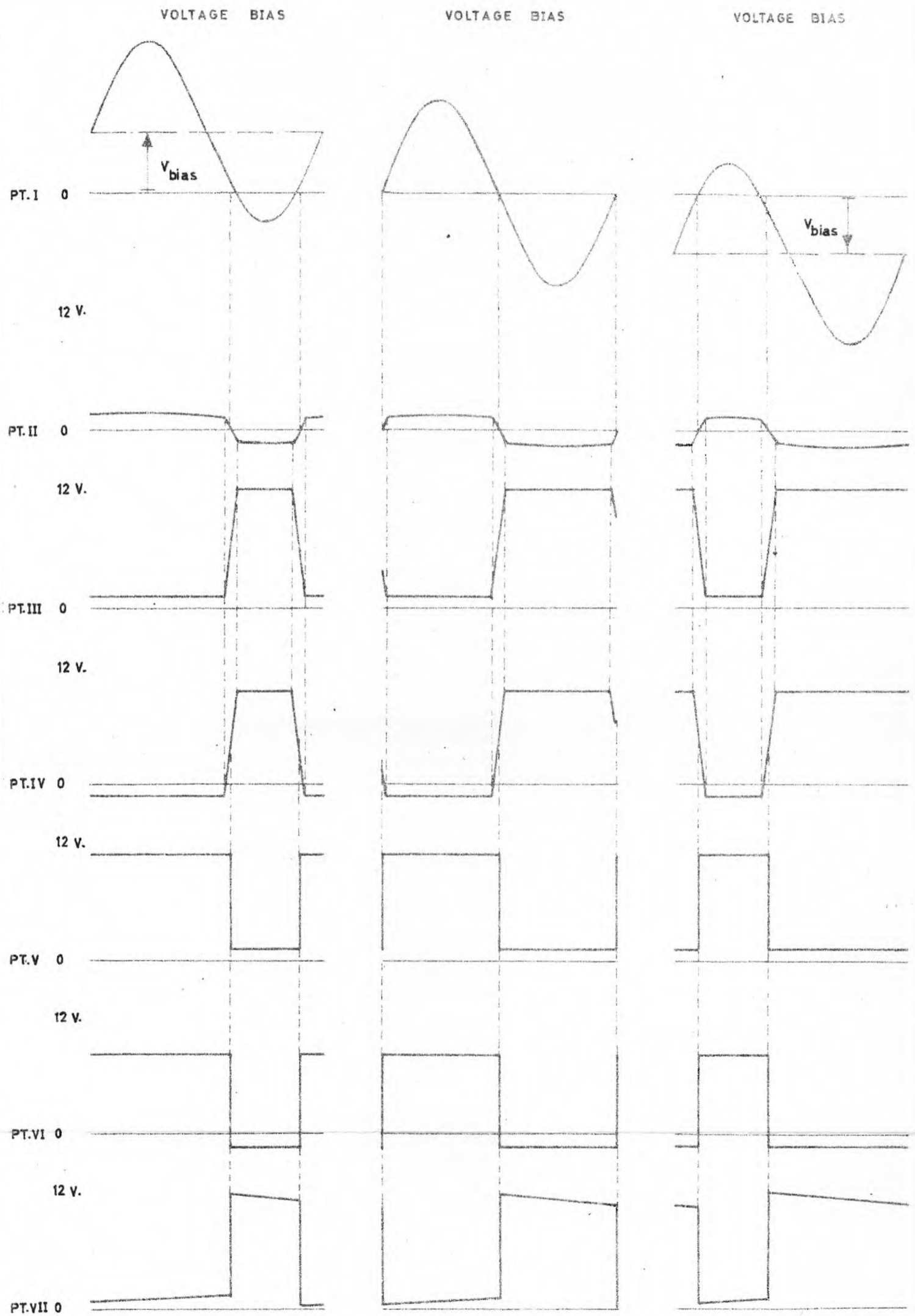


Fig.17

Wave-forms at various points of the driving circuit, shown in Fig.16 , for positive, zero, and negative d.c. bias

at its collector is a square-wave of magnitude slightly less than 12 volts with rise-time of about 2 u.sec. for carrier frequency of 50 c/s.

In order to cancel the effect of the net direct current flowing through the primary winding of  $T_2$ , a large capacitor  $c$ , inserted in series with it, may be used. Resistor  $R_9$ , is thus, employed to provide a discharging path for the capacitor during OFF period of transistor  $N_4$ . An alternative way is to use a third winding on the transformer  $T_2$ . This winding is energized by a direct voltage whose polarity is such that the resulting direct current effect opposes that of the primary winding. A variable resistance may be inserted in series to control that direct current to the required magnitude.

In deriving the transformer response equations in subsection (4.2.4),  $R_9$  and  $c$  were neglected just to avoid unnecessary complications at that stage. However, various equations can be easily modified to account for their presence according to the following points :

(i) If the capacitor value is high enough, the voltage built across it may be assumed negligible without causing serious errors. Consequently, all the expressions desired during ON period (subsection (4.2.4.1)) may be regarded as valid provided that the zero-axis of  $i_p(t)$  is shifted to coincide with the mean value of  $i_p(t)$  and  $i'_p(t)$  during a complete carrier cycle.

(ii) The effect of  $R_9$  only occurs during OFF period of the switch. This may be accounted for by replacing  $R_1$  by  $R_1 + R_9$ , in all the expressions of subsection (4.2.4.2). Again, to account for  $c$ , the zero axis of  $i'_p(t)$  should be considered as coinciding with the mean value of  $i'_p(t)$  and  $i_p(t)$  during a complete carrier cycle.

## 6.0. CONCLUSIONS.

It has been shown that 3-terminal synchronous switches, capable of operating with P.F.T. and N.F.T., are physically realizable. A superior circuit, employing switching transistors driven by pulse-transformer, has been described and its dynamic behaviour has been analyzed. Design criteria, which determine the limits of validity of various parameters, have been developed. A simple procedure for a comprehensive design of 3-terminal synchronous switch and an appropriate driving circuit, has been outlined with an illustrative example.

The feasibility of constructing widely controlled fly-time synchronous switches, immensely increases the scope of their application. It has led to the development of physically dissimilar chopper networks with identical responses by establishing the duality between P.F.T. and N.F.T. circuits.<sup>(1)</sup> It has also resulted in establishing the realizability of obtaining modified dynamic characteristics from various chopper networks by controlling the fly-time of the incorporated synchronous switches.<sup>(1)</sup>

The flexibility and simplicity, with which the presented synchronous switch can be operated and its fly-time be controlled and measured, suggests the possibility of its use to simulate mechanical switch operation with its unavoidable physical fly-time. Thus, this enables one to perform various studies which may explain the experimental anomalies, associated with mechanical switches, which cause actual results to differ from those predicted. Furthermore it may guide future work in which mechanical switches, despite their physical fly-time, be preferred, in some applications, to electronic switches.

## 7.0. ACKNOWLEDGMENT

The work presented in this paper was carried out under the supervision of Dr. D.G.O. Morris, D.Sc., M.I.E.E., Reader in



Electrical Engineering, Imperial College of Science and Technology, The author wishes to express his gratitude to Dr. Morris for his helpful guidance, constant encouragement and keen interest.

The author wishes to express his thanks to Dr. P.H.G. Allen, Ph.D., A.M.I.E.E., A.M.I.Mech.E., and members of the staff of power systems and machines at Imperial College for their invaluable help and constructive remarks.

### 8.0. REFERENCES.

1. KHALAFALLA, F.B. "Derived Chopper Networks and Methods of Modifying Their Responses", Power Systems Laboratory Report No. 68, Imperial College, January 1966.
2. KRUPER, A.P. "Switching Transistors Used as a Substitute for Mechanical Low-Level Choppers". Trans. A.I.E.E., E-C17, 141-144, March 1955.
3. BRIGHT, R.L. "Junction Transistors Used as Switches", Communications and Electronics, 111, 1955.
4. HURLEY, R.B. "Transistorized Low-Level Chopper Circuits". Electronic Industries and Tele.-Tech., 15, 42-43, 108, 110, 112, December 1956.
5. HURLEY, R.B. "Transistor Electronics", Chapter 20, New York, John Wiley & Sons, Inc., 1958.
6. KORN, G.A. and KORN, T.M. "Electronic Analog and Hybrid Computers". Chapter 6, McGraw-Hill, New York, 1964.
7. MITCHELL, B. and BELL, B. "The INCH (Integrated Chopper)". General Engineering Memo 7, National Semiconductor Corp., Danbury, Conn., June 1962.
8. MEYER-BRÖTZ, G. "Eigenschaften und Anwendungen von Flächentransistoren als Schalter". Telefunken Z., June 1960.

9. Massachusetts Institute of Technology Staff. "Magnetic Circuits and Transformers". John Wiley & Sons, Inc., New York, 1943.
10. LEE, REUBEN. "Electronic Transformers and Circuits". John Wiley & Sons, Inc., New York, 1947.
11. WIMETT, T.F., "Low-Power Pulse-Transformers". Report. R-122, Servomechanisms Laboratory, Massachusetts Institute of Technology, 1947.
12. GLASOE, G.N., and LEBACQZ, J.V. "Pulse Generators". Massachusetts Institute of Technology Radiation Laboratory Series, Vol. 5, Chapter 12, McGraw-Hill Book Company, Inc., New York, 1948.
13. MILLMAN, J. and TAUB, H. "Pulse and Digital Circuits". Chapter 9, McGraw-Hill, New York, 1956.
14. "High-Frequency Transistors for Computer and Switching Applications", Bulletin No. DL-S 60349, May, 1960. Texas Instruments Limited.

## 9.0. APPENDICES

### 9.1. Equivalent Circuits of Pulse-Transformer

Fig. (9.1) shows the complete equivalent circuit of a pulse-transformer taking into account the effective interwinding capacitance  $c$ , and the core loss which is represented by a shunt resistance  $R_c$  (9-13). The resistance  $R_1$  is the sum of the source impedance (assumed resistive) and the primary winding resistance.  $R_2$  is the sum of the load and the secondary winding resistances.

When the input signal is in the form of pulses, the differential equations describing the transformer behaviour can be appreciably simplified by dividing the solution into three parts: the first gives the response to the discontinuity near the front edge of the pulse, the second gives the response during the flat-top, and the third gives the response after the termination of the pulse. The complete response can thus be obtained by combining the three responses taking into account the proper boundary conditions.

In this way of analysis, the pulse-transformer is reduced to a number of approximate equivalent circuits corresponding to the different portions of the pulse. These equivalent circuits may be easily obtained from Fig. (9.1) by removing elements which have negligible effect. As a consequence, the rise-time response may be determined from the high-frequency equivalent circuit of Fig. (9.2), the response during the flat top of the pulse is obtained from the low-frequency equivalent circuit of Fig. (9.3). During the decay-time, the response may be calculated from the two equivalent circuits shown in Fig. (9.4). Where Fig. (9.4a) is only valid for the infinitesimal period in the immediate neighbourhood of the end of the pulse, and Fig. (9.4b), is applicable for the rest of the decay-time. If the source is disconnected at the end of the pulse, this can be represented by switches A and B being open-circuited. However, in some applications the source remains in the circuit but short-

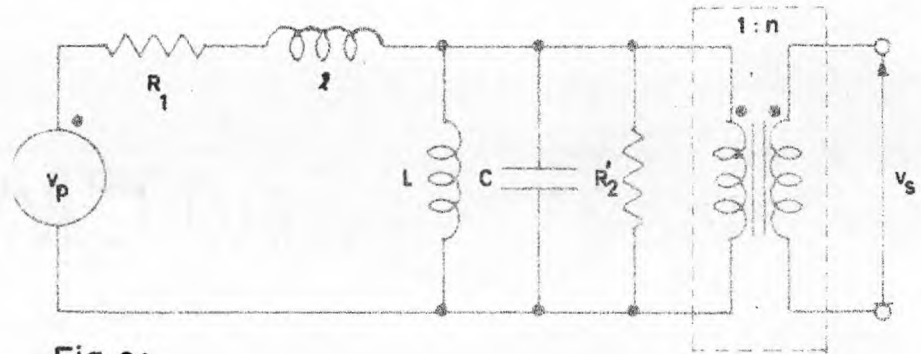


Fig. 9.1

Approximate equivalent circuit of a pulse-transformer including capacitances and resistances

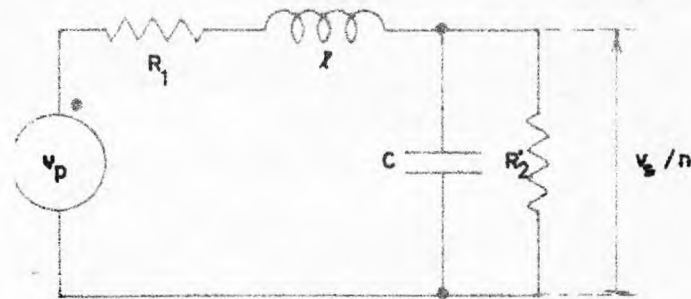


Fig. 9.2

Approximate equivalent circuit for the calculation of the rise-time response

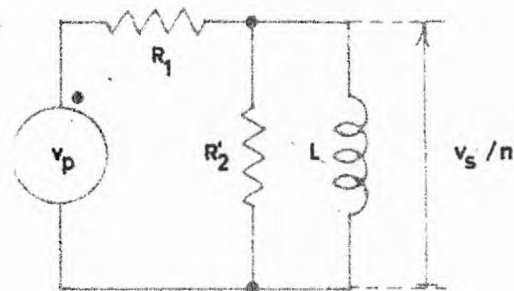
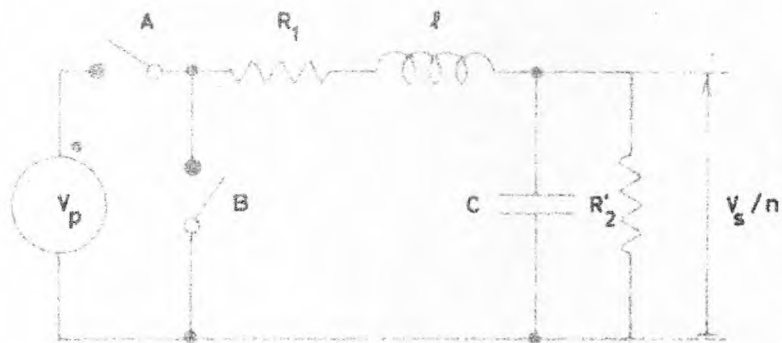
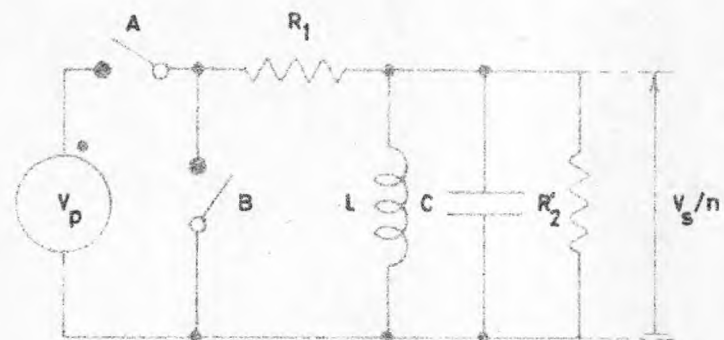


Fig. 9.3

Approximate equivalent circuit for the calculation of the flat-top response



(a) Circuit applicable in the immediate vicinity of the trailing edge of the pulse



(b) Circuit applicable for the remaining period of the decay-time

Fig.9.4

Approximate equivalent circuits used to calculate the decay-time response

circuited in which case it can be represented by switch B being closed.

9.2. Characteristics of Alloy-Junction Germanium Transistor  
Type 2N1302 (N-P-N)<sup>(14)</sup>,

(i) Absolute maximum ratings at 25°C ambient temperature

		Units
Collector-Base Voltage	(25) 30	V
Emitter-Base Voltage	25	V
Collector Current	300	ma
Total Device Dissipation	150	mw
Storage Temperature Range	-65 to + 100	°C

(ii) Electrical Characteristics at 25°C Ambient Temperature

Parameter and test conditions	Min.	Typ.	Max.	Unit
$I_{CBO}$ Collector Reverse Current $V_{CB} = +25 \text{ v} ; I_E = 0$	-	+3	+6	ua
$I_{EBO}$ Emitter Reverse Current $V_{EB} = +25 \text{ v} ; I_C = 0$	-	+2	+6	ua
$BV_{CBO}$ Collector-Base Breakdown Voltage $I_C = 100 \text{ ua}$	+25	-	-	v
$BV_{EBO}$ Emitter-Base Breakdown Voltage $I_E = 100 \text{ ua}$	+25	-	-	v
$h_{FE}$ DC Forward Current Transfer Ratio $I_C = 10 \text{ ma} ; V_{CE} = 1 \text{ v}$	20	50	-	
$h_{FE}$ DC Forward Current Transfer Ratio $I_C = 200 \text{ ma} ; V_{CE} = 0.35 \text{ v}$	10	-	-	
$V_{BE}$ Base-Emitter Voltage $I_C = 10 \text{ ma} ; I_B = 0.5 \text{ ma}$	+0.15	+0.30	+0.40	v
$V_{CE(sat.)}$ Collector-Emitter Saturation Voltage $I_C = 10 \text{ ma} ; I_B = 0.5 \text{ ma}$	-	+0.10	+0.20	v
$V_{pt}$ Punch-Through Voltage	+25	-	-	v
$C_{ob}$ Common-Base Output Capacitance $V_{CB} = +5 \text{ v} ; I_E = 0 ; f = 1 \text{ mc}$	-	-	20	uuf
$C_{ib}$ Common-Base Reverse-Bias Input Capacitance $V_{EB} = +5 \text{ v} ; I_C = 0 ; f = 1 \text{ mc}$	-	10	-	uuf
$f_{\alpha b}$ Common-Base Alpha Cut-off Frequency $V_{CB} = +5 \text{ v} ; I_E = 1 \text{ ma}$	3	4.5	-	mc

(iii) Switching Characteristics.

Switching Speeds (See Fig (9.5))			Unit
$t_d$	Delay Time	0.12	u.Sec.
$t_r$	Rise Time	0.70	u.Sec.
$t_s$	Storage Time	0.50	u.Sec.
$t_f$	Fall Time	0.80	u.Sec.
$t_t$	Total Switching Time	2.00	u.Sec.
$Q_s$	Stored Base Charge	1000	uu. Cb.



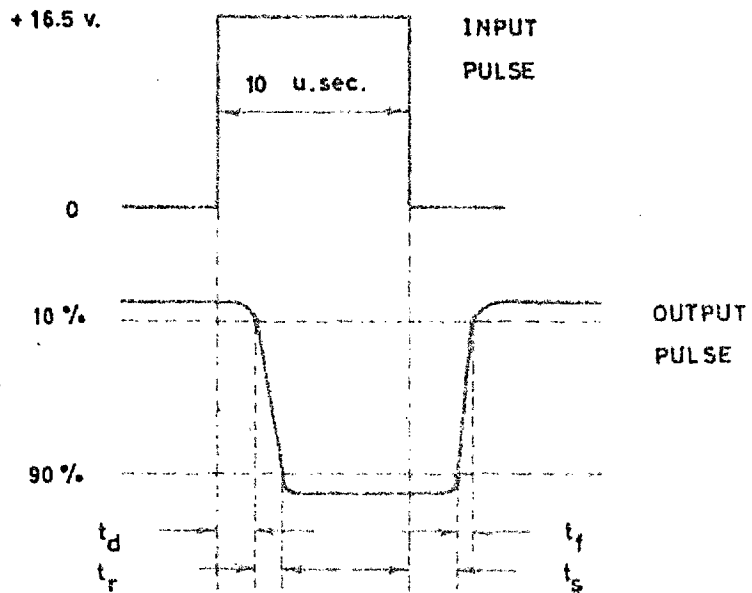
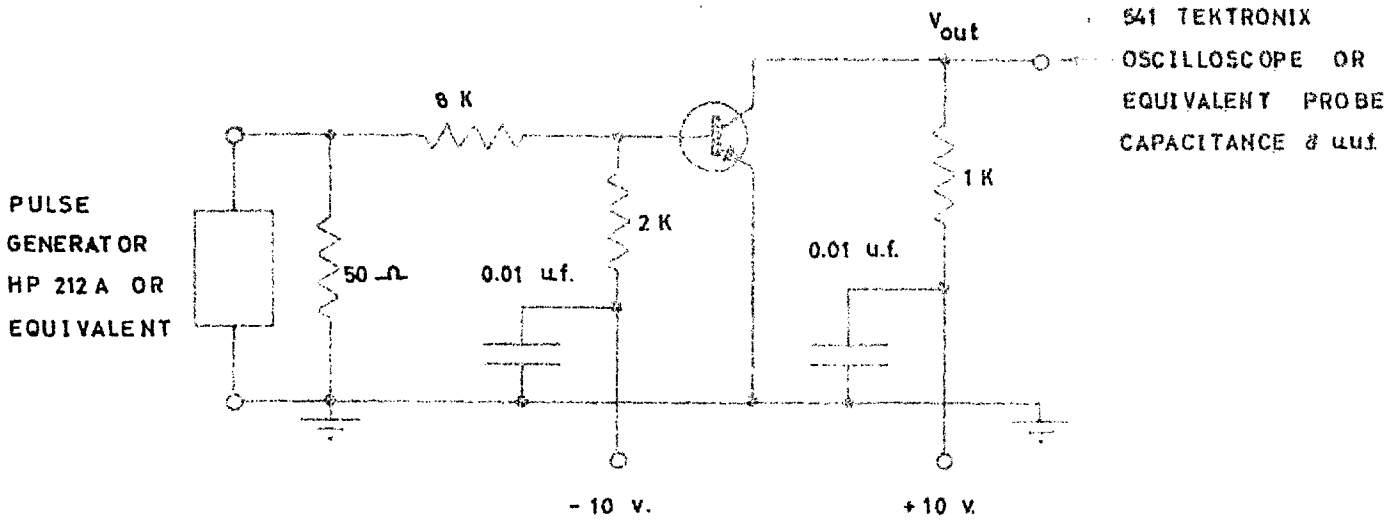


Fig.9.5 (14)  
Switching-speed test circuit

CHAPTER II

IMPERIAL COLLEGE OF SCIENCE AND TECHNOLOGY

---Department of Electrical Engineering---

Power Systems Laboratory Report No. 67

DERIVED CHOPPER NETWORKS AND METHODS OF MODIFYING  
\*\*\*\*\*

THEIR RESPONSES  
\*\*\*\*\*

F.B. Khalafalla

May, 1967

SYNOPSIS

A synthesis technique is developed to realize 3-terminal chopper networks whose transfer functions are equivalent to those of two general types of RC chopper networks. The method adopted is based on systematic application of the duality concept. The major contribution to the technique was gained by establishing the duality between positive and negative fly-time 3-terminal synchronous switches which form simplest units in the chopper network structure. To verify the equivalence between various derived chopper networks, their response equations have been derived and given in tables.

The paper also outlines unconventional methods to obtain modified responses of various chopper networks, by exploiting the synchronous switch potentialities, using 4-terminal structures of chopper networks, and by adding operational amplifiers and transformers.

CONTENT

- Synopsis.
- Contents
- List of Principal Symbols
- 1.0 Introduction
- 2.0 Synchronous Switch and Principle of Duality
  - 2.1 3-Terminal Synchronous Switch Representation
  - 2.2 Fly-Time and its Representation
  - 2.3 Equivalent Arrangement of 2-Terminal Switches
  - 2.4 Dual of 2-Terminal Synchronous Switch
  - 2.5 Dual of 3-Terminal Synchronous Switch
- 3.0 3-Terminal RC Chopper Networks and Their Equivalents
  - 3.1 Prototype Chopper Networks
  - 3.2 Derived Networks
    - 3.2.1 Dual Network
    - 3.2.2 Complement Network
    - 3.2.3 Dual-Complement Network
- 4.0 Derivation of Response Equations
  - 4.1 Single-Switch Double-Capacitor Chopper Network and its Derived Networks
    - 4.1.1 Voltage Energised Networks
    - 4.1.2 Current Energised Networks
  - 4.2 Response Equations of RC Prototype Chopper Networks
- 5.0 Modified Chopper Networks
  - 5.1 4-Terminal Chopper Networks
    - 5.1.1 Parallel Double-Switch Double-Capacitor Chopper Network and its Derived Networks
    - 5.1.2 Cascaded Inverted Double-Switch Double-Capacitor Chopper Network and its Derived Networks
    - 5.1.3 Triple-Switch Single-Capacitor Chopper Network and its Derived Networks.

- 5.2 Use of Full-Range of Fly-time Operation of  
Synchronous Switches
- 5.3 Use of Operational Amplifiers and Transformers
- 6.0 Conclusions
- 7.0 Acknowledgements
- 8.0 References
- 9.0 Appendix

LIST OF PRINCIPAL SYMBOLS

$t$	:	time (independent variable)
$s$	:	Laplace complex frequency variable
$T$	:	period of carrier wave, in seconds
$\omega$	:	carrier frequency, in radians/second
$\delta$	:	proportion of period during which the moving contact of the switch is in contact with only one of the fixed contacts
$a$	:	proportion of period during which the moving contact of the switch is either in contact with neither of the fixed contacts (P.F.T. mode of operation), or in contact with both of them (N.F.T. mode of operation).
$n$	:	integer number
$d$	:	width of moving contact of switch
$D$	:	distance between fixed contacts of switch
$n_1, n_2$	:	turns ratios of transformer
$A$	:	gain of amplifier
$v_1$	:	excitation voltage
$v_2, v_3, v_4, v_5$	:	output voltages of various chopper networks
$i_1$	:	excitation current
$i_2, i_3, i_4, i_5$	:	output currents of various chopper networks
$C$	:	capacitance associated with prototype and dual-complement chopper networks
$G, G_1, G_2, G_3$	:	conductances associated with prototype and dual-complement chopper networks
$L$	:	inductance associated with dual and complement chopper networks
$R, R_1, R_2, R_3$	:	resistances associated with dual and complement chopper networks

- $\tau, \tau_1, \tau_2, \tau_{e_{12}}, \tau_{e_1}, \tau_{e_2}, \tau_e$  ) : time constants associated with various  
chopper networks
- $R_f$  : feedback resistance
- $R_a$  : resistance in the parallel adding  
channel
- $R_b, R_c$  : adding resistances in series with  
chopper network

## 1.0 INTRODUCTION

In the field of carrier control systems, chopper networks have been found to be most advantageous type of compensators compared to other types when carrier frequency deviation is excessive. (1 to 8). Chopper Networks are mainly composed of electric passive elements interconnected by one or more carrier-driven 3-terminal synchronous switches. In previous papers, various configurations of chopper networks presented have been limited to:-

- (i) RC electric passive elements connected in simple structures.
- (ii) Synchronous switches operating with zero or positive fly-time.

The main purpose of this paper is to seek for different methods whereby configurations and responses of chopper networks may be developed and expanded. The practical feasibility of constructing 3-terminal synchronous switches, which can operate with positive and negative fly-time (9), has established the essential background upon which basis, extension of the principle of duality to chopper networks is made possible. Heuristic development of chopper network equivalence is greatly assisted by attaining the dual of the synchronous switch. However, chopper networks dealt with in this paper are limited to two types of electric passive element; RC or RL.



## 2.0 SYNCHRONOUS SWITCH AND PRINCIPLE OF DUALITY

### 2.1. 3-Terminal Synchronous Switch Representation

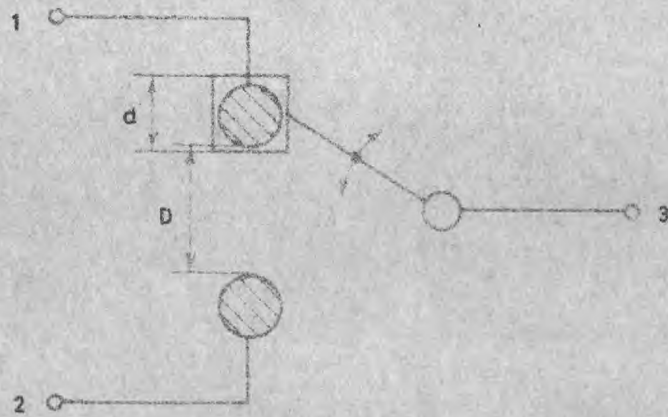
A simple representation may be achieved in the form of single-pole double-throw arrangement as shown in Fig. (1-a). In this, points 1 and 2 represent fixed contacts. A hinged link swings around point 3 with a fixed angle of travel at carrier frequency  $\omega$ . The head of the swinging link represents the moving contact which comes in contact with the fixed ones 1 and 2, successively, each for a period of  $\delta T$ .

### 2.2 Fly-Time and its Representation

The switch representation illustrated in Fig. (1-a) does not only describe its function but also symbolises its timing operation. Supposing that the size of the moving contact can possibly be changed, two modes of switch operation can be simulated:

- (i) If the width of the moving contact  $d$  is smaller than the distance between the fixed contacts  $D$ , a **positive** physical time will be required to bridge that distance. The term "Positive Fly-Time" (P.F.T.) may therefore be introduced to define this mode of operation. Fig. (1-b) shows the moving contact position as a function of time, under P.F.T. mode of operation. In this case, the following expressions apply

$$\begin{array}{ll}
 0 < d \leq D & 2.1.a ) \\
 0 < \delta \leq \frac{1}{2} & 2.1.b ) \\
 \frac{1}{2} > a \geq 0 & 2.1.c )
 \end{array}
 \quad \left. \vphantom{\begin{array}{l} 2.1.a \\ 2.1.b \\ 2.1.c \end{array}} \right\} 2.1$$



(a) Single-pole double-throw switch

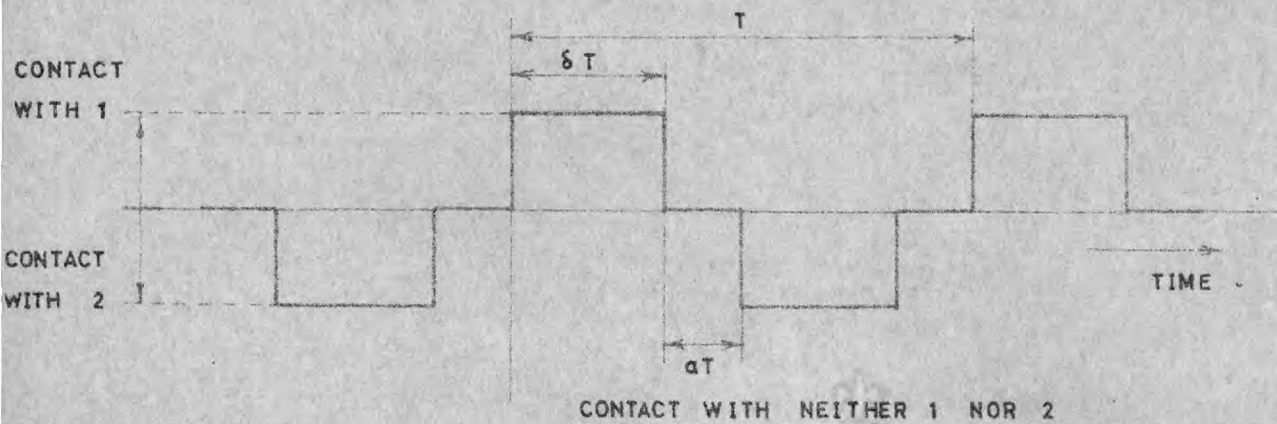
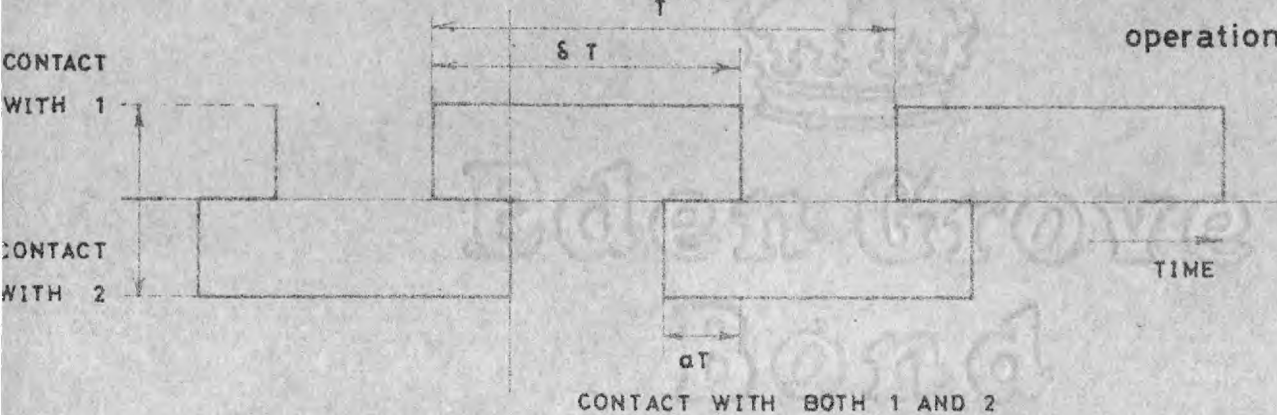
(b) Position of the moving contact related to time for R.F.T. mode of operation ( $0 < \delta \leq 0.5$ )(c) Position of the moving contact related to time for N.F.T. mode of operation ( $0.5 \leq \delta < 1$ )

Fig. 1

Representation of a 3-terminal synchronous switch and its state/time relationship

Where  $aT = \text{fly-time}$  2.2

- (ii) If the width of the moving contact  $d$  is larger than the distance between the fixed contacts  $D$ , an overlapping period of  $a.T$  will result in during which the moving contact is connecting both points 1 and 2 to point 3. The overlapping period may be defined as "Negative Fly-Time" (N.F.T.). Under this mode of operation, Fig. (1-C) shows the moving contact position as a function of time. In this case, the following expressions apply

$$\left. \begin{aligned} D &\leq d < \text{stroke distance} && 2.3.a ) \\ \frac{1}{2} &\leq \delta < 1 && 2.3.b ) \\ 0 &\geq a > -\frac{1}{2} && 2.3.c ) \end{aligned} \right\} 2.3$$

In this connection, it is evident that the mode of operation with Zero Fly-Time (Z.F.T.) is a common limiting condition for both P.F.T. and N.F.T. modes described above in which case only the equalities given by both expressions (2.1) and (2.3) hold.

### 2.3 Equivalent Arrangement of 2-Terminal Switches

By splitting point 3 into two connected ones, an alternative representation can be achieved, as shown in Fig. (2), in the form of double-pole single-throw arrangement. In this case, a delay period of  $T/2$  between identical operating conditions of the 2-terminal switches must be introduced. This implies that the two poles should swing in parallel. A link joining the middle points of the two poles may thus be used to satisfy that condition.

P.F.T. and N.F.T. modes of operation may also be represented in a similar manner as described in the preceding subsection.

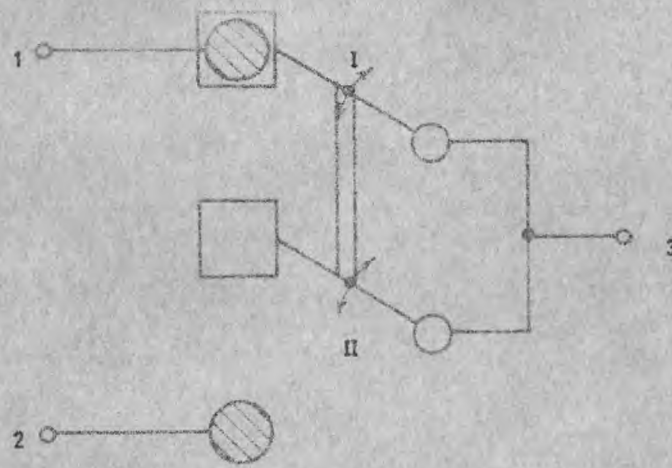


Fig.

Double-pole single-throw switch

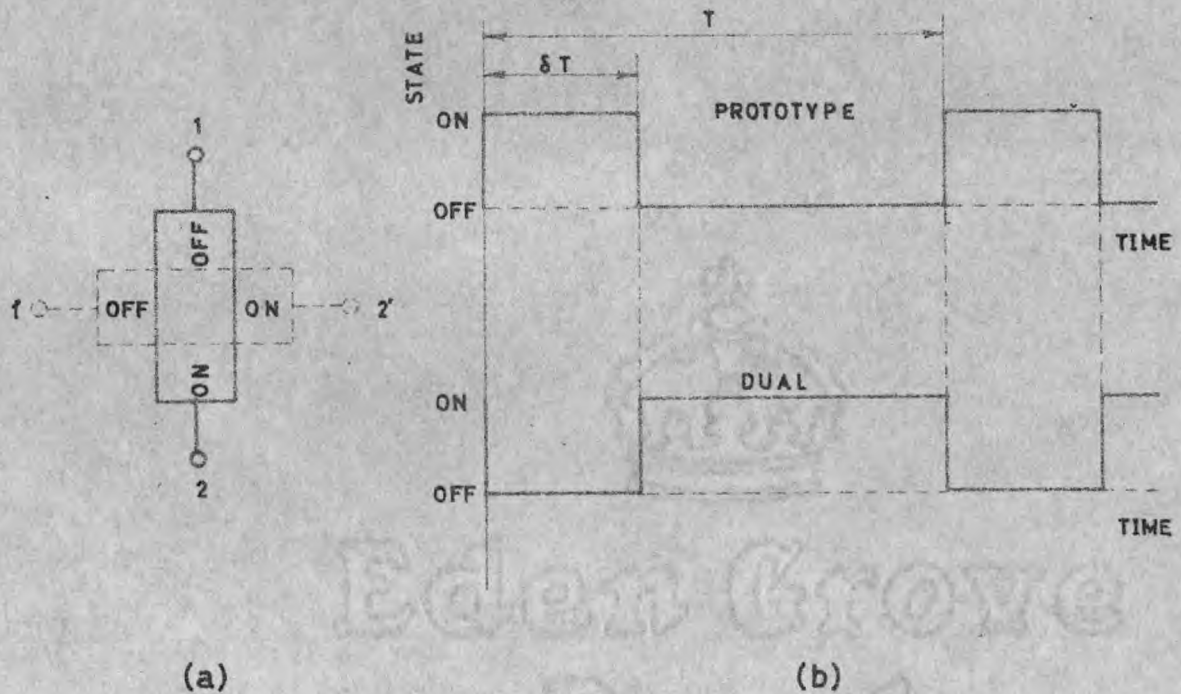


Fig. 3

(a) 2-terminal synchronous switch and its dual

(b) State/time relationship of the 2-terminal synchronous switch and its dual shown in (a)

#### 2.4 Dual of 2-Terminal Synchronous Switch

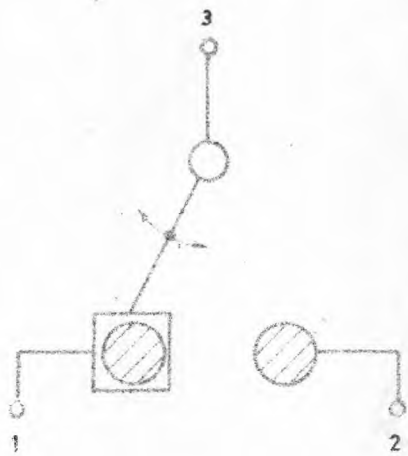
A review of circuit theory (10 to 16) shows that the same sequence of ideas and procedures characterizes both the loop and node methods of analysis, but with an inter-change in pairs of principal quantities and concepts involved. List of quantities and concepts, which play dual role, is given in the Appendix (9).

Since a zero current implies an open circuit and a zero voltage a short circuit, these two physical constraints are seen to be dual. Applying this simple criterion on the 2-terminal switch (ON-OFF), shown in solid lines 1-2 in Fig. (3-a), it is easy to prove that its dual is an OFF-ON switch as shown in the same figure in dashed line 1' - 2'. One may proceed by cutting the switch 1-2 orthogonally by several parallel lines. Since points 1-2 are solidly shorted during the ON period of the switch, then the dual according to the above criterion, may be represented as unconnected two points 1' and 2'. With similar reasoning, the dual corresponding to the OFF period, during which points 1 and 2 are unconnected, may be readily shown to be the two points 1' and 2' solidly connected. Combining the state of the joint between points 1' and 2' during ON and OFF periods, an OFF-ON 2-terminal switch may result. Figs. (3-b) and (3-c) show the state/time relationships of the 2-terminal synchronous switch and its dual respectively.

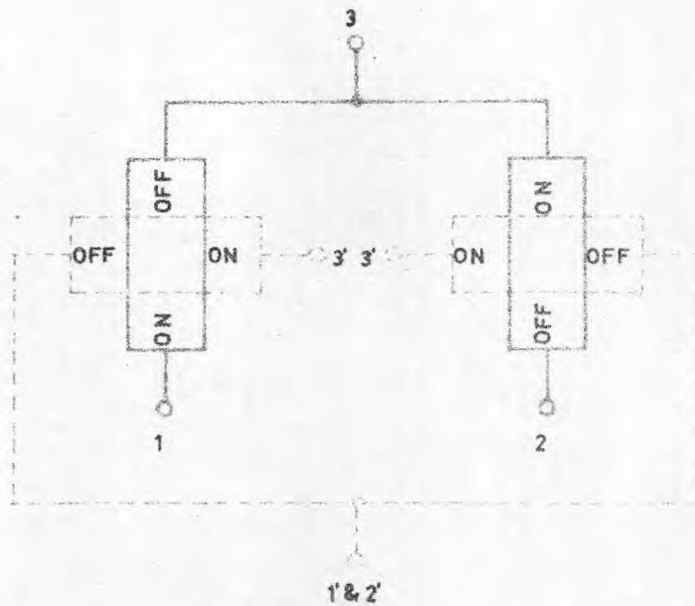
#### 2.5 Dual of 3-Terminal Synchronous Switch

Fig. (4-a) shows a 3-terminal synchronous switch operating with a fly-time  $aT$ , such that

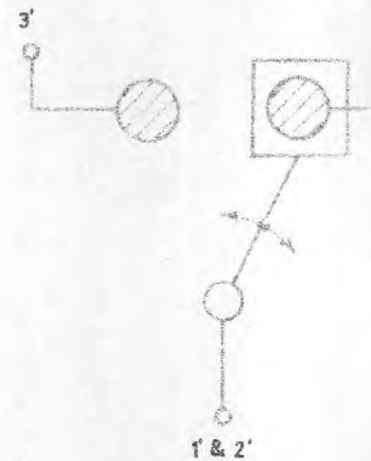
$$aT = \left(\frac{1}{2} - \delta\right) T \quad 2.4$$



(a) Prototype  
FLY-TIME =  $\alpha T$



(b) Prototype and dual



(c) Dual  
FLY-TIME =  $-\alpha T$

Fig. 4  
Illustration of the process of dual construction of  
a P.F.T. 3-terminal synchronous switch

Construction of its dual will be considerably simplified if its 2-terminal switch arrangement is used. This is drawn with solid line in Fig. (4-b). Applying similar technique to that described in Subsection (2.4), it can readily be shown that the dual is as that shown in the same figure with dashed line. The 2-terminal switches associated with the dual can be recomposed into a 3-terminal synchronous switch, operating with a fly-time equal to  $-aT$ , as shown in Fig. (4-c).

On this basis, P.F.T. and N.F.T. 3-terminal synchronous switches are shown to be dual.

### 3.0 3-Terminal RC Chopper Networks and Their Equivalents

In dealing with various networks, it has been found appropriate to adopt symbols for voltage and current generators similar to those given in Ref. (17). Dot notation is employed to define the polarities of various voltages and currents for its consistency and simplicity<sup>(18)</sup>. For the purpose of convenience, the input driving force, whether of voltage or current form, will be denoted by the proper symbol with post-subscript 1. The resulting responses, which accordingly are of voltage or current form, will have postsubscripts 2 and 3, the proper response of which may be selected accordingly to type of application; e.g. as to whether the chopper network is required as a phase-lag or phase-lead demodulating compensator for carrier control systems (7,8).

#### 3.1 Prototype Chopper Networks

Prototype chopper networks are arbitrarily chosen to contain RC electric passive elements and to be energised by a voltage source. For reasons that will be clarified in Subsection (5.2) only P.F.T. synchronous switches are going to

be used at the present stage.

Prototype networks may be conveniently classified according to number of 3-terminal synchronous switches and capacitors employed, as given below:

- (i) Single-switch double-capacitor type as shown in Fig. (5-a).
- (ii) Double-switch single-capacitor type as shown in Fig. (7-a).

In order to preserve the generality, each of  $G$  and  $G_2$  is considered to represent the parallel combination of load conductance and a general conductance, and  $G_1$  to represent the capacitor leakage conductance in parallel with a general conductance.

The response or behaviour of these prototype chopper networks may be described by establishing the relationship between the output voltages  $v_2$  and  $v_3$  and the known input voltage  $v_1$ . These relations are given, in Laplacian form, in table (4.3) for the interval

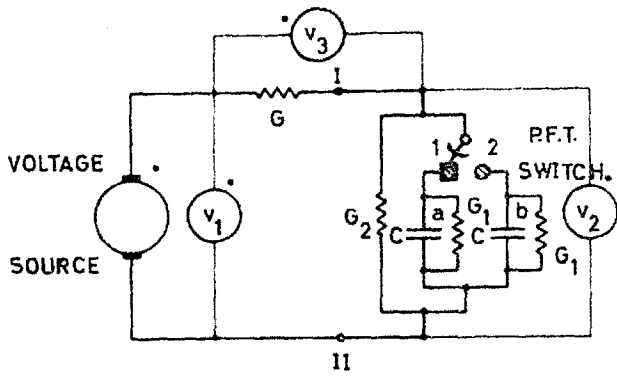
$$n T \leq t < (n + 1) T \quad 3.1.$$

where the initial values of voltages appearing across the capacitors still have to be expressed in terms of the input voltage in order to obtain complete response description. This is beyond the scope of the present paper and it is hoped that the complete analysis will be dealt with in a future paper.

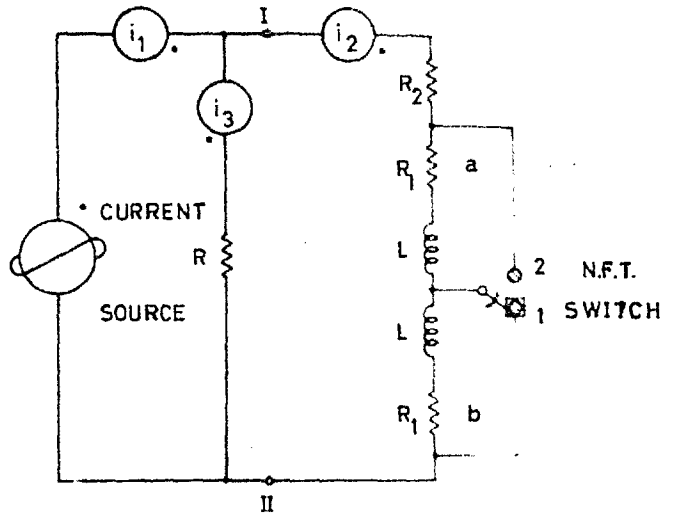


Voltage energisation

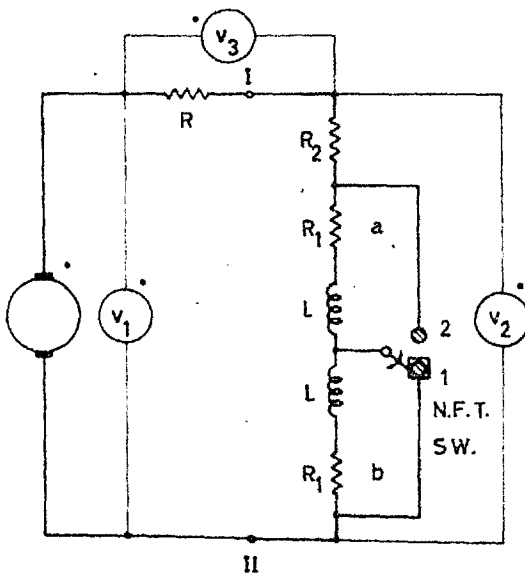
Current energisation



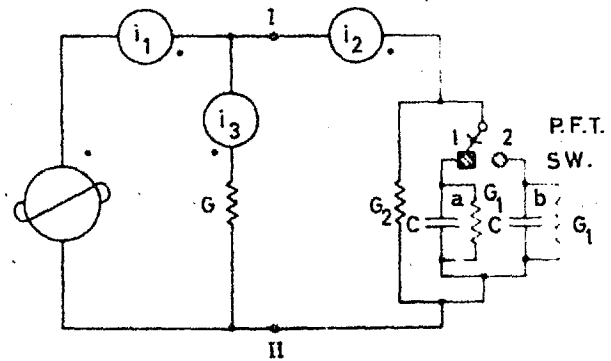
(a) Prototype



(b) Dual of prototype



(c) Complement of prototype



(d) Dual-complement of prototype

Fig. 5

Single-switch double-capacitor chopper network and its derived networks

### 3.2 Derived Networks

In network theory, one is concerned with three aspects; an excitation, a response and a network. As a consequence, three problems have been evolved as to find out one aspect when the other two are specified. Out of these problems the network synthesis, in which case an excitation and a response are specified while the network is to be found, plays a significant role in the modern network theory.

Depending on whether the given functions are specified in the time or in the frequency domain, different synthesis procedures have been developed (10 to 16). However, if a finite network is to be expected, the transfer function, formed from the ratio of the frequency domain functions of the response and the excitation, must fulfil the realizability conditions. These conditions, essentially, impose various constraints on the form of the transfer function which have led to the establishment of well known criteria of existence of solution for the case of linear networks (10 to 16).

With regard to chopper networks, it is extremely difficult to formulate their transfer functions in a rational form (quotient of polynomials in the complex frequency variable) for the following reasons:

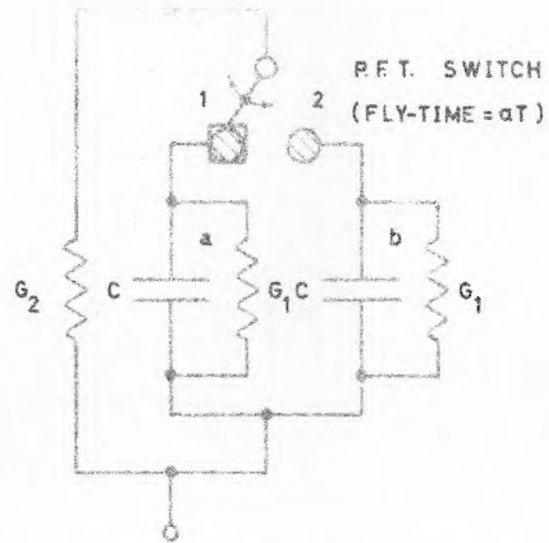
- (i) The excitation signal is in the form of suppressed-carrier amplitude modulated wave.
- (ii) Presence of synchronous switches which do not behave as linear elements (but behave as time-varying elements).
- (iii) The output is not a linear function of the input.

In the light of the above factors, it is evident that equivalent chopper networks can hardly be obtained by synthesis procedure. In this connection, however, the principle of duality can be very useful in avoiding the necessity of formulating the transfer function and the need of a synthesis procedure. It is therefore appropriate to discuss techniques of constructing the dual of chopper networks.

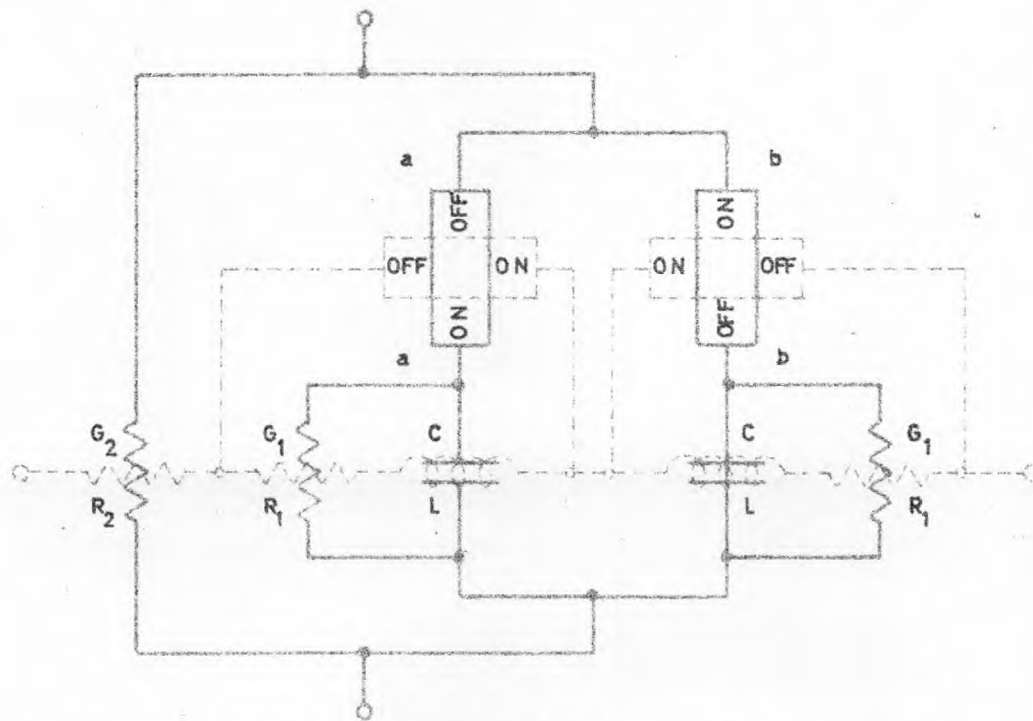
### 3.2.1 Dual Networks

Considering the RC prototype chopper networks shown in Figs. (5-a) and (7-a), it would appear, at the first sight, that construction of their duals is extremely complicated due to the presence of the 3-terminal synchronous switches. Yet, by decomposing the 3-terminal switch into its 2-terminal switch arrangement, the problem reduces to a simple straightforward one as the results of the techniques outlined in Subsections (2.4) and (2.5) can be readily used. To illustrate the usefulness of this method, dual construction of a part of the network of Fig. (5-a), which consists of branches a and b (where each branch consists of a capacitance  $c$  in parallel with a conductance  $G_1$ ), conductance  $G$  and a P.F.T. 3-terminal switch, is going to be discussed in more detail.

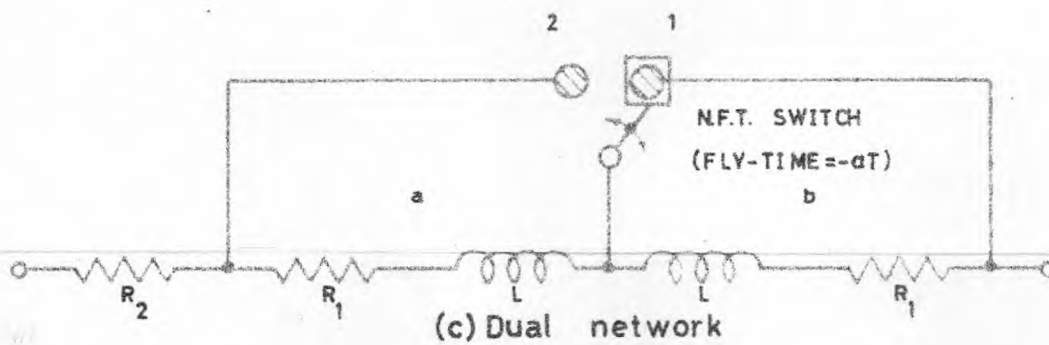
The part of the network of Fig. (5-a) in which we are interested is redrawn in Fig. (6-a). Fig. (6-b) illustrates the steps to be taken in constructing the dual. In this respect, the P.F.T. <sup>switch</sup> is decomposed into ON-OFF and OFF-ON switches using analogous procedure as that described in subsection (2.5); consequently the original network assumes the convenient configuration as shown in solid line. Having constructed the dual graph orthogonal to that of the prototype as shown in dashed line, it is easy to assign to its branches the dual of the elements in the respective branches of the original network: provided that the following quantities



(a) Prototype network



(b) Prototype and dual networks



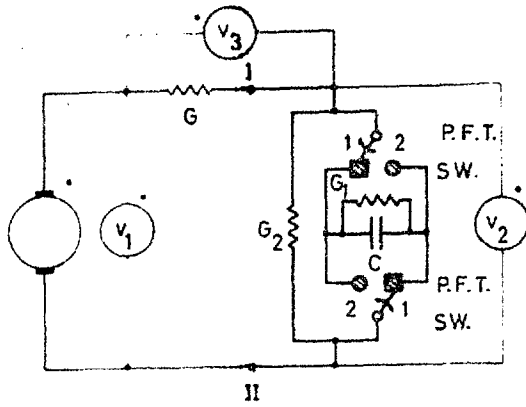
(c) Dual network

Fig.6

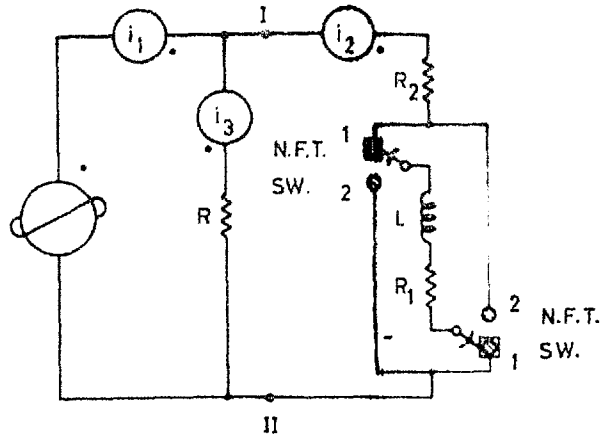
Illustration of the process of dual construction of a part of the chopper network shown in Fig.(5-a)

Voltage  
energisation

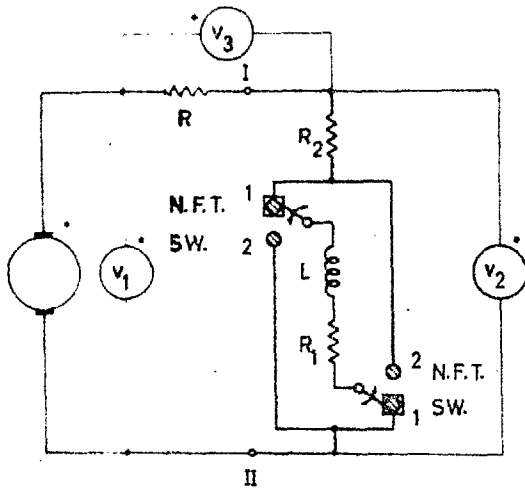
Current  
energisation



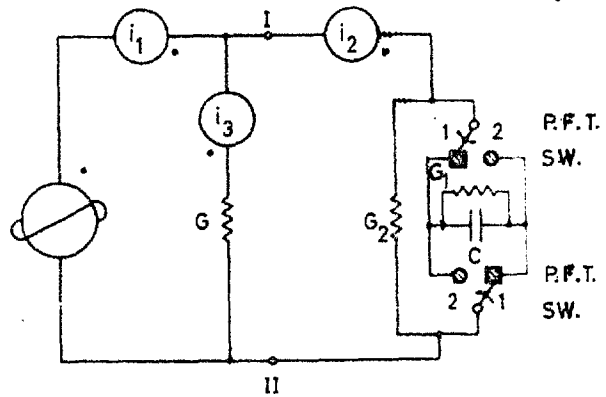
(a) Prototype



(b) Dual of prototype



(c) Complement of prototype



(d) Dual-complement of prototype

Fig. 7

Double-switch single-capacitor chopper network and its derived networks

and concepts are interchanged:

C	$\longleftrightarrow$	L	)	
G	$\longleftrightarrow$	R	)	
ON-OFF switch	$\longleftrightarrow$	OFF-ON switch	)	} 3.2
series connection	$\longleftrightarrow$	parallel connection	)	

According to Subsection (2.5), the resulting 2-terminal switches associated with the dual network can be recomposed into N.F.T. switch as shown in Fig. (6-c).

In the light of the simple technique described above, a systematic process of constructing the duals of chopper networks has been emerged. Bearing in mind that the dual of a voltage source is a current source, and also with the help of the above developed procedure, it is easy to construct the duals of the prototype chopper networks of Figs. (5-a) and (7-a) as shown in Figs. (5-b) and (7-b), respectively. As a verification, their current response functions are outlined in subsection (4.1.2) whose expressions are found to be identical in form to the respective voltage response functions of their corresponding prototype networks.

In this connection, it may be pointed out that the inductance  $L$ , appearing in the dual networks, is connected in series with resistance  $R_1$  which, in practice, may represent the inevitable inductor resistance in series with a general resistance. Another feature which may be worthwhile mentioning is the fact that if the dual networks were selected to be prototypes, their corresponding duals could be easily proved, following similar lines as those outlined above, to be exactly the originally selected prototypes.

### 3.2.2 Complement Network

Turning the attention to the dual networks shown in Figs. (5-b) and (7-b), it is observed that the line passing through points I and II divides conveniently the network into two parts; the left hand part consists of a current source  $i_1$  shunted by a resistance  $R$ , while the right hand part consists of a time varying impedance. It is therefore evident that Thevenin's theorem can be applied to convert the left hand part into an equivalent voltage source  $v_1$  in series with the same resistance  $R$  such that

$$v_1 = i_1 R \quad 3.3$$

The resulting networks are illustrated in Figs. (5-c) and (7-c) for the two respective duals under consideration. Expressions for the voltage response functions  $v_2/v_1$  and  $v_3/v_1$  have been established in Subsection (4.1.1.), are found to be identical, in form, with the complement of those pertinent to their respective prototype networks. On this basis, it is found appropriate to refer to these networks as "Complement Networks".

In this respect, it is obvious that the dual network can be derived back from its respective complement by applying Norton's theorem to its linear left hand part which contains the voltage source  $v_1$  in series with the resistance  $R$ .

### 3.2.3 Dual-Complement Network

Pursuing similar technique as that outlined in Subsection (3.2.1) it is possible to construct the dual of the complement network. Figs. (5-d) and (7-d) show the dual complement networks for the two chopper networks under consideration where the

associated 3-terminal switches are of the P.F.T. type. Again, expressions for the current response functions have been derived in Subsection (4.1.2), and are found to be identical in form, with the respective voltage response functions pertinent to the complement networks.

It may be worth noting that the dual complement network can be directly derived from its prototype by applying Thevenin's theorem to the portion containing the voltage source  $v_1$  and series resistance  $1/G$ . The inverse process is also true in which case Norton's theorem should be applied to the part of the dual-complement network containing the current source  $i_1$  and the shunt conductance  $G$  in order to obtain the prototype network.

#### 4.0 Derivation of Response Equations

Response equations of a network are expressions relating the desired output to the known input. In general, they may be specified either in the time or in the complex frequency domain. For linear networks, such relations can be directly derived from the node and mesh equations by solving them simultaneously, taking into account the initial conditions.

In dealing with chopper networks, the node and mesh equations have to be set up four times per carrier cycle. These correspond to intervals during which the incorporated synchronous switches assume a particular state and hence the chopper network can be treated as a linear network. The various equations applicable during a particular interval of carrier cycle are also valid during the corresponding intervals, as the time progresses, provided that the proper initial conditions are accounted for. To obtain these initial conditions as a discrete function of time requires a



long and complicated analysis which is not the immediate intention of this paper. However, to provide an adequate basis of comparison between various equivalent chopper networks, it is sufficient to derive the response equations for one complete carrier cycle in which the initial conditions can be left as constant parameters.

In order to illustrate the method of deriving the response equations, single-switch double-capacitor chopper network and its derived networks, shown in Fig. (5), are going to be considered as an example.

#### 4.1 Single-Switch Double-capacitor chopper network and its Derived Networks

##### 4.1.1 Voltage Energised Networks

During all intervals of carrier cycle the following mesh equation applies

$$v_1 = v_2 + v_3 \quad 4.1$$

##### (i) Prototype Network

This network is shown in Fig. (5-a) in which it is assumed that the switch is in contact with point 1 during the interval.

$$nT \leq t < (n + \delta)T, \quad 0.5 \leq \delta < 1 \quad 4.2$$

Setting up the node and mesh equations and rearranging, the following expressions can be easily obtained

$$v_2 = v_a \quad 4.3$$

$$v_3 = \frac{(G_1 + G_2)}{G} v_a + \frac{c}{G} \frac{d}{d_t} (v_a)$$

$$= \tau \left\{ \frac{1}{\tau_{e_{12}}} + \frac{d}{d_t} \right\} v_a \quad 4.4$$

$$0 = \left\{ 1 + \tau_1 \frac{d}{d_t} \right\} v_b \quad 4.5$$

Where  $v_a$  and  $v_b$  are voltages which appear across the capacitors in branches a and b respectively.

And  $\tau_1$ ,  $\tau_{e_{12}}$  are time constants defined as in the notes under table 4.2 (4.2).

During the interval

$$(n + \delta) \leq t < (n + \frac{1}{2}) T \quad 4.6$$

the switch is in the middle position. The corresponding relations can then be formulated as given below

$$v_2 = \frac{G}{G + G_2} v_1 \quad 4.7$$

$$v_3 = \frac{G_2}{G + G_2} v_1 \quad 4.8$$

$$0 = \left\{ 1 + \tau_1 \frac{d}{d_t} \right\} v_a \quad 4.9$$

$$0 = \left\{ 1 + \tau_1 \frac{d}{d_t} \right\} v_b \quad 4.10$$

During the interval

$$(n + \frac{1}{2}) T \leq t < (n + \frac{1}{2} + \delta) T \quad 4.11$$

the switch is in contact with point 2. Consequently, node and mesh equations can be derived which may be written as

$$v_2 = v_b \quad 4.12$$

$$v_3 = \tau \left\{ \frac{1}{\tau_{e_{12}}} + \frac{d}{d_t} \right\} v_b \quad 4.13$$

$$0 = \left\{ 1 + \tau_1 \frac{d}{d_t} \right\} v_a \quad 4.14$$

During the interval

$$(n + \frac{1}{2} + \delta) T \leq t < (n + 1) T \quad 4.15$$

the switch is again in the middle position. The corresponding relations are thus similar to those expressed by Equations (4.7) to (4.10).

(ii) Complement Network

The network is shown in Fig. (5-c) in which the associated switch is of N.F.T. type (dual to the P.F.T. switch associated with the prototype network). Node and mesh equations are going to be set up during the same intervals assigned to the prototype network, and rewritten in the convenient forms similar to those formulated above.

During the interval specified by Equation (4.2), the switch is in contact with only point 1. Hence, the corresponding relations can be easily derived which may be written as

$$v_3 = R i_a \quad 4.16$$

$$\begin{aligned} v_2 &= \frac{R_1 + R_2}{R} R i_a + \frac{L}{R} \frac{d}{dt} (R i_a) \\ &= \tau \left\{ \frac{1}{\tau_{e_{12}}} + \frac{d}{dt} \right\} R i_a \quad 4.17 \end{aligned}$$

$$o = \left\{ 1 + \tau_1 \frac{d}{dt} \right\} i_b \quad 4.18$$

Where  $i_a$  and  $i_b$  are currents flowing through the inductors in branches a and b respectively.

During the intervals specified by Equations (4.6) and (4.15) the switch is in contact with both points 1 and 2. Accordingly, the corresponding equations may be derived and expressed as below:

$$v_3 = \frac{R}{R + R_2} v_1 \quad 4.19$$

$$v_2 = \frac{R_2}{R + R_2} v_1 \quad 4.20$$

$$o = \left\{ 1 + \tau_1 \frac{d}{dt} \right\} i_a \quad 4.21$$

$$o = \left\{ 1 + \tau_1 \frac{d}{dt} \right\} i_b \quad 4.22$$

During the interval specified by Equation (4.11), the switch is in contact with only point 2. Hence,

$$v_3 = R i_b$$

$$v_2 = \frac{R_1 + R_2}{R} R i_b + \frac{L}{R} \frac{d}{dt} (R i_b) \quad 4.23$$

$$= \tau \left\{ \frac{1}{\tau_{e_{12}}} + \frac{d}{dt} \right\} R i_b \quad 4.24$$

$$0 = \left\{ 1 + \tau_1 \frac{d}{dt} \right\} i_a \quad 4.25$$

Solving the sets of equations pertinent to various intervals in terms of the voltage excitation  $v_1$  and then transforming the results into the complex frequency domain by applying Laplace transform; it is easy to obtain formulae for the voltages  $v_2$ ,  $v_3$ ,  $v_a$ ,  $v_b$  (for the prototype network) and  $v_2$ ,  $v_3$ ,  $R i_a$ ,  $R i_b$  (for the complement network) expressed in Laplacian form as given in table (4.2).

#### 4.1.2 Current Energised Networks

Being dual to the voltage energised networks, the following node equation is found applicable during all intervals of the carrier cycle

$$i_1 = i_2 + i_3 \quad 4.26$$

Pursuing an analogous procedure to that adopted in Subsection (4.11), it is possible to derive sets of equations corresponding to various intervals of one carrier cycle for the dual and dual complement networks as given in table (4.1).

If these sets of equations are solved in terms of the current excitation  $i_1$  and then Laplace transform is applied to the results; expressions for the currents  $i_2$ ,  $i_3$ ,  $i_a$ ,  $i_b$  (for the dual network) and  $i_2$ ,  $i_3$ ,  $G v_a$ ,  $G v_b$ , (for the dual complement network) can be obtained in Laplacian form as given in table (4.2).

TABLE (4.1)

Differential equations of the Dual and Dual-Complement of Single-Switch Double-Capacitor Chopper Network

Chopper Network Interval of Time	Dual Network Fig. (5-b)	Dual-Complement Network Fig. (5-d)
$nT \leq t < (n + \delta) T$	$i_2 = i_a$	$i_3 = G v_a$
	$i_3 = \tau \left\{ \frac{1}{\tau_{e_{12}}} + \frac{d}{dt} \right\} i_a$	$i_2 = \tau \left\{ \frac{1}{\tau_{e_{12}}} + \frac{d}{dt} \right\} v_b$
	$o = \left\{ 1 + \tau_1 \frac{d}{dt} \right\} i_b$	$o = \left\{ 1 + \tau_1 \frac{d}{dt} \right\} v_b$
$(n + \delta) T \leq t < (n + \frac{1}{2}) T$ and $(n + \frac{1}{2} + \delta) T \leq t < (n + 1) T$	$i_2 = \frac{R}{R + R_2} i_1$	$i_3 = \frac{G}{G + G_2} i_1$
	$i_3 = \frac{R_2}{R + R_2} i_1$	$i_2 = \frac{G_2}{G + G_2} i_1$
	$o = \left\{ 1 + \tau_1 \frac{d}{dt} \right\} i_a$	$o = \left\{ 1 + \tau_1 \frac{d}{dt} \right\} v_a$

TABLE (4.1) contd

Chopper Network Interval of time	Dual Network Fig. (5-b)	Dual-Complement Network Fig. (5-d)
	$o = \left\{ 1 + \tau_1 \frac{d}{d_t} \right\} i_b$	$o = \left\{ 1 + \tau_1 \frac{d}{d_t} \right\} v_b$
$(n+\frac{1}{2}) T \leq t <$ $(n+\frac{1}{2}+\delta) T$	$i_2 = i_b$	$i_3 = G i_b$
	$i_3 = \tau \left\{ \frac{1}{\tau_{e_{12}}} + \frac{d}{d_t} \right\} i_b$	$i_2 = \tau \left\{ \frac{1}{\tau_{e_{12}}} + \frac{d}{d_t} \right\} G v_b$
	$o = \left\{ 1 + \tau_1 \frac{d}{d_t} \right\} i_a$	$o = \left\{ 1 + \tau_1 \frac{d}{d_t} \right\} v_a$

TABLE (4.2)

Response Equations of Single-Switch Double-Capacitor Chopper Network and its Derived Networks, in Laplacian form.

Chopper Network/ Interval of Time	Prototype Fig. (5-a)	
$nT \leq t < (n+\delta)T$	$v_a(s)$	$\left\{ \frac{n v_1(s)}{\tau} / \left( s + \frac{1}{\tau_e} \right) \right\} + \left\{ n V_a / \left( s + \frac{1}{\tau_e} \right) \right\}$
	$v_2(s)$	$v_a(s)$
	$v_3(s)$	$\left\{ \frac{n v_1(s) (s + \frac{1}{\tau})}{\tau_{e12}} / \left( s + \frac{1}{\tau_e} \right) \right\} - \left\{ n V_a / \left( s + \frac{1}{\tau_e} \right) \right\}$
$(n+\delta)T \leq t < (n+\frac{1}{2})T$	$v_a(s)$	$\left\{ (n+\delta) V_a / \left( s + \frac{1}{\tau_1} \right) \text{ for } (n+\delta)T \leq t < (n+1)T \right\}$
	$v_2(s)$	$(n+\delta) v_1(s) \tau_2 / (\tau + \tau_2)$
	$v_3(s)$	$(n+\delta) v_1(s) \tau / (\tau + \tau_2)$
$(n+\frac{1}{2})T \leq t < (n+\frac{1}{2}+\delta)T$	$v_b(s)$	$\left\{ (n+\frac{1}{2}) \frac{v_1(s)}{\tau} / \left( s + \frac{1}{\tau_e} \right) \right\} + \left\{ (n+\frac{1}{2}) V_b / \left( s + \frac{1}{\tau_e} \right) \right\}$
	$v_2(s)$	$v_b(s)$
	$v_3(s)$	$\left\{ (n+\frac{1}{2}) v_1(s) (s + \frac{1}{\tau}) / \left( s + \frac{1}{\tau_e} \right) \right\} - \left\{ (n+\frac{1}{2}) V_b / \left( s + \frac{1}{\tau_e} \right) \right\}$
$(n+\frac{1}{2}+\delta)T \leq t < (n+1)T$	$v_b(s)$	$(n+\frac{1}{2}+\delta) V_b / \left( s + \frac{1}{\tau_1} \right) \text{ for } (n+\frac{1}{2}+\delta)T \leq t < (n+1)T$
	$v_2(s)$	$(n+\frac{1}{2}+\delta) v_1(s) \tau_2 / (\tau + \tau_2)$
	$v_3(s)$	$(n+\frac{1}{2}+\delta) v_1(s) \tau / (\tau + \tau_2)$



TABLE (4.2) contd.

Chopper Network Interval of Time	Dual of Prototype Fig. (5-b)	
$nT \leq t < (n+\delta)T$	$i_a(s)$	$\left\{ \frac{n i_1(s)}{\tau} / (s + \frac{1}{\tau_c}) \right\} + \left\{ n I_a / (s + \frac{1}{\tau_c}) \right\}$
	$i_2(s)$	$i_a(s)$
	$i_3(s)$	$\left\{ n i_1(s) (s + \frac{1}{\tau_{c12}}) / (s + \frac{1}{\tau_c}) \right\} - \left\{ n I_a / (s + \frac{1}{\tau_c}) \right\}$
$(n+\delta)T \leq t < (n+\frac{1}{2})T$	$i_a(s)$	$(n+\delta) \frac{I_a}{\tau_1} / (s + \frac{1}{\tau_1})$ for $T(n+\delta) \leq t < (n+1)T$
	$i_2(s)$	$(n+\delta) i_1(s) \tau_2 / (\tau + \tau_2)$
	$i_3(s)$	$(n+\delta) i_1(s) \tau / (\tau + \tau_2)$
$(n+\frac{1}{2})T \leq t < (n+\frac{1}{2}+\delta)T$	$i_b(s)$	$\left\{ (n+\frac{1}{2}) \frac{i_1(s)}{\tau} / (s + \frac{1}{\tau_c}) \right\} + \left\{ (n+\frac{1}{2}) \frac{I_b}{\tau_c} / (s + \frac{1}{\tau_c}) \right\}$
	$i_2(s)$	$i_b(s)$
	$i_3(s)$	$\left\{ (n+\frac{1}{2}) i_1(s) (s + \frac{1}{\tau_{c12}}) / (s + \frac{1}{\tau_c}) \right\} - \left\{ (n+\frac{1}{2}) \frac{I_b}{\tau_c} / (s + \frac{1}{\tau_c}) \right\}$
$(n+\frac{1}{2}+\delta)T \leq t < (n+1)T$	$i_b(s)$	$(n+\frac{1}{2}+\delta) \frac{I_b}{\tau_1} / (s + \frac{1}{\tau_1})$ for $(n+\frac{1}{2}+\delta)T \leq t < (n+\frac{3}{2})T$
	$i_2(s)$	$(n+\frac{1}{2}+\delta) i_1(s) \tau_2 / (\tau + \tau_2)$
	$i_3(s)$	$(n+\frac{1}{2}+\delta) i_1(s) \tau / (\tau + \tau_2)$

Table 4.2 continued

chopper network

interval of time	Complement of Prototype Fig. (5-c)	
$nT \leq t < (n+\delta)T$	$i_a(s)R$	$\left\{ n \frac{v_1(s)}{\gamma} / (s + \frac{1}{\gamma_e}) \right\} + \left\{ n I_a R / (s + \frac{1}{\gamma_e}) \right\}$
	$v_3(s)$	$i_a(s) R$
	$v_2(s)$	$\left\{ n v_1(s) (s + \frac{1}{\gamma_{e12}}) / (s + \frac{1}{\gamma_e}) \right\} - \left\{ n I_a R / (s + \frac{1}{\gamma_e}) \right\}$
$(n+\delta)T \leq t < (n+\frac{1}{2})T$	$i_a(s)R$	$(n+\delta) I_a R / (s + \frac{1}{\gamma_1})$ for $(n+\delta)T \leq t < (n+1)T$
	$v_3(s)$	$(n+\delta) v_1(s) \gamma_2 / (\gamma + \gamma_2)$
	$v_2(s)$	$(n+\delta) v_1(s) \gamma / (\gamma + \gamma_2)$
$(n+\frac{1}{2})T \leq t < (n+\frac{1}{2}+\delta)T$	$i_b(s)R$	$\left\{ (n+\frac{1}{2}) \frac{v_1(s)}{\gamma} / (s + \frac{1}{\gamma_e}) \right\} + \left\{ (n+\frac{1}{2}) I_b R / (s + \frac{1}{\gamma_e}) \right\}$
	$v_3(s)$	$i_b(s) R$
	$v_2(s)$	$\left\{ (n+\frac{1}{2}) v_1(s) (s + \frac{1}{\gamma_{e12}}) / (s + \frac{1}{\gamma_e}) \right\} - \left\{ (n+\frac{1}{2}) I_b R / (s + \frac{1}{\gamma_e}) \right\}$
$(n+\frac{1}{2}+\delta)T \leq t < (n+1)T$	$i_b(s)R$	$\left\{ (n+\frac{1}{2}+\delta) I_b R / (s + \frac{1}{\gamma_1}) \right\}$ for $(n+\frac{1}{2}+\delta)T \leq t < (n+\frac{3}{2})T$
	$v_3(s)$	$(n+\frac{1}{2}+\delta) v_1(s) \gamma_2 / (\gamma + \gamma_2)$
	$v_2(s)$	$(n+\frac{1}{2}+\delta) v_1(s) \gamma / (\gamma + \gamma_2)$

Table 4.2 continued

chopper network		Dual Complement of Prototype Fig. (5-d)	
interval of time	$(n+\delta)T \leq t < (n+1)T$	$v_a(s)G$	$\left\{ n \frac{i_1(s)}{\gamma} / (s + \frac{1}{\tau_c}) \right\} + \left\{ n V_a G / (s + \frac{1}{\tau_e}) \right\}$
	$t$	$i_3(s)$	$v_a(s) G$
	$t$	$i_2(s)$	$\left\{ n i_1(s) (s + \frac{1}{\tau_{c12}}) / (s + \frac{1}{\tau_c}) \right\} - \left\{ n V_a G / (s + \frac{1}{\tau_e}) \right\}$
$(n+\delta)T \leq t < (n+1)T$	$(n+\delta)T \leq t < (n+1)T$	$v_a(s)G$	$(n+\delta) V_a G / (s + \frac{1}{\tau_1})$ for $(n+\delta)T \leq t < (n+1)T$
	$t$	$i_3(s)$	$(n+\delta) i_1(s) \tau_2 / (\tau + \tau_2)$
	$t$	$i_2(s)$	$(n+\delta) i_1(s) \tau / (\tau + \tau_2)$
$(n+\frac{1}{2})T \leq t < (n+\frac{1}{2}+\delta)T$	$(n+\frac{1}{2})T \leq t < (n+\frac{1}{2}+\delta)T$	$v_b(s)G$	$\left\{ (n+\frac{1}{2}) \frac{i_1(s)}{\gamma} / (s + \frac{1}{\tau_c}) \right\} + \left\{ (n+\frac{1}{2}) V_b G / (s + \frac{1}{\tau_e}) \right\}$
	$t$	$i_3(s)$	$v_b(s) G$
	$t$	$i_2(s)$	$\left\{ (n+\frac{1}{2}) i_1(s) (s + \frac{1}{\tau_{c12}}) / (s + \frac{1}{\tau_c}) \right\} - \left\{ (n+\frac{1}{2}) V_b G / (s + \frac{1}{\tau_e}) \right\}$
$(n+\frac{1}{2}+\delta)T \leq t < (n+1)T$	$(n+\frac{1}{2}+\delta)T \leq t < (n+\frac{3}{2})T$	$v_b(s)G$	$(n+\frac{1}{2}+\delta) V_b G / (s + \frac{1}{\tau_1})$ for $(n+\frac{1}{2}+\delta)T \leq t < (n+\frac{3}{2})T$
	$t$	$i_3(s)$	$(n+\frac{1}{2}+\delta) i_1(s) \tau_2 / (\tau + \tau_2)$
	$t$	$i_2(s)$	$(n+\frac{1}{2}+\delta) i_1(s) \tau / (\tau + \tau_2)$

N.B.:

- (i) Presubscript when multiplied by the carrier period  $T$ ; the result defines the instant at which the Laplace transform is taken.
- (ii)  $V_a$  and  $V_b$  are the initial values of voltages appearing across the capacitors in branches a and b, respectively, at the instant indicated by their presubscripts.
- (iii)  $I_a$  and  $I_b$  are the initial values of currents in the inductors in branches a and b, respectively, at the instant indicated by their presubscripts.
- (iv) Time constants associated with various chopper networks in terms of their parameters.

<u>Time Constant</u>	<u>Prototype and its dual-complement chopper networks</u>	<u>Dual and complement of prototype chopper networks</u>
$\tau$	$\frac{C}{G}$	$\frac{L}{R}$
$\tau_1$	$\frac{C}{G_1}$	$\frac{L}{R_1}$
$\tau_2$	$\frac{C}{G_2}$	$\frac{L}{R_2}$
$\tau_{e_{12}}$	$\frac{C}{G_1 + G_2}$	$\frac{L}{R_1 + R_2}$
$\tau_{e_1}$	$\frac{C}{G + G_1}$	$\frac{L}{R + R_1}$
$\tau_{e_2}$	$\frac{C}{G + G_2}$	$\frac{L}{R + R_2}$
$\tau_e$	$\frac{C}{G + G_1 + G_2}$	$\frac{L}{R + R_1 + R_2}$

Table 4.3

Response equations, in Laplacian form, of R.C. prototype chopper networks.

R.C. prototype

Interval of time	Double-switch single-capacitor type Fig. (7-a)	
	$(n+1)\tau$	$v(s)$
$\downarrow$	$v_2(s)$	$v(s)$
$\downarrow$	$v_3(s)$	$\left\{ n v_1(s) (s + \frac{1}{\tau_{c12}}) / (s + \frac{1}{\tau_c}) \right\} - \left\{ n V / (s + \frac{1}{\tau_c}) \right\}$
$(n+\delta)\tau$	$v(s)$	$(n+\delta)V / (s + \frac{1}{\tau_1})$
$\downarrow$	$v_2(s)$	$(n+\delta)v_1(s) \tau_2 / (\tau + \tau_2)$
$\downarrow$	$v_3(s)$	$(n+\delta)v_1(s) \tau / (\tau + \tau_2)$
$(n+\frac{1}{2})\tau$	$v(s)$	$\left\{ (n+\frac{1}{2}) \frac{v_1(s)}{\tau} / (s + \frac{1}{\tau_c}) \right\} + \left\{ -(n+\frac{1}{2})V / (s + \frac{1}{\tau_c}) \right\}$
$\downarrow$	$v_2(s)$	$v(s)$
$\downarrow$	$v_3(s)$	$\left\{ (n+\frac{1}{2})v_1(s) (s + \frac{1}{\tau_{c12}}) / (s + \frac{1}{\tau_c}) \right\} - \left\{ (n+\frac{1}{2})V / (s + \frac{1}{\tau_c}) \right\}$
$(n+\frac{1}{2}+\delta)\tau$	$v(s)$	$(n+\frac{1}{2}+\delta)V / (s + \frac{1}{\tau_1})$
$\downarrow$	$v_2(s)$	$(n+\frac{1}{2}+\delta)v_1(s) \tau_2 / (\tau + \tau_2)$
$\downarrow$	$v_3(s)$	$(n+\frac{1}{2}+\delta)v_1(s) \tau / (\tau + \tau_2)$

**N.B.:** for explanations of symbols, see notes under table (4.2).

#### 4.2 Response Equations of RC Prototype Chopper Networks

On similar lines as those provided in Subsection (4.1), it is possible to derive the response equations of double-switch single-capacitor chopper network and its derived networks shown in Fig. (7). In order to avoid repetition, the response equations of only the prototype network are given, in Laplacian form, in table (4.3).

#### 5.0 Modified Chopper Networks

In the preceding sections, synchronous switches have been analysed and viewed from various angles resulting in a significant increase in their implementations which lend themselves to further exploitation. Also, with the establishment of the dual of synchronous switch and the development of systematic techniques of deriving equivalent chopper networks, coordinated basic knowledge is evolved which may be adopted to help in developing modified chopper network configurations and responses. In this respect, various possible exploitations are going to be discussed.

#### 5.1 4-Terminal Chopper Networks

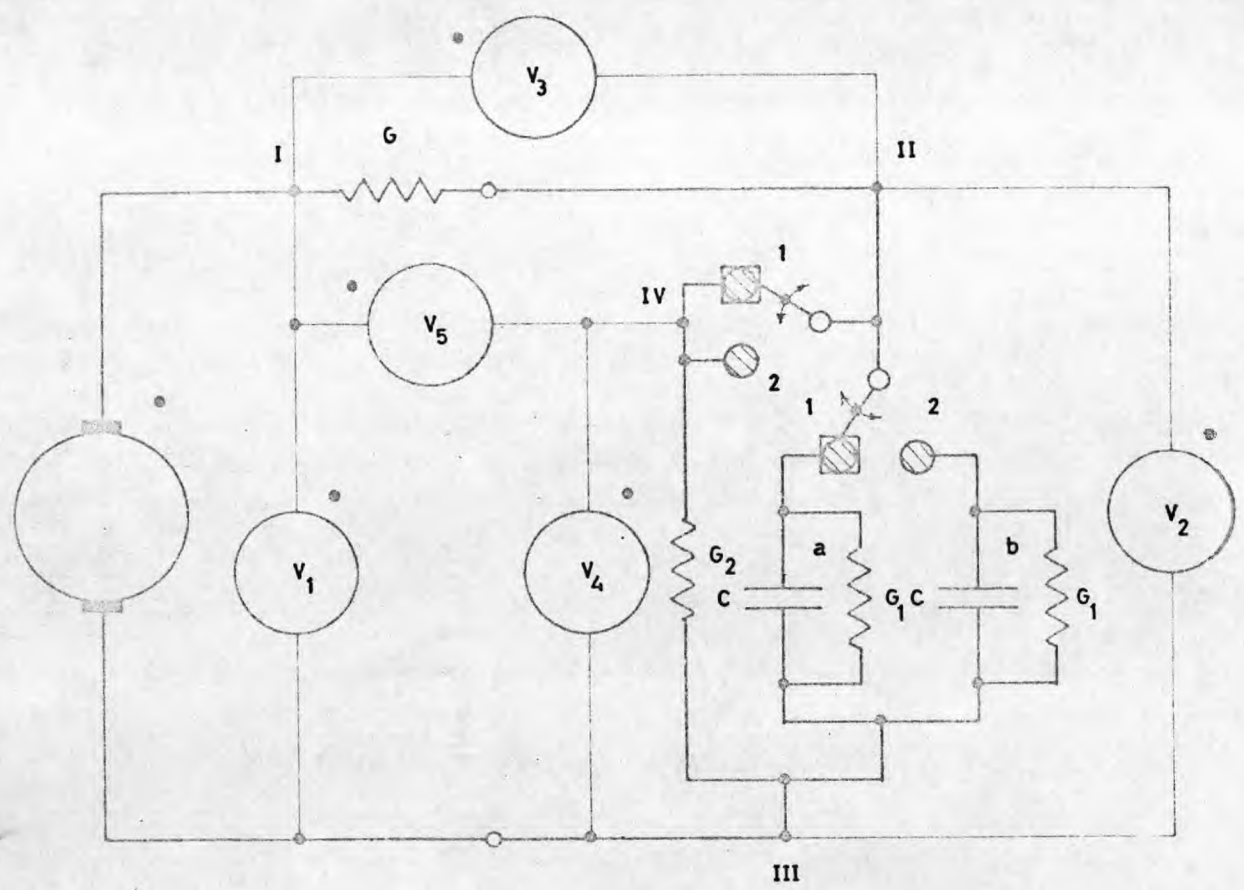
By employing an additional synchronous switch in the chopper networks of Figs. (5) and (7), three modified circuit arrangements can be easily derived. These modified networks are characterized by having an extra terminal which allows two new responses to be extracted. Besides, a slight modification takes place in the form of the remaining two responses due to the insertion of the additional switch.

### 5.1.1 Parallel Double-Switch Double-Capacitor Chopper Network and its Derived Networks

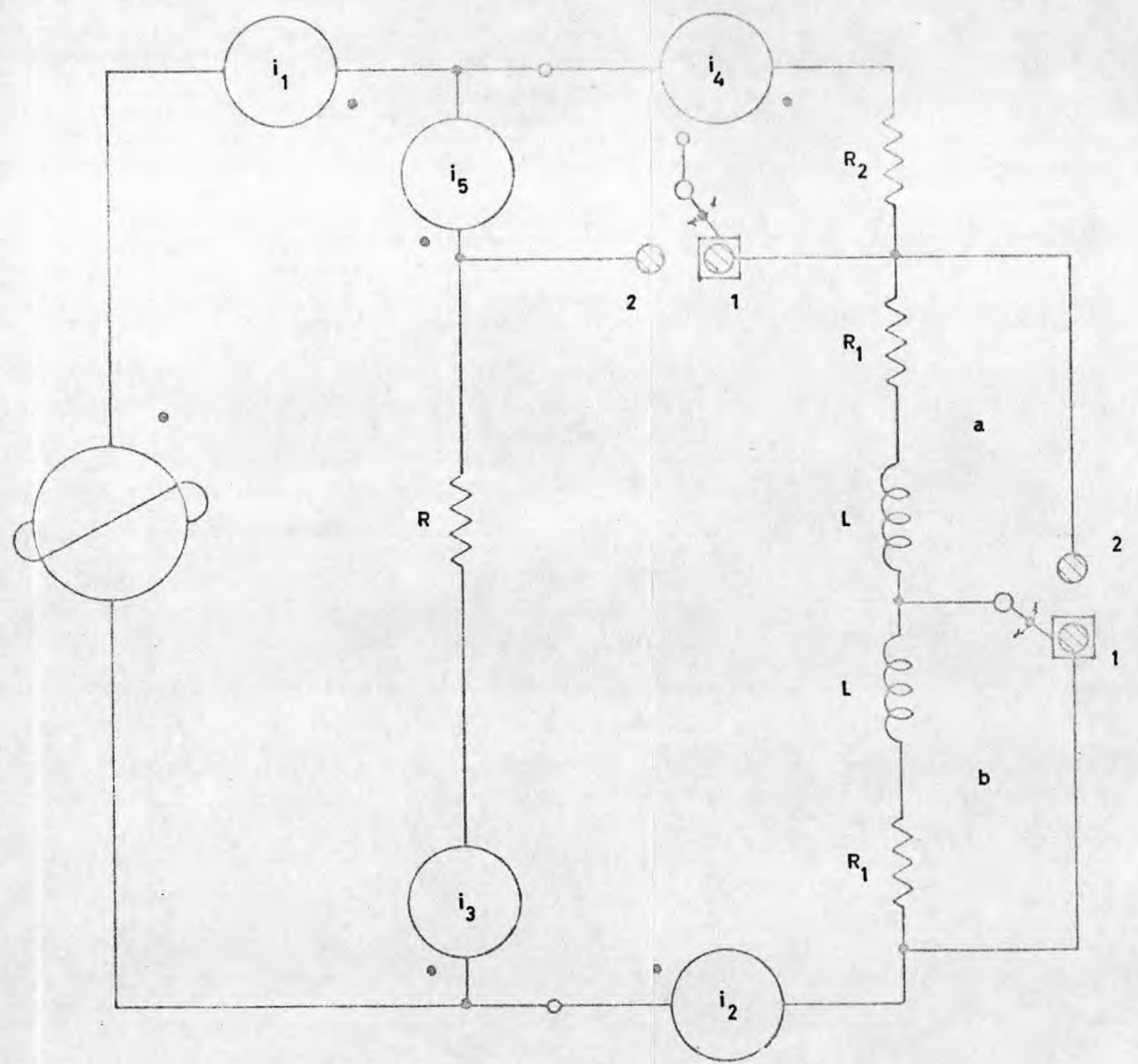
This network is a modification to the one of Fig. (5-a) in which an additional switch is inserted in cascade with  $G_2$  as shown in Fig. (8-a). The two associated switches are of similar type (P.F.T.) and operate in parallel (Parallelism refers, in this context, to the sequential movement of their moving contacts and not to their connection). Without the additional switch; voltages equal to  $\frac{G}{G + G_2} v_1$  and  $\frac{G_2}{G + G_2} v_1$  would appear across  $G_2$  and  $G$ , respectively, during the fly-time. The magnitude of either one of these voltages or both could be quite high to damage the corresponding conductances which may be representing load conductance. Therefore, the additional switch is shown to provide an adequate protection against such a possibility as it disconnects  $G_2$  and  $G$  from the rest of the network during the fly-time. This may also lead to minimization of the noise content in the useful output voltages.

With regard to the dual network, its construction can be achieved as shown in Fig. (8-b) with the help of the techniques outlined in Subsection (3.2.1). The H.F.T. switch, whose moving contact is unconnected, corresponds to the additional P.F.T. switch in the prototype network. During the fly-time its fixed contacts are short circuited which results in diverting the flow of the currents in  $R$  and  $R_2$  by bypassing them; thus protecting them against damaging current values.

With the present technique it is very difficult to derive complement and dual-complement networks which could simultaneously demonstrate the four outputs. However, by considering only three terminals at a time, the problem reduces



(a) Prototype



(b) Dual

Fig. 8

Parallel double-switch double-capacitor chopper network and its dual



to a standard one which can be easily tackled. Adopting this approach, the 4-terminal network of Fig. (8-a) may be viewed either as the 3-terminal network I, II, III (comprising  $v_1$ ,  $v_2$  and  $v_3$ ) or as the 3-terminal network I, IV, III (comprising  $v_1$ ,  $v_4$  and  $v_5$ ). These two 3-terminal networks coincide (i.e.  $v_2 = v_4$  and  $v_3 = v_5$ ) and their responses become identical to those of Fig. (5-a) if the associated synchronous switches operate with either zero or negative fly-time.

Considering the prototype network in terms of the three terminals I, II, III, it is easy to construct the dual, complement and dual-complement networks following similar pattern of treatment as before. The resulting networks are shown in Fig. (9).

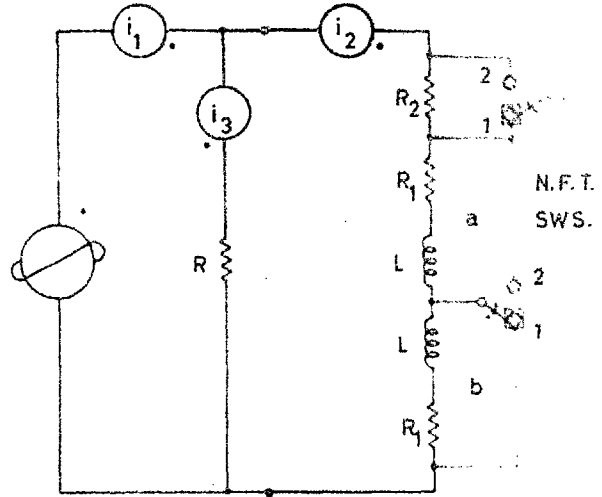
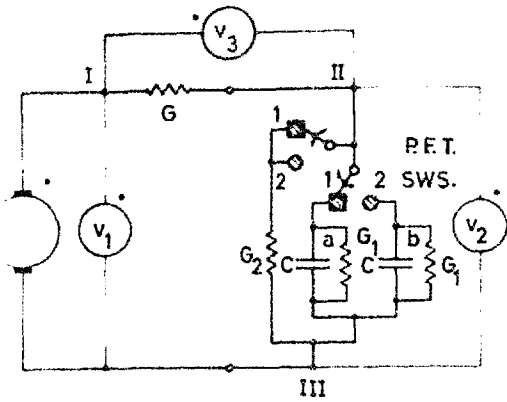
In the case the prototype network is considered in terms of the three terminals I, IV, III, it would be much convenient to rearrange its configuration in the way as illustrated in Fig. (10-a). In this, the additional switch is moved past the original switch to become connected in cascade without affecting the original behaviour of the network. The advantage gained from this rearrangement is to provide the simplicity with which derived networks can be deduced. These networks are shown in Fig. (10).

It is evident that the dual networks of Figs. (9-b) and (10-b) can also be directly derived from the general dual of Fig. (8-b) without referring to the prototype. The guiding thought behind this lies in the fact that by moving the N.F.T. switch, whose moving contact is unconnected, to become in parallel with either  $R_2$  or  $R$  is immaterial as far as the network behaviour is concerned. It is also noticed that the corresponding networks in Figs. (9) and (10) become identical

Voltage energisation

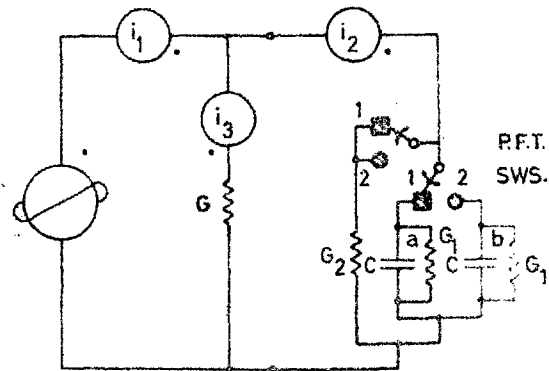
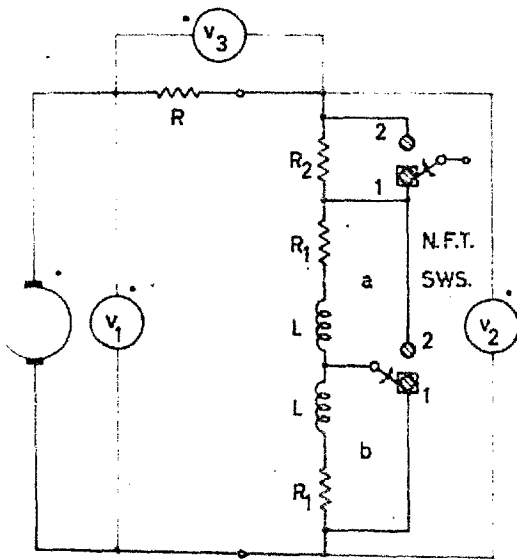
Current energisation

41



(a) Prototype

(b) Dual of prototype



(c) Complement of prototype

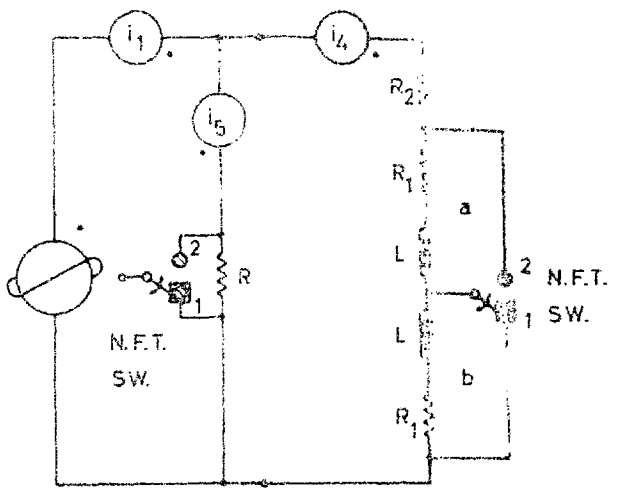
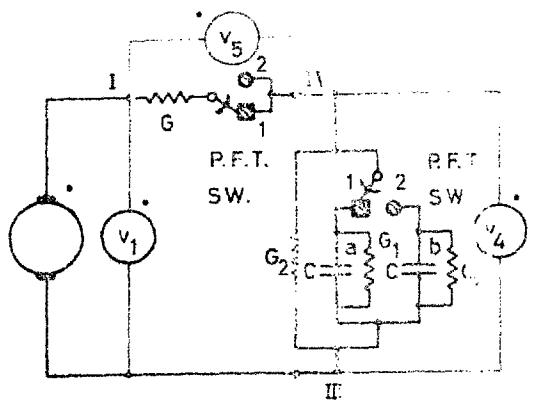
(d) Dual-complement of prototype

Fig. 9

Parallel double-switch double-capacitor chopper network and its derived networks (circuit is treated as a 3-terminal network I, II, III)

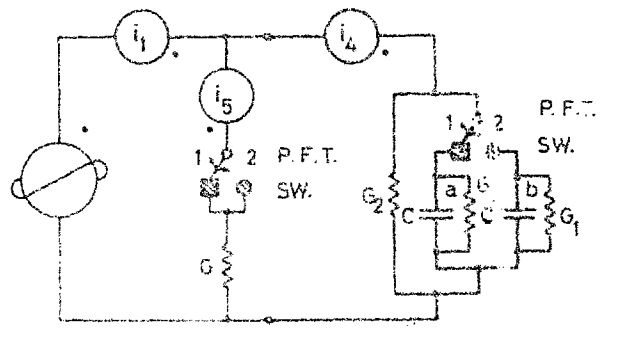
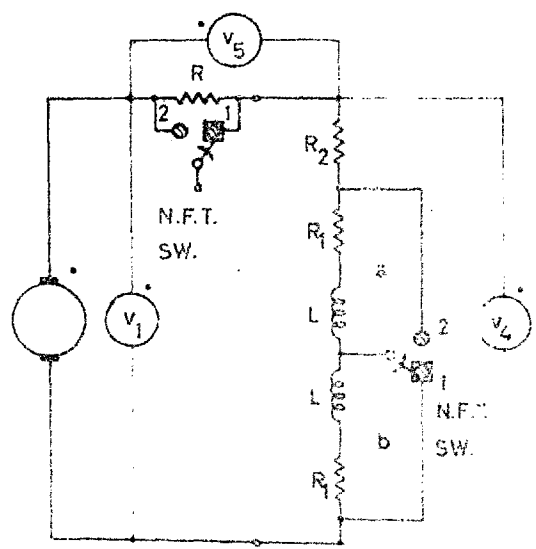
Voltage energisation

Current energisation



(a) Prototype

(b) Dual of prototype



(c) Complement of prototype

(d) Dual-complement of prototype

Fig. 10

Parallel double-switch double-capacitor chopper network and its derived networks (circuit is treated as a 3-terminal network I,IV,III)

when the synchronous switches, incorporated in the prototype, operate with either zero or negative fly-time.

The response equations of the prototype are given in Laplacian form in table (5.1). Detailed derivation of these equations as well as the corresponding ones of various derived chopper networks has been omitted as it is identical to that given in Section (4.0).

#### 5.1.2 Cascaded Inverted Double-Switch Double-Capacitor Chopper Network and its Derived Networks

This network is shown in Fig. (11) in which same number of electric passive elements and synchronous switches, as those used in the network of Fig. (8), are employed. However, the switches are connected in a different way which may be described as cascaded inverted connection.

Directing the attention to the prototype network, it is found to be a nonplanar type due to the presence of cross-over branches. Consequently, the principle of duality cannot directly be applied. However, by neglecting the branch which connects the voltmeter  $v_5$ ; the rest of the network becomes planar. Having done so, the dual network can then be constructed as shown in Fig. (11-b) where the current  $i_5$  corresponding to the voltage  $v_5$  in the prototype, cannot possibly be obtained. Fig. (12) illustrates the details of constructing the dual of the most complicated part of the network under consideration.

In the previous treatment, to preserve the circuit topology, the complement and dual-complement networks were considered instead of the equivalent and dual equivalent networks. The latter networks are exactly similar to the former ones provided that their corresponding output postsubscripts

TABLE (5.1)

Response equations, in Laplacian form, of  
parallel double-switch double-capacitor  
prototype chopper network:

Interval of time	Response Equations	
$nT \leq t < (n+\delta)T$	$v_a(s)$	$\left\{ \frac{n v_1(s)}{\tau} / (s + \frac{1}{\tau_c}) \right\} + \left\{ \frac{n V_a}{(s + \frac{1}{\tau_c})} \right\}$
	$v_2(s)$	$v_a(s)$
	$v_3(s)$	$\left\{ \frac{n v_1(s)}{\tau} (s + \frac{1}{\tau_{cl2}}) / (s + \frac{1}{\tau_c}) \right\} - \left\{ \frac{n V_a}{(s + \frac{1}{\tau_c})} \right\}$
	$v_4(s)$	$v_2(s)$
	$v_5(s)$	$v_3(s)$
$(n+\delta)T \leq t < (n+\frac{1}{2})T$	$v_a(s)$	$(n + \delta) \frac{V_a}{(s + \frac{1}{\tau_1})}$ for $T(n + \delta) \leq t < (n + 1) T$
	$v_2(s)$	$(n + \delta) v_1(s)$
	$v_3(s)$	o
	$v_4(s)$	o
	$v_5(s)$	$(n + \delta) v_1(s)$
$(n+\frac{1}{2})T \leq t < (n+\frac{1}{2}+\delta)T$	$v_b(s)$	$\left\{ (n + \frac{1}{2}) \frac{v_1(s)}{\tau} / (s + \frac{1}{\tau_c}) \right\} + \left\{ (n + \frac{1}{2}) \frac{V_b}{(s + \frac{1}{\tau_c})} \right\}$
	$v_2(s)$	$v_b(s)$
	$v_3(s)$	$\left\{ (n + \frac{1}{2}) v_1(s) (s + \frac{1}{\tau_{cl2}}) / (s + \frac{1}{\tau_c}) \right\} - \left\{ (n + \frac{1}{2}) \frac{V_b}{(s + \frac{1}{\tau_c})} \right\}$

TABLE (5.1) contd.

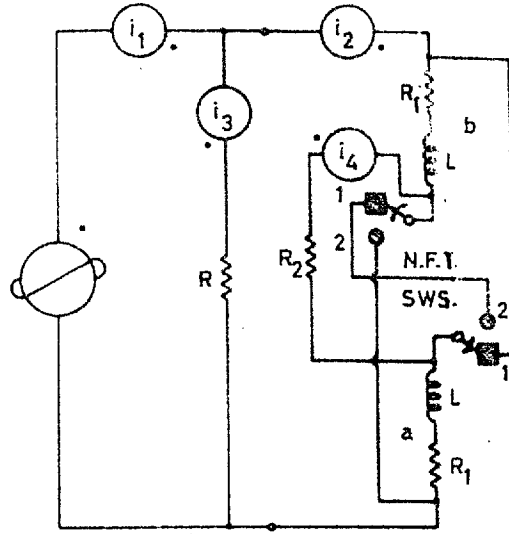
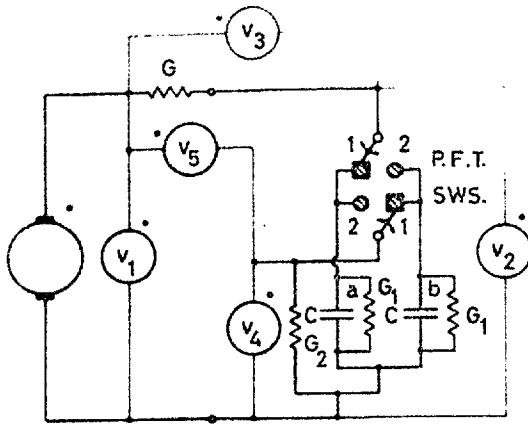
Interval of Time	Response Equations	
	$v_4(s)$	$v_2(s)$
	$v_5(s)$	$v_3(s)$
$(n + \frac{1}{2} + \delta)T \leq t < (n+1)T$	$v_b(s)$	$\left\{ (n + \frac{1}{2} + \delta) \frac{V_b}{(s + \frac{1}{\tau_1})} \right\}$ for $(n + \frac{1}{2} + \delta)T \leq t < (n + \frac{3}{2})T$
	$v_2(s)$	$(n + \frac{1}{2} + \delta) v_1(s)$
	$v_3(s)$	o
	$v_4(s)$	o
	$v_5(s)$	$(n + \frac{1}{2} + \delta) v_1(s)$

N.B.:

For explanations of symbols, see notes under table (4.2).

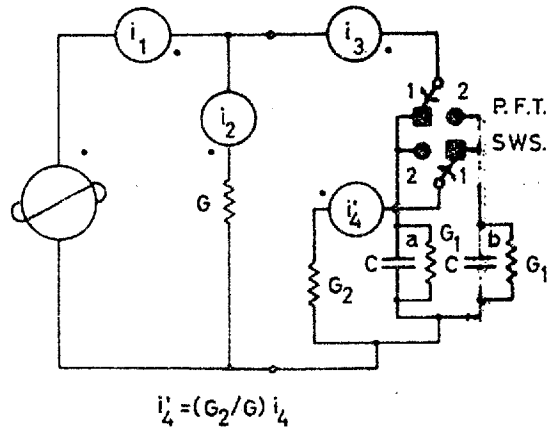
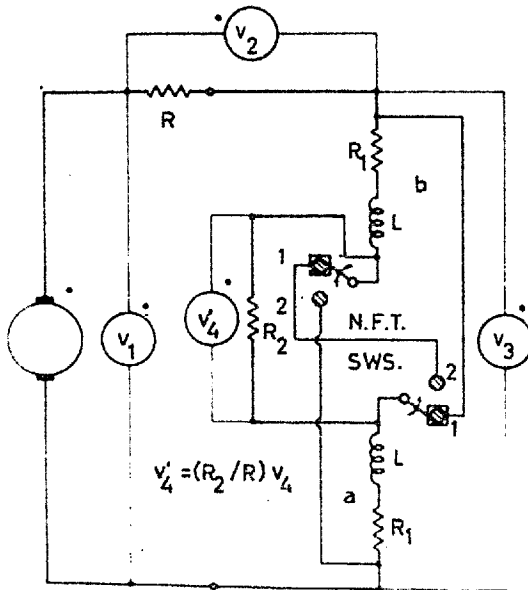
Voltage  
energisation

Current  
energisation



(a) Prototype

(b) Dual of prototype

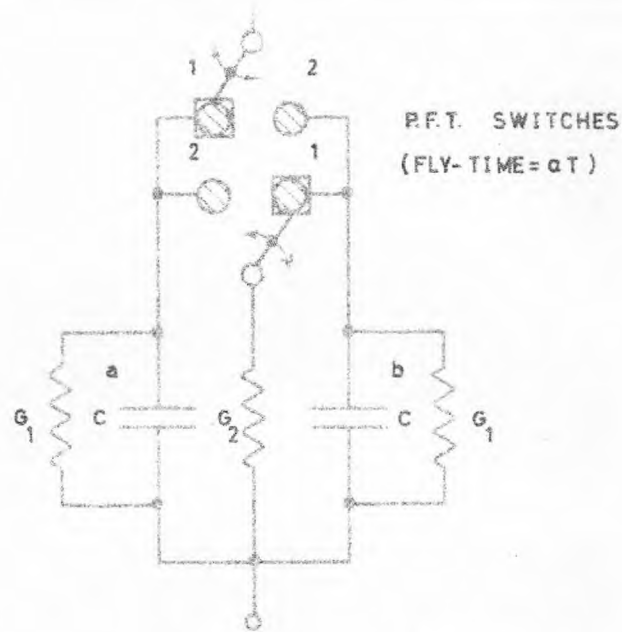


(c) Equivalent of prototype

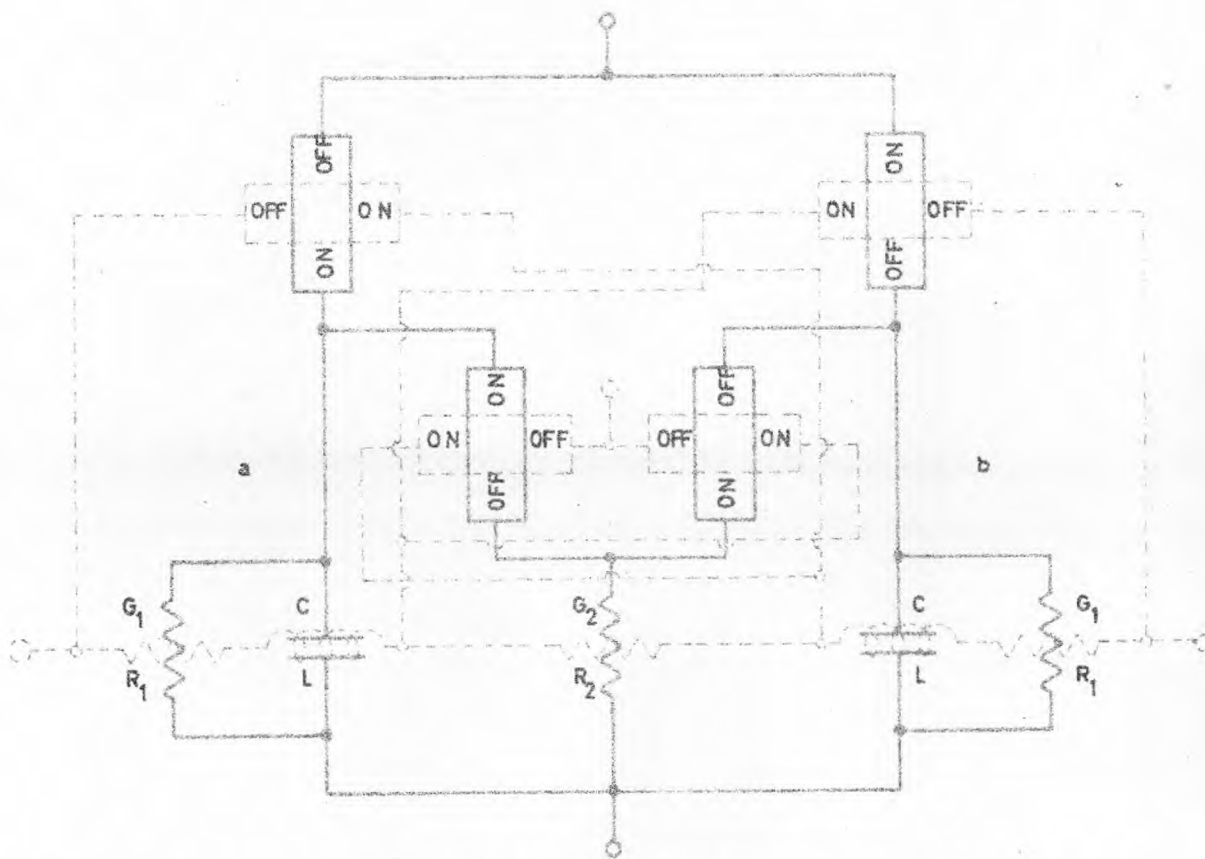
(d) Dual-equivalent of prototype

Fig.11

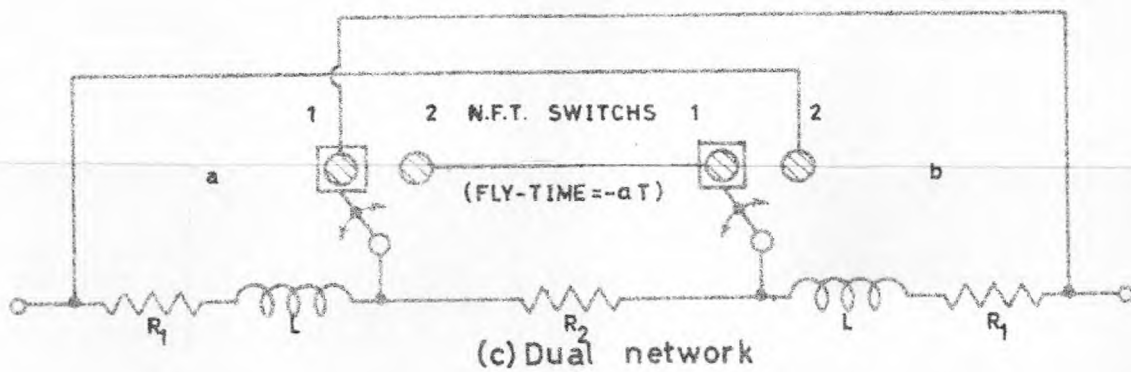
Cascaded inverted double-switch double-capacitor chopper network and its derived networks



(a) Prototype network



(b) Prototype and dual networks



(c) Dual network

Fig.12

Illustration of the process of dual construction of a part of the chopper network shown in Fig.(11-a)



2 and 3 are interchanged. Regarding the present network, it is found rather convenient to derive its equivalent and dual-equivalent networks for they yield, in addition, proportional outputs which are equivalent and dual-equivalent, in form, to the output  $v_4$  of the prototype. The factors of proportionality can be easily determined to be  $R_2/R$  and  $G_2/G$ , respectively. Table (5.2) gives the response equations of the prototype in Laplacian form.

### 5.1.3 Triple-Switch Single-Capacitor Chopper Network and its Derived Networks

This network results when an additional P.F.T. switch is inserted in cascade with  $G_2$  as shown in Fig. (13-a). Derived networks can be easily obtained by pursuing a parallel pattern of treatment as that adopted in Subsection (5.1.1). Fig. (13-b) shows the general dual network which corresponds to Fig. (8-b) in the case of parallel double-switch double-capacitor network. Figs. (13-c) and (13-d) illustrate the complement and dual-complement networks, respectively, which would yield the outputs corresponding to  $v_2$  and  $v_3$  if the dashed lines are neglected, and would yield the outputs corresponding to  $v_4$  and  $v_5$  if the networks are modified according to the dashed lines. Again, table (5.3) gives the response equations of the prototype in Laplacian form.

## 5.2 Use of Full-Range of Fly-Time Operation of Synchronous Switches

In the previous discussions, synchronous switches incorporated into various capacitor prototype chopper networks were limited to operate with either zero or positive fly-time.

TABLE (5.2)

Response equations, in Laplacian form, of cascaded inverted double-switch double-capacitor prototype chopper network

Interval of Time	Response Equations	
$nT \leq t < (n+\delta)T$	$v_a(s)$	$\left\{ n \frac{v_1(s)}{\tau} / \left( s + \frac{1}{\tau_{el}} \right) \right\} + \left\{ n V_a / \left( s + \frac{1}{\tau_{el}} \right) \right\}$
	$v_b(s)$	$n V_b / \left( s + \frac{1}{\tau_{el2}} \right)$
	$v_2(s)$	$v_a(s)$
	$v_3(s)$	$\left\{ n v_1(s) \left( s + \frac{1}{\tau_1} \right) / \left( s + \frac{1}{\tau_{el}} \right) \right\} - \left\{ n V_a / \left( s + \frac{1}{\tau_{el}} \right) \right\}$
	$v_4(s)$	$v_b(s)$
$(n+\delta)T \leq t < (n+\frac{1}{2})T$	$v_a(s)$	$(n + \delta) V_a / \left( s + \frac{1}{\tau_1} \right)$
	$v_b(s)$	$(n + \delta) V_b / \left( s + \frac{1}{\tau_1} \right)$
	$v_2(s)$	$(n + \delta) v_1(s)$
	$v_3(s)$	o
	$v_4(s)$	o
$(n+\frac{1}{2})T \leq t < (n+\frac{1}{2}+\delta)T$	$v_a(s)$	$(n + \frac{1}{2}) V_a / \left( s + \frac{1}{\tau_{cl2}} \right)$
	$v_b(s)$	$\left\{ (n+\frac{1}{2}) \frac{v_1(s)}{\tau} / \left( s + \frac{1}{\tau_{el}} \right) \right\} + \left\{ (n + \frac{1}{2}) V_b / \left( s + \frac{1}{\tau_{el}} \right) \right\}$

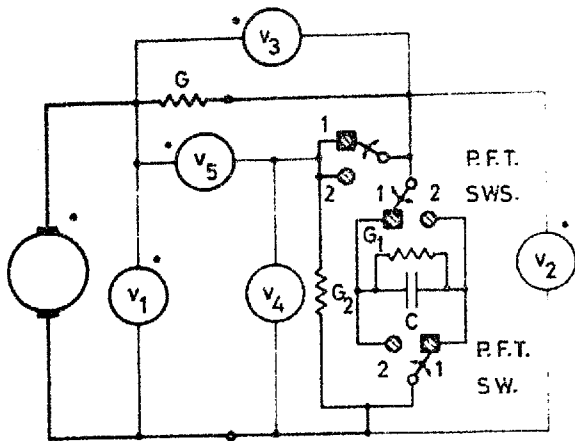
TABLE (5.2.) contd.

Interval of Time	Response Equations	
	$v_2(s)$	$v_b(s)$
	$v_3(s)$	$\left\{ (n+\frac{1}{2}) v_1(s) \frac{(s+1)}{\tau_1} / (s+\frac{1}{\tau_{e1}}) \right\} - \left\{ (n+\frac{1}{2}) v_b / (s+\frac{1}{\tau_{e1}}) \right\}$
	$v_4(s)$	$v_a(s)$
$(n+\frac{1}{2}+\delta)T \leq t < (n+1)T$	$v_a(s)$	$(n + \frac{1}{2} + \delta) v_a / (s + \frac{1}{\tau_1})$
	$v_b(s)$	$(n + \frac{1}{2} + \delta) v_b / (s + \frac{1}{\tau_1})$
	$v_2(s)$	$(n + \frac{1}{2} + \delta) v_1(s)$
	$v_3(s)$	o
	$v_4(s)$	o

N.B.:

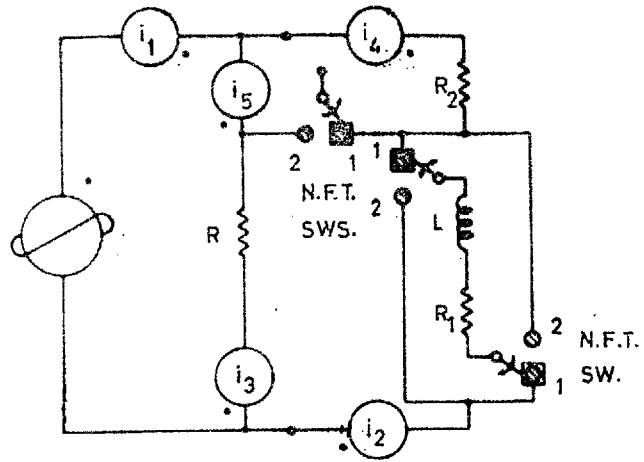
For explanations of symbols, see notes under table (4.2).

Voltage  
energisation

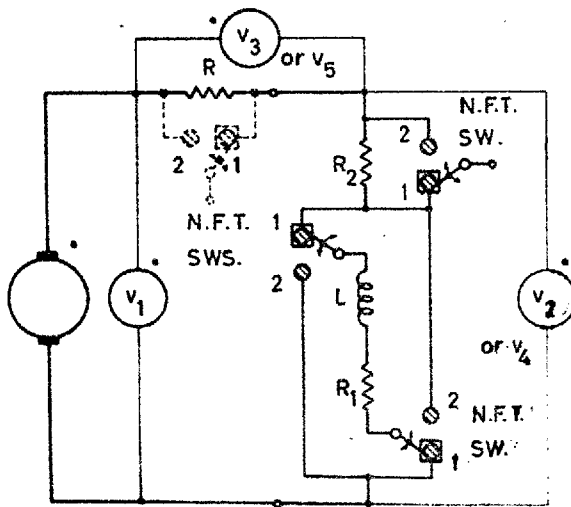


(a) Prototype

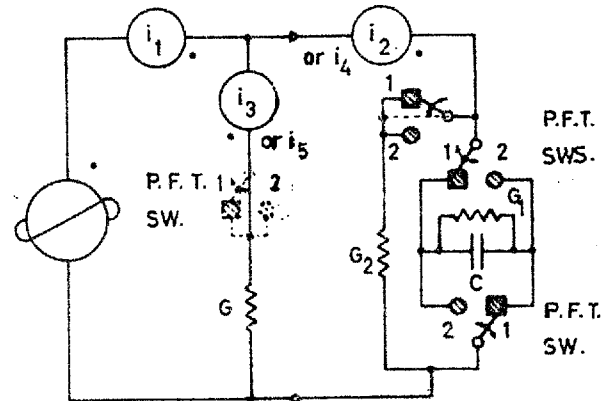
Current  
energisation



(b) Dual of prototype



(c) Complement of prototype



(d) Dual-complement of prototype

Fig. 13

Triple-switch single-capacitor chopper network and its derived networks

TABLE (5.3)

Response equations, in Laplacian form, of triple-switch  
single-capacitor prototype chopper network

Interval of Time	Response Equations	
$nT \leq t < (n+\delta)T$	$v(s)$	$\left\{ \frac{n v_1(s)}{\tau} / \left( s + \frac{1}{\tau_e} \right) \right\} + \left\{ n V / \left( s + \frac{1}{\tau_e} \right) \right\}$
	$v_2(s)$	$v(s)$
	$v_3(s)$	$\left\{ n v_1(s) \left( s + \frac{1}{\tau_{e12}} \right) / \left( s + \frac{1}{\tau_e} \right) \right\} - \left\{ n V \left( s + \frac{1}{\tau_e} \right) \right\}$
	$v_4(s)$	$v_2(s)$
	$v_5(s)$	$v_3(s)$
$(n+\delta)T \leq t < (n+\frac{1}{2})T$	$v(s)$	$(n + \delta) V / \left( s + \frac{1}{\tau_1} \right)$
	$v_2(s)$	$(n + \delta) v_1(s)$
	$v_3(s)$	o
	$v_4(s)$	o
	$v_5(s)$	$(n + \delta) v_1(s)$
$(n+\frac{1}{2})T \leq t < (n+\frac{1}{2}+\delta)T$	$v(s)$	$\left\{ \left( n + \frac{1}{2} \right) \frac{v_1(s)}{\tau} / \left( s + \frac{1}{\tau_e} \right) \right\} - \left\{ \left( n + \frac{1}{2} \right) V / \left( s + \frac{1}{\tau_e} \right) \right\}$
	$v_2(s)$	$v(s)$
	$v_3(s)$	$\left\{ \left( n + \frac{1}{2} \right) v_1(s) \left( s + \frac{1}{\tau_{e12}} \right) / \left( s + \frac{1}{\tau_e} \right) \right\} + \left\{ \left( n + \frac{1}{2} \right) V / \left( s + \frac{1}{\tau_e} \right) \right\}$

TABLE (5.3 contd.)

Interval of Time	Response Equations	
	$v_4(s)$	$v_2(s)$
	$v_5(s)$	$v_3(s)$
$(n + \frac{1}{2} + \delta)T \leq t < (n+1)T$	$v(s)$	$(n + \frac{1}{2} + \delta) \frac{V/(s + \frac{1}{\tau_1})}{\tau_1}$
	$v_2(s)$	$(n + \frac{1}{2} + \delta) v_1(s)$
	$v_3(s)$	o
	$v_4(s)$	o
	$v_5(s)$	$(n + \frac{1}{2} + \delta) v_1(s)$

N.B.:

For explanations of symbols, see notes under table (4.2).

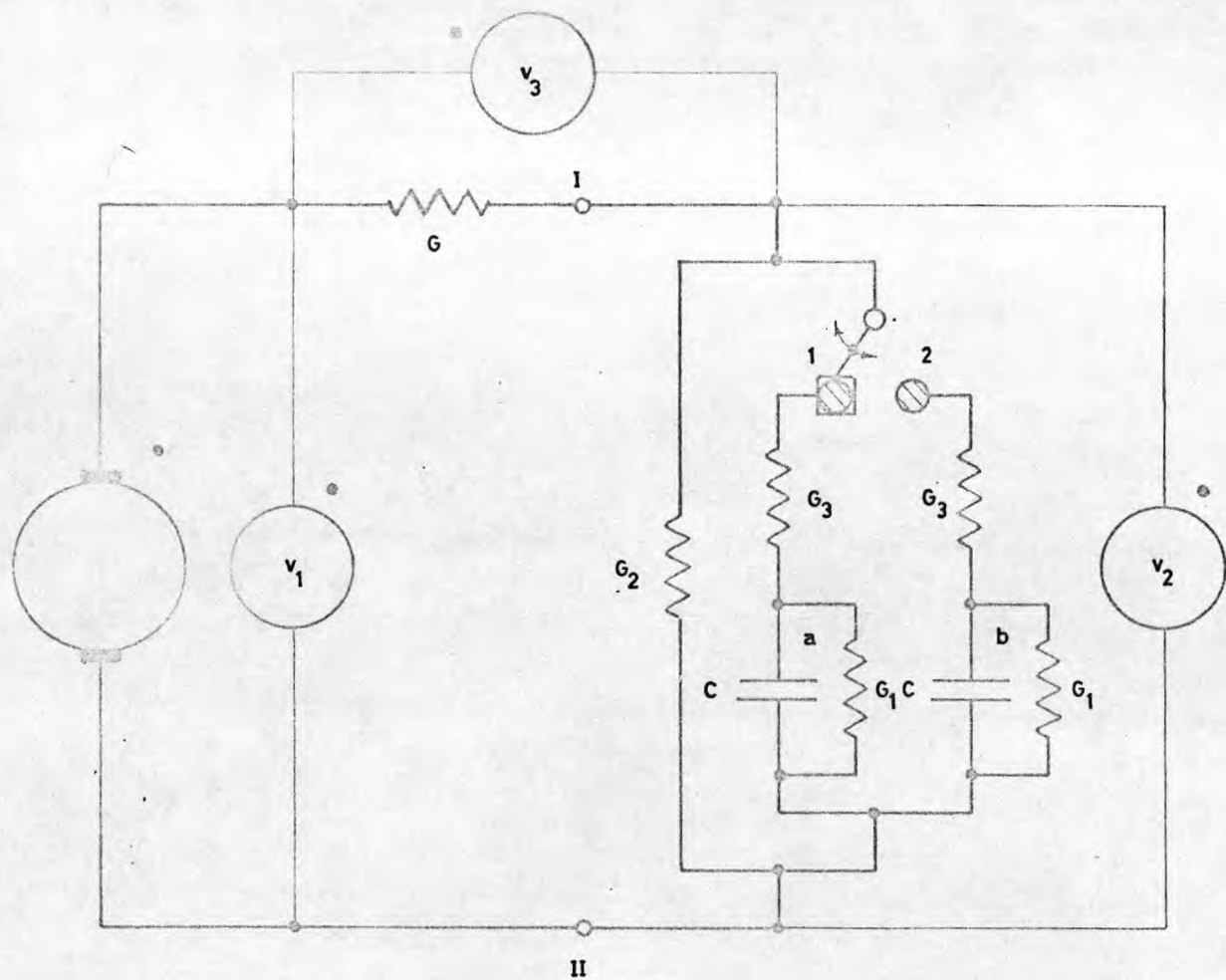
This is fundamentally because negative fly-time operation of the synchronous switches allows short circuiting of the capacitors, which may possess different finite charges, to take place. As a result, very high currents (theoretically infinity) would flow through the switches and damage them.

Therefore, in order to extend the practical operation of various synchronous switches in the N.F.T. region, it is necessary to add a current limiting resistor in series with each capacitor. Significant modification in various chopper network responses are expected as a consequence of inserting these limiting resistors as well as of the effect of N.F.T. operation of the synchronous switches. Keeping this in mind it is obvious that all previously discussed chopper network prototypes can be modified to allow full-range of fly-time operation of the synchronous switches. Corresponding modifications in various derived chopper networks have to be also made to prevent either open circuiting inductors, through which finite current are flowing, or short circuiting capacitors possessing finite charges, to take place.

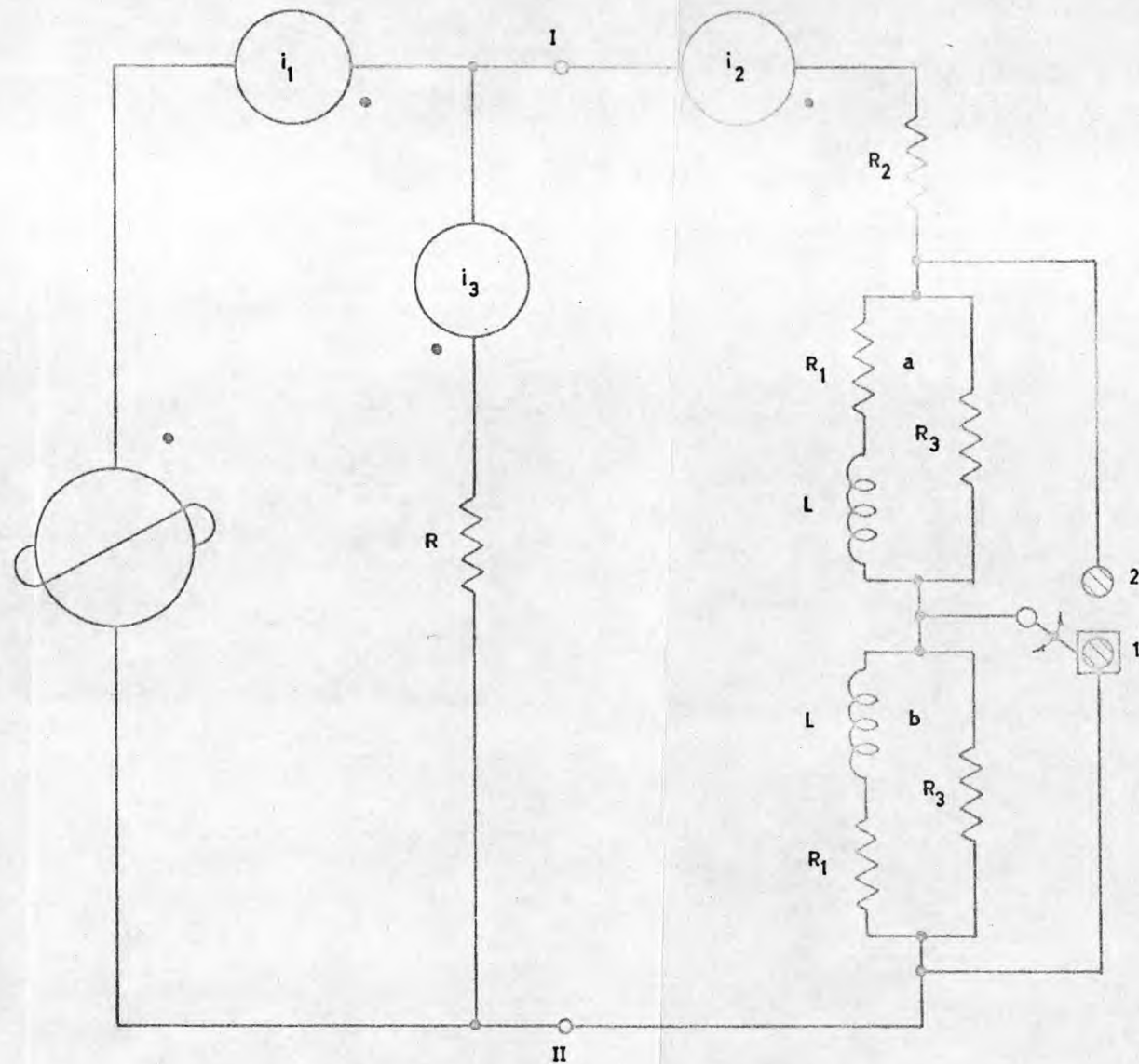
For the purpose of more clarification, the prototype and dual of single-switch double-capacitor network, shown in Figs. (5-a) and (5-b), are taken as an example. After the modifications these networks are re-illustrated in Figs. (14-a) and (14-b), respectively.

### 5.3 Use of Operational Amplifiers and Transformers

In the previous two subsections, it has been shown that realization of modified responses is feasible by means of either modifying the structure of various chopper networks or by making use of the full-range of fly-time variation of the incorporated



(a) Prototype



(b) Dual of prototype

Fig.14

Modified single-switch double-capacitor chopper network and its dual, practicable for full range of fly-time operation of synchronous switch



synchronous switches. A different technique of obtaining modified responses, based on the principle of adding or subtracting proportional quantities of the input and any particular output of the chopper network, is also possible <sup>(19)</sup>. The addition (or subtraction) operation of the two signals may be performed by means of a summing amplifier.

To demonstrate this technique, the single-switch double-capacitor chopper network of Fig. (5-a) is selected as an example. This is illustrated in Fig. (15) where the output expressions of  $v'_2$  and  $v'_3$  can be easily formulated as given below:

$$v'_2 = - \frac{1}{G_f} \left\{ G_a v_1 - A G_b v_2 \right\} \quad 5.1$$

$$v'_3 = - \frac{1}{G_f} \left\{ G_a v_1 - A G_c v_3 \right\} \quad 5.2$$

Where

$G_f$  is conductance of the feedback resistor

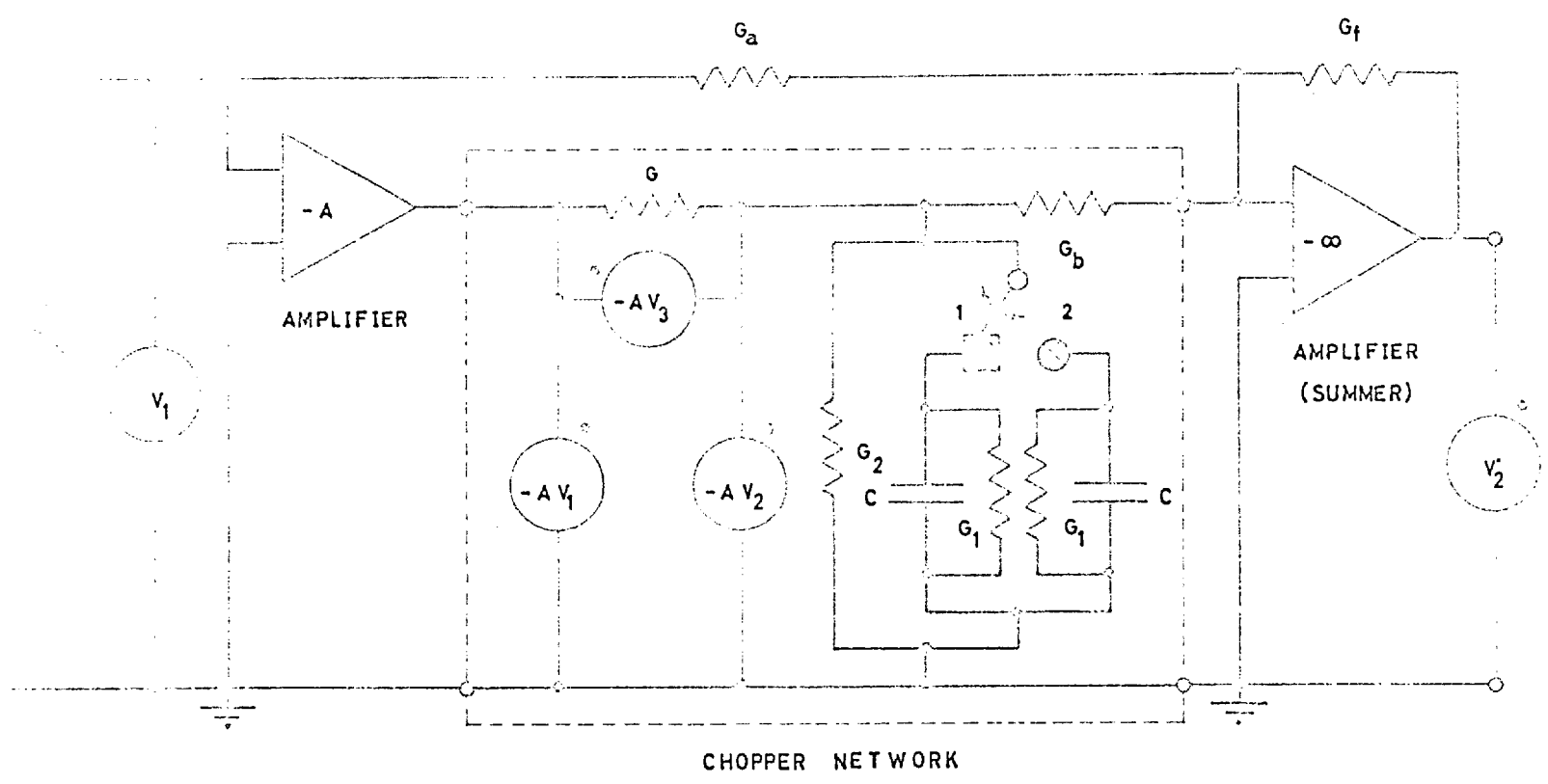
$G_a$  is conductance in the parallel adding channel

$G_b, G_c$  are conductances of the adding resistors in series with chopper network

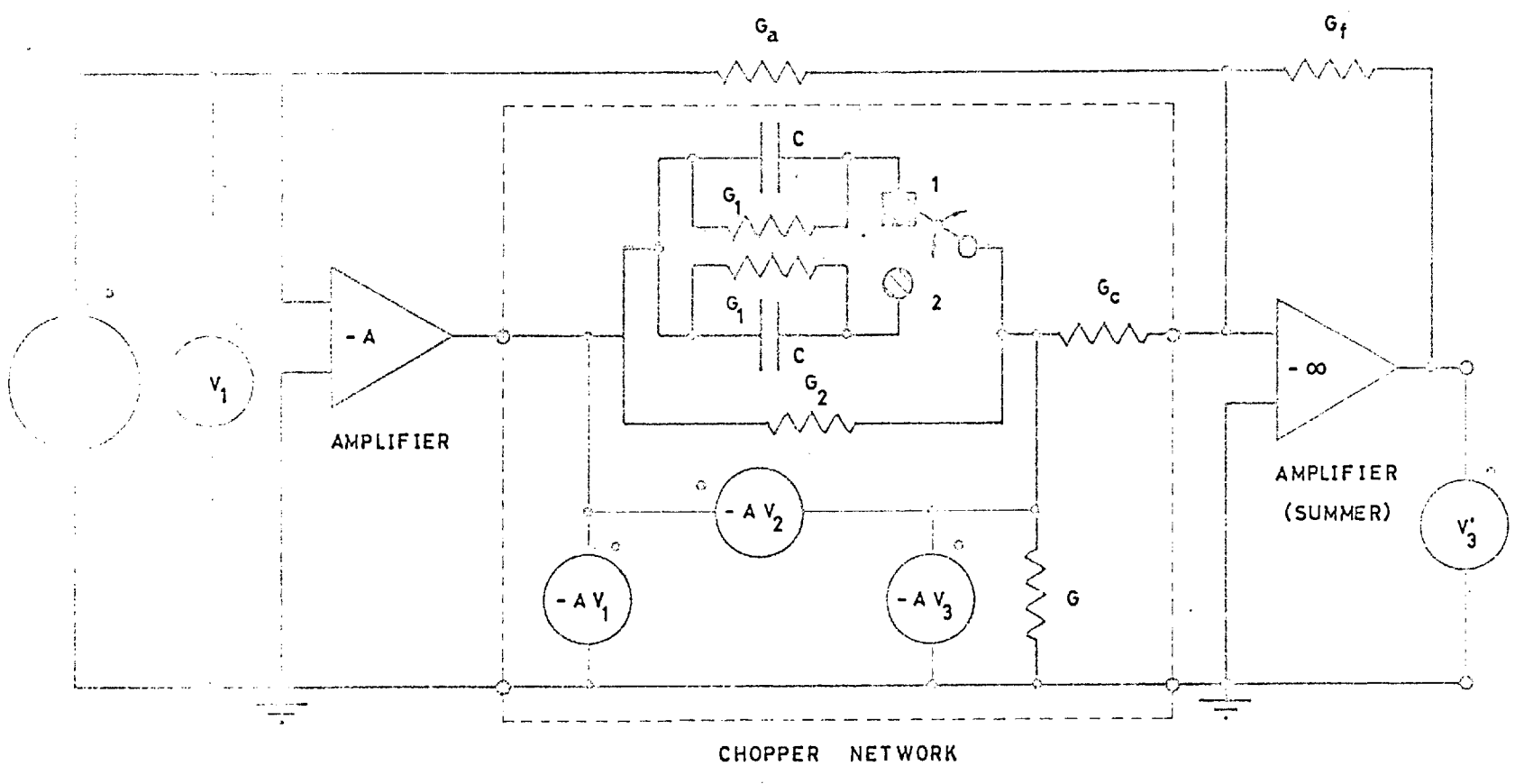
$A$  is the gain of the amplifier feeding the chopper network

From the expressions of  $v'_2$  and  $v'_3$ , it is evident that a wide range of modification is feasible not only by varying the ratios  $G_b/G_f$  and  $G_c/G_f$  but also by varying the amplifier gain  $A$  which may possess a positive or a negative sign (according to employed number of amplifier stages).

A less flexible arrangement is possible by utilizing centre-tapped transformer as shown in Fig. (16). Expressions



(a)



(b)

Fig.15  
Circuits illustrating the use of operational amplifiers for obtaining modified responses

for  $v_{o_1}$  and  $v_{o_2}$  may be written as

$$v_{o_1} = -R_f \left\{ \frac{n_1}{R_a} v_1 - \frac{n_2}{R_b} v_2 \right\} \quad 5.3$$

$$v_{o_2} = -R_f \left\{ \frac{n_1}{R_a} v_1 + \frac{n_2}{R_c} v_2 \right\} \quad 5.4$$

which imply that subtraction and addition of signals in the two parallel channels correspond to the arrangements (a) and (b) of Fig. (16), respectively.

In the case when only signal addition is required, it is possible to dispense with the amplifier A as well as with the transformer and the input signal is thus fed directly to the two parallel channels.

## 6.0 Conclusions

Special attention has been given to 3-terminal synchronous switch as an essential part of chopper networks. An increased insight into its functioning and timing operation has been derived from the simple mechanical representation described above. This representation has enabled the concept of fly-time in its positive and negative sense to be explained comprehensively in simple physical terms.

It has been shown that breaking 3-terminal switch into its most elementary form of 2-terminal switch is feasible. With 2-terminal switch, it was possible to apply the principle of duality resulting in another 2-terminal switch whose sequential operation is intimately related to that of the prototype. The achievement of these two steps has led to the extension of application of duality concept to 3-terminal switches which, in turn, paved the way for the development of systematic techniques

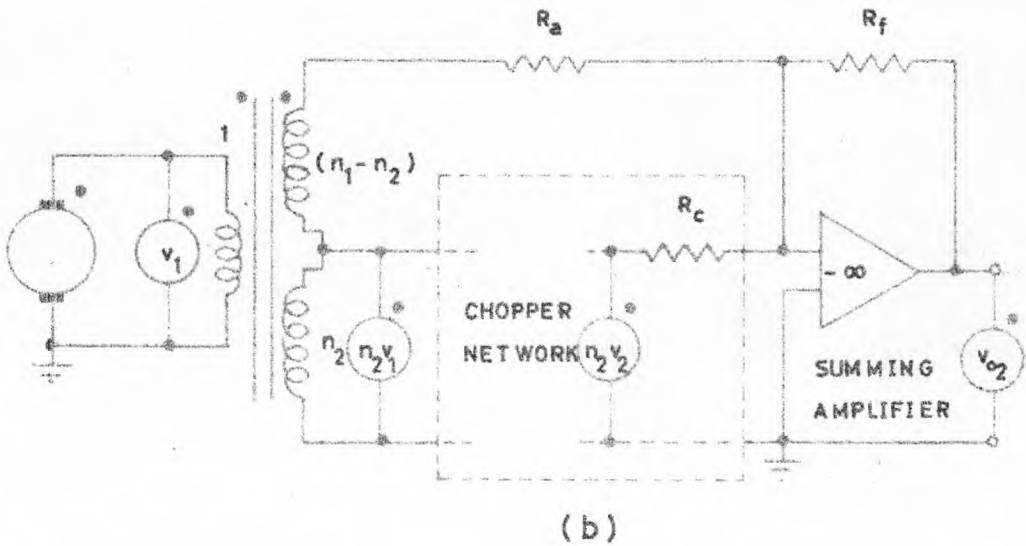
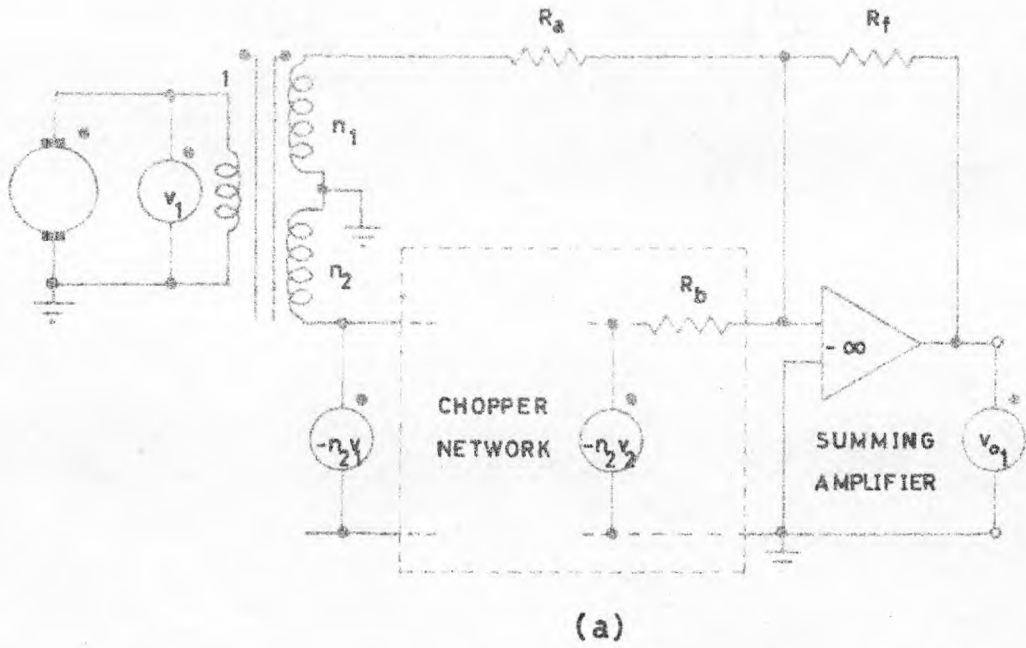


Fig. 16

Circuits illustrating the use of transformers for obtaining modified responses

for constructing the dual of chopper networks of complicated configurations.

Making use of the duality concept, Thevenin's and Norton's theorems, derivation of physically dissimilar chopper networks with identical responses have been realized. Substantial economy in computational effort is evident since the analysis of only one chopper network yields the behaviour of its analogous ones. Freedom in selecting either voltage or current forms for excitation and response signals of various chopper networks may result in an increased flexibility in many applications. Although the study in this paper has been limited to chopper networks comprising only two electrical passive elements RC or RL, however, it lays down the foundation for any further development of more elaborate configurations involving the three passive elements RLC.

It has been also shown that modified responses of various chopper networks can be realized not only by varying the values of passive elements but also by:

- (i) Modifying the chopper network structure with the use of additional number of synchronous switches which may be connected in different ways.
- (ii) Varying the fly-time operation of synchronous switches over its positive range as well as its negative range.
- (iii) Making use of operational amplifiers and transformers for adding or subtracting proportional quantities of the input and any particular output of the chopper network.

Finally, it is believed that the above treatment of the synchronous switches would considerably increase their potential

which could find a wider scope of application in many fields. With regard to the techniques developed concerning the realization of new configurations and responses of chopper networks, further exploitation is suggested. Extensive studies are also suggested to be directed towards the noise content and network economy on which basis various chopper networks may be compared.

#### 7.0 Acknowledgements

The work described in this paper was carried out under the supervision of Dr. D.G.O Morris, D.Sc., M.I.E.E., Reader in Electrical Engineering, Imperial College of Science and Technology. The author wishes to express his thanks to Dr. Morris for his helpful guidance, constant encouragement and keen interest.

The author also wishes to place on record his gratitude to Dr. P.H.G. Allen, Ph.D., A.M.I.E.E., A.M.I.Mech.E., and Dr. N.J. Short, Ph.D., for their invaluable assistance and constructive criticism.

#### 8.0 References

1. Murphy, G.J. and J.F. Egan. "The Analysis of Compensating Detectors for A.C. Control Systems", Proceedings, National Electronics Conference, Vol. 15, pp. 1056-65, 1959.
2. Murphy, G.J. and J.F. Egan. "The Analysis of Demodulating Compensating Networks", IRE Trans., on Automatic Control, Vol. AC-4, pp. 71-79, Dec., 1959.

3. Bohn, E.V. "Demodulator Lead Networks", IRE Trans., on Circuit Theory, Vol. CT-7, pp. 56-61, Mar., 1960.
4. Bohn, E.V. "A Simple Method for the Analysis of Demodulator Compensating Networks", Ibid., Vol. CT-8, pp. 306-11, Sept., 1961.
5. Weiss, G. "Synchronous Networks", Trans. IRE, PGAC, Vol. AC-7, No. 2, pp. 45-49, Mar., 1962.
6. Walker, F. and D.R. Wilson. "The Analysis of an R.C. Chopper Network", Electronic Engineering, pp. 111, 1965.
7. Knox, A. and G.J. Murphy. "A Method for The Design of Phase-Lead Demodulating Compensators for Use in Carrier Control Systems," I.E.E.E., Vol. AC-8, No. 4, 1963.
8. Murphy, G.J. and A. Knox. "A Method for the Design of a Phase-Lag Demodulating Compensator for Use in Carrier Control Systems," I.E.E.E., Trans. Applic. Industr., No. 73, pp. 252-7, July, 1964.

9. Khalafalla, F.B., "Design of a Transistor 3-Terminal Synchronous Switch and its Driving Circuit", Power Systems Laboratory Report No. 67, Imperial College, Jan., 1966.
10. Tuttle, D.F. "Network Synthesis"; Vol. 1, John Wiley & Sons, Inc., 1958.
11. Cauer, W. "Synthesis of Linear Communication Networks," Volumes I and II, McGraw-Hill Book Company, Inc., 1958.
12. Kuhn, E.S. and D.O. Pederson. "Principles of Circuit Synthesis", McGraw-Hill Book Company, Inc., 1959.
13. Guillemin, E.A. "Introductory Circuit Theory," John Wiley & Sons, Inc., 1960.
14. Guillemin, E.A. "Synthesis of Passive Networks," John Wiley & Sons Inc., 1962.
15. Hazony, D. "Elements of Network Synthesis," Reinhold Publishing Corporation, New York, 1963.
16. Van Valkenburg, M.E. "Introduction to Modern Network Synthesis," John Wiley & Sons, Inc., 1964.



17. Morris, D.G.O. "Mechanical Networks,"  
Correspondence, Journal  
I.E.E., May, 1955.
18. Morris, D.G.O. "Ideal Active Elements,"  
Journal I.E.E., Vol. 3,  
No. 29, pp. 272/3, May,  
1957.
19. Schlesinger, E.R. "Choppers Compensate A.C.  
Servos," Control Engrg.,  
11 (g), 113-114, Sept.,  
1964.

## 9.0 Appendix

List of dual quantities or concepts (13)

Current	voltage
branch current	branch voltage
mesh or loop	node or node pair
number of loop (l)	number of node pairs (n)
loop current	node-pair voltage
mesh current	node potential
link	tree branch
link current	tree-branch voltage
tree-branch current	link voltage
tie set	cut set
short circuit	open circuit
parallel paths	series paths